MARTIN MARIETTA ENERGY SYSTEMS LIBRARIES

3 4456 0365947 7

ORNL-3470
UC-25 – Metals, Ceramics, and Materials
TID-4500 (23rd ed.)

METALS AND CERAMICS DIVISION
ANNUAL PROGRESS REPORT
FOR PERIOD ENDING MAY 31, 1963

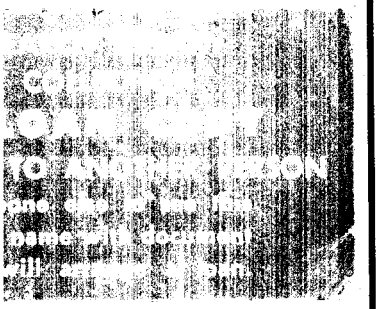

OAK RIDGE NATIONAL LABORATORY
operated by
UNION CARBIDE CORPORATION
for the
U.S. ATOMIC ENERGY COMMISSION

Printed in USA. Price: $3.50 Available from the
Office of Technical Services
U. S. Department of Commerce
Washington 25, D. C.

LEGAL NOTICE

This report was prepared as an account of Government sponsored work. Neither the United States, nor the Commission, nor any person acting on behalf of the Commission:

A. Makes any warranty or representation, expressed or implied, with respect to the accuracy, completeness, or usefulness of the information contained in this report, or that the use of any information, apparatus, method, or process disclosed in this report may not infringe privately owned rights; or

B. Assumes any liabilities with respect to the use of, or for damages resulting from the use of any information, apparatus, method, or process disclosed in this report.

As used in the above, "person acting on behalf of the Commission" includes any employee or contractor of the Commission, or employee of such contractor, to the extent that such employee or contractor of the Commission, or employee of such contractor prepares, disseminates, or provides access to, any information pursuant to his employment or contract with the Commission, or his employment with such contractor.

ORNL-3470

Contract No. W-7405-eng-26

METALS AND CERAMICS DIVISION ANNUAL PROGRESS REPORT

for Period Ending May 31, 1963

J. H Frye, Jr., Director
J. E. Cunningham, Assistant Director

DATE ISSUED

NOV 4 [illegible]

OAK RIDGE NATIONAL LABORATORY
Oak Ridge, Tennessee
operated by
UNION CARBIDE CORPORATION
for the
U. S. ATOMIC ENERGY COMMISSION

MARTIN MARIETTA ENERGY SYSTEMS LIBRARIES

3 4456 0365947 7

Summary

PART I. FUNDAMENTAL RESEARCH

1. Crystal Physics

Crystals of BeO greater than 2 mm on an edge have been grown from the solvent, molten V_2O_5. These crystals were purer by more than an order of magnitude and apparently more perfect than previously reported crystals grown from $Li_2O{\cdot}2WO_3$. Optically clear ThO_2 crystals up to 3 mm on an edge have been grown from unseeded ThO_2-$Li_2O{\cdot}2WO_3$ solutions. Similarly, crystals approaching 1 cm on an edge have been grown on rotating seeds. Single crystals of the incongruently melting compounds UAl_3 and UAl_4, with longest dimension of 1 mm, have been grown from U-Al melts. Detailed x-ray structural analysis of hydrothermally synthesized single crystals of $Cs_2O{\cdot}Fe_2O_3{\cdot}4SiO_2$ has permitted their assignment to the cubic space group $IA3d$.

2. Reactions at Metal Surfaces

Studies of the fundamental mechanisms of oxidation have continued, and the role played by stress in oxidation mechanisms has remained a topic of primary interest. The large surface stress accompanying the solution of oxygen in niobium was measured directly by the flexure of specimens oxidized on one side only. The recrystallization of anodic oxide films on niobium and tantalum was investigated to improve understanding of the mechanism of destruction of the protective qualities of thermally formed oxide films on these metals. A study of the influence of surface impurities on the state of strain in Cu_2O films and on the oxidation kinetics for copper provided additional information on the relation between strain and oxidation kinetics.

3. Spectroscopy of Ionic Media

The general-purpose multicenter Gaussian and one-center Slater expansion techniques for the computation of electronic wave functions in atoms, molecules, and crystals are being developed. The one-center codes have been employed in demonstrating that the "split p-orbital" method is unsatisfactory.

Absorption spectra of nickel(II) ion, measured in a variety of high-temperature solvents, have been interpreted in terms of ligand-field theory. Tetrahedral nickel(II) complexes, which are relatively rare, have been identified in molten organic salts, molten potassium chloride, molten cesium chloride, and molten dimethylsulfone with added chloride. It has also been shown that the nickel(II) ion exists in an octahedral, or distorted octahedral, field when dissolved in molten fluorides. The spectra of nickel(II) ion in oxo salt solvents, such as nitrate and sulfate, actually involve a large rhombic splitting of the orbital states that arise from the free-ion ^3P term, rather than the previously assumed octahedral symmetry.

The lowest-energy charge-transfer bands of nitrate and iodide ions have been accurately measured in molten-salt solvents for the first time. The effect of cation environment on oscillator strength has been measured for the lowest-energy transition of the nitrate ion. A procedure has been devised for calculating the concentrations of the two solute species for a family of solute equilibria of which the simplest is $4Bi^+ \rightleftharpoons Bi_4^{4+}$, which occurs in Bi-$BiCl_3$ solutions. Densities of several pure salts and salt mixtures have been measured.

4. Structure of Metals

Additions of oxygen, nitrogen, and carbon completely suppress twinning in columbium single crystals deformed in slow compression at 77°K, but hydrogen in concentrations up to 1000 ppm has no effect on frequency of twinning. The <001> component in the fiber texture of aluminum rods extruded at subzero temperature is due primarily to

fragments of original <001> grains. During low-temperature annealing, these fragments act as nuclei for recrystallization. Other recrystallized texture components occur, and there is a marked difference in temperature dependence of the nucleation rate and/or growth rate of the various components. Studies continue on inhomogeneous flow in polycrystals, the texture of irradiated copper, and the role of deformation twins in nucleating recrystallization.

5. Theory of Alloying

Galvanomagnetic properties of eight high-purity single crystals of tungsten have been measured. The magnetoresistance was quadratic in magnetic-field strength for all orientations of current and magnetic field investigated. This indicates that the Fermi surface of tungsten is closed and compensated. In agreement, Hall fields were found to be positive, large, and only moderately anisotropic. The largest transverse electric field was not the odd Hall field but was an electric field even with respect to magnetic-field reversal. Sharp peaks of this property occurred whenever the magnetic field was normal to the <112> or <113> directions.

The low-temperature specific heats of Hf-Zr alloys have been measured. The electronic density of states, deduced from the electronic specific heat coefficient, changed slowly and nearly linearly between zirconium and hafnium. The Debye temperatures decreased from zirconium to hafnium, but less rapidly than would be expected from atomic masses alone. This finding is in agreement with the greater cohesion and elastic properties in hafnium, arising from the same factors as cause the lanthanide contraction.

The solubility of lead in β-zirconium was found to reach 14.5 at. % at 1300°C, and this composition retains the body-centered cubic structure upon quenching. The first intermediate phase in the Zr-Pb system is Zr_5Pb, which probably has the β-tungsten structure. A eutectic occurs at 23 at. % Pb near 1400°C.

6. Physical Property Studies

Studies have continued on accurate methods of measuring the thermal conductivity of solids over a wide temperature range and on the influence of controlled variables on this property. Thermal conductivity data have been obtained on UO_2 at temperatures up to 1350°C in a radial-heat-flow apparatus. The linear temperature dependence of the thermal resistance suggests that the only significant heat-transport mechanism operative in UO_2 up to 1350°C is phonon conduction. Operation of the thermal comparator apparatus has been described analytically, and a series of systematic thermal conductivity determinations was initiated. Development proceeded on several measurement methods, including a quenching method to measure thermal diffusivity up to 1500°C, a direct-heating method to measure thermal conductivity up to 2000°C, a probe method to measure the thermal conductivity of powders up to 1000°C in a variety of atmospheres, and a technique to measure total hemispherical emittance up to 1200°C.

7. Basic Sintering Studies

Evaluation of the densification kinetics of ThO_2 powder compacts during the initial sintering (as the specimens are brought to temperature) indicates that material transport occurs by plastic flow (dislocation motion). The effect of heating rate on densification has been studied at much higher rates than previously, and a temperature-dependent end point has again been noted. These observations seemed to indicate that material transport due to dislocation motion during early stages of sintering was very rapid. Impurities appear to have caused the previously reported minimum in the densification rate as a function of temperature for ThO_2 powder compacts. Thoria containing CaO sintered and underwent creep at much lower temperatures than ThO_2 without additives.

8. Deformation of Crystalline Solids

An improved calorimeter for the measurement of stored energy during deformation of metals and alloys has been designed and constructed. Stored energy in a series of deformed copper-zinc alloys appears to be related to effects on short-range order.

With an electron microscope, dislocation density as a function of deformation has been measured for a series of dilute alloys of aluminum in nickel

previously studied with the calorimeter. Dislocation density for a given strain was independent of composition. However, the addition of aluminum appeared to suppress a cell structure observed in pure nickel.

The effect of strain rate on the drop of the yield point in iron showed that the yield point is due to the multiplication of dislocations and not to the unlocking of dislocations from their impurity atmospheres. Yield-point data on the copper-aluminum system have also been analyzed.

The low-temperature creep properties of alpha iron were studied. A direct determination showed the activation energy and activation volume to be independent of temperature, strain rate, and interstitial impurity content but dependent on stress.

9. X-Ray Diffraction of Crystalline Defects

X-ray diffraction studies of thin Cu_2O films grown on copper single crystals, in cooperation with the Reactions at Metal Surfaces Group, have continued. Films grown on the (311) copper surface had more nearly the same lattice constant as bulk Cu_2O, were less strained, and had less mosaic spread than those grown on the (110) surface. These results are consistent with the smaller epitaxial mismatch of the film with the substrate and the smaller oxidation rate as compared with films grown on the (110) surface.

10. X-Ray Diffraction Research

Service functions and research programs of the X-Ray Diffraction Group are reviewed. The determination of crystal structures for mixed-oxide compounds containing BeO and for iron-substituted minerals has progressed. The application of single-crystal diffraction techniques to the problem of radiation damage in BeO has confirmed the general hypotheses derived from powder data and added new details requiring more-sophisticated models of the damaged lattice. An x-ray diffraction experiment with Nb_3Sn showed no thermal instability or order-disorder transition up to 1000°C.

11. Metallurgy of Superconducting Materials

Since homogeneous materials must be obtained for both physical metallurgy studies and superconducting property determinations, segregation in alloys was studied. A casting technique was developed which produces only microsegregation. This segregation was eliminated in most of the alloys of the niobium-zirconium system by annealing at 1400°C for 4 to 24 hr. A metallographic technique was developed for making quantitative analyses of the compositions of the alloys over regions ranging from 0.5 μ to several centimeters in diameter. Preliminary tests indicate that this technique is applicable to Ti-, Zr-, Nb-, and Ta-base alloys.

Studies of the transformation kinetics and morphologies of niobium-zirconium alloys containing 25 to 40% Zr showed only the $\beta \longrightarrow \beta_1 + \beta_2$ reaction; no transformation to the equilibrium α_{Zr} + Nb structure occurred in one week at 400, 500, or 600°C. Composition had little effect on the incubation period for the transformation but did affect the time for completion of the transformation. Cold work accelerated the entire transformation. The maximum rate of transformation occurs at about 700°C for all compositions.

A nondestructive technique has been developed to determine the quality of long lengths of wire. The method uses a Keithley milliohmmeter to measure continuously the resistance of a ¼-in. section of the wire passing through the instrument. The cause of resistance variations of 10%, observed in some lots of commercial wire, is being investigated by superconducting property testing and destructive examination.

12. Electron-Microscope Studies

Observations of dislocation substructure, mechanical twins, and impurities in columbium and columbium-vanadium alloys have led to an explanation for the mechanical behavior of the body-centered cubic metals at low temperature.

Two annealing processes have been observed in single crystals of columbium deformed at room temperature. One process resembles homogeneous nucleation and migration of coincidence site boundaries. The other annealing process gives a gradual elimination of dislocations without boundary migration.

The formation and reversion of ω phase were followed in a Zr–15% Nb alloy, and many of the structural features of the early aging stages were clarified.

PART II. LONG-RANGE APPLIED RESEARCH

13. Zirconium Metallurgy

Studies of the α-zirconium solubility boundary in the Zr-Nb alloy system showed, by quantitative metallography, that a third phase might exist between the reported alpha and beta phases.

Single crystals of dimensions up to $1 \times 20 \times 75$ mm of zirconium and $1 \times 6 \times 30$–40 mm of Zircaloy-2 have been grown by traversing strip specimens past an electron beam that produces a hot zone 1 mm high and as wide as the strip.

The phase shift occurring on reflection of incident light at the oxide-metal interface of anodized oxide films in situ has been measured for both niobium and Zircaloy-2 over the spectral range of 3000 to 15,000 A. The refractive indices of oxide films on niobium, produced by anodizing, have been measured over the spectral range 3750 to 7000 A by two methods with excellent agreement. The combination of techniques enables very accurate measurement of film thickness.

A method was developed for semiquantitatively determining the preferred orientation in polycrystalline Zircaloy-2 by microhardness measurements.

14. Materials Compatibility

Oxygen as an impurity can have a significant effect on the compatibility of alkali metals with refractory metals. Oxygen partitions itself between the two metal phases in the proper ratio to attain the same chemical potential in the two metals. Using this thermodynamic fact, a method has been developed to predict the equilibrium distribution of oxygen between refractory and alkali metals. Theoretically calculated values of the distribution coefficient for several systems at 500 and 800°C have been compared with experimental results.

15. Solid Reaction Studies

Extensive experimental data on diffusion in body-centered cubic zirconium, titanium, and vanadium have demonstrated the inapplicability of the Arrhenius-type expression in describing the behavior of diffusion coefficients over wide temperature ranges. A program was initiated to study diffusion in solids in a temperature gradient. The effect of alpha bombardment on diffusion coefficients of Pb^{212} in silver is being determined. Diffusion rates of Nb^{95} in UO_2 have been determined from 1100 to 2100°C.

16. Fuel Element Development

All phases of the Fuel Element Development Program have been directed toward higher temperature operation.

In a new part of the program, aimed at fabricating fuel elements by vapor deposition techniques, pyrolytic graphite, tubing of several refractory metals, and various boron-carbon compositions including B_4C have been satisfactorily deposited. Fine-grained, randomly oriented tungsten tubing was fabricated with excellent control of the surface and dimensions.

A combined $(U,Th)O_2$ fuel produced by the sol-gel technique has been substituted for UO_2 in the development of an all-ceramic fuel element. High-quality, dispersion-type fuel bodies have been fabricated by spheroidizing the individual particles and coating them with BeO before cold pressing and sintering and are undergoing irradiation tests.

It has been shown that UO_4 is the volatile material lost during the reduction of UO_{2+x} in vacuum. The composition of the equilibrated (solid) oxide phase as a function of oxygen pressure was also determined.

By use of pure starting materials and careful prevention of surface contamination during processing, UC compacts having high and uniform densities have been obtained by low-temperature sintering. Additions of UAl_2 as a sintering aid have consistently yielded densities greater than 97% with sintering temperatures of only 1400°C and with 97% of the aluminum being removed during the processing.

Brazing alloys were developed that were capable of wetting and flowing on BeO and UO_2. Adequate bonding was obtained when UO_2 was brazed to a variety of metals, but some difficulty has been encountered with microcracking in the UO_2.

The reproducibility achievable in forming aluminum-base dispersion fuel plates has been greatly

increased by incorporation of a considerable amount of cold working into the fabrication sequence. The optimum fabrication temperature for such plates was shown to be 500°C when the effects of fabrication temperature on blistering and forming were balanced.

17. Mechanical Properties Research

This research is concerned with the effects of reactor coolant, multiaxial stress state, fatigue, and reactor irradiation on the mechanical properties of materials of interest to reactor technology. The mechanism by which hydrogen reduces the creep strength of nickel alloys has been elucidated by the discovery that the presence of hydrogen in nickel reduces the dislocation pinning stress. Prestraining, even to the small strains introduced in roller-leveling sheet or straightening tubing, has been shown to significantly reduce ductility of austenitic stainless steels. Austenitic stainless steels in CO_2 carburize readily if the chromium content is approximately 11%; at contents below about 5% or above 20%, carburization does not occur under the conditions studied.

States of stress other than simple uniaxial stressing have been studied for Inconel under low-cycle fatigue conditions at 820°C. The rupture time for this alloy could be related to the maximum principal stress and the effective stress computed from distortion energy theory.

An extensometer capable of measuring displacements to ± 0.0005 in. in a fast-neutron flux of 3×10^{13} *nv* has been developed and has been used in in-pile creep experiments on graphite.

18. Nondestructive Test Development

Nondestructive techniques are under continuous development for testing nuclear components, particularly by use of electromagnetic, ultrasonic, and penetrating radiation. A new phase-sensitive eddy-current instrument, operating in the frequency range 1 kc to 4 Mc, has greater applicability to thickness measurements than more conventional instruments. A mathematical model to aid design of improved electromagnetic probes is being programmed. Ultrasonic studies have led to development of a new device for inspecting brazed heat-exchanger joints. Low-voltage radiography has been extended to contact radiography capable of 500× magnification and useful for evaluating coated uranium carbide particles. Improved gamma- and x-ray transmission techniques are being developed for the determination of fuel-loading variations in fuel plates and rods. Existing test methods are being adapted to measurements of problem materials and measurements in radiation fields.

19. High-Temperature Materials

The High-Temperature Materials Program is developing knowledge for the design of advanced reactors that will use alkali metals as heat transfer and working fluids and either superalloys or refractory alloys as container materials.

At pressures as low as 3×10^{-7} torr, the interstitial content of 0.040-in.-thick Nb–1% Zr alloy specimens will increase 300 ppm in 1000 hr at 1200°C. Wrapping of specimens in molybdenum foil reduces the contamination. The creep rate of Nb–1% Zr alloy at 1000°C was found sensitive to pressure in the range 10^{-5} to 10^{-7} torr. The vapor pressure of type 316 stainless steel in high vacua has been determined to range from 3.4×10^{-9} torr at 760°C to 1.7×10^{-7} torr at 980°C. Oxide films on the stainless steel reduce the evaporation rate by approximately 50%.

Tube blanks have been fabricated from molybdenum alloys by extrusion and from niobium alloys by floturning.

The mode and depth of penetration of oxygen-contaminated niobium by lithium have been shown to depend on grain size and temperature, with penetration increasing as the grain size and temperature increase. A Haynes alloy No. 25 natural-circulation corrosion loop containing boiling potassium has been satisfactorily operated for 3000 hr at 870°C. Less than 0.1 mil was removed from the condenser and a small deposit of metal was seen in the cooler zones. Cracks were found in the Haynes alloy No. 25 and were attributed to thermal cycling associated with boiling instabilities. Stabilization of boiling of alkali metals (potassium and rubidium) has been achieved by 150°C initial local superheating of liquid in the boiler.

Vacuum creep tests have been conducted on Mo–0.5% Ti, Nb–40% V–1% Ti, and Nb–1% Zr in the temperature range 870 to 1300°C. The Nb–40%

V–1% Ti alloy is disconcertingly weak, even at a temperature of 870°C. The internal-friction spectrum of nitrogen-contaminated Nb–1% Zr alloys has been related to zirconium-nitrogen interactions.

A 2-ft-wide by 10-ft-high forced-circulation loop of Nb–1% Zr has been fabricated in an argon-filled chamber using 74 manual welds.

The total hemispherical emittance of Nb–1% Zr alloy was found to be sensitive to the contamination that occurs at 6 to 9×10^{-6} torr.

Nondestructive techniques have been applied to the inspection of molybdenum alloy tubing, and a new phase-sensitive eddy-current technique was used to inspect tapered stainless steel tubing.

PART III. REACTOR DEVELOPMENT SUPPORT

20. Gas-Cooled Reactor Program

Approximately 65% of the first core for the EGCR and all control rods have been received. Twelve of the twenty instrumented fuel assemblies for the EGCR core have been assembled. A nondestructive technique has been developed to detect nonbonding of the thermocouples to the cladding of these units.

Preliminary results on graphite cantilever beams under irradiation at 450°F have shown that the zero intercept and the linear creep rate vary linearly with stress.

Varied fuel elements and specimens have been fabricated for irradiation testing for advanced reactor concepts. Suitable procedures have been developed for arc welding end closures in beryllium tubes. A Ti–6 wt % Be alloy was found to have the best wetting behavior of brazing alloys for beryllium. The effects of external pressure, cladding thickness, and friction forces on interactions between UO_2 fuel and stainless steel cladding have been studied.

Pyrolytic-carbon-coated uranium carbide particles have been evaluated by measurement of several physical characteristics. The escape of fission-product Kr^{88} from the particles appeared to be related to the percentage of particles cracked during load tests and the coating thicknesses. Equipment capable of coating particles at up to 2000°C has been assembled. Uranium migration in coated-particle fuels heated to 1600 and 2000°C has been measured by neutron activation and by low-voltage radiography. Coated particles have retained fission gases excellently ($< 10^{-4}$% release at 1400°C) when care was taken not to rupture coatings.

Fueled-graphite spheres and bushings have been characterized. Dry chlorine gas at 800 to 1000°C markedly reduced exposed fuel, as measured by alpha counting, acid electrolysis, or neutron activation. Duplex pyrolytic-carbon coatings under irradiation have retained fission-product gases excellently. Only 1 to 2% of the coatings cracked on particles irradiated at 800 to 2100°F for up to 30 at. % burnup. Fueled graphite at 1500 to 1800°F irradiated to 2 at. % burnup retained Kr^{88} well (R/B $< 10^{-7}$%). Pyroxylin films have enabled measurement of the microhardness of pyrolytic-carbon coatings. These films retain the indenter impression; the pyrolytic-carbon coating is resilient and does not.

Irradiation at 650°C has produced a greater effect on strength and ductility of the British 20 Cr–25 Ni–Nb alloys than has irradiation at 750°C. Irradiation appears to have weakened or embrittled the end-closure weld region.

The metal cladding of UO_2 being irradiated appears to capture all energetic recoil atoms; the gases measured on postirradiation puncturing probably result from diffusion or from boiling out from the recoil tracks that penetrate the fuel surface.

The thermal conductivity of polycrystalline UO_2 has been found to fit a lattice-conduction heat-transport mechanism, at least to 1100°C.

Deposition of fission-product iodine and tellurium from uranium carbide at 800°C has been measured. The rate-controlling step in the deposition of I^{131} on stainless steel surfaces below 300°C appears to be diffusion through the helium sweep gas.

Nitrided type 304 stainless steel has been found to oxidize in impure helium at 1050°F. Thus under EGCR conditions the surface properties of the nitride case would be replaced by those of an oxide film.

A general interrelation has been observed between strength, density, hardness, and modulus of elasticity of graphite moderator materials. The compression modulus of elasticity was much smaller than the corresponding tensile modulus for all specimens tested.

21. Molten-Salt Reactor

The vapor of CF_4 has been found effectively nonreactive toward INOR-8 immersed in fuel salt at 600°C, but minor attack occurred at 700°C. The debilitating effect of fluoride-salt spillage on oxidation resistance of INOR-8 has been studied. The microstructure and composition of molybdenum were unchanged when it was tested with materials used in the Molten-Salt Reactor Experiment system.

The tube-to-tube sheet joints for the MSRE heat exchanger have been successfully accomplished by welding and back brazing with a gold-nickel alloy. Nondestructive ultrasonic and radiographic tests of the tube joints were developed and used. Procedures have been developed for welding INOR-8 to nickel, Inconel, and austenitic stainless steel. Room- and elevated-temperature tensile properties and creep properties have been measured for these weldments. Stress relieving at 1600°F was found to significantly improve the stress rupture and high-temperature ductility of INOR-8 weld metal.

Random heats of reactor-quality INOR-8 to be used in the MSRE have been found to have mechanical properties better than established design values. This alloy has been approved by the ASME Boiler and Pressure Vessel Code Committee. Evidence has been found in INOR-8 for a dynamic strain aging that is affected by the number of impurity atoms in solution available to interfere with dislocation motion.

Grade CGB graphite bars produced for the MSRE moderator met specifications except that they had a general cracked condition and some bars had densities as low as 1.82 g/cm^3. Despite this, the graphite had good mechanical strength and adequately low permeation to salt. Rapid thermal cycling between 390 and 1300°F did not damage the graphite or cause salt-impregnated cracks to propagate. Tensile strength of CGB graphite bars was found to average 5440 psi for flaw-free specimens and range down to 1510 psi for cracked specimens.

Mixtures of prereacted powders of Gd_2O_3–30 wt % Al_2O_3 have been successfully cold pressed and sintered into cylinders to 95% of calculated densities, but careful control of conditions is required because of distortion apparently due to the formation of intermediate compounds. Mixtures containing 20 wt % Al_2O_3 showed less distortion when sintered at higher temperatures and should be fabricated to specification more easily. Hot-pressed Gd_2O_3-Al_2O_3 sample control-rod elements, tested by thermal and mechanical stressing, cracked but did not crumble; and the metal container was not distorted.

The examination of capsules from various MSRP irradiation experiments has led to the development of a fission-gas sampling rig, equipment for in-pile gas sampling, and the discovery of fluorine as a radiolysis product. Metallographic examination of an INOR-8 capsule exposed to fuel salt for 1500 hr at a flux of 2×10^{13} and a temperature of 1400°C showed no evidence of fluorine gas attack or accelerated corrosion.

22. High-Flux Isotope Reactor

To achieve the required high performance in the High-Flux Isotope Reactor being built at ORNL, a unique fuel element and control rod have been developed.

Each fuel plate for this reactor contains a core with a fuel dispersion in one area and a burnable-poison dispersion in another, the contents of both varying nonlinearly across the width of the plate. A procedure has been developed and demonstrated to fabricate such cores in a single pressing in greater than 95% yield.

Fuel plates curved to the proper involute have now been reproducibly formed, principally by low-pressure marforming. Electrohydraulic reforming has successfully recovered out-of-tolerance plates. Reproducibility in forming has resulted principally from close control of the plate fabrication, particularly as to the variation in thickness, and from an increase in cold work.

Assembly of fuel elements to stringent tolerances by several techniques has been demonstrated. Various combinations of the basic procedures have been used: (1) plates spaced by bends on the outer edges and welded to each other, (2) mechanical attachment to inner support tube, and (3) inner- and/or outer-plate edges welded to tubular side plates that have been grooved to establish plate spacing. Sliding the fuel plates into longitudinal grooves in two concentric cylindrical side plates and attaching at both edges by circumferential welds has been selected as the production method.

Unusual nondestructive testing techniques have been developed to ensure adherence to tight

specifications. Entire plates are being inspected by x-ray attenuation to determine uranium distribution. Ultrasonic techniques have been developed to determine routinely $\frac{1}{16}$-in. nonbond areas, and eddy-current techniques have been developed to locate the core hump.

The two control rods are cylinders over 5 ft long surrounding the core, each comprising a strongly absorbing 40 vol % Eu_2O_3 dispersion, an intermediate 40 vol % tantalum dispersion, and two almost nonabsorbing zones of aluminum. Both europium oxide and tantalum have been found compatible with aluminum at 500°C, and large-size plates of both dispersions have been fabricated by roll bonding. Some crack propagation has been encountered forming the Eu_2O_3 dispersion plates.

23. Space Power Program

Materials have been evaluated and component-fabrication methods developed for some of the complex equipment required to demonstrate the feasibility of a boiling-potassium-cooled compact power reactor for use in space. Specific accomplishments include attachment of small-diameter thermocouples to electrical heaters, construction of large tapered-tube alkali-metal condensers, and brazing of bearings to shafts for rotating machinery.

24. Thorium Utilization Program

Because of the high radioactivity of isotopes produced during the irradiation of thorium, it is desirable to accomplish all the processing steps of a Th-U^{233} fuel cycle in a shielded and alpha-tight facility. A lightly shielded facility has been built, equipped, and tested for fabricating 1000 Zircaloy-2-clad fuel rods. Mixed ThO_2-UO_2 from the Chemical Technology Division's sol-gel process is remotely crushed, sized, vibratorily compacted into dense rods in Zircaloy-2 tubes, and sealed by welding. Fabrication equipment is being designed for a large, heavily shielded facility with no glove port access. Thorium-uranium oxide fuels produced by the sol-gel process and vibratorily compacted have shown superior irradiation performance.

Improvement of the high-temperature strength of thorium has been accomplished by alloying and dispersion hardening.

Several coatings to improve the attrition resistance of thoria pellets have been evaluated, and satisfactory pellets probably can be produced.

25. Advanced Test Reactor

Composite fuel plates containing 34 wt % U_3O_8 and 0.15 wt % B_4C dispersed in aluminum were roll clad with type 6061 aluminum. With careful control, plates have been rolled to the desired dimensional specifications. Fewer than 1% of the plates have been rejected for nonbonds. Chemical analysis has indicated reasonable control of fuel homogeneity.

A two-strike low-pressure marforming process has been developed for forming mass quantities of fuel plates. By improved assembly procedures, several fuel elements have been produced well within the tentative specifications.

A relationship has been developed for predicting recovery in cold-worked aluminum as a function of cold work, temperature, and time at temperature.

26. Army Package Power Reactors

Economical arc-melting procedures have been developed to produce dense, stable materials for control and burnable poison. These include both Eu_2O_3 and the newly developed corrosion-resistant compound $Eu_{5.3}MoO_{11}$. The new europium-molybdenum oxide has withstood exposure for more than 850 hr in 250°C water.

Dispersions of up to 40 wt % Eu_2O_3 in stainless steel have resisted exposures up to 4×10^{21} neutrons/cm^2. The corrosion resistance of these dispersions has been shown to be independent of irradiation exposure and to be primarily dependent on concentration.

In an SM-1 fuel element examined after 19.5 Mwyr of operation, changes in plate thickness were proportional to burnup. No matrix cracking or gross deterioration of the UO_2 was found. Cermet samples containing up to 26 wt % UO_2 sustained burnups of 2.6×10^{21} fissions/cm^3 at surface temperatures of 600°F with no loss of structural integrity. The density decreased linearly with burnup at a rate of 4.3% per 10^{21} fissions/cm^3.

27. Enrico Fermi Fast-Breeder Reactor

Procedures capable of brazing the Fermi core B fuel element in a single operation have been developed. Seven of these stainless steel UO_2-dispersion fuel elements have been fabricated.

Miniature specimens of the core B fuel plates have been examined after being irradiated in the MTR at temperatures of 700 to 1200°F for burnups up to 29%. Considerable swelling and microcracking of the matrices occurred in the samples irradiated to the higher burnups.

28. Water Desalination Program

Fuel fabrication costs have been estimated for the very large reactors proposed for water desalination. Fabrication of 18 metric tons of uranium per day into identical elements is an insignificant part of the cost of generating heat.

PART IV. OTHER PROGRAM ACTIVITIES

29. Thermonuclear Project

The sorption of seven gases by four types of vapor-deposited titanium, used in high-vacuum getter pumping, has been measured and interpreted. For the manufacture of high-quality magnets, high-performance superconducting joints are being developed and other aspects of the metallurgy of superconductors are being studied.

30. Transuranium Program

Equipment for the glove-box fabrication of Pu^{242} oxide targets for the High-Flux Isotope Reactor has been largely constructed and procured. In this equipment, the oxide is first pressed into pellets with an aluminum matrix and then loaded into a finned aluminum tube. The tube is sealed by automatic welding, hydrostatically collapsed on the pellets, and installed in a sleeve. Similar equipment is being designed for completely remote performance of the same operations with actinide oxides recycled from the reactor.

31. Postirradiation Examination Laboratory

Construction of the new High Radiation Level Examination Laboratory has been completed, and installation of equipment is in progress. For use in the HRLEL, the replication technique has been improved and expanded, the ultrasonic cleaning method has been modified to permit decontamination of large objects, an improved fission-gas sampler has been developed, a pinhole camera for autoradiographs has been built, a versatile gamma-ray spectrometer has been tested, and two shielded metallographs have been installed. Although not yet installed, the HRLEL x-ray diffractometer has been used on many samples not requiring shielded loading.

The Postirradiation Examination Group has been disbanded, and its functions have been transferred to the Operations Division.

Contents

SUMMARY iii

PART I. FUNDAMENTAL RESEARCH

1. CRYSTAL PHYSICS 3
   - Molten-Salt-Solution Crystal Growth 3
   - Erbium Manganese Oxide 4
   - Intermetallic Compounds 4
   - Hydrothermal Synthesis 4
   - Potassium Chloride Crystals 5

2. REACTIONS AT METAL SURFACES 6
   - Refractory-Metal Oxidation 6
   - Copper Oxidation Studies 8

3. SPECTROSCOPY OF IONIC MEDIA 11
   - Wave-Function Calculations 11
   - Complete Spin-Allowed Spectrum of 3*d* Orbital Transitions of Tetrahedral $NiCl_4^{2-}$ in Molten Salts 11
   - Tetrahedral Nickel Halogeno Complexes in Organic-Salt Melts 12
   - Nickel(II) Complexes in Molten Dimethylsulfone 12
   - Coordination of Fluoride Ions About Nickel(II) Ions in the Molten LiF-NaF-KF Eutectic Solvent 13
   - Spectra of Ni^{2+} in Molten Oxo Salts 13
   - Lowest-Energy Allowed Transitions of Nitrate and Iodide Ions in Molten Salts 13
   - Influence of Environment on the Oscillator Strength of the Lowest-Energy Transition of the Nitrate Ion 14
   - Equilibrium of Solute Species Formed When Bismuth Metal Is Dissolved in Molten Bismuth Trichloride 14
   - Densities of Some Molten-Salt Mixtures 15

4. STRUCTURE OF METALS 16
   - Effect of Interstitial Elements on Twinning in Columbium 16
   - Preferred Orientation in Irradiated Copper 16
   - Deformation Studies 16
   - Nature of the <001> Fiber Texture Component in Extruded Aluminum Rods 17
   - Primary Recrystallization Textures in Aluminum Extrusions 17
   - Behavior of Twin Boundaries During Annealing 18
   - Application of the Mössbauer Effect to Metallurgical Problems 18
     - Impurities in Grain Boundaries of Nickel 19
     - Precipitation of Cobalt in Aluminum 19
   - Comments on Stacking-Fault Energy of Thorium 19

5. THEORY OF ALLOYING 20

Galvanomagnetic Properties of Tungsten 20
Low-Temperature Specific Heats of Zirconium Alloys 23
The Lead-Zirconium Phase Diagram 26

6. PHYSICAL PROPERTY STUDIES 27

Thermal Conductivity Results 27
Radiative Property Results 28
Development of New Measuring Apparatus 28

7. BASIC SINTERING STUDIES 30

Temperature-Dependent Densification End Point 30
Minima in Thoria Densification Rate Curves 31
Properties of ThO_2 Containing CaO 32

8. DEFORMATION OF CRYSTALLINE SOLIDS 33

Dislocations in Deformed Ni-Al Alloys 33
Stored-Energy Measurements During the Deformation of Metals and Alloys 36
Yield Points 38
Low-Temperature Creep of Iron 39

9. X-RAY DIFFRACTION OF CRYSTALLINE DEFECTS 40

Thin Cu_2O Films on Copper Single Crystals 40

10. X-RAY DIFFRACTION RESEARCH 41

Routine Analyses 41
X-Ray Diffraction Effects from Irradiated Crystals of Beryllium Oxide 41
High-Temperature X-Ray Diffraction Experiment with Polycrystalline Nb_3Sn 44

11. METALLURGY OF SUPERCONDUCTING MATERIALS 45

Measurement of Compositional Segregation in Niobium-Zirconium Alloys by Anodization 45
Studies on Transformation Kinetics in Niobium-Zirconium Alloys 45
Improved Casting Techniques for Preparing Macrohomogeneous Ingots of Niobium-Zirconium Alloys 46
Development of Methods for Nondestructive Examination of Superconducting Wires 47
Equipment Development 48
Resistivity Apparatus 48
Nucleation Site and Velocity of Movement of the Superconducting-Normal Interface in Short-Wire Specimens 48

12. ELECTRON MICROSCOPE STUDIES 49

Direct Observation of Lattice Defects by Electron Microscopy 49
Transmission Electron Microscope Study of Dislocations and Deformation Twins in Columbium and Columbium-Vanadium Alloys 50
Effect of Impurities on Mechanical Twinning and Dislocation Behavior in Body-Centered Cubic Metals 51
Dislocations in Deformed and Annealed Niobium Single Crystals 51
Transmission Electron Microscopy of Omega Phase in a Zr–15% Nb Alloy 52

PART II. LONG-RANGE APPLIED RESEARCH

13. ZIRCONIUM METALLURGY 55

Zirconium-Niobium Alloys 55
A Preliminary Examination of the Formation and Utilization of Texture and Anisotropy in Zircaloy-2 56
Texture Determinations by Hardness Anisotropy in α-Zirconium Alloys 56
Preparation of Single Crystals of Zirconium and Zirconium Alloys 59
Zone-Refining of Zirconium and Zone-Leveling of Alloys 60
Oxide Film Studies 60

14. MATERIALS COMPATIBILITY 63

Oxygen Partitioning in Alakli-Metal–Oxygen–Refractory-Metal Systems 63
Determination of Oxygen in Potassium 64

15. SOLID REACTION STUDIES 67

Diffusion in Body-Centered Cubic Metals 67
Diffusion in a Temperature Gradient 69
Effect of Alpha Radiation on Diffusion of Lead in Silver 69
Diffusion of Nb^{95} in UO_2 71

16. FUEL ELEMENT DEVELOPMENT 75

Pyrolytic and Chemical Vapor Decomposition Studies 75
Ceramic Fuel Element Development 78
Fabrication Development 79
Irradiation Testing 79
Phase Relations in the Uranium-Oxygen System 79
Fabrication of Uranium Carbide Using a Volatile Sintering-Temperature Depressant 82
Ceramic Brazing 84
Aluminum Fuel Element Technology 85
Aluminum-Base Fuel Plates 85
Chemical Compatibility Studies on the UO_2- and U_3O_8-Aluminum Systems 87
Irradiation Testing of Aluminum-Base Fuel Dispersions of UAl, U_3O_8, and UC_2 in Aluminum-Clad Plates 87

17. MECHANICAL PROPERTIES RESEARCH 89

Influence of Hydrogen on the High-Temperature Creep Properties of Metals 89
Some Metallurgical Parameters Affecting Creep Ductility of Type 304 Stainless Steel 90
Effect of Chromium on the Carburization of Cr-Ni-Fe Alloys in CO_2 91
Effect of Stress State on High-Temperature Low-Cycle Fatigue 92
In-Pile Extensometer 92

18. NONDESTRUCTIVE TEST DEVELOPMENT 94

Electromagnetic Test Methods 94
Ultrasonic Test Methods 95
Penetrating-Radiation Methods 96
Low-Voltage Radiography and Microradiography 96
Gamma Scintillation Gaging 96
Inspection Development for Problem Materials 96
Development of Remote Inspection Techniques 96

19. HIGH-TEMPERATURE MATERIALS 98
Physical Metallurgy Studies 98
Contamination of Refractory Metals in High Vacua 98
Slow-Bend Creep Testing of Niobium-Base Alloys 101
Alloy Stability in High Vacua 104
Fabrication Development 106
Refractory-Metal Extrusion 106
Floturning of Refractory-Metal Tube Shells 108
Materials Compatibility 111
Corrosion of Refractory Metals by Lithium 111
Haynes Alloy No. 25—Boiling-Potassium Loop Test 112
Boiling-Potassium Stability Studies 114
Mechanical Properties 118
Materials Evaluation 118
Internal Friction in Nb—1% Zr Alloy 120
Refractory-Metal Joining 122
Component Fabrication 122
Physical Properties 122
Data Compilation and Correlation 122
Development of Measuring Equipment 123
Nondestructive Testing 124
Molybdenum Tubing 124
Tapered Tubing 125

PART III. REACTOR DEVELOPMENT SUPPORT

20. GAS-COOLED REACTOR PROGRAM 129
Introduction 129
EGCR Support 129
EGCR Instrumented Fuel Assembly Fabrication 129
EGCR Construction Support 130
Thermocouple-to-Tube Braze Joints 130
Graphite Cylinders 130
Stress-Rupture Tests on EGCR Clad Tubing 131
Creep of Graphite Under Irradiation 132
Microstructural Effects of Nitrogen Compounds in UO_2 on Type 304 Stainless-Steel-Clad Fuel Capsules 133
Advanced Fuel Elements 133
Irradiation Capsule Fabrication 133
Joining of Beryllium 134
Fuel-Cladding Interactions of Metal-Clad Fuel Elements During Thermal Cycling 134
Postirradiation Tensile Tests on Stainless Steels 136
Unclad Fuel Concepts 138
Evaluation of Coated Particles 138
Neutron-Activation Tests on Coated Particles 139
Evaluation of Fueled-Graphite Bodies 140
Graphite Fabrication 140
Unclad Reactor Concept Irradiation Experiments 141
Coated-Particle Examination 142
Fueled-Graphite Spheres 142

Metallographic Examination of Pyrolytic-Carbon-Coated and Uncoated $UC-UC_2$ Particles 143
Metallography of $(Th,U)C_2$ Fuel Particles 143
Microhardness Measurement of Pyrolytic-Carbon Coatings 143
Supporting Research 147
In-Pile Stress Rupture of UK Stainless Steel 147
Release of Fission Gas from UO_2 149
Thermal Conductivity Studies on UO_2 149
Thermal Conductivity Studies on Coated-Particle Fuels 150
Fission-Product Deposition Studies 150
Graphite-Metal Compatibility Studies 152
Contaminant Studies 152
Oxidation Studies of Nitrided Type 304 Stainless Steel 152
Mechanical Properties of Moderator Graphites 153
Neutron Flux Monitoring 155

21. MOLTEN-SALT REACTOR 157

Introduction 157
Fluoride-Salt Corrosion Studies 157
Corrosion Effects of CF_4 157
Effects of Fluoride-Salt Spillage 157
Molybdenum-Graphite Compatibility Tests in Fluoride Salts 158
MSRE Heat Exchanger Tube-to-Tube Sheet Attachments 158
Nondestructive Testing of MSRE Heat Exchanger Tube Joint 159
Welding Development for INOR-8 160
High-Temperature Creep of 82 wt % Au–18 wt % Ni Brazed Joints in Shear 161
Mechanical Properties of INOR-8 Alloy 162
ASME Boiler and Pressure Vessel Code Allowable Stresses for INOR-8 162
Reactor-Quality INOR-8 162
Influence of Prior Annealing on the Tensile Properties of INOR-8 164
Evaluation of MSRE Graphite 165
Mechanical Properties of MSRE Graphite 167
Examination of MSRE In-Pile Experiments 167
Metallographic Evaluation of INOR-8 Capsule in MTR-47-4 168
Sintering Characteristics of Gd_2O_3-Al_2O_3 Cylinders 170
Sample Control-Rod Element Testing 171

22. HIGH-FLUX ISOTOPE REACTOR 173

Introduction 173
Fuel Element 173
Core Fabrication 173
Fuel Plate Fabrication 175
Fuel Plate Forming 175
Assembly and Welding 177
Nondestructive Testing 181
Ultrasonic Nonbond Detection 182
Fuel Homogeneity 182
Core Orientation 183
Coolant Channel Spacing 183
Mechanical Properties of 6061-4043 Weldments at Elevated Temperature 184

Burnable Poisons 185
HFIR Metallurgical Engineering Assistance Program 187
HFIR Control Rods 187
Powder Metallurgy 187
Plate Rolling and Preforming 191
Thermal Conductivity 192

23. SPACE POWER PROGRAM 193

Introduction 193
Component Fabrication 193
Fabrication of Instrumented Clusters 193
Turbine Pump Fabrication 193
Fabrication of Heat-Transfer Equipment 194

24. THORIUM UTILIZATION PROGRAM 196

Introduction 196
Th-U^{233} Fuel-Rod Facility 196
Thorium-Uranium Fuel Cycle Development Facility 198
Remote Fabrication Equipment for Clad Oxide Fuels 201
Brookhaven National Laboratory Kilorod Welding Development 202
Vibratory-Compaction Studies 204
Irradiation Studies 205
Neutron-Activation Experiments on Mixed Oxides Produced by the Sol-Gel Process 205
In-Pile Tests of Mixed Oxides Produced by the Sol-Gel Process 205
Metallic Fuels 208
Dispersion Hardening of Thorium 210
Thoria-Pellet Development 212

25. ADVANCED TEST REACTOR 213

Introduction 213
Fuel Element Development 213
Powder Metallurgical Preparation of Fuel Cores 213
Fuel Plate Fabrication 215
Fuel Plate Forming 216
Fuel Element Assembly 217
Mechanical Properties 218
Nondestructive Testing 219

26. ARMY PACKAGE POWER REACTOR 221

Introduction 221
Control and Poison Materials 221
Europium Oxide Consolidation Studies 221
Europium Oxide Stability Studies 222
Irradiation Testing of Stainless-Steel-Clad Dispersions of Eu_2O_3 223
Fuel Materials 225
Postirradiation Examination of SM-1 Core 1 Fuel Elements 225
Postirradiation Examination of SM-2 Fuels Development Specimens 225

27. ENRICO FERMI FAST-BREEDER REACTOR 227

Introduction 227
Fuel Element Fabrication 227
Irradiation Testing of Fermi Core B Miniature Fuel Specimens 228

Capsule and Specimen Design 228
Operating History 229
Postirradiation Examination 229

28. WATER DESALINATION PROGRAM 232

Introduction 232
Fuel Fabrication Costs 233
Zircaloy-Clad Natural-UO_2 Elements 233
Zircaloy-Clad Plutonium-Depleted UO_2 233
Clad Uranium-Metal Elements 233
General Economic Studies 234

PART IV. OTHER PROGRAM ACTIVITIES

29. THERMONUCLEAR PROJECT 237

Introduction 237
Vacuum 237
Superconductivity 239
Engineering 239

30. TRANSURANIUM PROGRAM 240

Introduction 240
Transuranium Target Fabrication Equipment 240
Cubicle No. 3 241
Cubicle No. 2 241
Cubicle No. 1 243
Plutonium Target Fabrication Equipment 243
Pellet Pressing 243
Target End Closures 244
Welding 245
Brazing 245
Collapse of Target Tubes 246
Attachment of the Hexagonal Sleeve to the Finned Tubing 247
Résumé 247

31. POSTIRRADIATION EXAMINATION LABORATORY 248

Introduction 248
Development of Postirradiation Examination Techniques 248
Remote Replication 248
Ultrasonic Cleaning 249
Development of Remote Equipment 249
Installation of Shielded Metallographs 250

PAPERS, ORAL PRESENTATIONS, AND OPEN-LITERATURE PUBLICATIONS

PAPERS AND ORAL PRESENTATIONS GIVEN AT SCIENTIFIC AND TECHNICAL MEETINGS 255

PUBLICATIONS 260

ORGANIZATION CHART 265

Part I.
Fundamental Research

1. Crystal Physics

Progress in materials research is often dependent on the availability of single-crystal specimens of high perfection and controlled purity. The technology has not been developed for growing quality, laboratory-sized, single crystals of many desired materials. This program is one of exploring and developing crystal-growth processes, of growing quality crystals of controlled purity, of studying the basis of crystallization, and of determining the purity and perfection of grown crystals. The higher-quality crystals synthesized are being shared with other groups.

MOLTEN-SALT-SOLUTION CRYSTAL GROWTH

C. B. Finch G. W. Clark

Recently, it was found that BeO dissolved in and recrystallized from V_2O_5 melts. Crystals of BeO exceeding 2 mm on an edge have been grown from this solvent at 1100°C and apparently are of higher quality than those grown from alkali polytungstate melts. Only two impurities, silicon (100 ppm) and vanadium (200 ppm), were detected in these crystals by emission spectroscopy. This is more than an order-of-magnitude decrease in impurity level compared with BeO crystals grown from alkali polytungstate or polymolybdate melts. Another very helpful fact is that the volatilization of the V_2O_5 is much less than that of tungstate or molybdate melts.

The success with V_2O_5 as a solvent led to its consideration as a medium for the growth of other refractory-oxide crystals. This resulted in growth of millimeter-size crystals of Al_2O_3, HfO_2, $HfO_2 \cdot SiO_2$, $3BeO \cdot 2Al_2O_3 \cdot 6SiO_2$ (beryl),[1] and SnO_2.

Previous experiments[2] on the growth of BeO from $Li_2O \cdot 2WO_3$ over the temperature interval 1000 to 1300°C have been extended to determine the influence of each of the alkali ions in producing observed growth-habit modifications. The procedure has been that of slow cooling the melts charged with excess BeO in the form of polycrystalline pellets under similar conditions. Crystals from $Li_2O \cdot 2WO_3$ tend to form as pyramids and never as prisms; those from $Na_2O \cdot 2WO_3$ or $Rb_2O \cdot 2WO_3$ are mostly prisms with tapered ends. Melts containing potassium yielded complex multifaceted pyramids, and those containing cesium produced friable hexagonal plates. For BeO crystals grown from the solvent $Li_2O \cdot Na_2O \cdot 4WO_3$, the effect of Na^+ prevails over that of Li^+, yielding prisms. In an analogous fashion the effect of Li^+ prevails over that of K^+, yielding pyramids. For a mixture of Na^+ and K^+, both pyramids and prisms are formed.

Work continued on improving techniques and apparatus used in growing ThO_2 single crystals from the solvent $Li_2O \cdot 2WO_3$ at 1200 and 1300°C.[2] Optically clear crystals up to 3 mm on an edge have been grown[3] in unseeded melts. Also, medium-quality crystals approaching 1 cm on an edge have been grown on seeds in stirred melts. These crystals were grown at a temperature of 1220°C in melts having a temperature gradient of 11°C/cm between the nutrient and the seed. The maximum linear growth rate observed, without spurious nucleation on the seed, has been 0.05 mm/day in the <111> crystallographic direction. The only impurity detectable by spectrographic analysis in these crystals was 100 ppm Ca. This

[1] R. C. Linares, A. A. Ballman, and L. G. Van Uitert, *J. Appl. Phys.* **33**(11), 3209 (1962). Reported independently the growth of beryl from V_2O_5.

[2] G. W. Clark, C. B. Finch, O. C. Kopp, and J. J. McBride, *Metals and Ceramics Div. Ann. Progr. Rept. May 31, 1962*, ORNL-3313, p 181.

[3] C. B. Finch and G. W. Clark, "Growth of Thorium Dioxide Single Crystals from Lithium Ditungstate Solvent," submitted to the *Journal of Applied Physics*.

was a pleasant surprise in that no steps were taken to obtain high-purity starting materials.

In support of this work a portion of the ternary system Li_2O-WO_3-ThO_2 has been investigated. At least two incongruently melting compounds have been detected below 1200°C. One of these compounds has been isolated and is being identified.

ERBIUM MANGANESE OXIDE

G. W. Clark

Single crystals of the compound $ErMnO_3$ have been grown up to 1 cm long and 3 mm in diameter, using the oxyhydrogen-flame-fusion method (Verneuil), and as well-formed hexagonal platelets about 0.1 mm across, out of bismuth oxide melts at 1200°C. This compound is of interest in that it is ferroelectric as well as antiferromagnetic, and its structure is characterized by unusual five- and sevenfold coordination polyhedra about manganese and the rare-earth atoms.[4] An x-ray structural analysis of an $ErMnO_3$ crystal electrically polarized so as to contain one ferroelectric domain is in progress. Measurements of the ferroelectric hysteresis loop, the magnetic susceptibility, and the optical absorption of $ErMnO_3$ crystals are also under way.

INTERMETALLIC COMPOUNDS

J. J. McBride G. W. Clark

Five 1-mm-long single crystals of the incongruently melting compounds UAl_3 and UAl_4 have been grown. The procedure for growth of each has been much the same, but the temperature range and the composition of the starting material were appropriately selected. Melts of the desired uranium-aluminum mixture were cooled at a rate of 2°C/hr in a gradient of 10°C/cm over a temperature range where the specific compound was stable and were then cooled quickly to near room temperature. The orthorhombic UAl_4 crystals have been larger and perhaps of better quality than the cubic UAl_3. The UAl_4 crystals were prismatic in shape, with (110) faces dominant, whereas the UAl_3 grew for the most part as cubes. To obtain larger crystals, growth on seed crystals in a stirred melt is in progress.

Broad interest in the superconducting compound Nb_3Sn prompted the effort to grow single crystals of this intermetallic compound. One method tried was that of slow cooling a melt having the nominal composition Nb_3Sn. The charge, contained in a BeO crucible, was taken to a temperature of 2200°C and then lowered out of the hot zone by the Bridgman-Stockbarger method. The other method was that of dissolving niobium in a niobium-tin-rich melt at 1250°C and transporting the niobium down a temperature gradient to where the compound Nb_3Sn nucleates and grows. The resulting ingots have had single-phase Nb_3Sn regions, but grains have been submillimeter in size. Nevertheless, a polycrystalline sample was used for x-ray studies of lattice-parameter changes with temperature in the 500 to 1000°C range and is reported in Chap. 10 of this report.

HYDROTHERMAL SYNTHESIS

O. C. Kopp[5] G. W. Clark

A detailed x-ray structural analysis has been completed[6] of the hydrothermally synthesized $Cs_2O{\cdot}Fe_2O_3{\cdot}4SiO_2$ (an analog of the aluminum silicate mineral, pollucite) previously reported.[2] The substitution of Fe^{3+} for Al^{3+} in the crystal structure has permitted the assignment of the iron analog to the cubic space group *Ia3d*. This had not been possible for pollucite because of similar x-ray scattering factors for aluminum and silicon. Thus it is inferred that pollucite has the same cubic structure.

In addition to the previously reported synthesis of potassium-, rubidium-, and cesium-based iron micas,[2] crystals of an iron-substituted sodium-based micaceous material and a distinctly fibrous material have been synthesized. Cesium-iron mica has been prepared in sufficient quantity to permit chemical analysis. These data indicate that iron

[4] H. L. Yakel, W. C. Koehler, E. F. Bertaut, and E. F. Farrat, "On the Crystal Structure of the Manganese(III) Trioxides of the Heavy Lanthanides and Yttrium," accepted for publication in *Acta Crystallographica*.

[5] Consultant from the University of Tennessee.

[6] O. C. Kopp, L. A. Harris, G. W. Clark, and H. L. Yakel, *Am. Mineralogist* **48**(1,2), 100 (1963).

is present in both 2+ and 3+ valence states, and thus suggest that iron ions occupy both tetrahedral and octahedral sites. Optical absorption, magnetic susceptibility, and x-ray studies are in progress to test this hypothesis and to specify the crystal structure.

Very small crystals of MgO, BeO, TiO_2, and Al_2O_3 have been grown by dissolving and transporting these oxides in supercritical water systems. However, the proper conditions of temperature, pressure, and solvent have not been found for seeded crystal growth.

Difficulties in obtaining welded high-pressure closures on autoclave liners of low-carbon steel led to the development of a new type of closure. In this design, both ends of a thin-walled tube liner are sealed (using modified Bridgman seals) in such a way that one has rather easy access to the inside.[7]

[7] O. C. Kopp, G. W. Clark, and T. G. Reynolds, "A Replaceable Liner Type Autoclave with Modified Bridgman Closures," submitted to the *Review of Scientific Instruments*.

A newly designed autoclave which opens into two halves symmetrical about the tube axis permits easy access to removable liners. This increases greatly the freedom of choice of liner material and of type and concentration of solvent. This design accepts either a Bridgman- or welded-type closure.

POTASSIUM CHLORIDE CRYSTALS

J. J. McBride G. W. Clark

Potassium chloride crystals, averaging about 60 g each, were pulled from the melt in a dry nitrogen atmosphere, and etch-pit counts were taken on cleaved sections of the crystals with glacial acetic acid as etchant. Typical counts were about 10^6 pits/cm^2. Calcium- and strontium-doped KCl crystals were grown as specimens for use in color centers and in mechanical properties studies by the Solid State Division.

2. Reactions at Metal Surfaces

J. V. Cathcart
R. E. Pawel G. F. Petersen

Previous work[1-4] in this group demonstrated the existence of very large surface stresses in some oxidizing systems – as high, for example, as 50,000 psi in tantalum. Such stresses were shown to influence the oxidation kinetics of materials such as niobium and tantalum in a decisive fashion, and considerable evidence is accumulating that stresses in thin oxide films may play a significant role in the marked oxidation-rate anisotropy which many metals exhibit. Despite these facts, stress has generally been ignored as an important parameter in recent considerations of oxidation mechanisms. The research program described below represents an attempt to define more precisely the role which stresses, generated during the oxidation process, play in the oxidation mechanism.

The work is divided between two projects: The first is a study of refractory-metal oxidation, in which emphasis is placed on the influence of surface stresses on the protective qualities of the oxide. The second involves an investigation of the very early stages of the oxidation of copper single crystals, where epitaxially induced strains are particularly evident.

REFRACTORY-METAL OXIDATION

The technique, originally applied to tantalum,[4] of studying stress buildup during oxidation by measuring the flexure of thin metal specimens oxidized on one side only was extended to niobium, and it was shown that very high stresses are also generated in the course of this reaction. The model proposed for stress generation during the oxidation of tantalum also appears to be applicable to the case of niobium, particularly during the early stages of oxidation, where surface stresses in excess of 40,000 psi were shown to develop at 400 and 425°C at 1 atm oxygen pressure. The tendency for these specimens to deviate from pure bending at a critical stage in the oxidation process, however, prevented the application of the above stress model to the entire range of the data. The possible relation between this bending behavior and the breakdown of the protective oxide layer on niobium is the subject of continued investigation.

A source of considerable argument in the oxidation literature concerns the mechanism of protective-film breakdown on the refractory metals tantalum and niobium. The crux of the disagreement is the question of whether or not nonporous, mechanically stable films of the pentoxide can exist on the surfaces of oxidizing niobium and tantalum specimens. As part of a continuing effort to shed light in this important area, a study of the properties of anodically formed films was undertaken. Anodically formed amorphous pentoxide films up to several thousand angstroms thick can be formed at room temperature on these metals without any accompanying oxygen solution in the metal. Thus an investigation of the recrystallization of these films and of their characteristics during continued thermal oxidation offers the opportunity both for an evaluation of the stability of the films and for a comparative study of the effect of stress buildup, due to

[1] J. V. Cathcart, R. E. Pawel, and G. F. Petersen, *Metals and Ceramics Div. Ann. Progr. Rept. May 31, 1962*, ORNL-3313, p 185.

[2] B. S. Borie, C. J. Sparks, and J. V. Cathcart, *Acta Met.* **10**(8), 691–97 (1962).

[3] J. V. Cathcart, J. J. Epperson, and G. F. Petersen, *Acta Met.* **10**(8), 699–703 (1962).

[4] R. E. Pawel, J. V. Cathcart, and J. J. Campbell, "Stress Generation in Tantalum During Oxidation," accepted for publication in the *Journal of the Electrochemical Society*.

oxygen solution in the metal, on the properties of the oxide.

Initial studies of the recrystallization of the amorphous pentoxide films were made with films stripped from niobium and tantalum specimens. It was recognized that additional parameters would have to be considered for the recrystallization of films in intimate contact with the substrate metal, but, as described below, many important aspects of the recrystallization process may be inferred from the result obtained with stripped films. Only the results with tantalum oxide films are given, since the behavior of the niobium films was very similar.

Films ranging from 200 to 2000 A in thickness were stripped from an electropolished tantalum surface and mounted on standard electron-microscope specimen grids, and the structure of the as-stripped anodic films was studied by electron microscopy. Even at high magnification, very little structural detail was observed. Electron diffraction yielded the broad halos associated with extremely fine crystallite size or amorphous material.

Recrystallization of the amorphous films could be induced either by vacuum annealing or, in the microscope itself, by increasing the beam intensity. Distinguishing features of a recrystallized region were an increase in electron transmission and the appearance of a very high density of extinction contours. Figure 2.1 is an electron micrograph of a typical growth front of an "electron-beam-recrystallized" area. The recrystallized region is growing into the field from the left. In some cases, grain growth within a recrystallized region was observed, thus illustrating very graphically a fundamental metallurgical phenomenon.

The effect of thermal annealing on the anodic films was studied as a function of time and temperature. No evidence of recrystallization was observed for 225-A anodic films stripped from tantalum and held in vacuum for $\frac{1}{2}$ hr at temperatures to 550°C. At 600°C, a low density of crystallized areas was observed. In the initial stages, these areas were essentially single crystals having simple geometric shapes. Such a "nucleus" is shown in Fig. 2.2. Upon prolonged heating at

Fig. 2.1. Electron Micrograph of Growth Front of "Electron-Beam-Recrystallized" Region in a 225-A Anodically Formed Amorphous Oxide Film Stripped from a Tantalum Surface. 132,000X. Reduced 50%.

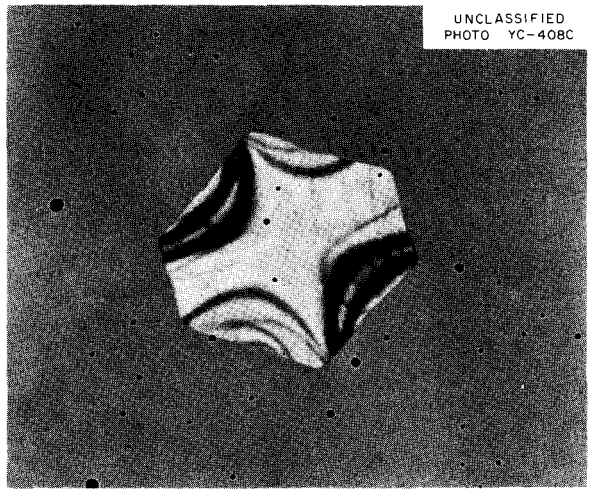

Fig. 2.2. Electron Micrograph of a Small Thermally Recrystallized Region in a 225-A Anodic Oxide Film Stripped from a Tantalum Specimen and Held in Vacuum for 30 min at 600°C. 34,000X. Reduced 40%.

600°C, a large proportion of the regions grew in the manner illustrated in Fig. 2.3. At higher temperatures the recrystallization process was proportionally accelerated. The recrystallization spectrum for anodic niobium oxide films of comparable thicknesses lies at least 100°C lower in temperature.

Parenthetically, it should be noted that the method of repeated stripping of anodic films of known thickness from a specimen surface, in principle, provides a very sensitive "microsectioning" technique for determining penetration curves in self-diffusion studies where radiotracer methods are used. Such an investigation has been initiated in cooperation with the Solid Reaction Studies Group of the Metals and Ceramics Division. The preliminary results look very encouraging, and the method shows particular promise for use in low-temperature diffusivity measurements as well as for studying possible "anomalous" diffusion rates sometimes associated with small penetration distances.

Fig. 2.3. Electron Micrograph of a Thermally Recrystallized Region in a 225-A Anodic Film Stripped from a Tantalum Specimen and Annealed for 18 hr at 600°C. 7400X. Reduced 58.5%.

COPPER OXIDATION STUDIES

Previous work showed the presence of very large, epitaxially induced strains in thin oxide films formed on copper single crystals.[2-3] During the past year, research in this area was designed to demonstrate the possible connection between these strains and the kinetics of the oxidation process. It was noted that the presence of small quantities of surface impurities could produce marked changes in both the rate of oxidation and the degree of strain anisotropy of the oxide films. A systematic investigation of impurity effects was therefore undertaken in the belief that a study of the changes thus produced in the characteristics of the oxide films would permit a correlation of strain state and oxidation rate.

The two impurities studied were CO_2 and CCl_4. These materials were added to purified oxygen in concentrations ranging from less than 1 ppm to about 1000 ppm. Both impurities produced significant changes in the oxidation rates of different crystallographic planes, although the influence of the CO_2 was considerably milder. At 250°C, the CO_2 additions produced a 50% increase in the oxidation rate of the (111) plane of copper but had relatively little effect on other crystal planes. Preliminary studies of the optical properties of the resulting Cu_2O films suggest that the prominent absorption edge for Cu_2O which lies in the visible spectrum is shifted slightly toward longer wavelengths in these films.

The effects from CCl_4 additions were much more drastic. Figures 2.4*a* and *b* show two copper single-crystal spheres oxidized under identical conditions except that, for the specimen in Fig. 2.4*b*, 1000 ppm CCl_4 was added to the oxidizing mixture 3 min after the initiation of oxidation. Not only was the overall rate of oxidation greatly increased, but the time required for CuO formation was reduced. On the other hand, when CCl_4 was introduced prior to the beginning of oxidation, the oxidation rates of virtually all crystal planes were reduced, the order of relative rates was changed, and the morphology of the oxide was altered.

It was observed that the effects produced by both contaminants were dependent on the order in which they and oxygen were admitted to the system. When CO_2 was introduced into the oxidation chamber 2 or 3 min after the start of oxidation,

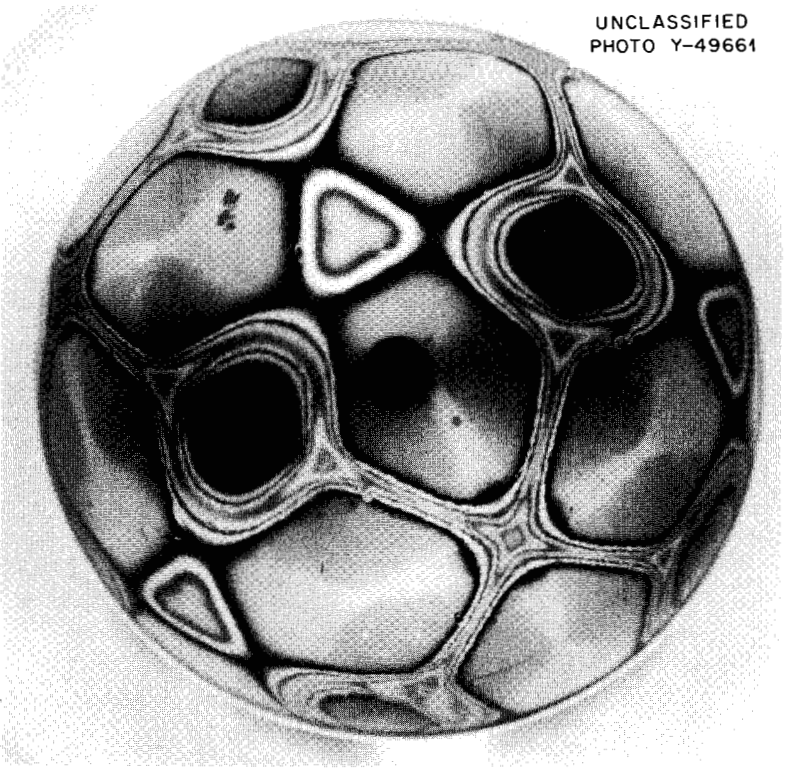

Fig. 2.4*a*. Copper Single-Crystal Sphere Oxidized in Purified Oxygen for 30 min at 250°C. 7X. Reduced 14%.

Fig. 2.4*b*. Copper Single-Crystal Sphere Oxidized in Oxygen Plus 1000 ppm CCl_4 for 30 min at 250°C. 7X. Reduced 14%.

it produced no effect. Likewise, as indicated above, a different set of changes resulted in the oxidation characteristics of copper in the presence of CCl_4, depending on whether or not the copper surface was covered with oxide at the time the CCl_4 was introduced.

These results immediately suggest a possible relation between oxidation kinetics and the strain state of the oxide. Impurities adsorbed on an oxide-free copper surface would be expected to alter the character of the subsequently produced oxide-metal interface, thus altering the epitaxial forces which are primarily responsible for the existence of strains in these thin oxide films. Other explanations, of course, are also possible, and examinations of the films by x-ray diffraction (in cooperation with the X-Ray Diffraction Group of the Metals and Ceramics Division), by electron microscopy, and with the polarizing spectrometer are currently in progress in an effort to characterize more fully the changes occurring in the oxide films.

3. Spectroscopy of Ionic Media

WAVE-FUNCTION CALCULATIONS

H. W. Joy

The previously described general-purpose multicenter Gaussian expansion code for atomic and molecular wave functions is functioning on the IBM 7090, though not in an optimum manner, for it is currently limited to a set of nine basic functions and has not been exhaustively checked for accuracy. Various improvements are being made. It is planned to extend the code for use in the computation of energy bands in solids.

General-purpose one-center expansion techniques have also been developed. These construct an approximate atomic or molecular wave function in terms of generalized[1] Slater-type orbitals, all based on a single point as origin:

$$N_r r^{n-1} e^{-\zeta r} S_l^m(\theta,\phi) , \qquad (1)$$

where $N_r r^{n-1} e^{-\zeta r}$ is the ordinary r-dependent part of a Slater-type orbital but with both ζ and n as parameters, and $S_l^m(\theta,\phi)$ is a real spherical harmonic. Such expansions are useful for molecules, primarily because of the significant reduction in computing time per integral they allow.

The one-center methods are being applied in calculations on the carbon atom and the CH_3^- ion to test Dewar's "split p-orbital" method.[2] Here, it was necessary to construct integral codes not only for the functions (1) but, in order to include Dewar's use of each lobe of a p-type function as a separate orbital, for functions which employ the absolute value of a function $S_l^m(\theta,\phi)$. The work, while still incomplete, has already shown the method to be unsatisfactory when applied rigorously.[3] In the course of this work, a new computer-based technique for evaluating integrals involving products of associated Legendre functions was found.[4]

[1] R. G. Parr and H. W. Joy, *J. Chem. Phys.* **26**(2), 424 (1957).

[2] M. J. S. Dewar and N. L. Hojvat, *J. Chem. Phys.* **34**(4), 1232 (1961).

[3] A. F. Saturno, H. W. Joy, and L. C. Snyder, "Computations to Evaluate Dewar's Split P-Orbital (SPO) Method," to be published in the *Journal of Chemical Physics.*

[4] H. W. Joy, *J. Chem. Phys.* **37**(12), 3018 (1962).

COMPLETE SPIN-ALLOWED SPECTRUM OF 3*d* ORBITAL TRANSITIONS OF TETRAHEDRAL $NiCl_4^{2-}$ IN MOLTEN SALTS

C. R. Boston G. P. Smith

The complete spin-allowed spectrum of 3*d* orbital transitions for $NiCl_4^{2-}$ in solution in molten salts at high temperatures was observed.[5] These measurements include the ${}^3T_1(F) \rightarrow {}^3T_2(F)$ transition near 4000 cm^{-1}, which, though rarely observed, is an important diagnostic test for tetrahedral Ni^{2+} complexes. The $NiCl_4^{2-}$ spectrum was observed for solutions of $NiCl_2$ in CsCl and KCl melts.

Three spin-allowed orbital transitions are predicted for tetrahedral Ni^{2+} complexes, ${}^3T_1(F) \rightarrow {}^3T_2(F)$, ${}^3A_2(F)$, ${}^3T_1(P)$. Measurement of all three transitions is required to check ligand-field theory. This has not previously been accomplished except in crystals. Liehr and Ballhausen[6] calculated the energies of these transitions, including spin-orbit fine structure, as functions of Dq. The observed spectrum fits the Liehr and Ballhausen calculations for a Dq of about 370 cm^{-1} and also agrees

[5] C. R. Boston and G. P. Smith, *J. Am. Chem. Soc.* **85**(7), 1006 (1963).

[6] A. D. Liehr and C. J. Ballhausen, *Ann. Phys. (N.Y.)* **6**(2), 134 (1959).

with that measured by Weakliem[7] for Ni^{2+} impurity ions at tetrahedral sites in a Cs_2ZnCl_4 crystal.

The measurements near 4000 cm^{-1} at high temperature were made possible by the development of a spectrophotometer of new design.

TETRAHEDRAL NICKEL HALOGENO COMPLEXES IN ORGANIC-SALT MELTS

T. R. Griffiths[8] G. P. Smith

When the spectra of nickel compounds in solution are examined, almost invariably an octahedral configuration about nickel is found. Relatively few tetrahedral complexes of nickel(II) are known, but some evidence exists for organo-nickel complexes in the solid state containing tetrahedral nickel. The spectra of nickel halides in molten organic salts were thus measured.

The results obtained are shown in Table 3.1 and are in good agreement with theory for tetrahedral nickel. The band at 4000 cm^{-1} is poorly resolved, owing to solvent absorption. Charge-transfer bands for $NiBr_4^{2-}$ and NiI_4^{2-} of complex shape have been measured in the visible region, and computational calculations are planned on these before the work is submitted for publication.

[7]H. A. Weakliem, *J. Chem. Phys.* **36**(8), 2117 (1962).

[8]On leave of absence from N.E. Essex Technical College, Colchester, England.

NICKEL(II) COMPLEXES IN MOLTEN DIMETHYLSULFONE

C. H. Liu[9] G. P. Smith

Dimethylsulfone is of interest as a solvent because of its kinship to the sulfate ion and because

[9]Summer participant in 1962 from Brooklyn Polytechnic Institute.

Table 3.1. Peak Positions and Extinction Coefficients for Tetrahedral Nickel Halogeno Complexes in Various Organic-Salt Melts

Solvent	Nickel Halide Added	Temperature (°C)	Peak Position, $h\nu_{max}$ (cm^{-1})[a]					
Aniline hydrochloride	$NiCl_2$	210	7550	11,630	*b*	14,180	15,480	*b*
Diethylamine hydrochloride	$NiCl_2$	245	7490	11,610	*b*	14,170	15,550	*b*
Tetraphenylarsonium chloride	$NiCl_2$	247	7410	11,590	*b*	14,140	15,410	*b*
Tributylbenzylphosphonium chloride	$NiCl_2$	165	7440 [20.2]	11,650 [7.0]	12,500[c]	14,140 [189.3]	15,370 [188.7]	16,200[c]
Tributyl-2,4-dichlorobenzylphosphonium chloride	$NiCl_2$	134	7410 [19.5]	11,590 [6.8]	*b*	14,160 [164.2]	15,360 [164.8]	*b*
Tetrabutylammonium bromide	$NiCl_2$ and $NiBr_2$	120	7110 [24]	10,720		13,290 [215]	14,340 [217]	15,300[c]
Tetrapentylammonium bromide	$NiCl_2$ and $NiBr_2$	117	7140	10,720	*b*	13,030	14,180	*b*
Tetrabutylammonium iodide	$NiCl_2$	161	6970 [45]	10,380[d]	*b*	11,330 [364]	12,120 [413]	*b*
Tetrahexylammonium iodide	NiI_2	122	7030 [50]	10,380[d]		11,370 [369]	12,120 [396]	13,720[c]

[a]Values in brackets are extinction coefficients, ϵ_{max}.

[b]Not resolved because solvent curve was not subtracted for solution curve by Calcomp Plotter.

[c]Shoulder.

[d]Very weak.

it is expected to be a weakly complexing medium. We have been able to use melts of this material to prepare halide complexes of nickel(II) which elude preparation in more strongly coordinating solvents such as water. The investigation is still in a preliminary stage, and only a few general conclusions can be drawn.

Nickel(II) ions, introduced in any of several nickel compounds (such as anhydrous nickel sulfate), form approximately octahedral solvo complexes with molten dimethylsulfone. The complexes are characterized by a low value of the cubic crystal-field parameter. When halide ions are added, it is possible (by spectroscopic methods) to follow the formation of complexes containing successively more halide ions until the limiting (all-halide) complex is formed. This proves to be a tetrahedral NiX_4^{2-} (X = Cl, Br, I) ion.

COORDINATION OF FLUORIDE IONS ABOUT NICKEL(II) IONS IN THE MOLTEN LiF-NaF-KF EUTECTIC SOLVENT

J. P. Young[10] G. P. Smith

The spectrum of solutions of NiF_2 in the molten eutectic salt 46.5 mole % LiF–11.5 mole % NaF–42.0 mole % KF was measured between 5000 and 30,000 cm^{-1} at a melt temperature of 525°C. Nickel(II) ions were shown to exist in an octahedral, or distorted octahedral, field of fluoride ions. Ligand-field parameters were $Dq = -660$ cm^{-1} and $B \approx 950$ cm^{-1}. Band intensities were near normal for octahedral nickel(II) complexes, in contrast to other octahedral-like spectra for nickel(II) in molten salts, which are anomalously intense.

SPECTRA OF Ni^{2+} IN MOLTEN OXO SALTS

G. P. Smith C. H. Liu[9]
T. R. Griffiths[8]

The spectra of Ni^{2+} in molten nitrate[11] and sulfate[12] salts have been interpreted as due to octahedral fields about the nickel ions. However, the intensities of the bands are too high to be satisfactorily explained as vibronic or magnetic dipole transitions.[13] Consequently, we have been reinvestigating this problem under conditions of better spectral resolution and over wider wavelength ranges. The work is by no means complete, but it is already obvious that some of the supposedly octahedral spectra involve, in fact, a rhombic splitting of the orbital states which arise from the free-ion ^3P term and that the splitting is very large.

LOWEST-ENERGY ALLOWED TRANSITIONS OF NITRATE AND IODIDE IONS IN MOLTEN SALTS

G. P. Smith C. R. Boston
D. W. James[14]

Charge-transfer bands for molten salts that occur at wavelengths near 200 mμ are of considerable theoretical interest. However, they are difficult to measure accurately for two reasons: First, most materials that might be used as solvents absorb strongly in this region, and, second, instrumental errors increase rapidly at the short wavelength limit (186 mμ in this case) of the spectrophotometer. Thus, previous attempts to measure charge-transfer bands in molten salts have been unsuccessful.[15,16]

These difficulties have been largely overcome in this work by choosing solvents with low absorbance in the wavelength region of interest and using extremely short path lengths (24 μ). To reduce the usual instrumental errors in this region, a spectrophotometer having excellent stray-light characteristics was employed.

The charge-transfer band for NO_3^- ion was measured in $LiClO_4$ solvent at 251°C. The band occurred at 195 mμ, with an extinction coefficient of 8730 liters $mole^{-1}$ cm^{-1}, and had an oscillator strength of 0.34. These values fall within the

[10] Analytical Chemistry Division.

[11] D. M. Gruen and R. L. McBeth, *J. Phys. Chem.* **63**(3), 393 (1959).

[12] K. E. Johnson and T. S. Piper, *Discussions Faraday Soc.* **32**, 32 (1962).

[13] J. Ferguson, Bell Telephone Laboratories, Murray Hill, N.J., private communication.

[14] Visitor from New Zealand.

[15] J. Greenberg and B. R. Sundheim, *J. Chem. Phys.* **29**(5), 1029 (1958).

[16] B. Cleaver, E. Rhodes, and A. R. Ubbelohde, *Discussions Faraday Soc.* **32**, 22 (1962).

range reported for other polar and nonpolar solvents near room temperature.

The charge-transfer band for I^- ion was measured in LiCl-KCl eutectic at 357°C. The band, when corrected for overlap with the next higher energy band, occurred at 208 mμ, with an extinction coefficient of 9670 liters $mole^{-1}$ cm^{-1}, and had an oscillator strength of 0.285. These results compare favorably with results obtained for a KI-doped KCl crystal[17] if one assumes a larger cavity size for the iodide ion in a molten salt.[18] Results of this study are being prepared for publication.

INFLUENCE OF ENVIRONMENT ON THE OSCILLATOR STRENGTH OF THE LOWEST-ENERGY TRANSITION OF THE NITRATE ION

G. P. Smith D. W. James[14]
C. R. Boston

The lowest-energy transition of the nitrate ion is forbidden by the rule of LaPorte but may be observed as a weak band with peak intensity at about 300 mμ. The effect of changing the cation composition of pure nitrate melts on the energy of the absorption peak has been previously studied[19,20] as a possible means of direct measurement of ionic interaction forces. This research has been extended to determine the effect of changes in the cationic environment on the oscillator strength, f, of the band.

The determination of the oscillator strength of the weak nitrate band requires separation of the band from the adjacent steeply rising absorption edge. This separation has been performed using the Oracle and the CDC 1604 electronic computer. The effect of changing either the cation composition of the melt or its temperature has been investigated, and, although the study is incomplete, certain qualitative features are apparent. The results were correlated with the quantity Φ given by

$$\sum_i \left(\frac{Z_i}{r_i}\right) N_i ,$$

where Z_i is the cationic charge, r_i is the cationic radius, and N_i is the electrical equivalent fraction, all of the ith species. As Φ decreases from lithium to potassium, the oscillator strength steadily decreases, whereas for lower Φ values, f remains essentially constant. When two salts are mixed, the oscillator strength varies linearly between the values for the two pure salts. Thus a mixture of 83% $CsNO_3$–17% $LiNO_3$ has an oscillator strength of 1.44×10^{-4} at 350°C, whereas pure potassium nitrate, which has the same value for Φ, at the same temperature has an f number of 0.94×10^{-4}. The temperature coefficient of oscillator strength is independent of Φ and is of the order of $1 \times 10^{-7}/°C$.

Analysis of the data to give more-quantitative information regarding temperature coefficients and the effect of mixed-cation environments is currently proceeding and will be reported at a later date.

EQUILIBRIUM OF SOLUTE SPECIES FORMED WHEN BISMUTH METAL IS DISSOLVED IN MOLTEN BISMUTH TRICHLORIDE

C. R. Boston G. P. Smith
L. C. Howick[21]

Until recently the molecular constitution of the liquid phases of bismuth–bismuth trihalide systems was an unsolved problem which attracted much research and debate.[22] During the past two years, the large uncertainty in the identification of the solute species for dilute solutions of bismuth metal in molten bismuth trichlorides has been substantially reduced by spectroscopic research at ORNL and by emf research by L. E. Topol and R. A. Osteryoung at North American

[17] H. Mahr, *Phys. Rev.* **125**(5), 1510 (1962).

[18] M. Smith and M. C. R. Symons, *Trans. Faraday Soc.* **54**, *346 (1958).*

[19] G. P. Smith and C. R. Boston, *J. Chem. Phys.* **34**(4), 1396 (1961).

[20] G. P. Smith and C. R. Boston, *Discussions Faraday Soc.* **32**, 14 (1962).

[21] Summer participant in 1961 from the University of Arkansas.

[22] For reviews see: D. Cubicciotti, *J. Chem. Educ.* **37**(10), 540 (1960); S. J. Yosim *et al.*, *J. Phys. Chem.* **63**(2), 230 (1959); and N. H. Nachtrieb, *Ibid.* **66**(6), 1163 (1962).

Aviation Corporation, Canoga Park, Calif. Spectroscopic research previous to that of the present year has been reported.[23]

During this year a procedure was devised for extracting from spectrophotometric data the concentration of the two solute species formed when metallic bismuth is dissolved in molten $BiCl_3$. The functional relation between these concentrations was found to be in accord with a family of solute equilibria of which the simplest was $4Bi^+ = Bi_4^{4+}$. The equilibrium constant K_N was computed to have a value of 3.8×10^6 at 264°C. This is within experimental error of the value 2.7×10^6 obtained by a previous emf study.

This research is described in an article which has been submitted for publication.[24]

DENSITIES OF SOME MOLTEN-SALT MIXTURES

D. W. James[14] C. H. Liu[9]
T. R. Griffiths[8]

Molten-salt densities are required to express other physical quantities, including the intensity of light absorption, on a molar basis. Since such data are rather sparse, this group has a continuing program to measure molten-salt densities as required for the support of its spectroscopic program.

Densities were determined as functions of temperature for the following salts: tributylbenzylphosphonium chloride;[25] tributyl-2,4-dichlorobenzylphosphonium chloride;[25] tetra-*n*-butylammonium bromide; tetra-*n*-butylammonium iodide; tetra-*n*-hexylammonium iodide; mixtures of $LiNO_3$ and $CsNO_3$ containing 35.4, 49.9, and 80.1 mole % $LiNO_3$; mixtures of $NaNO_3$ and $RbNO_3$ containing 20.6, 39.9, 59.9, and 80.0 mole % $NaNO_3$; 50 mole % $NaNO_3$–50 mole % KNO_3; and 80.0 mole % Li_2SO_4–20.0 mole % K_2SO_4.

This research is covered by two papers submitted for publication.[26,27]

---

[23] C. R. Boston and G. P. Smith, *J. Phys. Chem.* **66**(6), 1178 (1962).

[24] C. R. Boston and G. P. Smith, "Spectra of Dilute Solutions of Bismuth Metal in Molten Bismuth Trihalides. II. Formulation of Solute Equilibrium in Bismuth Trichloride," submitted to the *Journal of Physical Chemistry.*

[25] Donated by the Virginia-Carolina Chemical Corporation, Richmond, Va.

[26] D. W. James and C. H. Liu, "Densities of Some Molten Alkali Nitrate and Sulphate Mixtures," submitted to the *Journal of Chemical Engineering Data.*

[27] T. R. Griffiths, "Densities of Some Molten Organic Quaternary Halides," submitted to the *Journal of Chemical Engineering Data.*

4. Structure of Metals

EFFECT OF INTERSTITIAL ELEMENTS ON TWINNING IN COLUMBIUM[1]

C. J. McHargue H. E. McCoy

Single crystals of columbium containing various levels of oxygen, nitrogen, carbon, or hydrogen were deformed by slow compression and impact loading at −196°C. For the slow deformation rates, 1500 to 1900 ppm O_2, 500 ppm N_2, or 150 to 200 ppm C completely suppressed mechanical twinning. Hydrogen in concentrations to 1000 ppm had no apparent effect on ease of twinning. Impact loading caused twins to form at all levels of contamination studied, and cleavage cracking on {100} planes occurred in specimens having higher interstitial contents.

PREFERRED ORIENTATION IN IRRADIATED COPPER

C. J. McHargue J. C. Ogle

The study of preferred orientation in copper irradiated to 10^{19} neutrons/cm^2 in the ORR continued. Postirradiation treatments include (1) cold rolling 91%; (2) cold rolling 91%, annealing ½ hr at 500°C; (3) annealing for 1 hr at 300°C, cold rolling 91%; and (4) annealing for 1 hr at 300°C, cold rolling 91%, annealing for ½ hr at 500°C.

Pole figures for the {200} and {111} planes were obtained by the ORNL method during the report period. Texture components were tentatively assigned from inspection of these charts.

The irradiated and rolled copper has a strong component near (001) [100], and the remainder of the material has orientations between (123) $[\bar{5}\bar{2}3]$, (110) $[1\bar{1}2]$, and (112) $[11\bar{1}]$. The cube component is much sharper in the rolled and annealed specimen, but there is also a second unidentified component.

The as-rolled copper that was annealed before rolling had a strong (110) $[1\bar{1}2]$ component and a small amount of an unidentified component. The annealed texture contained mostly (001) [100] and a small amount of near (123) $[1\bar{2}1]$.

These results are unexpected in view of Smallman's statements that the brass-type texture $\left((110)\ [\bar{1}12]\right)$ should be developed.[2] In particular, the origin of the strong cube component in the as-rolled specimens is unexplained. Since the textures are complex, further x-ray data will be obtained, and axis distribution charts ("inverse" pole figures) will be determined.

DEFORMATION STUDIES

R. E. Reed, Sr. R. A. Vandermeer

Microstructures of aluminum rods almost always contain small, irregular particles which appear to be grain fragments. If these are portions of original grains, they may provide clues to the way in which inhomogeneous flow occurs. It has been thought that such debris originated at grain boundaries as a result of deformation band formation.

A single crystal of aluminum with a longitudinal axis near <001> was extruded to a 0.250-in.-diam rod (extrusion ratio 9:1). Metallographic examination showed the structure to be similar to that observed in polycrystalline specimens. Since such a structure is not characteristic of grain-boundary effects, it may be related to the inhomogeneous stresses of the extrusion process. Further experiments are expected to show whether such a

[1] Abstract of paper accepted for publication in *Transactions of the Metallurgical Society of AIME.*

[2] A. H. Cottrell, "Point Defects and the Mechanical Properties of Metals and Alloys at Low Temperatures," p 3 in *Vacancies and Other Point Defects in Metals and Alloys,* Institute of Metals, London, 1958.

structure is characteristic of orientations only near <001> and to give information on its relation to the relative stability of this orientation with respect to an applied stress.

It is usually assumed in texture studies that the major change in dimensions determines the preferred orientation. Thus, Barrett[3] implies that rods formed by rolling, drawing, extrusion, or swaging will have similar textures. Data obtained in this program indicate, however, that there are differences which may be significant when used to analyze theories of texture formation.

Aluminum rods were made from billets which had a near <001> texture by extrusion and by swaging. Fiber axis distributions were determined for a variety of reductions. Comparisons of these textures suggest that the <001> orientation may be more stable during deformation by swaging than by extrusion. There is a greater tendency for material with orientations along the <100> zone to move toward <001> during swaging.

NATURE OF THE <001> FIBER TEXTURE COMPONENT IN EXTRUDED ALUMINUM RODS[4]

R. A. Vandermeer C. J. McHargue

The <001> fiber texture component, found in aluminum rods extruded at subzero temperatures, was shown to consist of a debris of particles of various sizes having extremely irregular shapes dispersed in a nonuniform way throughout a matrix of the <111> orientation. Evidence was presented which indicated that the <001> texture component was not a result of recrystallization but rather was due to a fragmentation of the grains comprising the original extrusion billet. It was argued that this fragmentation arose because of the macroscopically inhomogeneous nature of deformation and flow during extrusion. Both x-ray line-broadening measurements and electron microscopy observations indicated that, after extrusion, regions having <001> orientations were in a state of relatively less strain and distortion than <111> regions, suggesting that the former have undergone less plastic deformation.

A <001> fiber texture component was also found after complete recrystallization of specimens from this aluminum rod. Approximately one-third of the recrystallized volume had this orientation. It was shown that the <001> fragments, that formed during the extrusion process, acted as nuclei for recrystallization; that is, the grain boundaries separating these fragments from the matrix were capable of migration during annealing.

Electron transmission microscopy observations and x-ray line-broadening measurements indicated that <001> regions in these aluminum extrusions recover at a much more rapid rate than <111> oriented regions at annealing temperatures up to 187°C.

PRIMARY RECRYSTALLIZATION TEXTURES IN ALUMINUM EXTRUSIONS

R. A. Vandermeer C. J. McHargue

In addition to the <001> recrystallization texture, there are several other preferred orientations that appear in aluminum rods extruded at subzero temperatures and annealed at temperatures up to 270°C. These recrystallization fiber texture components may be described in terms of the following indices: a spread of orientation between <114> and <012>; scattered <235>; and <111>. In addition to the <001> component, all these texture components are present after complete recrystallization at 270°C. X-ray orientation determinations of the largest recrystallized grains found after annealing at temperatures up to 187°C revealed that grains with orientations between <114> and <012> were the most predominant. These grains were observed to have a very rapid rate of growth until they reached a size of about 150 μ; thereafter they grew only very slowly. At annealing temperatures of 230°C and above, however, the largest recrystallized grains were of the <235> orientation. These grains were five to ten times larger than the <114> to <012> grains at these temperatures. These results suggest that there is a marked difference in the temperature dependence of either the rate of nucleation or rate of growth, or both, between these preferred orientation components.

[3] C. S. Barrett, "The Structure of Cold-Worked Metal," pp 414–41 in *Structure of Metals*, 2d ed., McGraw-Hill, New York, 1953.

[4] Abstract of paper to be submitted to *Transactions of the Metallurgical Society of AIME*.

The kinetics of recrystallization in these aluminum extrusions were not simple. Temperatures of at least 230°C were needed to give complete recrystallization. At lower temperatures, recrystallization occurred rapidly at first and then gradually slowed down until, for all practical purposes, it ceased. The fraction of recrystallization at which the process stopped decreased with the annealing temperature. A recovery anneal of 200 hr at 105°C did not alter the kinetics of recrystallization at 230°C to any appreciable extent.

An etch-pit analysis, combined with the x-ray orientation determinations, was used to establish the orientation relations between recrystallized grains and the matrix into which they were growing. It was found that all the recrystallized grains of the <114> to <012> and <235> orientations that were examined tended to have a low-index direction [<001>, <011>, or <111>] in common with the deformed matrix. In fact, the amount of rotation needed to bring the orientation of these grains into a common orientation with the matrix was very close to some of the special orientations described by Aust[5] and Kronberg and Wilson.[6] This suggests that the grain boundaries of these recrystallized grains may be coincident site boundaries.

After complete recrystallization the <001> oriented areas are composed of a network of subgrain boundaries; the subgrains are in the order of 15 to 50 μ in size. This was established by metallographic and x-ray back-reflection Laue photographs.

BEHAVIOR OF TWIN BOUNDARIES DURING ANNEALING

J. C. Ogle

A study of the behavior of deformation twin boundaries during annealing should give information on the nature of recrystallization nuclei, anisotropy of growth rates, and relative interfacial energies for various internal surfaces. Such a study was initiated on twins formed in pure niobium at low temperatures.

An orientation effect was noted for twinning tendency in crystals deformed at 77°K if precautions were taken to minimize the amount of nonuniform compression. Compression directions near <100> caused extensive slip but no twinning, whereas those near <111> caused profuse twinning. Calculation of the resolved shear stresses shows that {110} slip should be favored for the former orientations and twinning for the latter. Twinning always occurred on the {112} <11$\bar{1}$> system, and in every case the most profuse set of twins corresponded to the member of that family that had the highest resolved shear stress. Where twinning occurred on more than one {112} plane, this criterion applied to only the most active system. In some cases twins were observed on systems for which the calculated resolved shear stress was very low.

During annealing, new grains often nucleate at intersections of twins. Orientations are being determined to see if the new grain is related to either of the twins. In specimens where there are many closely spaced parallel twin bands, the usual behavior is for the matrix between the twins to be absorbed by lateral growth of the twinned regions. In other instances, new grains were found to nucleate at the twin-matrix interface of isolated twins. Almost none of the new grains are equiaxed, and marked differences in growth rates are apparent. Isolated twins sometimes contracted and disappeared (or were absorbed by the matrix).

A few observations were made on thin films by electron transmission microscopy. Significant differences in dislocation density and arrangement were observed in the matrix and twins and at various structural features within the twins; however, not enough specimens have been studied yet to correlate these observations with the other ones.

APPLICATION OF THE MÖSSBAUER EFFECT TO METALLURGICAL PROBLEMS

G. V. Czjzek[7]

The recoilless emission and absorption of gamma rays (Mössbauer effect) are extremely sensitive to the surroundings of the emitting or absorbing nucleus. This makes it possible to use the corresponding atoms as local probes to investigate structural features and processes in solids. Two series of experiments were started using the Mössbauer effect in Fe^{57} obtained by beta capture of Co^{57}.

[5] K. T. Aust, *Trans. Met. Soc. AIME* **221**(4), 758 (1961).

[6] M. L. Kronberg and F. H. Wilson, *Trans. Met. Soc. AIME* **185**(8), 501 (1949).

[7] Visitor from Germany.

Impurities in Grain Boundaries of Nickel

A layer of Co^{57} was electrolytically deposited on a thin foil of fine-grained nickel. The specimen was then diffusion-annealed for eight days at 300°C in a hydrogen atmosphere. Successive layers of the material were removed by electropolishing. After each polishing step, an autoradiograph of the specimen was made and the Mössbauer spectrum was taken. After the first polishing, the autoradiograph showed a practically homogeneous distribution of the Co^{57}. The Mössbauer spectrum consisted of the characteristic six lines of Fe^{57} dissolved in nickel. After each of the next three polishing steps, the autoradiographs showed an increasing inhomogeneity of the distribution, and in some parts grain boundaries were outlined. The Mössbauer spectrum showed a pronounced decrease of the above lines, and new lines appeared which have weak intensity and cannot be clearly resolved. Although a quantitative evaluation is not yet possible, it appears that the density of *s* electrons at the Fe^{57} nuclei is greater for iron in grain boundaries than for iron dissolved in the nickel lattice. The internal magnetic field is probably smaller in the grain boundaries.

Precipitation of Cobalt in Aluminum

A layer of Co^{57} was deposited on a thin foil of high-purity (99.999%) aluminum. The specimen was diffusion-annealed for 3 hr at 630°C in a hydrogen atmosphere. After the specimen was electropolished, a Mössbauer spectrum was taken with a stainless steel absorber. The spectrum consisted of a single line with center at 2.6×10^{-6} ev, with a small asymmetry. This asymmetry increased when the specimen was annealed at 335°C. If the main line (with the theoretical Lorentz form) is subtracted from the spectrum, it can be seen that the asymmetry is due to a second line whose center is shifted with respect to the main line by about 2.4×10^{-6} ev. After the specimen was reannealed for 2 hr at 630°C and quenched in water at room temperature, the line returned to its original form. From this it is concluded that the line with center at 2.6×10^{-6} ev is due to Fe^{57} dissolved in aluminum, the second line at 0.2×10^{-6} ev being due to Fe^{57} in a precipitated nonmagnetic phase, probably Co_2Al_9. A series of annealing-quenching treatments at different temperatures has been started to determine the kinetics of the precipitation process.

COMMENTS ON STACKING-FAULT ENERGY OF THORIUM[8]

J. O. Stiegler C. J. McHargue

Lightly deformed thorium foils were examined by electron transmission microscopy. Tangled dislocations forming cell walls were observed, but no stacking-fault fringes or cross slip was seen. These observations suggest that the stacking-fault energy of thorium is approximately equal to that of silver.

[8] Abstract of published note: *Acta. Met.* 11(3), 225 (1963).

5. Theory of Alloying

GALVANOMAGNETIC PROPERTIES OF TUNGSTEN

J. O. Betterton, Jr. D. S. Easton

The Lifshitz, Azbel', and Kaganov[1] and Lifshitz and Peschanskii[2] theory of high-field galvanomagnetic properties has been successful in many metals for study of the topology of the Fermi surface. In metals such as sodium with a closed Fermi surface, the Lifshitz theory predicts the observed early saturation of magnetoresistance and the nearly isotropic magnetoresistance and Hall constants. In other metals with open Fermi surfaces, such as copper, silver, and gold, this theory correctly predicts an unlimited increase in magnetoresistance and high anisotropy whenever open trajectories occur. For metals where the numbers of electrons and holes are equal, theory gives quadratic field dependence of the magnetoresistance for all field directions. The transverse voltage will contain anisotropic terms in H and H^2 which are not simply related to the geometry of the Fermi surface. These metals are called "compensated" metals. Finally, many metals such as Sn, Pb, Ga, Cd, and Zn have open Fermi surfaces and are compensated. Since the field dependence is H^2 everywhere, singularities associated with open orbits are found[3] by their characteristic variation with the angle between the current and open orbit direction.

Tungsten, because of its availability in high-purity form, was chosen first from among the groups IV-A, V-A, and VI-A transition elements which will be studied. Table 5.1 lists the source, residual resistivity, resistance ratio, average $\omega\tau$,

[1] I. M. Lifshitz, M. la Azbel', and M. I. Kaganov, *Zh. Eksperim. i Teor. Fiz.* **31**, 63 (1956); *Soviet Phys. JETP (English Transl.)* **4**, 41 (1957).

[2] I. M. Lifshitz and V. G. Peschanskii, *Zh. Eksperim. i Teor. Fiz.* **35**, 1251 (1958); *Soviet Phys. JETP (English Transl.)* **12**, 875 (1959).

[3] N. E. Alekseevskii, Yu. P. Gaidukov, I. M. Lifshitz, and V. G. Peschanskii, *Zh. Eksperim. i Teor. Fiz.* **39**, 1201 (1960); *Soviet Phys. JETP (English Transl.)* **12**, 837 (1961).

Table 5.1. Characteristics of Tungsten Single Crystals Used in Galvanomagnetic Studies

Source	$\rho_{317°K}/\rho_{4°K}$	$\rho_{4°K}$ (ohms/cm)	$\overline{\omega\tau}$ (1 electron/atom at 30 kilogauss)	Orientation
		$\times 10^{-9}$		
Westinghouse	14,000	0.43	68	1.5° from <100>
Linde	900	7.4	4	7° from <100>
Westinghouse	20,000	0.28	104	1.5° from <110>
General Electric	1,000	6.0	5	1° from <110>
General Electric	1,200	5.3	6	5° from <111>
Linde	1,300	4.8	6	1° from <111>
Materials Research	6,000	0.97	30	4° from <210>
General Electric	1,400	4.2	7	<1° from <211>

and orientation of the eight crystals which have been measured. The purity of these crystals, particularly those made by H. Sell of the Westinghouse Electric Corporation, was excellent. As an indication of this, the resistivity of these tungsten crystals increased by factors between 10^2 and 10^5 on application of 30-kilogauss fields, and the effective fields ($B\rho_{317°K}/\rho_{4°K}$) were as great as 6×10^8 gauss. The resistivity, Hall electric field, and transverse even field are shown in polar coordinates in Fig. 5.1. The resistivity (measured $\|$ the current, $\perp$ magnetic field) is plotted as the outer curve of the upper row of diagrams, with values corresponding to the vertical scale. The Hall field (measured $\perp B \perp J$) is defined as the transverse electric field which is odd with respect to magnetic-field reversal. This component is plotted in the central portion of the upper row of diagrams, with the scale indicated horizontally. Finally, the lower row of graphs represents the electrical field ($\perp J \perp B$) which is even with respect to magnetic-field reversal, each graph according to a common scale indicated on the lower right. In these diagrams the magnetic field rotates in the plane of the paper; the radius of the curve represents the magnitude of the property, plotted against the angle and direction of the magnetic field. Resistivity and Hall field are always positive, but in the transverse even graphs (lower row) a negative sign, plotted by reversing the direction of the radius, frequently occurs.

In agreement with prior measurements[4–9] on less pure crystals and with more recent measurements by Fawcett,[10] the resistivity of tungsten is only moderately anisotropic with a near-quadratic field dependence in all field directions. The field dependence was measured at minima and maxima of resistivity, with no evidence of saturation up to effective fields of 6×10^8 gauss. In terms of Lifshitz theory, there is no indication of open orbits and the resistivity behavior of tungsten is characteristic of a compensated metal with equal numbers of holes and electrons at the Fermi surface.

The Hall fields were always positive and large and not everywhere linear in field. At the points where they are linear, the Hall constants were in a range 20 to 100 $\times$ 10^{-11} M^3/As, with largest values appearing when the current was near the <110> crystallographic axis. The curves shown for the current directions <211> and <210> are not believed to show a significant anisotropy because of errors caused by the rapidly changing transverse even voltages, which were measured with them. In the <100>, <110>, and <111> crystals there is an inverse relationship between peaks in the Hall field and minima of the resistivity. The strong anisotropy which would be expected from open trajectories is not seen, and these diagrams with moderate anisotropy support compensated, closed surfaces. The positive values confirm the existence of holes in tungsten, which would be essential for compensation. On the other hand, large and quite anisotropic transverse even properties are observed,[11] as shown in lower diagrams of Fig. 5.1. The effects decrease in size with the crystals whose current axes are close to the (100), (110), or (111) axis in agreement with crystal symmetry, which would require a transverse even effect to vanish when the current is perfectly aligned and the field is perpendicular to the current.

All of the crystals were at least 1 to 5° from the nominal axis, as shown in Table 5.1, except the <210> crystal, which was 7° from this axis and shows the largest transverse even effect. The peaks occur for those magnetic field directions whose normal planes always contain a <112> or <113> direction.

---

[4] E. Justi and H. Scheffers, *Physik. Z.* **37**, 700 (1936); **38**, 891 (1937).

[5] E. Grüneisen and H. Adenstedt, *Ann. Physik* **31**(8), 714 (1938).

[6] W. J. de Haas and J. deNobel, *Physica* **5**(5), 449 (1938).

[7] J. deNobel, *Physica* **15**, 532 (1949); **23**, 261, 349 (1957).

[8] J. O. Betterton, Jr., and D. S. Easton, "Nb-Nb_3Sn and Nb-Zr Superconducting Coils in an Iron-Core Magnet," pp 348–57 in *Proceedings of the International Conference on High Magnetic Fields, Cambridge*, November 4–7, *1961*, MIT Press, Cambridge, and Wiley, New York, 1962.

[9] J. O. Betterton, Jr., and D. S. Easton, *Metals and Ceramics Div. Ann. Progr. Rept. May 31, 1962*, ORNL-3313, p 198.

[10] E. Fawcett, *Phys. Rev.* **128**(1), 154 (1962).

[11] J. O. Betterton, Jr., and D. S. Easton, "Magnetoresistance and Transverse Voltage, That Is Even with Respect to the Field, in Tungsten," paper presented at the American Physical Society Meeting, Stanford, Calif., Dec. 26–29, 1962 [abstract published: *Bull. Am. Phys. Soc.* **7**, 618 (1962)].

UNCLASSIFIED
ORNL-DWG 63-3355

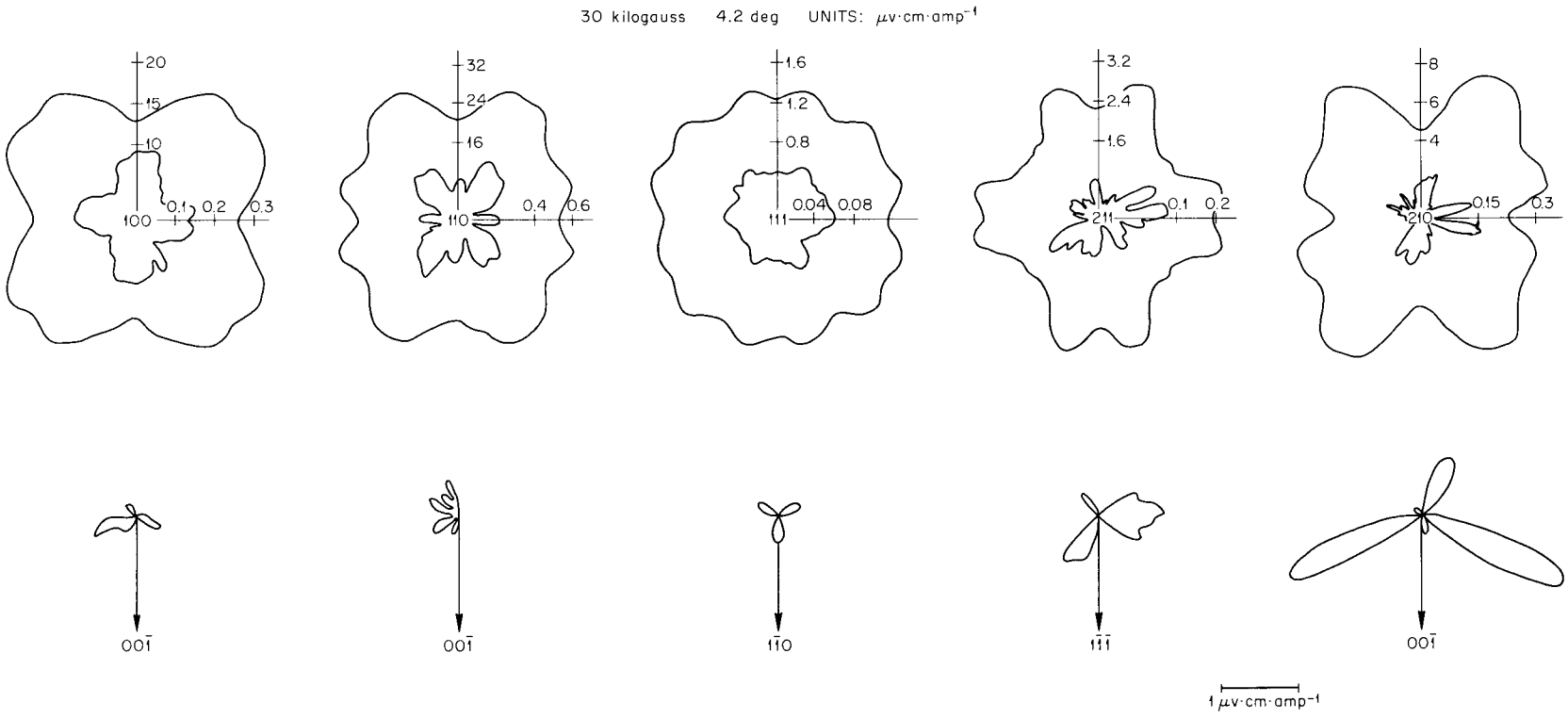

Fig. 5.1. Polar Diagrams of the Resistivity, Hall Field, and Transverse Even Field in Tungsten.

Transverse even effects have been observed in Bi, Ga, Cu, and Sn.[12-15] Klauder and Kunzler[14] proposed that the voltage components of the even electric field vector were indeed the components of the open trajectories. In copper, they were able to show that these components gave the correct directions of open trajectories. Thus, for a metal with open trajectories the even voltages should be an important aid in the interpretation of the Fermi surface. The Lifshitz theory predicts the appearance of even transverse voltages in compensated metals. In the compensated metal tin, Kachinskii found transverse even peaks in field directions normal to open orbits, but in contrast to copper, the open voltages had appreciable values in directions of elongated closed orbits adjacent to the open orbit directions. He proposed that these voltages were due to the appearance of closed orbits elongated in one direction and oriented so that the direction of elongation is not parallel or perpendicular to the current. In tungsten this would suggest elongated orbits on the Fermi surface <112> and <113> directions, but if this were true it is not clear then why the magnetoresistivity did not show a small range of open orbits.

The odd and even electric fields were also measured transverse to the current and parallel to the magnetic field. These fields were an order of magnitude smaller than the fields ($\perp J \perp B$) above and have not been plotted. The small magnitude of these components is an indication that the Fermi surface of tungsten is not highly anisotropic.[16]

On the basis of earlier magnetoresistance measurements, both Chambers[17] and Fawcett[10,18] had pointed out that tungsten had a closed and compensated Fermi surface. The present experiments confirm this situation after investigation of other current directions and at higher effective fields. The galvanomagnetic properties are in agreement with the electronic specific heat coefficient, which has a small value of 0.75 mj/deg^2, corresponding to a small Fermi area in this metal.[19] Theoretical energy band calculations for the transition metal chromium, by Asdente and Friedel,[20] show that the density of states distribution divides into two parts: one of low energy, which interacts more spatially, and one of high energy, which is more atomic in nature. According to the galvanomagnetic properties, the high- and low-energy parts of the tungsten band structure overlap in energy only slightly with the low-energy bands, filled to such an extent that they are closed surfaces, and with high-energy bands, closed because they contain so few electrons. A modification of the Asdente and Friedel electronic structure of chromium-type metals proposed by Lomer[21] agrees with the galvanomagnetic properties, having closed holes in the fourth band and closed pockets of electrons in the fifth and sixth bands.

Further changes in this model for tungsten may be required if the transverse even voltages really indicate elongations of the Fermi surface in the <112> and <113> directions. A comparison in this respect should be made with the cyclotron resonance measurements of Fawcett,[22] which show a cyclotron mass minimum of 0.84 for orbits when the applied magnetic field is near <111> in the <110> plane of tungsten, the mass increasing as the field deviates from the normal to the <111>.

LOW-TEMPERATURE SPECIFIC HEATS OF ZIRCONIUM ALLOYS

J. O. Betterton, Jr. J. O. Scarbrough

Transition metal alloys can be considered in different ways, depending on the property studied. Pauling and others, who are concerned with chemical binding, treat the localized region of nearest neighbors and use valency numbers which

[12] R. A. Connell and J. A. Marcus, *Phys. Rev.* **107**(4), 940 (1957).

[13] W. A. Reed and J. A. Marcus, *Phys. Rev.* **126**(4), 1298 (1962).

[14] J. Klauder and J. Kunzler, *Phys. Rev. Letters* **6**(4), 179 (1961).

[15] V. N. Kachinskii, *Soviet Phys. "Doklady" (English Transl.)* **5**(6), 1260 (1961).

[16] J. M. Ziman, *Electrons and Phonons*, p 518, Oxford University Press, London, 1960.

[17] R. G. Chambers, p 118 in *Fermi Surface* (ed. by W. A. Harrison and M. B. Webb), Wiley, New York, 1960.

[18] E. Fawcett, *Phys. Rev. Letters* **7**(10), 370 (1961).

[19] M. Horowitz and J. Daunt, *Phys. Rev.* **91**(5), 1099 (1953).

[20] M. Asdente and J. Friedel, *Phys. Rev.* **124**(2), 384 (1961).

[21] W. M. Lomer, *Proc. Phys. Soc.* **80**(514), 489 (1962).

[22] E. Fawcett and W. M. Walsh, Jr., *Phys. Rev. Letters* **8**(12), 476 (1962).

include all the binding electrons. This viewpoint is successful for binding energies but is not so useful for electrical properties. Matthias, in considering superconducting compounds, defines an electron/atom parameter as the difference in atomic number, so that essentially all the electrons outside the inert-gas shell and including the filled *d* shells of the B-subgroup elements are involved in his predictions of superconducting transition temperature. The model, however, which is most frequently used is the rigid-band model. This model concerns itself with *k* values of the electrons and states that the impurity does not disturb the distribution of states present in the pure metal, other than through addition or subtraction of occupied states near the Fermi level. With two bands or subbands of different spin, the situation is the same only the bands may be shifted rigidly relative to one another during alloying or application of magnetic field. Nothing was said about the disposition of charge in real space, but Friedel pointed out[23] that screening electrons would effectively subtract states as well as electrons from the bottom of the band, leaving the situation unchanged as to the number of occupied states at the Fermi level. The success of the rigid band in a qualitative way may also be due to a cancellation of some of the larger effects by a pseudo potential,[24] which cancels the large lattice potential in many pure metals. Thus, different conditions for orthogonalization to the closed-shell electrons in different atoms in the alloy tend to minimize the differences in potential between the atoms and make the assumptions workable for some alloying systems.

With transition metal alloys with B-subgroup elements, the rigid-band model requires modification in order to explain the zero valency of transition elements in many alloys. This was noted as early as 1931 by Ekman in γ-brass phases involving transition metals. Alloys of hexagonal zirconium with B-subgroup elements Ag, Cd, In, Sn, and Sb are another example of this phenomenon.

When zirconium is alloyed with tin, each constituent of the alloy would normally be expected to contribute four electrons, and zirconium properties such as electronic specific heat and the axial ratio, which depend on the position of the Fermi surface, would be expected to change only slightly. Actually, large changes are observed;[25,26] with Ag, Cd, In, Sn, and Sb added in constant amounts the electronic specific heat and the axial ratio increase linearly with a solute valency. The small effects with silver and the large effects with antimony suggest that, actually, only a small number of valency electrons are being contributed to the distribution by the zirconium. Since studies of the cohesion of elements in the Periodic Table suggest that all four zirconium electrons are effective in the metallic binding, a distinction is made between zirconium *d*-type electrons and *s*-*p*-type electrons, putting these electrons into separate bands. Most of the four electrons in zirconium are assumed to be of 4*d* type, and electrons in these states are assumed to have little probability of being in the atomic cells of the solute atoms when these solute atoms have completed filled groups of 4*d* electrons. The replacement of a zirconium atom with one of these solute atoms then removes two 4*d* states and approximately four electrons, with a net change of about zero as far as the Fermi surface is concerned. In support of this, the electrical resistance[27] of the same alloys at 4.2°K is approximately $d\rho/dx = 16 + 1.4n$, when x is atomic percent solute of valence n, and one can see that the main effect is not the screening of the excess charge n on the solute but the strong scattering of the *d*-band holes, which would be proportional to the number of such holes and x.

The electronic and lattice specific heats of the solutes Ag, Cd, In, Sn, and Sb have been discussed in detail in a recent paper,[25] where it was shown that in addition to the above model there is an alternate model which assumes that the main effect is due to shifts in the relative positions of the *s*- and *d*-type bands during alloying and which

[23] J. Friedel, *Advan. Phys.* **3**(12), 446 (1954).

[24] V. Heine, *The Fermi Surface* (ed. by W. A. Harrison and M. B. Webb), pp 279–89, Wiley, New York, 1960.

[25] G. D. Kneip, Jr., J. O. Betterton, Jr., and J. O. Scarbrough, "Specific Heats of Zirconium Alloys," submitted to the *Physical Review*.

[26] J. O. Betterton, Jr., and D. S. Easton, "Lattice Constants of Alpha-Zirconium Alloys with Additions of Ag, Cd, In, Sn, and Sb," paper presented at the Annual Meeting of the Metallurgical Society of AIME, St. Louis, Missouri, February 19–23, 1961 [abstract published: *J. Metals* **13**, 86 (1961)].

[27] J. O. Betterton, Jr., and D. S. Easton, "Electrical Resistivities of Zirconium with Dilute Additions of Ag, Cd, In, Sn, and Sb," pp 270–73 in *Proceedings of the VII International Conference on Low Temperature Physics* (ed. by G. M. Graham and A. C. Hollis Hallett), University of Toronto Press, 1961.

could also account for the alloying effects of these elements on the electronic specific heat. Recent calculations of the electronic structure of zirconium, which are in good agreement with the electronic specific heat of pure zirconium[28] but which do not show a rising $N(\epsilon)$ curve with increasing electron-to-atom ratio in zirconium, have been made by Altmann and Bradley.[29] This effect may be characteristic of alloying zirconium with B-subgroup elements rather than a characteristic of a pure zirconium band structure.

Further investigation of the above is intended by a study of zirconium with A-subgroup alloys. Such A-subgroup elements from the transition periods have incomplete *d* shells and would be expected to combine with zirconium in a more normal fashion. Alloys have been prepared with niobium and molybdenum, and plans are under way to prepare alloys with scandium. The alloys with elements titanium and hafnium, from the same column in the Periodic Table as zirconium, are also under study. The first results have been obtained for Zr-Hf alloys and are shown in Fig. 5.2.

[28]G. D. Kneip, Jr., J. O. Betterton, Jr., and J. O. Scarbrough, "Low-Temperature Specific Heats of Titanium, Zirconium, and Hafnium," to be published in the *Physical Review*.

[29]S. L. Altmann and C. J. Bradley, *Phys. Letters* 1(8), 336 (1962).

The electronic specific heats change nearly linearly and slowly between hafnium and zirconium. The effects of dilute additions of Ag, Cd, In, Sn, and Sb have been superimposed on the hafnium curve, Fig. 5.2, to show the relative size of the effects. Although zirconium and hafnium should be similar in electronic structure, with hexagonal crystal structure, with nearly the same axial ratio (1.59), and nearly the same lattice constants, the nuclear charge has almost doubled in the case of hafnium and the 4*f* shell of electrons has been completed. The effect of these changes is smaller than the above valency effects and may be due either to a gradually increasing interaction between the valency electrons from zirconium to hafnium or to a displacement of the energy of the *s*-type band relative to the *d*-type band due to the greater density of *s*-type wave function near the increased nuclear charge of hafnium.

The Debye temperatures of Hf-Zr alloys obtained from the low-temperature lattice specific heats are shown in Fig. 5.3, where they are compared with the quantity $KM^{-1/2}$, which shows the effect of atomic mass M for an isotropic, central-force solid[30] with constant elastic properties and atomic volume of zirconium. The comparison between the two curves shows that the Debye temperature does not decrease as much with hafnium additions as would be indicated by the atomic mass changes and that average forces between the atoms are rising steadily with hafnium. This is believed to

[30]J. C. Slater, *Introduction to Chemical Physics*, pp 234–38, McGraw-Hill, New York, 1939.

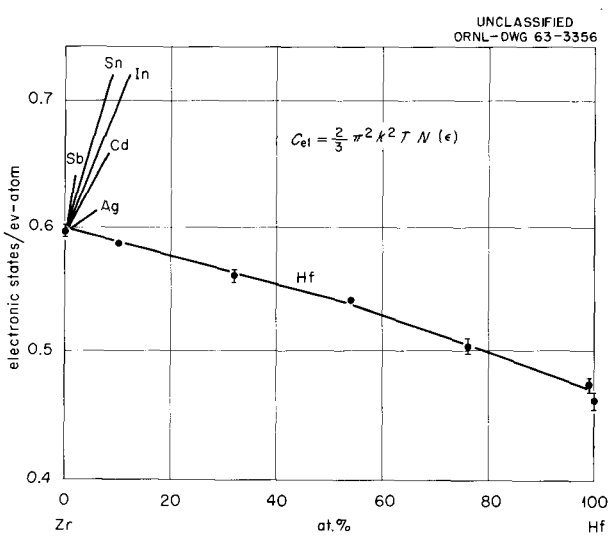

Fig. 5.2. Density of Electronic States in Hf-Zr and in B-Subgroup Zirconium Alloys.

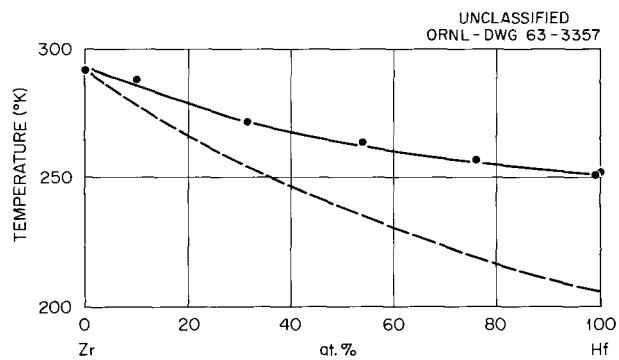

Fig. 5.3. Debye Temperatures of Hf-Zr Alloys Compared with Isotropic Model with Mass and Volume Changes Only.

be due to the increased cohesion in hafnium, resulting from the lanthanide contraction. Similar evidence for increased binding energy, as well as derivatives of the binding energy, may be seen in the abnormally high α/β transformation temperature and melting temperature in hafnium relative to zirconium. Values of the elastic constants of single crystals of titanium, zirconium, and hafnium have recently been measured by Fisher[31] and show the elastic constants of hafnium to be considerably greater than those of zirconium. Fisher's calculations of θ_D from his elastic constants are in excellent agreement with Debye temperature[29] measured in this research for pure titanium and zirconium.

THE LEAD-ZIRCONIUM PHASE DIAGRAM

J. O. Scarbrough J. O. Betterton, Jr.

The alpha phase has previously been shown[32] to form peritectoidally in this system at 5 at. % Pb and 890°C. The beta solubility extends to at least 14.5 at. % Pb at 1300°C, where the body-centered cubic structure is retained upon quenching small specimens. An intermediate phase occurs at the approximate composition Zr_5Pb, which according to preliminary x-ray study is of β-tungsten structure. The portion of the diagram between 14.5 and 23% Pb has not been finally established. A eutectic occurs near 23 at. % Pb and 1400°C, one component of which has been identified as Zr_5Pb_3. The Zr_5Pb alloys with β-tungsten structure are of interest as superconductors, since the Zr_5Pb alloy according to Matthias' rules should have a reasonably high transition temperature.

[31] E. S. Fisher, *Bull. Am. Phys. Soc.* **8**(1), 65 (1963).

[32] G. D. Kneip, Jr., J. O. Scarbrough, and J. O. Betterton, Jr., *Metals and Ceramics Div. Ann. Progr. Rept. May 31, 1962*, ORNL-3313, p 202; a preliminary Zr-Pb diagram from the present experiments has been shown: B. Lustman and F. Kerze, Jr., *Metallurgy of Zirconium*, p 462, McGraw-Hill, New York, 1955.

6. Physical Property Studies

D. L. McElroy

T. G. Kollie W. Fulkerson

These studies concern the accurate measurement of the thermal conductivity (k) of solids over a wide temperature range and the influence of controlled variables on this property. These tests will be used to elucidate heat-transport mechanisms operative at high temperatures and to provide data for studying the interaction of the transport mechanism with lattice defects. There is evidence that at high temperatures heat-transfer mechanisms supplementary to the normal phonon processes may be important in nonmetallic crystals.[1] The nature of some of these mechanisms is such that they are best characterized by high-temperature k measurements. However, other related physical properties, such as electrical conductivity, specific heat, and thermal radiative properties, must be measured in order to identify and separate other mechanisms. Enough information to quantitatively test existing theories can be obtained only by using several independent methods to measure a series of related properties of the same sample or a group of samples.

THERMAL CONDUCTIVITY RESULTS

Measurements begun last year on UO_2 pressed and sintered to 93.4% of theoretical density were extended to 1350°C in the improved radial-heat-flow apparatus.[2] The results obtained (reported in Part II, Chap. 19, this report), although not as refined as desired, represent a considerable improvement and extension in this measuring method. The study of UO_2 is continuing, not only because it is a material of nuclear interest, but also because there is particular interest in, and controversy over, the mechanism of heat-transport operative in this solid at high temperatures.[3,4] In particular, recent single-crystal data[5] indicate that other mechanisms of heat transport besides phonon conduction (such as infrared transmission and/or ambipolar diffusion) are operative above 600°C. However, the only allowable conclusion from the limited UO_2 data obtained by this group is that no significant auxiliary heat-transport mechanisms are operative up to 1350°C. This poses the interesting problem of establishing why such auxiliary mechanisms are important in the single crystal, but not in the polycrystal, sintered body. This problem will be the subject of further study which will involve higher-temperature k measurements, as well as auxiliary electrical and optical measurements, on UO_2.

Two analytical approaches describing the heat transfer which occurred during operation of the thermal comparator[6] were successfully pursued. Both models showed that the sphere response is proportional to the specimen thermal conductivity if the specimen-sphere contact area is maintained sufficiently small and constant for all specimens. These conditions were ensured by slight equipment

[1]Communication of this evidence has been expedited by two invitational conferences on thermal conductivity, one held at Battelle Memorial Institute in 1961 and one held at the National Research Council in 1962. The third conference in this series, to be held in Gatlinburg, Tenn., Oct. 16–18, 1963, is being coordinated by the Physical Properties Studies Group.

[2]T. G. Godfrey, T. G. Kollie, and D. L. McElroy, *Am. Soc. Metals, Trans. Quart.* **55**(3), 749–51 (1962).

[3]J. L. Bates, *Nucleonics* **19**(6), 83 (1961).

[4]J. E. May *et al.*, *Observations on the Thermal Conductivity of UO_2*, AECL-1641 (November 1962).

[5]J. L. Daniel *et al.*, *Thermal Conductivity of UO_2*, HW-69945 (September 1962).

[6]D. L. McElroy, T. G. Kollie, and W. Fulkerson, *Metals and Ceramics Div. Ann. Progr. Rept. May 31, 1962*, ORNL-3313, pp 135–37.

modifications. Furthermore, the sphere response was made more sensitive by operating in nitrogen rather than in helium; and calibration curves were established using a single sphere on small specimens of known thermal conductivity at 40, 75, and 125°C. Since the apparatus yields rapid k determinations on small specimens, it is ideal for studies which involve comparison of a group of samples that show a systematic variation of some property.

An example of this is afforded by data taken on Al-Gd_2O_3 composites of different compositions. Thermal conductivity was measured at 75°C on cold-pressed pellets, ¼ in. in diameter by ¼ in. in length, of aluminum powder containing 0, 10, 15, 20, and 25 vol % Gd_2O_3. The thermal conductivity of the pellets decreased rapidly with increasing Gd_2O_3. This change was much more than would be expected if the aluminum were the continuous phase. The Rayleigh-Maxwell relation for calculating the thermal conductivity of two-phase structures was applied, assuming the dispersed phase to be aluminum and the continuous phase to be Gd_2O_3. The calculated values agreed with the measured values, and photomicrographs of the pellets substantiated the above assumption. In addition, the thermal conductivity of a small specimen of uranium sulfide was measured at 40, 75, and 125°C and was shown to be approximately 25% greater than that of UO_2.

The Wiedemann-Franz-Lorentz relation between the thermal (k) and electrical (σ) conductivities and the absolute temperature, $k/\sigma = LT$, was examined for the pure metals Nb, Mo, Ta, and W and ten of their nearest neighbors. Because σ for pure metals decreases with increasing temperature, it is usually assumed that k decreases with increasing temperature. However, the temperature dependence of k of group IV-A metals is virtually zero; that of the group V-A series, positive; and that of group VI-A, negative; while the temperature dependence of iron is negative, and that of yttrium is positive. These changes are due to the electronic portion of k; and, although the electrical resistivity (ρ) temperature relation is a positive monotonic function of temperature, this is not necessarily true for thermal conduction due to electrons. By assuming a linear temperature dependence for σ or ρ and by differentiating the above expression with respect to temperature, one can obtain an expression for dk/dt:

$$\frac{dk}{dt} = \frac{L}{\rho_0}\left[\frac{(1 - \alpha T_0)}{(1 + \alpha t)^2}\right],$$

where ρ_0 is the electrical resistivity at T_0 (273°K), and t is the temperature in degrees centigrade. The value of this expression may be positive, negative, or zero, depending on the magnitude of α, the temperature coefficient of ρ. When values for α of these groups of metals are substituted in the derived expression, the measured temperature dependence of thermal conductivity for these pure metals is adequately predicted.

RADIATIVE PROPERTY RESULTS

The total hemispherical emittances of several materials are reported in Part II, Chap. 19, this report. This represents an initial effort toward understanding the radiative properties of solids and their relation to other physical properties. This understanding is needed to design high-temperature equipment and to obtain precise temperature measurements by optical means at high temperatures.

DEVELOPMENT OF NEW MEASURING APPARATUS

High-temperature experiments are characterized by many difficulties which result from temperature-transducer limitations and materials-compatibility problems. For a given system, these difficulties can cause excessive determinate errors as well as systematic errors which are hard to detect. Thus, in addition to the above-mentioned techniques, several overlapping methods of k measurement in the temperature range 100 to 2000°C are being developed. These independent methods provide this program with considerable flexibility, as well as the possibility of internal checks on the various methods. These methods allow measurements over a wide range of conductivities, varying from low-conductivity powders to high-conductivity metals. Other related physical properties at high temperatures may be measured with much of the same

equipment used in the thermal conductivity measurements. During the past year, significant progress was made on the development of a hot-probe apparatus, a quenching apparatus, and a direct-heating apparatus.

The hot-probe apparatus allows the measurement of the thermal conductivity of powders in a vacuum or in a variety of gaseous environments up to 1000°C. This class of materials represents a logical extension and special case of the studies on heat flow in multiphase heterogeneous material in which a number of variables are easily changed. In this technique, a cylindrical probe made from a material of high thermal conductivity and having a large length-to-diameter ratio is inserted in the powder to be measured; the probe is heated by a constant electrical current. The temperature rise of the probe is related to the thermal conductivity of the powder. The initial temperature of the powder is controlled by a special tube furnace which was uniformly bifilar wound for 24 cm. Critical placement of shaped, external radiation shields at each end of the furnace yielded a 14-cm-long isothermal zone which was at least 10 times as long as that of an unshielded furnace.[7]

The direct-heating apparatus[8] was fabricated and assembled and is currently being tested. This apparatus will be used to measure the thermal conductivity of solids to about 2000°C. The apparatus consists of a large vacuum chamber which contains a tantalum sheet furnace for indirect heating of a tubular specimen positioned along the axis of the furnace. Electrodes are attached to each end of the specimen to allow direct heating. The thermal conductivity is determined from suitable power and temperature measurements. Scott[9] used this technique on UO_2 between 800 and 1150°C. The vacuum chamber is provided with sight ports so the specimen temperature can be measured optically. Although the principal objective is to measure thermal conductivity, this apparatus is extremely versatile and should also provide the means for measuring high-temperature emissivity, specific heat, electrical conductivity, and thermoelectric power.

The quenching apparatus was redesigned to ensure maintenance of adequate operating conditions and to allow two methods to be used to determine thermal diffusivity to 1500°C. Both methods require measuring the temperature change of the specimen in a fluidized bed. By one method a preheated specimen is quenched in the bed and thus subjected to a sudden increase or decrease in surface temperature. In the other method the specimen is held in the fluidized bed, and the specimen surface temperature is increased at a predetermined rate. After slight equipment modifications, the fluidized bed could also be used as the heating medium for an adiabatic wall in the direct measurement of specimen specific heat. The latter is needed to obtain thermal conductivity values from the thermal diffusivity results.

[7]Neils Engel, "A Device to Control the Temperature Profile in Tubular Furnaces," a technical note submitted to the *Review of Scientific Instruments.*

[8]D. L. McElroy, T. G. Kollie, W. Fulkerson, T. G. Godfrey, and H. W. Godbee, "Progress Report on Thermal Conductivity Measurements at the Oak Ridge National Laboratory," pp 17–29 in *Proceedings of the Second Conference on Thermal Conductivity, October 10, 11, and 12, 1962,* Division of Applied Physics, National Research Council, Ottawa, Ontario, 1963.

[9]R. Scott, *The Thermal Conductivity of* UO_2, AERE M/R 2526 (March 1958).

7. Basic Sintering Studies

C. S. Morgan C. S. Yust

The rapid advance of reactor and other technology in recent years has called for materials with improved high-temperature properties. Ceramic materials prepared by sintering techniques are often best suited for use, particularly with respect to high-temperature tolerance. These studies of sintering fundamentals are intended to advance basic understanding of the mechanism of material transport during sintering, especially in ceramics (such as UO_2 and ThO_2) which have the fluorite structure.

Although many investigators believe that the results of model studies indicate material transport to be principally by volume diffusion, the studies reported here indicate that the initial densification of certain materials occurs primarily by dislocation movement.

TEMPERATURE-DEPENDENT DENSIFICATION END POINT

The study of the densification kinetics of ThO_2 powder compacts has continued. The temperature-dependent densification end point, which has been previously reported in ThO_2 and noted to be independent of the rate of heating,[1] was investigated at heating rates much greater than those utilized in the original work. Very thin powder compacts, supported on small-diameter sapphire rods with a thermocouple located immediately adjacent to the pellet, were inserted into a hot furnace at a speed adjusted to give the desired heating rate. In this manner, heating rates as high as 150°C/sec, as indicated by the thermocouple, were obtained when the maximum temperature to which the compact was heated was 1200°C. Upon reaching temperature, the compacts were withdrawn from the furnace. As shown in Fig. 7.1, there is a slight decrease in density with increasing heating rate, but the density change is extremely small compared to the difference in time at each temperature. The density decrease noted may be due, at least in part, to failure of the interior of the compact to reach the indicated temperature.

The temperature-dependent densification end point can be explained in terms of a plastic-flow model of material transport.[2] Consider two identical sets of two spheres making point contact which are being heated (Fig. 7.2). At temperature T_1, the sintering process between the two spheres has just started; at a higher temperature, T_2, the weld necks have grown, and the sphere centers have

[1] C. S. Morgan and C. S. Yust, *Met. Div. Ann. Progr. Rept. May 31, 1961*, ORNL-3160, p 40.

[2] C. S. Morgan and C. S. Yust, "Material Transport During Sintering of Fluorite Structure Materials," submitted to the *Journal of Nuclear Materials*.

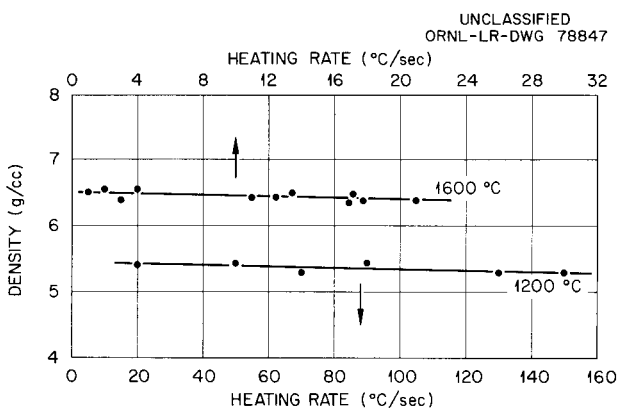

Fig. 7.1. Density vs Heating Rate for Thoria Powder Compacts Brought to Temperature. (No hold at temperature.)

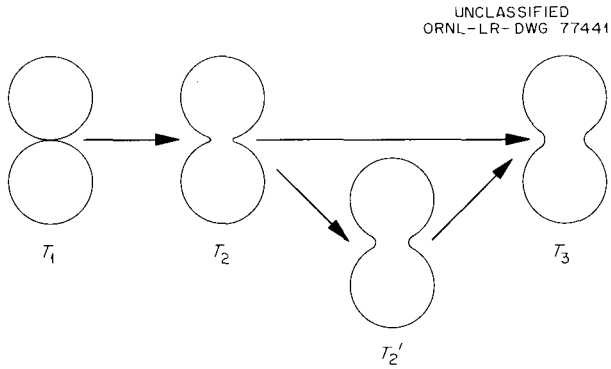

Fig. 7.2. Schematic Diagram of Spheres Sintering.

moved closer together. The temperature of the first set of spheres is increased at a steady rate, going from T_1 through T_2 to T_3. On reaching T_3, the first set of spheres has a geometrical state, as shown in the figure. The second set of spheres is held at temperature T_2, where the dislocation motion that can rapidly take place is quickly completed since the growth of the neck lowers the stress below the level required for continued dislocation motion. Further sintering must be by volume-diffusion transport of material or by dislocation glide after climb to a more favorable position. The isothermal sintering causes the second set of spheres to attain the condition indicated in the figure as T_2'. Heating this set of spheres to T_3 now results in a lower rate of densification during heating because the enlargement of the neck radius during isothermal heating reduces the magnitude of the forces causing dislocation motion. Further rapid sintering by extensive dislocation movement does not take place until the stress required to move dislocations has fallen below the level of stress now existing in the neck. The temperature at which this occurs is approximately the temperature at which the first set of spheres would have had the same extent of sintering, that is, the same neck geometry. On the assumption that this temperature is lower than T_3, there is little difference in extent of sintering when T_3 is reached, even though the heating times may have differed widely.

It is thought that failure to achieve a heating rate that is sufficiently rapid to cause compacts to reach temperature before reaching the sintered density characteristic of that temperature is a reflection of two factors: (1) densification during the heatup period is predominantly by plastic flow not requiring substantial contribution by processes involving diffusion; and (2) once movement is initiated, the movement of dislocations effecting the plastic flow is so rapid as to appear infinite in terms of these sintering measurements. Thus, the densification rate is controlled by the start of movement of dislocations, which in turn is triggered by the rising temperature.

MINIMA IN THORIA DENSIFICATION RATE CURVES

Data obtained during the report period indicate that impurities may cause the minimum observed in the densification rate vs temperature curve for ThO_2 powder compacts.[1] The curve designated "standard" ThO_2 in Fig. 7.3 is typical for all batches of ThO_2 prepared by the usual oxalate precipitation from $Th(NO_3)_4$ containing about 400

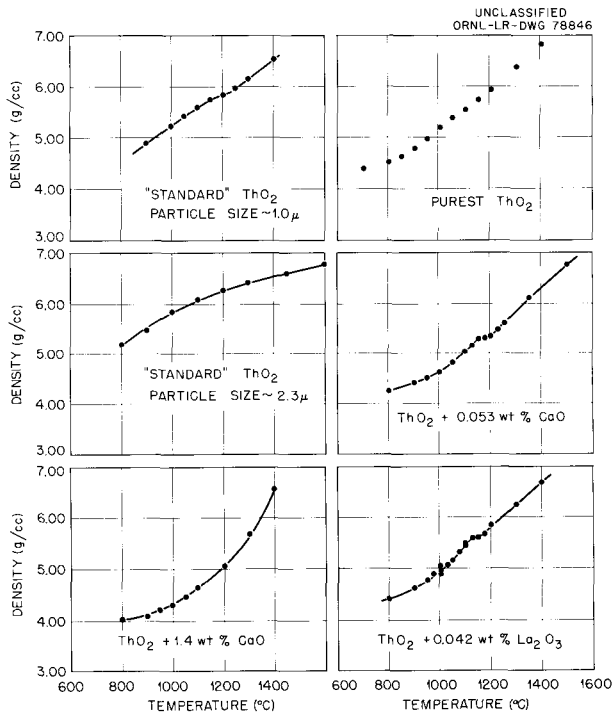

Fig. 7.3. Densification vs Temperature Curves for Compacts of Thoria Powder Preparations Brought to Temperature at 2°C/sec. (No hold at temperature.)

ppm of impurities. The small, but definite, inflection around 1200°C in the density vs temperature curve is a manifestation of the densification rate minimum. Thorium dioxide prepared from the same $Th(NO_3)_4$ by a modified procedure involving a long digestion of thorium oxalate in the supernatant liquid before filtration had larger and more-rounded particles. The sintering curve for this material does not have an inflection. Thorium dioxide prepared from the purest $Th(NO_3)_4$ available had particle size and shape similar to "standard" ThO_2 but did not have an inflection; ThO_2 preparations from the pure $Th(NO_3)_4$ containing small quantities of coprecipitated ions (lanthanum, calcium, or iron) did have an inflection. Increasing the quantity of coprecipitated impurity caused the inflection to vanish, as is seen in the data for ThO_2 containing 1.4 wt % CaO.

The data thus show a definite relation between the minimum and the impurity-ion content, although the mechanism of the impurity effect is not certain. Sintering studies with NaCl revealed a minimum in the densification rate curve at approximately the same temperature at which Eshelby *et al.*[3] found a maximum in the yield stress vs temperature curve for this material. Eshelby attributed the maximum in the yield stress to variation of impurity-ion interaction with dislocations as a function of temperature. The minima in densification rate curves for ThO_2 and NaCl may result from a similar effect. (Literature reports indicate that NaCl powder will not densify.[4] However, it was found that, if the NaCl has sufficiently small particle size and is kept dry, it densifies substantially when brought rapidly to temperature.)

[3]E. D. Eshelby *et al.*, *Phil. Mag.* **3**(25), 75 (1958).

[4]W. D. Kingery and M. Berg, *J. Appl. Phys.* **26**(10), 1205 (1955).

PROPERTIES OF ThO_2 CONTAINING CaO

Thoria containing 1.35 wt % CaO forms a solid solution having essentially the same unit cell size as pure ThO_2. Preliminary measurements on the solid solution indicate that the self-diffusion coefficient of thorium determined by measuring the penetration of Th^{230} was about twice as large as that in "standard" ThO_2. Compressive creep of a bushing containing the added CaO occurred at approximately one-tenth the stress required to cause creep of thoria without added calcium at 1450°C. The sintering of ThO_2 containing the 1.35 wt % CaO was found to proceed much more rapidly than the sintering of pure thoria. When heated to a specific temperature and immediately cooled, the compacts achieved a density which is characteristic of the temperature and is independent of the heating rate. In addition, the variation in densification rate with temperature variations was indicative of material transport by plastic flow, as in the case of pure-thoria compacts. These results suggest a model in which the presence of the calcium ions causes an increased initial sintering rate but does not cause diffusion to become the rate-controlling mechanism.

8. Deformation of Crystalline Solids

DISLOCATIONS IN DEFORMED Ni-Al ALLOYS

J. A. Wheeler, Jr. C. K. H. DuBose
J. O. Stiegler

To understand further the means by which energy is stored in a crystal lattice during deformation, it is desirable to have some idea of how the density and distribution of dislocations vary as deformation proceeds. Therefore the dislocation densities of some Ni-Al alloys were measured as a function of strain by means of transmission electron microscopy. The material used was the same as that used for stored-energy measurements.[1] The compositions studied were Ni, Ni–1 wt % Al, Ni–4 wt % Al, and Ni–5.5 wt % Al. Samples were prepared from $\frac{3}{8}$-in.-diam rod rolled to 20 mils and annealed in vacuum at 950°C. The Ni–5.5 wt % Al alloy was quenched in water; the others were cooled slowly. Tensile deformation was done on an Instron tensile machine at a crosshead speed of 0.05 in./min at 23°C. The gage length of all samples was approximately 3 in. Elongation was measured by using scribes across the surface of the sample.

Thin foils about 2500 A thick, suitable for transmission electron microscopy, were prepared by the window technique[2] of electropolishing using stainless steel cathodes and an electrolyte composed of 86 ml H_3PO_4, 10 g CrO_3, and 5 ml H_2SO_4. The electropolishing cell was operated at a current density of 0.8 to 1 amp/cm^2 at 6 to 7 v. The thin foils were mounted in the biaxial tilting stage and examined in a Hitachi (HU-11) electron microscope operated at 100 kv.

Dislocation densities were determined by the line intercept method. The dislocation distributions varied to some extent with film thickness; consequently, photographs were made only of very thick areas, indicated by intense diffuse scattering of electrons. Since it was generally impossible to move dislocations in these areas by means of the electron beam, film thicknesses could not be measured directly. An estimated thickness of 2500 A was used in all this work. In experiments in which dislocations were moved, these foils were more than 2000 A thick; it is doubtful that appreciable transmission would occur if the foils were more than 3000 A thick. All results reported here are the average of at least three measurements on areas generally more than 4 μ square.

In Fig. 8.1 the results are plotted as dislocation density ρ in cm/cm^3 against true strain ϵ.

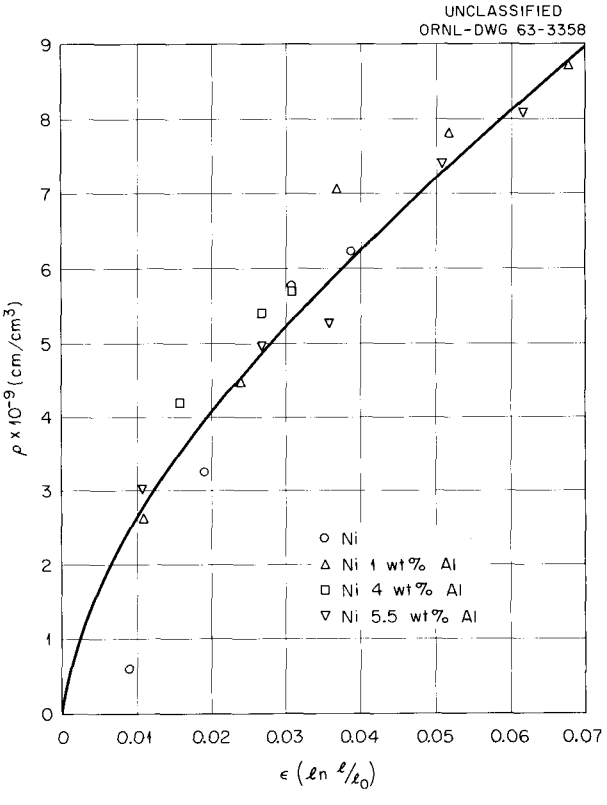

Fig. 8.1. Dislocation Densities of Ni-Al Alloys Deformed at 23°C.

[1] R. O. Williams and J. A. Wheeler, Jr., *Metals and Ceramics Div. Ann. Progr. Rept. May 31, 1962*, ORNL–3313, p 183.

[2] Thomas Gareth, *Transmission Electron Microscopy of Metals*, p 154, Wiley, New York, 1962.

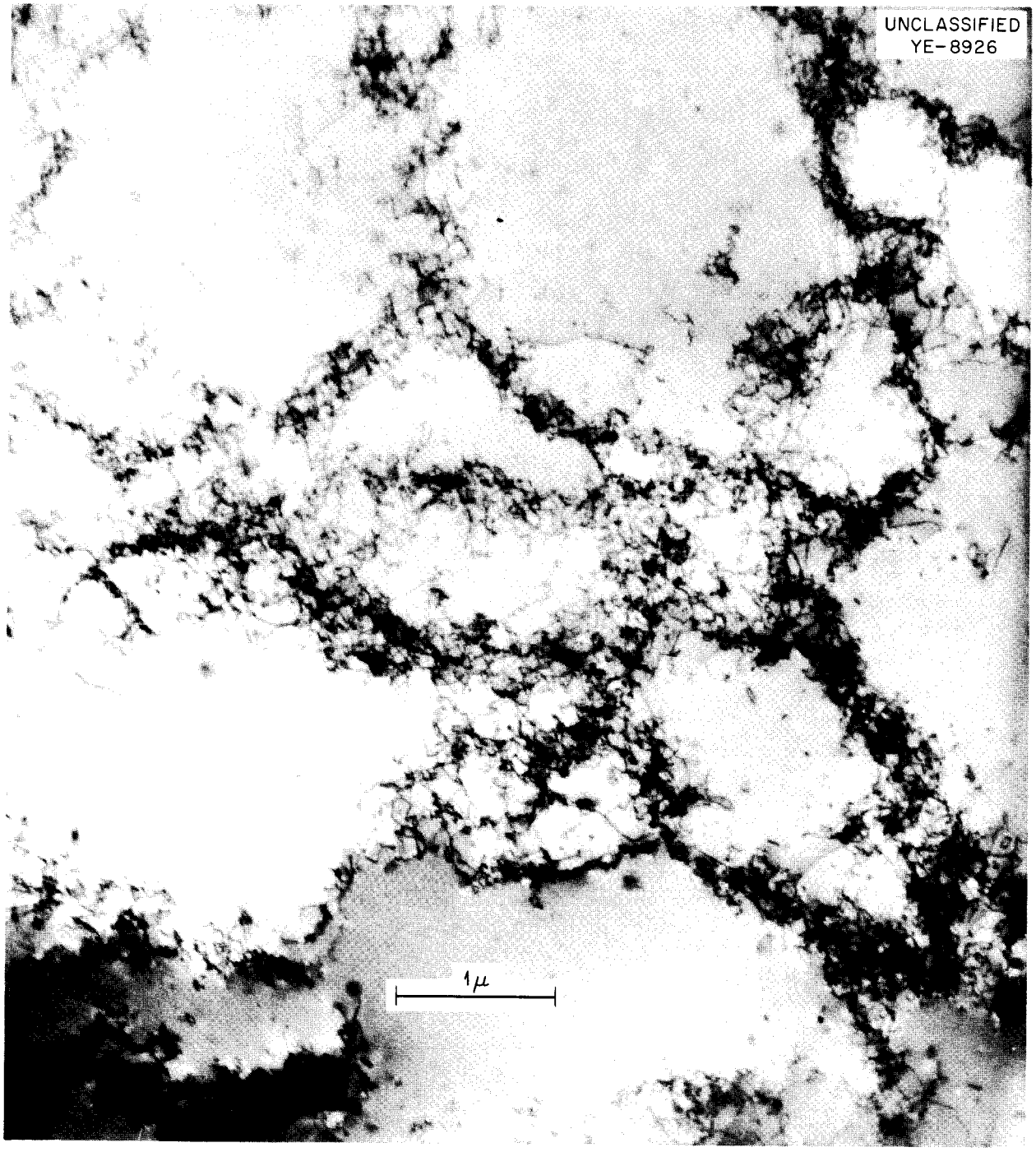

Fig. 8.2. Dislocation Structure of Pure Nickel Deformed at 23°C to $\epsilon = 0.039$. $\rho = 5.4 \times 10^9$ cm/cm^3.

Considering the reliability of the method, these results indicate that the dislocation density for a given amount of strain is independent of alloy composition. Another important feature is the fact that the dislocation density is definitely not a linear function of strain, even at these very low strains. Considerable curvature is observed which is approximately parabolic beyond $\epsilon = 0.01$. Similar behavior is observed for body-centered cubic iron.[3] Using a least-squares analysis and forcing the curve to go through the origin, the results can best be described by the expression

$$\rho = 4.7 \times 10^{10} \epsilon^{0.6} .$$

The curve of this equation is shown as the solid line in Fig. 8.1.

During deformation, a cell structure develops very early in nickel. This structure is typified by a high density of dislocations in the cell walls; but the interior of the cells is relatively free of dislocations. With the addition of aluminum, development of the cell walls is retarded. This is illustrated in Figs. 8.2, 8.3, and 8.4, which are electron micrographs of Ni, Ni–1 wt % Al, and Ni–5.5 wt % Al after nearly equal strains. The nickel shows a well-developed cell structure; the Ni–1 wt % Al, a cell structure which is somewhat less developed than that of the nickel; and the Ni–5.5 wt % Al, no cell structure (at least at these low strains), but rather an array of isolated, relatively straight dislocations. This effect has been observed in face-centered cubic alloys by others[4] and seems to be due to the lowering of the stacking fault energy with additions of an alloying element.

[3] A. S. Keh, *Direct Observations of Imperfections in Crystals*, p 213, Interscience, New York, 1962.

[4] A. Howie, *Direct Observations of Imperfections in Crystals*, p 283, Interscience, New York, 1962.

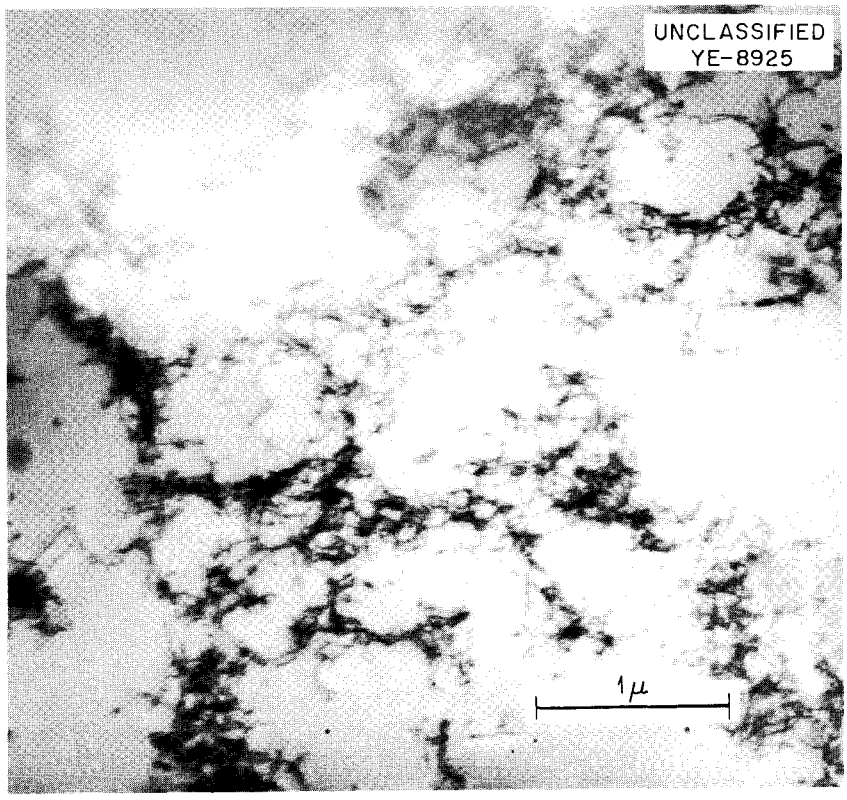

Fig. 8.3. Dislocation Structure of Ni–1 wt % Al Deformed at 23°C to $\epsilon = 0.037$. $\rho = 7.0 \times 10^9$ cm/cm^3.

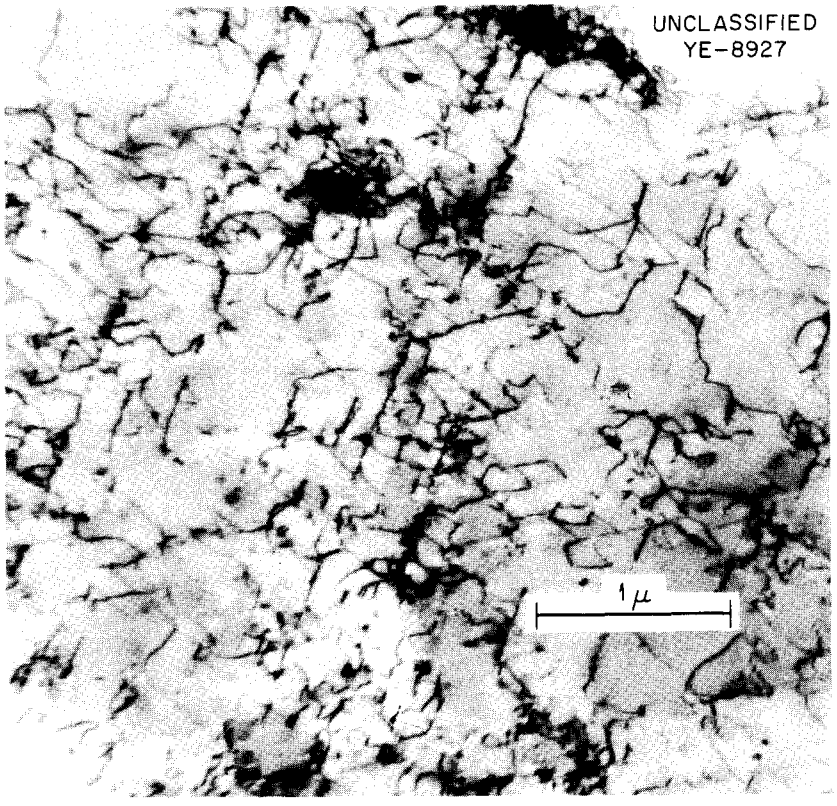

Fig. 8.4. Dislocation Structure of Ni–5.5 wt % Al Deformed at 23°C to $\epsilon = 0.036$. $\rho = 4.9 \times 10^9$ cm/cm^3.

STORED-ENERGY MEASUREMENTS DURING THE DEFORMATION OF METALS AND ALLOYS

R. O. Williams

Major accomplishments during the year have been the construction and operation of a new calorimeter, results on the grain-size effect in copper, additional results on copper-zinc alloys, and some results on copper single crystals.

Although the new calorimeter (Fig. 8.5) is based on the same principle as earlier models,[5] it represents a significant simplification and gives improved operation. Due to the new design and other improvements, it was possible to obtain good data at room temperature with CCl_3F. This had not been possible before. This new design is to be described elsewhere.[6]

The data for the copper-zinc system are summarized in Fig. 8.6. The data for 24°C have not been included but will fall slightly below those for 243°K. Although no detailed interpretation of these data has been made, it is assumed that the large increase in stored energy with increasing zinc content is due to the destruction of short-range order which exists in these alloys. The maxima between 20 and 25% zinc provide some support for this idea.

Figure 8.7 shows the stored energy vs strain of copper samples having three different grain sizes. It is evident that any grain-size effect is small, although no clear trend is established since the values for the intermediate grain size lie above those for the other two sizes.

It would be desirable to have good data on the stored energy in single crystals, since the deformation of single crystals is much simpler and

[5]R. O. Williams and J. A. Wheeler, Jr., *Met. Div. Ann. Progr. Rept. May 31, 1961,* ORNL–3160, p 20.

[6]R. O. Williams "A Liquid-Gas Film Calorimeter for Deformation of Metals," to be published in *Review of Scientific Instruments.*

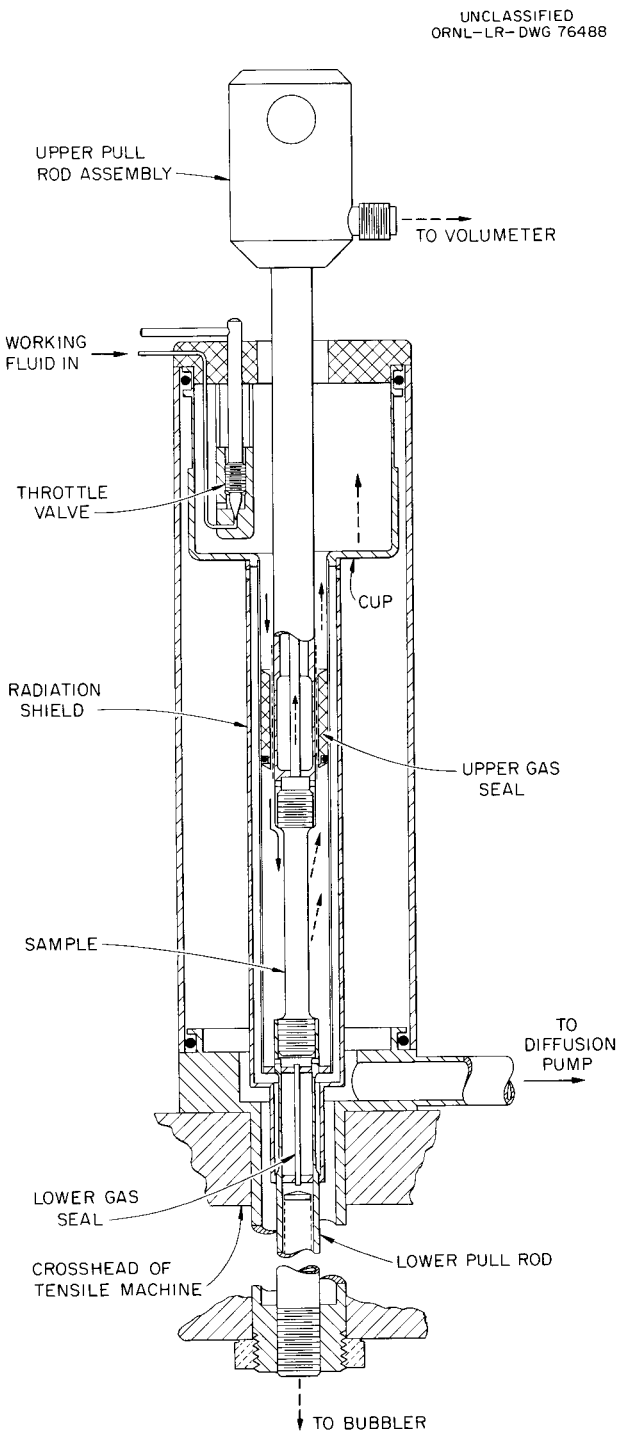

Fig. 8.5. A Liquid-Gas Film Calorimeter for Deformation of Metals.

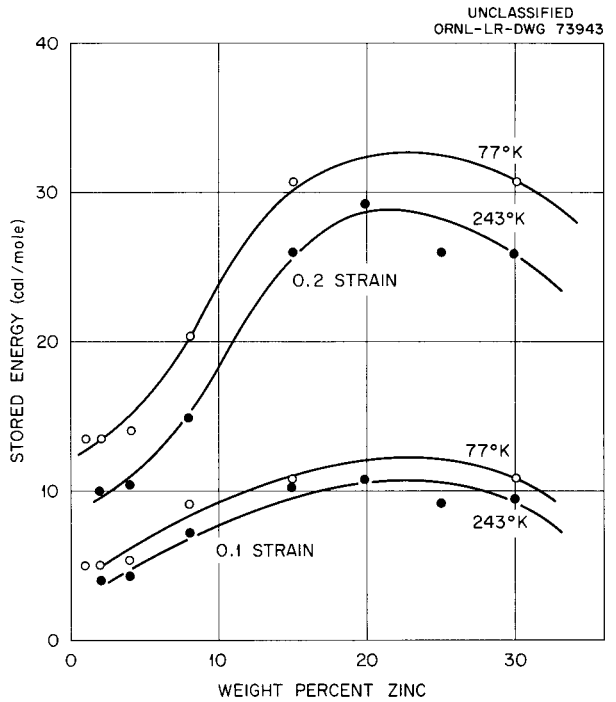

Fig. 8.6. The Stored Energy in Copper-Zinc Alloys as a Function of Strain and Temperature.

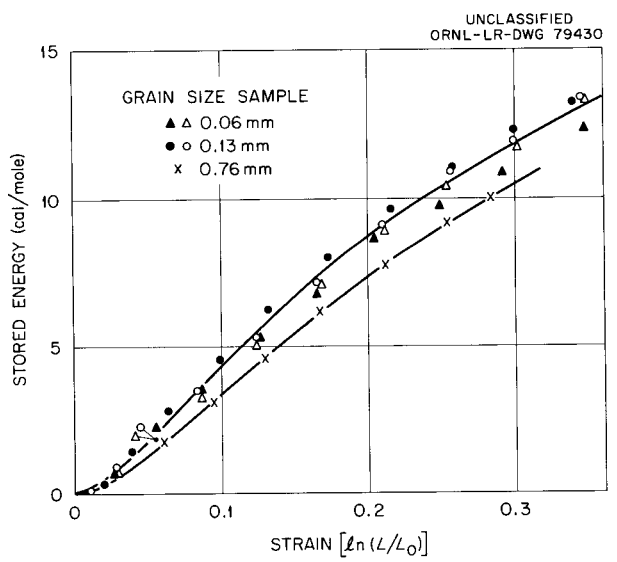

Fig. 8.7. Stored Energy of Deformation in Copper Samples with Different Grain Sizes.

better understood. The technique referred to above lacks sufficient sensitivity to make such measurements at low strains, because so little heat is liberated. In one experiment the temperature rise of the single crystal during deformation has been measured with a thermocouple, a method used much earlier by Farren and Taylor.[7] The present investigation represents refinements of instrumentation and technique; but, although this method has excellent sensitivity (values as low as 0.001 cal/mole can be easily detected), the overall accuracy is not too good. The results from two copper samples having orientations approximately in the middle of the unit triangle are shown in Fig. 8.8. As would be expected, at low strains the initial rates of storage are very low compared with those of polycrystals (Fig. 8.7); but at higher strains they are similar to initial polycrystal storage rates. (Shear strain should be divided by about 2.4 to make it comparable to tensile strain.)

[7]W. S. Farren and G. I. Taylor, *Proc. Roy. Soc. (London)*, A**107**, 422 (1925).

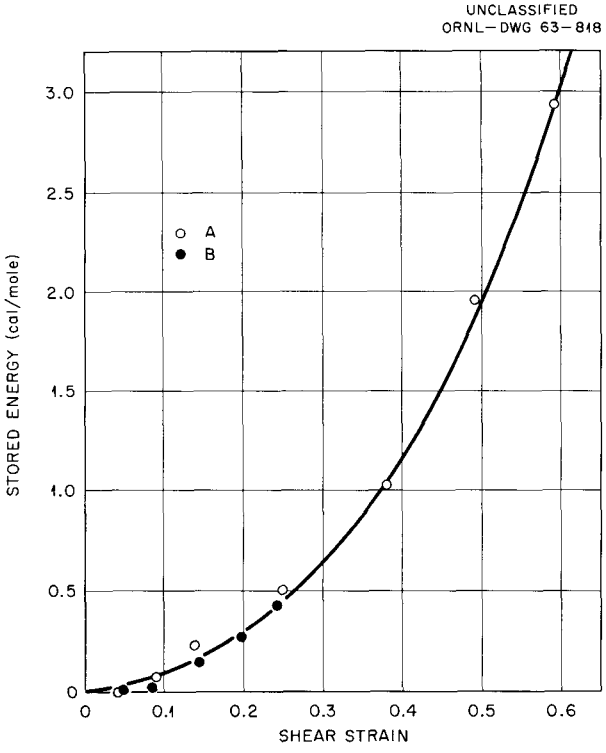

Fig. 8.8. The Stored Energy of Deformation for Two Copper Single Crystals.

YIELD POINTS

R. J. Arsenault

The effect of strain rate on the yield-point drop (upper yield stress minus lower yield stress) in Ferrovac E iron was investigated,[8] and typical results are shown in Fig. 8.9. The slope of the curve in Fig. 8.9 is related to the activation volume of yield-point mechanism. The value obtained from the slope is in good agreement with the activation volumes measured by the differential strain rate technique; and since the activation volumes agree, both yielding and plastic flow occur by the same mechanism. Therefore the yield point is due to the multiplication of dislocations, not to the unlocking of dislocations from their impurity atmospheres (Cottrell theory).

An analysis was made of data obtained on the copper-aluminum[9] system, where the yield point is attributed to short-range order. Again, agreement was found between the activation volumes. Further work is planned for both body-centered and face-centered cubic metals in relation to yield points and activation volumes.

[8]R. J. Arsenault, "Comments on the Yield Point in Iron," submitted to *Acta Metallurgica*.

[9]T. Koppenaal and M. E. Fine, *Trans. AIME* **221**(6), 1178 (1961).

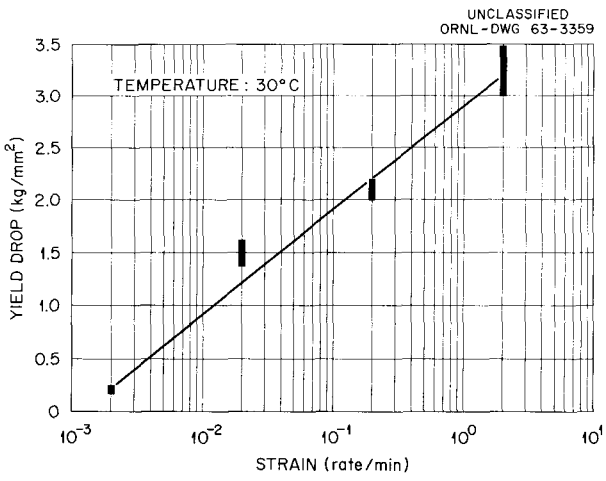

Fig. 8.9. The Yield Drop as a Function of Strain Rate.

LOW-TEMPERATURE CREEP OF IRON

R. J. Arsenault

The low-temperature creep properties of alpha iron were investigated[10] in the temperature range −185° to −20°C and in the stress range 0 to 30 kg/cm^2. The activation energy and activation volume were measured directly and were found to be independent of temperature, strain rate, grain size, and interstitial impurity content, but a function of stress. Figures 8.10 and 8.11 show the stress dependence of the activation energy and volume respectively.

There are difficulties in analyzing the experimental results in terms of all the various proposed rate-controlling mechanisms. Although there is major disagreement between the theoretical treatment for the formation of a double kink overcoming the Peierls-Naborro forces and experimental results (i.e., the theory predicts that the activation volume is not a function of stress, but experimental results indicate that it is a function of stress), this mechanism is preferred. Further theoretical treatment is required before any final decision can be made concerning the rate-controlling mechanism.

[10] R. J. Arsenault and J. Weertman, "Low-Temperature Creep of Alpha Iron," paper presented at the Annual Meeting, AIME, Dallas, Texas, Feb. 24–28, 1963, and will be submitted to the *Transactions of the Metallurgical Society of AIME.* Abstract published: *J. Metals* **5**(1), 88 (1963).

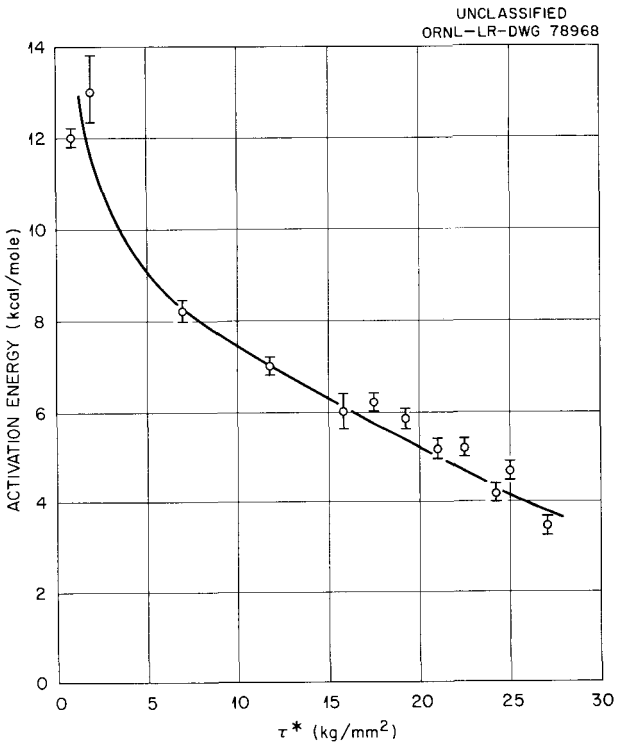

Fig. 8.10. Activation Energy as a Function of Stress.

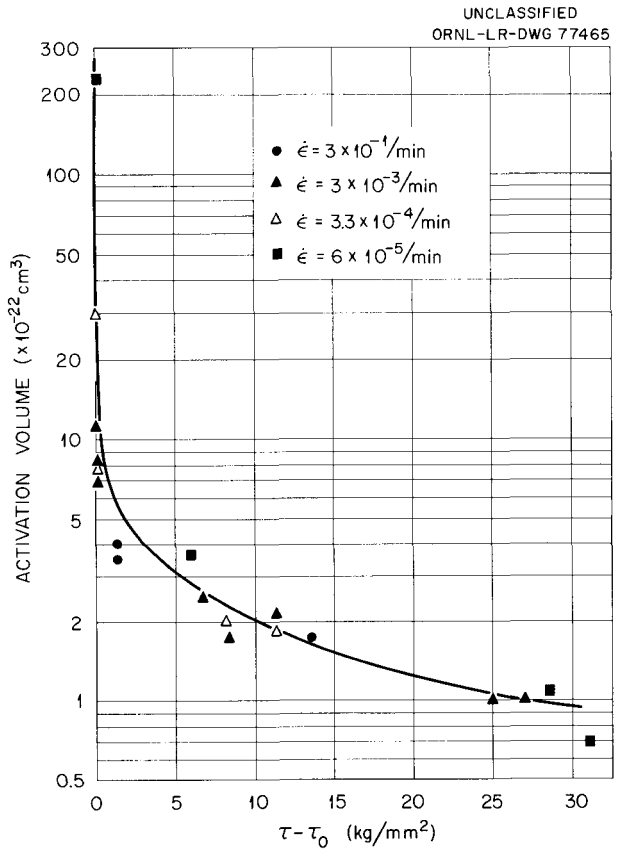

Fig. 8.11. Activation Volume as a Function of Stress.

9. X-Ray Diffraction of Crystalline Defects

THIN Cu_2O FILMS ON COPPER SINGLE CRYSTALS

B. S. Borie

C. J. Sparks J. V. Cathcart

In an attempt to understand the differences in oxidation kinetics of various crystallographic surfaces of copper, several Cu_2O films grown on (311) surfaces of copper single crystals have been investigated by x-ray diffraction methods. These mosaic single-crystal films were prepared and examined using techniques previously described.[1-3]

The average lattice parameters of the Cu_2O films which grow with their (110) parallel to the (311) copper surface are plotted against the thickness as determined by integrated intensity measurements in Fig. 9.1. Since bulk Cu_2O has a lattice spacing of $d_{110} = 3.019$ A, it is seen that the thin oxide films are expanded normal to their surface. In comparison, the oxide films grown on the (110) copper surface are expanded almost twice as much as the films grown on the (311) copper surface. Previous analyses of the oxide films on (110) copper surfaces led to the conclusion that epitaxial forces between the copper substrate and oxide film caused the observed strains.[4] The oxide films were compressed in the plane of the surface, since the copper lattice is smaller than that of the oxide. This results in an expansion of the oxide normal to the surface. A possible explanation for the lesser expansion of the oxide films grown on the (311) surface of copper may be found in the smaller epitaxial mismatch between the film and substrate.

Mosaic spread of the Cu_2O films grown on the (311) face of copper single crystals is much less (by about a factor of 2 to 4) than that of films grown on the (110) surfaces of copper. This fact leads to a greater diffracted intensity since a larger volume of the film is oriented to diffract at a particular 2θ setting. With the additional use of automatic step-scanning x-ray equipment, it is possible to detect and measure the x-ray diffraction maxima from films as thin as four atomic layers approximately equal to 10 A.

Analysis of the data on the Cu_2O films grown on the (311) surfaces of copper is not complete as yet, but, apparently, this face of copper gives rise to an oxide film with less strain than the faster-oxidizing (110) surface of copper.

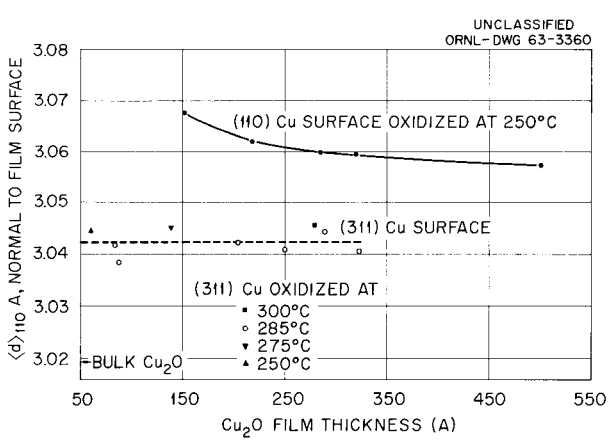

Fig. 9.1. Lattice Parameters of Cu_2O Films Grown on (311) and (110) Copper Surfaces for Different Film Thickness.

[1] J. V. Cathcart, J. E. Epperson, and G. F. Petersen, *Acta Met.* **10**(8), 699 (1962).

[2] B. S. Borie, *Acta Cryst.* **13**, 542 (1960).

[3] B. S. Borie and C. J. Sparks, *Acta Cryst.* **14**, 569 (1961).

[4] B. S. Borie, C. J. Sparks, Jr., and J. V. Cathcart, *Acta Met.* **10**(8), 691 (1962).

10. X-Ray Diffraction Research

ROUTINE ANALYSIS

O. B. Cavin R. M. Steele
L. A. Harris H. L. Yakel

The X-Ray Diffraction Group examined about 550 samples submitted for routine analyses during the past year. In addition to its usual cold-laboratory services, the Group this year activated a shielded diffraction goniometer for the examination of radioactive specimens.[1]

In addition to more common problems involving phase identification, crystal orientation, stress measurements, crystallite-size estimations, and lattice-parameter determinations, diffraction data for several previously unreported compounds have been gathered. Those for which accurate compositions may be fixed by chemical analyses and for which unit cell parameters have been deduced include the following:

K_3ErCl_6 Face-centered cubic; $a_0 = 9.76 \pm 0.01$ A; $(NH_4)_3FeF_6$ type. Powder data;[2] but single crystals are easily grown. One weak reflection would be indexed as 732,651.

$ReBr_3$ Monoclinic; $a_0 = 15.75 \pm 0.02$ A; $b_0 = 10.59 \pm 0.01$ A; $c_0 = 9.50 \pm 0.01$ A; $\beta = 117.4 \pm 0.1°$; U = 1407 ± 6 A^3; cell is A face-centered. Single-crystal data.[2] Refractive indices normal to **b** are about 2.16.

K_2ReF_6 Hexagonal; $a_0 = 5.86 \pm 0.01$ A, $c_0 = 4.60 \pm 0.01$ A. Possible β_2-K_2ThF_6 structure. Powder data.[2]

ReF_3 Tetragonal; $a_0 = 8.59 \pm 0.02$ A, $c_0 = 7.37 \pm 0.01$ A. Powder data.[2]

Diffraction studies of mineral structures in which iron replaces aluminum have continued, with an examination of mica $RbFe_3{}^{2+}(Si_3, Fe^{3+})O_{10}(OH)_2$. Single-crystal data indicate a monoclinic unit cell with $a_0 = 5.37 \pm 0.06$ A, $b_0 = 9.36 \pm 0.06$ A, $c_0 = 10.57 \pm 0.06$ A, $\beta = 100.5 \pm 0.3°$. With the assumption that the structure is based on that of a common biotite mica (type 1M,[3] space group $C2/m$), an attempt will be made to fix the iron atom positions.

The determination of the crystal structure of $Ca_2Be_3O_5$ progressed through the statistical analysis of the diffraction data, the calculation of the $P(u, v)$ Patterson projection and the $P(u, v, 0)$ Patterson section, and the assignment of tentative calcium ion positions. In the course of this analysis a computer program (FORTRAN) for the statistical analysis of diffraction data was assembled and is currently being tested. Some observations on multiple scattering effects in equi-inclination Weissenberg diffraction geometry were also published.[4]

X-RAY DIFFRACTION EFFECTS FROM IRRADIATED CRYSTALS OF BERYLLIUM OXIDE[5]

H. L. Yakel B. S. Borie

Single crystals of beryllium oxide, grown from a Cs_2MoO_4 melt,[6] have been irradiated to 3.6×10^{21} *nvt* (fast) at 50°C in the Engineering Test Reactor. Physical properties of the irradiated crystals have been measured, and x-ray diffraction patterns have

[1] H. L. Yakel, *Metals and Ceramics Div. Ann. Progr. Rept. May 31, 1962*, ORNL-3313, p 130.

[2] CuKα radiation, $\lambda = 1.5418$ A.

[3] S. B Hendricks and M. E. Jefferson, *Am. Mineralogist* **24**(12), 729 (1963).

[4] H. L. Yakel and I. Fankuchen, *Acta Cryst.* **15**, 1188 (1962).

[5] Abstract of paper to be submitted for presentation at the International Conference on Beryllium Oxide, AAEC Research Establishment, Lucas Heights, NSW, Australia, October 21–25, 1963.

[6] Crystals were grown by C. B. Finch of the Metals and Ceramics Division, Oak Ridge National Laboratory.

been obtained. The physical appearance of an irradiated crystal is contrasted with similar unirradiated crystals in Fig. 10.1.

The diffraction data tend to confirm previous results from polycrystalline compacts of BeO irradiated to high doses at low temperatures. An interpretation of these earlier data in terms of random interstitial agglomerates[7] would seem to be in general agreement with the single-crystal observations.

[7]H. L. Yakel and B. S. Borie, "Structural Changes in Irradiated BeO," to be published in *Acta Crystallographica.*

The sensitivity of single-crystal techniques has shown several diffraction phenomena previously unobserved in the powder data (Fig. 10.2). These include (1) the presence of continuous streaks of diffracted intensity parallel to **c*** along rows with $h - k \neq 3n$; (2) clear resolution of a minimum in the intensity distributions between sharp and diffuse components of reflections $hk \cdot l$ with l odd; and (3) quantitative differences in the breadths of reflections $hk \cdot l$ with l even (but not zero), depending on h and k values.

Spacing measurements on the single-crystal patterns indicate an a_0 parameter of 2.702 ± 0.002 A, in good agreement with the a_0 parameter measured

UNCLASSIFIED
Y-47372

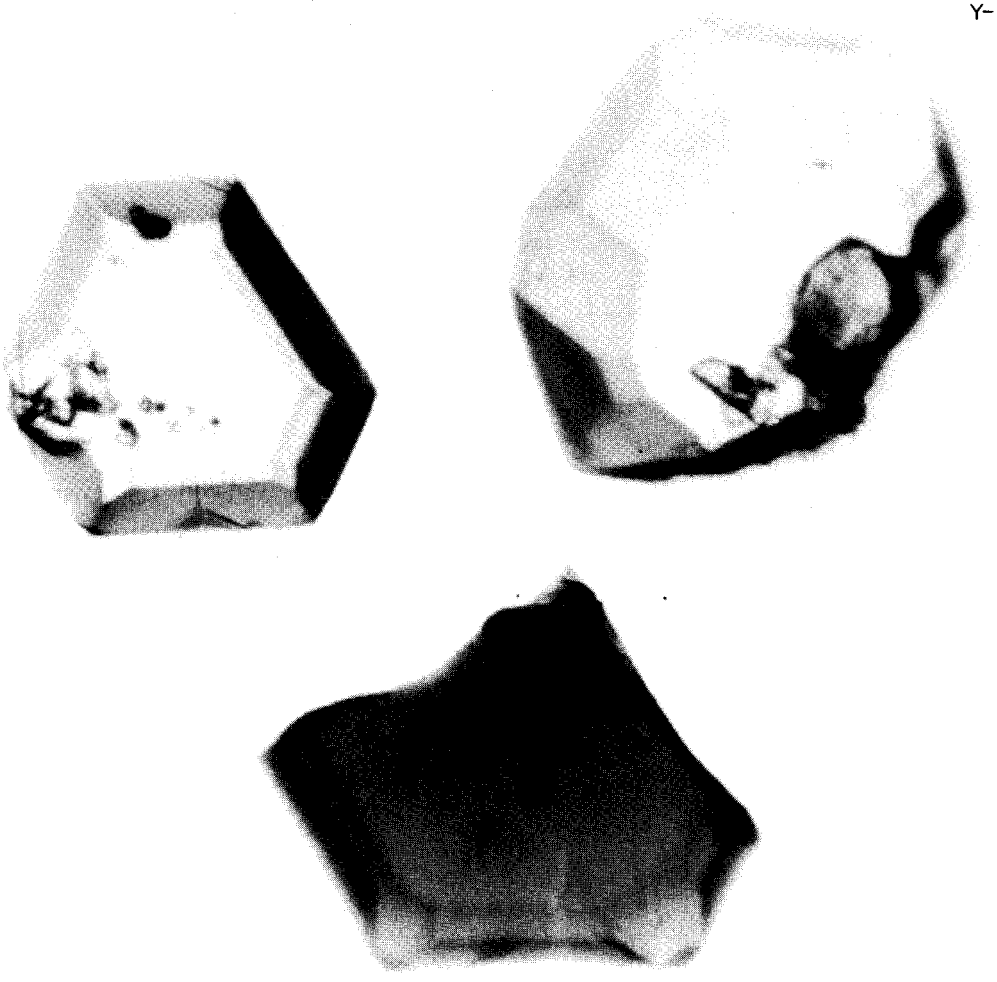

Fig. 10.1. Two Unirradiated Crystals of BeO (Upper) and a Similar Crystal Irradiated to 3.6×10^{21} *nvt* (Fast) at 50°C. All crystals grown from a Cs_2MoO_4 melt. Maximum crystal width = 0.7 mm.

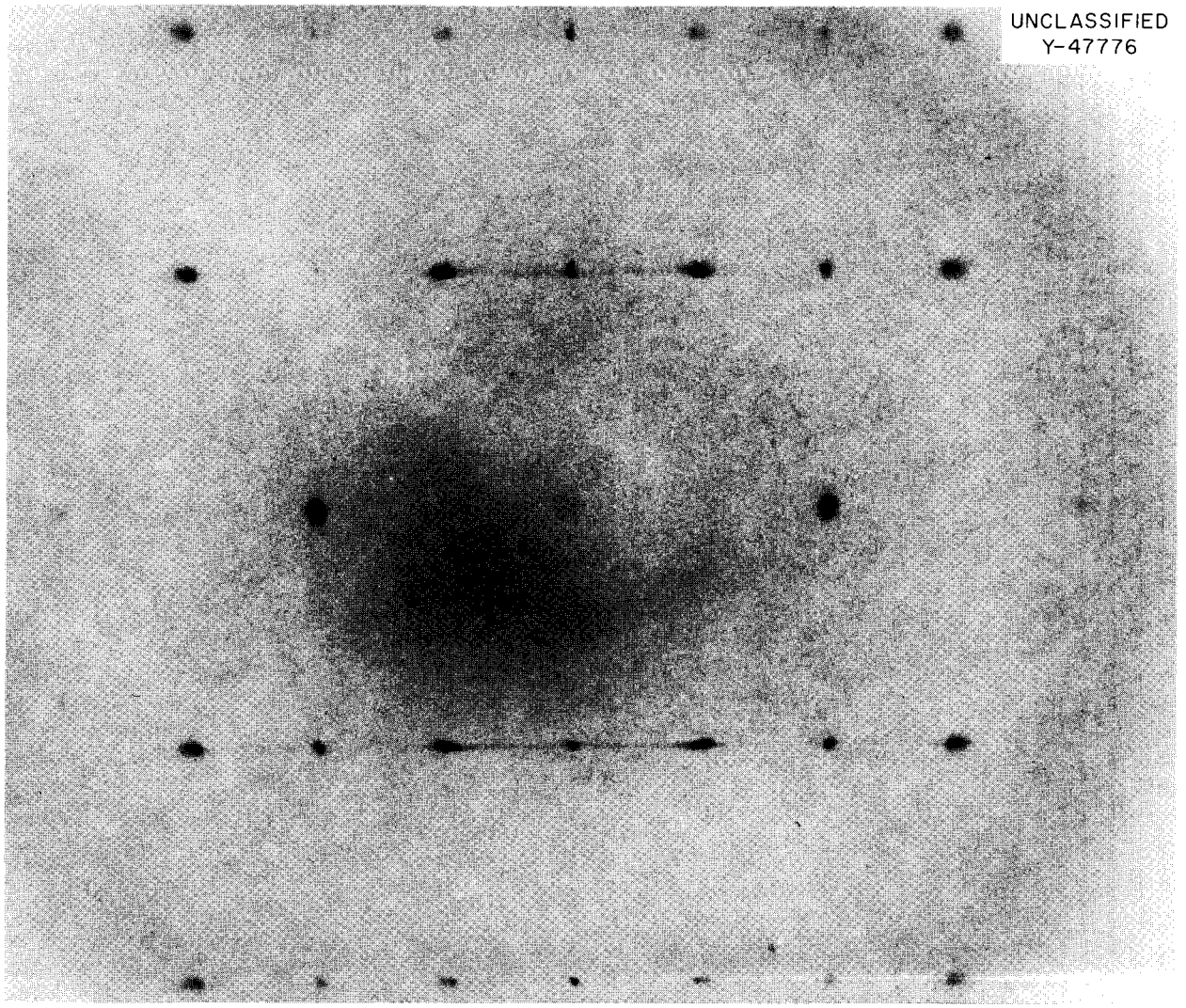

Fig. 10.2. The $h0 \cdot l$ Section of Reciprocal Space for a Beryllium Oxide Crystal Irradiated to 3.6×10^{21} nvt (Fast) at 50°C. c* is vertical. Precession photograph taken with monochromatic MoKα radiation (λ = 0.7107 A), $\mu = 25°$, r_s = 15 mm.

from polycrystalline BeO given equivalent irradiation treatment. Spacings dependent on $|\mathbf{c}^*|$ exhibit the irregular behavior noted in the powder data, which was interpreted as displacements of intensity maxima or centroids from reciprocal lattice points. If the displacement hypothesis is correct, the c_0 parameter of an irradiated crystal cannot be computed without a consideration of the lattice disturbances producing the diffraction effects. If the model of the irradiated BeO lattice proposed on the basis of the powder data is applied to the single-crystal data, the c_0 parameter would be 4.42 ± 0.01 A.

The density of the irradiated BeO crystals was measured by a flotation method to be 2.880 ± 0.001 g/cm^3. This represents a decrease of 4.3% from the density of unirradiated crystals. With the agglomerate expansion and probability parameters deduced from the powder data and with lattice parameters in the irradiated and unirradiated conditions

taken as a_0 = 2.702 A, c_0= 4.42 A, and a_0 = 2.6979 A, c_0 = 4.3772 A,[8] respectively, the predicted density decrease is 5.3%.

Current attempts to refine the model of the damaged BeO lattice are directed at the explanation of the new diffraction phenomena observed from irradiated single crystals. Lattice disturbances near agglomerate edges and existence of ordered structures within agglomerates are considered possible sources of these effects.

HIGH-TEMPERATURE X-RAY DIFFRACTION EXPERIMENT WITH POLYCRYSTALLINE Nb_3Sn

H. L. Yakel

In order to contribute to the solutions of questions concerning the thermal stability and/or possible disordering of the intermetallic compound Nb_3Sn, a high-temperature x-ray diffraction study of a polycrystalline single-phase Nb_3Sn (nominal) specimen was initiated. This material was obtained from G. W. Clark, Crystal Physics Group, Metals and Ceramics Division, Oak Ridge National Laboratory (Chap. 1 of this report). A Unicam S.150 high-temperature diffraction camera was used in the experiment, which covered the temperature range 20 to 975°C; Cu $K\alpha$ (λ = 1.5418 A) radiation was employed. The specimen was contained in a thin-walled quartz capillary and was maintained at each temperature of interest for a minimum of 75 hr.

A summary of the lattice parameter vs temperature data is given in Fig. 10.3. The difference between the parameters at 20°C before and after the experiment may be ascribed to evaporative loss of tin, solution of excess niobium, reaction with the capillary walls, or any combination of these. Despite the uncertainty introduced by this effect, the following conclusions may be drawn.

There is no significant indication of thermal instability in the material studied up to 1000°C. Intensities of pairs of reflections critically dependent on the lattice-site occupation were followed in an effort to find a possible order-disorder transition. No such transition could be detected.

The lattice parameters of the compound between 500 and 975°C may be used in the expression

$$a_0(T) = a_0(T_0)[1 + \alpha(T - T_0) + \beta(T - T_0)^2]$$

to obtain the thermal expansion coefficients

$$\alpha = (7.40 \pm 0.01) \times 10^{-6}/\text{deg} ,$$

$$\beta = (1.76 \pm 0.02) \times 10^{-9}/\text{deg}^2 .$$

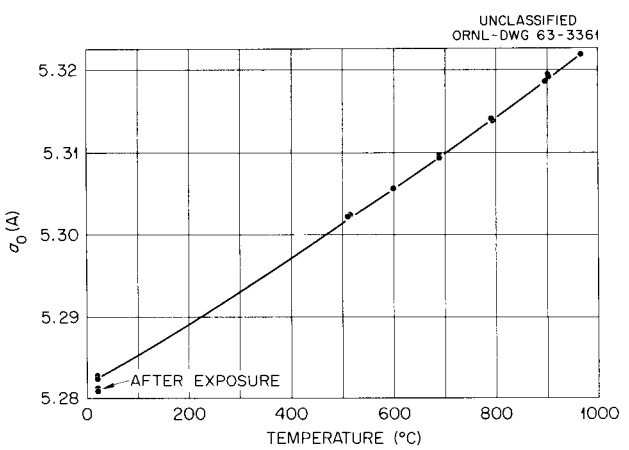

Fig. 10.3. Lattice Parameters of Nb_3Sn as a Function of Temperature Between 20 and 975°C. A smooth curve has been arbitrarily drawn through the data points.

[8] B. Bellamy, T. W. Baker, and D. T. Livey, *J. Nucl. Materials* **6**(1), 1 (1962).

11. Metallurgy of Superconducting Materials

The recent discovery of several materials that remain superconductive at magnetic-field strengths of 80,000 to 100,000+ gauss has created an interest in the use of these materials to make large-volume, high-field-strength solenoid magnets for use in power generation and transmission, plasma containment in fusion reactors, bubble chambers and particle accelerators, particle shielding for space vessels, and large experimental laboratory equipment. Engineering applications of the superconducting properties range from construction of frictionless bearings to motors, electronic computer elements, and precessionless gyroscopes. Among the kinds of information required are: (1) theory of design of superconducting magnets; (2) the physics of high-field superconductors; (3) the true nature of the superconducting filamentary structure and its relation to the morphology of the material; (4) how to make electrical joints between pieces of superconducting material that will have the properties of the parent material in high fields; and (5) the effects of metallurgical variables on the normal and superconducting properties of superconductive materials (the principal subject of the program of this group).

MEASUREMENT OF COMPOSITIONAL SEGREGATION IN NIOBIUM-ZIRCONIUM ALLOYS BY ANODIZATION

M. L. Picklesimer

A metallographic technique was developed to quantitatively determine the composition of regions ranging from 0.5 μ or less to centimeters in diameter in Nb-Zr alloys having compositions ranging from 20 to 50% Zr. It is an extension of the anodizing technique previously developed for phase identification in zirconium-base alloys. A metallographically prepared specimen and a set of standard specimens of known and proven compositions and homogeneity are anodized at 78 v. The colors produced at 78 v vary from yellow to red to blue as the composition varies from 50 to 20% Zr. The sensitivity is such that variations of as little as 1% Zr can be readily detected and measured. The technique was quantitatively proven by microbeam x-ray fluorescence and microdrilling for solution spectroscopy analyses of the standard and test specimens. This new technique was used to show that the macro- and microsegregation present in as-cast Nb-Zr alloys can be as much as 8% Zr. For example, the composition in nominally Nb–25% Zr specimens varied from (24 ± ½)% Zr to (32 ± ½)% Zr over regions varying from microns to centimeters in length.

Preliminary tests indicate that the technique can be successfully used on Ti-, Zr-, Nb-, and Ta-base alloys.

STUDIES ON TRANSFORMATION KINETICS IN NIOBIUM-ZIRCONIUM ALLOYS

G. R. Love M. L. Picklesimer

Transformation kinetics of Nb-Zr alloys containing 25 to 40% Zr were studied for variable time, temperature, composition, and prior treatment. Arc-cast alloys, with significant microscopic segregation, were swaged to 0.100 in. in diameter (approximately 75% reduction in area) and sectioned into ¼-in. lengths. Half of the sections were recrystallized at 1050°C for ½ hr. Tentative time-temperature-transformation diagrams were made for alloys containing 30, 35, and 40% Zr in both the cold-worked and recrystallized conditions. The time-temperature-transformation diagrams for cold-worked Nb–40% Zr and for the same Nb–40% Zr alloy after a 1050°C anneal (above the two-phase field) are presented in Figs. 11.1 and 11.2 respectively. Typical "C" type curves were obtained, with the maximum rate of transformation occurring at about 700°C. The kinetics of the transformation to the equilibrium phases present below 610°C

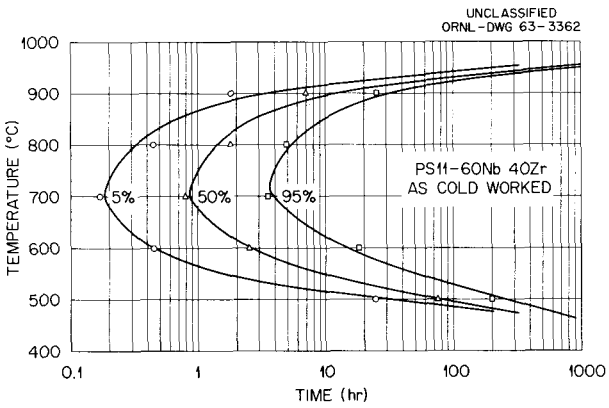

Fig. 11.1. Time-Temperature-Transformation Diagram for Cold-Worked Nb–40% Zr Alloy.

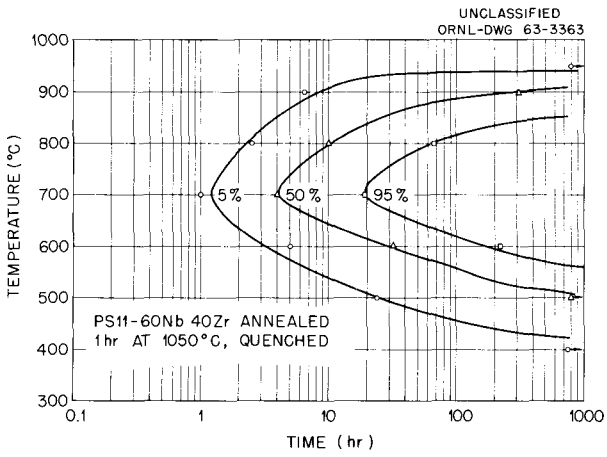

Fig. 11.2. Time-Temperature-Transformation Diagram for Annealed Nb–40% Zr Alloy.

are quite slow; no decomposition was observed in any specimen of this series in one week. Cold work significantly decreased the incubation time and increased the reaction rate at all temperatures.

Guided by these tentative time-temperature-transformation diagrams, a more complete and quantitative study of transformation kinetics using homogeneous alloys was begun. Preliminary data indicate that the principal effect of the inhomogeneities present in the earlier specimens of these alloys was to prolong the time between initiation and completion of the transformation.

The kinetics of the transformation $\beta \rightarrow \beta_1 + \beta_2$ do not seem to vary significantly with the average composition of the inhomogeneous samples used in the early study except as to completion times (95% complete: 3.5 hr in a 40% Zr alloy, 15 hr in a 30% Zr alloy).

The transformation data will be used to prepare specimens having known interlamellar spacings and lamellar compositions to allow examination of the effect of these variables on the superconducting properties of the aggregate.

IMPROVED CASTING TECHNIQUES FOR PREPARING MACROHOMOGENEOUS INGOTS OF NIOBIUM-ZIRCONIUM ALLOYS

G. R. Love

A major problem associated with the metallurgical study of superconducting alloys is that of chemical inhomogeneity of the alloys. Conventional cold-hearth arc casting produces ingots having compositional variations greater than 5% from top to bottom of the ingot and as much as 8% from grain boundary to grain center for any grain in the ingot. Heat treatment of the cast material does not, in general, remove these inhomogeneities. Cold-hearth electron-beam zone leveling was attempted to improve the cast homogeneity but was not successful.

A casting technique was developed (in cooperation with the Melting and Casting Group) which is remarkably successful in reducing the as-cast segregation in these alloys. An arc-cast button of the desired average composition is prepared by standard techniques. The button is then transferred to a suspended copper hearth which has a recess for the button and a small hole through the bottom of the recess. A second copper mold is placed below the suspended hearth; this mold is remote from the arc and remains cold relative to the melt. A casting is made by arc-melting the alloy button in the upper hearth (leaving a solid "skull" over the hole in the upper hearth), holding it molten for a few seconds to homogenize the liquid, and then quickly raising the power of the arc to melt through the skull, thus allowing the molten metal to drop directly into the cold mold, where it is very quickly solidified. The as-cast grain size of such an ingot is quite small; macrosegregation along the ingot is eliminated; and microsegregation of the coring type is greatly reduced.

Homogenization experiments conducted in evacuated, argon-filled quartz capsules using the "skull-cast," or "drop-cast," ingots showed that for alloys containing more than 40% Zr, microsegregation could be eliminated by annealing at 1400 ± 10°C for 4 hr. A detectable variation in composition remained after 24 hr at 1400°C for those alloys which contained 35% Zr or less. Specimens of an Nb–33% Zr ingot were annealed at 1400 ± 10°C for 24, 48, 72, and 168 hr. Reasonable homogeneity was observed at 168 hr, but an impurity phase was found in the grain boundaries, increasing in amount with increasing time. Since the impurity phase embrittles and contaminates the alloy, the maximum permissible annealing time at 1400°C in quartz capsules is one day.

Further studies on homogenization of such ingots will be carried out in a high-vacuum cold-wall furnace which is expected to achieve vacuums of 10^{-8} torr or better at ingot temperatures above 2000°C.

DEVELOPMENT OF METHODS FOR NONDESTRUCTIVE EXAMINATION OF SUPERCONDUCTING WIRES

E. E. Barton G. R. Love

A significant degradation of current-carrying ability is observed as the length of a superconducting test sample is increased, particularly when it is wound into a solenoid. Short-wire tests of as-received Nb-Zr wire in transverse magnetic fields show current densities greater than 10,000 amp/cm^2 in fields in excess of 50,000 gauss. A multiturn coil of the same wire in the same field will carry only about one-half that current density. One possible explanation of this degradation is that a long length of test wire contains an assortment of defects randomly located along the wire. Therefore the longer the length tested, the greater the probability that it contained defects which limited current density. Such defects can be (1) a decrease in cross section; (2) nicks, folds, laps, longitudinal grooves, and cracks; (3) tensile fractures in the core; and (4) compositional variations across the diameter and/or along the length. Since commercial production of homogeneous ingots of the Nb-Zr alloys of interest and fabrication of these ingots into wire are extremely difficult, it is plausible to expect such defects.

In the present study, it is very important to know the quality of test wires. Many test specimens must be cut from one length of wire, and they must be comparable in composition, cold work, diameter, and cross section.

A device was constructed to measure continuously the resistance of a ¼-in. increment of wire for wire lengths up to 5000 ft. The wire was passed at carefully controlled speeds through four sliding contacts which were weighted to give an approximately constant contact load and which were electrically connected to a Keithley model 503 milliohmmeter in the familiar four-lead method of measuring resistance. The resistance was recorded on a strip-chart recorder which had a chart speed known relative to the wire speed. The combined error in the measuring and recording system was no greater than 2% of the instantaneous value of wire resistance (nominally 0.3 ohm).

Test wires of commercially produced tantalum and Nichrome V were examined with the equipment. In no case was the variation in resistance observed to be as much as 2%, and the reproducibility for any given length was at least ±1%. One lot of commercially produced Nb-Zr superconducting wire was examined and found to have no variation in 50 ft greater than instrumental error. A second lot, from another manufacturer, exhibited variations as great as 10% in resistance, with a reproducibility of at least 1%. Since part of the resistance variation could have been due to a surface film (oxide scale, die lubricant, etc.), the test wire was pickled to remove 0.00025 in. from the diameter (5% reduction in area); and resistance was again measured over the same length. The second determination showed the same variations at each point along the wire, although offset from the original value by about 5% (due to the decreased cross section). This illustrates that the observed variations were due to varying properties in the wire.

Using the survey equipment, a number of short-length samples which have significantly higher or lower resistance were selected for testing for superconducting properties and for later destructive examination to determine the cause of the resistance variation.

EQUIPMENT DEVELOPMENT

E. E. Barton

Resistivity Apparatus

Resistivity measurements during programmed heating and cooling cycles and/or during isothermal treatment usually permit rapid determination of approximate time-temperature-transformation diagrams. Such data are used to select isothermal heat treatments of metallographic specimens for quantitative metallography. The present resistivity apparatus has been designed around a Keithley model 503 milliohmmeter, a commercial instrument which has the desired range and sensitivity for resistance measurement. The specimen is heated in a high-vacuum atmosphere (approximately 10^{-8} torr) in a low-thermal-mass resistance furnace constructed of tantalum sheet coated with sprayed high-purity alumina and wound with tantalum wire. A programmed power control for the furnace permits heating and cooling rates from approximately 1 to 16°C/min and isothermal transformation of the specimen at any desired temperature from 100 to about 1400°C. A voltage divider network permits conversion of the Keithley output so that an X-Y recorder plots resistivity vs temperature or time (the data desired) to an accuracy of 1% without continuous manual monitoring.

Nucleation Site and Velocity of Movement of the Superconducting-Normal Interface in Short-Wire Specimens

Determination of the critical-current magnetic-field curve for a short-wire specimen of a superconducting material provides data for evaluating the effects of metallurgical variables on the superconducting properties. However, the test has a serious shortcoming – it is not known where the superconducting-normal transition interface is nucleated in the specimen. Thus doubt is created as to whether the superconducting properties of the specimen are being determined or whether the evaluation is of joints to normal-state material, defects or inhomogeneities in various sections of the wire, or the point of highest external field.

A technique using a resistive network on the sample and a dual-beam oscilloscope is being developed to detect the location and direction of movement of the initial site of the superconducting-normal transition interface. A block diagram of the circuitry is shown in Fig. 11.3. During a test, the oscilloscope is triggered by the first pulse to arrive; the image is photographed; and the sequence and direction of pips on the oscilloscope are analyzed to determine the location and direction of movement of the superconducting-normal interface. Preliminary tests proved the feasibility of this method.

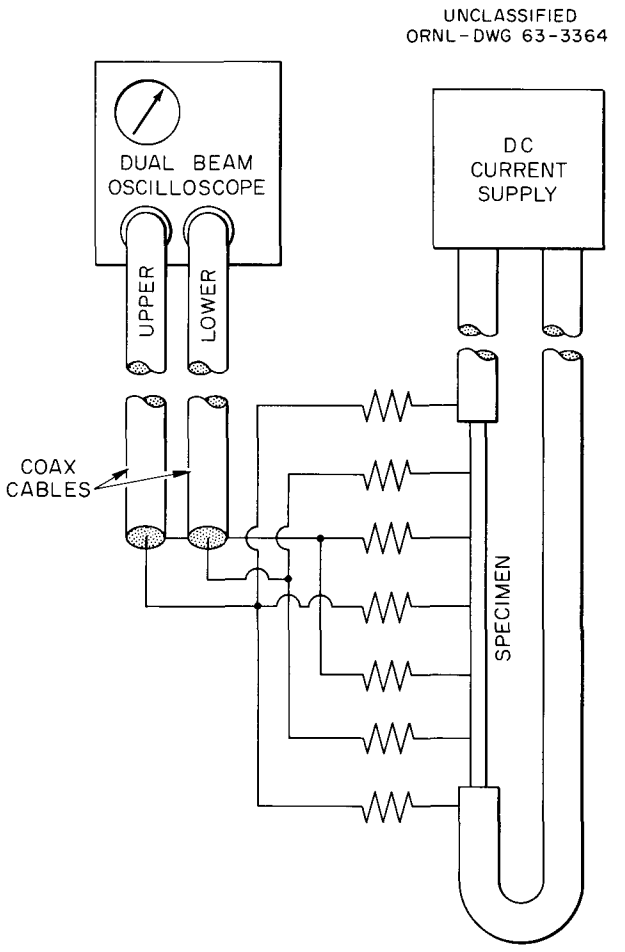

Fig. 11.3. Block Diagram of Equipment Circuitry. Resistive network for determining nucleation site of superconducting-normal interface.

12. Electron Microscope Studies

DIRECT OBSERVATION OF LATTICE DEFECTS BY ELECTRON MICROSCOPY

J. O. Stiegler

The transmission electron microscope technique is currently being used to investigate problems in plastic deformation, annealing, and aging of various pure metals and alloys. Particular emphasis is being placed on deformation twinning studies of body-centered cubic metals. Preliminary observations indicate that completely different substructures characterize materials that twin during deformation from those that do not. This is illustrated in Figs. 12.1 and 12.2, which are transmission electron micrographs of pure niobium and an Nb–40 wt % V alloy after room temperature deformation by cold rolling. Under these conditions niobium failed to twin, but the alloy twinned readily. An Nb–20 wt % V alloy deformed at room temperature failed to twin and had a dislocation substructure similar to that shown in Fig. 12.1. The same alloy deformed at liquid nitrogen temperature twinned readily and showed a dislocation substructure similar to that of Fig. 12.2. Thus, lowering the temperature of deformation appears to affect dislocation behavior in the same way as increasing the alloy

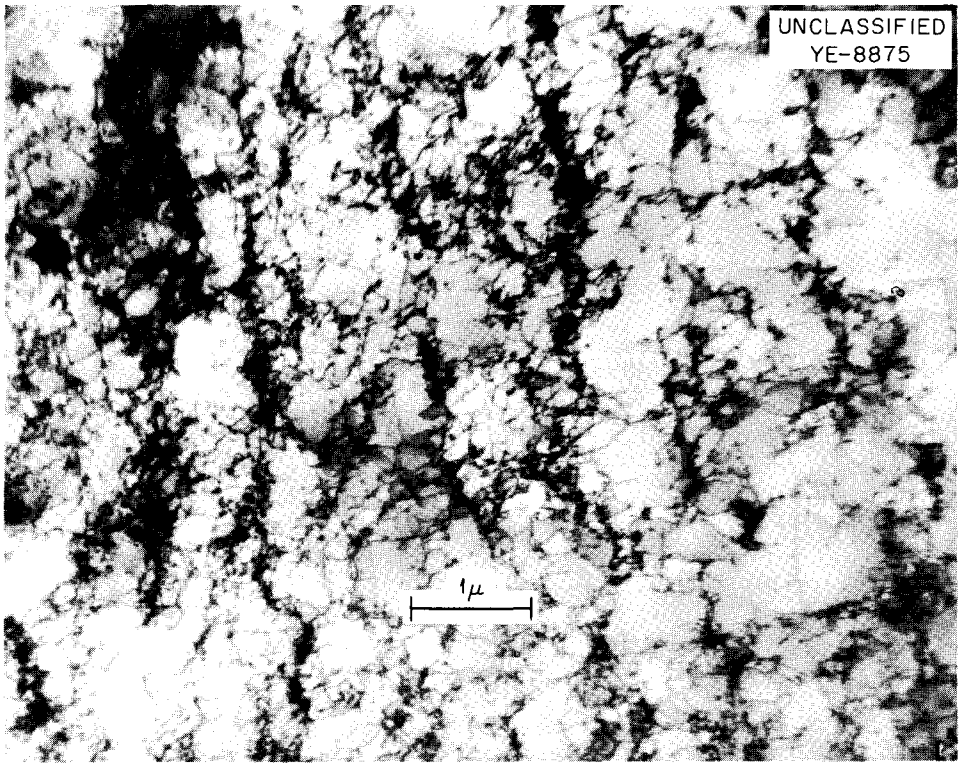

Fig. 12.1. Transmission Electron Micrograph of Dislocations in Niobium Deformed at Room Temperature. 16,000X.

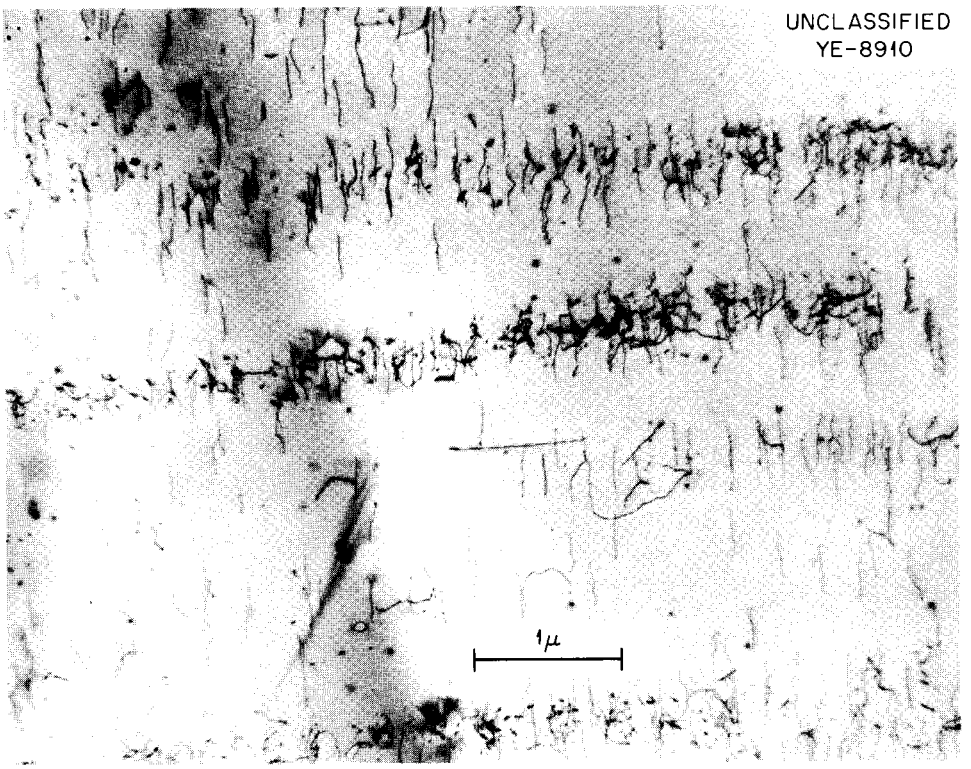

Fig. 12.2. Transmission Electron Micrograph of Dislocations in Nb–40 wt % V Alloy Deformed at Room Temperature. 20,000X.

content. The differences in dislocation substructure suggest that the lattice frictional stress on dislocations is increased and that the ability of dislocations to cross slip is decreased. This, in turn, is thought to lead to centers of stress concentration in the material which nucleate the twinning process.

There is no evidence that the stacking-fault energy is lowered by either the alloying or the lowered temperature of deformation. In fact, the joggy nature of dislocations and abundance of loops after these treatments suggest that the stacking-fault energy remains very high.

Interstitials are observed to precipitate on the grown-in dislocation network after recrystallization anneals. It is believed that these precipitates cause tangling of the slip dislocations which breaks up potential centers of stress concentration and thus inhibits twinning.

These studies are being extended to group VI-A metals and their alloys. An effort is being made to compare structures in tungsten-rhenium alloys that twin during deformation with the substructures in the niobium-vanadium alloys. The electronic effects postulated to account for the enhanced twinning behavior of the tungsten-rhenium alloys cannot be responsible for the similar behavior in the niobium-vanadium system. If behavior in the two systems can be shown to be caused by identical factors, it should be possible to produce ductile tungsten alloys with elements more common than rhenium.

TRANSMISSION ELECTRON MICROSCOPE STUDY OF DISLOCATIONS AND DEFORMATION TWINS IN COLUMBIUM AND COLUMBIUM-VANADIUM ALLOYS[1]

J. O. Stiegler C. J. McHargue

The addition of vanadium to columbium results in a remarkable modification of mechanical be-

[1]Paper presented at the Annual Meeting of the AIME, Dallas, Texas, Feb. 24–28, 1963 [abstract published: *J. Metals* 15(1), 91 (1963)].

havior and microstructure as observed by transmission electron microscopy. In pure columbium the dislocations produced by deformation were found to tangle together and form the well-known cell structure early in the deformation process; under the action of the electron beam, they moved readily along irregular paths, indicative of frequent cross slip. In the Cb–40% V alloy the deformation dislocations were confined to bands in which they ultimately acquired irregular shapes. Many loops lay in the bands, but no distinct cells were formed by deformations as high as 20%. Dislocations moved reluctantly under the action of the electron beam and always along straight lines, suggesting that cross slip occurs infrequently. Regular dislocation networks were formed in annealed Cb–40% V foils; however, no alternate extended and contracted nodes were observed. This indicates that the stacking-fault energy of this alloy is moderately high.

Deformation twins formed in the Cb–40% V alloy always had blunt ends. Notches in the twins contained intense dislocation tangles. In some cases the twins were observed to run between the bands of slip dislocations, apparently nucleated by stress concentrations produced by the bands. Microtwins produced by deformation of the thinned foils were also observed; they exhibited contrast effects typical of pileups of partial dislocations.

EFFECT OF IMPURITIES ON MECHANICAL TWINNING AND DISLOCATION BEHAVIOR IN BODY-CENTERED CUBIC METALS[2]

J. O. Stiegler C. J. McHargue

Mechanical twins were observed after low-temperature deformation of pure body-centered cubic metals and after room-temperature deformation of certain solid-solution alloys. In both cases the presence of interstitials inhibited the twinning process or transferred it to lower temperatures. In this paper, dislocation substructures, as observed by transmission electron microscopy, are reported for materials that twin during deformation and contrasted with substructures in materials that fail to twin. Differences are interpreted in terms of an increased lattice frictional stress and a reduced ability of dislocations to cross slip in high alloys or during low-temperature deformation. Mechanisms by which these effects alter the twinning behavior are discussed. There is evidence that the stacking-fault energy is not lowered by alloying. It is further argued that stress concentrations resulting from the altered dislocation configuration are responsible for the enhanced twinning in the alloys. In addition, a raised cleavage strength and increased ability to hold interstitials in solution may act to prevent brittle fracture. The inhibiting effect which interstitials exert on twinning is explained in terms of interstitial precipitates providing sites where dislocation tangles may form and thus break up potential centers of stress concentration.

Transmission electron microscope observations of a Cb–40% V alloy are described which show that the twins generally run entirely across the grains in lightly deformed materials. Twins may be nucleated in a grain by other twins in adjacent grains intersecting their common boundary or by stress concentrations produced by the dislocation substructure. Dislocations, which are probably generated by the grain boundaries, multiply by a cross-slip mechanism.

These observations suggest that solid-solution alloys of the refractory metals can be developed which have superior strength and, because of their ability to twin, may be fabricated readily at room temperature.

[2]Abstract of paper presented at AIME Conference on Deformation Twinning held at the University of Florida, Gainesville, Florida, March 21, 22, 1963. Paper will be published in the proceedings of the Conference; also, ORNL TM-542 (May 28, 1963).

DISLOCATIONS IN DEFORMED AND ANNEALED NIOBIUM SINGLE CRYSTALS[3]

J. O. Stiegler C. K. H. DuBose
R. E. Reed, Sr. C. J. McHargue

Dislocation configurations in deformed and annealed niobium single crystals were observed by transmission electron microscopy. Grown-in dislocations were observed to act as sinks for

[3]Abstract of paper to be published in *Acta Metallurgica.*

interstitials; this action retarded climb during annealing and possibly made the dislocations immobile during deformation. Three-dimensional walls of dislocation tangles formed early in the deformation process and surrounded cells relatively free of dislocations. During the initial annealing stages, dislocations in the cell walls rearranged themselves to form well-defined small-angle boundaries between adjacent cells. After 1 hr at 700°C, a few recrystallized grains, rotated 20 to 30° about [111] from the surrounding cell structure, were observed. These grains may have nucleated and grown due to the coincidence of lattice sites between them and the unrecrystallized material. The growth rate decreased appreciably as the grains grew into material which did not bear this special orientation relationship with the recrystallized grain. Regions in which these grains were not nucleated recrystallized without a change in orientation by the gradual sweeping out of dislocations.

[4]Abstract of paper submitted to *Journal of Nuclear Materials.*

TRANSMISSION ELECTRON MICROSCOPY OF OMEGA PHASE IN A Zr–15% Nb ALLOY[4]

J. O. Stiegler J. T. Houston
M. L. Picklesimer

Transmission electron microscopy was used to follow the formation and reversion of the metastable omega phase in a Zr–15% Nb alloy. In a fully aged specimen the omega phase is shown to consist of noncoherent platelets approximately 1000 A in diameter and approximately 200 A thick, probably lying on {111} planes of the retained beta phase. The platelets form a regular three-dimensional network having an average spacing of approximately 1000 A. Regions of retained beta phase contain a line structure similar to that observed in specimens aged at lower temperatures when the omega phase is believed to be coherent. Aging of the foils in the electron microscope resulted in partial reversion of the noncoherent platelets and formation of the coherent structure. Possible mechanisms for the formation of the two types of omega phase are discussed along with an explanation of the changes in mechanical properties that accompany their formation.

Part II.
Long-Range Applied Research

13. Zirconium Metallurgy

Studies of zirconium-base alloys of potential use as structural materials in several water-cooled and/or -moderated reactor systems are being conducted along several lines of research. The principal research projects presently under way are: (1) studies of the physical metallurgy, consisting of transformation kinetics and morphologies, mechanical properties, phase diagrams where necessary, and heat-treatment response; (2) the development, evaluation, and utilization of preferred orientation and strain anisotropy in α-zirconium alloys during fabrication, and the utilization of the yield stress anisotropy in increasing the permissible design stresses in structures; (3) the determination of the effects of composition, temperature, and environment on the oxidation-corrosion rates in the thin film stages of oxide growth; and (4) a study of the effects of alloy composition and oxidation environment on the structural properties of thin oxide films in situ.

ZIRCONIUM-NIOBIUM ALLOYS

P. L. Rittenhouse M. L. Picklesimer

Binary and ternary alloys of zirconium containing 0.5 to 2.5% Nb are being studied at several installations because they appear to be superior to Zircaloy-2 in strength and hydrogen absorption characteristics and have equal corrosion resistance in water. These properties, however, are realized only when the alloys are in heat-treated conditions that are difficult to reproduce between various lots of material. Prediction and explanation of the properties resulting from heat treatment, and their control in production runs, require an accurate knowledge of the Zr-Nb phase diagram. The alpha solubility boundary is in dispute, the maximum solubility of niobium in α-zirconium being reported as 4 to 6.5% Nb (refs 1,2) by dynamic methods and 0.5 to 2% Nb (refs 3–6) by metallographic methods.

Last year it was reported that resistivity measurements indicated a maximum solubility of 6% Nb in α-zirconium, but that metallographic examination of isothermally treated specimens contradicted this result. A careful metallographic study of Zr-Nb alloys of from 0.2 to 15% Nb has since been made. Specimens of each alloy were isothermally heat treated at temperatures from 400 to 900°C, and other specimens of each alloy were held in a temperature gradient approximately linear between 500 and 900°C for two-week periods in each case. Metallographic examination indicated a maximum solubility of 1% Nb in α-zirconium at 600°C for both types of specimens. Quantitative metallography of these same specimens, however, indicated discontinuities in the plots of percent second phase vs temperature at constant average composition. Such discontinuities can occur only if there exists a hitherto unsuspected three-phase region or intermediate phase. The presence of at least three phases in specimens containing more than 3% Nb has been shown by anodizing. It is believed that another phase may exist between the reported alpha and beta phases, but no conclusive evidence has yet been obtained.

---

[1] B. A. Rogers and D. F. Atkins, *Trans. AIME* **203**(9), 1034 (1955).

[2] Yu. F. Bichkov, A. N. Rozanov, and D. M. Skorov, *J. Nucl. Energy* **5**, 402 (1957).

[3] O. S. Ivanov and V. K. Grigorovich, *Proc. U.N. Intern. Conf. Peaceful Uses At. Energy, 2nd, Geneva, 1958* **5**, 34 (1958).

[4] V. S. Emelyanov, Y. G. Godin, and A. I. Evstyukhin, *J. Nucl. Energy* **6**, 266 (1957–58).

[5] A. G. Knapton, *J. Less-Common Metals* **2**, 113 (1960).

[6] H. Richter *et al.*, *J. Less-Common Metals* **4**, 252 (1960).

A PRELIMINARY EXAMINATION OF THE FORMATION AND UTILIZATION OF TEXTURE AND ANISOTROPY IN ZIRCALOY-2[7]

M. L. Picklesimer

Anisotropy of mechanical properties in Zircaloy-2 due to preferred orientation has caused many difficulties in the fabrication and utilization of mill products. There has been little effort spent in examination, analysis, or control of the development of preferred orientation in Zircaloy-2. The promise of an appreciable increase in permissible design stresses in structures of this material requires that a thorough study be made of the problem. This paper represents a preliminary examination of the development and utilization of texture preparatory to an experimental study of anisotropy in Zircaloy-2 tubing.

The development of preferred orientation during manufacture of Zircaloy-2 plate, strip, and tubing is qualitatively analyzed in terms of the plastic strain undergone, the modes of deformation operative, the anisotropy of flow strengths, and the effects of forming forces of the rolls or dies. The problem of forming structural shapes from anisotropic mill products is discussed, and the utiliza- of the anisotropy of mechanical properties is considered.

TEXTURE DETERMINATIONS BY HARDNESS ANISOTROPY IN α-ZIRCONIUM ALLOYS

P. L. Rittenhouse

Since thin-walled tubing of large diameter which will allow high design stress levels is being considered for use in several water-cooled and/or -moderated reactors, the studies of strain anisotropy in Zircaloy-2 plates[8,9] are being extended to such tubing. It is important to determine the texture and strain anisotropy at various stages of fabrication and to determine the variation of textures from end to end and from the inside wall to the outside wall of each piece of tubing. The determination of this number of individual textures becomes prohibitively tedious, difficult, and costly by x-ray diffraction techniques. A method of quantitative determination of texture by hardness anisotropy is being developed.

The hardness anisotropy in several materials[10-13] has been studied using the Knoop method. This has an elongated diamond pyramid microindenter which makes an impression in the form of a parallelogram having one diagonal about seven times as long as the other. The Knoop indenter is used because it is less symmetrical than other types and is more sensitive to variations of hardness with direction. The hardness anisotropy is determined by making successive hardness impressions, between which the long axis of the indenter is rotated relative to some reference direction in the surface. The results are usually interpreted semiquantitatively by correlation with orientation factors for slip and/or twinning.

The anisotropy of five schedules of Zircaloy-2 of known preferred orientation was studied by measurement on three orthogonal planes. These planes were perpendicular to the rolling, transverse, or normal fabrication directions and are identified as $\bar{R}$, $\bar{T}$, and $\bar{N}$ planes respectively. The results in all cases were consistent with the known textures. A representative result is shown in Fig. 13.1*a* for a material (schedule 8, Part II of ref 8) which had a texture approximating that of a single crystal (a concentration of basal poles in the normal direction 6.5 times random). It is expected that equations can be derived to allow a reasonable determination of the orientation and intensity of the texture from such data.

Results from similar measurements on the $\{10\bar{1}0\}$, $\{11\bar{2}0\}$, and (0001) planes of a single

[7]Abstract of published paper: sec 13 in *Proceedings of the USAEC Symposium on Zirconium Alloy Development, Castlewood, Pleasanton, California, Nov. 12–14, 1962*, GEAP-4089, vol II (Nov. 30, 1962).

[8]P. L. Rittenhouse and M. L. Picklesimer, *Metallurgy of Zircaloy-2: Part I – The Effects of Fabrication Variables on the Anisotropy of Mechanical Properties*, ORNL-2944 (Oct. 13, 1960); *Part II – The Effects of Fabrication Variables on the Preferred Orientation and Anisotropy of Strain Behavior*, ORNL-2948 (Jan. 11, 1961).

[9]M. L. Picklesimer, *Metals and Ceramics Div. Ann. Progr. Rept. May 31, 1962*, ORNL-3313, p 156.

[10]F. W. Daniel and C. G. Dunn, *Trans. Am. Soc. Metals* **41**, 419 (1949).

[11]M. Schwartz, S. K. Nash, and R. Zeman, *Trans. AIME* **221**(3), 554 (1961).

[12]C. Feng and C. Elbaum, *Trans. AIME* **212**(1), 47 (1958).

[13]N. A. Hill and J. W. S. Jones, *The Crystallographic Dependence of Low Load Indentation Hardness in Beryllium*, AERE-R-3215 (1960).

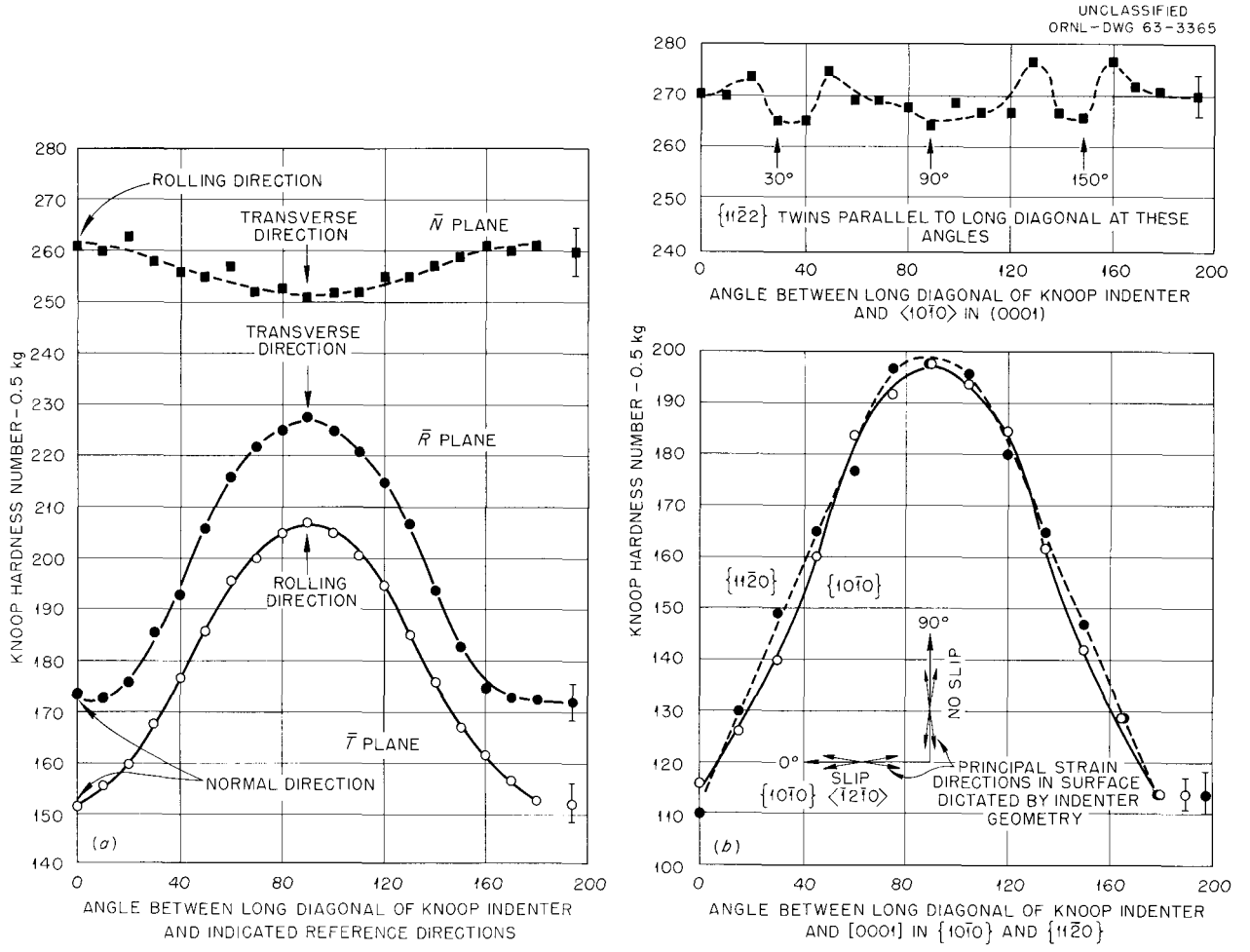

Fig. 13.1. Hardness Anisotropy in Zircaloy-2. (*a*) Schedule 9; (*b*) single crystal.

crystal of Zircaloy-2 are shown in Fig. 13.1*b*. The variation in hardness on the {10$\bar{1}$0} and {11$\bar{2}$0} planes is the result of the variation of the resolved shear stress for {10$\bar{1}$0} <$\bar{1}$2$\bar{1}$0> slip with direction of the indenter, this being a maximum when the long axis of the Knoop indenter is parallel to the [0001] direction and essentially zero when it is perpendicular to that direction. Variations in hardness on the basal plane are more subtle and depend on the combination of orientation factors for the six {10$\bar{1}$2} twin planes with respect to the indenter.

For impressions on the prism faces of the single crystal of Zircaloy-2, it was observed that the ratio of the long to the short diagonal (theoretically 7.11 and measured on lead as 6.9 for this indenter) varied from 5.2 when the long diagonal was parallel to the [0001] direction to 7.4 when it was perpendicular to the same direction. This behavior is a reflection of the higher elastic limit for compression in the [0001] direction,[9] and, since much more elastic recovery occurred in the [0001] direction, the indicated hardnesses are too high.

The elastic recovery is emphasized if a cone indenter is used to make the hardness impressions. The surface pileup and deformation occurring around the impression of a cone indenter on (0001) and {10$\bar{1}$0} planes in a single crystal of Zircaloy-2 are shown in Fig. 13.2*a* and *b*. The surface pileup in directions perpendicular to the [0001] direction (Fig. 13.2*a*) is due to {1010}

UNCLASSIFIED
Y-50135

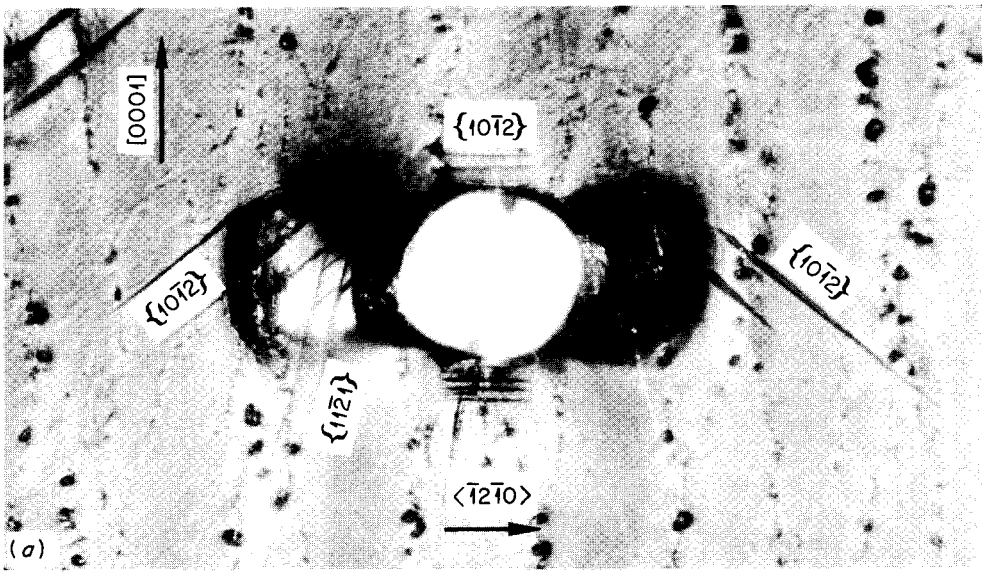

Fig. 13.2. (*a*) **Plastic Pileup and Twinning Around a Cone Impression on {10$\bar{1}$0} Prism Plane in Zircaloy-2 Single Crystal;** (*b*) **{10$\bar{1}$2} Twinning Around Cone Impression on (0001) Basal Plane in Zircaloy-2 Single Crystal. 300X.**

{$\bar{1}$2$\bar{1}$0} slip. The twins perpendicular to the [0001] direction are {10$\bar{1}$2} twins, presumably formed on release of the load; those at approximately 50° to that direction are of the {$\bar{1}$0$\bar{1}$2} type formed during loading; and those about 15° to it are of the {11$\bar{2}$1} type, also formed during loading. The twins occurring around the cone impression made in the basal plane of the specimen and shown in Fig. 13.2*b* are of the {10$\bar{1}$2} type, all six possible orientations being observed. It is important to note that the <10$\bar{1}$0> and <$\bar{1}$2$\bar{1}$0> directions can be immediately identified.

PREPARATION OF SINGLE CRYSTALS OF ZIRCONIUM AND ZIRCONIUM ALLOYS

J. C. Wilson

A new method was developed for the rapid production of single crystals of α-zirconium and its alloys. Previous methods using long-time alpha anneals with[14] and without[15] periodic excursions into the β-temperature range require several weeks to produce small specimens of zirconium which have considerable substructure. These methods have not been successful for the alpha alloys. The method herein described requires less than one day and can be used for the alloys as well. Large single crystals of Zircaloy-2 have been produced for the first time.

Specimens 1 to 3 mm thick, 10 to 25 mm wide, and 10 to 25 cm long are traversed past an electron beam that heats the metal to 1000 to 1400°C in a zone less than 1 mm high across the width of the strip. Heat conduction and radiation losses cause a temperature gradient of about 300°C/cm to exist on each side of the heated zone. Traverse rates range from 2 to 50 mm/hr. All experiments have been conducted with an electron beam power of less than 150 w and in a vacuum of 2×10^{-7} torr or better. Zirconium specimens have been initially in either a cold-worked or annealed condition, but the best results for Zircaloy-2 have been obtained if it was first β-quenched. Some of the results are shown in Fig. 13.3.

At present, zirconium crystals 1 mm thick, having an area of about 10 cm^2 and more, can be readily grown in a strip specimen having a total area of about 40 cm^2. The maximum size of crystals produced to date of Zircaloy-2 is $1 \times 6 \times 30$–40 mm and of zirconium is $1 \times 20 \times 75$ mm.

Severe warping and twisting of the strips usually occur if only a few grains are formed across the width of the strip, being more severe in Zircaloy-2 than in iodide zirconium. Back-reflection Laue photographs show the crystals to have a reasonable degree of perfection. More recent experiments showed that one grain can be forced to occupy the

[14] J. P. Langeron and P. Lehr, *Compt. Rend.* **243**, 151 (July 9, 1956).

[15] E. J. Rapperport, *Acta. Met.* **3**(3), 208 (1955).

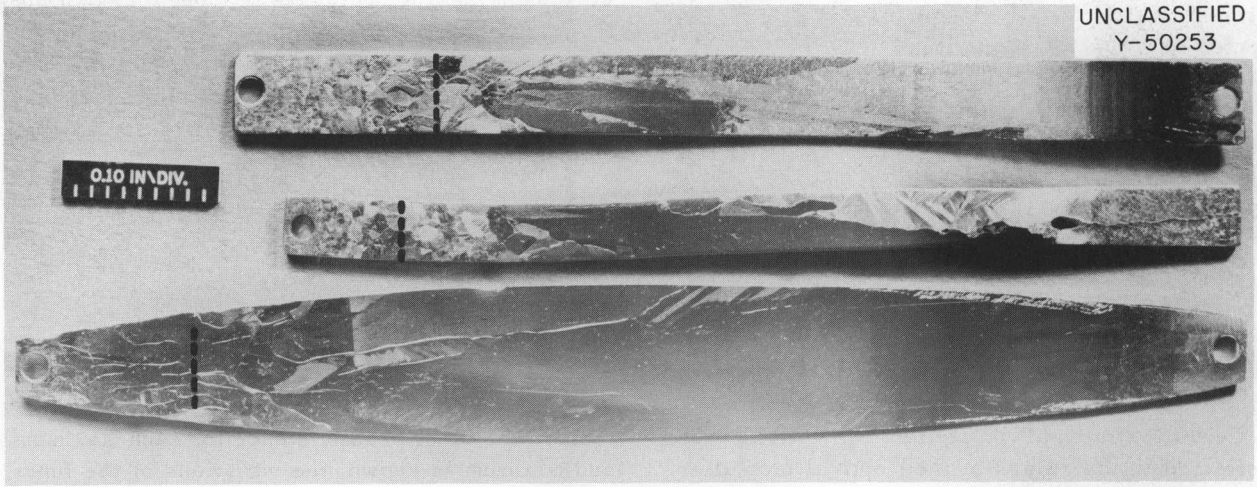

Fig. 13.3. Single Crystals of Zirconium and Zircaloy-2 Produced by the Electron Beam Technique. Specimens were not polished or etched after crystal growth; brightness and texture variations are due to thermal etching, transformation relief, and orientation relative to the oblique light source used for photography. Undulations in the plane of the strips and twist about the longitudinal axis are present but do not show in this photograph. The superposed lines indicate the initial position of the electron beam. The beam was traversed from left to right as oriented above. Top – arc-melted iodide zirconium; traverse rate, 12 mm/hr. Center – Zircaloy-2, initially β-quenched from 1030°C; traverse rate, 12 mm/hr. Bottom – high-purity iodide zirconium, as deposited and rolled; traverse rate varied from 10 to 40 mm/hr.

entire width of the strip, and more perfect crystals are expected as a result. No strong tendency for growth of grains of specific orientations was observed.

In Zircaloy-2 the grains having basal poles near the normal to the strip were observed to have a lineage structure of intermetallic precipitates on planes parallel to the basal pole and 20° from the $(1\bar{2}10)$ plane. This structure was observed only in grains having the basal pole near the strip normal.

ZONE-REFINING OF ZIRCONIUM AND ZONE-LEVELING OF ALLOYS

J. C. Wilson

Preliminary zone-refining experiments were carried out on iodide zirconium, using the equipment of Materials Research Corporation, Orangeburg, New York, to determine the feasibility of electron beam floating-zone refining of large zirconium bars and to furnish material for the initial crystal-growth experiments.

Swaged iodide zirconium rods up to $^7/_{16}$ in. in diameter were zone refined (maximum of four passes) without difficulty despite the fact that the electron gun was designed for rods $^1/_4$ in. in diameter or less. Metallographic examination of selected portions of the refined rods showed that single crystals of α-zirconium up to 50 mm long occupied as much as half the cross section of the rod. Back-reflection Laue photographs showed these crystals to be less perfect than those grown by the solid-state method described above.

OXIDE FILM STUDIES

J. C. Banter

Certain structural properties of materials are reflected in the values of their optical properties. For thin film oxides on metals, these properties may include strain in the film and the characteristics of the defect structures resulting from strain and/or nonstoichiometry in the film. Experiments based on interference techniques have been designed to determine the optical properties of oxide films in situ. The initial experiments have been conducted with anodically formed oxide films.

The spectral reflectivity of anodized Zircaloy-2 and niobium specimens was determined as a function of the wavelength, λ, of the incident light over the spectral range 2000 to 28,000 A with a double-beam recording spectrophotometer. Due to interference, the reflected light exhibits minima at those wavelengths where

$$nT \cos r - \frac{\delta\lambda}{4\pi} = (2m - 1)\lambda \ , \qquad (1)$$

and maxima where

$$nT \cos r - \frac{\delta\lambda}{4\pi} = \frac{m}{2}\lambda \ , \qquad (2)$$

with

n = refractive index of the oxide film at wavelength λ,

T = thickness of the oxide film,

r = the angle of refraction into the film,

δ = the phase shift occurring on reflection at the oxide-metal interface,

m = the order of the interference.

The oxide films were then isolated from the metal, either by stripping the film from the niobium or dissolving the metal away from the film for Zircaloy-2. Their transmission spectra were then determined over the same spectral range. The transmitted light also exhibits interference; but, for this case, the equations simplify to, for minima,

$$nT = \frac{(2m - 1)}{4}\lambda \qquad (3)$$

and, for maxima, to

$$nT = \frac{m}{2}\lambda \ . \qquad (4)$$

Since the order of interference for each maximum and minimum is known, the variations of the functions nT and $nT \cos r - (\delta\lambda/4\pi)$ with wavelength can be determined. The result is shown in Fig. 13.4. Since r is quite small, $\cos r$ is approximately equal to 1. The difference between the two curves at any wavelength can then be set equal to the term $-\delta\lambda/4\pi$, allowing the phase shift, δ, to be calculated. The results of such calculations for anodized niobium and Zircaloy-2 oxide films are shown in Fig. 13.5.

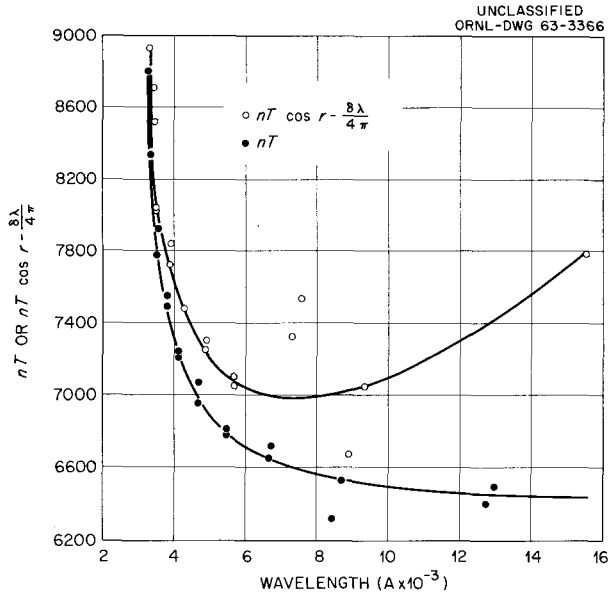

Fig. 13.4. Variation of the Functions nT and nT cos $r - (\delta\lambda/4\pi)$ with Wavelength Measured on Niobium Specimen Anodized at 150 v.

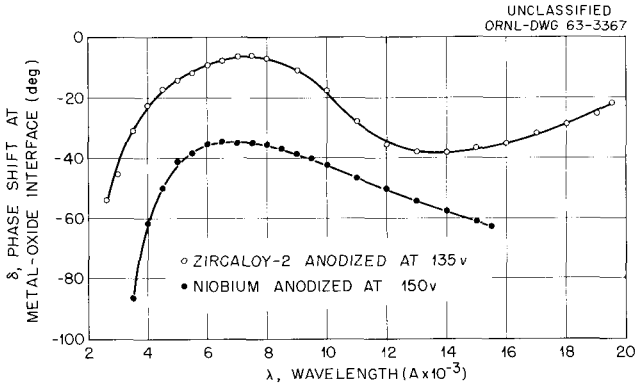

Fig. 13.5. Phase Shift on Reflection from the Metal-Oxide Interface as Calculated from Interference Data.

The values for the phase shift are only qualitative at wavelengths longer than 7000 A due to the lack of a sufficient number of points to properly define the interference functions in this region. This situation can be remedied by using thicker films. The reflection curve also appears to exhibit anomalous behavior between 7000- and 9000-A wavelengths. This may be due to an inherent instrumental error or it may be due to absorption by the metal substrate. It will be investigated further.

The refractive indices of the niobium oxide films were measured in situ by the Brewster angle method[16] over the spectral range 3750 to 7000 A. The refractive indices outside this range were determined by calculating the film thickness at one wavelength within the range, using the experimentally determined value for n and the appropriate value of nT taken from the curve presented in Fig. 13.4 and dividing the values for nT at other wavelengths by this thickness. This gave the desired values of refractive index over the spectral range of 3000 to 13,000 A.

The refractive indices of the stripped niobium oxide film were also determined by a total reflection method using a strontium titanate single-crystal lens on a polarizing spectrometer. Within

[16] L. Young, *Anodic Oxide Films*, pp 188–89, Academic Press, London and New York, 1961.

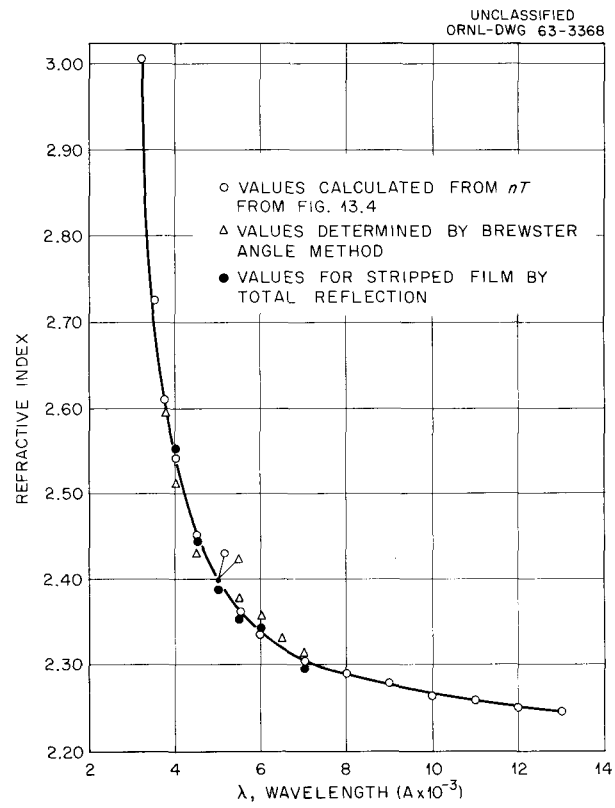

Fig. 13.6. Variation of Refractive Index with Wavelength of Oxide Film on Niobium Specimen Anodized at 150 v.

experimental error, the refractive indices determined by the two methods were identical. The results of such measurements are shown in Fig. 13.6.

The thickness of the niobium film was then calculated at each wavelength corresponding to a maximum or minimum in the reflected or transmitted intensities, using the interference equations and the appropriate values of δ and n taken from the curves. The thickness calculated from the reflection data was 2879 ± 50 A and that from the transmission data was 2884 ± 40 A.

Attempts to strip the oxide film from zirconium and Zircaloy-2 specimens for refractive index measurements were not successful. Determination of the refractive indices of the oxide film in situ is difficult due to the necessity for achieving intimate optical contact between the oxide and the strontium titanate lens. This method, however, may be the only solution since the Brewster angle method cannot work due to absorption in the oxide film in the spectral range in which this method can be employed.

The methods used have resulted in a highly accurate (±1.5%) determination of the oxide film thickness on a niobium specimen. The accuracy of such a measurement will, however, probably vary with film thickness.

Attention will now be directed toward refining and improving the experimental techniques so that they may be applied more generally, and especially to oxide films on a metal substrate, as a function of film thickness, oxidizing environment, and composition of the oxide and the substrate metal.

14. Materials Compatibility

OXYGEN PARTITIONING IN ALKALI-METAL–OXYGEN–REFRACTORY-METAL SYSTEMS

A. P. Litman J. R. DiStefano

Impurities such as oxygen, nitrogen, hydrogen, or carbon in either a refractory metal or an alkali metal can have a significant effect on compatibility of the components in an alkali-metal–refractory-metal system. In some cases the impurity concentrations sufficient to cause deleterious effects are only a few hundred parts per million – levels which might be present in high-purity metals.

Two mechanisms which have been proposed to explain the effects of impurities are the formation of complexes in the solid metal and the removal of soluble or loosely adherent compounds by a flowing liquid metal. In addition, a more subtle form of corrosion can also occur because of the tendency of impurities to migrate between solid and liquid metal in order to attain the same chemical potential in the two metals. In the case of oxygen in refractory-metal–alkali-metal systems, this problem is especially important for two reasons: (1) low oxygen concentrations are difficult to obtain and maintain in these metals; and (2) at the temperatures required for many applications, oxygen diffusion rates are high. In some systems a deleterious effect of oxygen partitioning is an unfavorable modification of the mechanical properties of the refractory metal. Another possible result is the plugging of cooler regions of flowing systems by precipitated alkali-metal oxides if sufficient quantities of oxygen have been leached from the refractory metal.

Using available thermodynamic and solubility data, it is possible to predict the equilibrium distribution of oxygen in refractory-metal–alkali-metal systems.[1] The equilibrium distribution of oxygen should be a constant, κ_T, at a given temperature; it is expressed by

$$\frac{C_B}{C_A} = \exp\left[\frac{\Delta F_f^\circ(A \text{ oxide}) - \Delta F_f^\circ(B \text{ oxide})}{RT}\right] \times \frac{(C_B)_s}{(C_A)_s} = \kappa_T ,$$

where C_B and C_A represent the concentration of oxygen in the refractory metal and the alkali metal respectively; ΔF_f°(oxide) is the standard free energy of formation of the refractory-metal or alkali-metal oxide; and $(C_B)_s$ and $(C_A)_s$ are the oxygen solubilities in B or A at temperature T. Calculations of κ_T have been made at 500 and 800°C; and these data, along with experimental coefficients developed to date, are presented in Table 14.1.

The calculated coefficients differed by several orders of magnitude when compared to experimental values. These differences may be due to nonideality of the dilute oxygen–alkali-metal solution; to the small, but finite, solubility of the refractory metal in potassium; or to uncertainties in the analytical procedures for determining oxygen in alkali metals. In addition to providing useful corrosion information, the equilibrium oxygen distribution between a refractory and an alkali metal can, in some cases, be used in purification studies and as an analytical tool to determine the oxygen concentration in the alkali metal. A description of studies to determine oxygen in potassium by using empirically determined distribution coefficients follows.

[1] J. R. DiStefano and E. E. Hoffman, "Corrosion Mechanisms in Refractory-Metal–Alkali-Metal Systems," pp 10–11, paper to be presented at the AGARD conference on refractory metals, The Science and Technology of Tungsten, Tantalum, Molybdenum, Niobium and Their Alloys, Oslo, Norway, June 23–29, 1963.

Table 14.1. Calculated and Experimental Values for κ_T for Some Refractory-Metal–Oxygen–Alkali-Metal Systems

System	$\kappa_T = \frac{C_O \text{ in Refractory Metal}}{C_O \text{ in Alkali Metal}}$			
	Calculated		Experimental	
	500°C	800°C	500°C	800°C
Nb-O-Li	5×10^{-11}	1×10^{-7}		0.025
Nb-O-Na	1×10^{3}	4×10^{2}		
Nb-O-K	5×10^{5}	3×10^{4}	0.5–1.2	0.1–0.3
Ta-O-Li	3×10^{-11}	3×10^{-8}		<1
Ta-O-Na	6×10^{2}	1.5×10^{2}	6–26[a]	2–18[a]
Ta-O-K	3×10^{5}	1×10^{4}		
Mo-O-Li	7×10^{-22}	5×10^{-16}		
Mo-O-Na	1×10^{-8}	2×10^{-6}		
Mo-O-K	7×10^{-6}	1×10^{-4}		
W-O-Li	1×10^{-21}	3×10^{-16}		
W-O-Na	2×10^{-8}	2×10^{-6}		
W-O-K	1×10^{-5}	2×10^{-4}		
Zr-O-Li	3	4		
Zr-O-Na	1.6×10^{10}	1.7×10^{10}		
Zr-O-K	6×10^{11}	1×10^{12}		~7

[a]G. E. Raines, C. V. Weaver, and J. H. Stang, *Corrosion and Creep Behavior of Tantalum in Flowing Sodium*, BMI-1284, p 13 (Aug. 21, 1958).

Determination of Oxygen in Potassium

A. P. Litman G. Goldberg[2]

An accurate and reproducible procedure for determining the oxygen concentration in potassium is needed for corrosion, purification, and solubility studies. Gettering plus vacuum fusion,[3] vacuum distillation,[4] and a modified mercury amalgamation[5,6] method were studied during this past year to evaluate these procedures as methods for analyzing oxygen in potassium.

The gettering plus vacuum fusion method consists of gettering the oxygen in potassium with an active metal such as zirconium and then analyzing the zirconium by vacuum fusion. Calculations[7] have shown that the transfer of oxygen from potassium to zirconium is such that, at equilibrium, the ratio of oxygen in zirconium to oxygen in potassium should be a constant, κ_T, at any temperature, T. Experiments have demonstrated that $\kappa_{815°C} \cong 7$ for the Zr-O-K system. Therefore, if a sample of potassium containing an unknown concentration of oxygen is equilibrated with zirconium that contains a known concentration of oxygen, the final oxygen concentration of the zirconium and knowledge of the distribution coefficient for

[2]Analytical Chemistry Division.

[3]P. H. Goble, W. M. Albrecht, and M. W. Mallett, "Determination of Oxygen in Sodium," *Progress Relating to Civilian Applications During 1957*, BMI-1173, p 67 (February); BMI-1181, p 70 (April); BMI-1189, p 59 (May); BMI-1201, p 55 (June).

[4]R. Thacker, *The Determination of the Oxygen Content in Liquid Metals*, IGR-TN/C 609 (June 1957).

[5]G. Goldberg, *Anal. Chem. Div. Ann. Progr. Rept. Dec. 31, 1962*, ORNL-3397, p 50.

[6]L. P. Pepkowitz and W. C. Judd, *Anal. Chem.* **22**(10), 1283 (1950).

[7]J. R. DiStefano and E. E. Hoffman, "Corrosion Mechanism in Refractory-Metal–Alkali-Metal Systems," pp 10–11, paper to be presented at the AGARD conference on refractory metals, The Science and Technology of Tungsten, Tantalum, Molybdenum, Niobium and Their Alloys, Oslo, Norway, June 23–29, 1963.

this system can be used to determine the original oxygen concentration in the potassium. Recent tests have demonstrated oxygen recoveries of approximately 90% from potassium by this method when the oxygen addition Nb(O) was approximately 800 ppm. Disadvantages of the method are the relatively high cost and the long time necessary for each analysis. However, the method does have excellent possibilities as an absolute method to use in checking the accuracy of methods more suited for routine analysis.

The vacuum distillation method for determining oxygen in potassium is based on the removal of potassium metal from a sample of potassium containing dissolved oxygen and/or potassium oxides by distilling the metal at elevated temperature under vacuum and leaving K_2O as the distilland. The oxygen concentration in the potassium can then be determined by acidimetric titration or flame photometric analysis of the distilland. Calculations[8] have shown that up to 350°C the equilibrium partial pressure of oxygen due to dissociation of K_2O is negligible. Thermodynamic data suggest that no interferences should be expected from the initial presence of the higher oxides of potassium or of KH in the potassium. However, the presence of trace amounts of Na, Ca, Mg, Ti, Zr, and C could reduce K_2O and lead to low oxygen values if the analysis of the distilland does not include the concentrations of the oxides of these impurities. In addition, compounds such as KOH, K_2CO_3, KF, and KCl initially present in the potassium could result in high oxygen values, since they would remain in the distilland. Preliminary studies have shown that sodium is the only major impurity which must be considered in determining the oxygen concentration in potassium samples by this method. Recent experiments have demonstrated good agreement between the results obtained by gettering plus vacuum fusion and those obtained by vacuum distillation on portions of the same potassium samples, in which the oxygen concentration varied from approximately 50 to 800 ppm. In addition, when the oxygen concentration in potassium was $\leq$100 ppm, the methods of gettering plus vacuum fusion, vacuum distillation, and mercury amalgamation all show good agreement.

[8]G. W. Horsley, *The Purification of Commercial Potassium*, AERE M/R 1371 (January 1954).

Table 14.2. Oxygen Recovered from Potassium by the Mercury Amalgamation Method as a Function of Oxygen Source and Equilibration Temperature

Oxygen Source	Oxygen Added (ppm)	Equilibration Temperature (°C)	Equilibration Time (hr)	Oxygen Recovered[a] (%)
Nb(O)	800	815	100	19
K_2O	620	70	0.25	110
	585, 505	400	48, 48	12, 36
	540, 575	600	48, 48	32, 37
KO_2	780	70	0.25	16
	890, 945	200	48, 48	8, 8
	830, 835	600	48, 48	44, 45
HgO	505	70	0.25	6
	465, 435	200	48, 48	13, 14
	555, 435	400	48, 48	27, 43
	480, 360, 460	600	48, 72, 48	24, 40, 52
	435	800	48	81

[a]Based on K_2O as the assumed residue after amalgamation.

Considerable emphasis has been placed on adapting the mercury amalgamation method[5] to potassium because of the relatively simple analytical procedure involved and the good precision consistently demonstrated on Na, NaK, and K samples. Mercury is used in the amalgamation procedure to physically separate the alkali metal from the alkali-metal oxide. Oxygen can be calculated after acidimetric titration or flame photometric determination of the total alkali-metal concentration in the oxide residue. The accuracy of the mercury amalgamation method has been studied as a function of temperature and oxygen source. Oxygen concentrations in the potassium were varied from 170 to 950 ppm; and, to avoid the problem of sample segregation, the entire potassium sample was analyzed in every case. The oxide species recovered after amalgamation was assumed to be K_2O. The results are detailed in Table 14.2 and show low percentage recoveries in every case, with the exception of a test in which K_2O was added to potassium just above the melting point of the metal and analyzed immediately. Possible reasons for the low recoveries obtained have been discussed.[9] These results indicate that less emphasis should be placed on mercury amalgamation as a method for determining oxygen in potassium.

The studies described are part of a joint program with the Analytical Chemistry Division.

---

[9]A. P. Litman and G. Goldberg, ORNL-3420, pp 238–41 (classified).

15. Solid Reaction Studies

T. S. Lundy J. I. Federer
W. K. Biermann[1] D. Heitkamp[1]
J. F. Murdock

DIFFUSION IN BODY-CENTERED CUBIC METALS

Extensive experimental work has continued on measuring diffusion coefficients in body-centered cubic metals. Wide temperature ranges have been investigated so that the previously reported[2,3] nonlinear Arrhenius-type behavior could be evaluated further. This behavior is illustrated in Fig. 15.1, where straight-line plots would have been obtained if the Arrhenius-type equation $D = D_0 \exp(-Q/RT)$ with constants D_0 and Q had been obeyed. The nonlinearity of these plots for the cases where wide temperature ranges have been covered is obvious not only for diffusion in β-titanium and β-zirconium but also for diffusion in single crystals of vanadium. The latter is significant, for it demonstrates that the enhanced diffusion coefficients at low temperatures are not caused only by some defect structure produced by the solid-state transformations that occur in both titanium and zirconium when they are heated to diffusion temperatures. The data for Nb^{95} in niobium are preliminary in nature and will be extended to lower temperatures so that any curvature will be evident.

The meaning of the deviations from Arrhenius-type behavior for diffusion in body-centered cubic metals is not clear. Arrhenius,[4] in his paper from which the equation evolved, emphasized that the activation energy was constant only to a first approximation. Experimental determinations over short temperature intervals have falsely implied that the values of D_0 and Q are necessarily constant with temperature. As a result, theoretical treatments have magnified the significance of the relative values of D_0 and Q for different systems. These treatments have generally assumed that one mechanism of diffusion in a given system is characterized by constant values for D_0 and Q regardless of the temperature range of the measurements. Thus it is natural to describe the data presented in Fig. 15.1 by summing as many terms of the form $D_0 \exp(-Q/RT)$ as is necessary to give the determined curvature and to associate a mechanism of diffusion with each such term. Further experimental work is necessary to determine the correct interpretation of the problem.

One of the suggestions for explaining the observed curvature is that the enhanced diffusion rate at the lower temperatures may be due to dislocation pipe short circuiting. Electron microscope studies of the annealing of heavily cold-worked vanadium foil have shown that dislocations cannot survive thermal treatments in excess of 1000°C for 1 hr.[5] Thus the much longer diffusion anneal at the lowest temperature (approximately 8½ days at 1000°C) for vanadium should have resulted in no significant enhanced diffusion due to dislocation pipes. Since tantalum retains high dislocation densities after short anneals at temperatures up to 1200°C, it has been suggested[5] that measurements be made in both annealed and cold-worked tantalum to determine the contribution

[1] Visitor from Germany.

[2] T. S. Lundy *et al.*, *Metals and Ceramics Div. Ann. Progr. Rept. May 31, 1962*, ORNL-3313, p 145.

[3] T. S. Lundy and J. I. Federer, *Diffusion of Zr^{95} in Body-Centered Cubic Iodide Zirconium*, ORNL-3339 (Aug. 22, 1962).

[4] Svante Arrhenius, *Z. Physik. Chem.* (*Leipzig*) **4**, 226 (1889).

[5] J. O. Stiegler, private communication.

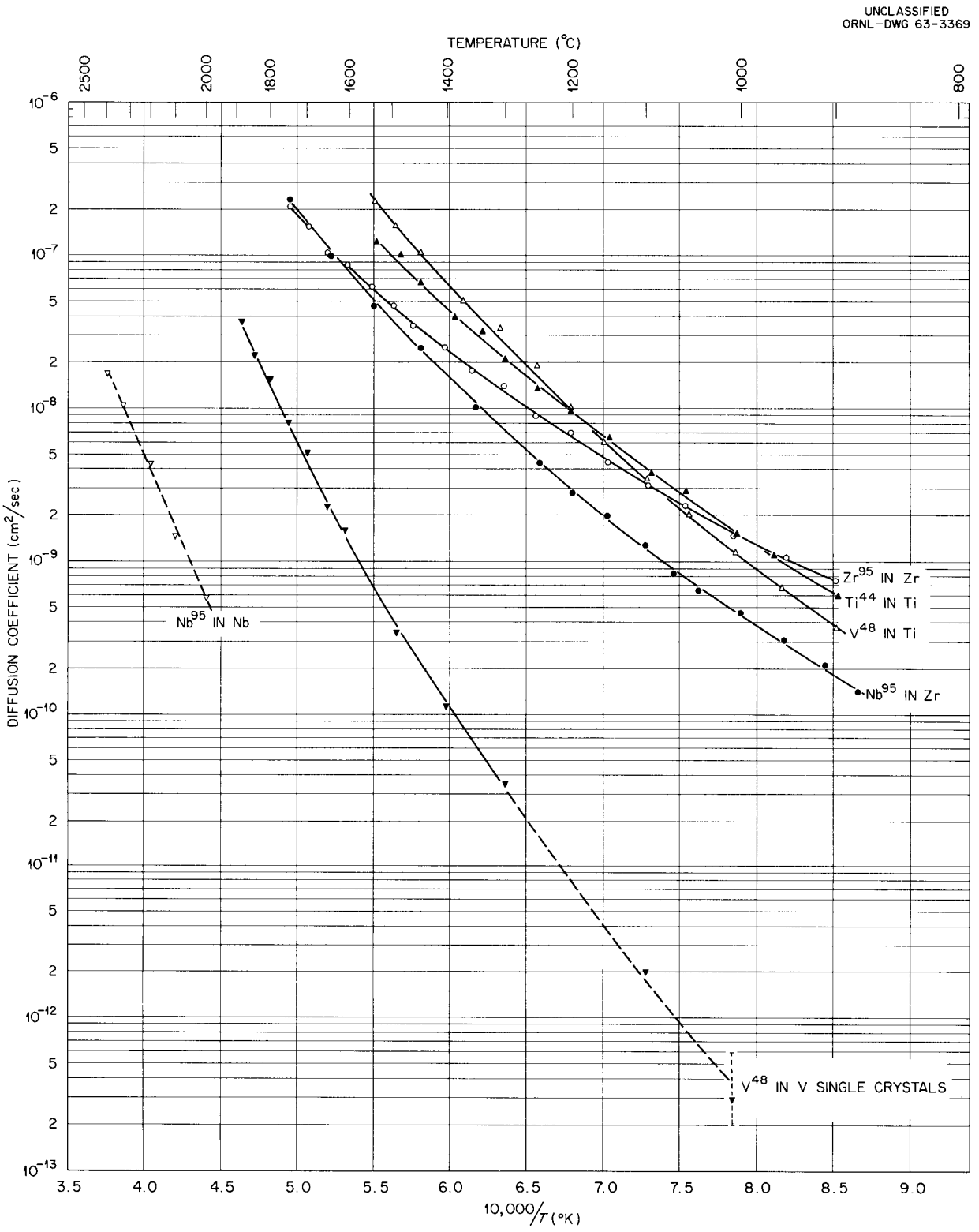

Fig. 15.1. Diffusion in Body-Centered Cubic Metals.

of dislocations to diffusion coefficients. Such experiments are now being performed in conjunction with the Reactions at Metal Surfaces Group, Part I, Chap. 2, this report. These experiments, in which a newly developed anodizing and stripping technique for removing very thin sections (as small as 100 A of metal) is used, allow determination of diffusion coefficients in the range 10^{-14} to 10^{-17} cm^2/sec.

DIFFUSION IN A TEMPERATURE GRADIENT

A program was initiated to study diffusion in solids in a temperature gradient. The interest in this problem stems from nuclear applications where, in recent years, metals and ceramics have been subjected to much higher temperature gradients than before. These gradients have influenced some of the important solid-state reactions, and it is important to gain a better understanding of such influences.

When an initially homogeneous two-component system is placed in a temperature gradient, a concentration gradient will occur. This phenomenon is called the Ludwig-Soret effect. The effect has been studied extensively in gases and liquids but very little in solids. Because of the small quantity of data, a quantitative theory of thermal gradient diffusion has not been established for solids. In the present work, the diffusion of small amounts of tracer atoms in silver in a temperature gradient is being studied.

The technique being used to study the Ludwig-Soret effect in silver involves the following steps: (1) uniformly distributing a small amount of tracer in the silver specimen; (2) placing the diffusion specimen between two tungsten disks – the upper one heated and the lower one cooled in order to maintain a large temperature gradient; and (3) sectioning to determine the activity profile in the specimen after annealing for a long time in the temperature gradient.

From the measured redistribution of the tracer, it is possible to obtain data on the transport heat of the solute atoms. Since the different theoretical approaches to the treatment of diffusion in a temperature gradient are especially concerned with the interpretation of the transport heat and its connection with energies of isothermal diffusion, the measured values can be compared with the well-known activation energies of migration and formation of defects in silver.

EFFECT OF ALPHA RADIATION ON DIFFUSION OF LEAD IN SILVER

During irradiation of metals with energetic particles, an excess number of defects can be produced. If the excess steady-state defect concentration is larger than the defect concentration in thermodynamic equilibrium, the diffusion, which is directly related to the number of defects, will be enhanced. These diffusion effects have been studied extensively by indirect methods (for instance, resistivity measurements), but not yet by direct tracer techniques. Usually the generation rate of excess defects at temperatures in the normal self-diffusion range is not high enough to lead to an observable enhancement of diffusion. However, at lower temperatures the presence of these excess defects may play an important role in certain irreversible solid-state reactions of interest in nuclear technology.

In this study an attempt is being made to measure the enhancement of diffusion at relatively low temperatures – below the normal range for measuring self-diffusion by a direct tracer technique. This is possible by using the highly sensitive recoil method developed by Hevesy and Seith.[6] Based on the extremely small range of alpha recoil atoms in solids, this method permits measurement of diffusion coefficients in the range 10^{-15} to 10^{-18} cm^2/sec. The diffusion enhancement due to the alpha particle bombardment from a 10-curie source of Po^{210} will be measured.

In these experiments a thin layer of alpha-active atoms is deposited on the surface of the sample. Both before and after diffusion has taken place, the alpha recoil atoms of the tracer which escape the surface are counted. A suitable alpha-active tracer, the recoil atoms of which are also radioactive and have a reasonable half-life, is Pb^{212}. Lead-212 decays via Bi^{212} to Tl^{208} (shown in the decay scheme of Th^{228}, Fig. 15.2). Thallium-208 is the alpha recoil atom of Bi^{212}, not of the tracer Pb^{212}; however, if there is radioactive equilibrium between Pb^{212} and Bi^{212}, the activity of Tl^{208} is an exact measure of Pb^{212} concentration. The

[6] G. V. Hevesy and W. Seith, *Z. Physik* **56**, 790 (1929).

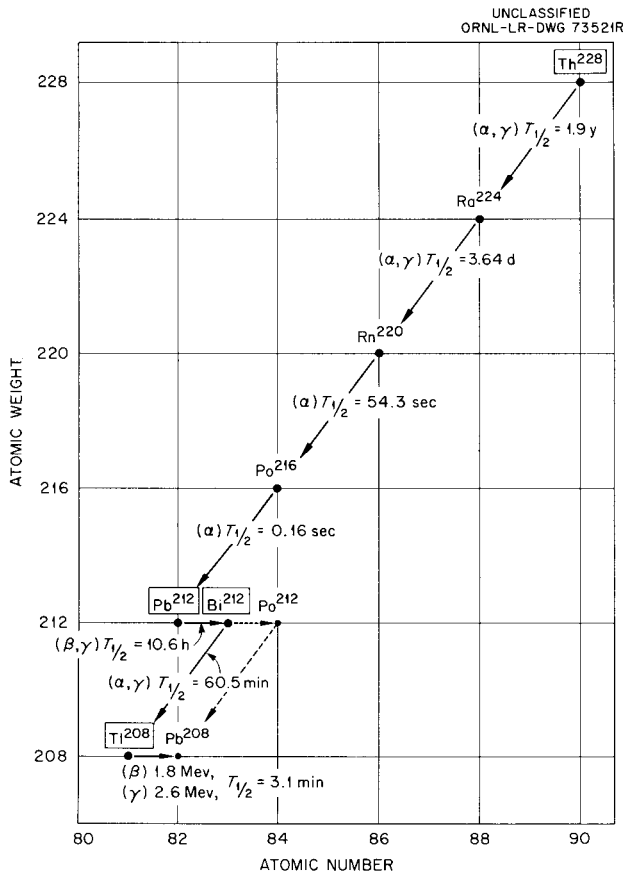

Fig. 15.2. Decay Scheme of Th^{228}.

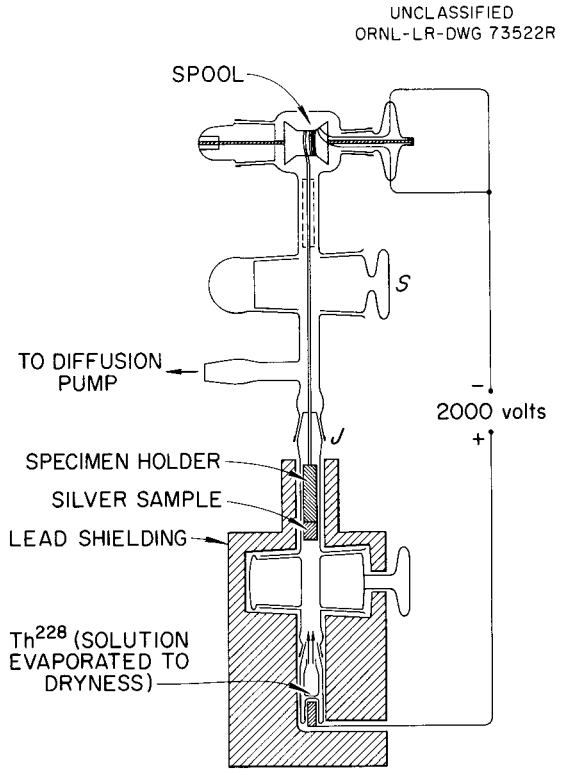

Fig. 15.3. Apparatus for Collecting Pb^{212}.

number of Tl^{208} recoils that can be counted decreases very rapidly with diffusion time because of the small recoil range (approximately 40 mμ in silver). The experimental procedure involves the following main steps:[7]

1. Preparing the specimen – Single crystals of silver (99.999% pure) are used. The surface is chemically polished carefully to remove the distorted area (checked by taking a Laue pattern).
2. Collecting Pb^{212} on the surface of the silver specimen – A Th^{228} source approximately equivalent to 3 mg of radium is encapsuled in a Pyrex container (Fig. 15.3). An electric field of 200 v/cm is applied to collect the Rn^{220} recoil atoms which are in the volume between the sample and the source.
3. Measuring the surface concentration of Pb^{212} by means of the Tl^{208} recoil activity – The sample is precisely fixed by an open Pyrex tube at a distance of 1 mm above a copper plate (Fig. 15.4). An electric field of 200 v/mm collects the Tl^{208} recoils (half-life, 3.1 min) on the copper plate, which can then be quickly moved below the G-M tube by an electromagnet.
4. Diffusion annealing the specimen – A uniform temperature is maintained by a temperature-controlled furnace (Fig. 15.5). Experiments are now being performed to measure the diffusion coefficient without irradiation and to measure its dependence on temperature.

[7]During steps 2–5, the silver sample, fastened by a specimen holder, is always kept under helium gas or in a vacuum to prevent the surface from being oxidized. The sample is always raised above stopcock *S* (Figs. 15.2–15.4) by means of a spool, and the stopcock is closed when ground joint *J* must be disconnected for the next step.

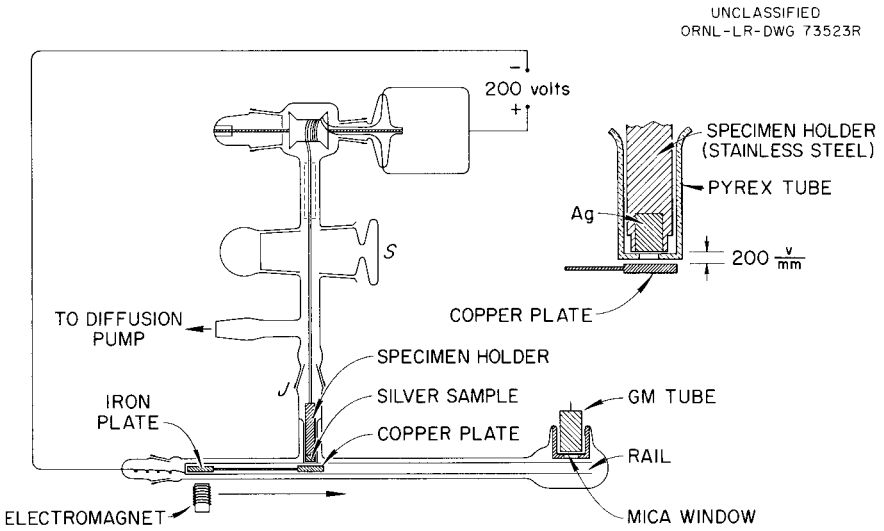

Fig. 15.4. Apparatus for Collecting and Measuring Tl^{208} Recoil Atoms.

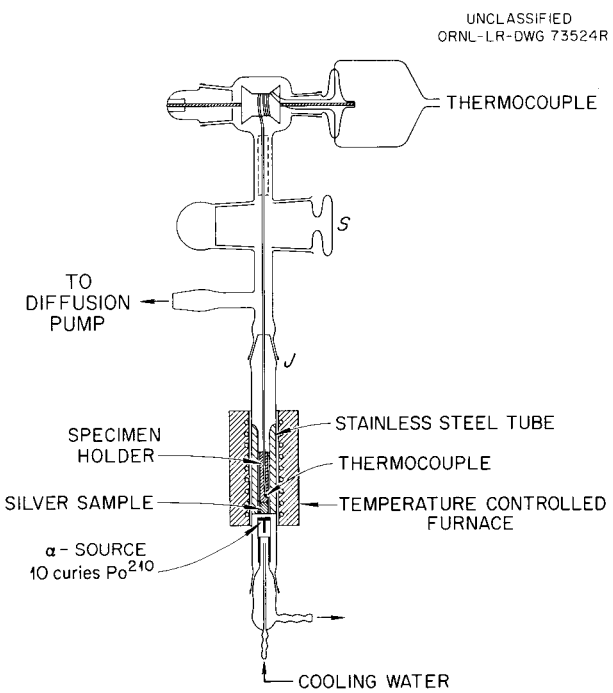

Fig. 15.5. Apparatus for Performing Diffusion Annealing Under Irradiation.

5. Diffusion annealing and irradiating the specimen – The Po^{210} alpha source is to be placed 1 mm below the sample (see Fig. 15.5). In this arrangement the 10-curie alpha source, which is covered with a 0.00027-in. stainless steel foil, provides a flux of approximately 2×10^{11} alpha particles cm^{-2} sec^{-1} which bombards the surface of the sample. The range of these alpha particles is much greater than the range of the Tl^{208} atoms. Thus the whole diffusion zone is damaged. The source is cooled to minimize vaporization of the polonium.

DIFFUSION OF Nb^{95} IN UO_2

Diffusion of Nb^{95} in pressed and sintered UO_2 pellets and in fused, large-grained crystals of UO_2 has been studied over the temperature range 1096 to 2100°C. The techniques of specimen preparation, isotope placement, and treatment of sectioning data have been described previously.[8,9] Fused UO_2 supplied by Spencer Chemical Company was found to be generally unsuitable for these experiments because of the presence of a secondary phase and a large number of cracks. Coarse-grained, fused UO_2 supplied by the Norton Company contained less secondary phase and very few cracks. The Norton UO_2 was used in these

[8] T. S. Lundy *et al.*, *Met. Div. Ann. Progr. Rept. May 31, 1961*, ORNL-3160, p 43.

[9] T. S. Lundy *et al.*, *Metals and Ceramics Div. Ann. Progr. Rept. May 31, 1962*, ORNL-3313, p 146.

tests, even though the specimens did contain considerable macroscopic porosity that necessitated careful selection procedures.

According to the boundary conditions of these experiments, if diffusion occurs by a single volume transport mechanism, plots of ln Nb^{95} activity vs distance squared (x^2) should be linear. However, the activity profiles for all pressed and sintered UO_2 specimens annealed between 1096 and 2100°C were characterized by two distinct segments: (1) an initial portion with a large Nb^{95} gradient that was curved concave upwards and (2) a linear portion beginning at a distance of about 50 μ from the surface and extending to the limit of Nb^{95} penetration. Activity profiles for fused UO_2 specimens were similar to those for pressed and sintered UO_2, except the linear portions were not always well defined. Typical plots determined for pressed and sintered pellets and fused specimens are shown in Fig. 15.6. The actual curvatures of the initial portions are better illustrated in Fig. 15.7, where the x^2 scale is expanded.

Although the shapes of the activity profiles are not readily interpreted in terms of mechanism(s), diffusion coefficients were calculated from the linear portions of the plots; and the values are presented in Table 15.1. These data show that the diffusion coefficients of Nb^{95} in pressed and sintered UO_2 increase with increasing temperature between 1265 and 1600°C but attain an approximately constant value of 2×10^{-8} cm^2/sec in the temperature range of 1700 to 2100°C. Diffusion coefficients of Nb^{95} in fused UO_2 increase with increasing temperature between 1100 and 2010°C, but the temperature dependence cannot yet be adequately described.

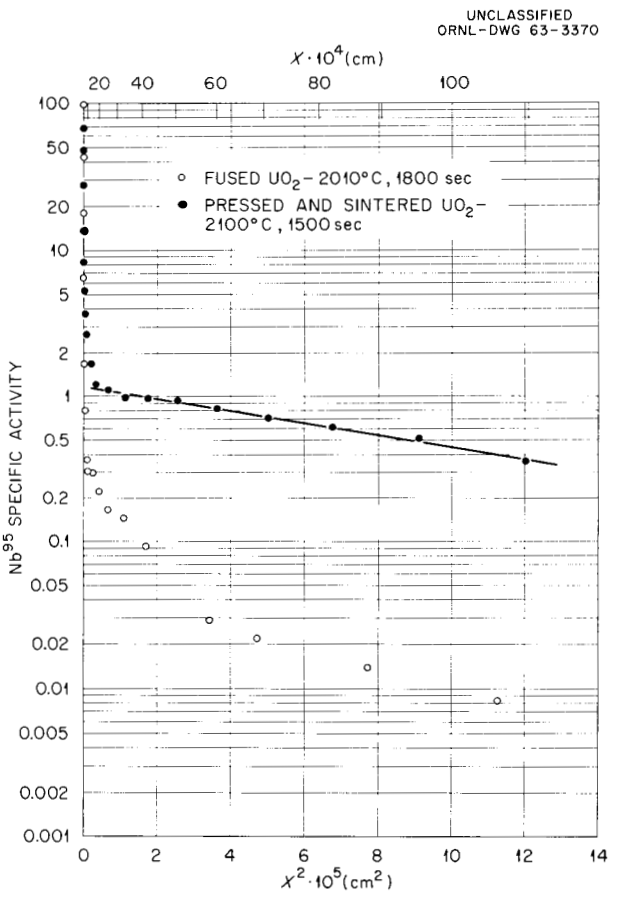

Fig. 15.6. Activity Profiles for Diffusion of Nb^{95} in UO_2.

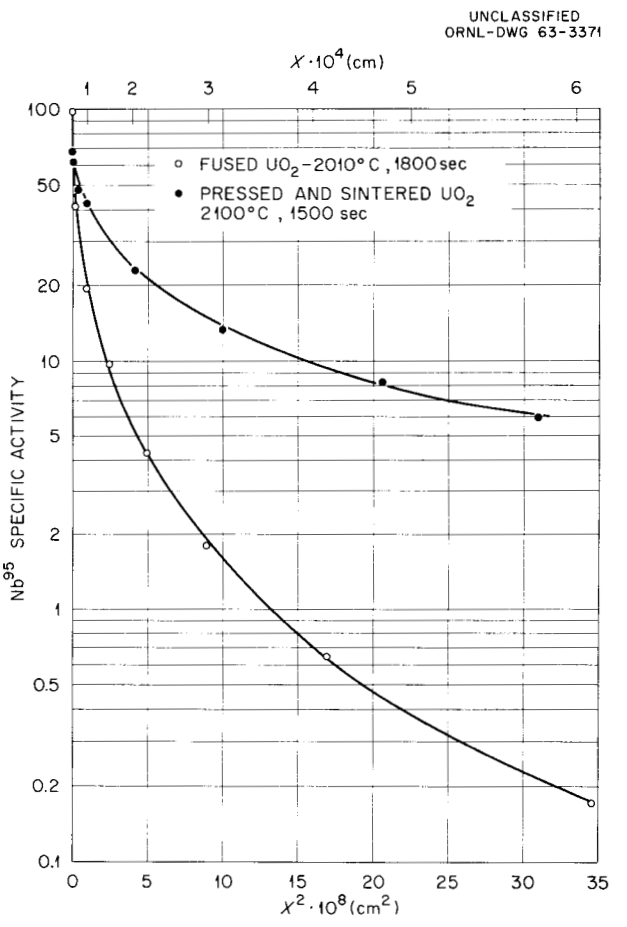

Fig. 15.7. Activity Profiles for Diffusion of Nb^{95} in UO_2.

Table 15.1. Summary of UO_2-Nb^{95} Diffusion Experiments

Specimen	Temperature (°C)	Time (sec)	Atmosphere	Diffusion Coefficient (cm^2/sec)
		$\times 10^{-3}$		
Pressed and sintered UO_2 pellets	1096	148.62	H_2	7.99×10^{-11}
	1100	143.52	H_2	2.47×10^{-11}
	1265	29.10	H_2	1.71×10^{-11}
	1302	22.20	Ar	3.48×10^{-11}
	1320	32.46	H_2	6.56×10^{-11}
	1360	21.60	H_2	9.72×10^{-11}
	1380	21.90	H_2	4.82×10^{-11}
	1400	14.55	Ar	4.77×10^{-10}
	1405	11.46	Ar	4.96×10^{-10}
	1525	6.54	Ar	1.83×10^{-9}
	1595	3.81	Ar	1.37×10^{-8}
	1695	3.30	Ar	1.18×10^{-8}
	1805	1.62	Ar	1.93×10^{-8}
	1895	2.37	Ar	2.15×10^{-8}
	1980	25.20	Ar	1.64×10^{-9}
	2010	1.80	Ar	1.48×10^{-8}
	2030	1.83	Ar	3.05×10^{-8}
	2100	1.50	Ar	1.63×10^{-8}
Fused crystals of UO_2	1100	143.52	H_2	2.47×10^{-11}
	1320	32.46	H_2	1.07×10^{-10}
	1570	14.40	Ar	1.08×10^{-10}
	2010	1.80	Ar	1.75×10^{-9}

Activity profiles similar to those shown in Fig. 15.6 have been reported for diffusion of U^{235}, U^{233}, Y^{91}, Zr^{95}, and Pm^{147} in pressed and sintered UO_2 specimens analyzed by sectioning.[10–12] Diffusion coefficients were calculated from the activity profiles in the last study[12] by approximating the data near the surface with a straight line. The method of surface activity decrease was used almost exclusively in the other two studies.[10,11] The diffusion coefficients obtained by either method are several orders of magnitude smaller than values obtained for Nb^{95} diffusion at comparable temperatures in the present work.

In this study, diffusion coefficients were not calculated from the initial portion of the activity profiles. Figure 15.7 clearly illustrates the

[10] A. B. Auskern and J. Belle, *J. Nucl. Mater.* **3**(3), 311 (1961).

[11] Roland Lindner and Franz Schmitz, *Z. Naturforsch.* **16**(a), 1373 (1961).

[12] Franz Schmitz and Roland Lindner, *Z. Naturforsch.* **16**(a), 1096 (1961).

curvature of the data, even near the surface of the specimen. In addition, the Fisher theory predicts that pure grain-boundary diffusion is characterized by a linear function of x, rather than x^2, as shown in Fig. 15.6, the second portion of the plots for pressed and sintered UO_2. The relatively high diffusion coefficients that were obtained and the fact that a large fraction of the total Nb^{95} activity was always found near the surface of the specimen suggest that grain boundaries or other structural defects were responsible for the linear portion of the activity profiles for both types of UO_2.

The possibility of an oxygen gradient influencing the penetration characteristics was studied by an experiment in which the lattice parameter of UO_2 as a function of distance from the surface of a diffusion specimen was determined by x-ray diffraction techniques.[13] The lattice parameter is sensitive to the oxygen-to-uranium ratio,[14] but only the lattice parameter corresponding to an oxygen-to-uranium ratio of 2.001 (5.4710 ± 0.0005 A) was found up to the limit of Nb^{95} penetration.

---

[13]Work performed by O. B. Cavin of the X-Ray Diffraction Group.

[14]W. A. Young *et al.*, *An X-Ray and Density Study of Nonstoichiometry in Uranium Oxides*, NAA-SR-6765 (Mar. 30, 1962).

16. Fuel Element Development

While the goals of the Fuel Element Development program remain the development of new fuel or cladding materials and the improvement in the performance of existing concepts, the actual program is changing. As in most fuel element programs, the emphasis is shifting to higher temperatures, although in some cases the term is relative, that is, aluminum elements at >400°F (204°C). This shift is most evident in the incorporation during the past year of a new program aimed at fabrication of refractory-metal fuel elements by vapor deposition techniques.

PYROLYTIC AND CHEMICAL VAPOR DECOMPOSITION STUDIES

R. L. Heestand C. F. Leitten, Jr.

A program has been initiated to study the deposition parameters and physical characteristics of refractory metals, fuels, and their compounds when synthesized by pyrolytic and chemical vapor decomposition techniques. The prime objective of this program is to investigate techniques for the direct fabrication of uranium compounds from the gaseous uranium halides and their subsequent cladding with refractory metals to achieve finished fuel element geometries. Perfecting of such a technique should result in very low fuel cycle costs.

An apparatus, shown in Fig. 16.1, was assembled so that deposition parameters of the various system components could be studied. The process consists of flowing a gas or mixture of gases over a resistance-heated mandrel at a given temperature, pressure, and flow rate to determine deposition parameters. The apparatus consists of a resistance-heated graphite mandrel as a deposition substrate, flowmeters for regulation of component gas flows, and a vacuum pump to maintain a negative system pressure. Table 16.1 lists the reactants used and compounds resulting from current investigations.

Initial investigations of deposition rates for pyrolytic graphite were made in order to predict carbon deposition rates for subsequent carbides. Variations in temperature and flow rates gave deposition rates which could be varied from 1 mil/hr at 1400°C to 23 mils/hr at 2000°C. Graphite samples were prepared under varying conditions and were turned over to the Ceramics Laboratory for use in the GCR program.

To evaluate the behavior of the system before operating with uranium hexafluoride, other metallic halides were studied. Hydrogen reduction of molybdenum pentachloride, tantalum pentachloride, and tungsten hexafluoride to the metals was carried out, and, since tungsten was of particular interest as a refractory-metal cladding, a more extensive examination of tungsten deposition was conducted.

Tungsten deposits were made over the range of 500 to 1100°C under partial vacuums of 10 to 20 mm with deposition rates varying from 1 to 40 mils/hr. Figure 16.2 shows the comparison of the microstructure of a tubular specimen deposited at 1000°C and a similar specimen deposited at 800°C. The specimen deposited at 1000°C shows a highly columnar grain structure, and x-ray diffraction patterns indicate a high degree of orientation; while the specimen deposited at 800°C shows a fine grain structure and a low degree of preferred orientation.

Deposition of tungsten has also been carried out inside copper tubes, both to give larger specimens of material and to prove the feasibility of fabricating such tubing as a containment material or diffusion barrier.

By use of a progressive hot-zone furnace, tubes of $\frac{3}{4}$ in. OD × 0.20 in. wall thickness × 14 in. long, such as shown in Fig. 16.3, have been fabricated. These experiments demonstrate the feasibility of fabricating lengths of tungsten tubing having a uniform wall thickness. Material balances indicate deposition efficiencies in excess of 90%.

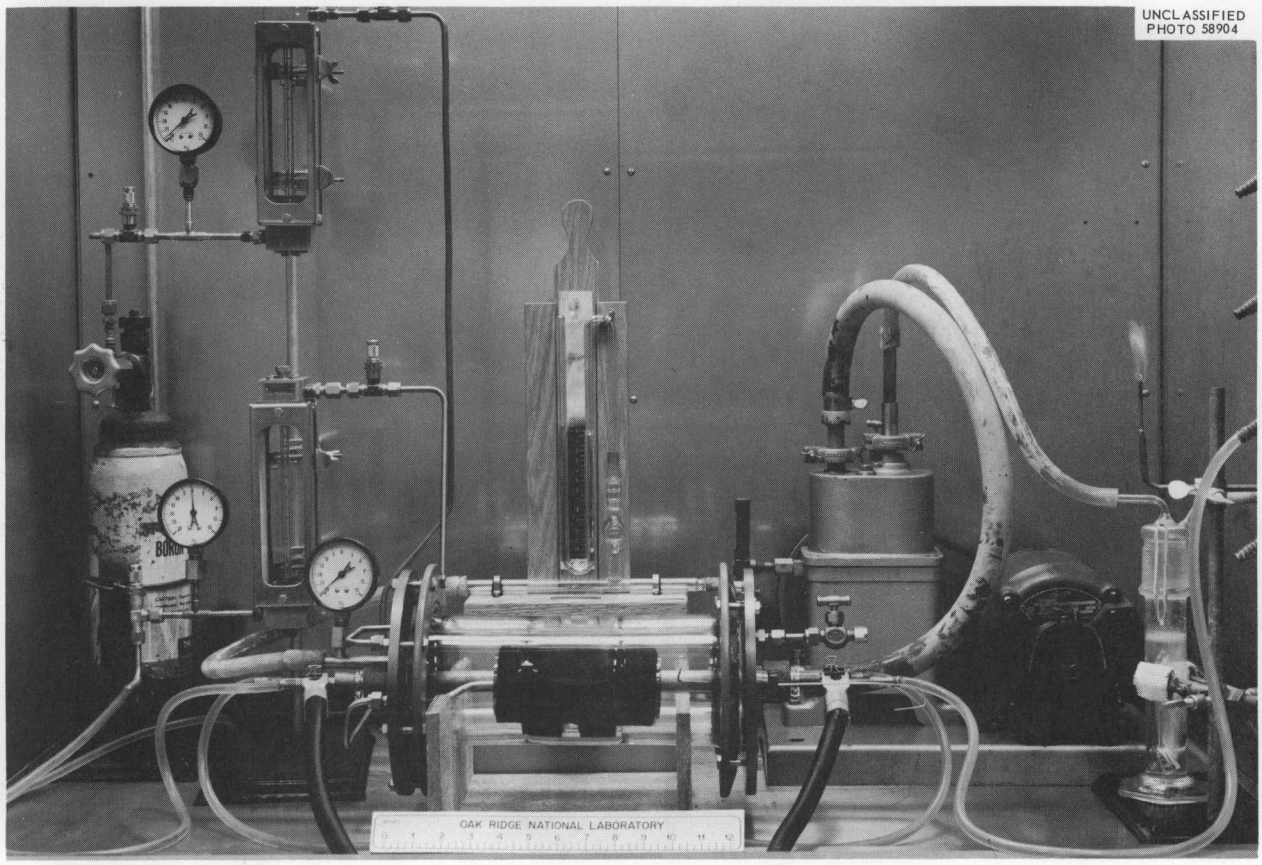

Fig. 16.1. Apparatus for Study of Deposition Parameters.

Table 16.1. Reactants and Pyrolytic Materials

Reactants	Temperature (°C)	System Pressure (torrs)	Resulting Deposits
$CH_4 + H_2$	1200–2000	10–20	Pyrolytic graphite
$CH_4 + WF_6 + H_2$	1900–2025	10–20	Ditungsten carbide
$WF_6 + H_2$	500–1100	5–20	Tungsten
$MoCl_5$[a] $+ H_2$	800–1000	10	Molybdenum
$TaCl_5$[a] $+ H_2$	900–1000	20	Tantalum
CH_4[a] $+ UF_6 + NH_3$			Possible UC_2-U_2N_3
$CH_4 + UF_6 + H_2$			UF_4

[a]Maximum and minimum deposition parameter limits have not been determined.

UNCLASSIFIED
PHOTO 60011

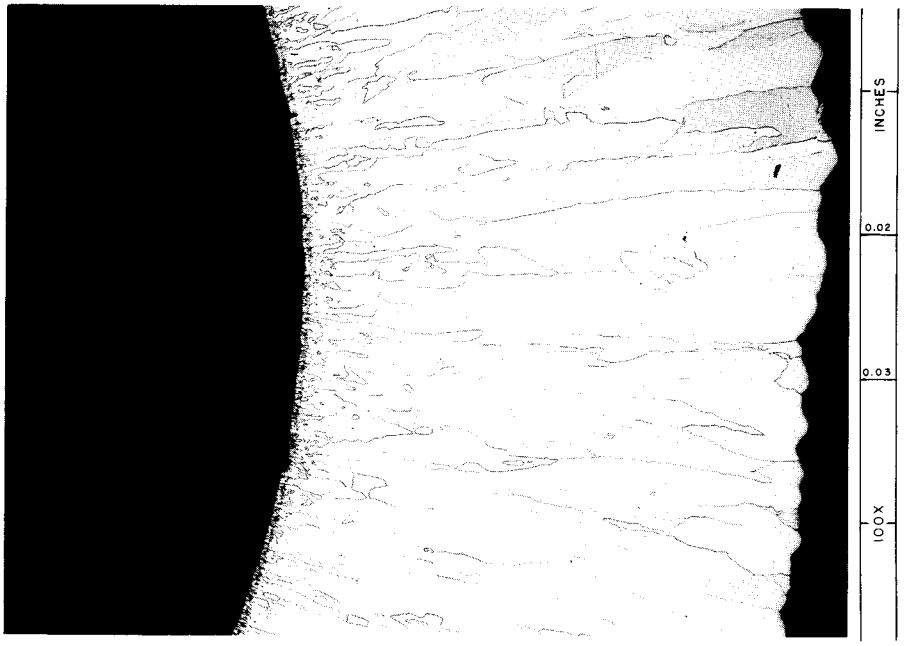

1000°C 0.040 in./hr Y-48192

800°C 0.016 in./hr Y-48191

ETCHED $NH_4OH + H_2O_2$

Fig. 16.2. Effect of Deposition Variables on the Structure of Pyrolytic Tungsten. Reduced 26.5%.

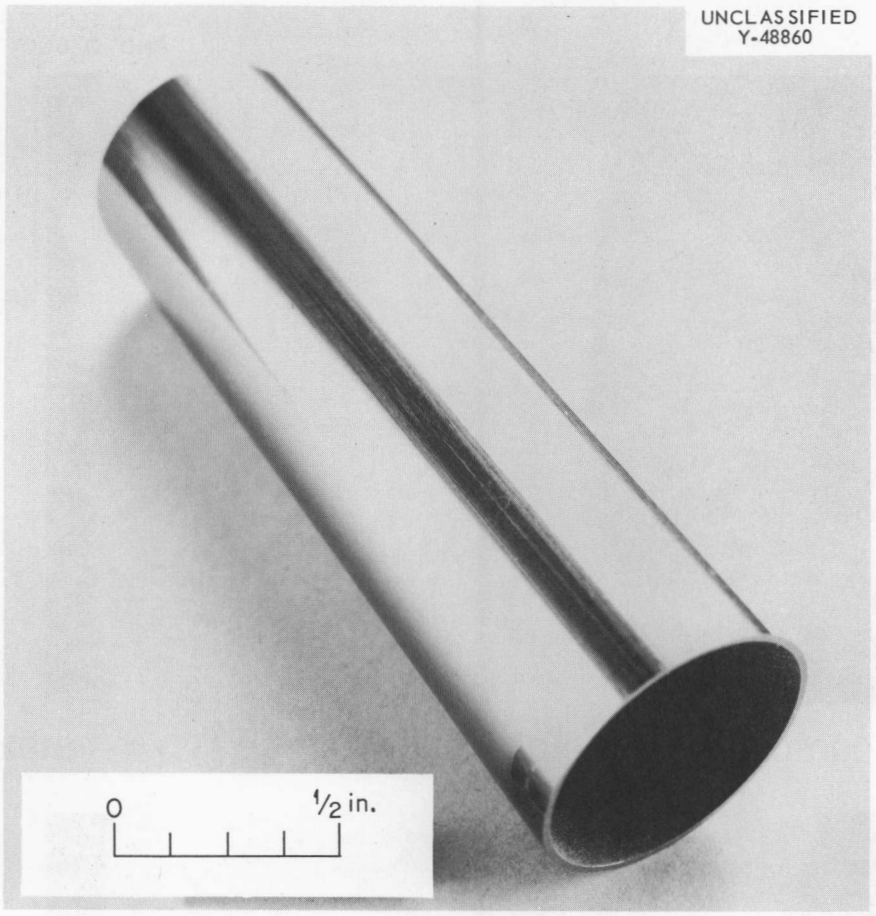

Fig. 16.3. Tungsten Tube, ¾ in. diam × 0.020 in. Wall Thickness × 14 in. Long, Deposited in Cold-Drawn Copper at 650°C. Deposition rate 4 mils/hr.

Tubes down to ½ in. diam × 0.002 in. wall thickness have been fabricated by these techniques. Other shapes would, of course, be applicable.

Early attempts to obtain uranium carbide by reduction of uranium hexafluoride with hydrogen in the presence of methane were unsuccessful due to the complete conversion of UF_6 to UF_4. Further studies of this reaction are being made using ammonia as a source of monatomic hydrogen. Deposits using this technique have been made; however, no positive identification of the uranium compounds has been made.

CERAMIC FUEL ELEMENT DEVELOPMENT

A. T. Chapman R. L. Hamner
R. E. Meadows

This program for developing an all-ceramic fuel element for use in advanced high-temperature gas-cooled reactors has continued with the development of fueled beryllium oxide elements. Emphasis has, however, been switched from UO_2 to the use of $(U,Th)O_2$ fuels. The fuel is still being incorporated as large (100 to 150 μ) particles in a BeO matrix. To minimize losses in uranium, which will

increase as the operating temperatures are increased, studies on loss mechanisms from UO_2 and on the phase relationships in the uranium-oxygen system have continued.

Fabrication Development

The substitution of $(U,Th)O_2$ for UO_2, as the fuel to be used in this program, has necessitated a review of the fabrication techniques previously developed.[1] Considerable differences are found in the physical properties of these two oxides.

A $(U,Th)O_2$ sol-gel product prepared by the ORNL Chemical Technology Division was selected as the most promising starting material for $(U,Th)O_2$ solid solution. This selection was based on a comparative evaluation made of $(U,Th)O_2$ mechanical mixtures of sinterable powders and $(U,Th)O_2$ powders derived from coprecipitation processes. The sol-gel product becomes essentially a homogeneous $(U,Th)O_2$ solid solution and attains a density of 98 to 99% of theoretical upon heating to 1100°C in air. It has a linear shrinkage from the as-dried state to the ultimate density of approximately 25%, which makes it compatible with the shrinkages of BeO matrices. Because of its hard, brittle nature, however, the sol-gel material could not be spheroidized by the air-tumbling process[1] developed for spheroidizing powder granules.

A technique was developed for spheroidizing the sol-gel products based on their characteristic solubility in water in the as-dried condition. The technique consists of drying the gel at 80°C, crushing the cake formed to yield granules of a given sieve-size fraction, moistening the granules with an alcohol-water mixture, then tumbling in a closed cylindrical container for approximately 16 hr. Spheroidizing is achieved by the tumbling action of the granules during a controlled solutioning action of the alcohol-water mixture on the granules.

By coating individual fuel particles followed by conventional cold-pressing and sintering techniques, a technique was developed to produce fueled BeO bodies containing discretely dispersed fuel particles. Coating of the particles was accomplished by saturating the particles with a liquid, preferably alcohol, then slowly adding dry, −140 mesh BeO powder to the moistened granules as they were tumbled in a rotating cylinder. By this process, BeO required for compositions up to 70 vol % can be applied rather uniformly and almost completely to the fuel particles as shown in Fig. 16.4. The type of dispersion obtained by cold-pressing and sintering BeO-coated $(U,Th)O_2$ spheroidal particles is shown in Fig. 16.5.

Irradiation Testing

In a joint program with the Gas-Cooled Reactor Project, specimens containing 30 vol % UO_2, prepared by conventional blending and cold-pressing and sintering techniques,[1] were irradiated at approximately 2100°F (1148°C) in a helium sweep-gas experiment in the ORR. The density of the specimens was 93% of theoretical. Fuel particle preparation consisted of spheroidization of granulated UO_2 powder by an air-tumbling technique followed by partial sintering for microstructural control. Initial values of release rate to birth rate for relatively long-lived fission gases – Kr^{87} (78 min) to Xe^{133} (5.3 days) – were high, being on the order of 10^{-3}.

A fueled BeO specimen containing 30 vol % spheroidal $(U,Th)O_2$ particles which was fabricated by coating the individual fuel particles with BeO powder prior to cold pressing, as described in the above, was evaluated by neutron activation. The fractional release of Xe^{133} from this specimen after irradiation at approximately 200°F for 5×10^{14} fissions was less than 1×10^{-6} during post-irradiation heating for 3 hr at 2000°F (1093°C) in hydrogen.

Phase Relations in the Uranium-Oxygen System

Studies in the uranium-oxygen system were continued with emphasis on the loss of uranium from UO_{2+x} as well as on the phase relations. A series of experiments were performed that confirmed the preliminary results reported last year,[2] which indicated that during the reduction in vacuum of

[1] R. L. Hamner, *Metals and Ceramics Div. Ann. Progr. Rept. May 31, 1962*, ORNL-3313, p 68.

[2] A. T. Chapman and R. E. Meadows, *Metals and Ceramics Div. Ann. Progr. Rept. May 31, 1962*, ORNL-3313, p 69.

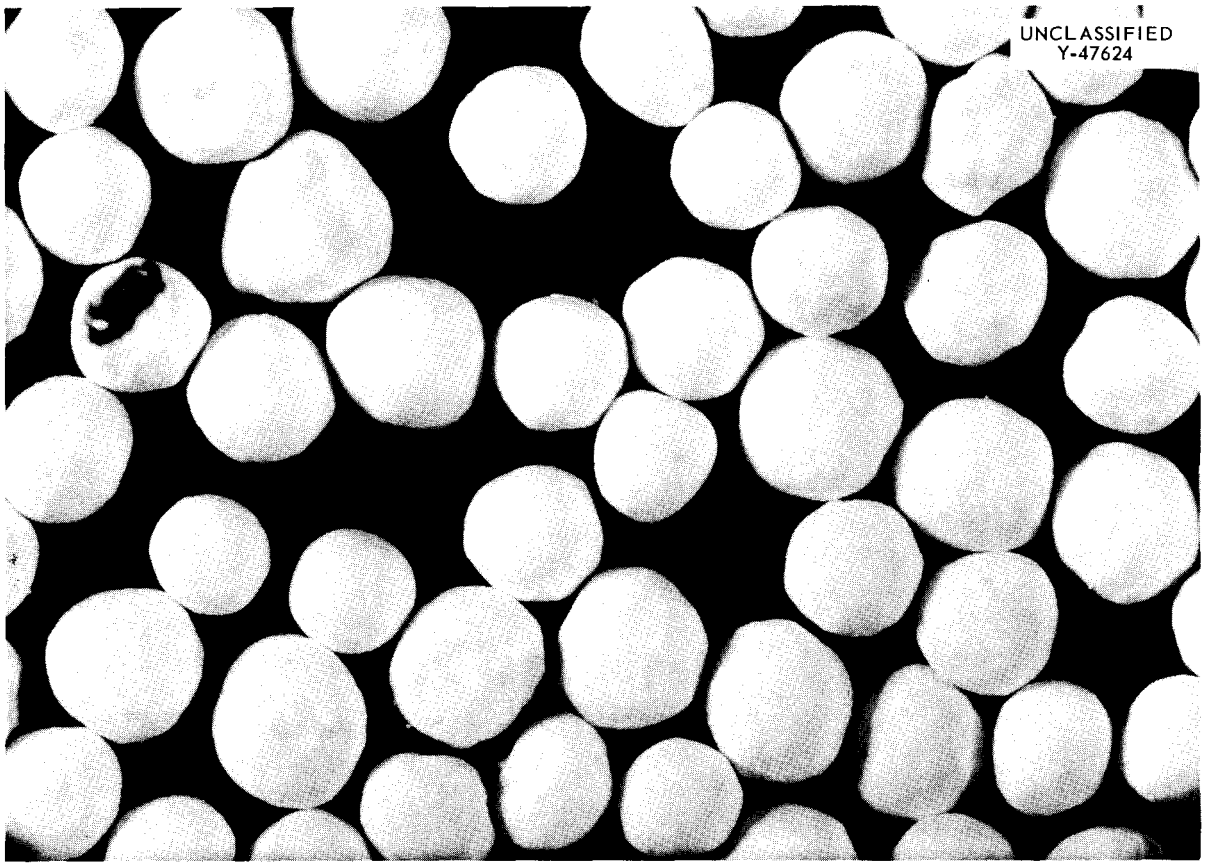

Fig. 16.4. Spheroidal Particles of UO_2 Coated with BeO Powder. 35X.

UO_{2+x} $(0.02 > x > 0.00)$ to the equilibrium composition of $UO_{2.00}$, a volatile material with a composite O/U ratio of 4 is produced. The experiments reported previously did not provide positive identification of the vapor-phase components.

The thermogravimetric behavior of UO_{2+x} in a controlled oxygen pressure is presented schematically in Fig. 16.6. This figure indicates that, after an initial oxidation of $UO_{2.00}$ to the equilibrium O/U ratio, there is a continual loss of material from UO_{2+x} which occurs at essentially a constant rate. During this process, the O/U ratio of the residual material remains constant. This reaction may be described as

$$UO_{2+x}(s) + z\,\frac{(2-x)}{2}\,O_2(g) \rightarrow zUO_4(g) + (1-z)UO_{2+x}(s)\ . \quad (1)$$

The choice of $UO_4(g)$ as the volatile uranium species rather than a combination of $UO_3(g)$ and $\frac{1}{2}\,O_2(g)$ is based on (1) the constancy of O/U ratio of the volatile component from materials of varying starting O/U ratios; (2) the effect of temperature on the reaction; (3) effusion cell data; and (4) some limited mass spectrographic information. Experiments at 1800 to 2000°C indicate that reaction (1) is responsible for the volatilization of uranium from $UO_{2.00}$ even in the very low oxygen pressures associated with system pressures of 10^{-5} to 10^{-6} torr.

During the course of this study the composition of the equilibrated (solid) oxide phase was determined as a function of oxygen pressure. These results are presented in Fig. 16.7. It is to be noted that the isocomposition lines representing O/U ratios below 2.15 are based on a minimum of experimental evidence. The line corresponding to

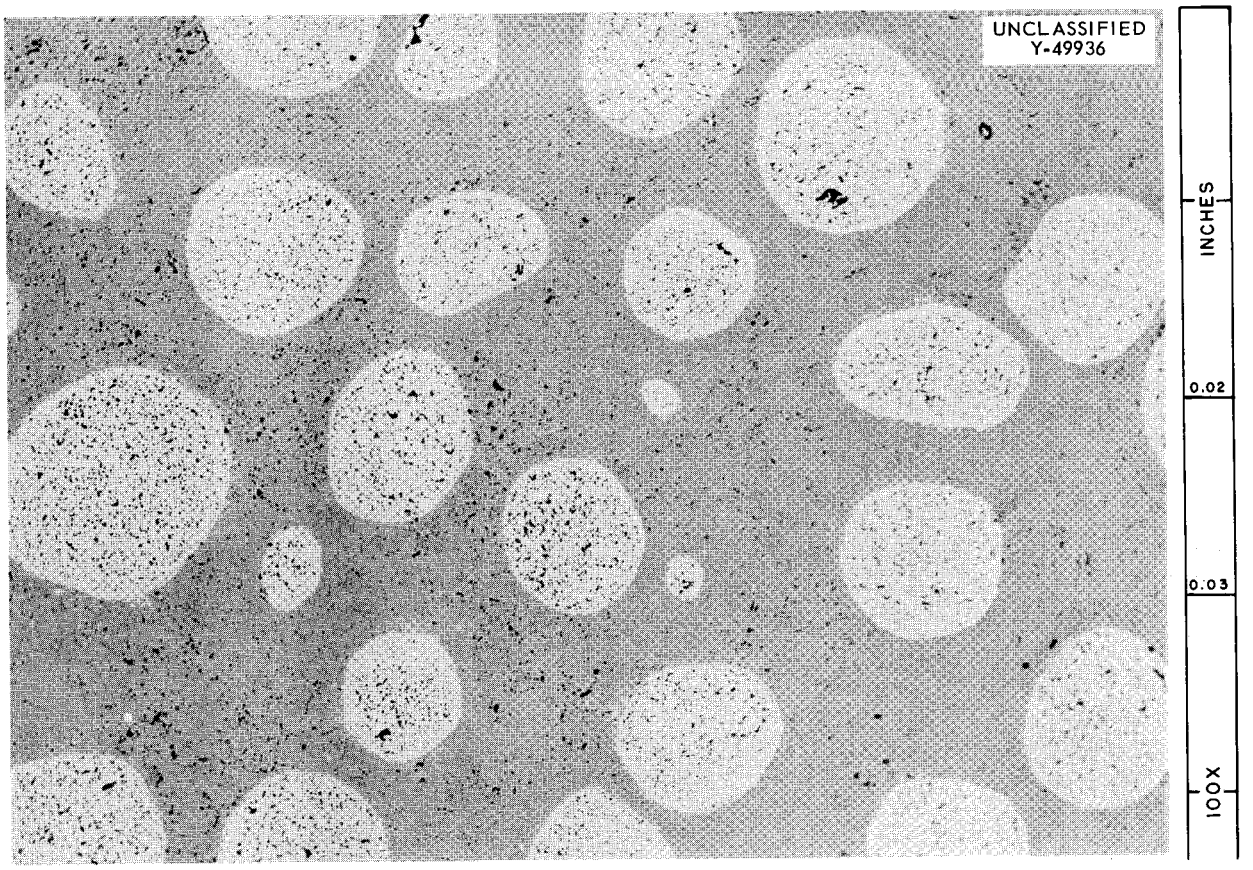

Fig. 16.5. Polished Section of 150 to 250 μ $(U,Th)O_2$ Particles (Light Phase) Dispersed in a BeO Matrix (Dark Phase). As polished. 100X.

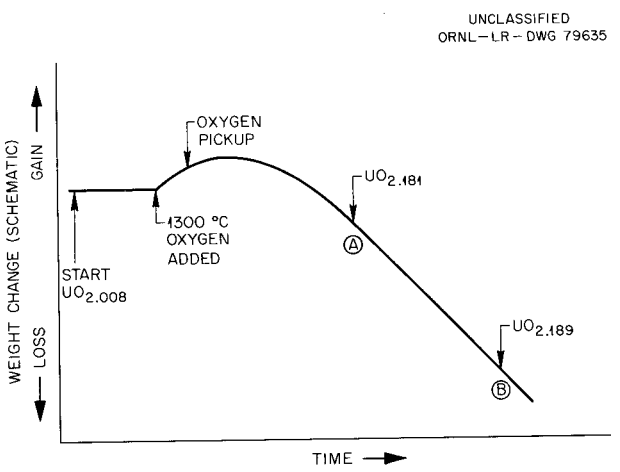

Fig. 16.6. Thermogravimetric Behavior of UO_{2+x} Heated to 1300°C in an Oxygen Pressure of 0.10 mm Hg.

the coexistence of UO_{2+x} and U_3O_{8-y} may be expressed analytically as

$$\log p_{O_2}\,(\text{atm}) = \frac{-18{,}050}{T(^\circ\text{K})} + 9.110\ .$$

The data upon which Fig. 16.7 is based were determined under conditions where the volatile phase was continually removed from the sample site and condensed in cooler regions of the furnace. This diagram is valid, therefore, only under conditions where the pressure of $UO_4(g)$ is low.

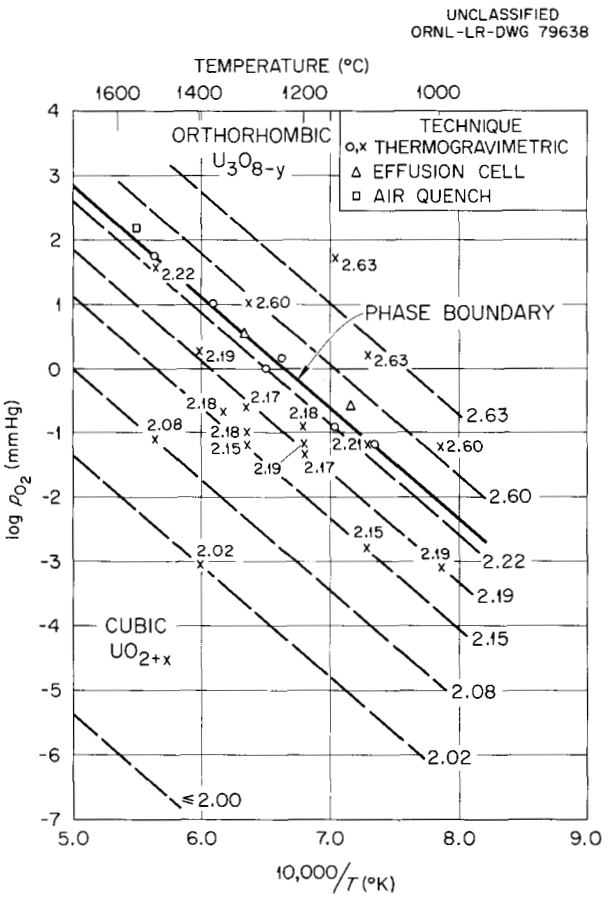

Fig. 16.7. The Relation of Oxygen Pressure and Temperature to Compositions Between $UO_{2.00}$ and $UO_{2.67}$ in the Uranium-Oxygen System.

FABRICATION OF URANIUM CARBIDE USING A VOLATILE SINTERING-TEMPERATURE DEPRESSANT

J. P. Hammond

Uranium carbide continues to show promise as a fuel for power and space reactors and especially for the thermionic systems. However, its fabrication looms as a serious problem since, to achieve acceptable densities, sintering temperatures in the range of 1800 to 2000°C are required. At such temperatures, uranium is usually lost by volatilization resulting in an undesirable hyperstoichiometric microstructure. A process has been developed on a pilot basis for fabricating dense high-quality uranium carbide at low temperatures of 1350 to 1400°C. Whereas the method uses UAl_2 as a fabrication aid, it is eliminated as a result of sintering in a 10^{-6} to 10^{-7} torr vacuum, giving an essentially all-uranium monocarbide structure. The basic principles of the technique were described previously.[3]

Using the general techniques previously developed, but with close control to avoid any surface contamination of the powders, has resulted in large improvements in final density. Table 16.2 gives recent results for the UC(4.8C)–7½ wt % UAl_2 system, while Fig. 16.8 shows a representative microstructure. The theoretical densities ranged from 97.1 to 98.5%, showing a considerable improvement over those reported previously.

As shown in the table, the starting material came from several castings and the pellets were fired in several different batches, indicating the procedure is capable of yielding consistent results.

Aluminum removal during vacuum sintering, as reflected by the low aluminum contents reported (Table 16.2) and the absence of any appreciable secondary constituent in the microstructure (Fig. 16.8), was effective for each of the firing schedules attempted and for both the 7- and 13-g pellet sizes. The aluminum contents reported correspond to removal of from 97 to 99% of the initial aluminum.

The data indicate that the starting carbide material is very low in oxygen and nitrogen. Milling for 48 hr followed by exposure in the argon-filled vacuum dry box results in substantial increase in the amounts of these contaminants with no large additional increases during firings. While no analyses were made, it is thought that even larger increases must have occurred in the previous samples that sintered to the lower densities. Although the carbon analyses given in the table are judged accurate to only about ±0.12%, the control of carbon in the cast material is probably accurate to ±0.03%.[4]

---

[3] J. P. Hammond and J. D. Sease, *Metals and Ceramics Div. Ann. Progr. Rept. May 31, 1962*, ORNL-3313, p 94.

[4] D. T. Bourgette, *Preparation of Stoichiometric Uranium Monocarbide Cylinders*, ORNL TM-309 (Oct. 4, 1962).

The factors shown to have the greatest effect upon fabrication results in terms of both density and aluminum removal were quality of the starting materials used and the extent of contaminant pick-up in processing. Carbon in the starting uranium monocarbide should be held close to the stoichiometric amount (4.8 ± approximately 0.05 wt %) and the oxygen and nitrogen kept as low as practicable.

Table 16.2. Fabrication Results on the UC(4.8C)–7½ wt % UAl_2 System[a]

Pellet No.	Order of Firing	Casting No.	Pellet Weight (g)	Firing Procedure (hr)	Firing Procedure (°C)	Fired Density (% theo)	Chemical Analysis (wt %) Al	C	O_2	N_2	Phases Present (by x ray)
109	1	C-67	6	3	1350	97.1					
110	1	C-67	6	3	1350	97.1	0.050	4.59[b]			All UC[c]
115	2	C-67	6	3	1350	97.5					
116	2	C-67	6	3	1350	97.5					
113	2	C-68	6	3	1350	97.9					
114	2	C-68	6	3	1350	98.5					
137	3	C-73	6	3	1400	98.2	0.017	4.60[b]	0.14	0.0047	All UC
138	3	C-73	6	3	1400	98.2					
139	4	C-73	13	3	1350	98.0					
140	4	C-73	13	3	1350	97.8					
135	3	C-73	13	3	1400	98.2	0.034	4.56[b]			All UC
136	3	C-73	13	3	1400	98.2					
141	5	C-72	13	3	1400+	97.8	0.054	4.58	0.22	0.0097	
				1	1500						
142	5	C-72	13	3	1400+	97.8					
				1	1500						
143	5	C-72	13	3	1400+	97.2					
				1	1500						
(Analyses on two of the carbide starting materials)											
(As-cast)		C-73						4.70	0.0005	0.0005	
(Powder)		C-73						4.85	0.099	0.0045	
(As-cast)		C-72						4.77	0.0071	0.0028	
(Powder)		C-72							0.23	0.011	

[a]Powder milled 48 hr, pressed as ½-in.-diam pellets at 25 tsi, and sintered at temperature in vacuum (10^{-6} to 10^{-7} torr).

[b]Average of two determinations.

[c]Lattice parameter = 4.956 A compared to 4.961 A for pure UC.

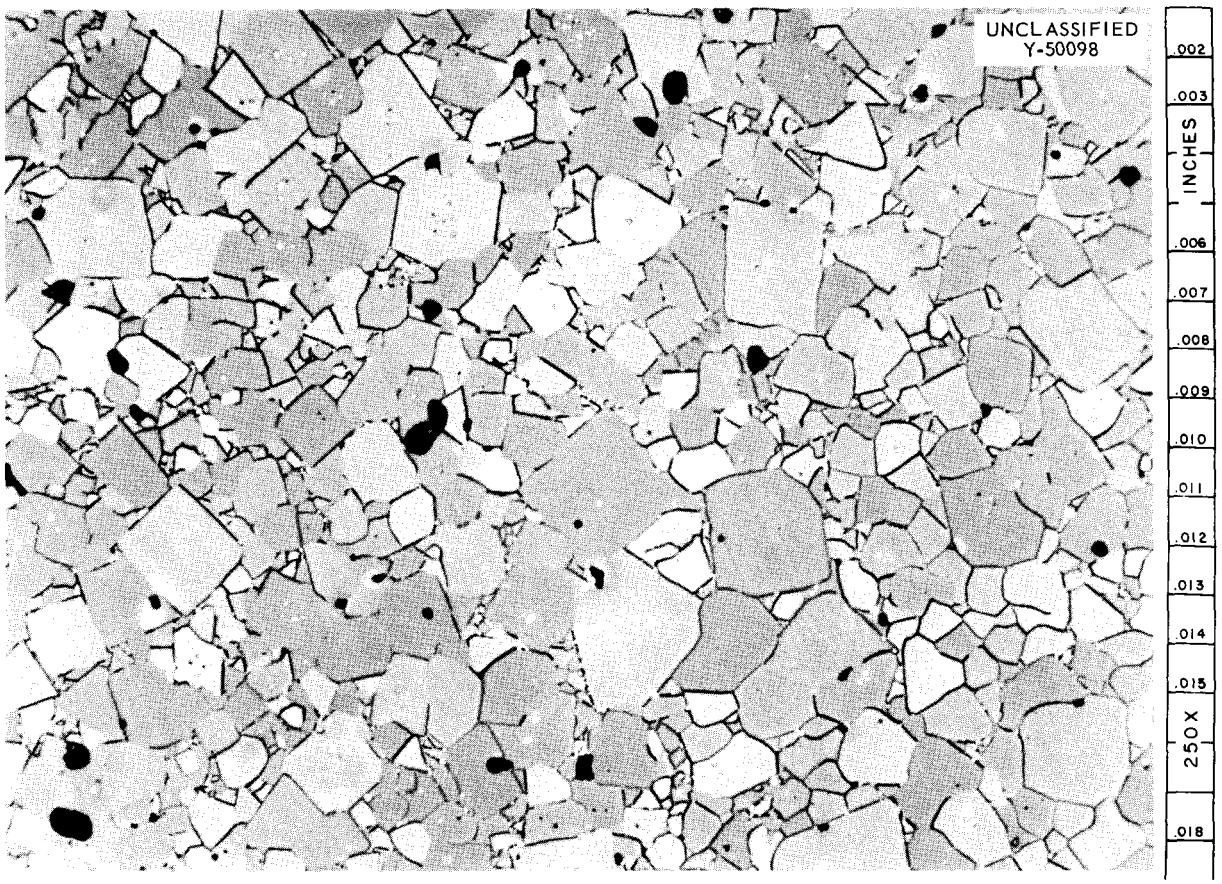

Fig. 16.8. Dense UC Structure Obtainable with UAl_2 Additive. Pellet No. 138 in Table 16.2; density is 98.2. Etchant: 30 HNO_3–30 H_2O–30 acetic.

CERAMIC BRAZING

C. W. Fox G. M. Slaughter

A program to develop suitable procedures for brazing ceramic materials is continuing.[5] The lack of procedures capable of making joints suitable for high-temperature use, and especially joints suitable for reactor use, has been a detriment to the fabrication of all-ceramic fuel elements. Heat transfer in more conventional fuel elements could also be improved by bonding the fuel to the cladding. A report describing the results of preliminary studies, together with a discussion of the unique test assemblies that have been constructed, has been issued.[6]

Phases of this program directly related to fuel element development include the brazing of uranium dioxide and beryllium oxide. Brazing alloys tested included those developed at ORNL as well as promising material developed at other installations. The results of wetting studies on these ceramics are presented in Table 16.3. It is evident that beryllium oxide is somewhat more difficult to wet than UO_2.

The more promising alloys were used for additional studies which consisted of preparing brazed joints of UO_2 to other materials (i.e., niobium, zirconium, aluminum oxide, etc.). Although adequate bonding occurred in most of the joints tested, some cracking in the UO_2 resulted, probably as a result of differential expansion. Additional work

[5]C. W. Fox, *Metals and Ceramics Div. Ann. Progr. Rept. May 31, 1962*, ORNL-3313, pp 120–21.

[6]C. W. Fox, *Progress Report – Brazing of Ceramics*, ORNL TM-413 (Nov. 8, 1962).

Table 16.3. Results of Wettability Tests of Brazing Alloys on UO_2 and BeO

Brazing Alloy (wt %)	Flow Point (°C)	Remarks
		UO_2
49Ti–49Cu–2Be	1000	Good wetting and flow; no cracking of UO_2
68Ti–28Ag–4Be	1100	Fair wetting and flow; no cracking of UO_2
75Zr–23Cu–2Be	1150	Poor wetting and flow; UO_2 cracked
95Zr–5Be	1060	Good wetting and flow; no cracking of UO_2
48Ti–48Zr–4Be	1050	No wetting or flow
46Ti–46Pd–6Al–2Be	1150	Poor wetting and flow
82Zr–6Ni–6Cr–6Fe[a]	1150	Good wetting and flow; no cracking of UO_2
Ni-clad Ti[b]	1050	Good wetting and flow
		BeO
49Ti–49Cu–2Be	1000	Good wetting and flow
68Ti–28Ag–4Be	1100	Fair wetting and flow
95Zr–5Be	1060	No wetting or flow
48Ti–48Zr–4Be	1050	No wetting or flow
82Zr–6Ni–6Cr–6Fe	1150	No wetting or flow
Ni-clad Ti	1050	Excellent wetting and flow
Nicrobraz 10 (Ni-P)	1020	No wetting or flow

[a]British patent 890,971.
[b]Commercial alloy; Little Falls Alloys, Inc.

is being performed with UO_2 of a higher density to determine if this cracking can be prevented or minimized.

ALUMINUM FUEL ELEMENT TECHNOLOGY

Aluminum-Base Fuel Plates

J. H. Erwin M. M. Martin
C. F. Leitten, Jr.

In recent years, studies have been conducted for the purpose of understanding the effects of various fabrication parameters on the quality of high-strength aluminum-base fuel plates and on their subsequent formability and reactor performance. This program has proved beneficial to the development of high-quality fuel components for application in high-flux, high-performance research reactors. During the past year, the major efforts on aluminum plate fabrication have been aimed directly at and, more, supported by the HFIR and ATR projects and have been covered in Part III, Chaps. 22 and 25 respectively.

Emphasis in this program was placed on studying the effects of hot-rolling temperature and cold reduction on the blistering tendency in type 6061 aluminum-clad fuel plates and on the subsequent forming characteristics of the plates. Previous work[7,8] has shown that the problems encountered

[7]M. M. Martin, J. H. Erwin, and C. F. Leitten, Jr., "Fabrication Development of the Involute-Shaped High Flux Isotope Reactor Fuel Plates," pp 268–89 in *Research Reactor Fuel Element Conference, September 17–19, 1962, Gatlinburg, Tennessee*, TID-7642, Book 1 (1963).

[8]M. M. Martin *et al.*, *Metals and Ceramics Div. Ann. Progr. Rept. May 31, 1962*, ORNL-3313, pp 83–86.

in forming high-strength aluminum-clad plates to close tolerances related to the quality of the plate, in particular to the thickness and microstructural variations encountered in the roll-bonding process. Metallographic and x-ray diffraction analyses on fuel plates fabricated by the best techniques available revealed that, after thermal treatment, gross differences in texture and grain size existed along the length of the plates. The shaping of these plates resulted in nonreproducible plate curvatures, and thus, when working to close tolerances, a relatively high rejection rate (approximately 50%). Conversely, commercial type 6061 aluminum of uniform grain size reproducibly formed within the close tolerances.

Since the hot-rolling temperature and degree of cold reduction affect the grain size in heat-treated type 6061 aluminum, both of these parameters were felt worthy of further investigation. To more nearly duplicate the conditions to be encountered in forming fuel plates, compacts were assembled and fabricated with typical reduction schedules. These compacts consisted of Alclad 6061 covers on Alclad 6061 centers. Twenty unfueled compacts of type 6061-F aluminum were hot rolled in the range 400 to 500°C and subsequently were cold reduced 7.4, 19.4, and 31.5%. A summary of typical data obtained from two representative lines after marforming these various plates is shown in Table 16.4. As indicated in the table, all plates were heat treated at 500°C and furnace cooled prior to forming at a constant pressure of 1600 psi with an available 3.875-in. involute-shaped HFIR die. It is apparent in Table 16.4 that the formability of the plates can be improved by either decreasing the hot-rolling temperature or increasing the percentage of cold reduction. In general, the formability of type 6061-O aluminum was found to

Table 16.4. Formability of Type 6061-O Composite Plates as a Function of Hot-Rolling Temperature and Percent Cold Reduction

Plate Treatment[a]	No. of Plates	R = 2.731 in.			R = 3.563 in.			Percentage Rejection from Blistering
		Max Spread in Readings	Average Spread	Variance S	Max Spread in Readings	Average Spread	Variance S	
Commercial plate								
6061 annealed	20	10	9.1	2.75	8	5.9	1.50	<5
Hot rolled at 400°C								
7.4% cold reduction	18	14	11.4	3.00	9	7.6	2.17	32
19.35% cold reduction	19	5	4.0	1.16	3	2.3	0.69	
31.5% cold reduction	19	6	4.9	1.51	4	2.4	0.83	
Hot rolled at 450°C								
7.4% cold reduction	19	12	7.0	2.03	7	4.9	1.41	15
19.35% cold reduction	19	9	6.4	2.00	5	4.0	1.22	
31.5% cold reduction	19	5	3.1	0.97	4	2.3	0.70	
Hot rolled at 500°C								
7.4% cold reduction	18	22	19.3	5.66	15	13.1	3.71	5
19.35% cold reduction	19	10	7.9	1.85	7	5.3	1.40	
31.5% cold reduction	19	7	5.3	1.77	4	2.6	0.85	

[a]All plates heat treated 500°C and furnace cooled after cold rolling; plates were formed with a 3.875-in. involute die at 1600 psi.

be best at the 450°C temperature and at cold reductions greater than 7.4%.

Although the formability of type 6061-O aluminum was shown to improve at the lower hot-rolling temperatures, the blistering tendency of the composites was observed to increase as the hot-rolling temperature decreased. As indicated in Table 16.4, a 32% blister rejection rate was observed in plates fabricated at 400°C as compared to only 5% in plates roll clad at 500°C. The majority of blisters noted in these plates were of the nonbond type, since they appeared in the clad-frame interface. Metallographic examination of the plates verified this observation. Metallurgical bonding was not achieved in plates fabricated at 400°C, as manifested by the discontinuous nature of the interfacial grain growth at the clad-frame boundaries. Continuous grain growth was noted in the plates fabricated at 500°C. However, it must be kept in mind that last year it was shown that a marked change in the nature of the oxide and a corresponding large increase in blistering occurs at temperatures slightly above 500°C. Work is now in progress in an effort to correlate the fabrication practices used with plate texture and grain size and with the mechanical properties.

The preliminary results obtained in this study were subsequently used in fabricating plates for both the HFIR and ATR fuel elements. The plates were hot rolled at 500°C to minimize blistering and were cold reduced 20% to improve formability. The subsequent marforming of these plates resulted in reproducible fuel plate curvatures with yields in excess of 95%.

Chemical Compatibility Studies on the UO_2- and U_3O_8- Aluminum Systems

C. F. Leitten, Jr. T. S. Lundy

For the past several years the chemical compatibility of the UO_2- and U_3O_8-aluminum systems has been under study. These studies have encompassed the effects of temperature, time, oxide preparation, sample preparation, and heat-treating atmosphere. However, interpretation of the test results has been difficult because of the interdependency of these variables.

Recent studies have suggested that other factors not initially considered could have a pronounced effect on the test results. The presence of trace amounts of the stearic acid–CCl_4 lubricant used in compacting these initial dispersions was found to promote reaction of either UO_2 or U_3O_8 with aluminum. Refined studies indicate that it is the presence of chloride in the compact that accelerates the reaction. Such chloride-bearing lubricants have been widely used in the powder metallurgy compaction of aluminum-base dispersions. It thus appears that precautions should be taken to minimize the presence of chloride in these types of compatibility studies.

Irradiation Testing of Aluminum-Base Fuel Dispersions of UAl, U_3O_8, and UC_2 in Aluminum-Clad Plates

C. F. Leitten, Jr. A. E. Richt
R. J. Beaver

The evaluation[9] of irradiation effects in aluminum-clad dispersions of 64 wt % UAl_3, 63 wt % U_3O_8, and 60 wt % UC_2 in aluminum was completed. Examination of samples irradiated to the maximum burnup confirmed the previous results obtained from samples with less burnup.[10] In summary, these studies showed that high-uranium-investment fuels containing U_3O_8 and UAl_3 dispersions in aluminum should perform reliably in low-temperature research reactors. The dimensional stability of both fuel systems under irradiation is considered acceptable even after burnup exceeding 7.5×10^{20} fissions/cc (84% U^{235} depletion). Reactions were noted between the fissile compound and the aluminum matrix in both fuel systems; however, they did not appear to cause adverse effects on the dimensional stability of the aluminum-clad fuel plates. Thermal treatment of samples irradiated to

[9] A. E. Richt, C. F. Leitten, Jr., and R. J. Beaver, "Radiation Performance and Induced Transformation in Aluminum-Base Fuels," pp 469–88 in *Research Reactor Fuel Element Conference, September 17–19, 1962, Gatlinburg, Tennessee*, TID-7642, Book 2 (1963).

[10] C. F. Leitten, Jr., *Metals and Ceramics Div. Ann. Progr. Rept. May 31, 1962*, ORNL-3313, p 80.

approximately 60% U^{235} burnup resulted in no evidence of blistering or gross swelling in either fuel material even after 24 hr at 1000°F (538°C).

Although a volume increase was noted in the UC_2-aluminum specimens after irradiation, the high impurity content observed in the specimens is suspected as the cause of the poor performance of this material. Metallographic examination of the specimens after irradiation strongly indicated that the UC_2, per se, when dispersed in an aluminum matrix, is capable of high burnup with no unusual irradiation damage effects.

17. Mechanical Properties Research

INFLUENCE OF HYDROGEN ON THE HIGH-TEMPERATURE CREEP PROPERTIES OF METALS

H. E. McCoy, Jr.

Previous reports[1-3] have related the fact that the creep properties of several nickel-base alloys are inferior in a hydrogen environment as compared with those observed in an argon environment. The important characteristics of this environmental effect are that (1) the influence of hydrogen is manifested through an increase in the secondary creep rate and a decrease in the time for the initiation of tertiary creep, (2) the magnitude of the effect becomes greater as the strain rate decreases, and (3) the rupture ductility is not significantly altered. Recent studies have been directed toward learning more about the mechanism whereby hydrogen influences the deformation behavior.

It was pointed out previously[1] that Inconel, "A" nickel, and several binary alloys containing various amounts of iron, nickel, and chromium are deleteriously influenced by hydrogen. Several other materials have been tested in argon and hydrogen environments during the past year to determine how universal the hydrogen influence is. The results of tests on polycrystalline copper of 99.999+% purity showed that the rupture life of this material is much less in hydrogen than in argon. Again, the general features listed in the first paragraph were apparent. High-purity electron-beam zone-refined nickel was tested both as single crystals and in the cold-worked and recrystallized state. It was found that this material was also adversely influenced by hydrogen. Type 304 stainless steel and Armco iron have been evaluated under several sets of test conditions and appear to have equivalent creep properties in argon and in hydrogen.

Several nickel specimens have been tested under conditions where the test environment was periodically cycled between argon and hydrogen. It was found that, following a period of about 50 hr after the environment was changed, the material assumed a creep rate characteristic of the particular environment.

Although it was previously postulated that the role of hydrogen was to decrease the surface energy of nickel and hence increase the growth rate of voids during creep, observations during the past year have caused doubt as to this being the rate-controlling mechanism. Specimens of the electron-beam zone-refined nickel, which were found to exhibit markedly lower creep resistance in hydrogen than in argon, were found not to contain voids after having undergone as much as 20% strain.

Electron-transmission-microscopy studies, conducted under the direction of J. O. Stiegler of the Metallography Group, have shed much light upon what the actual role of hydrogen is in metals. High-temperature creep tests were run using thin nickel strips (3 × 0.060 × 0.0015 in.). These tests were carried out in an analytical balance in which the environment could be controlled. The foil specimens were subsequently thinned and examined in the electron microscope. It was found that the specimens tested in hydrogen contained only a few isolated dislocations, all of which moved readily under the influence of the electron beam. The dislocation density was considerably higher in the foils tested in an argon

---

[1] H. E. McCoy, W. R. Martin, and R. L. Stephenson, *Met. Div. Ann. Progr. Rept. May 31, 1961,* ORNL-3160, pp 86–90.

[2] H. E. McCoy, *Metals and Ceramics Div. Ann. Progr. Rept. May 31, 1962,* ORNL-3313, pp 40–42.

[3] H. E. McCoy, "Influence of Various Gaseous Environments on the Creep-Rupture Properties of Nuclear Materials Selected for High-Temperature Service," pp 263–96 in *Conference on Corrosion of Reactor Materials, June 4–8, 1962, Proceedings,* vol I, International Atomic Energy Agency, Vienna, 1962.

environment than in those tested in hydrogen. Dislocation tangles were present, and it was found that the dislocations could not be made to move in these specimens. A further observation was that, if the specimens tested in hydrogen were annealed at 200°C in vacuum to remove the hydrogen, the dislocations became immobile under the electron beam.

Although several questions remain unanswered, the present indication is that the presence of hydrogen inhibits dislocation–impurity-atom interactions. The observations that the dislocations in the specimens tested in hydrogen are rendered immobile by removing the hydrogen and that the hydrogen effect is cyclic discount the possibility of impurities being removed from the metal by the hydrogen. Rather, it seems that impurities already present are being redistributed so that they effectively pin the dislocations when argon is present but not when hydrogen is present. It may be that the hydrogen atoms form clusters around the impurity atoms and keep them from being drawn into the stress fields of the dislocations. Another possibility is that the hydrogen atoms may, as a result of their mobility, occupy all the available sites along the dislocations. This would reduce the degree of misfit between the dislocation and the lattice, and the stress field of the dislocations would become less. Hence the interactions between impurity atoms and dislocations would become less effective. Work is continuing in an effort to pinpoint the exact mechanism.

SOME METALLURGICAL PARAMETERS AFFECTING CREEP DUCTILITY OF TYPE 304 STAINLESS STEEL

W. R. Martin

The ductility of reactor-fuel cladding materials has recently become more important than in the past because of the design of fuel elements having very thin cladding. One of the present criteria for the fuel element is that the cladding material must undergo plastic deformations without fracturing. It is therefore desirable to optimize the creep ductility of the cladding material prior to its use in the fuel element. Two material conditions affecting the creep ductility are cold work and the method of melting. The present investigation is concerned with the magnitude of the effect of these variables.

Table 17.1 shows that creep ductility at 815°C, as measured by the total elongation, is greatly reduced by cold rolling. Table 17.2 demonstrates that the method of prestraining apparently does not alter the creep ductility. The total elongation for a given rupture time appears to be the same, regardless of the method of prestraining.

The creep testing of single-vacuum consumable-electrode melted type 304 stainless steel in uniaxial tension at 815°C indicates that the ductility of the vacuum-melted material is 20 to 25% greater than that of the air-melted material. However, the

Table 17.1. Comparison of Stress Rupture and Creep Ductility at 815°C of Cold-Worked and Annealed Type 304 Stainless Steel in an Argon Environment

Stress (psi)	Rupture Time (hr)		Total Elongation (%)	
	Annealed[a]	Cold Worked[b]	Annealed[a]	Cold Worked[b]
7000	98	191	20.3	7.0
6000	177	330	23.4	4.7
5500	326	529	17.2	3.9
4000	1634	1390	15.6	3.0
3500	3353	1900	10.9	5.3

[a]Annealed 1 hr at 1900°F (1030°C) in H_2.
[b]Cold work: 5% by cold rolling.

Table 17.2. Stress Rupture and Creep Ductility at 815°C of Air-Melted Type 304 Stainless Steel as a Function of Room-Temperature Prestrain

Prestrain (%)	Stress – 7000 psi		Stress – 4000 psi	
	Time to Rupture (hr)	Total Elongation (%)	Time to Rupture (hr)	Total Elongation (%)
0	98	20.3	1634	15.6
5	134	12.1	1227.2	2.75
10	161	4.7		
20	221	1.6		

stress necessary to cause rupture in 1000 hr at 815°C for a vacuum-melted heat is 65 to 80% of that required for air-melted heats.

EFFECT OF CHROMIUM ON THE CARBURIZATION OF Cr-Ni-Fe ALLOYS IN CO_2

W. R. Martin

Compatibility problems of stainless steels with gaseous environments have been investigated at ORNL and at several other laboratories during the past several years. This work has revealed that some stainless steels, type 304 stainless steel in particular,[4] are carburized when exposed at elevated temperature to CO_2. However, iron is decarburized when exposed to similar conditions, and some other stainless steels exposed to CO_2 are not carburized. The current program is to investigate what alloying constituents or combination of alloying constituents are necessary to cause carburization of iron-base alloys. Preliminary studies[5] indicated that the chromium content was related to the carburization phenomenon. Studies were made of the carburization in CO_2 of iron alloys containing 1 to 10 wt % Cr, and the degree of carburization increased with increasing chromium. These studies have been expanded to include a wider range of chromium content. Laboratory heats have been prepared for iron-base alloys containing 7 to 28% Cr and 8 to 10.7% Ni.

The temperature dependence of the carburization of these alloys is given in Fig. 17.1, and the effect of time at temperature is demonstrated in Fig. 17.2. The alloys increased in carbon content with increasing time at temperature. The magnitude of the carburization as a function of chromium content is seen to exhibit a maximum at about 11% Cr.

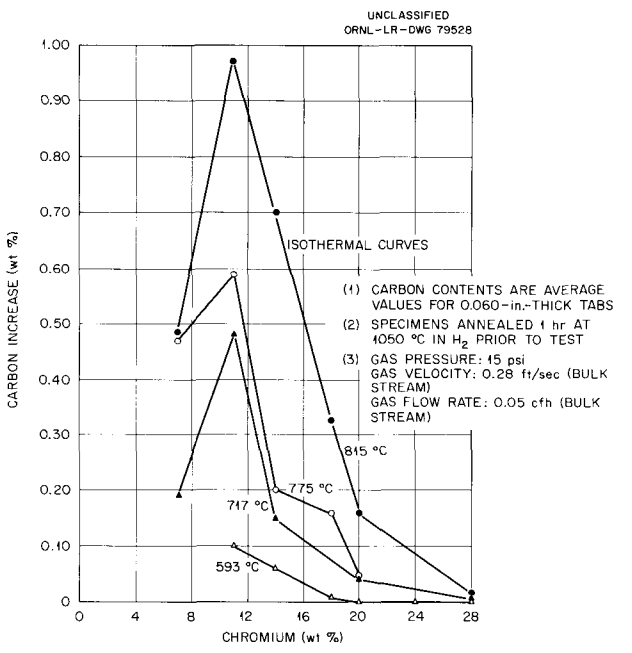

Fig. 17.1. Effect of Chromium Content on the Carburization of Cr–8% Ni–Fe Alloys Annealed for 1000 hr in Flowing Carbon Dioxide.

[4]W. R. Martin and H. E. McCoy, *The Effect of CO_2 on the Strength and Ductility of Type 304 Stainless Steel at Elevated Temperatures,* ORNL TM-339 (Sept. 27, 1962); also *Corrosion* **19**(5), 157t–64t (May 1963).

[5]H. E. McCoy, *Metals and Ceramics Div. Ann. Progr. Rept. May 31, 1962,* ORNL-3313, p 39.

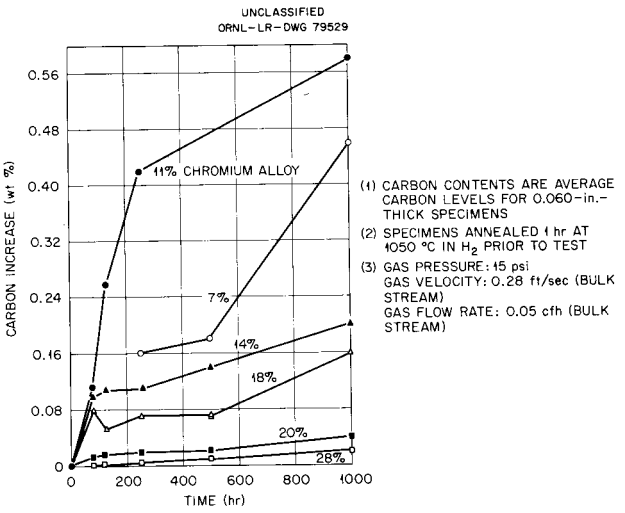

Fig. 17.2. Effect of Chromium Content on the Carburization of Cr–8 wt % Ni–Fe Alloys in Flowing Carbon Dioxide at 775°C.

In general, the amount of carburization increased as the degree of oxidation increased for these Fe-Cr-Ni alloys. It is postulated that increasing the chromium content of the alloy increases the carburization potential of the material, but that the kinetics of the carburization reaction are related to the oxidation process. Since the oxidation rates are decreased by increasing the chromium content, longer times or higher temperatures are required to carburize the alloys containing large chromium contents. One can postulate further that minor constituents in a given heat of material that decrease the rate of oxidation may also result in decreased carburization.

EFFECT OF STRESS STATE ON HIGH-TEMPERATURE LOW-CYCLE FATIGUE

C. R. Kennedy

The behavior of Inconel at 820°C under several realistic dynamic-stress states has been studied. The purpose of this work was to critically evaluate present criteria used to solve low-cycle fatigue problems and to demonstrate their applicability to the more-complex situations. This work has been reported in detail,[6] and the results are summarized here.

[6]C. R. Kennedy, *The Effect of Stress State on High-Temperature Low-Cycle Fatigue,* ORNL-3398 (Mar. 7, 1963).

The results obtained from these tests have been correlated with the results of previous static- and dynamic-stress tests. This investigation has furnished a general approximation for solving complex creep problems involving both static- and dynamic-stress states. The general solution is based on the developed relation

$$t_r = \left(\frac{B}{\bar{\sigma}}\right)^{\beta} \left(\frac{\bar{\sigma}}{\sigma_1}\right), \qquad (1)$$

where

t_r = time to rupture,

$\bar{\sigma}$ = effective stress,

σ_1 = maximum principal stress,

B, β = constants,

and on Minor's damage-accumulation hypothesis. The damage accumulation, however, was shown to be independently additive in each principal stress axis.

Other results obtained from the investigation are:

1. A method for generating true stress-rupture data from constant-load data was obtained.
2. The effect of cyclic stresses on strain rate was demonstrated.
3. A method for determining the magnitude of the frequency effect on the number of cycles to failure was developed for the case where the plastic-strain range is used as a criterion for fracture.
4. A method was found to determine the magnitude of the stress-state effect on the cycles to failure when the plastic-strain range is used as a criterion for fracture.

IN-PILE EXTENSOMETER

W. W. Davis

A linear, variable carbon-film resistor has been successfully developed as an in-pile extensometer. The resistor as purchased was altered only to substitute ceramic parts for those made of plastic and to provide attachment of the variable contact to the extensible element in the experiment. Figure 17.3 shows the placement of the extensometer in an in-pile creep test on graphite in which an overall strain sensitivity of 10^{-6} in./in.

is realized. The resistor, as used in the circuit described below, has a firm displacement sensitivity of 10^{-4} in., which should make it useful in tensile-creep tests of most ductile metals.

The associated circuit is shown in Fig. 17.4. It is a bridge-type balanced circuit in which displacement of the contact on the extensometer resistor (R_1) is calibrated against the change of dial reading on the ten-turn linear resistor (R_2) when balance is restored. The circuit is essentially independent of battery voltage and of any uniform change of resistance in R_1 with temperature or radiation damage. Since the total resistance across the in-pile resistor has changed very little in use and the neutron flux is nearly constant over the length of the resistor, the displacement data obtained are considered quite reliable.

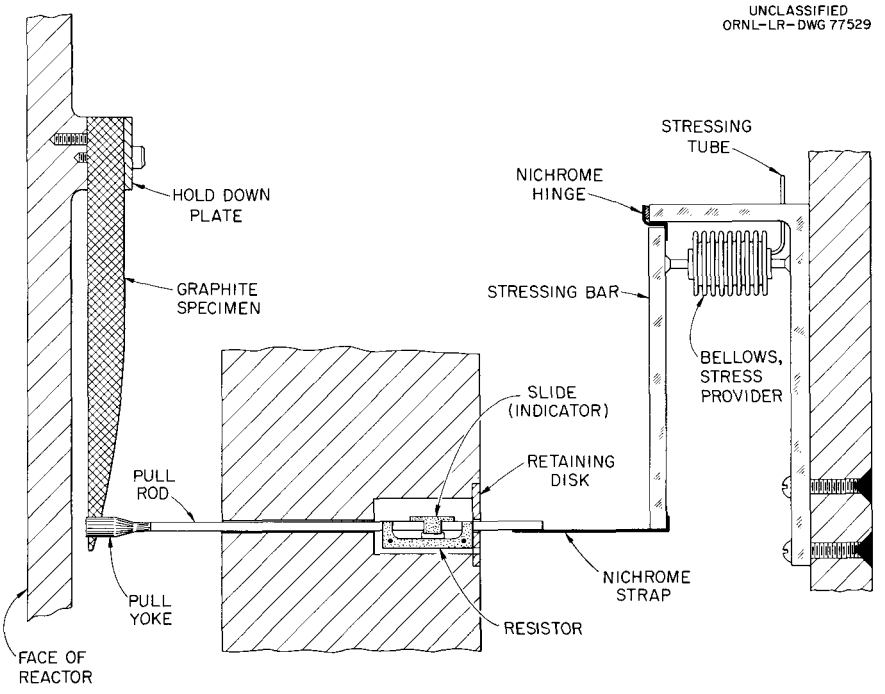

Fig. 17.3. Extensometer Placement in an Experiment.

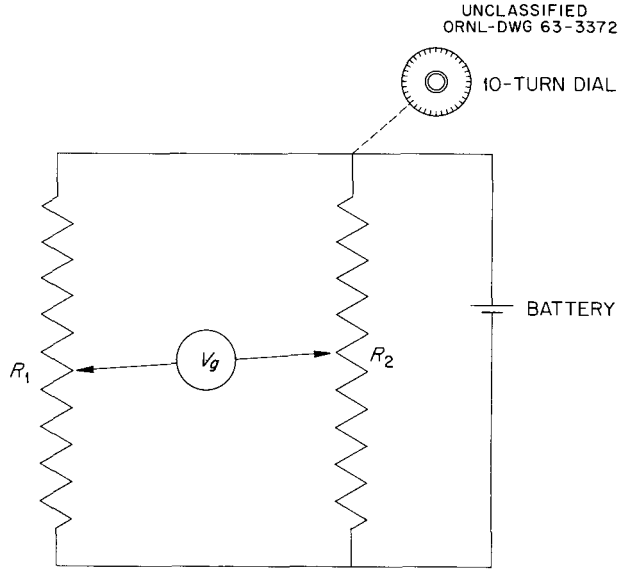

Fig. 17.4. Electric Circuit of a Resistance Extensometer.

18. Nondestructive Test Development

ELECTROMAGNETIC TEST METHODS

C. V. Dodd

Research and development concerning electromagnetic phenomena have continued on analytical and empirical bases. This has included both application of known phenomena for the development of new techniques and development of new instrumentation in an attempt to overcome shortcomings in the method. The study of spacing measurements[1] has continued on improved probes for interplate spacing (measuring coolant-channel dimensions in such fuel elements as those used in the HFIR and ATR), tubing inner diameter, and interrod measurements. The improved probes should be simple to fabricate and sturdier and more accurate than previous models. As part of the program on spacing measurements and as an aid to all eddy-current inspections, both empirical and analytical studies are in progress on the determination of coil impedance of an eddy-current probe coil as a function of coil dimensions, frequency, specimen conductivity and permeability, and coil-to-specimen spacing. The mathematical solution is being programmed for computer operation; after completion of the programming, values for a number of typical cases will be determined. As a result of this study, given the fixed value of the electrical properties of the specimen and any necessary mechanical restrictions, ideal custom-coil design and frequencies can be computed for any given evaluation problem. This should result in better eddy-current inspection with less time spent for the fabrication of improper coils.

Design and fabrication work for the prototype phase-sensitive eddy-current instrument[2] has been completed. This instrument measures the amount of phase shift between initial and detected electromagnetic waves. This phase shift is related to the properties of the test specimen. Figure 18.1 is a block diagram of the instrument. The Schmitt trigger modules which are in both the driver- and receiver-coil circuits operate a flip-flop circuit. Output of the flip-flop is thus proportional to the phase difference between driven and detected signals. Appropriate signal processing allows the data to be presented on a meter or strip-chart recording. To date, calibration studies have indicated that the instrument is operable in the frequency range 1 kc to 4 Mc. By monitoring phase changes rather than amplitude variations, the inspections are relatively insensitive to variations in coil-to-specimen spacing. It has been possible to evaluate greater specimen thicknesses than could have been evaluated with more conventional equipment. This system has already been applied successfully to several inspection problems that could not be resolved with existing instruments.

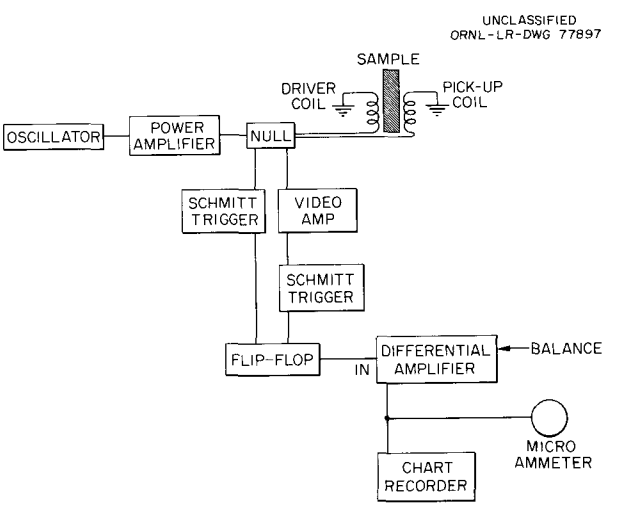

Fig. 18.1. Block Diagram of Phase-Sensitive Eddy-Current Instrument.

[1] C. V. Dodd and R. W. McClung, *Metals and Ceramics Div. Ann. Progr. Rept. May 31, 1962,* ORNL-3313, pp 49–50.

[2] C. V. Dodd, "Applications of a Phase-Sensitive Eddy-Current Instrument," paper submitted to *Nondestructive Testing.*

ULTRASONIC TEST METHODS

K. V. Cook R. W. McClung

The studies of ultrasonic behavior in thin sections have been directed toward development of techniques to detect nonbond areas in clad structures.[3] Through-transmission studies have continued on flat fuel plates and sheet and duplex tubing. One- and two-crystal reflection methods have been studied for application to a number of difficult inspection problems. For instance, a two-crystal system complete with scanning mechanisms has been developed to detect nonbond in brazed tube-to-header heat exchanger joints (see Fig. 18.2). The white inspection probe, which contains both a transmitter crystal and a receiver crystal, fits into the base of the tube joint to be inspected. The two metal legs of the mechanism fit into other adjacent tube bores to provide stability and rigidity throughout the inspection procedure. Scanning of the bonded interface can be performed longitudinally (in the axial direction) with circumferential indices at the end of each scan or circumferentially with longitudinal indices. The latter technique has been more commonly used. The data potentiometers provide both circumferential and longitudinal data on the position of the probe. This allows a servo-driven recorder to be used in automatically producing a plan view or map of the detected nonbond areas. Such a system has been used to evaluate the MSR heat exchanger brazing. Metallographic sectioning of typical joints indicated a test sensitivity capable of finding $\frac{1}{32}$-in.-diam nonbonds. In all of the nonbond studies, considerable effort has been applied to the development of more realistic reference standards for quantitative evaluation of discontinuities.

[3] R. W. McClung and K. V. Cook, "Ultrasonic Detection of Nonbond in Clad Structures," paper submitted for presentation at the International Conference on Nondestructive Testing, London, Sept. 9–13, 1963, and for publication in the proceedings.

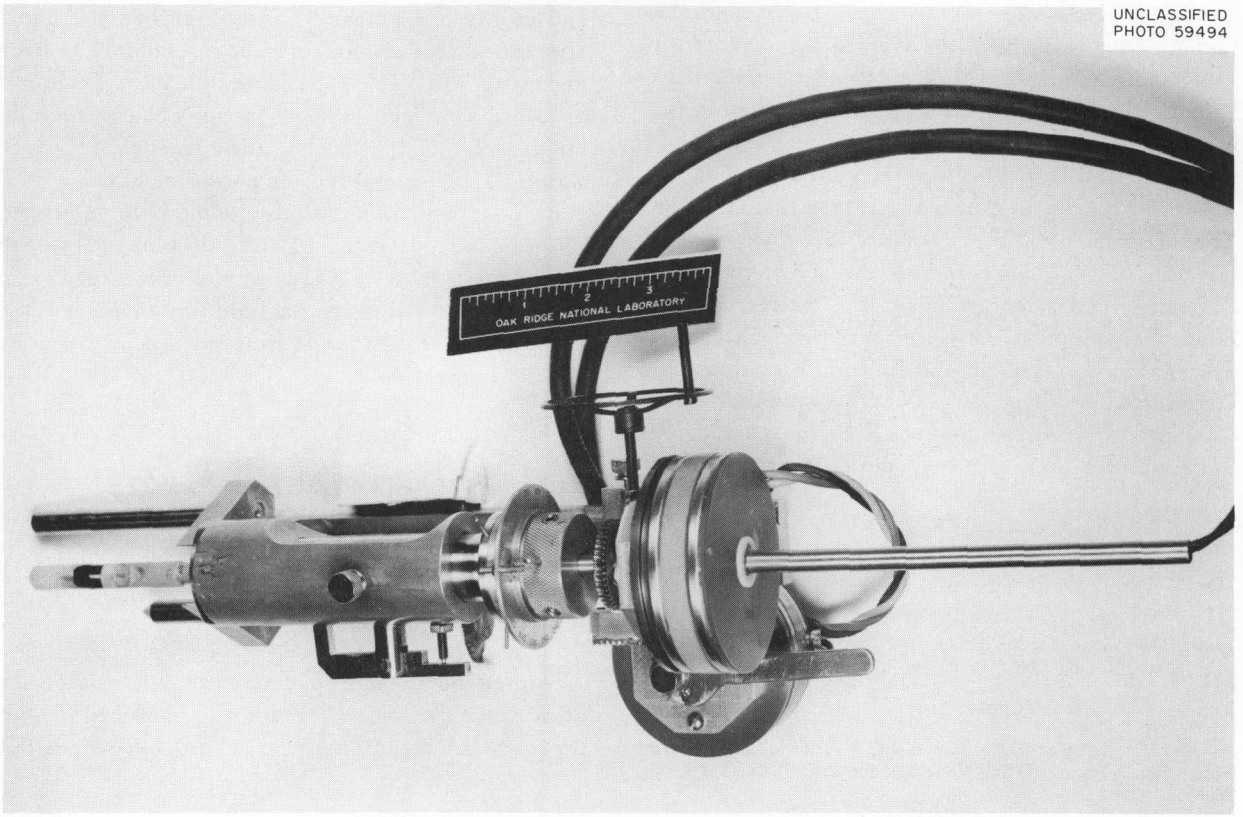

Fig. 18.2. Mechanical Device for Ultrasonic Scanning of Brazed Heat Exchanger Joints.

PENETRATING-RADIATION METHODS

Low-Voltage Radiography and Microradiography

R. W. McClung

The study of low-voltage radiographic parameters and the exhaustive data collected have allowed the establishment of optimum radiographic techniques for simple shapes of aluminum, steel, beryllium, and graphite.[4] Extension of these techniques has allowed contact microradiography[5] using high-resolution photographic plates. Useful magnification of 500X has been possible on the radiographs, with the attainable resolution being approximately 1 μ. Thus far, a principal benefit of the system has been the evaluation of coated uranium carbide particles.

Gamma Scintillation Gaging

B. E. Foster S. D. Snyder

Techniques have been developed which use through-transmission Co^{60} irradiation to determine fuel-loading variation in vibratory-compacted or swaged fuel rods.[6] The assembled equipment has been utilized as a tool for quality evaluation during compaction studies and has served as a model for production-inspection installations.

Studies on the use of x-ray transmission for the measurement of fuel concentration variations in flat fuel plates[7] have led to the development of advanced instrumentation for the performance of x-ray transmission measurements and data processing. In the fuel rod and fuel plate evaluations, a principal problem has been the development of adequate reference and calibration standards. Because of a lack of homogeneity in all standards manufactured similar to actual fuel rod or plate, substitute homogeneous materials having comparable x- or gamma-ray attenuations are being studied. For instance, Pb-Sn alloys are being considered as substitutes for UO_2-ThO_2-filled fuel rods; U-Al eutectic alloys, tool steel, and aluminum are being evaluated as potential standards for fuel plate inspection.

A versatile mechanical scanner[8] has been developed and fabricated for use in penetrating-radiation studies on fuel-bearing components. This equipment is shown in Part III, Fig. 22.6.

INSPECTION DEVELOPMENT FOR PROBLEM MATERIALS

R. W. McClung K. V. Cook

Nondestructive test development for materials that are difficult to inspect has included studies on molybdenum, graphite, and tantalum. Ultrasonics have been of particular value in the inspection development for refractory-metal bar, sheet, plate, and tubing. Some study has concerned the use of alternate materials as reference standards to avoid damaging the very expensive alloys. Technique development for graphite shapes has included radiography, eddy currents, and ultrasonics. Several materials being studied for potential use as solid-state couplants in ultrasonic methods have allowed efficient transmission of the ultrasound into the very porous material and, at the same time, have served as a sealant to exclude unwanted moisture from the material when it is immersed in water during the inspection.

DEVELOPMENT OF REMOTE INSPECTION TECHNIQUES

R. W. McClung K. V. Cook
C. V. Dodd

Studies have continued toward the development of techniques for radiography of materials in the presence of a radioactive background. Work thus

---

[4] R. W. McClung, *Nondestructive Testing* **20**(4), 248–53 (1962).

[5] R. W. McClung, "Studies in Contact Microradiography," paper to be presented at Annual Meeting of the American Society for Testing Materials, Atlantic City, N. J., June 23–28, 1963, and submitted to *Materials Research and Standards.*

[6] B. E. Foster and S. D. Synder, *Metals and Ceramics Div. Ann. Progr. Rept. May 31, 1962,* ORNL-3313, pp 50–51.

[7] R. W. McClung, pp 337–59 in *Research Reactor Fuel Element Conference, September 17–19, 1962, Gatlinburg, Tennessee,* TID-7642, Book 1 (1963).

[8] *Oak Ridge National Laboratory Status and Progress Report, March 1963,* ORNL-3436, p 5.

far has included radiography of an aluminum step wedge and a subsequent double exposure with varying amounts of background radiation of different energy. Evaluation of the fogged film on the basis of penetrameter sensitivity will enable establishment of the tolerance for such fogging exposure. There is considerably greater tolerance for the higher energy rays because of the reduced efficiency of the x-ray film at these energies. Many of the eddy-current and ultrasonic techniques are being developed with the added criterion that performance be possible in a remote facility.

19. High-Temperature Materials

W. C. Thurber

The High-Temperature Materials Program seeks to provide base-line metallurgical information on a time schedule that will permit reactor designers to make intelligent, well-founded decisions as to the feasibility and practicability of advanced reactor concepts. The program generally centers on materials problems associated with alkali-metal-cooled systems that use refractory alloys as container materials. This provides a framework within which to select the most meaningful research and development tasks. Some attention has also been directed to examination of stainless steels and superalloys for containment of alkali metals under less-severe conditions.

Promising refractory alloys are being evaluated as to fabricability, weldability, compatibility with boiling and nonboiling alkali metals, physical metallurgical behavior, quality, environmental contamination potential, and mechanical and physical properties. Some significant portions of the work have been covered elsewhere[1,2] and are not included in this report.

PHYSICAL METALLURGY STUDIES

Contamination of Refractory Metals in High Vacua

H. Inouye

The properties of refractory metals are significantly influenced by trace quantities of oxygen, carbon, and nitrogen. The determination of their properties therefore requires precise control of the atmosphere in which they are heated, since interstitial solution of these elements readily occurs. This investigation was undertaken to assess the contamination characteristics of refractory metals exposed to trace quantities of atmospheric impurities for extended periods at high temperatures.

Preliminary results have shown that for niobium the permissible concentrations of impurity gases are in the range 0.01 to 0.001 ppm (10^{-5} to 10^{-6} torr) for exposure times of about 100 hr.[3] Subsequent experiments have shown that, when the exposure time at 800 to 1200°C is approximately 1000 hr, the permissible concentrations of impurity gases are in the range of 10^{-4} ppm (10^{-7} torr).[4] Because these impurity concentrations present an unsurmountable analysis and control problem when they are present in an inert gas, it was concluded that high vacua were necessary to control the contamination of metals similar to niobium.

During this reporting period, a more-detailed study of the factors influencing contamination of refractory metals was undertaken. These factors included the metal surface-to-volume ratio, the test material, the effectiveness of sacrificial foil wraps, and the composition of the residual gases. A summary of the experimental results is given below.

The effect of the metal surface-to-volume ratio on the contamination was determined on specimens of Nb–1% Zr, nominally 0.020 and 0.040 in. thick, that were exposed for 984 hr to the residual gases in a vacuum system operating at a pressure of 5.6×10^{-7} torr. It was assumed that under the test conditions the rate of contamination was controlled by the concentration of the impurity gases and that by comparison the diffusion rates of the impurities into the metal were sufficiently high

[1] ORNL-3337, pp 111–73, Oct. 2, 1962 (classified).

[2] ORNL-3420, pp 173–246, May 6, 1963 (classified).

[3] H. Inouye, ORNL-3270, pp 121–23, Apr. 26, 1962 (classified).

[4] H. Inouye, ORNL-3337, pp 130–32, Oct. 2, 1962 (classified).

so as not to affect the sticking probability of the gases on the metal surfaces. With these boundary conditions, the extent of contamination should be directly proportional to the metal surface area, and ΔC, the change in the impurity concentration, is therefore inversely proportional to the specimen thickness. If ΔC_1 is the total change in the impurity concentration (O, C, and N) in a metal of thickness t_1, resulting from reactions with the residual gases, and ΔC_2 is the change for the same metal of thickness t_2, the ΔC_1-ΔC_2 ratio should be equal to the t_2-t_1 ratio. To further satisfy the assumptions, the change in the specimen weight per unit area should be independent of the thickness. The results of such calculations based on the increase in the oxygen, carbon, and nitrogen contents of Nb–1% Zr are shown in Table 19.1. The excellent correlation shown by the data indicates that contamination of Nb–1% Zr does indeed vary directly with the surface-to-volume ratio.

The data summarized in Table 19.2 indicate that good agreement exists between contamination as predicted by weight change and as measured analytically. The former method thus provides a rapid and low-cost tool for the assay of contamination.

The reactivity of four refractory metals exposed for 1000 hr at 2.7×10^{-7} torr is shown in Fig. 19.1. For comparison purposes, it was necessary to normalize the data on the basis of equivalent metal thicknesses. The reported results are therefore a measure of the contamination in a specimen 0.1 cm (0.0394 in.) thick contaminated from one side.

Each datum on the curves represents the net interstitial change for a specimen. A breakdown of the net change for Nb–1% Zr in Fig. 19.2 shows that oxygen accounts for over 80% of the contamination and that the balance is due to carbon. Under the same test conditions, the hydrogen, oxygen, carbon, and nitrogen content of unalloyed molybdenum decreased. Hydrogen and nitrogen were removed from tantalum, and only the oxygen content of niobium increased. The compositions of the residual gases to which these metals were exposed are listed in Table 19.3. The source of oxygen contamination is the CO, CO_2, and H_2O, whereas the carbon is derived from several gas

Table 19.2. Comparison of the Contamination of Nb–1% Zr by Weight Change and by Chemical Analysis[a]

Test Temperature (°C)	Total Contamination (ppm)	
	By Weight Change	By Analysis
578	−21	15
744	40	58
896	40	105
1009	195	192
1130	252	254
1182	482	287
1190	492	404

[a]1000 hr at 2.7×10^{-7} torr.

Table 19.1. Influence of Specimen Thickness on the Contamination of Nb–1% Zr Alloy[a]

Temperature (°C)	Thickness Ratio, t_2/t_1	Concentration Change Ratio, $\Delta C_1/\Delta C_2$	Weight Change (mg/cm^2)	
			Thickness, t_1	Thickness, t_2
856	1.94	1.91	0.138	0.132
988	1.54	1.50	0.185	0.183
1081	1.92	2.01	0.266	0.243
1135	1.98	1.97	0.292	0.274
1201	1.94	1.72	0.540	0.552

[a]984 hr at 5.6×10^{-7} torr.

species. Nitrogen contamination does not appear to be a problem. This may be due to the possibility that the mass 28 component was mainly CO; therefore the nitrogen partial pressure was quite low.

The effect of sacrificial foil wraps of Mo, Ta, and Nb–1% Zr on lowering the contamination of Nb–1% Zr gave the unexpected results shown in Fig. 19.3. On the basis of the reactivity of each of these metals, it was anticipated that the most-reactive metal foils would provide the most protection; however, since the least-reactive metal provided the greatest protection, a property other than "gettering" ability appears to be responsible for the observations. It is estimated that at 1200°C, molybdenum wrapping reduces the contamination of Nb–1% Zr by a factor of 7, tantalum wrapping by a factor of 4, and Nb–1% Zr wrapping by a factor of 3.

A test has been made to determine the reactivity of nitrogen with Nb, Nb–1% Zr, Ta, Mo, and TZM (Mo–0.5% Ti–0.1% Zr–0.08% C). Specimens of

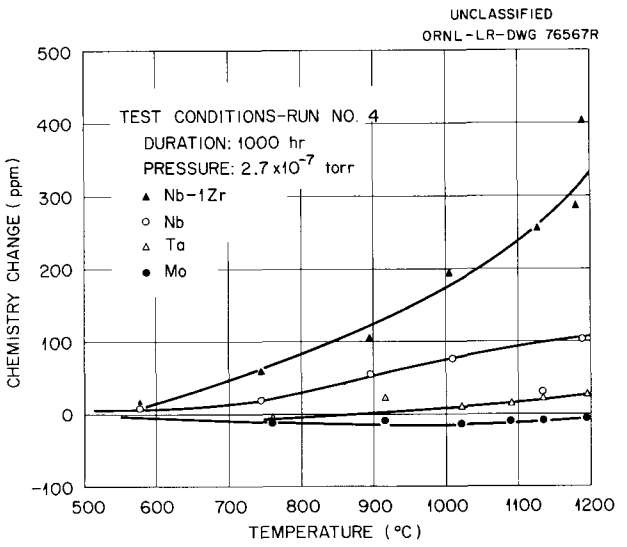

Fig. 19.1. Comparative Reactivities of Refractory Metals in High Vacua.

Table 19.3. Analysis of the Residual Gases in a Pyrex-Mullite System at 2.7×10^{-7} Torr

Species	Composition (%)	Partial Pressure (torrs)
H_2	53	1.4×10^{-7}
CH_4	3.2	8.6×10^{-9}
H_2O	19.0	5.1×10^{-8}
Hydrocarbon	5.9	1.6×10^{-9}
$N_2 + CO$	15	4.0×10^{-8}
O_2	0.1	2.7×10^{-10}
CO_2	4.5	1.2×10^{-8}

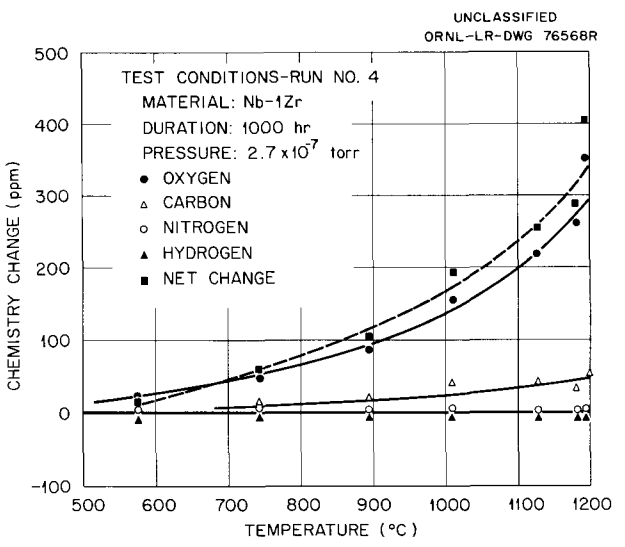

Fig. 19.2. Contamination of Nb–1% Zr Alloy in High Vacua.

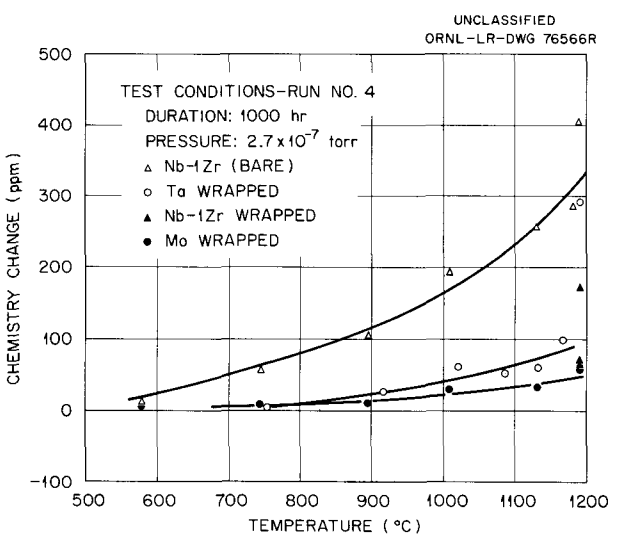

Fig. 19.3. Effect of Sacrificial Foil Wraps on the Contamination of Nb–1% Zr.

these metals were exposed to a nitrogen overpressure of 6.6×10^{-7} torr and a base pressure of 2.4×10^{-7} torr at temperatures of 618 to 1202°C for 1000 hr. Weight-change determinations show that nitrogen does not influence the order of the reactivity of the various metals. As in prior tests the observed reactivities decreased in the order Nb–1% Zr, Nb, Ta, and Mo; TZM was intermediate between molybdenum and tantalum. Both molybdenum and TZM lost weight at all temperatures, whereas Nb–1% Zr, Nb, and Ta showed weight increases. On the basis of weight-change measurements, it appears that total contamination in a nitrogen atmosphere of 6.6×10^{-7} torr is about equivalent to that in a vacuum of 2.7×10^{-7} torr (see Table 19.3).

The changes observed in the nitrogen content of Nb–1% Zr as a result of exposure to nitrogen at 6.6×10^{-6} torr are listed in Table 19.4. Both the nitrogen content and the sticking probability increased uniformly with temperature.

Table 19.4. Reactivity of Nb–1% Zr with Nitrogen for 1000 hr at 6.6×10^{-7} Torr

Temperature (°C)	Nitrogen Increase		Sticking Probability
	(mg/cm^2)	(ppm)[a]	
			$\times 10^{-4}$
618	0.0039	5	0.93
780	0.0030	4	0.71
934	0.0062	7	1.48
1040	0.0199	23	4.74
1113	0.0239	28	5.67
1154	0.0282	33	6.70
1155	0.0367	43	8.72
1178	0.0338	40	8.0
1191	0.0410	48	9.75
1198	0.0472	55	11.2
1202	0.0453	53	10.8

[a]Based on specimen thickness of 0.1 cm (0.0394 in.) contaminated from one side.

Slow-Bend Creep Testing of Niobium-Base Alloys

T. K. Roche

The slow-bend creep test previously described[5] is presently being used for two purposes: (1) for qualitatively screening materials as to their elevated-temperature strength and (2) for studying the effect of test pressure on the creep behavior of the Nb–1% Zr alloy under slow-bend conditions. In this test a small specimen of rectangular cross section is suspended as a cantilever beam and is loaded to a preselected outer fiber stress after reaching the test temperature; the deflection of the sample is then measured as a function of time. The apparatus is completely under vacuum. Variable pressure is obtained in the apparatus by regulating the amperage to the diffusion-pump heaters, thus regulating the pumping speed.

An example of data obtained for the purpose of screening materials is shown in Fig. 19.4. These tests, carried out at 1200°C with an initial outer fiber stress of 8000 psi, indicate the superiority of Nb–1% Zr to the Nb-V alloys.

Three tests for investigating the effect of testing pressure on the creep behavior of Nb–1% Zr under slow-bend conditions have been completed. The tests were carried out for 504 hr at 1000°C with initial outer fiber stress of 12,500 psi and with pressure ranges of 3 to 7×10^{-8}, 3.2 to 7.4×10^{-6}, and 1.6 to 6×10^{-5} torr. Differences were noted in the time-deflection curves for the tests (Fig. 19.5), which could be correlated with the increase in interstitial content (contamination) of the specimens, stemming from increasing test pressures. The general characteristics of each curve were for the specimens to experience a period of "steady-state" deflection during the first stages of test, followed by a decrease in deflection rate to test termination. A partial exception to this generalization was observed during the test carried out at 1.6 to 6×10^{-5} torr. After a pronounced decrease in deflection rate following the steady-state period, a rapid increase in deflection took place over a relatively short time period (during which the system pressure was observed to increase to 1.6×10^{-4} torr for an unknown length of time). This, in turn, was followed by a deflection-rate decrease. Pre- and

[5]T. K. Roche, *Metals and Ceramics Div. Ann. Progr. Rept. May 31, 1962,* ORNL-3313, p 57.

posttest chemical analyses and metallographic notes on the specimens are presented in Table 19.5. Also included are observations made on a specimen that was heated to the test temperature but not stressed. Results from this sample are indicative of the contamination that can be expected in all specimens during heatup.

A tentative explanation of the time-deflection curves can be based on the difference in contamination experienced by the specimens as a result of the pressure variable. With the test at 3×10^{-7} to 7×10^{-8} torr as a reference, it was noted that the steady-state deflection rate increased with testing pressure. This fact is attributed to an increase in contamination rate with increasing pressure and to a corresponding increase in structural instability of the specimens through diffusion of interstitials and precipitation

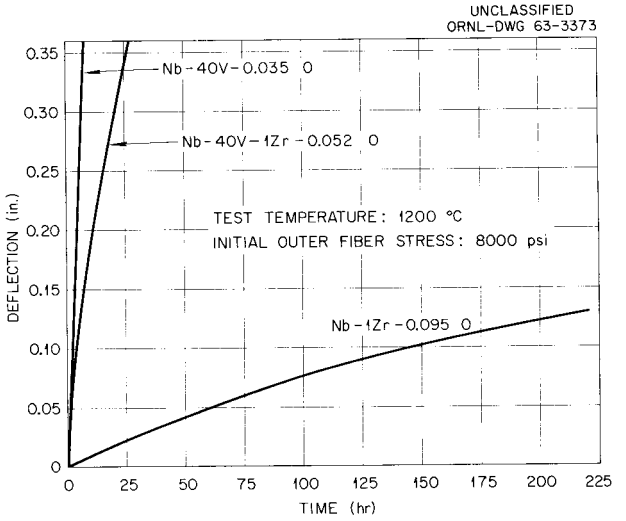

Fig. 19.4. Deflection-Time Curves for Three Niobium-Base Alloys in Slow-Bend Creep Tests.

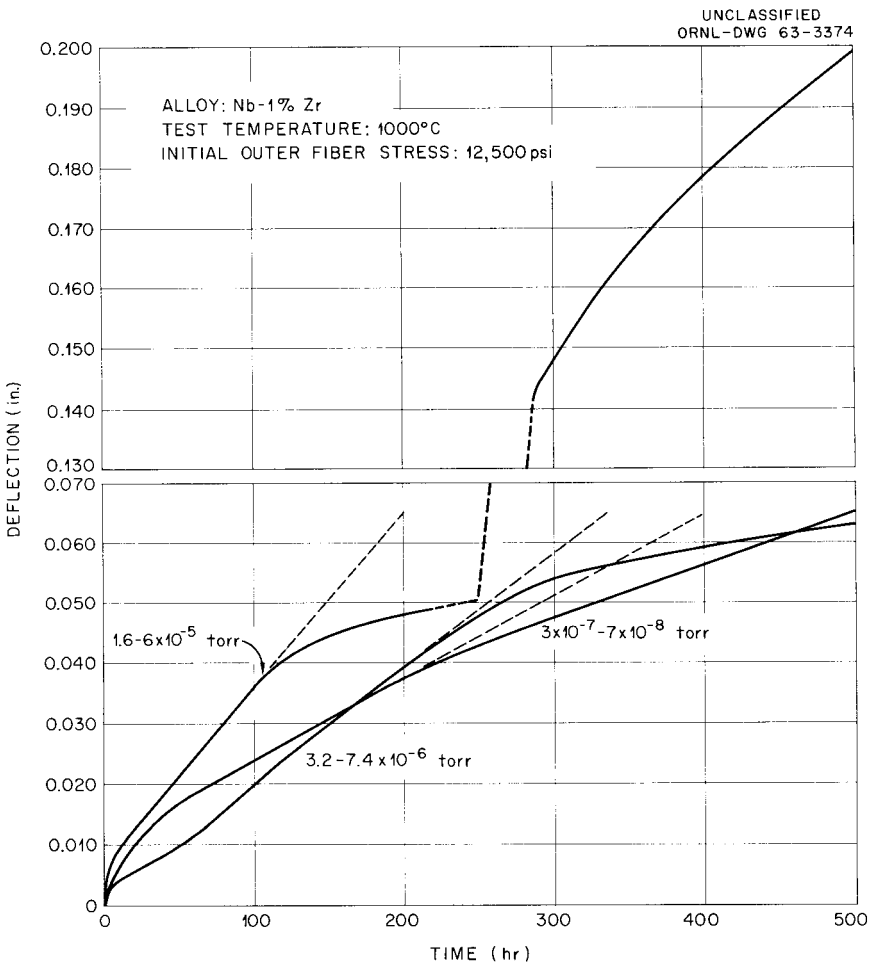

Fig. 19.5. Effect of Test Pressure on the Slow-Bend Creep Deflection of Nb–1% Zr Alloy.

Table 19.5. Pre- and Posttest Chemical Analyses and Metallographic Notes on Nb–1% Zr Slow-Bend Specimens

Test temperature: 1000°C
Initial outer fiber stress: 12,500 psi
Test duration: 504 hr
Thickness of specimen: 0.1 cm
Approximate exposed surface area of specimen: 3.39 cm^2 (0.525 $in.^2$)

Specimen	Zr (%)	Analysis (ppm)				Increase in Interstitials During Test (ppm)				Calculated Increase in Specimen Weight During Test		Metallographic Notes
		C	O	H	N	C	O	H	N	(g)	(mg/cm^2)	
Annealed 2 hr at 1200°C[a]	0.60 ±0.03	120	510	<1	210							Pepperlike precipitate (ZrO_2)
Tested at 3×10^{-7} to 7×10^{-8} torr		250	690	<1	220	130	180	0	10	0.00047	0.138	Pepperlike precipitate (ZrO_2)
Annealed 2 hr at 1200°C[b]	0.63 ±0.03	70	480	3	220							Pepperlike precipitate (ZrO_2)
Heated to 1000°C (not bend tested)		290	540	3	230	220	60	0	10	0.00041	0.121	Pepperlike precipitate (ZrO_2)
Tested at 3.2 to 7.4×10^{-6} torr		440	4,000	4	270	370	3,520	1	50	0.0058	1.710	Pepperlike precipitate (ZrO_2) and small amount of additional phase (NbO)
Tested at 1.6 to 6×10^{-5} torr		290	19,700	61	330	220	19,220	58	110	0.0284	8.377	Pepperlike precipitate (ZrO_2) and large amount of additional phase (NbO)

[a]Annealed control for specimen tested at 3×10^{-7} to 7×10^{-8} torr.
[b]Annealed control for specimens heated to 1000°C – not tested; tested at 3.2 to 7.4×10^{-6} torr; tested at 1.6 to 6×10^{-5} torr.

of new phases (e.g., ZrO_2). A major part of the subsequent decrease in deflection rate could result from dispersion strengthening by stabilized precipitated particles. It thus appears significant that the decrease in deflection rate became more pronounced at the higher test pressure, as shown by a comparison of the deflection rates for the final 50 hr of the tests carried out at 3×10^{-7} to 7×10^{-8} torr and 3.2 to 7.4×10^{-6} torr. A similar effect was noted on the test at 1.6 to 6×10^{-5} torr during the period from 100 to 250 hr. The rapid increase in deflection rate after approximately 250 hr for the test at 1.6 to 6×10^{-5} torr is not completely understood at present; however, it is felt to be related to instabilities caused by gross contamination.

Alloy Stability in High Vacua

D. T. Bourgette

It has been reported that the solid-state evaporation rates of iron-, nickel-, and cobalt-base alloys increase with increasing chromium concentration and increasing temperature.[6] Owing to advanced technology and because of the adequate compatibility of type 316 stainless steel with boiling potassium at elevated temperatures, it was selected for further evaporation studies.

By the use of a free-evaporation technique, both oxidized and polished specimens ranging from 0.013 to 0.018 cm in thickness and from 15 to 18 cm^2 in area were subjected to pressures from 5×10^{-7} to 5×10^{-9} torr at temperatures of 760°C (1400°F) to 982°C (1800°F) for times from 500 to 3700 hr. The results for type 316 stainless steel are illustrated by the log evaporation rate vs reciprocal temperature plot in Fig. 19.6 (curve *A*). In all tests it was observed that the evaporation rates of oxidized specimens were lower than those of polished specimens.[7,8] A comparison of curves *A* and *B* in Fig. 19.6 indicates the effects of oxidation prior to test. A similar effect was observed for nickel- and cobalt-base alloys. By use of the Langmuir free-evaporation equation and on the assumption that the evaporation coefficient is unity (as for a pure metal), the vapor pressure of type 316 stainless steel has been calculated to be 3.42×10^{-9} torr at 760°C (1400°F) and 1.67×10^{-7} torr at 982°C (1800°F).

Figure 19.7*a* and *b* illustrates the surface and cross-sectional microstructure of originally polished type 316 stainless steel resulting from a 500-hr test at 982°C (1800°F) and 5×10^{-7} torr. It is obvious from the surface roughness that evaporation rates can be based only on apparent or initial surface area. Note further the formation of a new phase at the surface of the sample and the formation of subsurface voids. The same

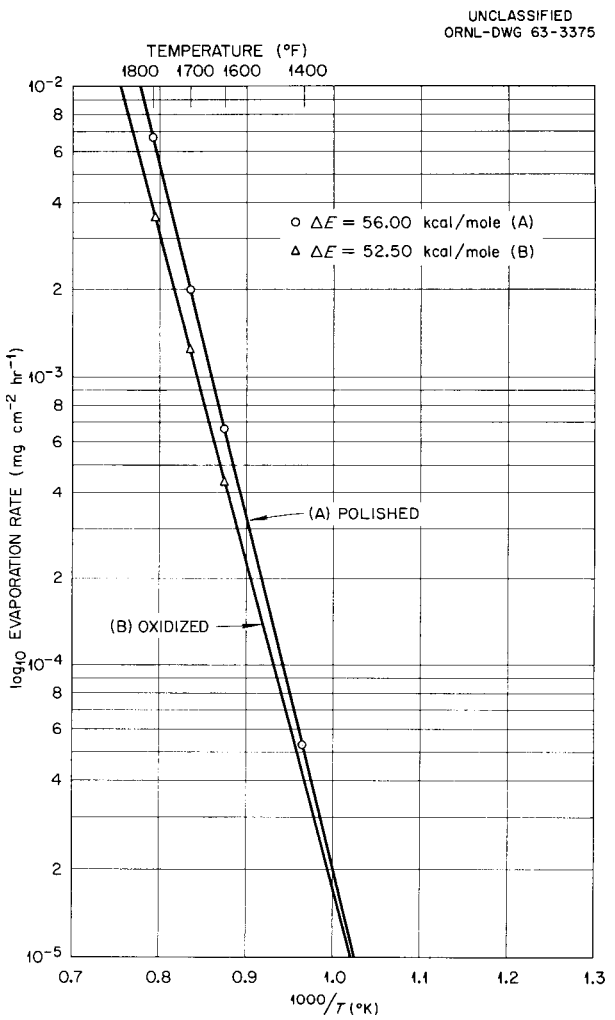

Fig. 19.6. Evaporation Rates of Type 316 Stainless Steel Between 5×10^{-7} to 5×10^{-9} torr.

[6]D. T. Bourgette, *Metals and Ceramics Div. Ann. Progr. Rept. May 31, 1962,* ORNL-3313, p 59.

[7]D. T. Bourgette, ORNL-3337, pp 136–37, Oct. 2, 1962 (classified).

[8]D. T. Bourgette, ORNL-3420, pp 202–06, May 6, 1963 (classified).

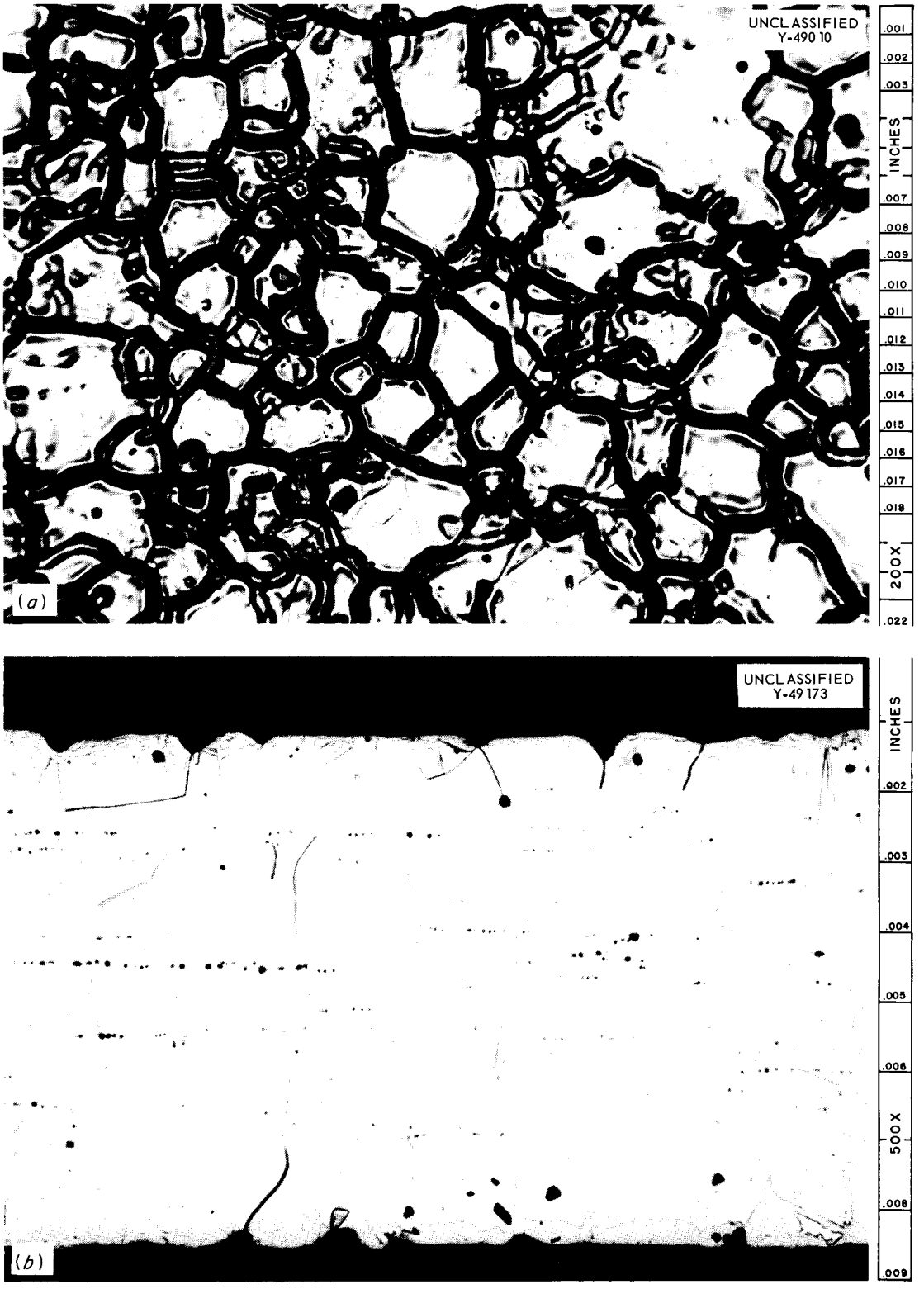

Fig. 19.7. (*a*) Unetched Surface and (*b*) Etched Cross Section of Type 316 Stainless Steel Illustrating Evaporation Losses at 982°C (1800°F) and 5×10^{-7} torr. Note resulting ferrite and subsurface void formation. Etchant: glyceria regia. Reduced 13%.

Fig. 19.8. Type 316 Stainless Steel Oxidized in Air at 820°C (1500°F) and Subsequently Evaporated at 1800°F (982°C) at 5×10^{-7} torr. Etchant: glyceria regia.

general microstructure occurs at lower temperatures when the test duration is increased to 900 hr or more.

Figure 19.8 shows the microstructure of an oxidized sample which was evaporated at 982°C (1800°F). An increase in the number and size of the subsurface voids and increased grain-boundary broadening over the nonoxidized condition presented in Fig. 19.7*b* may be observed. It is believed that this is caused by the reaction of oxides with the carbon in the alloy. The surface phase existing after the test has been identified as ferrite.

Creep-rupture data indicate that type 316 stainless steel becomes stronger as the evaporation time at 870°C (1600°F) is increased to at least 1400 hr under pressures of 5×10^{-7} to 5×10^{-9} torr. Microstructural studies revealed the presence of sigma phase, carbides, and subsurface voids, and it is felt that these structural interruptions caused the stress-rupture life of the alloy to be increased.

FABRICATION DEVELOPMENT

Refractory-Metal Extrusion

R. E. McDonald

The majority of molybdenum alloy tubing available in the United States is currently being produced by warm drawing of billets produced from drilled, wrought stock. An alternate approach to provide feed material for the drawing operation involves the production of tube shells by extrusion. To test this concept, extrusion billets of unalloyed Mo, TM (Mo–0.5% Ti), and TZM (Mo–0.5% Ti–0.1% Zr–0.08% C) have been prepared (Fig. 19.9).

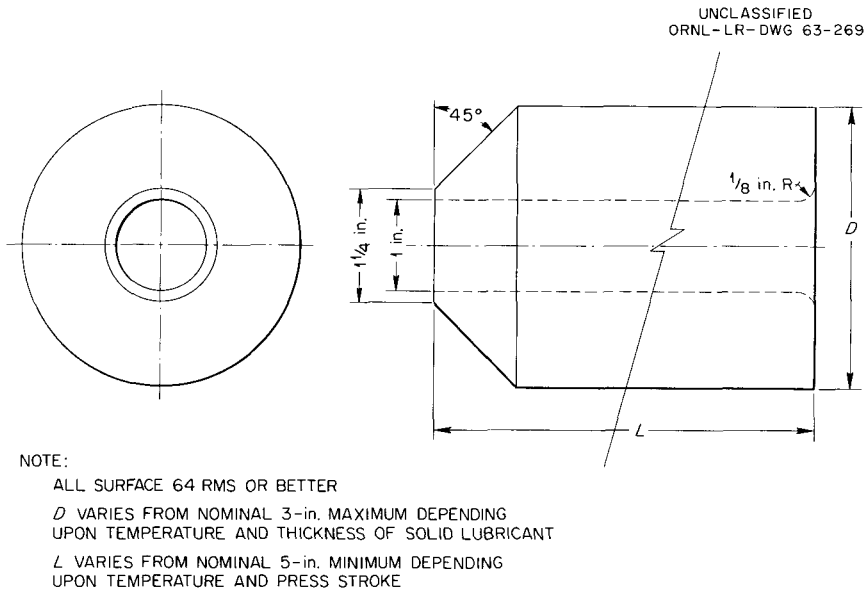

Fig. 19.9. Tube Shell Extrusion Billet.

The tooling selected for the molybdenum-base alloy extrusions was similar to that developed at ORNL for extruding nickel-molybdenum alloys.[9] However, modifications were made to compensate for higher temperatures and pressures. A schematic view of the extrusion press container, showing the assembled tooling, is presented in Fig. 19.10. The 90° conical die and mandrel stem were coated with zirconia and polished to a mirror finish.

Prior to extruding the molybdenum billets, two AISI-1018 mild-steel billets were extruded to evaluate the tooling and to establish the sequence of operations. No difficulties were encountered in either of these extrusions. To date, two unalloyed molybdenum billets have been extruded. The initial molybdenum billet was coated with a slurry of Corning No. 7810 glass to a thickness of approximately 0.030 in. and extruded at 1760°C (3200°F), with a reduction ratio of 8.8:1. The second unalloyed billet was coated in the same manner but extruded at 1593°C (2900°F), with a reduction ratio of 8.8:1. Although both extrusions were successful, lubrication difficulties which affected the surface finish of the tube shells were encountered. At 1760°C (3200°F) the viscosity of the glass was low, causing the glass to be ejected from the container during the initial billet upset. Reducing the extrusion temperature resulted in improved surface finish, since more uniform lubrication was achieved. An overall view of the two molybdenum tube shells along with the two mild-steel extrusions is shown in Fig. 19.11.

Tube blanks for warm drawing (1.040 in. OD × 12 in. long with 0.125-in.-thick walls) have been prepared by machining. Prior to drawing, the blanks will be nondestructively inspected for soundness, and test samples will be examined metallographically. Chemical analyses were taken on the as-received and extruded molybdenum (see Table 19.6). It is apparent that a slight increase in oxygen content occurred as a result of extrusion but that changes in carbon, nitrogen, and hydrogen were negligible.

[9] M. R. D'Amore and H. Inouye, *The Extrusion of Composite Tubes,* ORNL CF-56-4-123 (Apr. 18, 1956).

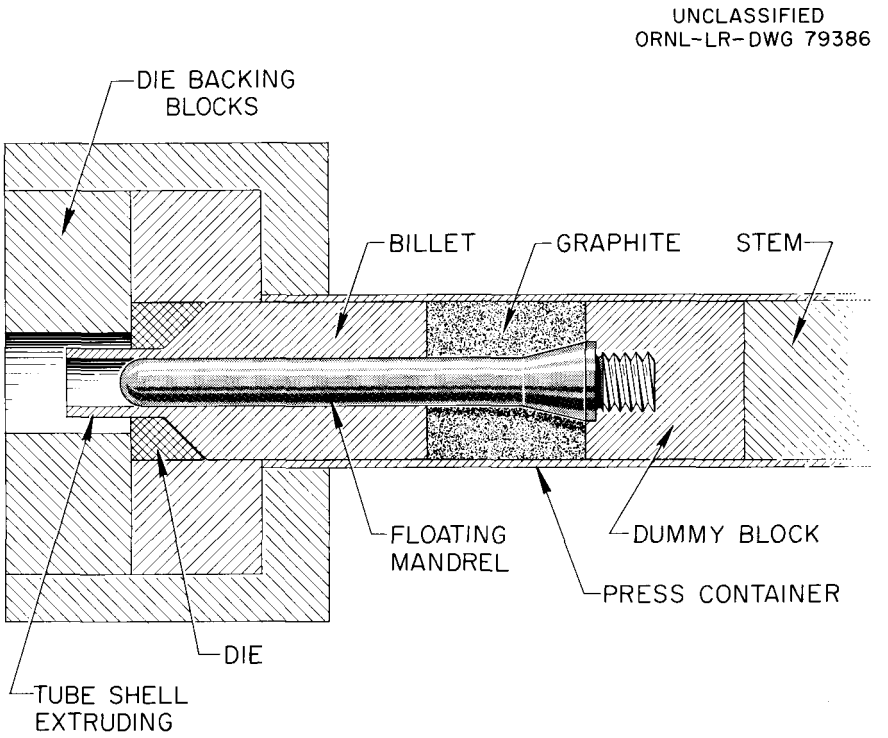

Fig. 19.10. Schematic View of the Assembled Extrusion Tooling.

Table 19.6. Interstitial Impurity Content of a Molybdenum Billet

Impurity Content (ppm)	As-Received, Hot Rolled	Extruded, 1760°C (3200°F)
Carbon	200	220
Oxygen	15	72
Nitrogen	10	11
Hydrogen	1	5

Floturning of Refractory-Metal Tube Shells

R. E. McDonald C. F. Leitten, Jr.

The production of refractory-metal tubing by the conventional tube-shell extrusion and drawing techniques presents several inherent difficulties. The high temperatures normally encountered in extruding the basic tube shells pose problems in tooling design, lubrication, and contamination. In addition, the required conditioning of the extruded tube shell substantially reduces the material yield. To circumvent these problems, floturning is being investigated as an alternate method for fabrication of tube shells.

Floturning is a mechanical working operation in which the material being worked is reduced in thickness by a shearing action, causing the material to flow uniformly along the mandrel (Fig. 19.12). The process is normally performed at room temperature.

Studies were conducted with the Nb–1% Zr alloy to establish the feasibility of floturning refractory-metal tube shells and to investigate the basic process parameters. Two wrought Nb–1% Zr hollow cylinders (2 in. OD × $1\frac{1}{2}$ in. ID × 5 in. long) were machined from bar stock. The billets were first annealed and then floturned in a single pass (~50% reduction) using different feed rates and mandrel speeds. On the basis of results from these trial runs, it was concluded that an acceptable floturning process could be developed.

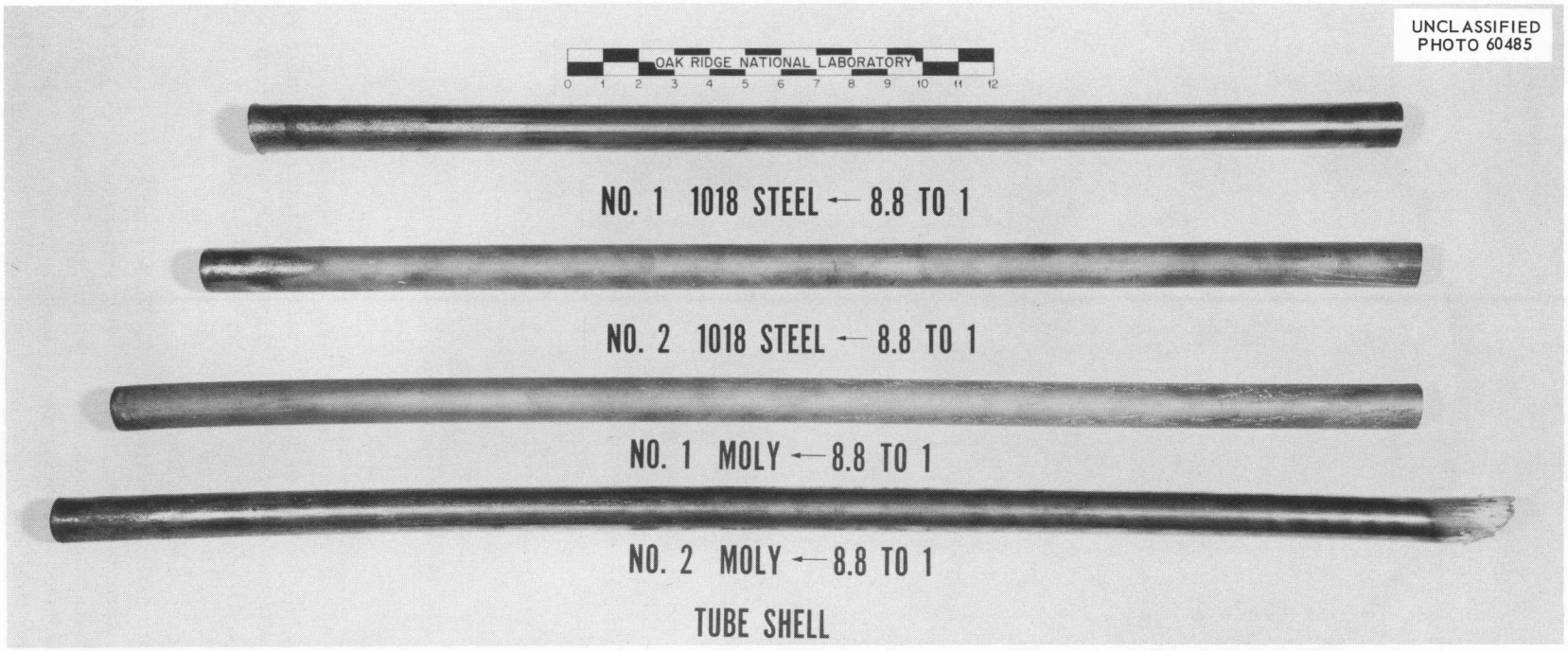

Fig. 19.11. Overall View of the Extruded Tube Shells. Surface of No. 1 molybdenum shell conditioned by sandblasting. Surface of No. 2 molybdenum shell conditioned by stainless-wire brushing.

UNCLASSIFIED
ORNL-LR-DWG 78912

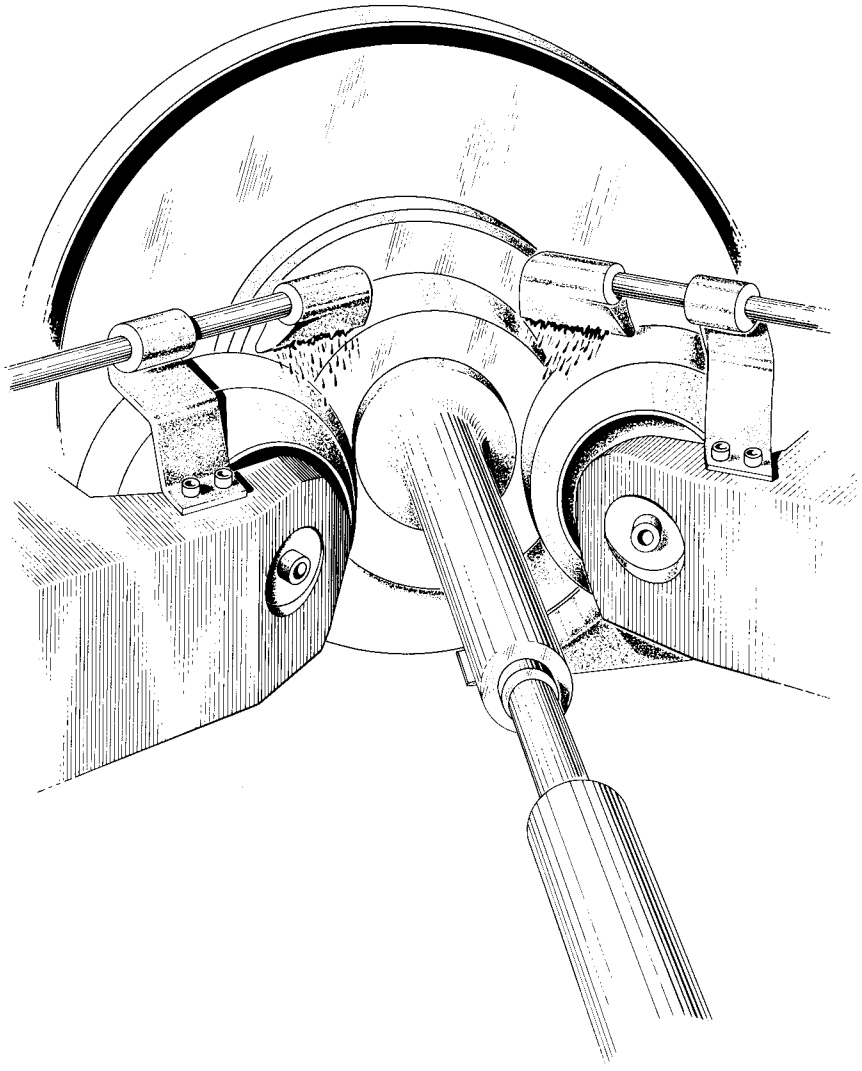

Fig. 19.12. Schematic Drawing of Floturning Process.

Since the ultimate goal of the process is to floturn cast refractory-metal billets without intermediate hot working, an attempt was made to directly process a cast Nb–1% Zr ingot. The ingot was vacuum homogenized at 1537°C (2800°F) for 1 hr and machined into a cylinder of identical dimensions to the wrought material previously processed. The billet was then floturned, using the parameters established for the wrought material. Some problems arose from the heavy reduction employed; however, after the reduction rate was decreased and the feed rate was adjusted, a satisfactory surface was obtained. It is felt that the floturning of cast ingots can be improved by using centrifugally cast cylinders in which a uniform, equiaxed grain structure exists.

These initial tests indicate that tube shells with surface finishes satisfactory for subsequent drawing can be produced by this process. A high material yield appears to be possible with the process, particularly if cast refractory-metal cylinders can be processed directly.

MATERIALS COMPATIBILITY

Corrosion of Refractory Metals by Lithium

J. R. DiStefano

The most serious compatibility problem in refractory-metal–lithium systems has been found to be related to the presence of oxygen in some refractory metals.[10,11] Oxygen concentrations in excess of 300 ppm can cause the rapid penetration of niobium or tantalum by lithium at temperatures from 300 to 1200°C. The mechanism of this corrosion process is not thoroughly understood, but the principal variables affecting the extent of lithium penetration (at a constant oxygen concentration) have been found to be temperature and, to a lesser degree, grain orientation.

During the past year, experiments with the Nb-O-Li system have continued in an effort to better understand the nature of the corrosion process. One of the variables studied was grain size; the results of this investigation are shown in Fig. 19.13. At 400°C the mode of penetration

[10] J. R. DiStefano, *Metals and Ceramics Div. Ann. Progr. Rept. May 31, 1962,* ORNL-3313, p 29.

[11] J. R. DiStefano and E. E. Hoffman, "Relation Between Oxygen Distribution and Corrosion in Some Refractory-Metal–Lithium Systems," pp 431–49 in *Conference on Corrosion of Reactor Materials, June 4–8, 1962, Proceedings,* vol II, International Atomic Energy Agency, Vienna, 1962.

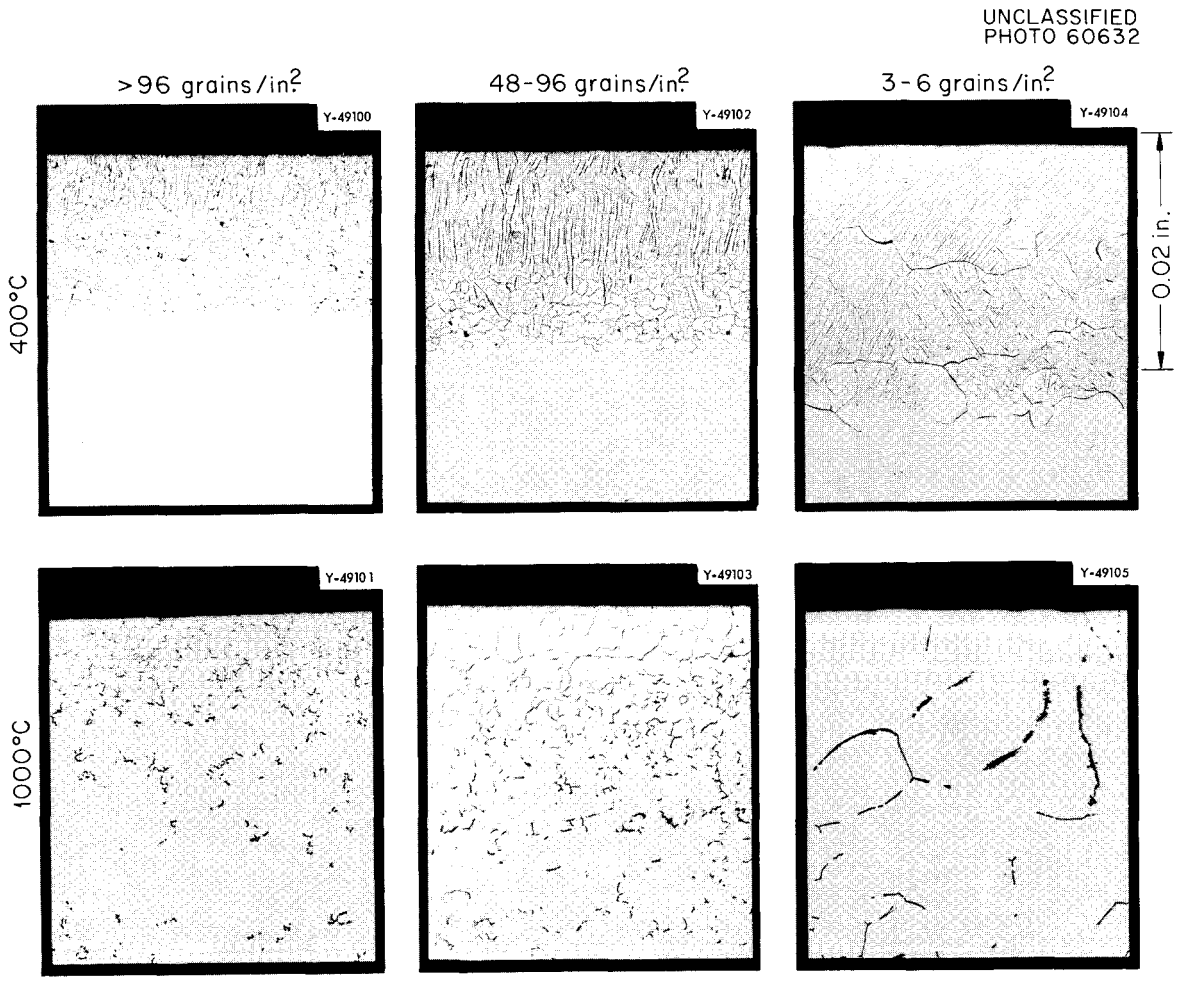

Fig. 19.13. Effect of Grain Size and Test Temperature on Corrosion of Niobium by Lithium.

changed from primarily grain-boundary corrosion to transcrystalline corrosion as the grain size increased. At 1000°C, penetration was entirely along grain boundaries and occurred to a greater depth than that in the 400°C tests. Since lithium penetration is related to the oxygen concentration in the niobium, these results indicate that grain boundaries are preferential sites for oxygen segregation. At low temperatures, certain crystallographic planes also appear to be areas of high oxygen concentration.

If lithium penetration is related to oxygen segregation, then the introduction of dislocations into a niobium single crystal might produce areas where oxygen can accumulate. In order to test this hypothesis, a test was conducted with two niobium single crystals, each containing 1700 ppm of oxygen and each having the same orientation. One crystal was annealed at 1800°C, and the other was cold-rolled to 20% reduction in thickness prior to exposure of both to lithium at 500°C. Conflicting results were obtained in two sets of experiments of this type; therefore, it is not apparent at this time whether a relation exists between deformation and corrosion.

In addition to lithium penetration, oxygen transfer from niobium to lithium has also been found to occur. Preliminary data indicate that the equilibrium distribution of oxygen between niobium and lithium at 800°C is approximately 1 to 40, that is,

$$\frac{C_{O \text{ in Nb}}}{C_{O \text{ in Li}}} = 0.025 .$$

This value is considerably larger than the value of 1×10^{-7} predicted from thermodynamic calculations.[12]

Future studies will include tests to further investigate the effect of deformation on corrosion and to measure more accurately the equilibrium distribution of oxygen between niobium and lithium at several temperatures.

Haynes Alloy No. 25–Boiling-Potassium Loop Test

E. E. Hoffman D. H. Jansen

Potassium is one of the more-attractive alkali metals being considered as a working fluid in Rankine-cycle turbogenerator power systems for the production of electrical power for space applications. Recent corrosion tests have been conducted with systems using natural-circulation boiling potassium contained in loops fabricated of Inconel (80% Ni–14% Cr–6% Fe) and Haynes alloy No. 25 (50% Co–20% Cr–15% W–10% Ni–3% Fe). The primary purpose of these loop tests was to determine the dissolution and deposition rates of these alloys in the condenser and subcooled liquid regions of a two-phase alkali-metal system. The corrosion rates were determined by measuring weight changes on accurately machined sleeve-type inserts that lined the walls of the condenser and subcooler.

The loop design and test conditions for the Haynes alloy No. 25 loop were similar to those for the Inconel–boiling-potassium test.[13] The nominal boiler and condenser temperature was 870°C (1600°F) during a test duration of 3000 hr, while the lowest temperature in the subcooler of this loop was 730°C (1350°F). The flow rate was maintained at 180 g/min (24 lb/hr), this being equivalent to a vapor velocity of 50 fps in the ½-in. sched-40 vapor carry-over line. A condensing rate of approximately 0.55 g cm^{-2} min^{-1} was obtained.

Boiling instabilities that occurred during the test resulted in frequent temperature and pressure fluctuations in the system, as indicated in Fig. 19.14. The temperature was measured in a thermocouple well located just below the liquid-vapor interface in the condenser. As shown in the figure, pressure surges due to flashing of superheated liquid in the boiler were followed by temperature rises as large as 70°C (125°F). These surges occurred on an average of every 90 sec. Recent findings on boiling instabilities and methods of suppressing them from a series of refluxing-capsule tests are reported in "Boiling-Potassium Stability Studies," which follows in this chapter.

The principal mass-transfer effects noted in this test were deposits at the liquid-vapor interface in the boiler and in the subcooled liquid region

[12] J. R. DiStefano and E. E. Hoffman, *Corrosion Mechanisms in Refractory-Metal–Alkali-Metal Systems*, ORNL-3424 (in press).

[13] E. E. Hoffman and D. H. Jansen, *Metals and Ceramics Div. Ann. Progr. Rept. May 31, 1962*, ORNL-3313, pp 29–31.

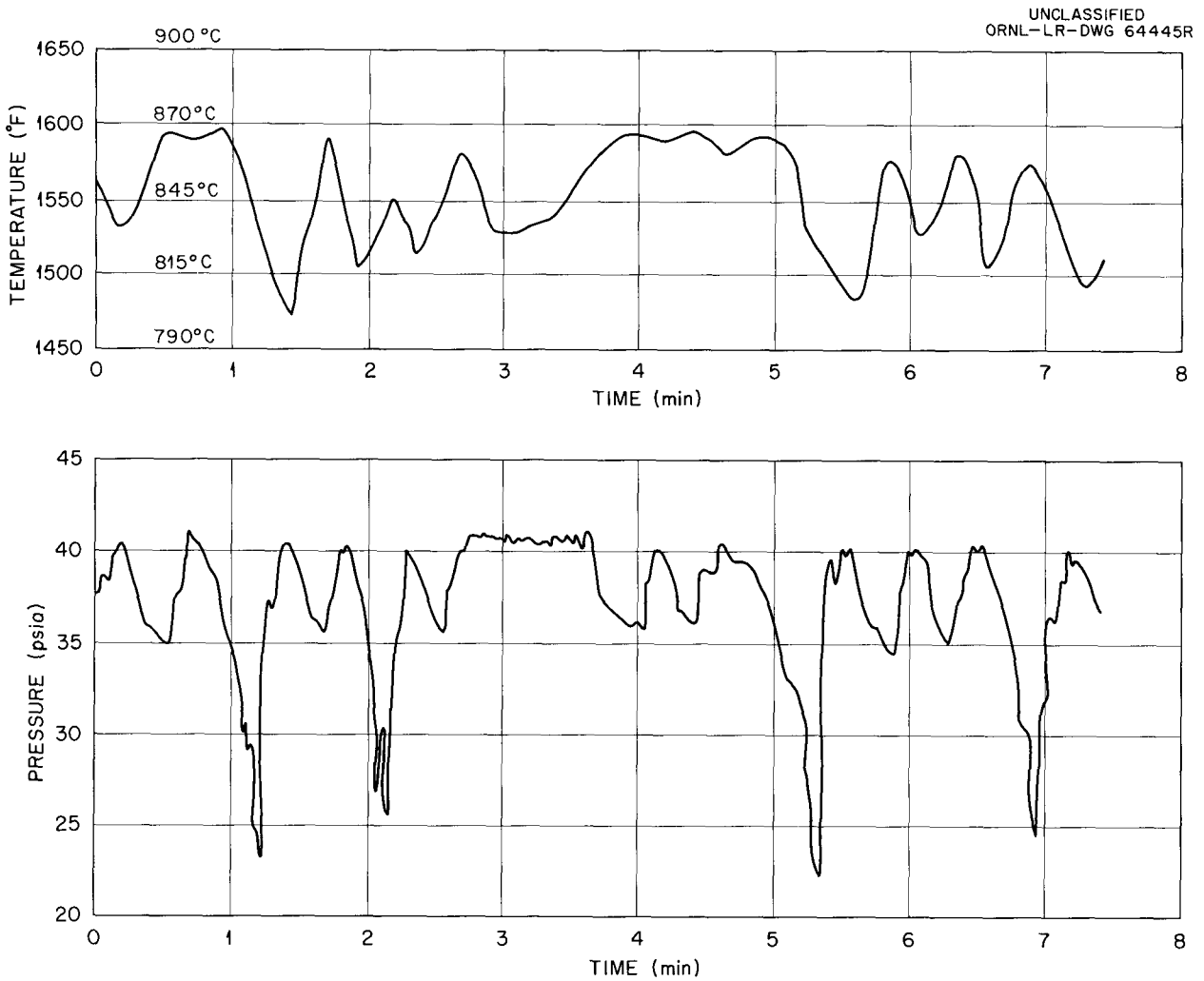

Fig. 19.14. Temperature-Pressure Profile for Haynes Alloy No. 25–Boiling-Potassium Loop Test.

of the system. A narrow band of metallic deposition approximately 0.040 in. thick was found in the boiler. The chemical analysis of this deposit indicated that it was preferentially enriched in cobalt (Table 19.7). X-ray analysis identified the deposit from the subcooler as the chromium carbides $Cr_{23}C_6$ and Cr_7C_3. Results of a microprobe analysis indicate no selective leaching of the major constituents (Co, Cr, W, Ni, and Fe) of the alloy from the condenser wall.

Weight-change determinations on the inserts that lined the condenser and subcooled liquid sections of the loop showed a uniform removal of approximately 1.2 mg/cm^2 (<0.0001 in. uniform surface

Table 19.7. Analyses of Mass-Transferred Deposit Found in Boiler of Haynes Alloy No. 25 Loop Test

Location of Deposit	Chemical Analyses[a] (wt %)				
	Co	Cr	Ni	Fe	W
Liquid-vapor interface, boiler	65	7	14	2	11
Nominal composition	50	20	10	3	15

[a]Adjusted to 100%.

removal) in the condenser and a maximum weight gain of 6.2 mg/cm^2 in the subcooler. This weight gain was associated with a metallic deposit approximately ½ mil thick.

The results of chemical analyses revealed a transfer of carbon from the condenser to the subcooled region, as indicated in Table 19.8. A comparison of the chemical analyses of turnings from the insert walls and of the total cross sections of the tensile specimens that were suspended in the boiler section of the loop indicates that a major portion of the carbon picked up in the subcooled liquid region came from the liquid region of the boiler. This carbon transfer is attributed to liquid carry-over when flashing occurred in the boiler.

The most-severe corrosion observed in the loop was 2-mil-deep subsurface voids at the liquid level in the boiler. Attack in the vapor carry-over line [870°C (1600°F)] was limited to a surface roughening and scattered subsurface voids to a maximum depth of 1 mil.

The results obtained from tests of tensile specimens suspended in various regions of the loop and control specimens heat-treated in argon indicate that the exposure to potassium resulted in slight increases in the room-temperature ductility of specimens from the hottest regions of the loop and in slight decreases in the room-temperature ductility of specimens from the subcooled liquid regions of the loop.

The most serious damage to the loop material was cracking that occurred in the weld zones of the inserts in the vapor region of the condenser. These cracks were attributed to thermal fatigue induced by alternating surges of potassium vapor. Cracks were found also in the vicinity of the liquid-vapor interface of the boiler. Since cracks were observed only in those regions of the boiler that suffered alternate exposure to liquid and vapor, this damage too is believed to have occurred as a result of thermal fatigue induced by an oscillating liquid level that was in turn caused by the unstable boiling conditions (see Fig. 19.15).

In summary, the dissolution and deposition rates obtained in this test were lower than those observed in an earlier test of Inconel under similar test conditions. If methods can be devised to stabilize boiling in these systems and thus eliminate the thermal-fatigue problem, it appears that Haynes alloy No. 25 is a promising material for applications requiring potassium containment at temperatures of approximately 900°C (1650°F).

Table 19.8. Carbon Analyses on Turnings Machined[a] from Haynes Alloy No. 25 Inserts Following 3000 hr of Exposure to Potassium

Specimen Number and Location	Temperature of Specimen During Test (°C)	Temperature of Specimen During Test (°F)	Carbon Content[b] (wt %)
Insert No. 8, condenser region	870	1600	0.09
Insert No. 28, subcooled liquid region	670	1250	0.45
Insert No. 40, preheated liquid region	730	1350	0.47
As-received material			0.09

[a]Nine mils machined from inner surface of pipe wall.
[b]Each value is the average of a minimum of three determinations on each sample.

Boiling-Potassium Stability Studies

E. E. Hoffman

For several years, corrosion-testing programs have been under way at this Laboratory and elsewhere to determine the compatibility of container metals with two-phase liquid metals at elevated temperatures. The compatibility evaluations have been complicated to varying degrees by liquid-metal carry-over from the boiler region of these systems during periods of unstable boiling. Typical thermal and system pressure fluctuations that have been observed in natural-circulation boiling-potassium loops are illustrated in Fig. 19.14. The frequency of these instabilities generally increased with system temperature, but major instabilities every few minutes were typical in systems operating at 870°C, the most-common boiler test temperature. Observations of system pressure and thermal conditions indicated that the unstable boiling could be characterized by two principal periods: (1) an interval during which simultaneously the boiler-liquid temperature rose,

UNCLASSIFIED
PHOTO 56852

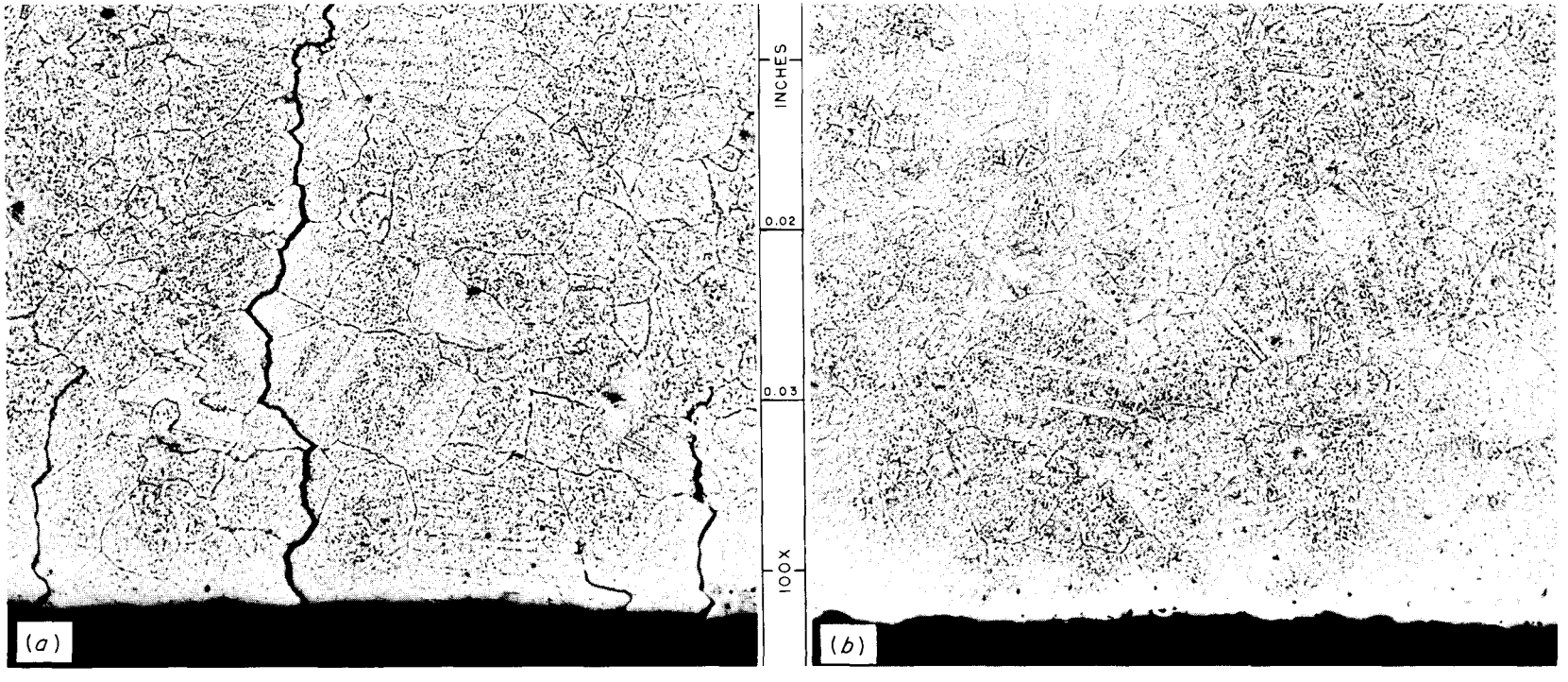

Fig. 19.15. Sections Cut from Wall of Boiler Section of Haynes Alloy No. 25 Loop. (*a*) Section in contact with vapor. (*b*) Section taken where liquid level fluctuations occurred. Etchant: modified aqua regia. 100X. Reduced 8%.

the condenser temperature fell, and the system pressure dropped far below the saturation pressure, followed by (2) an audible "bump" associated with flashing of the superheated liquid in the boiler which resulted in a rapid drop in boiler-liquid temperature, a rise in condenser temperature, and an increase in system pressure to the saturation value. The most notable complications introduced into the compatibility studies by these instabilities are the unknown mass-transfer effect(s) of the liquid carry-over on condenser dissolution and subcooler deposition and, even more serious, the failure of these systems by thermal fatigue. The effects of boiling alkali-metal instabilities on thermal-fatigue cracking have been discussed in previous reports.[14–17] During the test program, numerous changes in the design of the natural-circulation loop were effected in a futile attempt to stabilize boiling. The major changes included more-uniform heating of the boiler (sodium jacket), decreasing the vapor velocity (larger boilers), and varying the amount of liquid preheat.

Since lack of nucleation seemed to be responsible for the boiling instabilities described above, a test program has been conducted to evaluate the effectiveness of various devices in promoting nucleation of vapor bubbles in alkali metals. Only the salient results of these studies will be cited here since the details will be presented in a forthcoming topical report.

The boiling-stability studies were conducted in refluxing capsules of the type shown in Fig. 19.16. The capsules used in these studies were fabricated from Haynes alloy No. 25. Localized superheating of the potassium was obtained by means of a 0.050-in.-diam hot finger (or well of potassium) located at the bottom of the capsule in a rod heated with a gas flame. The gas flame was found to be an effective means of making rapid and easily controlled temperature adjustments in the $\frac{1}{4}$-in.-diam rod. The bulk of the heat input to the capsule (approximately 800 w for 870°C operation) was supplied by the cylindrical resistance heater that surrounded the boiler region. This test configuration made it possible to effect large variations in the hot-finger temperature while holding the bulk liquid temperature, as measured in the thermocouple well, at a reasonably constant value. It should be noted in the following discussion that the hot-finger temperature is measured $\frac{1}{4}$ in. away from the tip of the potassium well and therefore is believed to be considerably higher than the container-metal temperature at the solid-liquid (or vapor) interface. For this reason the temperature differences reported (hot-finger temperature minus boiler-liquid temperature) are larger than the true ΔT at the interface.

The effect of localized superheating of potassium in a refluxing capsule by means of the hot-finger technique is illustrated in Fig. 19.17. The liquid and vapor temperatures of the potassium are plotted as a function of time, with the heat input to the boiler essentially constant at approximately 800 w. It may be noted that, as the hot-finger temperature was increased, periodic boiling continued until a critical finger temperature of approximately 995°C was reached. At this temperature, continuous boiling began, and the liquid and vapor temperature differential decreased from approximately 200°C to 25°C and remained constant until the temperature of the finger was decreased to approximately 865°C. At this finger

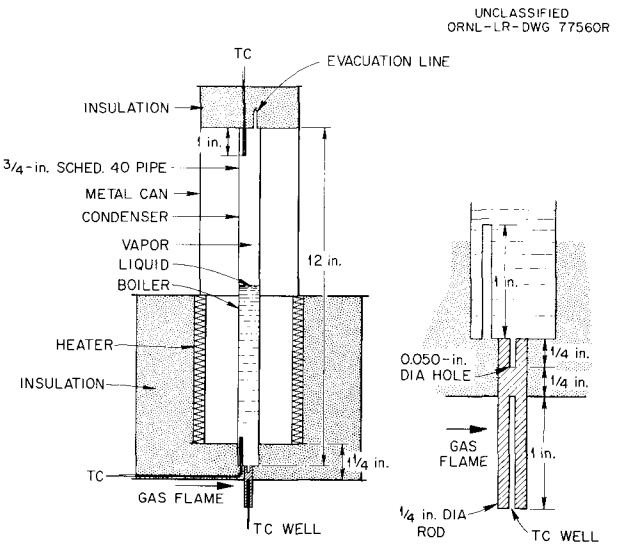

Fig. 19.16. Refluxing Test Capsule.

[14] E. E. Hoffman and D. H. Jansen, ORNL-3270, pp 91–101 (classified).

[15] D. H. Jansen and E. E. Hoffman, ORNL-3337, pp 113–16 (classified).

[16] D. H. Jansen and E. E. Hoffman, ORNL-3420, pp 222–27 (classified).

[17] E. E. Hoffman, "Boiling Alkali Metal and Related Studies," pp 15–24 in *NASA-AEC Liquid Metals Corrosion Meeting, December 7–8, 1960, Washington, D.C.*, NASA TN-D-769 (February 1961).

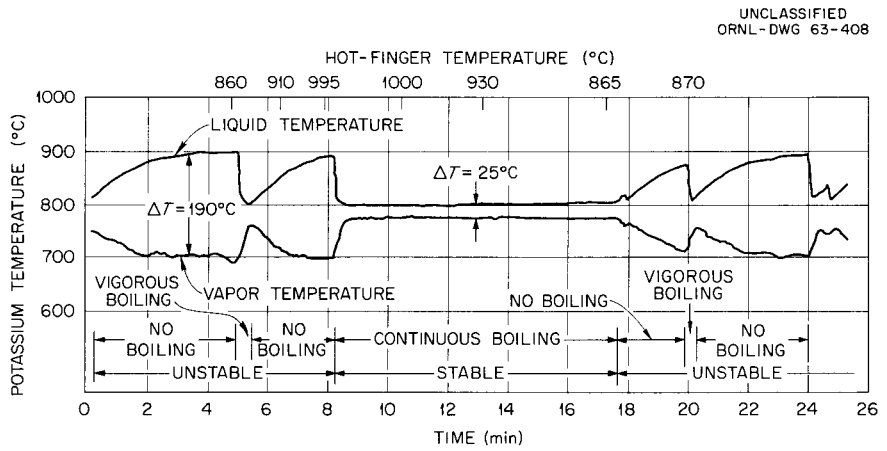

Fig. 19.17. Effect of Hot-Finger Temperature on the Boiling of Potassium in a Refluxing Capsule.

temperature, boiling in the capsule again became unstable. This unstable condition continued until the hot-finger temperature was once more increased to approximately 1000°C. Of special interest is the observation that the ΔT (between the hot-finger temperature and the average liquid temperature) required to initially stabilize boiling was approximately 150°C, whereas a ΔT of approximately 70°C was sufficient to maintain the the stable (or continuous) boiling conditions.

The extent of boiling at various times is also indicated in Fig. 19.17. This was determined by means of a contact microphone used in conjunction with an amplifier, a tape recorder, and a millivolt recorder. The sounds associated with boiling were recorded and plotted, and these observations proved to be more sensitive than temperature measurements in following the activity inside the capsule.

The hot-finger temperature required to stabilize the boiling of potassium was studied over a liquid temperature range from 800 to 1050°C, and, over the entire range, a ΔT between the hot-finger temperature and the average liquid temperature of approximately 150°C was required to establish continuous (stable) boiling. Also, over this temperature range, decreasing the ΔT to approximately 60°C resulted in the reestablishment of the unstable condition. Recent studies have been conducted to accurately measure the temperature of the hot finger and the liquid to obtain more-precise values of the ΔT required to achieve stable boiling. In these studies a metal-sheathed thermocouple formed the bottom of the potassium well in the hot finger. These results indicate that a ΔT of 50 to 60°C is required to obtain and maintain bubble nucleation at the hot finger. An additional observation in these experiments was that the "bump" frequency during unstable boiling increased as the liquid temperature increased, from one every several minutes at an average liquid temperature of 840°C to four per minute at a liquid temperature of 1050°C. The temperature variation in the liquid during an unstable cycle decreased from values as high as 100°C at an average liquid temperature of 840°C to less than 10°C at 1050°C.

A similar experiment to that described above for potassium was conducted with rubidium. Since rubidium has a higher vapor pressure than potassium at a given temperature, it was anticipated that the characteristic instabilities found in potassium would be shifted to lower temperatures for rubidium. This was found to be the case. The results of one hot-finger experiment on the rubidium capsule are given in Fig. 19.18. The instability pattern noted for rubidium under these temperature conditions was similar to that noted for the potassium test at higher temperatures (higher than those illustrated in Fig. 19.17). A temperature difference of approximately 200°C between the liquid and the hot finger was required to stabilize boiling; decreasing this ΔT to approximately 60°C resulted in the onset of the unstable condition.

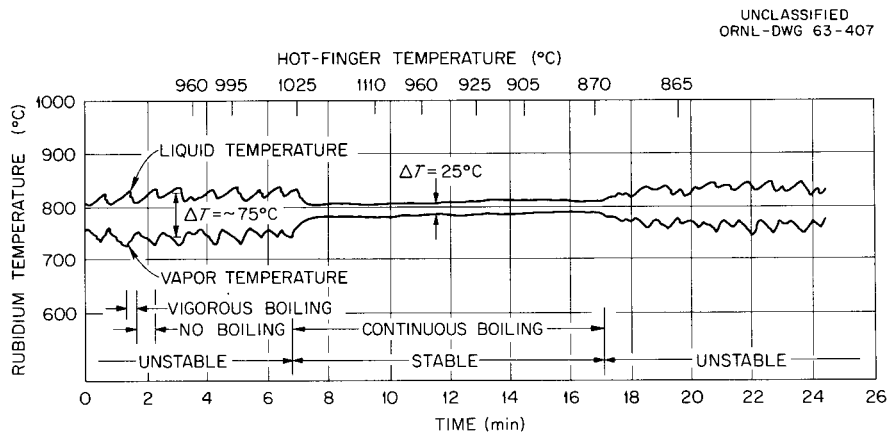

Fig. 19.18. Effect of Hot-Finger Temperature on the Boiling of Rubidium in a Refluxing Capsule.

In both the potassium and rubidium hot-finger experiments discussed above, the temperature gradient (150 to 200°C) required to initially stabilize boiling at a given liquid temperature was found to be considerably larger than the temperature gradient (70 to 100°C) required to maintain the stable condition.

A number of other "devices" have been evaluated as possible stabilizers for two-phase potassium systems. These have included (1) an ebullition tube immersed in the boiler liquid, (2) pointed rods resting on the bottom surface of the capsule, and (3) a small addition (2 wt %) of a lower-boiling-point alkali metal (rubidium) to potassium in a natural-circulation boiling-potassium loop. The pointed rods and alkali-metal addition were found to be totally ineffective in suppressing the boiling instabilities. The ebullition tube, while apparently improving the stability, was not as satisfactory as the hot finger. As a result of these studies, hot-finger bubble nucleators will be incorporated into future compatibility tests.

MECHANICAL PROPERTIES

Materials Evaluation

R. L. Stephenson H. E. McCoy

This program has two basic objectives. The first is to generate, for design purposes, mechanical property data on promising commercially available refractory-metal alloys. The second objective is to gain a better understanding of how certain metallurgical variables influence the mechanical behavior of refractory metals. This includes parameters such as fabrication history, heat treatment, and changes in concentration and distribution of interstitial impurities. A major portion of the effort to date has been expended on the construction of equipment suitable for conducting mechanical property tests at elevated temperatures without contaminating these reactive materials. A test chamber with a small internal tantalum heater was designed for this purpose and is shown schematically in Fig. 19.19. Alumina-tube test chambers with external heating have also been used with reasonable success but do not appear to have the same ultimate capability. To date, work has been completed on alloys of Mo–0.5% Ti, Nb–40% V–1% Ti, and Nb–1% Zr and is summarized in the ensuing paragraphs.

Studies of the Mo–0.5% Ti alloy were initially undertaken primarily because of the availability of test material. However, it was also felt that the state of knowledge with respect to the long-time stress-rupture behavior of this material and the influence of metallurgical variables such as fabrication procedure and heat treatment was ill-defined. Figure 19.20 shows the stress-rupture properties of Mo–0.5% Ti (heat No. KDTM-507) at 1090, 1200, and 1315°C. Several points are also included for another heat (KDTM-678C) of material having the same nominal composition.

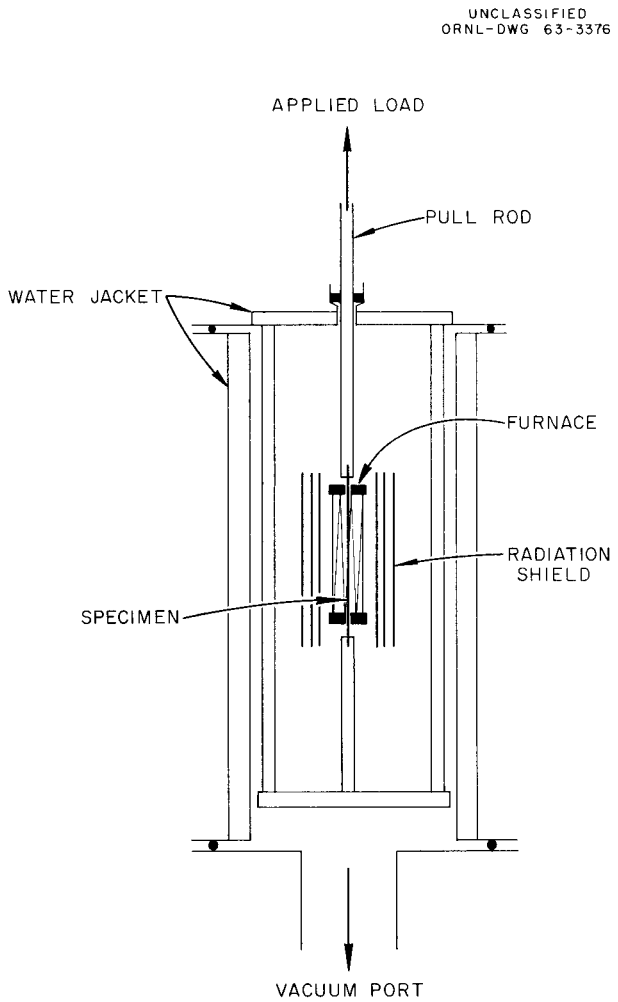

Fig. 19.19. Schematic Drawing of High-Temperature Creep-Testing Apparatus.

Studies by Semchyshen *et al.*[18] have shown an Mo–1.25% Ti–C alloy to be sensitive to the carbon-to-titanium ratio. Vendors' analyses indicated that the carbon-to-titanium ratio (expressed in weight percent) of the first heat of material used in the present work was 0.043 and that of the second heat was 0.059. Since the ratio is higher for the weaker material, the large strength difference must be related to other variables.

Future efforts on this material will be directed toward determining the effectiveness of gas carburization as a strengthening process and the effects of anisotropy on the high-temperature creep strength.

Nb–40% V–1% Ti Alloy. – In spite of excellent fabricability and weldability[19] and impressive elevated-temperature tensile strengths,[20] niobium-vanadium alloys have been shown[21] to have unsatisfactory creep properties at 1090°C. This, however, does not preclude the possibility of these alloys having satisfactory strengths for intermediate-temperature applications such as waste-heat radiators in space reactors. Accordingly, a small quantity of Nb–40% V–1% Ti was obtained for creep testing at 870°C. Table 19.9 shows the creep-rupture properties obtained.

From these data it can be stated that the Nb–40% V–1% Ti at 870°C is scarcely equal in rupture strength to Nb–1% Zr at 1090°C. Furthermore, the rupture ductilities of the Nb–40% V–1% Ti alloy specimens are greater than 150%, and, to be realistic in the design of structural members, an additional penalty must be paid with this alloy if the design is strain-limited.

Nb–1% Zr Alloy. – The main objective of this program is to evaluate the importance of several variables on the high-temperature mechanical properties of the Nb–1% Zr alloy. The variables include (1) test temperature, (2) prior annealing treatment, (3) amount of prior cold deformation, (4) orientation of test piece with respect to the rolling direction, and (5) the effectiveness of carburization and nitriding as strengthening processes. The primary reasons that Nb–1% Zr alloy was chosen for this work are its availability in lots having fairly reproducible properties and the current interest in this alloy as a reactor structural material.

Results of several tests run on as-received material are summarized in Fig. 19.21. The history of this material is as follows: billet to 0.160-in. sheet, unknown; 0.160 to 0.100-in. sheet, rolled at 425°C; and 0.100 to 0.060-in. sheet, cold-rolled. From the limited data currently available, the exact effects of contamination (primarily

[18] M. Semchyshen, R. Q. Barr, and E. Kalns, *Arc-Cast Molybdenum and Tungsten-Base Alloys,* Climax Molybdenum Company of Michigan, November 1962.

[19] B. R. Rajala, R. J. Van Thyne, and D. W. Levenson, *Improved Vanadium-Base Alloys,* ARF 2165-6 (Dec. 1, 1959).

[20] B. R. Rajala, F. C. Holtz, and R. J. Van Thyne, *Improved Vanadium-Base Alloys,* ARF 2210-2 (April 1961).

[21] B. R. Rajala and R. J. Van Thyne, *Improved Vanadium-Base Alloys,* ARF 2191-6 (Nov. 30, 1960).

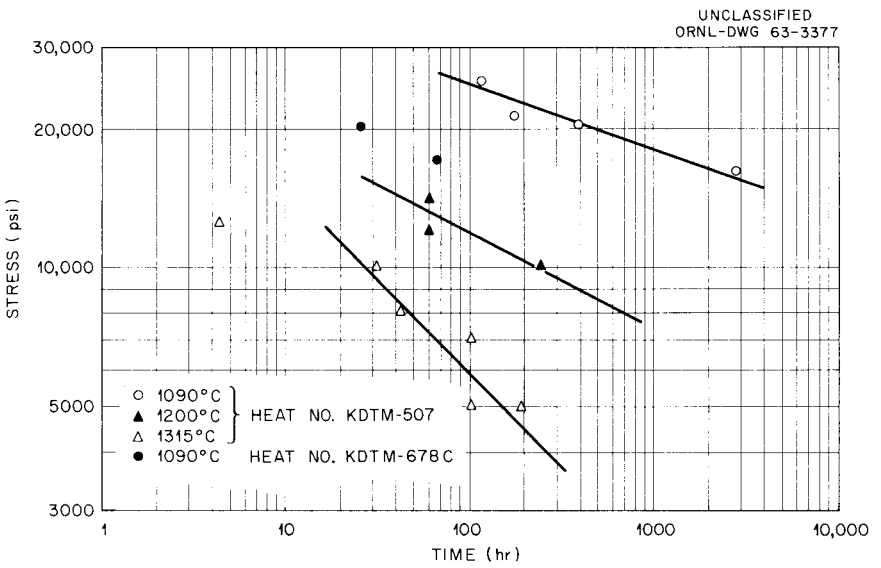

Fig. 19.20. Stress-Rupture Properties of Mo–0.5% Ti.

Table 19.9. Creep-Rupture Properties of Nb–40% V–1% Ti at 870°C

Test No.	Stress (psi)	Time (hr) to 1% Creep	2% Creep	5% Creep	10% Creep	Rupture
2409	6,000	5.4	11.2	31.5	70.0	399.6
2355	8,000	4.9	11.2	33.5	73.0	515.9
2353	10,000	0.35	0.9	9.6	33.6	395.9
2438	10,000	2.4	5.6	15.4	32.3	245.4
2354	12,000	1.3	3.4	10.5	23.0	80.4

oxygen) during testing cannot be ascertained. However, it appears that the rupture life is not particularly sensitive to moderate amounts of contamination. Based on the two transverse tests run to date, there appears to be little difference in the rupture properties of specimens taken either transverse or parallel to the rolling direction.

Internal Friction in Nb–1% Zr Alloy

R. L. Stephenson H. E. McCoy

Internal friction is being used to investigate the behavior of interstitials in niobium-zirconium alloys in order to explain the aging phenomena that are observed in this alloy.[22,23] In order to quantitatively interpret aging data, it is necessary to carry out background studies on specimens of unalloyed niobium containing only nitrogen or oxygen and on specimens containing various amounts of zirconium and nitrogen or oxygen. The results of studies on Nb-O and Nb-Zr-O alloys have been reported.[24]

[22]D. O. Hobson, *A Preliminary Study of the Aging Behavior of Wrought Columbium–1% Zirconium Alloys*, ORNL-2995 (Jan. 6, 1961).

[23]D. O. Hobson, *Aging Phenomena in Columbium-Base Alloys*, ORNL-3245 (Mar. 16, 1962).

[24]R. L. Stephenson, ORNL-3337, pp 162–64, Oct. 2, 1962 (classified).

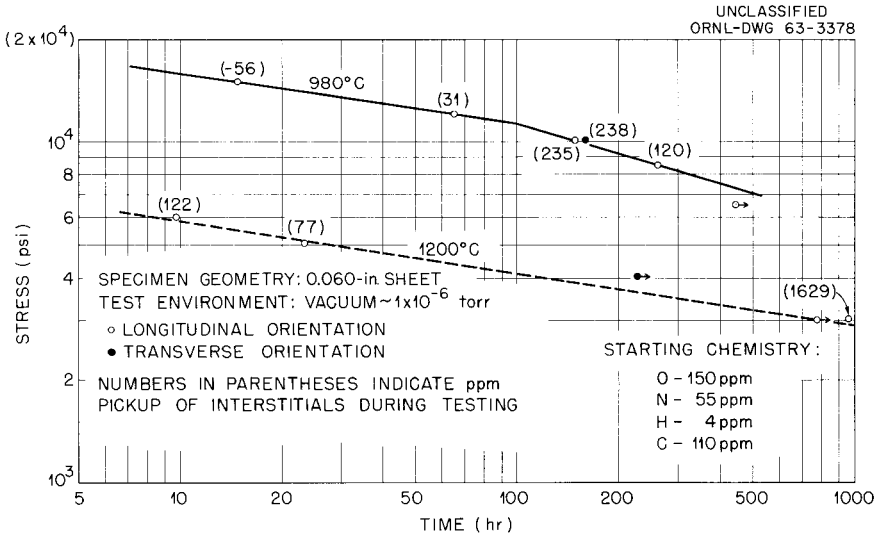

Fig. 19.21. Stress-Rupture Properties of Nb–1% Zr Alloy at 980 and 1200°C.

Figure 19.22 shows the internal-friction spectrums of an Nb–0.7% Zr specimen containing primarily nitrogen; the effect of aging on the peak heights is quite apparent. The peaks at approximately 160 and 220°C are due to oxygen and have been discussed previously.[24] It is known[25] that the peak at approximately 300°C is due to the stress-induced motion of nitrogen atoms. The newly observed peaks at approximately 380 and 480°C are also thought to be related to nitrogen, and their identification is the object of current experiments.

It can be seen from Fig. 19.22 that initially all peaks decrease on aging; but on further aging, the ordinary nitrogen peak (at ~300°C) increases in height. From studies with niobium-nitrogen alloys, it appears that the presence of zirconium is necessary for the peaks to be observed at 380 and 480°C. It, therefore, seems possible that these peaks are due to the stress-induced motion of nitrogen atoms among abnormal interstices created by the presence of the larger zirconium atoms. If one tentatively assumes the validity of this model, the foregoing observation can be explained in the following manner. Nearly all the available zirconium has been consumed in the formation of oxide and nitride precipitate, not leaving sufficient abnormal sites for the remaining nitrogen atoms. They are therefore forced to occupy the normal interstitial positions and thus produce a higher normal nitrogen peak. When specimens of unalloyed niobium containing nitrogen are aged, a broad peak appears at approximately 570°C. Preliminary observations indicate

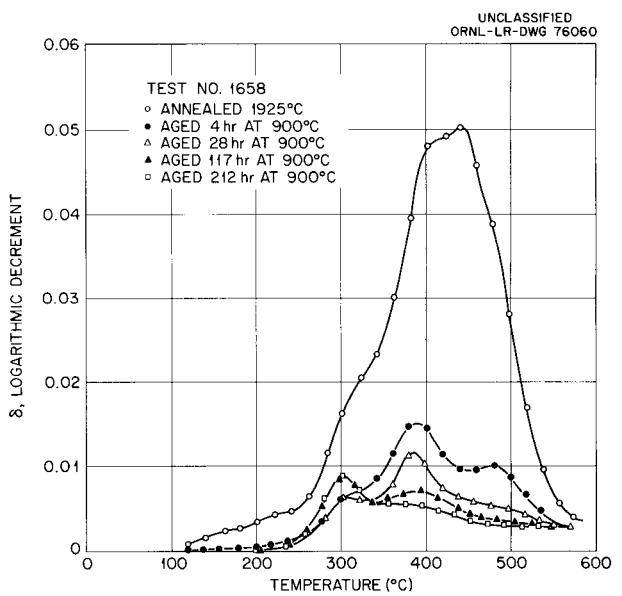

Fig. 19.22. Effect of Aging on Internal Friction Spectrum of Nb–0.74% Zr Containing 4900 ppm Nitrogen and 1600 ppm Oxygen.

[25] R. W. Powers and M. V. Doyle, *Trans. AIME* **209**, 1285 (October 1957).

that the height of the peaks is proportional to the quantity of nitride precipitate. When large amounts of nitrogen are present, however, it appears that below a certain minimum amount (~770 ppm) a different behavior is observed.

Work is continuing on the identification of these three unexplained peaks and on the direct determination of the effect of particular interstitials on mechanical properties.

REFRACTORY-METAL JOINING

Component Fabrication

E. A. Franco-Ferreira

A large loop for liquid-metal corrosion testing was fabricated of Nb–1% Zr alloy. An overall view of the completed loop is shown in Fig. 19.23*a*. The total height of the loop is approximately 10 ft, and its width is approximately 2 ft, making it the largest refractory-metal structure ever fabricated at ORNL.

All welding of the loop was done by a specially qualified welder of the Engineering and Mechanical Division under the constant supervision of the Welding and Brazing Group. The welding was carried out in a large inert-atmosphere chamber which initially could be evacuated to a pressure of 10^{-5} torr and then backfilled with high-purity argon. Atmospheric purity was constantly monitored using Nb–1% Zr sample welds for chemical analyses. These samples showed that impurity levels in the completed welds did not greatly exceed the normal levels in the as-received base material.

Because of the inherent difficulties associated with welding in a chamber, many special measures had to be taken. Since the loop was large and cumbersome, the proper sequencing of welds was quite important in order to ensure accessibility of all joints. In addition, owing to the need for maintaining proper alignment of the parts and the difficulty of manually holding the parts during tack-welding, special jigs were required to position each joint. A closeup view of several of the completed joints is shown in Fig. 19.23*b*.

It was found that joint design requirements differed considerably from those used for stainless steel. In all cases, larger joint gaps and more shallow bevels were required. A total of 74 separate welds were produced in the loop.

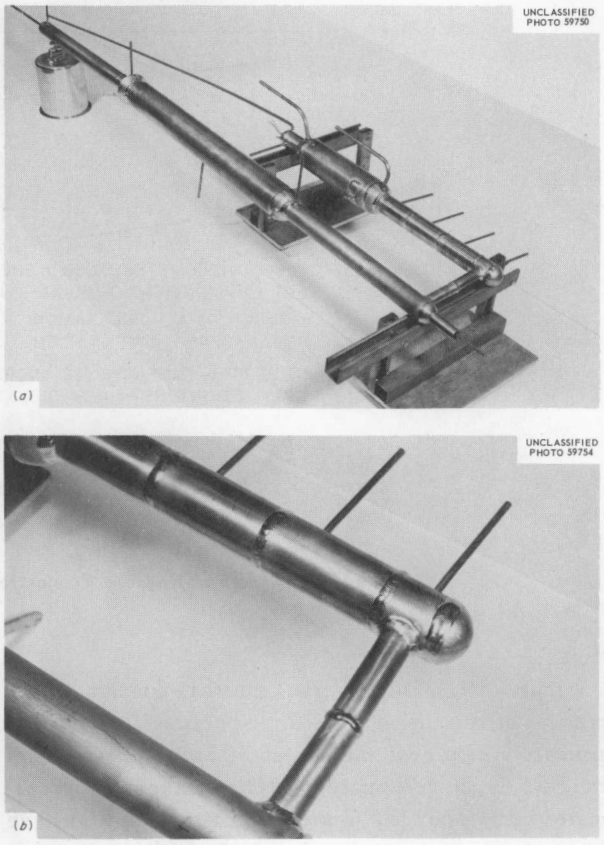

Fig. 19.23. (*a*) Overall View of Nb–1% Zr Alloy Loop; (*b*) Closeup Showing Several Completed Welds.

PHYSICAL PROPERTIES

This phase of the program has two goals relative to the materials of interest: (1) to compile and correlate existing high-temperature thermophysical property data and (2) to develop equipment and measure high-temperature thermophysical properties.

Data Compilation and Correlation

D. L. McElroy

A survey to compile the existing knowledge on the thermophysical properties of the pure metals Nb, Mo, Ta, and W and ten of their nearest neighbors was completed. The first draft of this survey has been tabulated, and, as expected, data were

missing for many of these properties in the temperature range of interest; however, the available information provides a reasonable first approximation for certain design calculations. An analysis of these data showed that a Wiedemann-Franz-Lorentz (W-F-L) relation was applicable for these pure metals. In particular, the temperature dependence of thermal conductivity can be obtained by differentiation of the W-F-L relation. This analysis shows that the magnitude of the temperature coefficient of the electrical resistivity determines whether k increases or decreases with increasing temperature, as described in Part I, Chap. 6.

Development of Measuring Equipment

D. L. McElroy

Progress was made on apparatus of potential use for this program including the total hemispherical emittance apparatus described below and the direct-heating apparatus and the hot-probe apparatus described in Part I, Chap. 6. The temperature dependence of the total hemispherical emittance was obtained by two methods: one employs an instrumented strip specimen, heated electrically, and the other uses an instrumented hollow cylindrical specimen, which totally encloses an axial heater. The specimens are heated in a black-body vacuum chamber held at a constant temperature. The strip specimen data also yield electrical resistivity values. Measurements were made on two types of stainless steel and an Nb–1% Zr alloy. Table 19.10 lists the results on type 310 stainless steel cylinders and on a type 316 stainless steel strip specimen. The values for type 316 stainless steel were 7 to 15% above those for the type 310 stainless steel specimen, and both showed a linear increase with temperature. An etched type 310 stainless steel sample and an etched and oxidized sample had total hemispherical emittance values 25% and 300% higher, respectively, than the unetched specimen. Table 19.11 lists the results obtained on two strips of Nb–1% Zr alloy in a vacuum of 6 to 9×10^{-6} torr and on a cylindrical specimen in a vacuum of 2 to 3×10^{-6} torr. Above 600°C the total hemispherical emittance of all the specimens increased because of oxidation, and the effect was more pronounced the higher the temperature. In general, the results on the hollow-cylinder-type specimen agree with those on the strip-type specimen. Further measurements are in progress on the Nb–1% Zr alloy at lower pressures.

Table 19.10. Total Hemispherical Emittance Values of Stainless Steel

Temperature (°C)	Type 310 Stainless Steel Cylinders			Type 316 Stainless Steel Strip
	As Received	Etched	Etched and Oxidized	As Received
100	0.153	0.200	0.485	0.175
200	0.167	0.214	0.542	0.184
300	0.181	0.299	0.572	0.195
400	0.195	0.241	0.594	0.208
500	0.206	0.255	0.610	0.222

Table 19.11. Total Hemispherical Emittance Values of Nb–1% Zr Alloy Specimens

Temperature (°C)	Strip Specimen No. 1		Strip Specimen No. 2 Pretreated at 800°C		Cylindrical Specimen No. 5	
	On Heating	On Cooling	On Heating	On Cooling	On Heating	On Cooling
100	0.134				0.107	0.117
200	0.134	0.207			0.117	0.132
300	0.133	0.214	0.215	0.237	0.127	0.145
400	0.132	0.228	0.227	0.247	0.137	0.159
500	0.137	0.235	0.240		0.146	0.172
600	0.172	0.249	0.252	0.269	0.156–0.178[a]	0.186
700	0.232	0.265	0.266		*b*	0.220
800	0.275		0.280	0.315		0.250
900			0.270	0.334		
1000			0.298			
1100			0.341			
1200			0.382			

[a]Drift with time.
[b]Heater failed.

NONDESTRUCTIVE TESTING

Most of the nondestructive testing activity has been directed toward the evaluation of tubing, including various sizes of molybdenum and molybdenum-alloy tubing and tapered stainless steel tubing. In general, this has involved the use of standard techniques to determine their applicability to new materials and configurations, with a minimum of effort on the development of new techniques.

Molybdenum Tubing

R. W. McClung

Several batches of ⅜-, ½-, and ¾-in.-OD molybdenum and Mo–0.5% Ti tubing have been nondestructively evaluated. Some of the tubing had been fabricated by warm drawing of vacuum-melted and drilled billets; the rest was prepared from vacuum-melted, hot-rolled, drilled, and honed billets. The techniques that have been applied include fluorescent penetrants, resonance and pulse-echo ultrasonics, and radiography. The drilled and honed tubing, which included both ½- and ¾-in. diameters, was found to have the best overall quality. On the ½-in.-diam tubing, the only discontinuities were a few shallow pinholes detected in the outer surface by penetrants. Wall-thickness values determined by resonance ultrasonics indicated that the material was within the commercial ±10% tolerance, and the greatest variations from a nominal 0.025-in. wall were 0.0229 and 0.0268 in. One large crack and two inner-surface gouges were found in the ¾-in.-diam honed tubing.

The ⅜- and ¾-in.-OD tubing fabricated by warm drawing contained the greater number of objectionable flaws, with the ¾-in.-diam lots being inferior to the ⅜-in.-diam lots. Several deep cracks (some of which extended completely through the wall) were found in both the alloyed and unalloyed ¾-in.-diam tubing. Some of these were on the tubing ends. In addition, the larger tubing had a very rough inner surface. The best

of the warm-drawn tubing was $\frac{3}{8}$-in.-diam Mo–0.5% Ti, in which only one crack was detected. Several cracks were found on the unalloyed $\frac{3}{8}$-in.-OD tubing. Wall-thickness variations from the nominal 0.020 in. exceeded the standard commercial tolerance of 10% in both the $\frac{3}{4}$- and $\frac{3}{8}$-in.-OD material.

Tapered Tubing

R. W. McClung C. V. Dodd

Several lengths of type 316 stainless steel tapered tubing were received for studies to determine the applicability of existing nondestructive-testing techniques. The tubes have a nominal outer diameter of 0.700 in. at one end and 0.300 in. at the other. The wall thickness is nominally 0.050 in. throughout.

A short calibration study with resonance ultrasonics indicated that accurate thickness measurements can be made over the entire diameter range of this tubing, with no need for instrument recalibration. Actual wall-thickness readings ranged from 0.047 to 0.051 in.

Two eddy-current probes, which previously had been fabricated for the measurement of tubing inner diameters,[26] were applied to the tapered tubes. These newly developed probes have the capabilities of measuring diameters over a span approximately 15 to 20% of the diameter. This is in contrast to pneumatic gaging, where the limit of the span is approximately 0.004 in. With the smaller probe, inside-diameter measurements were made at $\frac{1}{2}$ and 6 in. from the small end; with the larger probe, measurements were made at $\frac{1}{4}$, 12, and 24 in. from the large tubing end. Measurements on the small end indicated that the specified tolerances were not met, with the diameter generally being too large; measurements on the large end were frequently from 0.001 to 0.004 in. below tolerance.

A newly developed phase-sensitive eddy-current instrument[27] is being applied to the tapered tubing. One approach used a test probe containing one $\frac{1}{8}$-in.-diam coil and two 0.050-in.-diam coils placed on the tubing outer surface. A varying signal level as a function of tube length indicated that changes in inner diameter were affecting the overall signal level. A new test probe has been fabricated for through-transmission testing with one coil in the tube bore and the other on the outer surface. Preliminary spot checks have indicated that accurate wall-thickness measurements can be made with this system. It is anticipated that the same system can also detect the presence of cracks.

---

[26] C. V. Dodd and R. W. McClung, *Fuel Element Coolant Channel and Other Spacing Measurements by Eddy-Current Techniques*, ORNL TM-129 (Mar. 20, 1962).

[27] C. V. Dodd and R. W. McClung, *Metals and Ceramics Div. Ann. Progr. Rept. May 31, 1962*, ORNL-3313, p 49.

Part III.
Reactor Development Support

20. Gas-Cooled Reactor Program

A. E. Goldman

INTRODUCTION

The materials effort under way in support of the Gas-Cooled Reactor Program at the Oak Ridge National Laboratory (ORNL) consists in support for the Experimental Gas-Cooled Reactor (EGCR), experimental studies for advanced, clad gas-cooled reactor fuel elements, development of unclad ceramic fuel elements, and corollary supporting research studies. Major activities in each of these support areas during the past year are presented below, along with pertinent background information.

EGCR SUPPORT

The EGCR, now under construction at Oak Ridge, is an outgrowth of conceptual design studies by Kaiser Engineers, Allis-Chalmers, and ORNL. The reactor core consists of stainless-steel-clad, 2.46% enriched UO_2 fuel in a graphite-moderated core structure contained within a carbon-steel pressure vessel. The plant is being constructed by the H. K. Ferguson Company, and ORNL is responsible for procurement of the fuel and control rod assemblies.

The fuel assemblies consist of seven-element clusters of UO_2 bushings clad with 0.020-in.-thick type 304 stainless steel. The cluster is supported within a 1-in.-thick graphite sleeve that has an outside diameter of 5 in., an inside diameter of 3 in., and a stacked length of 29 in. The UO_2 bushings are 0.707 in. OD × 0.323 in. ID × 0.740 in. long. The design lifetime of the assemblies is conservatively set at 10,000 Mwd/metric ton. The nominal peak operating temperature of the stainless steel cladding is about 1500°F.

Manufacture of the initial fuel loading for startup of the EGCR is continuing at the Atomic Fuel Department of the Westinghouse Electric Corporation. All critical phases of work are being monitored to ensure compliance with the standards specified on materials and workmanship. Approximately 65% of the fuel assemblies (from the Atomic Fuel Department, Westinghouse) have been received at ORNL. The total cost associated with fabrication of the fuel assemblies will be $55 per kilogram of contained uranium metal.

All 25 control rods for the EGCR have been received at ORNL and are now stored at the EGCR site. They are 20 ft long, $3\frac{1}{4}$ in. OD, and have an absorber length of 15 ft. The rods are made in 5-ft-long segments and are supported by a central stainless steel rod that is flexible enough to ensure its entry into the core. Each absorber segment is made up of 3-in.-high annular rings of hot-pressed B_4C encased in copper-plated stainless steel tubing and is vented to the primary coolant system through stainless steel filters. The design life of the rods is more than 20 years.

EGCR Instrumented Fuel Assembly Fabrication

E. A. Franco-Ferreira

Reactor operation plans call for monitoring the temperature of the core components in selected channels through instrumented fuel assemblies. The Welding and Brazing Laboratory is fabricating the instrumented fuel assemblies to be used.[1,2] For the initial core loading, these consist of four instrumented fuel stringers for reactor insertion plus one spare stringer. Each fuel

[1] R. L. Senn, W. G. Cobb, and E. A. Franco-Ferreira, *GCRP Semiann. Progr. Rept. Sept. 30, 1962*, ORNL-3372, pp 67–74.

[2] R. L. Senn, W. G. Cobb, and E. A. Franco-Ferreira, *GCRP Semiann. Progr. Rept. Mar. 31, 1963*, ORNL-3445 (in press).

stringer contains four instrumented seven-rod fuel assemblies. The assemblies are equipped with thermocouples which measure fuel central temperature, fuel cladding temperature, coolant temperature, and graphite-sleeve temperature. To date, twelve clusters (three stringers) have been completed.

Figure 20.1 is a top view of an instrumented fuel assembly. The thermocouples that can be seen measure fuel central temperature, fuel cladding temperature, and coolant temperature. The thermocouples that measure the graphite-sleeve temperature are installed at the time that the individual assemblies are assembled into stringers. This stage of the assembly work is performed by personnel of the Reactor Division.

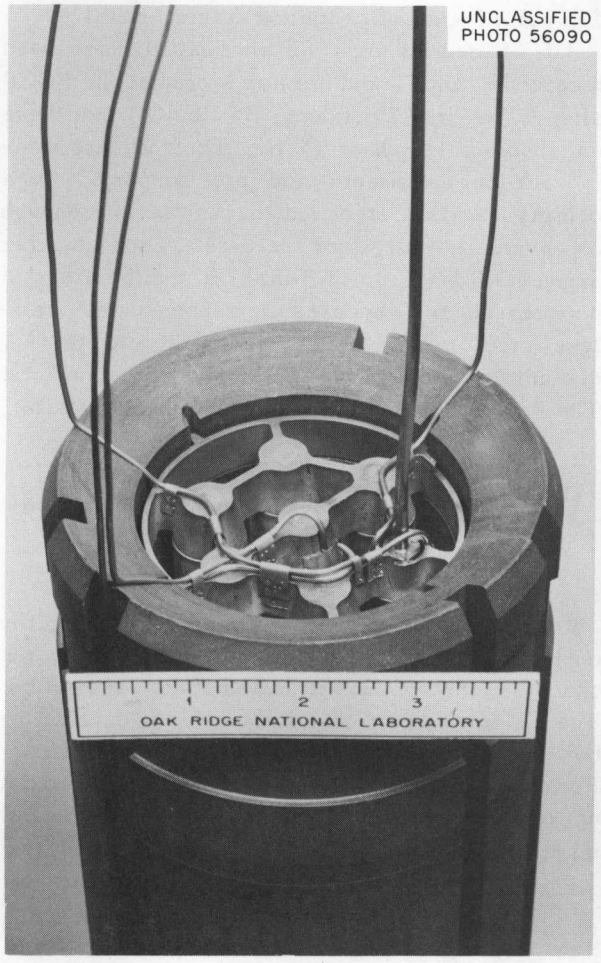

Fig. 20.1. Instrumented Fuel Assembly, Showing Complexity of Thermocouple Attachment.

EGCR Construction Support

G. M. Slaughter E. A. Franco-Ferreira

Metallurgical assistance was provided to the EGCR project in various phases related to construction.[3,4] This included help in brazing components for thermocouple penetrations through the pressure vessel and preparations for the fabrication of dissimilar-metal welds in the primary coolant piping. These welds of ferritic steel to stainless steel will be made at ORNL in view of the difficulties encountered by the outside subcontractor.

Thermocouple-to-Tube Braze Joints

K. V. Cook

A nondestructive testing technique has been developed and applied to the detection of nonbonding in the braze joints between thermocouples and fuel-element cladding for the instrumented fuel assemblies.[5] The ultrasonic technique establishes a "ringing" reflection pattern[6] in the capsule wall. A well-bonded joint will damp the ringing; a poorly bonded joint will have little, if any, effect on the ringing phenomenon.

Graphite Cylinders

R. W. McClung

Nondestructive testing studies[7] were conducted on several $4\frac{1}{2}$-in.-diam graphite cylinders removed from EGCR moderator columns. Evaluation techniques included radiography, eddy current, and ultrasonics. The only obvious discontinuities were several small crack-like indications noted during radiography. The eddy-current technique

---

[3]E. A. Franco-Ferreira, *GCRP Semiann. Progr. Rept. Sept. 30, 1962,* ORNL-3372, pp 85–86.

[4]E. A. Franco-Ferreira, *GCRP Semiann. Progr. Rept. Mar. 31, 1963,* ORNL-3445 (in press).

[5]K. V. Cook, *GCRP Semiann. Progr. Rept. Mar. 31, 1963,* ORNL-3445 (in press).

[6]K. V. Cook and R. W. McClung, "Development of Ultrasonic Techniques for the Evaluation of Brazed Joints," *Welding J.* **41**(9), 404-s–408-s (1962).

[7]R. W. McClung, *GCRP Semiann. Progr. Rept. Mar. 31, 1963,* ORNL-3445 (in press).

performed to detect nonlaminar flaws near the surface found no such discontinuities. The ultrasonic transmission properties were so variable that no interpretation could be made of the data.

Stress-Rupture Tests on EGCR Clad Tubing

J. T. Venard

Sixteen brazed fuel-element cladding tubes were obtained from Westinghouse for use in generating representative stress-rupture data. These tubes had midplane spacers that were copper-brazed in place, using a cycle of 10 min at 2035°F (max) in hydrogen.

Plain specimens $3\frac{3}{4}$ in. long and spacer specimens 5 in. long were cut from these tubes and are being tested in air and in flowing argon.

A plot of logarithmic tangential stress vs logarithmic time to rupture for the completed tests on plain specimens is shown as Fig. 20.2. The dashed lines represent stress-rupture results previously obtained on another heat of type 304 stainless steel (as received) tested in air.[8]

At 1300, 1500, and 1800°F, the data indicate no significant difference in the stress-rupture strengths of the two heats of material. No difference was noted in the results of testing in air or argon. At 1800°F the two EGCR heats seem to be stronger than the previously reported material. This effect may be due to specimen size and cannot be evaluated accurately as yet.

[8] J. T. Venard, *Stress-Rupture Properties of Type 304 Stainless Steel Tubing,* ORNL TM-535 (in press).

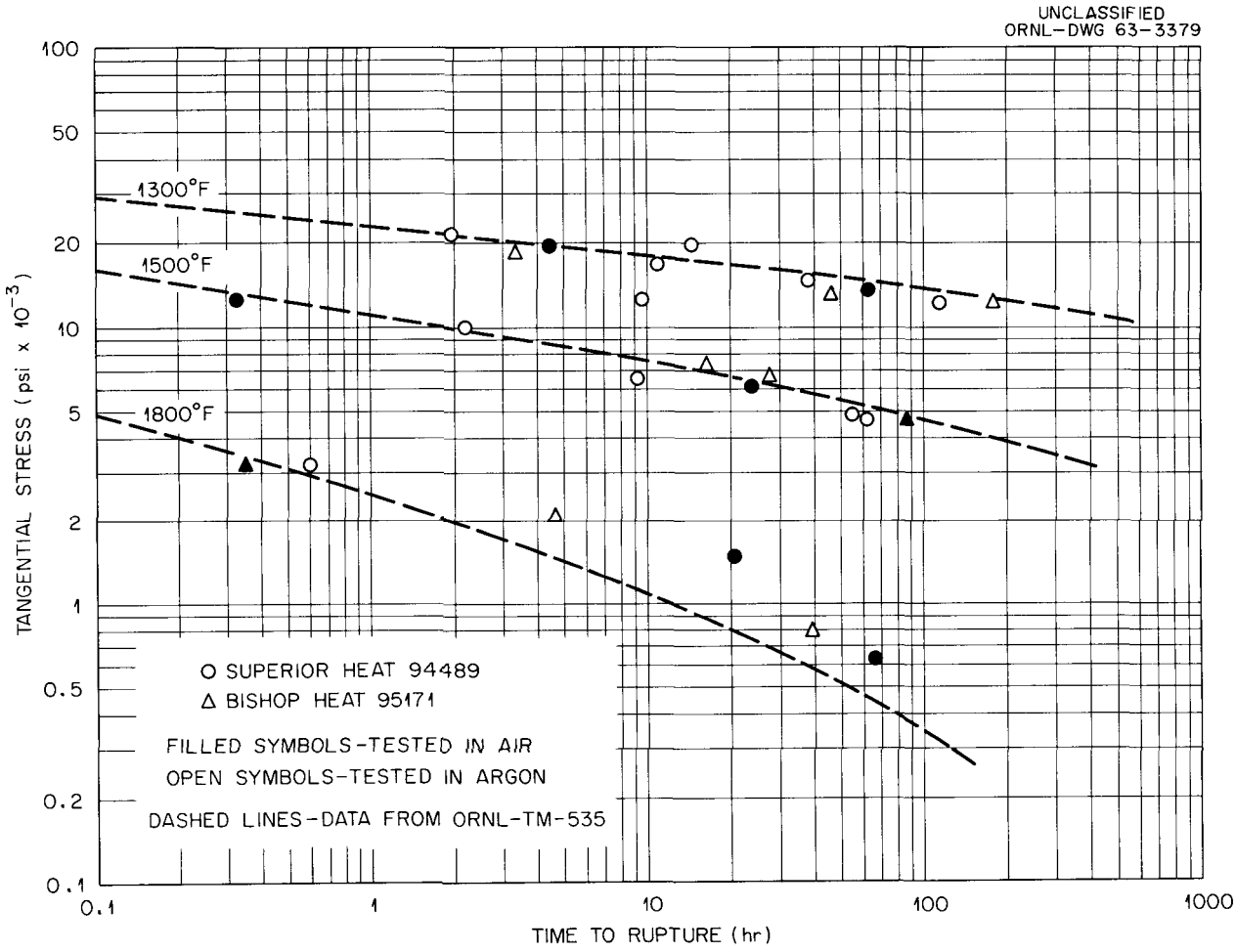

Fig. 20.2. Stress-Rupture Tests on EGCR Clad Tubing.

Strain-at-fracture data on the EGCR heats follow the same general trend with time and compare in magnitude to that obtained on the previously tested material. The grain size for the EGCR heats is approximately ASTM-5 and again is similar to the material previously tested.

Creep of Graphite Under Irradiation

C. R. Kennedy

The irradiation-induced shrinkage of graphite will introduce strains that are much larger than graphite can absorb without fracturing, unless internal-stress concentrations can be reduced through irradiation-induced creep. A parabolic cantilever-beam creep experiment has been placed in the Oak Ridge Research Reactor (ORR) to determine the creep characteristics of graphite and to determine whether graphite can absorb large strains through irradiation-induced creep.

To date, the experiment has been under test for 2350 hr irradiation. The test temperature of the specimens is 450°F, varying about ±40°F in each beam and about ±50°F from beam to beam. Measurement of the flux is in progress; however, it is estimated to be about 1 Mwd/adjacent ton per hour of exposure. The experimental details are described in Part II, Chap. 17.

The results of the creep tests are given in Figs. 20.3, 20.4, and 20.5. Figure 20.3 illustrates the actual creep curves obtained during irradiation, showing the large primary stage of creep. The primary stage can be measured by the zero intercept; these values, compared with values obtained from unirradiated control specimens, are given in Fig. 20.4. The linear creep rates, compared with data obtained from unirradiated control tests, are given in Fig. 20.5.

It is obvious that both the zero intercept (a measure of the primary creep) and the linear creep rate vary linearly with stress. The creep rates under irradiation, however, are still quite low, and it is not practical to extend this experiment to obtain creep strains similar to those expected in the EGCR. The levels of stress will be increased by 50% after 2600 hr exposure and maintained for 4000 hr exposure; the experiment will then be removed from the reactor. It is expected that the maximum creep strain sustained at that time will be 0.2%.

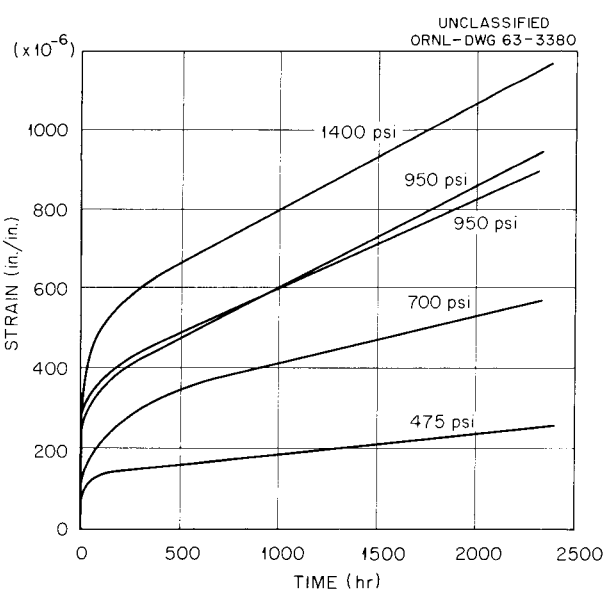

Fig. 20.3. Creep of AGOT Graphite Under Irradiation – ORR 104.

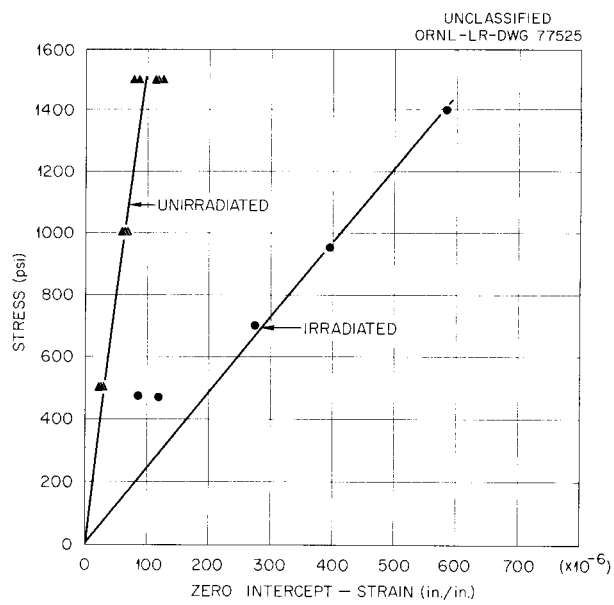

Fig. 20.4. Effect of Irradiation on the Creep of AGOT Graphite.

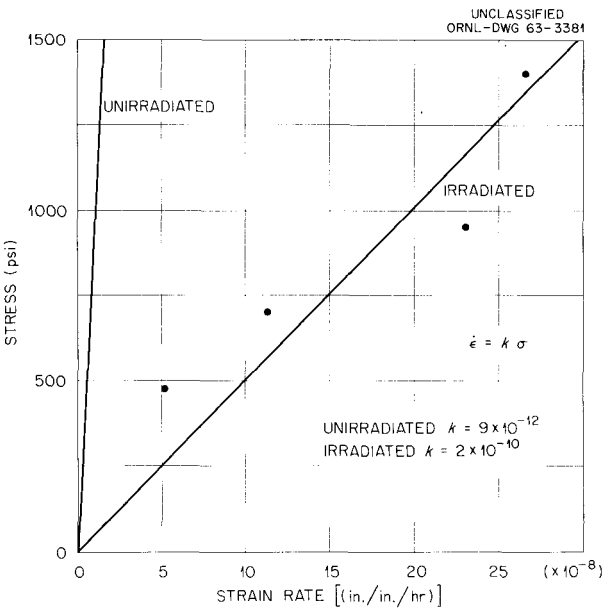

Fig. 20.5. Effect of Irradiation on the Creep Rate of AGOT Graphite.

Microstructural Effects of Nitrogen Compounds in UO_2 on Type 304 Stainless-Steel-Clad Fuel Capsules

E. L. Long, Jr.

Evidence of microstructural changes in type 304 stainless-steel-clad fuel capsules that could be related to nitrogen compounds in UO_2 was seen in the first group of EGCR prototype fuel capsules. This UO_2 had a nitrogen impurity level as high as 1900 ppm in the form of UN_2 with traces of UN. Metallographic examination of the irradiated capsules revealed that a precipitate had formed in the inner surface regions of the cladding to a depth of approximately 0.01 in. It was not until the second group of EGCR prototype capsules had been examined that the presence of this precipitate could be related to the nitrogen content of the UO_2; the fuel for the second group of elements analyzed less than 30 ppm of nitrogen. There was no evidence of a precipitate in the cladding of the second group of elements.[9]

Perhaps the most graphic illustration of the relation between the nitrogen content of UO_2 and the quantity of nitrides formed in the adjacent cladding was seen in three Maritime experimental assemblies.[10] No precipitates were observed in the cladding when the contained UO_2 had a nitrogen impurity level of less than 80 ppm. The "pearlitic" intergranular nitride precipitates formed during the brazing cycle in the fabrication of the fuel-rod clusters, not during the relatively low-temperature irradiation exposure.

Metallographic examination of the EGCR prototype fuel capsules irradiated in the Engineering Test Reactor (ETR) for extended periods of time has also shown the desirability of using a UO_2 fuel with low nitrogen levels. The cladding of two of these capsules failed; failure was attributed to a combination of the original nitrogen content of the UO_2, which resulted in a heavy precipitate in the inner surfaces of the cladding, and overpowering of the elements during irradiation.[11,12] The precipitates in the cladding of one of the ETR capsules were recently identified by x-ray diffraction as CrN and Cr_2N.

ADVANCED FUEL ELEMENTS

In order to take advantage of the EGCR as a test bed for advanced fuel concepts and of the extensive information gained from the design and construction of the EGCR, studies have been carried out on advanced concepts. Cladding materials and fuel-element designs are being studied that will promote increased efficiency as a result of higher outlet coolant temperatures, increased heat flux ratings, and/or reduced thermal-neutron absorption in the core.

Irradiation Capsule Fabrication

E. A. Franco-Ferreira

Work on the advanced gas-cooled reactor program includes the design and irradiation testing of

[9] J. G. Morgan *et al.*, *GCR Quart. Progr. Rept. June 30, 1961*, ORNL-3166, pp 133–34.

[10] E. L. Long, Jr., *Maritime Reactor Program Ann. Progr. Rept. Nov. 30, 1962*, ORNL-3416, pp 95–102; see especially Fig. 4.17, p 97.

[11] D. F. Toner *et al.*, *GCR Quart. Progr. Rept. Mar. 31, 1962*, ORNL-3302, pp 96–101; see especially Fig. 5.42, p 101.

[12] J. G. Morgan *et al.*, *GCRP Semiann. Progr. Rept. Mar. 31, 1963*, ORNL-3445 (in press).

advanced fuel-element concepts.[13,14] The irradiation testing is normally carried out on single capsules which are exposed in the ORR. The Welding and Brazing Laboratory has the primary responsibility for the fabrication of these irradiation capsules. The incorporation of the capsules into the various testing rigs is carried out by the Reactor Division. This year's work has included seven ORR loop No. 1 elements, ten ORR poolside capsules, and six coated-particle capsules, as well as the gas-shroud assemblies for all the loop elements.

A typical advanced fuel element for irradiation in the ORR loop No. 1 facility is shown in Fig. 20.6. This element has a roughened external cladding surface to provide increased heat transfer. Four thermocouples, which are brazed to the element cladding internally, can be seen at the left of the figure. The roughened surface is produced by copper-brazing a spirally wrapped small-diameter wire to the outer surface of the tube.

Joining of Beryllium

R. G. Gilliland

The lack of knowledge about the joining of beryllium has limited the use of this material in nuclear applications. Suitable procedures have been developed for welding end closures in beryllium tubes, and a description of this work has been reported.[15] An investigation of the wetting behavior of liquid metals on beryllium has also been performed in order to provide more information on brazing.[16–18]

The wetting behavior of several metals was investigated at 50 and 100°C above their melting points in argon and in vacuum. The general experimental method employed sessile-drop techniques for the evaluation of wettability and associated parameters. The liquid-vapor and -solid surface tensions, the work of adhesion, and the coefficient of spreading were determined for those systems exhibiting only minor alloying to permit a means of qualitatively measuring the wettability of beryllium by these metals. The results indicated that the Ti–6 wt % Be alloy produced the lowest liquid-vapor and -solid surface tensions and the highest work of adhesion and spreading coefficients. This alloy thus appeared to have the best overall wetting characteristics of those tested.

Fuel-Cladding Interactions of Metal-Clad Fuel Elements During Thermal Cycling

W. R. Martin

Progressive longitudinal extension of clad ceramic-fueled elements during thermal cycling has been reported previously.[19] The required condition for elongation of the elements during thermal cycling is contact between cladding and fuel. In the EGCR fuel elements this condition is achieved by collapse of the cladding about the fuel due to external pressure or radial expansion of the fuel in excess of the diametral expansion of the cladding, or a combination of the two. Recent efforts have been directed toward understanding the mechanism by which these elements are strained and the conditions for which progressive ratchetting is observed. Three areas have been experimentally investigated: (1) the effect of cladding wall thickness, (2) the effect of contact pressure between fuel and cladding, and (3) the effect of frictional forces between cladding and fuel.

[13] E. A. Franco-Ferreira, *GCRP Semiann. Progr. Rept. Sept. 30, 1962,* ORNL-3372, pp 81–83.

[14] E. A. Franco-Ferreira, *GCRP Semiann. Progr. Rept. Mar. 31, 1963,* ORNL-3445 (in press).

[15] R. G. Gilliland and G. M. Slaughter, *Welding J.* **42**(1), 29–36 (1963).

[16] R. G. Gilliland, *GCRP Semiann. Progr. Rept. Sept. 30, 1962,* ORNL-3372, pp 314–16.

[17] R. G. Gilliland, *GCRP Semiann. Progr. Rept. Mar. 31, 1963,* ORNL-3445 (in press).

[18] R. G. Gilliland, *Investigation of the Wettability of Various Pure Metals and Alloys on Beryllium,* ORNL-3438 (May 29, 1963).

[19] W. R. Martin and J. R. Weir, *Dimensional Behavior of the Experimental Gas-Cooled Reactor Fuel Element at Elevated Temperatures,* ORNL-3103 (July 19, 1961).

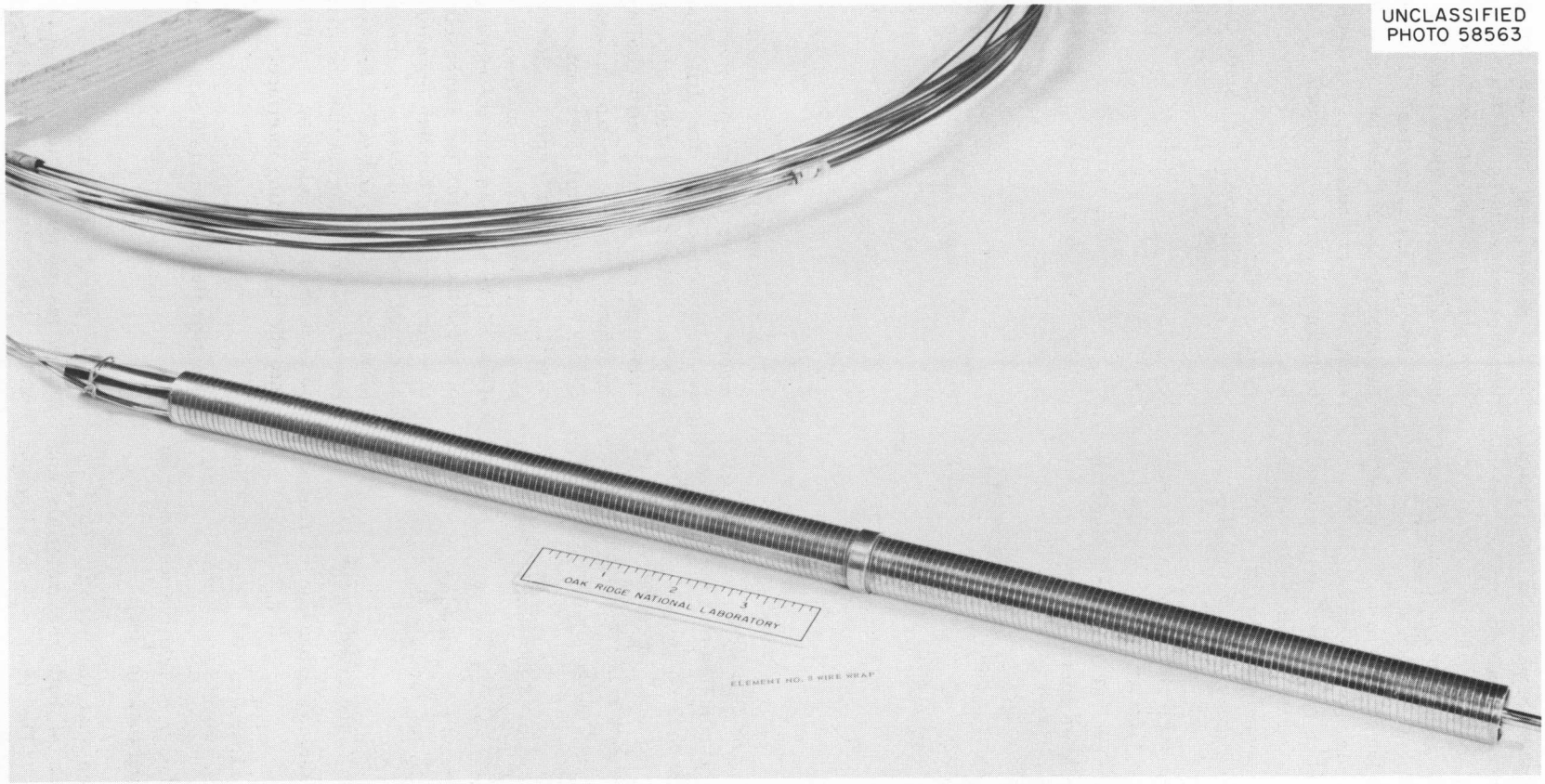

Fig. 20.6. Advanced Fuel Element for Irradiation in ORNL Loop No. 1 Facility.

The effect of coolant pressure on the plastic strain per cycle is as follows:

Coolant Pressure (psi)	Plastic Strain per Cycle (in./in.)
50	1.0×10^{-6}
200	1.3×10^{-5}
300	4.8×10^{-5}
400	$(4.7 \pm 2.3) \times 10^{-5}$

Reducing the cladding thickness increases the plastic strain per cycle as shown below:

Cladding Thickness (in.)	Plastic Strain per Cycle (in./in.)
0.020	1.1×10^{-4}
0.010	$(1.8 \pm 0.2) \times 10^{-4}$
0.015	1.3×10^{-4}
0.005	3.3×10^{-4}

Analysis of the data indicates that the magnitude of cladding strain depends on two factors. There must be sufficient frictional force between cladding and fuel to restrict relative movement, and a difference must exist in the thermal expansion of fuel and cladding.

The total strain introduced into the cladding can be represented mathematically as

$$E_t = (E''_{\text{fuel}} - E'_{\text{clad}}) - e_s ,$$

where

E_t = total strain in the cladding (in./in.),

E''_{fuel} = effective thermal expansion of the fuel (in./in.),

E'_{clad} = thermal expansion of the cladding (in./in.),

e_s = slippage factor or relative movement of cladding and fuel (in./in.).

It can be observed that the quantity $(E''_{\text{fuel}} - E'_{\text{clad}})$ is a function of both the materials and thermal conditions. The term e_s, or slippage factor, is a function of the frictional force between cladding and fuel and can be determined from the static coefficient of friction and the contact pressure. The static coefficient of friction between UO_2 and stainless steel has been measured for low contact pressures. The data obtained by the gravity-loading method in a helium environment at a pressure of 15 psi as a function of temperature are given below:

Temperature (°C)	Static Coefficient of Friction
18	0.34
100	0.34
300	0.33
500	0.38
600	0.42
700	0.46
800	0.50
900	0.30

The mechanism for the extension of clad elements suggests that progressive extension is due to a difference in the frictional force during heating and cooling. If the slippage factor is the same during heating and cooling, the strains introduced on heating are reversed on cooling. Hence, the element does not elongate progressively with each cycle. However, the strain reversal in each cycle may lead to fatigue failure. Thus it can be seen that the metallurgical lifetime of the cladding can be increased by decreasing the difference in thermal expansion of fuel and cladding and by decreasing the frictional force between cladding and fuel. Frictional forces may be reduced by ensuring that the cladding does not contact the fuel and/or by introducing a lubricant into the fuel-cladding interface.

Postirradiation Tensile Tests on Stainless Steels

W. R. Martin J. W. Woods

The effect of irradiation on the mechanical properties of austenitic stainless steels is currently being investigated using postirradiation tensile tests. Although other typical tensile-test

Fig. 20.7. Irradiation Assembly for Subsize Tensile Specimens.

measurements also will be made, the two measurements of primary importance are yield strength and uniform elongation.

For a given material the irradiation conditions being investigated are irradiation temperatures between 250 and 1400°F for an integrated flux of 7×10^{20} (>1 Mev). The postirradiation tensile-test conditions will also be varied in order to determine the effect of strain rate and test temperature.

The metallurgical variables being investigated are grain size and method of preparation (vacuum vs air melting).

Two hundred subsize tensile specimens of types 304 and 347 stainless steel have been irradiated, and the corresponding out-of-pile control specimens have been heat-treated. A typical in-pile irradiation assembly is shown in Fig. 20.7. Post-irradiation tensile tests will begin soon.

UNCLAD FUEL CONCEPTS

The unclad ceramic fuel concept offers the advantages of simplicity of fuel-element design, ease of fuel handling, suitability for high-temperature operation, and good neutron economy; it suffers the disadvantage that some fission-product activity may enter the coolant system. Work has been carried out on the general development of all-ceramic gas-cooled reactors. The primary objectives were investigation of the fabrication characteristics and behavior of coated fuel particles and graphite matrices.

Evaluation of Coated Particles

E. S. Bomar

Thirty-seven lots of pyrolytic-carbon-coated uranium carbide particles from five vendors were evaluated during this period. Information on visual appearance, coating thickness, coated-particle size, fuel content, and isotopic analysis was reported. A number of other property measurements were made as part of the search for a basis for characterizing fuel particles with respect to in-pile performance, and the loads required to crush individual particles from 56 lots of particles were measured.[20,21] A variation on measuring the crushing load for individual particles was tried. A "uniform" load was applied to a monolayer of approximately 5000 particles. The prorated load per particle sufficient to rupture coatings showed fair agreement with the minimum value found for measurements made on individual particles.

Microradiography was extensively employed to obtain coating-thickness and fuel-particle dimensional measurements.[20,21] This technique was also used to obtain qualitative fuel-migration data. Differences in response to heat treatment of a series of specimens prepared by one vendor showed that variations in manufacturing methods can influence response to fuel migration. Treatment in chlorine-bearing argon was found to remove superficial contamination from the surface of heat-treated coated particles.

The measurements of exposed fuel were reported[21] for 18 additional samples of coated-particle lots, in both the as-received and thermal-cycled conditions. Contrary to earlier experience,[22] the majority of these samples failed to unequivocally meet the requirements for exposure of no more than 5×10^{-3}% of the contained fuel.

The various measurements made on coated particles were examined for possible correlation with in-pile performance. An apparent dependence was found for particle performance expressed as the *R/B* ratio for Kr^{88}, the percentage of cracked coatings observed on crushing load tests, and particle coating thickness. The relation observed for the percentage of cracked coatings vs particle coating thickness was shown.[23]

Equipment was assembled during this period for preparation of pyrolytic-carbon coatings on fuel particles at temperatures to 1400°C. A limited number of coating experiments were performed.

---

[20] E. S. Bomar, F. L. Carlsen, Jr., J. L. Cook, R. J. Gray, and L. A. Harris, *GCRP Semiann. Progr. Rept. Sept. 30, 1962,* ORNL-3372, pp 184–85.

[21] E. S. Bomar, F. L. Carlsen, Jr., J. L. Cook, and R. J. Gray, *GCRP Semiann. Progr. Rept. Mar. 31, 1963,* ORNL-3445 (in press).

[22] R. L. Beatty, E. S. Bomar, F. L. Carlsen, Jr., and J. L. Cook, *Metals and Ceramics Div. Ann. Progr. Rept. May 31, 1962,* ORNL-3313, p 70.

[23] E. S. Bomar, F. L. Carlsen, Jr., J. L. Cook, R. J. Gray, and L. A. Harris, *GCRP Semiann. Progr. Rept. Sept. 30, 1962,* ORNL-3372, pp 187–92; see especially Fig. 10.7, p 191.

It was established, however, that at 1400°C the structure of the pyrolytic-carbon coating can be varied from laminar to columnar, or combinations of these, by altering the composition and/or flow rate of the methane-argon atmosphere. A second apparatus, capable of coating at temperatures to 2000°C, was designed and fabricated.

Neutron-Activation Tests on Coated Particles

R. B. Fitts J. L. Scott

Present studies of pyrolytic-carbon-coated fuel particles are directed toward the evaluation of the fission-product-retention characteristics of these fuels when produced by different techniques and to the establishment of operational temperature limits for various particles with respect to their retention properties. These factors are determined by low-temperature neutron activation and subsequent heat treatment to obtain the retention characteristics of the fuels at various temperatures. The experimental techniques have been described previously.[24,25]

Earlier work on fission-product retention of particles with laminar, columnar, and duplex pyrolytic-carbon coatings revealed that all three types retain xenon up to 1800°C. However, Ba^{140} and Ag^{111} were found to migrate rapidly through coatings at 1200 and 1000°C respectively.[26,27] This caused concern that uranium might also migrate through the coatings.

A series of tests has been conducted using fuel elements containing coated particles to determine whether such uranium migration exists.[28] These tests involved the comparison of the xenon release from samples which were heat-treated prior to irradiation, in order to cause uranium migration, with the release from identical samples which received no preirradiation heat treatment. Higher releases of xenon were obtained after 1600 and and 2000°C preirradiation heat treatments and were due to uranium migration to within the recoil range of the coating surface or into the matrix of the fuel element. Low-voltage radiographic examination of heat-treated, unirradiated pyrolytic-carbon-coated particles substantiated the presence of uranium which had migrated into the coatings from the fueled cores.[29] It was also observed that the probability of coating failure during high-temperature annealing appears to be enhanced by a prior acid-leaching treatment. Additionally, the coatings are apparently sensitized during uranium migration so that coating failure by delamination will begin after 24 hr in a moist (0.6 vol %) helium atmosphere. This type of failure is believed to result from the attack of water vapor on uranium which has penetrated the coatings, thereby allowing the successive escape of pockets of fission gas that have been trapped within the coating laminae.

These results strongly suggest that uranium migration is a problem in coated-particle reactor fuels for high-temperature (>1500°C) use. As a result of this study, a more-detailed investigation of this phenomenon is being made.

Studies are continuing on the fission-gas-retention properties of pyrolytic-carbon-coated particles as received as well as after their manufacture into fueled-graphite spheres. The data that have been obtained show that good retention of fission gases ($<10^{-4}$% release) may be obtained with coated particles when careful manufacturing techniques are employed. Unsupported coated particles with low ($<10^{-3}$% of total uranium in sample) surface contamination and low (<0.2% of total uranium in sample) amounts of exposed uranium, as determined by HNO_3 leach, will retain fission gas well at 1400°C.[30,31] Fueled-graphite spheres made by various manufacturers and containing similar coated particles have been tested at 1000°C for 24 hr.[31] These show excellent retention of fission gas if the particle

[24] *GCR Quart. Progr. Rept. Dec. 31, 1959,* ORNL-2888, pp 68–72.

[25] D. F. Toner and J. L. Scott, *Am. Soc. Testing Mater., Spec. Tech. Publ.* **306**, 86–89 (1961).

[26] J. L. Scott, D. F. Toner, and R. E. Adams, *GCRP Quart. Progr. Rept. June 30, 1961,* ORNL-3166, p 87.

[27] J. L. Scott and R. E. Adams, *GCRP Quart. Progr. Rept. Mar. 31, 1962,* ORNL-3302, pp 183–84.

[28] J. L. Scott, R. E. Adams, R. B. Fitts, and R. A. Bowman, *GCRP Semiann. Progr. Rept. Sept. 30, 1962,* ORNL-3372, pp 194–98.

[29] E. S. Bomar and R. W. McClung, *GCRP Quart. Progr. Rept. Mar. 31, 1962,* ORNL-3302, pp 167–72; J. L. Scott and R. E. Adams, *GCRP Quart. Progr. Rept. Mar. 31, 1962,* ORNL-3302, p 181.

[30] J. L. Scott and R. E. Adams, *GCRP Quart. Progr. Rept. Mar. 31, 1962,* ORNL-3302, pp 179–80.

[31] R. B. Fitts, *GCRP Semiann. Progr. Rept. Mar. 31, 1963,* ORNL-3445 (in press).

coatings have not been ruptured during manufacture. Ruptured coatings yield high amounts of exposed uranium when leached with HNO_3.

Evaluation of Fueled-Graphite Bodies

Preirradiation examination was performed on 42 lots of specimens (bushings, cylinders, and $1\frac{1}{2}$-in.-diam spheres) from four vendors.

An improvement in visual appearance and control of dimensions was found during this period as the several suppliers obtained fabrication experience. Indications are that a sphere diametral tolerance of ±0.032 in. can be met easily and possibly reduced. Requirements for bulk density of 1.70 g/cm^3 and net carbon density of 1.65 g/cm^3 can be met or exceeded with little difficulty.[32] Surface irregularities resulted from the protrusion of coated particles and, in some instances, die marks. Use of a molded unfueled shell usually resulted in improved surface finish, although variable unfueled shell thicknesses were observed. Fuel particles appeared, in some instances, in the "unfueled" shell, as a result of irregularities in the shape of the fueled insert or of entrainment of a few particles in the shell mixture.[32] Unfueled shells were also provided by machining graphite spheres, into which molded inserts were placed. Closures were made with plugs bonded in place with a carbonaceous cement.

Radiography and metallography were employed to determine fuel-particle distribution. Distribution was quite variable; however, uniform results were found in some specimens, showing that this requirement can be met. Radiography as presently employed is a marginal means of observing fuel distribution for a spherical geometry when only small variations in fuel concentration are present.

The integrity of coated particles in spheres was determined by alpha counting, acid electrolysis, and neutron-activation measurements. Exposed uranium, as determined by acid electrolysis, ranged from 0.002 to 16.5% of the contained uranium. The high values were for specimens for which excessive molding pressures had been used. In general, the Xe^{133} release values obtained from neutron-activation tests showed a direct dependence on the amount of exposed uranium present.

The possible use of dry chlorine gas as a means of removing exposed fuel from fueled-graphite spheres was studied. Treatment for up to $9\frac{1}{2}$ hr at 800 to 1000°C in flowing chlorine-argon mixtures effected a marked, if not complete, removal of exposed fuel.[33]

Metallographic examinations disclosed structural variations which reflect differences in vendor fabrication practice. The graphite matrices varied in texture from relatively dense to very porous, and significant differences in binder content were evident. The grains of the graphite filler ranged from very fine and equiaxed to platelike.

Brittle-ring tests were made on samples from fueled and unfueled bushings. The addition of coated particles was found to reduce the strength by a factor of 3. A difference in adhesion between coated particles and matrix was observed. The variation ranged from superficial bonding to that sufficient to cause cracks to propagate through the coated particles.

Graphite Fabrication

J. M. Robbins R. L. Hamner
A. J. Taylor

The concept of using soft molding materials for fabricating graphite spheres[34,35] was abandoned. Investigation established that such materials do not closely approximate isostatic pressure when confined under a uniaxial load. An experiment was designed and completed to assess the effects of forming pressure and of fuel concentration on coated-particle damage. It was shown that only minor damage was encountered up to approximately 24 vol % fuel loading and forming pressures up to 6000 psi. At higher pressures, coated-particle

[32] E. S. Bomar, F. L. Carlsen, Jr., J. L. Cook, and R. W. McClung, *GCRP Semiann. Progr. Rept. Sept. 30, 1962*, ORNL-3372, pp 203–07.

[33] E. S. Bomar, F. L. Carlsen, Jr., J. L. Cook, and R. W. McClung, *GCRP Semiann. Progr. Rept. Mar. 31, 1963*, ORNL-3445, Table 10.10 (in press).

[34] A. J. Taylor and J. M. Robbins, *Metals and Ceramics Div. Ann. Progr. Rept. May 31, 1962*, ORNL-3313, p 73.

[35] J. M. Robbins and A. J. Taylor, *GCRP Quart. Progr. Rept. Mar. 31, 1962*, ORNL-3302, pp 184–86.

damage became significant for all fuel concentrations.[36] Machined-shell concepts for fueled-graphite spheres are being investigated. Equipment and materials were ordered, and experiments were initiated for investigating the effect of shell thickness on the impact resistance of fueled-graphite spheres.

Specimens were fabricated for the 08-6S experiment in the ORR poolside facility. The specimens consisted of loosely bonded fuel cores of approximately 40 vol % natural graphite and approximately 60 vol % pyrolytic-carbon-coated uranium carbide particles encapsulated in machined graphite shells.[37]

Unclad Reactor Concept Irradiation Experiments

F. L. Carlsen, Jr.

Four types of irradiation facilities have been used in this program. The Low Intensity Test Reactor (LITR) static capsules and the ORR-B9 instantaneous fission-gas-release facility were used for unsupported pyrolytic-carbon-coated uranium carbide particles. The ORR poolside facility was used to test capsules containing fueled-graphite bushings and spheres, and similar capsules were used to test fueled-graphite cylinders and unsupported coated particles in the Materials Test Reactor (MTR) at Arco, Idaho. The ORR and MTR facilities employed helium sweep gas to measure the in-pile release of fission-product gases. In addition, two new facilities are being readied for fueled-graphite irradiations – an eight-ball static capsule (which will be installed in the F1 position in the ORR core) and the ORR loop No. 2 facility. During the past year, the Ceramics Laboratory assisted in the preparation of 11 irradiation experiments. The results of the irradiation experiments were reported regularly during the past year[38–40] and are summarized here.

Excellent fission-gas retention was observed from unsupported pyrolytic-carbon-coated uranium carbide particles having the duplex microstructure shown in Fig. 20.8. Coated particles of this type have been irradiated at temperatures of 800 to 2100°F and to burnups of 30 at. %, with cracking of only 1 to 2% of the coatings. The duplex coated particles exhibit better performance than other types of coated particles, as shown in Fig. 20.9. The superior performance of the duplex coated particles was confirmed in static capsule experiments.[40] The properties of coated particles that appear to significantly affect their performance are as follows:

1. *Microstructure* – Duplex coated particles perform better than either laminar- or columnar-coated particles.
2. Shape – Coatings on particles with angular shapes and doublet or dumbbell shapes show poor performance relative to those on spheroidal particles.
3. Coating Thickness – Performance is better for the thicker coatings.

The experiments on graphite fuel elements have shown that coated particles can be incorporated into graphite matrix elements without damage to the coated particles. The fission-gas-release rates at temperatures of 1500 to 1800°F have been very low (R/B for Kr^{88}, $<10^{-10}$) in an experiment on $1\frac{1}{2}$-in.-diam spheres after a burnup of 2 at. %.[39]

Graphite fuel elements from three vendors have been irradiated. A total of 24 fueled-graphite bushings, each 0.6 in. OD × 0.25 in. ID × 0.5 in. long, supplied by one vendor were irradiated in two ORR poolside facility capsules. Four bushings in one capsule and 12 in the other were found to be cracked. Cracking was not observed on 12 similar bushings supplied by a second vendor or in a larger cylinder (1 in. OD × 0.25 in. ID × 1.5 in. long) supplied by a third vendor.

The properties of the bushings that appear to be responsible for the poor performance are non-uniform fuel distribution, low fracture strength, and poor bonding to the coated particles.

[36] J. M. Robbins and A. J. Taylor, *GCRP Semiann. Progr. Rept. Mar. 31, 1963*, ORNL-3445 (in press).

[37] J. M. Robbins and A. J. Taylor, *GCRP Semiann. Progr. Rept. Sept. 30, 1962*, ORNL-3372, p 201.

[38] D. F. Toner *et al.*, *GCRP Semiann. Progr. Rept. Sept. 30, 1962*, ORNL-3372, pp 213–50.

[39] J. G. Morgan *et al.*, *GCRP Semiann. Progr. Rept. Mar. 31, 1963*, ORNL-3445 (in press).

[40] W. O. Harms, *Coated-Particle Fuel Development at the Oak Ridge National Laboratory*, ORNL TM-431 (Feb. 14, 1963).

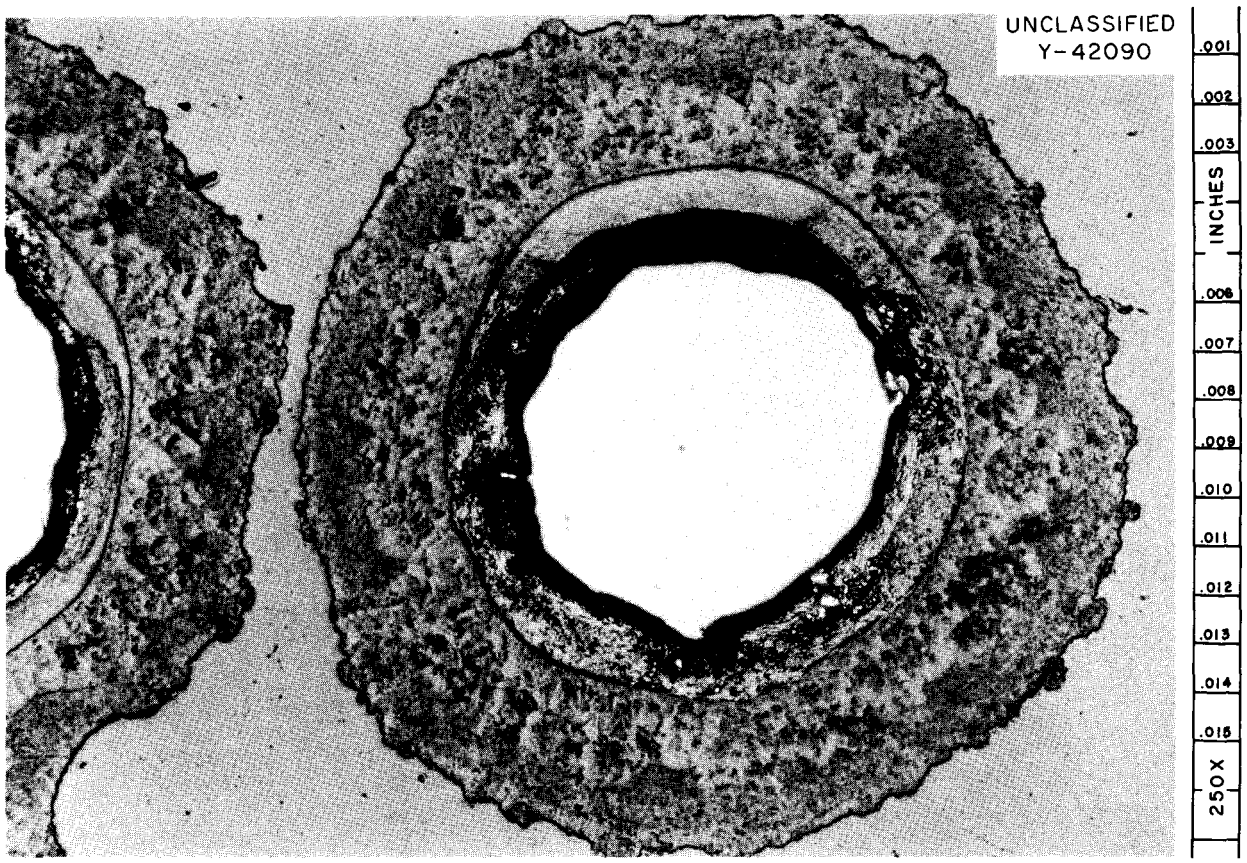

Fig. 20.8. Unsupported Pyrolytic-Carbon-Coated Uranium Carbide Particles, Illustrating Duplex Coating Structure.

Coated-Particle Examination

R. W. McClung

Microradiography[41] has continued as a service to the Ceramics Laboratory for the evaluation of graphite-coated uranium carbide particles. Advanced application of this technique has been made for the postirradiation examination of several particles.[42] The very high radiation level being emitted by the particle (approximately 3000 r/hr beta and 120 r/hr gamma) necessitated a modification of the normal exposures. However, by increasing the x-ray energy from 10 to 50 kvp, the exposure time was shortened from 75 min to 70 sec. Although this caused an expected decrease in normal image quality, it did allow 200× viewing of a particle which otherwise could not have been examined.

Fueled-Graphite Spheres

R. W. McClung

Preliminary radiographic studies have been performed on fueled-graphite spheres to determine the feasibility of this technique as an evaluation tool.[43] With the use of approximate x-ray energies, qualitative evaluation of fuel homogeneity can be made on machined or molded fuel balls. Lower

[41] R. W. McClung, *GCRP Quart. Progr. Rept. Mar. 31, 1962,* ORNL-3302, pp 165–67.

[42] E. S. Bomar and R. W. McClung, *GCRP Semiann. Progr. Rept. Sept. 30, 1962,* ORNL-3372, pp 181–83.

[43] E. S. Bomar, F. L. Carlsen, Jr., J. L. Cook, and R. W. McClung, *GCRP Semiann. Progr. Rept. Sept. 30, 1962,* ORNL-3372, pp 207–08.

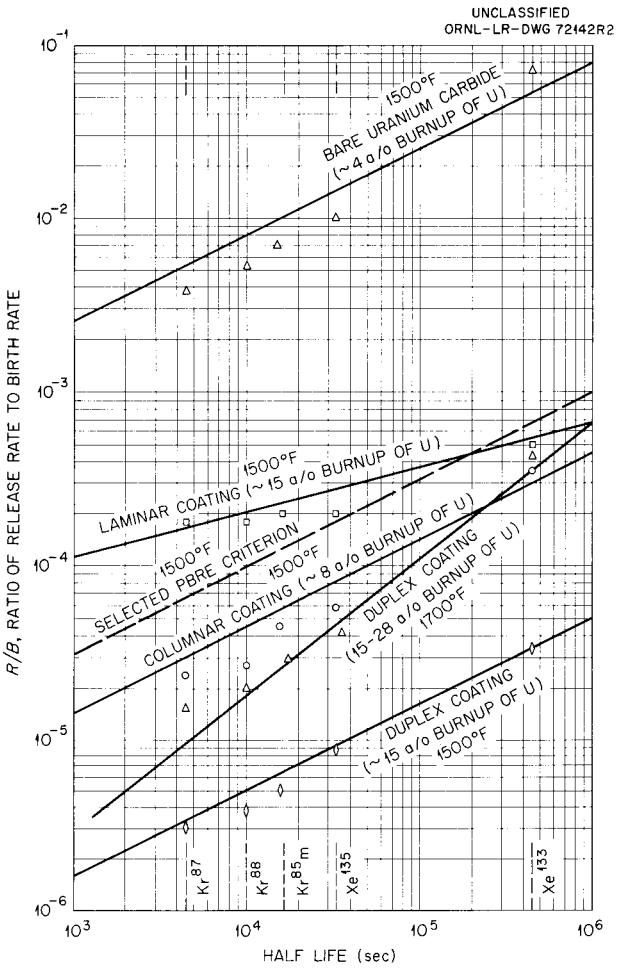

Fig. 20.9. Relation Between R/B and Half-Life for Release of Inert Gases from Pyrolytic-Carbon-Coated Uranium Carbide Particles at 1500°F, 1700°F, and High Burnup.

energies allow thickness measurements to be made on unfueled shells.

Metallographic Examination of Pyrolytic-Carbon-Coated and Uncoated UC-UC_2 Particles

R. J. Gray C. K. H. DuBose

Samples of commercially produced pyrolytic-carbon-coated and uncoated uranium carbide particles from three vendors have been examined metallographically. The purpose was to evaluate the microstructure of the particle in the as-received condition, after various heat treatments, and after fabrication in a graphite matrix. The factors studied included coating integrity, identification of reaction products, and presence of any extraneous phases.

The results of this investigation indicate that many ranges of microstructures can be expected, and should aid in the interpretation of postirradiation examination.[44]

Metallography of $(Th,U)C_2$ Fuel Particles

T. M. Kegley, Jr. B. C. Leslie

The pyrolytic-carbon-coated fuel particles of $(Th,U)C_2$ can be metallographically polished using the technique developed for UC_2 fuel particles.[45] The specimen mount containing the coated particles is ground successively through 320, 400, and 600 silicon carbide papers and then vibratorily polished on a nylon cloth using a slurry of Linde "A" alumina abrasive and silicone oil.[46]

It was observed that the thorium content of the $(Th,U)C_2$ fuel particles greatly influences the etching behavior of the fuel particles. A fuel particle with a Th/U ratio of 2 is so reactive that it will etch in a very few minutes when exposed in air. On the other hand, a fuel particle with a Th/U ratio of 0.6 requires immersion for 5 min in a solution of equal parts of HNO_3, CH_3COOH, and H_2O, which will etch UC_2 fuel particles in 20 to 30 sec.

Figure 20.10 compares the etched microstructures of $(Th,U)C_2$ fuel particles with Th/U ratios of 2 and 0.6. Figure 20.11 shows the microstructure of the particles with a Th/U ratio of 0.6 at 500×.

Microhardness Measurement of Pyrolytic-Carbon Coatings

T. M. Kegley, Jr. B. C. Leslie

A method was developed for determining the microhardness of the pyrolytic-carbon coatings deposited on nuclear fuel particles. Indentation

[44] C. K. H. DuBose and R. J. Gray, *Metallographic Examination of Pyrolytic-Carbon Coated and Uncoated Uranium Carbide Particles,* ORNL TM-521 (in press).

[45] C. K. H. DuBose and R. J. Gray, *Metallography of Pyrolytic-Carbon Coated and Uncoated Uranium Carbide Spheres,* ORNL TM-91 (Mar. 21, 1962).

[46] Dow-Corning 702 diffusion pump fluid.

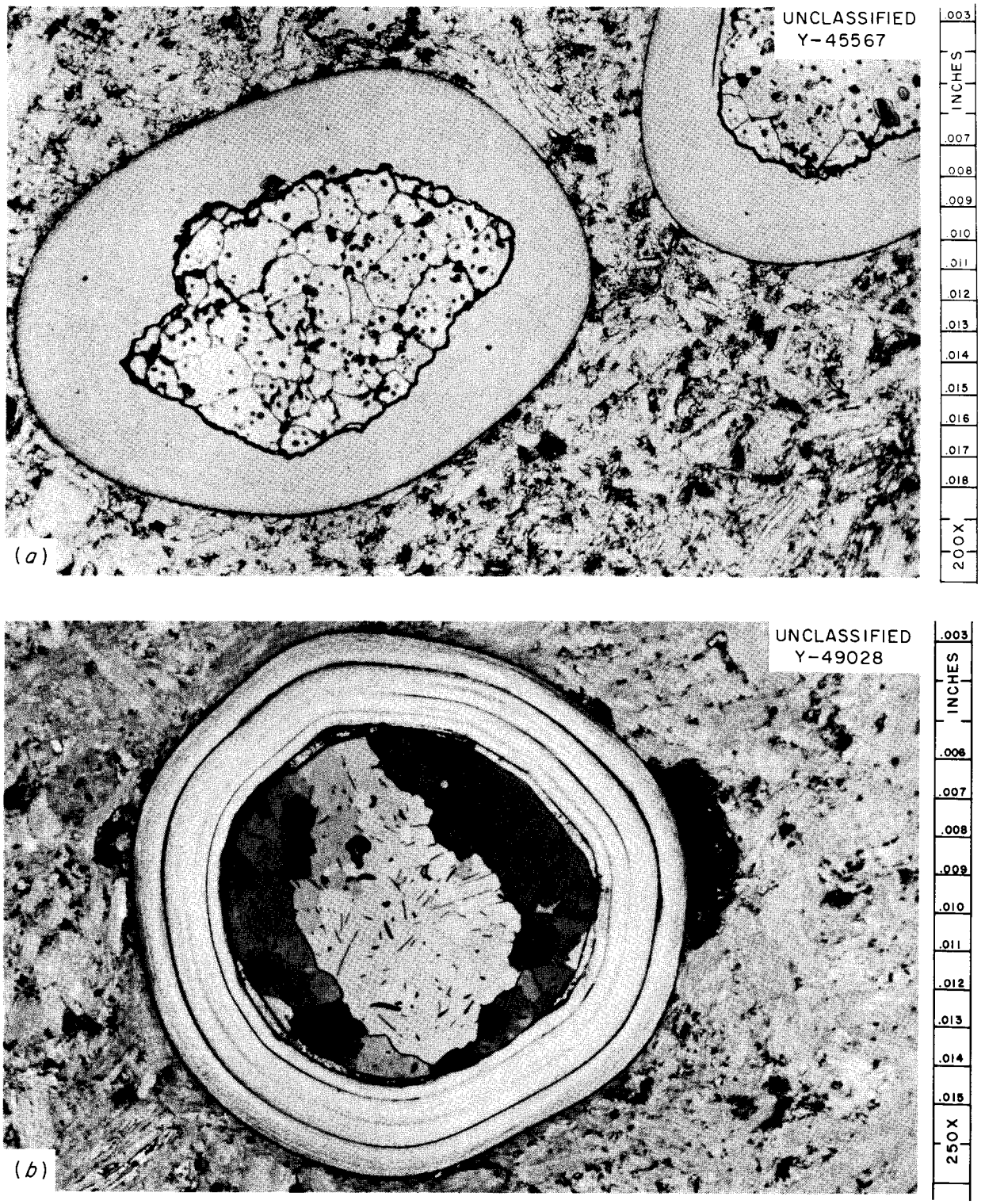

Fig. 20.10. Pyrolytic-Carbon-Coated $(Th,U)C_2$ Fuel Particles in Graphite. (*a*) Fuel particles with a Th/U ratio of 2 after etching in air for 5 min. 200X. (*b*) Fuel particles with a Th/U ratio of 0.6 after etching 5 min with a solution of equal parts of HNO_3, CH_3COOH, and H_2O. 250X.

Fig. 20.11. Pyrolytic-Carbon-Coated $(Th,U)C_2$ Fuel Particles with a Th/U Ratio of 0.6. As etched 5 min with equal parts of HNO_3, CH_3COOH, and H_2O.

Table 20.1. Microhardness of Pyrolytic-Carbon Coatings Deposited on Uranium Carbide Fuel Particles

Indenter Direction	Diamond Pyramid Hardness – G[a] (100-g Load)			
	3M-102-A Laminar	3M-SP-2 Laminar	NCC-AD Columnar[b]	NCC-G Columnar[b]
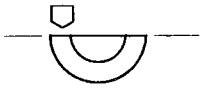	Range 186–204 Average 197	Range 115–150 Average 126	Range 51–63 Average 59	Range 70–81 Average 76
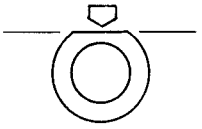	Range 183–198 Average 192	Range 97–122 Average 109	Range 38–48 Average 43	Range 78–85 Average 80

[a]Suffix G is added to indicate that the hardness determined is an elastic hardness.
[b]Duplex laminar-columnar coating, but hardness indentations were made on columnar portion.

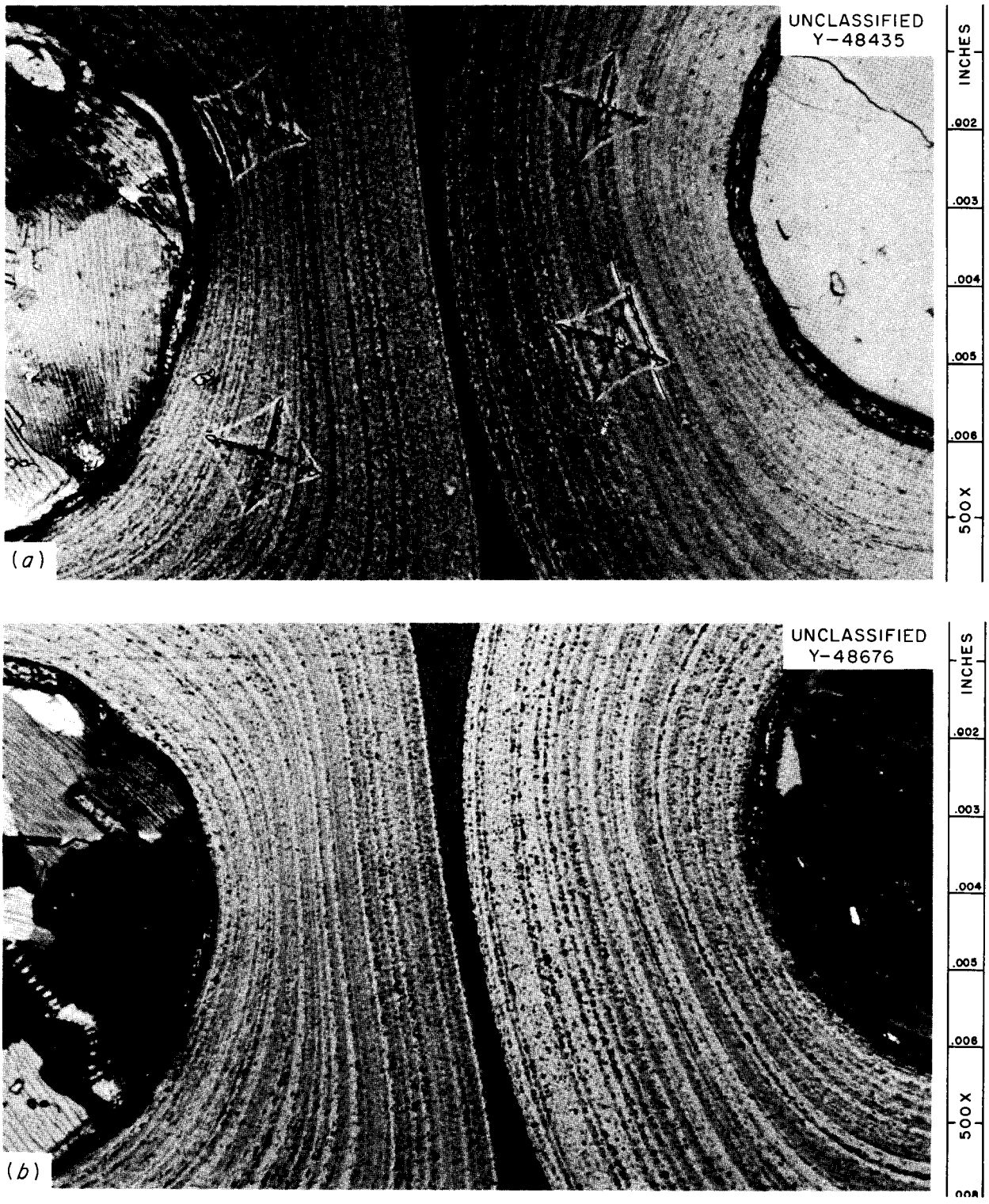

Fig. 20.12. Microhardness Indentations on Pyrolytic-Carbon Coating of Uranium Carbide Fuel Particles from Batch 3M-SP-2. (*a*) Before removal of pyroxylin film. (*b*) After removal of pyroxylin film. Uranium carbide fuel particles have been etched with HNO_3, CH_3COOH, and H_2O; but particles in top photograph appear brighter because of reflection from pyroxylin film. 500X.

microhardness tests made in the usual manner cannot be used because of the resiliency of the pyrolytic-carbon coating.

A pyroxylin film placed on the surface of the polished specimen containing the coated particles retains an impression of the diamond pyramid indenter for measurement. The pyroxylin film was formed on the specimen by placing a drop of 5% pyroxylin amyl acetate solution on the specimen and then spreading the drop evenly over the polished surface with a cotton swab. The amyl acetate solvent then evaporates, leaving the pyroxylin film.

Figure 20.12*a* shows indentations made in the pyrolytic-carbon coating before removal of the pyroxylin film, and Fig. 20.12*b* shows the same area after its removal. Examples of the microhardness values for particles from four other batches of pyrolytic-carbon-coated uranium carbide fuel particles are given in Table 20.1.

SUPPORTING RESEARCH

Supporting research, which can be expected to ultimately assist the GCR program, has been carried out in a variety of fields.

In-Pile Stress Rupture of UK Stainless Steel

J. T. Venard

As part of the AGR/EGCR Exchange Program, a series of stress-rupture tests have been run on British 20 wt % Cr–25 wt % Ni–Nb stainless steel tubing in poolside positions at the ORR. The neutron flux rate in these positions is approximately 2×10^{13} *nv* (> 1 Mev).

Log stress vs log time-to-rupture results for the two irradiation experiments completed are shown in Fig. 20.13. The out-of-pile control curves are shown for comparison.

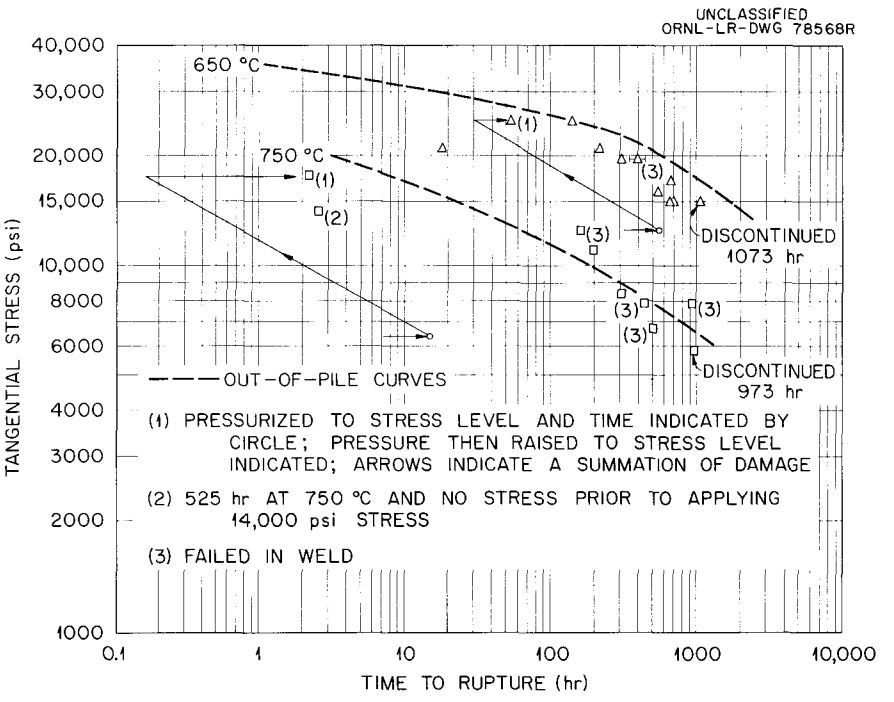

Fig. 20.13. Results of In-Pile Tube Burst Tests on UK 20 wt % Cr–25 wt % Ni–Nb Alloy; As Received and Welded; He–1% O_2.

Table 20.2. Results of In-Pile Tube Burst Tests on UK 20 wt % Cr–25 wt % Ni–Nb Alloy at 650°C

Tangential Stress (psi)	Time to Rupture (hr)	Average Tangential Strain (%)	Out-of-Pile Time to Rupture (hr)	Out-of-Pile Average Tangential Strain (%)	Location of Fracture
15,000	661	0.4	2400	4.0	Gage length
15,000	701	0.9	2400	4.0	Gage length
15,000	1073[a]	1.0	2400	4.0	
16,000	552	0.4	1800	6.0	Gage length
17,000	675	0.7	1350	7.0	Gage length
19,500	310	0.7	660	8.0	Gage length
19,500	400	0.7	660	8.0	Weld
21,000	18	0.6	450	10.0	Gage length
21,000	219	2.2	450	10.0	Gage length
25,000	25		140	11.0	Gage[b]
25,000	140	2.6	140	11.0	Gage length

[a]Discontinued.

[b]Specimen stressed at 12,500 psi for 556 hr; stress raised to 25,000 psi; specimen split open on rupturing.

Table 20.3. Results of In-Pile Tube Burst Tests on UK 20 wt % Cr–25 wt % Ni–Nb Alloy at 750°C

Tangential Stress (psi)	Time to Rupture (hr)	Average Tangential Strain (%)	Out-of-Pile Time to Rupture (hr)	Out-of-Pile Average Tangential Strain (%)	Location of Fracture
5,800	973[a]	3.6	2000	6.0	
6,700	504	2.9	950	7.0	Weld
7,800	440	2.8	540	8.0	Weld
7,800	934	6.8	540	8.0	Weld
8,300	306	9.8	430	9.0	Gage length
11,000	194	8.6	125	10.0	Gage length
12,500	160	4.2	66	15.0	Weld
14,000	2.5	10.5	37	16.0	Gage[b]
17,500	2.0	2.8	9	18.0	[c]

[a]Discontinued.

[b]Specimen irradiated 525 hr at 750°C with no stress prior to applying 14,000 psi.

[c]Specimen stressed at 6400 psi for 15 hr; stress raised to 17,500 psi; fracture location was not determined during hot-cell examination.

Tables 20.2 and 20.3 summarize the in-pile results for time to rupture and strain at rupture. Again representative out-of-pile results have been noted for comparison.

The data indicate that irradiation at 650°C results in a greater effect on the strength and ductility of this alloy than does irradiation at 750°C; for example, at 650°C the in-pile stress for rupture in a given time is approximately 85% of the out-of-pile stress, and the strains at fracture are approximately 30% of out-of-pile values. At 750°C these values are approximately 95 and 60% respectively.

It should be noted that a large percentage (25%) of the specimens tested in-pile failed at the closure welds. Since <1% of the control specimens failed in this manner, there is good reason to suspect that irradiation has weakened or embrittled the weld region. This question has not been resolved; however, efforts are being made to identify and evaluate the various parameters involved. Extensive metallography on irradiated and control specimens is presently under way, and future experiments will be designed with the weld problem in mind.

Release of Fission Gas from UO_2

R. B. Fitts

An investigation of the release of fission gas from UO_2 is being carried out to determine the mechanisms of gas escape from this material. A knowledge of these escape mechanisms is necessary for the better understanding and interpretation of the results of neutron-activation tests and the general problem of fission-gas release from reactor fuels.

The release of fission gas during low-temperature neutron-activation testing may be divided into two general areas. Significant gas release occurs at temperatures below 100°C only during neutron activation. Release also occurs at higher temperatures during postirradiation annealing. The release during irradiation establishes a gas-concentration gradient which is the initial condition for high-temperature release. This is the only apparent relation between the two areas.

The release of fission gas during irradiation and the variables present in the normal neutron-activation test have been the primary facets of this problem investigated to date. The results of this work have shown that essentially all the energetic recoil atoms released are captured and retained by the solid material surrounding the fuel.[47] Essentially none of these recoils are stopped by the atmosphere of the test capsule. The fission gas found in the capsule by postirradiation puncturing is probably due to irradiation-enhanced diffusion or the boiling out of gases in recoil tracks which penetrate the surface of open pores. The details of this process are now being examined.

Thermal Conductivity Studies on UO_2

T. G. Godfrey D. L. McElroy

Measurements of the thermal conductivity of 93.4% dense, pressed and sintered UO_2 were extended to 1200, 1300, and 1350°C in the improved radial-heat-flow apparatus[48] during the third, fourth, and fifth runs respectively. Results from the first two runs to 800 and 875°C were reported elsewhere.[49] The results may be described to ±1% between 200 and 1000°C for all the runs by an equation of the form:

$$k = \frac{\rho/\rho_t}{A + BT}, \qquad (1)$$

where ρ is the specimen density, ρ_t is the theoretical density, T is the absolute temperature in °K, and A and B are constants whose values are given in Table 20.4 for each of the five runs. This behavior of k is that expected for a semiconductor above its Debye temperature, where lattice conduction is the dominant heat-transport mechanism.

At the maximum temperature reached on initial heating, runs 3 and 4 were terminated by component failures in the system. By use of better construction materials and by other design improvements, the system was successfully operated to 1350°C

[47] R. B. Fitts, *GCRP Semiann. Progr. Rept. Mar. 31, 1963*, ORNL-3445 (in press).

[48] D. L. McElroy, T. G. Godfrey, and T. G. Kollie, *Am. Soc. Metals, Trans. Quart.* **55**(3), 749–51 (September 1962).

[49] T. G. Godfrey and D. L. McElroy, *Metals and Ceramics Div. Ann. Progr. Rept. May 31, 1962*, ORNL-3313, pp 74–76.

in run 5, and data were obtained on cooling from this temperature. In addition, the design used in run 5 allowed certain diagnostic tests to be executed which showed the need to further improve the uniformity of the specimen temperature to ensure purer radial heat flow.

Values of k higher than those predicted from Eq. (1) were obtained above 1100°C in runs 3, 4, and 5. However, on cooling from 1350°C during run 5, the k values obtained were consistently higher than those obtained on heating, and furthermore, the cooling data could again be fitted by Eq. (1) with the constants reported in Table 20.4. This hysteresis effect could be due to an irreversible change in the specimen or to a systematic error. The fact that the cooling data obey Eq. (1) suggests that the deviation from this relation observed on heating cannot be due to any auxiliary heat transport mechanism. Such mechanisms have been proposed to explain recent UO_2 single-crystal thermal conductivity data.[50]

Table 20.4. Constants for the Linear Relation Between Thermal Resistance ($1/k$) of UO_2 and Temperature

Run	A (cm °K^{-1} w^{-1})	B (cm/w)
1st heating	6.565	0.02033
2d heating	5.130	0.02157
3d heating	5.555	0.02183
4th heating	4.505	0.02363
5th heating	5.728	0.02185
5th cooling	6.182	0.02003

Thermal Conductivity Studies on Coated-Particle Fuels

W. Fulkerson D. L. McElroy

An apparatus for measuring the thermal conductivity of powders under controlled atmospheric environments to temperatures as high as 1000°C was constructed. In this hot-probe method a ⅛-in. tantalum tube is immersed in an isothermal powder specimen. The thermal conductivity of the powder can be related to the rate at which the temperature of the tube increases when the tube is heated by a constant power input. The specimen is contained in a special furnace, creating a flat temperature profile, and is enclosed in a chamber which can be evacuated or filled to a pressure of 2 atm. Following check-out of the apparatus using MgO powder, measurements will be made on pyrolytic-carbon-coated uranium carbide particles.

Fission-Product Deposition Studies

J. L. Scott

Most studies on fission-product release carried out to date have involved the measurement of the release rates of the inert gases xenon and krypton. Relatively little work has been done on the other fission-product species. In unclad fuel systems, such as HTGR and AVR, contamination of the primary coolant circuit with long-lived gamma emitters is a prime consideration. It is necessary, therefore, that quantitative information be obtained on the rates of release of other species from such fuels. Concurrently, the mechanism of transport of activity and the locus of deposition of individual fission products can be determined. Such information will result in improved reactor designs with better control over the deposition of fission products.

A small loop has been developed for obtaining the rates of release of species such as I^{131}, Ba^{140}, Sr^{89}, and Te^{132} from unclad fuels and the loci of deposition of these species on reactor materials at elevated temperatures. The loop has been previously described in detail.[51] Except for the test section the loop consists of ⅜-in. stainless steel tubing and contains a flowmeter, a diaphragm-type circulating pump, and a bypass leading to a liquid-nitrogen-cooled charcoal trap which is continuously monitored for Xe^{133}. The test section consists of a 30-in. length of ¾-in.-diam, 0.020-in.-thick stainless steel tubing. Other materials may be substituted or used as inserts within the stainless steel tubing if desired. A

[50] J. L. Daniel, J. Matolich, Jr., and H. W. Deem, *The Thermal Conductivity of UO_2*, HW-69945 (September 1962).

[51] J. L. Scott, *GCRP Semiann. Progr. Rept. Mar. 31, 1963*, ORNL-3445 (in press).

small resistance furnace is used to heat a 6-in. length of the test section to temperatures as high as 1000°C. Twelve thermocouples are welded to points along the length of the tube for measurement of the temperature gradient. Silver- and copper-impregnated charcoal traps are placed at both ends of the test section to confine the radioactive species to the test section.

Three tests have been run to date. In two tests the fission-product source was neutron-activated spherical uranium carbide particles in an AGOT graphite bottle. In the third test the source was neutron-activated UO_2 particles contained in a graphite bottle. In two tests, one containing UO_2 and the other containing uranium carbide, the fuel temperature did not exceed 650°C. In both tests, there was insufficient fission-product release, other than noble gases, to permit quantitative analysis of the distribution of activity on the deposition tube. It is believed that the major species released, Te^{132} and I^{131}, were absorbed by the graphite bottle.

Even though low release rates of iodine and tellurium were observed in these experiments, one should not infer that similar events would happen in a reactor. Since the samples experienced only 1 to 5×10^{14} fissions, there were no more than about 3×10^{13} atoms of any one fission-product isotope present at any time. At the much higher doses experienced in a reactor, the absorption sites might well become saturated so that these species might be released to the coolant.

For the third test the fuel temperature was 800°C, and there was sufficient oxygen present to convert some of the uranium carbide to UO_2. Under these conditions, I^{131} and Te^{132} were found to be released in gross quantities. The total fractional release values were 0.06 for Te^{132}, 0.41 for I^{131}, and 0.42 for Xe^{133}.

The loci of deposition of I^{131} and Te^{132} were a strong function of temperature. Although traces of I^{131} and Te^{132} were found at the hottest points on the deposition tube, most of the Te^{132} was found at a point 11 in. from the bottom of the tube. At this location the tube-wall temperature was 600°C. The I^{131} was found to begin deposition in more than trace amounts at 440°C and showed a very intense maximum at 300°C. The I^{131} distribution was found to fit a curve of the form:

$$\frac{df}{dx} = \frac{\alpha\beta}{\beta - \alpha}(e^{-\alpha x} - e^{-\beta x}) , \qquad (2)$$

where df/dx = the fraction of I^{131} deposited per unit length, x = the distance along the tube, and α, β = constants. The actual values of α and β were $\alpha = 0.51\ cm^{-1}$, and $\beta = 0.19\ cm^{-1}$. Theoretical analysis showed that

$$\alpha = \frac{\Delta H_a (T_0 - T_f)}{R T_0 T_f l} , \qquad (3)$$

where

ΔH_a = heat of absorption of the species on the wall (cal/mole),

R = gas constant (cal $°K^{-1}$ $mole^{-1}$),

T_0 = temperature at onset of deposition (°K),

T_f = temperature when deposition is complete (°K),

l = distance along tube between T_0 and T_f (cm).

From this relation the heat of absorption was computed to be 26.2 kcal/mole. The constant β is given by

$$\beta = \frac{4K_d}{DV} , \qquad (4)$$

where K_d = deposition rate constant (cm/sec), D = tube diameter (cm), and V = linear gas velocity (cm/sec). From relation (4), K_d was found to have a value of 2.57 cm/sec. For laminar flow,

$$K_d = \frac{48 D_g}{11 D} , \qquad (5)$$

where D_g is the gaseous diffusion coefficient (cm^2/sec). If D_g is assumed to be 1 cm^2/sec for I^{131} in helium, K_d = 2.42 cm/sec.

The excellent agreement between the estimated and measured values of K_d suggests that the rate-controlling step in the deposition process for I^{131} on stainless steel below about 300°C is the rate of diffusion of the isotope through the helium to the metal surface. The agreement between experiment and theory also suggests that "dust" particles were not involved in the transport and deposition processes for the particular experiment performed.

Graphite-Metal Compatibility Studies

J. H. DeVan B. Fleischer

Carbon transport from graphite to mating type 304L stainless steel surfaces has been observed at temperatures as low as 1000°F.[52] Studies carried out in vacuum show that this transport is the result of direct reaction between the metal and graphite and that the rate of carburization is roughly proportional to the contact pressure.[53] By extrapolating carburization data obtained at 1100°F, the threshold contact pressure required to produce detectable carburization in 1000 hr appears to be about 100 psi.

The linear relation between carbon transfer and contact pressure is believed to be associated with changes in the effective area of surface contact produced by changes in pressure; that is, higher contact pressures serve to iron out surface irregularities, particularly in the graphite, and thereby increase the concentration of carbon atoms adjacent to the metal surface. The overall effect can be compared to the increased reaction rate which is observed in a gas-metal system when the pressure of the reacting gas is increased.

Tests are in progress to substantiate the concept that the effect of contact pressure is indeed mechanical and not related to the activation energy of the carburization reaction. To accomplish this, diffusion couples of stainless steel and graphite are initially placed under a relatively high contact load. The contact pressure is then reduced, and the diffusion anneal is started. Carburization rates of these specimens will be compared with the rates of specimens which were held continuously under the higher or the lower pressures.

Contaminant Studies

B. Fleischer

Studies of impurity-induced corrosion reactions related to helium-cooled reactors have been extended from the effects of gaseous contaminants to those of solid impurities. Such impurities stem from many sources, but, most importantly, they result from the deliberate or inadvertent introduction of lubricants, rust-resistant coatings, and tube-drawing compounds.[54] Among the impurities investigated thus far are high-temperature lubricants, vapor-phase rust inhibitors, and chloride salts. All tests have been conducted with type 300 series stainless steels in impure helium at temperatures from 1100 to 1400°F.

Tests of lubricants[55] have involved possible corrosion effects arising from direct contact of a petroleum grease (Cosmoline 1094) with heated metal surfaces and from the vapor transport of decomposition products of oils and greases to core components. Although compatibility problems caused by direct contact of greases appear minor over the temperatures investigated, carburization effects arising from vapor decomposition place a stringent limitation on the volume of lubricant that can be permitted in the helium coolant.

Chloride salts and vapor-phase inhibitors are being investigated from the standpoint of their influence on the intergranular oxidation of iron-base alloys by impure helium.[56] Initial studies of these contaminants have shown no catastrophic effects on oxidation in helium at temperatures up to 1400°F.

Oxidation Studies of Nitrided Type 304 Stainless Steel

J. H. DeVan B. Fleischer

Compatibility studies are in progress to evaluate the oxidation behavior of nitrided type 304 stainless steel in high-temperature helium containing oxidizing impurities. Nitriding is utilized to increase the wear and erosion resistance of stainless steel bearing and nozzle surfaces in the EGCR. Initial oxidation exposures of cylindrical specimens with varying nitride thicknesses were carried out for 1000 hr in impure helium at 1050°F. The oxidation rates of as-received nitrided specimens were significantly higher than those for bare type 304 stainless steel. However, the rates decreased as outer portions of the nitride case were removed.

---

[52] B. Fleischer, *GCRP Quart. Progr. Rept. Mar. 31, 1962*, ORNL-3302, p 53.

[53] B. Fleischer, *GCRP Semiann. Progr. Rept. Mar. 31, 1963*, ORNL-3445 (in press).

[54] J. H. DeVan, *Catastrophic Oxidation of High-Temperature Alloys*, ORNL TM-51 (Nov. 10, 1961).

[55] B. Fleischer, *GCRP Semiann. Progr. Rept. Sept. 30, 1962*, ORNL-3372, pp 84–85.

[56] B. Fleischer, *GCRP Semiann. Progr. Rept. Mar. 31, 1963*, ORNL-3445 (in press).

The experiments indicate that the surface properties of a nitride case would give way to those of an oxide film under EGCR temperature and coolant conditions.

Mechanical Properties of Moderator Graphites

C. R. Kennedy

A program to determine the properties necessary to utilize graphite for optimum performance as a moderator material has been initiated. To date, specimens from eight bars of various grades and extrusion sizes have been tested. The results obtained from tensile tests are given in Table 20.5. Density and hardness values were obtained from end pieces cut from each specimen after tensile testing.

The 18 × 18 in. block of AGOT graphite is similar to the EGCR moderator material, and the core materials are actually those removed from EGCR columns. The specimens taken from the 18 × 18 in. graphite block were removed from a quarter section of the block and should be representative of the strength variation across the block. Specimens taken from the cores represent only a fixed position in the block; however, they represent the variation along the length of the blocks. As seen in Table 20.5, the average axial strengths and standard deviation, both across and along the blocks, are quite large and similar in value. The higher density value given for the 18 × 18 in. blocks results from selection of the specimens near the surface of the block, where the density is higher.

UNCLASSIFIED
PHOTO 62369

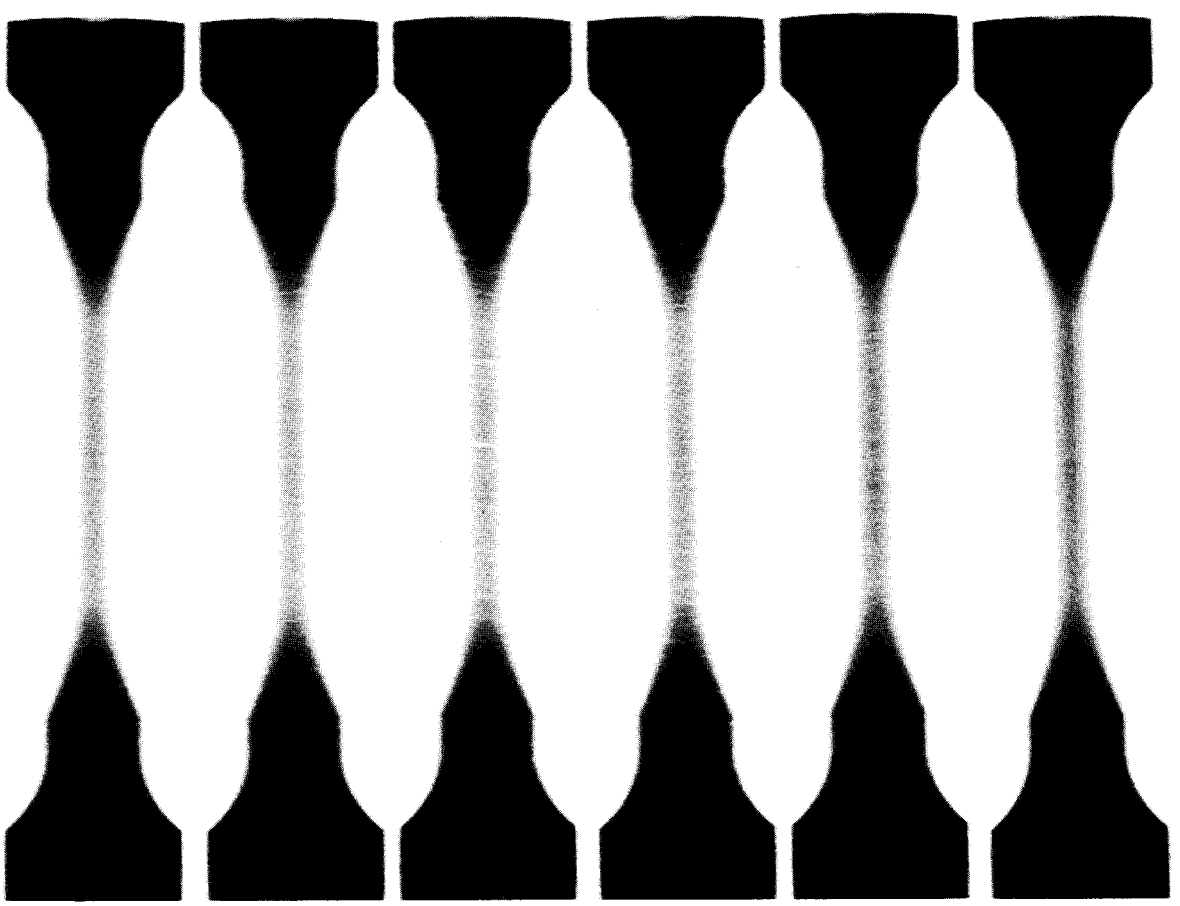

Fig. 20.14. Radiograph of Grade TSX Graphite Tensile Specimens – Orientation in the Normal 2 Direction.

Table 20.5. Results of Tensile Testing of Graphite

Grade	Average Fracture Stress (psi)	Standard Deviation (psi)	Average Fracture Strain (%)	Standard Deviation (%)	Average Modulus of Elasticity (psi)	Standard Deviation (psi)	Average Bulk Density (g/cm^3)	Standard Deviation (g/cm^3)	Linear Scale Hardness No.	Standard Deviation	Number of Specimens
					$\times 10^6$	$\times 10^6$					
Parallel to Extrusion Axis											
AGOT ($4\frac{3}{8} \times 4\frac{3}{8}$ in.)	2260	140	0.18	0.02	1.73	0.15					13
AGOT ($4\frac{3}{8} \times 4\frac{3}{8}$ in.) (lot 1074)	2180	240	0.20	0.63	1.54	0.17	1.727	0.019	13.07	0.64	24
AGOT (18 × 18 in.)	1630	440	0.14	0.04	1.48	0.19	1.723	0.006	10.02	0.35	23
AGOT (core 246)	1480	290	0.19	0.04	1.09	0.18	1.642	0.006	7.50	0.21	33
AGOT (core 266)	1580	390	0.16	0.04	1.29	0.15	1.681	0.008	9.36	0.37	35
AGOT (core 272)	1700	280	0.18	0.04	1.06	0.22	1.690	0.010	8.94	0.50	35
CSGBF ($4\frac{3}{8} \times 4\frac{3}{8}$ in.)	1980	300	0.19	0.03	1.47	0.14	1.651	0.016	12.55	0.59	15
TSX (6 × 6 in.)	2940	270	0.16	0.05	2.51	0.39	1.730	0.014	11.35	0.44	24
Normal 1 to Extrusion Axis											
AGOT ($4\frac{3}{8} \times 4\frac{3}{8}$ in.) (lot 1074)	1710	330	0.32	0.07	0.68	0.04					11
AGOT (18 × 18 in.)	730	150	0.15	0.03	0.73	0.08					12
CSGBF ($4\frac{3}{8} \times 4\frac{3}{8}$ in.)	1080	380	0.21	0.06	0.72	0.10					12
TSX (6 × 6 in.)	1340	590	0.28	0.14	1.03	0.14					5
Normal 2 to Extrusion Axis											
AGOT ($4\frac{3}{8} \times 4\frac{3}{8}$ in.) (lot 1074)	1440	340	0.27	0.07	0.69	0.04					10
AGOT (18 × 18 in.)	940	400	0.15	0.07	0.83	0.11					9
CSGBF ($4\frac{3}{8} \times 4\frac{3}{8}$ in.)	1120	320	0.22	0.06	0.71	0.09					12
TSX (6 × 6 in.)	370	55	0.07	0.02	0.70	0.06					4

The smaller blocks of AGOT graphite reflect a greater degree of integrity when compared with the larger extrusion sizes. The average axial strength is higher, and the standard deviations are smaller. It is interesting to note that, with one exception, the standard deviation decreased as the strength increased. This implies that not only is there a defect distribution but also there is a defect intensity variable that must be considered in a statistical treatment of the fracture characteristics of graphite.

A comparison of the transverse properties demonstrates that rotational symmetry about the extrusion axis is not always present. The material exhibiting the most symmetry is grade CSGBF, and the worst material is grade TSX graphite. All the materials which demonstrate this lack of symmetry contain varying degrees of preferred orientation of cracks. This is quite obvious in radiographs of specimens of the TSX grade shown in Fig. 20.14.

There appear to be general interrelations between the strength and density, hardness, and the modulus of elasticity values. The most sensitive variable relating to the strength, which does not appear to be grade sensitive, is the modulus of elasticity. This relation is shown in Fig. 20.15, which includes data from all grades and orientations. The interrelation appears favorable for the parallel specimens; however, the transverse specimen data exhibit much scatter. This transverse scatter is probably caused by cracks and their orientation in the bar.

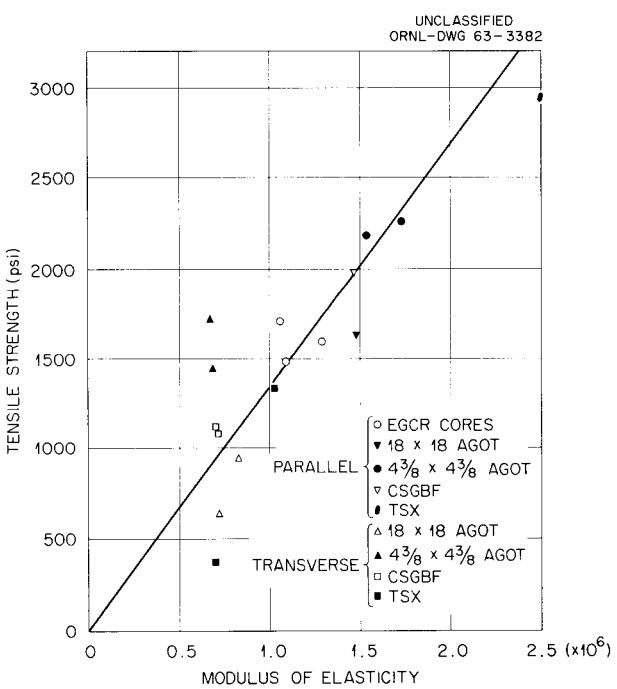

Fig. 20.15. Modulus of Elasticity vs Tensile Strength of Moderator Graphites.

Compression tests have been performed on three blocks of graphite, and the results are given in Table 20.6. The ratio of the strengths of the two grades of AGOT graphite is essentially the same in compression as in tension. The main apparent difference is in the modulus of elasticity measurement. The modulus was measured with resistance strain gages for the 18 × 18 in. block specimens and with a deflectometer for the 1074 graphite. The deflectometer measurements cannot be expected to be as accurate and will always be on the low side. It is, however, quite obvious that the compression modulus of elasticity is much smaller than the tensile modulus.

Examination of the compression results obtained from testing the TSX material reveals that the effect of the internal cracks has changed the direction of maximum strength. This can be rationalized on the basis that the tensile strains in compression are normal to those in tension, and less tensile strain can be expected in the L_1 direction.

Neutron Flux Monitoring

J. C. Zukas

To properly evaluate radiation-damage effects in neutron-irradiated structural materials, some knowledge of the shape and intensity of the neutron flux spectrum is primal. Accordingly, measurements are being made in the ORR B-8 core position and the P-5 and P-6 poolside facilities using threshold and thermal flux detectors. In the B-8 core position, where water cooling is easily achieved, dilute samples of Np^{237}, U^{238}, cobalt alloy, and zone-refined nickel wire (all sealed in quartz ampoules and inserted in cadmium thermal-neutron shields) are positioned vertically inside the experiment exposure can. Bare nickel, cobalt alloy, and triple-distilled sulfur samples are spaced between adjacent shields just beyond the region of thermal flux depression. The P-5

Table 20.6. Results of Compression Testing of Graphite

Grade	Average Fracture Stress (psi)	Standard Deviation (psi)	Average Fracture Strain (%)	Standard Deviation (%)	Average Modulus of Elasticity (psi)	Standard Deviation (psi)	Number of Specimens
					$\times 10^6$	$\times 10^6$	
Parallel to Extrusion Axis							
AGOT ($4\frac{3}{8} \times 4\frac{3}{8}$ in.) (lot 1074)	6140	276	2.15	0.41	0.65	0.16	14
AGOT (18 × 18 in.)	4510	490	1.21	0.15	0.90	0.08	12
Normal 1 to Extrusion Axis							
TSX (6 × 6 in.)	4950	451	3.30	0.58	0.36	0.07	7
Normal 2 to Extrusion Axis							
TSX (6 × 6 in.)	5410	232	5.32	0.57	0.19	0.04	4

and P-6 exposure cans will be modified to permit water cooling of cadmium shields.

The integrated fast flux above about 0.6 Mev can be measured using the fission reaction of Np^{237} and counting a suitable fission product such as Ba^{140} or Zr^{95}. To do this, however, consideration must be given to all possible chains of reaction which can result in these fission products. A computer code[57] has been written to handle these simultaneous reactions and will be applied to both Np^{237} and U^{238} fission threshold detectors.

A second computer program[58] is available to calculate the flux measured with nickel. This program considers the thermal cross sections as well as the fluctuations in reactor power. In the case of the nickel (n,p) reaction, two isomers of cobalt which have very large thermal cross sections are produced. If the thermal flux is known, or if simultaneous measurement of the thermal flux can be achieved, perhaps unshielded nickel can be used and suitable corrections may be made for thermal burnout. The thermal flux is being determined at present, using bare and shielded cobalt, and the results will be used to establish the reliability of shielded vs bare nickel monitors. For the B-8 core position the peak flux, measured with nickel, appears to be about 3×10^{13} neutrons cm^{-2} sec^{-1}; and the peak flux (thermal plus epicadmium), measured with bare cobalt, is about 2×10^{14} neutrons cm^{-2} sec^{-1}. Additional sampling may result in refinement of these values.

---

[57] D. R. Vondy, *Development of a General Method of Explicit Solution to the Nuclide Chain Equations for Digital Machine Calculations*, ORNL TM-361 (Oct. 18, 1962).

[58] Available from V. O. Haynes, Reactor Division.

21. Molten-Salt Reactor

A. Taboada

INTRODUCTION

The major effort of this program is presently devoted to the design, construction, and operation of the Molten-Salt Reactor Experiment (MSRE)[1] in an attempt to demonstrate the feasibility of this concept for central-power stations and to provide experience with the engineering (operability, dependability, serviceability, and safety) and materials compatibility of the reactor under conditions of long-term operation.

The MSRE is a high-temperature (1300°F), low-pressure (50 psi) system designed to provide a thermal output of 10 Mw. A fuel mixture of LiF-BeF_2-ZrF_4-UF_4 is circulated through a cylindrical, 5-ft-diam reactor vessel (containing a graphite matrix) to a heat exchanger, where heat is transferred to a non-fuel-bearing fluoride salt. This secondary salt coolant then discharges heat to the atmosphere through a salt-to-air heat exchanger.

All portions of the reactor in contact with salt are fabricated from the Ni-Cr-Mo alloy (INOR-8) that was specifically developed to resist corrosion by fluoride salts and still maintain good elevated-temperature strength. The core matrix consists of unclad, low-permeability graphite stringers that form vertical channels for fuel-salt flow.

The materials support work for this program has been limited to those problems affecting the successful completion of the MSRE and includes metallurgical assistance to other divisions working toward this aim as well as the materials development and testing work that follows.

[1] A. L. Boch *et al.*, "The Molten-Salt Reactor Experiment," pp 247–92 in *Symposium on Power Reactor Experiments, Vienna, October 23–27, 1961*, vol I, International Atomic Energy Agency, Vienna, 1962.

FLUORIDE-SALT CORROSION STUDIES

J. H. DeVan

Corrosion Effects of CF_4

In-pile capsule tests of the MSRE fuel salt have disclosed that under certain circumstances the formation of CF_4 may be induced in graphite-containing fluoride-salt reactor systems.[2] Accordingly, corrosion studies were continued to determine the effects of CF_4 exposure on MSRE core materials. After tests in CF_4 vapor[3] were completed, studies of INOR-8 coupons were conducted in fuel salt of the composition LiF-BeF_2-ZrF_4-ThF_4-UF_4 (70-23-5-1-1 mole %) and with CF_4 vapor passed continuously through or over the fluoride salt. The experiments were operated at 600 and 700°C for 700 and 1000 hr respectively. The results of these and the earlier vapor experiments indicated that CF_4 was effectively nonreactive toward INOR-8 at 600°C but that minor attack was promoted by CF_4 in the presence of fluoride salt at 700°C. At least part of the attack at 700°C was attributable to hydrolysis of CF_4 by moisture in the system, based on the presence of trace amounts of CO and CO_2 in the off-gas stream.

Effects of Fluoride-Salt Spillage

Studies of the oxidation behavior of INOR-8 have been extended to investigate the debilitating effects of fluoride-salt spillage on oxidation resistance. The purpose of the experiments is to establish the temperature level at which the

[2] R. B. Briggs *et al.*, *MSRP Progr. Rept. Aug. 31, 1961*, ORNL-3215, p 96.

[3] J. H. Devan, *Metals and Ceramics Div. Ann. Progr. Rept. May 31, 1962*, ORNL-3313, pp 23–25.

fluxing action of fluoride salts can lead to catastrophic attack of INOR-8 in oxygen-containing environments. The environment under study consists of nitrogen with varying additions of wet and dry air. Initial exposures were carried out in $\frac{3}{4}$-in.-diam INOR-8 tubes partially filled with salt and mounted horizontally. Plugging of inlet and outlet gas lines, however, required that tests be shifted to a larger vessel in which the capsules could be employed as fluoride-containing boats. Tests are in progress at 650°C with gas mixtures ranging from 100% N_2 to 100% air.

Molybdenum-Graphite Compatibility Tests in Fluoride Salts

The compatibility of molybdenum with materials in the MSRE system was evaluated using two INOR-8 thermal convection loops circulating the fuel mixture $LiF-BeF_2-ZrF_4-ThF_4-UF_4$ (70-23-5-1-1 mole %).[4,5] A graphite cylinder containing INOR-8 and Mo–0.5% Ti specimens was placed at the heater outlet of each loop and was maintained at the maximum salt temperature, 1300°F. The salt and graphite volumes in the two loops were in the ratio 2:1 and 1:1 respectively. The duration of each test was approximately 5500 hr.

Examination of the INOR-8 specimens that had contacted molybdenum and graphite revealed light pitting by the fuel mixture and scattered carburization in areas adjacent to graphite. The molybdenum specimens showed no change in either microstructure or chemistry (including areas which contacted graphite) when compared to as-received material. However, tensile tests of the specimens indicated a very low room-temperature ductility. A similar condition was found to exist in the sheet stock used to fabricate the specimens, and the cause of embrittlement was subsequently traced to surface contaminants present in the as-received material. Additional tests of molybdenum specimens having special surface treatments are now in progress under conditions identical to the first test series.

[4]R. B. Briggs *et al.*, *MSRP Progr. Rept. Aug. 31, 1961*, ORNL-3215, pp 96–99.

[5]R. B. Briggs *et al.*, *MSRP Semiann. Progr. Rept. Feb. 28, 1962*, ORNL-3282, pp 74–77.

MSRE HEAT EXCHANGER TUBE-TO-TUBE-SHEET ATTACHMENTS

R. G. Donnelly C. H. Wodtke

A high-integrity design for the tube-to-tube-sheet joints of the MSRE primary heat exchanger was developed, and procedures for effecting these joints were established and successfully utilized in the actual fabrication of the component. The MSRE U-tube heat exchanger is designed with all tube ends ($\frac{1}{2}$ in. diam, 0.042 in. wall) joined to a $1\frac{1}{2}$-in.-thick tube sheet 18 in. in diameter. Fabrication of this 7-ft-long component with 326 tube-to-tube-sheet joints was complicated by the necessity of absolute leak-tightness during service in an environment of molten-fluoride salts at 1300°F. The complete unit was constructed of INOR-8.

Because extremely high integrity was needed for the joints, a welded and back-brazed design (shown in Fig. 21.1) was chosen for the tube-to-tube-sheet joint. This design provided a double

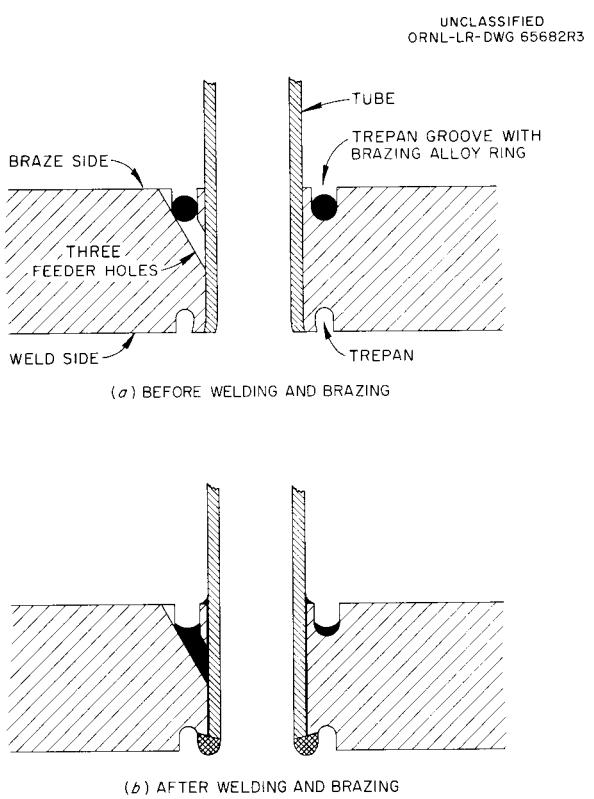

Fig. 21.1. Tube-to-Tube-Sheet Joint Designed for MSRE Heat Exchanger.

seal between the fuel and coolant salts to minimize leakage. Back brazing also served to reinforce the weld in case of inadvertent defects and eliminated the crevice and notch effect commonly encountered in tube-to-header welds. The trepan design with three feeder holes was used for the brazing joint to eliminate the possibility of preferential runoff of the brazing alloy onto the thin-walled tube, which would reach temperature before the heavy tube sheet. The corrosion-resistant, ductile brazing alloy (82 wt % Au–18 wt % Ni) selected for this application was placed in the trepan grooves before assembly of the tubes into the tube sheet.

To ensure adequate strength of the brazed joints, Miller-Peaslee shear-test specimens were fabricated and tested at room temperature and at the reactor operating temperature of 1300°F. Joints tested at room temperature had a minimum shear strength of 68,800 psi and an average of 73,000 psi, whereas those tested at 1300°F in air exhibited minimum and average shear strengths of 12,500 and 18,100 psi respectively. These strengths were considered adequate for the application, since the braze was to serve primarily as a seal and not as a load-carrying joint.

With the aid of trepan grooves on the weld side of the tube sheet, low-restraint edge welds were made with a special-built, semiautomatic, gas–tungsten-arc torch. This, in effect, eliminated the problems usually associated with welding thin-walled tubes to heavy-section tube sheets. Studies[6] were made to determine the conditions necessary to satisfy minimum weld penetration requirements and also the requirement of minimum weld metal "roll-over" which could constrict the coolant flow through the tubes.

Special procedures that emphasized cleanliness were prepared for the handling, assembly, welding, and radiography of the MSRE tube bundle. These operations were accomplished in approximately four weeks.

Brazing was carried out in an all-welded retort containing dry hydrogen. By the use of a large gas-fired furnace at a commercial brazing concern, the whole unit could be heated to brazing temperature, the temperature variations over the unit being limited between 1835 and 1885°F. Thus the possibility of distortion and excessive grain growth was minimized. Visual, radiographic, and dye-penetrant inspection of the welds revealed no defects whatsoever. Ultrasonic inspection of the brazed joints revealed only scattered porosity, and all joints exhibited excellent braze fillets. Also, the tube bundle as a whole was found to be helium leak-tight. The completed tube bundle is shown in its welding fixture in Fig. 21.2.

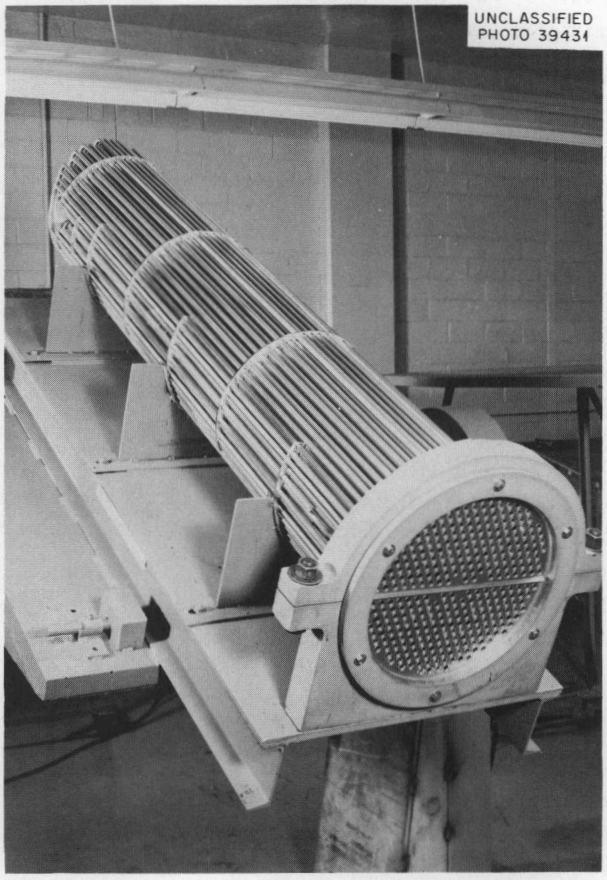

Fig. 21.2. MSRE Heat Exchanger in Welding Fixture.

NONDESTRUCTIVE TESTING OF MSRE HEAT EXCHANGER TUBE JOINT

K. V. Cook C. H. Wodtke

Methods of inspecting tube joints were developed that are applicable to the MSRE heat exchanger. These include radiography of the

[6] R. B. Briggs *et al., MSRP Semiann. Progr. Rept. Aug. 31, 1962,* ORNL-3369, pp 88–92.

weldments and an ultrasonic Lamb-wave technique for inspecting the brazed joints.

Test welds were examined with both x-ray and iridium sources under a variety of conditions and with curved strips of film placed in the tubes at the welds. Of those tested, the optimum radiographic conditions found for the heat exchanger weld were:

X-ray energy	160 kv
Film to focal distance	48 in.
Incident angle	30–35°
Time	2.5 min
Film type	M

Four to six exposures were required to completely inspect each weld; however, the tube arrangement on the MSRE heat exchanger allows several tube welds to be radiographed at one time. The defects observed were somewhat distorted because of the method of film placement; however, pores several mils in diameter were detected.

The ultrasonic Lamb-wave technique, developed for the evaluation of bonding in brazed tube joints, utilizes a small probe that fits inside the $\frac{1}{2}$-in.-diam tube. The probe contains two piezoelectric crystals that serve as ultrasonic generator and receiver respectively. The proper ultrasonic frequency and beam incident angles were determined, and a custom probe was designed and fabricated. A mechanical device was designed that provides for uniform scanning of the probe in the tube and thus ensures complete inspection coverage.

An evaluation of the MSRE heat exchanger using these methods indicated that the brazing operation was successful. The unit was generally bright and clean, and full fillets existed. Ultrasonic inspection revealed no nonbond areas large enough to cause a leak path or significant mechanical weakening. Some indications comparable to a $\frac{3}{32}$-in.-diam standard were noted that will be further investigated to ensure acceptability.

WELDING DEVELOPMENT FOR INOR-8

R. G. Gilliland

The design of the MSRE required that numerous dissimilar joints be fabricated. Consequently, welding procedure specifications were prepared and qualification tests were completed for INOR-8 to stainless steel, to nickel, and to Inconel. Test specimens were prepared from the qualification test welds for room- and elevated-temperature testing using the nickel-base filler material Inco 82 [67 Ni, 20 Cr, 2.5 Nb, 0.75 Ti, 0.3 Ta (wt %)]. The results of the room-temperature tensile tests using transverse specimens are presented in Table 21.1. The room- and elevated-temperature tensile test results for samples taken from the INOR-8 to type 347 stainless steel joints are presented in Table 21.2. Tests were performed at room temperature, 1000°F, and 1200°F on transverse samples of this joint. All joints of these dissimilar-metal welds exhibited satisfactory integrity, and all failures occurred outside the weld-metal area in the nickel, Inconel, and stainless steel base metal.

Elevated-temperature creep tests on transverse samples from the welds of INOR-8 to type 347 stainless steel were made at 1000°F and 1200°F,

Table 21.1. Results of Room-Temperature Tests on Dissimilar-Metal Welds Using Inco 82 Filler Material

Weld	Tensile Strength (psi)	Yield Strength (psi)	Elongation (%/2 in.)
INOR-8 to Inconel	98,200	52,900	29
INOR-8 to nickel	65,200	39,300	29
INOR-8 to type 347 stainless steel	95,500	58,200	22

Table 21.2. Room- and Elevated-Temperature Tensile Tests of INOR-8 to Type 347 Stainless Steel Dissimilar Welds Using Inco 82 Filler Material

Temperature (°F)	Tensile Strength (psi)	Yield Strength (psi)	Elongation (%/2 in.)
Room	95,500	58,200	22
1000 (538°C)	61,700	39,000	9
1200 (648°C)	51,700	35,800	8

and the results are shown in Table 21.3. Preliminary examination of the tested specimens indicated that all failures occurred at the stainless steel–Inco 82 interface. Very little strain, as indicated by reduction in area, was seen in these specimens. Those specimens that ruptured on loading did so in the type 347 stainless steel base material.

Table 21.3. Elevated-Temperature Creep Tests of INOR-8 to Type 347 Stainless Steel Dissimilar Welds Using Inco 82 Filler Material

Specimen No.	Test Temperature (°F)	Stress Level (psi)	Rupture Time (hr)
1–5	1000	60,000–105,000	Ruptured on loading
6	1000	55,000	186
7	1000	50,000	931
8	1200	39,000	13
9	1200	35,000	14
10	1200	29,000	128
11	1200	25,000	222
12	1200	22,000	320

Table 21.4. Elevated-Temperature Creep Tests of INOR-8 Transverse Weld Specimens in the As-Welded and Stress-Relieved Conditions

(Test temperature, 1300°F; stress, 27,500 psi)

Sample Condition	Rupture Time (hr)	Total Strain (%)
As welded	113.9	4.5
As welded	79.1	6.6
Stress relieved	234.2	12.5
Stress relieved	243.9	12.5

The effect of a stress-relieving treatment on the stress-rupture properties of INOR-8 weld metal has also been determined. Two samples were tested in the as-welded condition and two in the stress-relieved (2 hr at 1600°F) condition. The resulting data are presented in Table 21.4 for tests at 1300°F and a stress level of 27,500 psi. It is evident that the stress-relieving treatment improved the overall properties of the weldment, probably because of a redistribution of microconstituents such as grain-boundary carbides.

HIGH-TEMPERATURE CREEP OF 82 wt % Au–18 wt % Ni BRAZED JOINTS IN SHEAR

R. G. Donnelly W. R. Martin

In the event that the MSRE dump tank is to be replaced, it has been proposed that the connected INOR-8 piping be remotely rejoined by brazing with the 82 Au–18 Ni (wt %) alloy.[7] In order to obtain strength data on joints of this type, Miller-Peaslee shear-test specimens were fabricated and tested in short-time shear and stress to rupture.

All specimens were tack-welded prior to alloy preplacement to maintain a nominally zero joint clearance. The alloy, in the form of powder mixed with an acrylic binder, was then preplaced at the joints, and the specimens were furnace brazed. Brazing was carried out at 1850°F in a dry helium atmosphere for 10 min. After the specimens were brazed, they were machined to a brazed-joint gage length of 0.125 in. and ground to a joint width of 0.115 in. The short-time shear strengths at 1300°F are presented in Table 21.5.

The creep data obtained at 1300°F are presented in Table 21.6. The short-time creep strengths are low when one considers the strength values obtained by short-time mechanical property tests. The correlation of time to rupture for the tests at stresses equal to or greater than 2070 psi is excellent. However, the time to rupture at stress levels below 2070 psi is much in excess of that predicted from the shorter-time creep tests. The phenomenon is not simply a function of stress. Test 7 was stressed at 1030 psi for 2113 hr, at which time the stress was increased to 2070 psi.

[7] R. B. Briggs *et al.*, *MSRP Semiann. Progr. Rept. Feb. 28, 1962*, ORNL-3282, pp 84–86.

One would predict from damage theory that the rupture life would be equal to or less than 2.9 hr. The test ruptured after 2070 hr at the higher stress. The stress-rupture curve for the braze alloy at 1300°F resembles that observed for an alloy in which a time-dependent reaction, such as age hardening, is occurring.

Table 21.5. Miller-Peaslee Shear Strength Data at 1300°F

Base metal, INOR-8
Brazing alloy, 82 Au–18 Ni (wt %)
Brazing temperature, 1850°F
Brazing time, 10 min
Testing atmosphere, air

Specimen No.	Testing Temperature (°F)	Shear Strength (psi)
6	1300	16,020
7	1300	16,260
8	1300	17,025
9	1300	15,940
10	1300	15,345

Table 21.6. Shear Creep of Gold-Nickel-INOR-8 Braze at 1300°F

Test	Stress (psi)	Time to Rupture (hr)	Maximum Rupture Life Predicted from Short-Time Test (hr)
1	20,000	<0.0003	
2	6,900	0.01	
3	4,140	0.1	
4	2,070	2.9	
5	1,740	760.1[a]	30
6	1,380	3400	100
7	1,030	2312.8[b]	700
8	1,030	4000.2[a]	

[a]Still in test.

[b]Discontinued. Test reloaded to 2070 psi after 2312.8 hr and test ruptured after 2070 hr.

Examination of the phase diagram for Au-Ni suggests that an order-disorder reaction may be the cause of creep results observed. It is postulated that the material was quenched from the brazing temperature at a rate such that ordering could not occur or that the alloy was disordered as a result of specimen preparation (cold working). It is assumed that the ordering reaction is sluggish and hence requires time at temperature. Furthermore, it is assumed that the ordered structure[8] and two-phase region are stronger than the disordered structure, as is normally the case. Hence, in these creep tests, at stresses for which the time to rupture of the disordered material is less than that to complete the ordering, the specimen ruptures. Conversely, at low stresses the increased time to rupture of the disordered material permits the ordering reaction; hence the time to rupture is significantly increased. These data indicate that more information is needed on the high-temperature creep of this alloy in shear.

MECHANICAL PROPERTIES OF INOR-8 ALLOY

ASME Boiler and Pressure Vessel Code Allowable Stresses for INOR-8

J. T. Venard W. J. Leonard

The properties of INOR-8 were reviewed by the ASME Boiler and Pressure Vessel Code Committee, and this material was approved for code construction in code case 1315, subject to the allowable stresses in Table 21.7. These values now supersede previous design values established for the MSRE.

Reactor-Quality INOR-8

J. T. Venard W. J. Leonard

Mechanical properties are being determined on random heats of INOR-8, from which MSRE reactor components have been fabricated, to evaluate the effects of large-scale production and improved quality requirements. Some tensile tests and

[8]L. S. Darken and R. W. Gurry, *Physical Chemistry of Metals*, p 85, McGraw-Hill, New York, 1953.

Table 21.7. Maximum Allowable Stresses for INOR-8 Reported by ASME Boiler and Pressure Vessel Code

Temperature (°F)	Maximum Allowable Stress (psi)	
	Material Other than Bolting	Bolting
100	25,000	10,000
200	24,000	9,300
300	23,000	8,600
400	21,000	8,000
500	20,000	7,700
600	20,000	7,500
700	19,000	7,200
800	18,000	7,000
900	18,000	6,800
1000	17,000	6,600
1100	13,000	6,000
1200	6,000	3,500
1300	3,500	1,600

stress-rupture tests were completed and are reported.

The tensile properties of two heats, 5075 and 5081, of MSRE plate were determined in the range 70 to 1800°F. These results are given in Table 21.8. The values quoted for ultimate tensile strength and 0.2% yield strength are averages from four specimens, two from each heat of material, with one specimen being cut parallel to the plate rolling direction and one normal to the rolling direction. The two heats behaved similarly except for elongation and reduction in area at high temperatures, and no variation in properties was noted between directions in the original plate.

Figure 21.3 shows stress-rupture results to date for heat 5055 in air. A few longer-time tests on this heat are presently running, and stress-rupture testing has begun on heats 5075 and 5081.

These tests indicate a significant improvement in the mechanical properties of these heats when compared to design values established for MSRE on prior material.

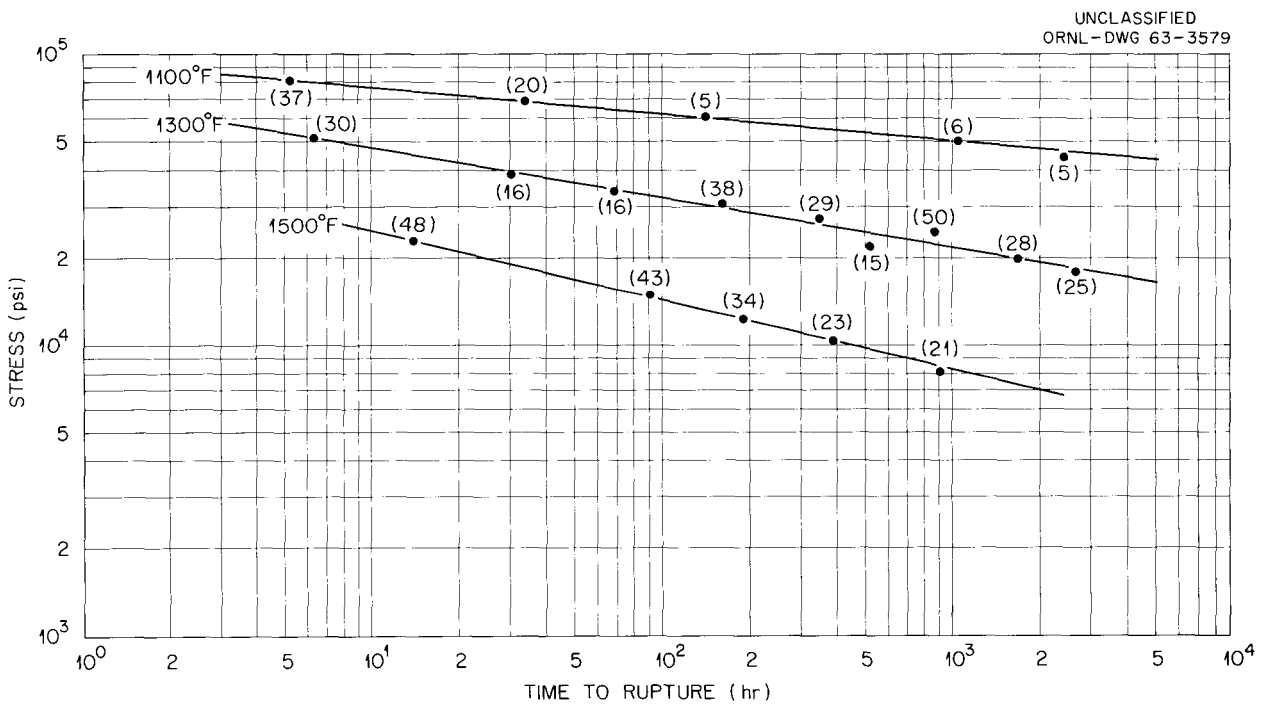

Fig. 21.3. INOR-8 Heat 5055 Stress Rupture in Air. Numbers in parentheses indicate total creep strain (%). Specimens cut parallel to plate rolling direction – tested as machined.

Table 21.8. Average Tensile Properties for INOR-8

Temperature (°F)	Ultimate Tensile Strength (psi)		0.2% Yield Strength (psi)		Elongation (%)		Reduction in Area (%)	
	Heat 5075	Heat 5081	Heat 5075	Heat 5081	Heat 5075	Heat 5081	Heat 5075	Heat 5081
70	113,600		46,500		53		54	
600	103,300		36,000		55		50	
800	100,100		35,000		53		52	
1000	96,000		33,200		53		46	52
1200	74,800		32,600		22	36	28	36
1400	61,600		31,800		21	30	23	30
1600	36,400		31,600		23	40	25	43
1800	20,300		20,000		28	28	29	29

Influence of Prior Annealing on the Tensile Properties of INOR-8

H. E. McCoy

It has been reported, "Welding Developments for INOR-8," this chapter, that heat treatment significantly improved the rupture life and ductility of INOR-8 at 1300°F. In order to gain a better understanding of the influence of prior heat treatment on INOR-8 alloy (Ni, 7% Cr, 17% Mo, 5% Fe, 0.06% C), a brief program was undertaken using tensile tests and subsequent metallographic examination as evaluation tools. The results of this study to date, involving heats 5075 and SP-25, can be summarized as follows.

1. The fracture ductility goes through a minimum as a function of temperature at approximately 1600°F.
2. The minimum ductility (measured at 1600°F) decreases with increasing solution annealing temperature. Although the ductility changes were quite large, the strength changes were only minor.
3. The minimum ductility (measured at 1600°F) can be improved by following the high-temperature solution anneal with an anneal in the temperature range 1400 to 1800°F. Again the strength changes were small relative to the ductility changes.
4. The rate of cooling from the solution annealing temperature was found to be important. After a 1-hr anneal at 2300°F, cooling rates of 200, 8.1, 4.2, and 2.0°F/min were used. The elongations at fracture at 1600°F were, respectively, 7.5, 32.0, 39.0, and 42.0%.
5. Two specimens were solution annealed at 2300°F and strained at room temperature. They were subsequently tested at 1600°F. The rupture ductility improved significantly with prior strain, with elongations of 7.5, 10.5, and 26.5% being observed for 0, 5, and 20% strains.
6. Serrated stress-strain curves were obtained at all test temperatures from 1200 to 1600°F except for the prestrained specimens.
7. No well-defined yield points were observed. Tensile tests in which the specimens were loaded, unloaded, aged, and reloaded failed to produce a yield point.
8. Metallographic observations revealed that even the anneal for 1 hr at 2400°F was not the solution anneal for this material.
9. The major microconstituents were (*a*) a relatively large precipitate with particles as large as 1 mil in diameter and located in stringers parallel to the working direction of the material; (*b*) a fine precipitate no larger than 0.1 mil in diameter and randomly located; and (*c*) a very fine, sometimes lamellar, precipitate which was associated with the grain boundaries of the material. The first constituent was found by means of microprobe analysis and appeared to be

significantly higher in molybdenum than the matrix, but was not identified further. The second constituent was believed to be metal carbide. The third constituent was not identified but, based on its etching characteristics, was believed to be different from the first two.

10. The third microconstituent was the only metallographic feature that appeared to be influenced by the various annealing treatments used.

The observations that have been made are indicative of dynamic strain aging in which impurity atoms interfere with the motion of dislocations. The fact that serrated stress-strain curves were observed over such a large temperature range indicates that several impurities may be responsible for the observed strain aging. The effect of increasing the solution annealing temperature may be that of increasing the number of impurity atoms in solution and hence free to interfere with dislocation motion. The influence of slow cooling or of annealing at a temperature lower than the solution annealing temperature may be that of reducing the number of impurity atoms in solution. The role of cold working may be that of producing additional dislocations which make flow easier or of producing nucleation sites onto which the impurity atoms precipitate while the test specimen is being heated. The absence of serrations in the stress-strain curves for these specimens favors the latter possibility.

The above explanation is not complete at this stage of this study and is speculative in many respects. It is felt that a satisfactory explanation of these observations will include an answer to the basic question of why most nickel-base alloys show a ductility minimum as a function of temperature.

EVALUATION OF MSRE GRAPHITE

W. H. Cook

Grade CGB graphite bars selected from material produced for the MSRE moderator were evaluated to secure advanced information as to the acceptability of the material for reactor use. The material met most specification[9] requirements except that it had a general cracked condition and some bars had low bulk densities. The effects of these deviations on mechanical properties and salt permeation were determined, and the cracked condition was characterized.

Examinations were made of two base-stock graphite bars and four bars of completely processed graphite supplied by the vendor. The base-stock graphite had a bulk density of 1.66 g/cm^3, which increased to 1.82 to 1.88 g/cm^3 in the final fabrication operations. The majority of the bars had bulk densities of approximately 1.85 g/cm^3. The microstructure of the completely processed graphite was found to be relatively complex. It appears to be a fine-grained graphite fabricated from at least four different sources of carbon.

The chemical composition of the graphite was within the limits specified, as shown in the comparison of the specified and determined values in Table 21.9.

Visual and radiographic techniques were used to study the cracks in the graphite.[10] The majority of the cracks were 0.001 in. (25 μ) to 0.002 in. (50 μ) thick, $\frac{1}{8}$ to $1\frac{1}{4}$ in. wide, and less than 3 in. long. These cracks tended to be near the longitudinal axes of the bars. It is calculated that cracks that intersect the external surfaces of the bars will fill with molten salt at a pressure difference of approximately 20 psig.

The base-stock graphite examined was essentially free of cracks, and only two short, closed cracks were detected radiographically. A microscopic examination made on completely processed graphite showed the impregnating material in some of the cracks, indicating that some cracking occurred at processing steps earlier than the final one.

A comparison was made of the permeation by molten salt and mercury of base stock and finished graphites under the conditions given in Table 21.10. The results are summarized in Table 21.11. These data show that permeation of grade CGB graphite by mercury or by molten salts is within specification limits. It is significant to note that (1) the 150-psig molten-salt pressure used in the standard permeation screening test for graphite is approximately three times the maximum expected in the MSRE and (2) the molten

[9] *Tentative Specification for Graphite Bar for Nuclear Reactors*, MET-RM-1 (May 10, 1961).

[10] R. B. Briggs *et al.*, *MSRP Semiann. Progr. Rept. Jan. 31, 1963*, ORNL-3419, pp 70–71.

Table 21.9. Comparison of the Purity Requirement for MSRE Graphite with Various Grades of Graphite

Constituent	Maximum Specified[a] (wt %)	Found (wt %)		
		CGB-Y[b]	TS-281[c]	CGB[c]
Ash	0.07	0.015	0.018	0.0005
Boron	0.0001	0.00022	0.00006	0.00008
Vanadium	0.01		0.0049	0.0009
Sulfur	0.0050		<0.0005	<0.0005
Oxygen, cm^3 (STP) of CO released per 100 cm^3 of graphite	30		7.0	6.0

[a] *Tentative Specification for Graphite Bar for Nuclear Reactors,* MET-RM-2 (May 10, 1961).
[b] A sample from a single bar.
[c] A composite sample from three separate bars.

Table 21.10. Test Conditions for Standard Permeation Screening Tests

Test Conditions	Molten-Salt[a] Test	Mercury Test
Temperature, °F	1300	70
Test period, hr	100	20
Pressure, psig[b]	150	470

[a] $LiF-BeF_2-ThF_4-UF_4$ (67-18.5-14-0.5 mole %).
[b] Specimens are in an evacuated state when they are placed into test.

Table 21.11. Permeation of Various Grades of Graphite by Mercury and Molten Salts[a]

Graphite Grade	Graphite Bulk Density (g/cm^3)	Weight Gain of Graphite Permeated with Mercury (%)	Bulk Volume of Graphite Permeated with Salt (%)
CGB-X	1.83	0.44(1)	0.0_2
CGB-Y	1.85		0.0_4
CGB	1.85(5)	1.92(3)	0.1_8(9)
TS-281	1.88	1.23(1)	0.2_1
CGB-B	1.66		21.4

[a] All values are averages of three, except the numbers in parentheses, which are the number of values averaged.

salt that permeated the graphite in the screening test was found only at the external surfaces and in crack fissures. The latter indicates that the pore structure of the graphite is fine enough to prevent impregnation by the molten salt.

Laboratory thermal-cycling tests were made on grade CGB graphite with salt-impregnated crack fissures to determine if damage would occur at conditions simulating the drain, cool, and reheat of the MSRE core.[11]

The thermal-cycling tests were made on 2-in.-long transverse sections cut from a machined grade CGB graphite bar in a zone having a relatively high concentration of cracks.

Two specimens each were impregnated with $LiF-BeF_2-ThF_4-UF_4$ (67-18.5-14-0.5 mole %) at 1300°F during 100-hr exposures at 50 and 150 psig; 50 psig was selected because it is approximately the maximum pressure expected in the

[11] R. B. Briggs *et al., MSRP Semiann. Progr. Rept. Jan. 31, 1963,* ORNL-3419, pp 71–74.

reactor. The average bulk volume of the specimens permeated by the salt was 0.08% at 50 psig and 0.13% at 150 psig.

The highest-salt-impregnated specimen of each pressure was subjected to 100 thermal cycles in argon in which the specimen temperature was increased from 390 to 1300°F in the first 9 min of each cycle. After this treatment there were no detectable changes in the appearance of the graphite or the lengths of the cracks.

Two high-temperature, one-cycle tests were made in a manner similar to that described above. These were made to determine the effect on graphite with salt-impregnated cracks under a qualitative simulation of a hot spot in the MSRE. The specimen temperature was increased from 390°F to 1830°F in 30 min. The impregnating salt, which was principally confined to cracks in the specimens, represented 0.17 and 0.36%, respectively, of the bulk volumes of each of two specimens. After the thermal-cycle treatment, there were no detectable changes in the appearance of the graphite or the lengths of the cracks. These results indicate that a hot spot in the reactor probably would not cause the salt to expand and break the graphite. More rigorous tests are planned to evaluate this.

MECHANICAL PROPERTIES OF MSRE GRAPHITE

W. H. Cook

Tensile[12] and flexural strengths were determined on specimens of grade CGB graphite to be used for the MSRE.

Cylindrical tensile specimens were machined with their longitudinal lengths parallel to the graphite bars. Specimens that were not appreciably affected by cracks yielded an average strength of 5440 psi and a modulus of elasticity of 3.1×10^6 psi. The specimens that demonstrated a definite effect of internal cracks had a minimum strength of 1510 psi and an average strength of 2940 psi.

A ring specimen technique was used to measure the tensile strengths transverse and parallel to the length of the grade CGB bars. The results were higher than those obtained with the cylindrical tensile specimens. This is probably due to higher stress gradients in the ring specimens. The 5440 psi obtained with the cylindrical specimens is considered to be the more accurate tensile strength parallel to the lengths of flaw-free grade CGB graphite. Using the ring specimen test data as a guide, transverse tensile strength would be approximately 75% of the longitudinal strength, or 4000 psi.

Flexural strengths were determined on four square bar specimens cut longitudinally from a severely cracked bar. These, tested as simple beams with third point loading, yielded an average strength of 4580 psi and a modulus of elasticity of 2.4×10^6 psi. The minimum strength value was 3462 psi.

The specification requires that the minimum longitudinal tensile and flexural strengths of specimens from the MSRE graphite bars shall be greater than 1500 and 3000 psi respectively. The minimum values obtained in the results exceeded these requirements.

Although all the inspection planned for the MSRE graphite has not been completed, the information obtained to date indicates that the material meets the needs of the MSRE moderator.

[12] R. B. Briggs *et al.*, *MSRP Semiann. Progr. Rept. Jan. 31, 1963*, ORNL-3419, pp 74–75.

EXAMINATION OF MSRE IN-PILE EXPERIMENTS

A. R. Olsen

During the past year, the Postirradiation Examination Laboratory (PIE) has contributed a number of services in the postirradiation examination of specimens and capsules from the ORNL in-pile experiments MTR-47-3, -47-4, and -47-5 that were run to demonstrate the compatibility of the MSRE system under irradiation. As reported previously,[13] the MTR-47-3 capsules were examined and dismantled in the Battelle Memorial Institute hot cells. The coupons and samples of the salt along with sections from each of the capsules were then transferred to the 4501 facility, where the coupons were carefully examined and photographed through the stereomicroscope.

[13] R. E. McDonald and J. R. Parrott, *Metals and Ceramics Div. Ann. Progr. Rept. May 31, 1962*, ORNL-3313, p 127.

As a result of these examinations, a detailed program of scale analysis, weight-loss determinations, dimensional checking, auto- and x-radiography, and metallography was developed. This work is 80% complete, and some results have been reported.[14–17]

The MTR-47-3 work was deliberately delayed to permit the complete examination of the MTR-47-4 experiment since this experiment more nearly resembled reactor conditions. This examination included the removal of the capsule array from the surrounding water jacket and sodium bath, dismantling of the array, dimensional and visual checking of each capsule, fission-gas recovery and analysis, autoradiography (Part IV, Chap. 31, this report), and capsule disassembly and sectioning with appropriate fuel-salt recovery and sampling.

A special fission-gas sampling rig was developed for these capsules. By use of this equipment, the first evidence of the evolution of fluorine from previously irradiated solid salt was developed.[14–17] As a result of the unexpected recovery of the fluorine and its subsequent reaction within the glass collection system, it was necessary to revise the gas sampling system. The glass portions were rebuilt, and a second all-metal prefluorinated collection and sample distribution system was built and inserted between the glass system and the in-cell puncturing device (Part IV, Chap. 31, this report). By use of the modified system, one small and three large irradiated capsules and one each of the unirradiated controls were punctured. The large quantities of fluorine recovered appear to be a function of the fuel burnup.

Since other evidence indicated that the fluorine gas was not present during irradiation at high temperatures, experiment 47-5 was devised and irradiated. This experiment permitted the periodic sampling of gas during irradiation. The results confirmed the conclusions derived from the 47-4 examination. Currently the 47-5 capsules are in the 4501 hot-cell facilities, and the two capsules designed for in-pile gas sampling are being monitored for the gas-evolution rate at temperatures varying from −70°C to as high as +88°C. The results of these experiments have not yet been fully analyzed. When this work is completed, the assembly will be dismantled, and examinations similar to those conducted on the capsules from 47-4 will be made.

METALLOGRAPHIC EVALUATION OF INOR-8 CAPSULE IN MTR-47-4

E. J. Manthos

Capsule 24 from in-pile experiment MTR-47-4[18] was examined metallographically at magnifications up to 1000 for evidence of F_2 gas attack and for possible accelerated corrosion due to irradiation. The INOR-8 container was exposed to fuel for 1500 hr at a flux of 2×10^{13} and temperatures to 1400°F.

Preliminary evaluation of the capsule at low magnification indicated no general attack of the magnitude expected from F_2 at elevated temperatures. All surface areas, including the salt-vapor interface, appeared to be uniformly unaffected. No bulging or distortion of the container was noted, as might be caused by the high pressures of F_2 potentially present at elevated temperatures. A thin, nonmetallic film that was easily removed was found on the inside metal surface but did not occur in sufficient quantity to analyze.

High-magnification examinations were made of longitudinal sections of the capsule wall in the vapor region and at various locations exposed to salt (including the interface, where maximum corrosion was expected, and the weldment). No attack, either uniform or preferential, was observed in any of these specimens. Figures 21.4*a–c* show the typical appearance of a longitudinal view of the interior surfaces of the capsule. The only surface irregularity present was due to rough machining in the cylindrical wall and was also evident in the control specimen that was not irradiated. This surface of the irradiated capsule was difficult to etch because of recrystallization to fine grains of work-hardened areas.

[14] S. S. Kirslis *et al.*, *Reactor Chem. Div. Ann. Progr. Rept. Jan. 31, 1962*, ORNL-3262, pp 20–26.

[15] R. B. Briggs *et al.*, *MSRP Semiann. Progr. Rept. Aug. 31, 1962*, ORNL-3369, pp 100–116.

[16] F. F. Blankenship *et al.*, *Reactor Chem. Div. Ann. Progr. Rept. Jan. 31, 1963*, ORNL-3417, pp 17–34.

[17] R. B. Briggs *et al.*, *MSRP Semiann. Progr. Rept. Jan. 31, 1963*, ORNL-3419, pp 80–93; 106–7.

[18] R. B. Briggs *et al.*, *MSRP Semiann. Progr. Rept. Aug. 31, 1962*, ORNL-3369, pp 100–116.

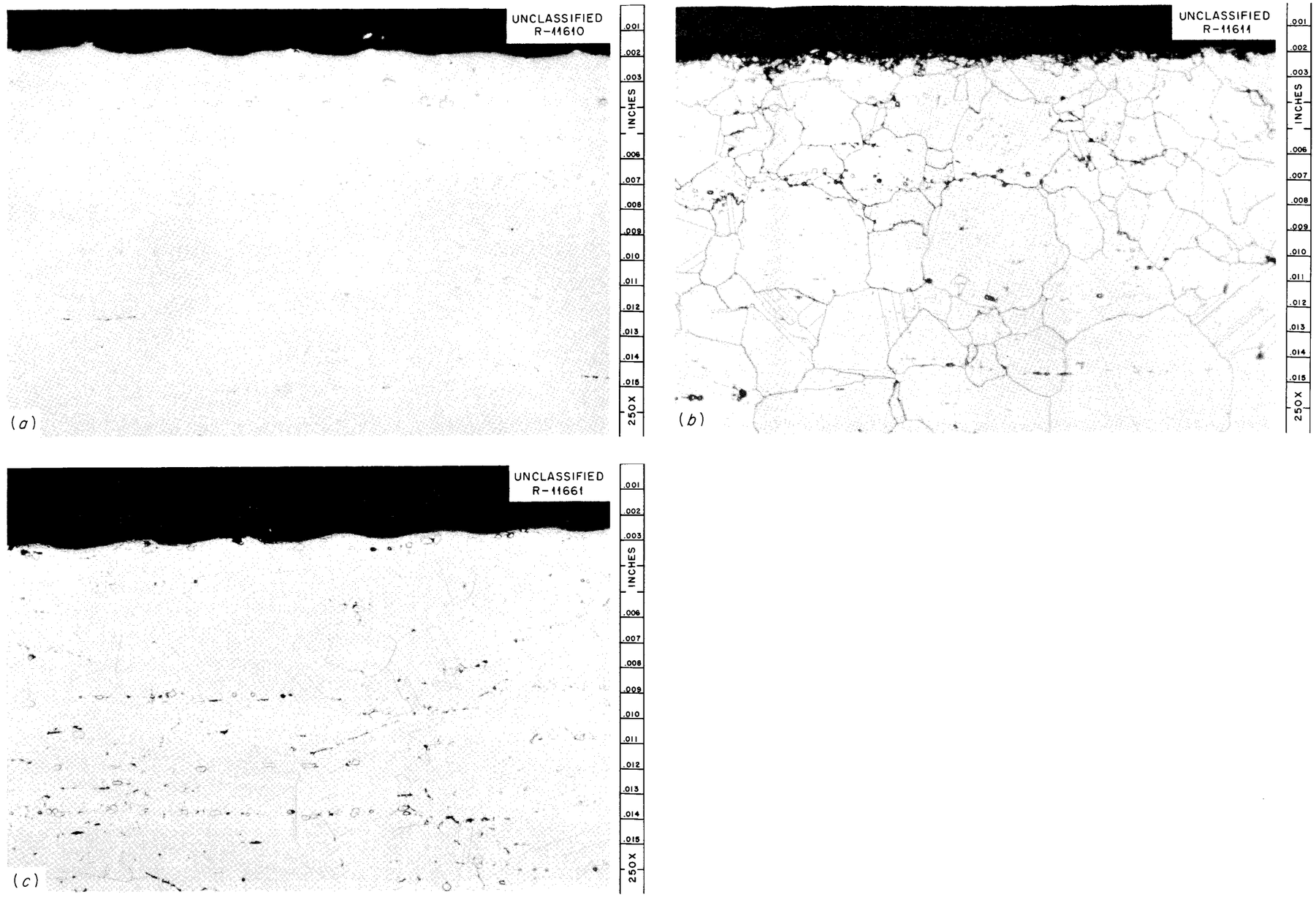

Fig. 21.4. Longitudinal View of Interior Surfaces of Wall from Capsule 24. (*a*) As polished. (*b*) Etchant: aqua regia. (*c*) Control, etchant: aqua regia. Reduced 10%.

Transverse sections of the capsule wall were examined for uniform surface removal, the expected method of F_2 corrosion. A section (shown with a control specimen in Fig. 21.5) measured 0.050 in. in thickness as compared to 0.0495 in. for the control, indicating no loss of wall.

It was evident from the metallographic examination that the severe attack normally expected when nickel alloys are exposed to F_2 at the test conditions was not present.

SINTERING CHARACTERISTICS OF Gd_2O_3-Al_2O_3 CYLINDERS

A. J. Taylor

A study was begun to develop the fabrication procedures necessary to make thin-walled cylinders of Gd_2O_3 and Gd_2O_3-Al_2O_3 mixtures. These cylinders are of interest as control-rod elements for the MSRE and are being designed to withstand

UNCLASSIFIED
PHOTO 60623

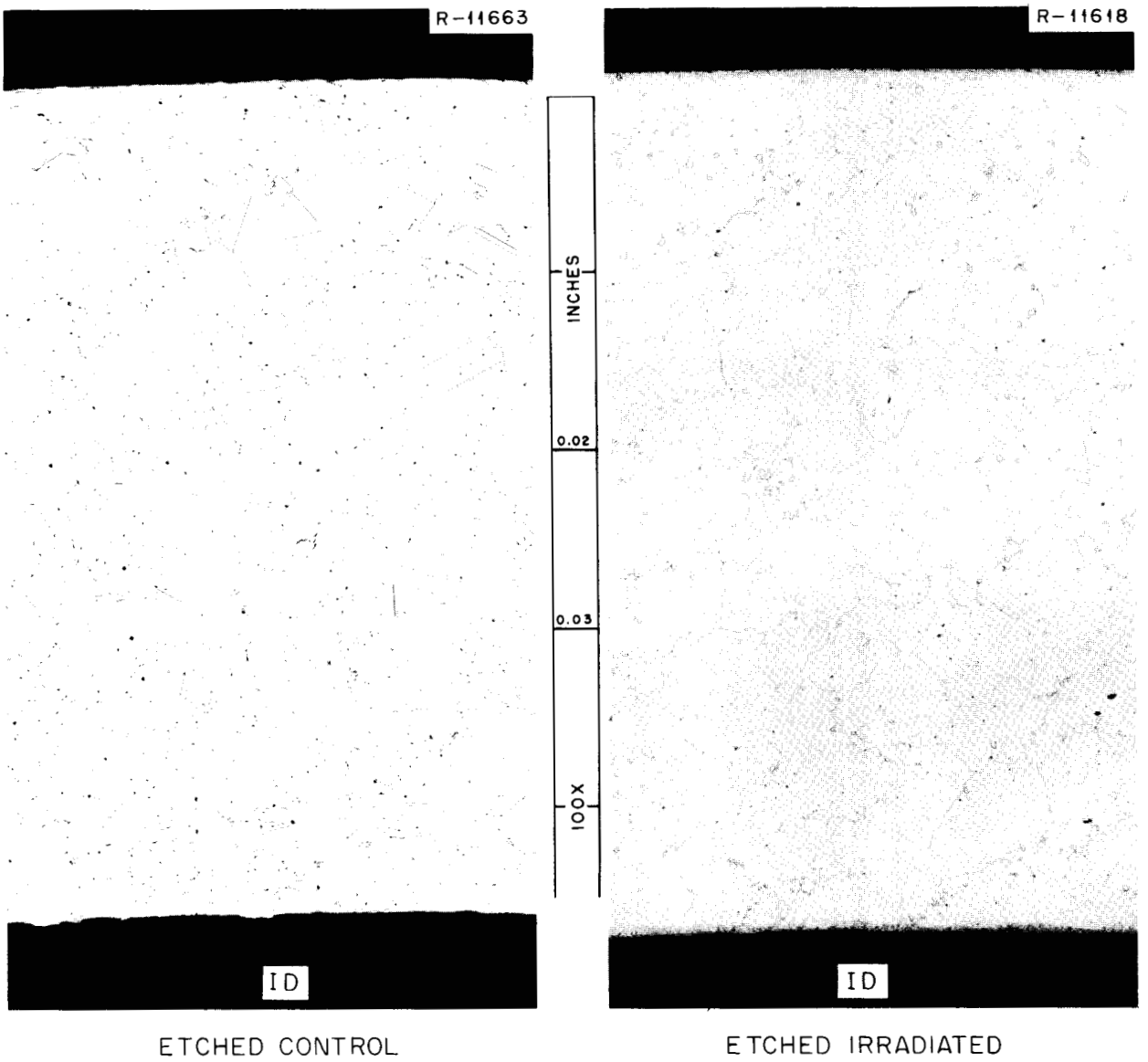

Fig. 21.5. Transverse Section of INOR-8 Capsule Wall.

a nitrogen atmosphere contaminated with air and moisture at temperatures up to 1400°F. The addition of 30 wt % Al_2O_3 was specified to minimize hydrolysis and subsequent deterioration of the Gd_2O_3.

Preliminary experiments[19] were made on pellets containing 0, 20, and 30 wt % Al_2O_3 to determine density and shrinkage data. It was observed that the cold-pressed mechanical mixtures melted when heated to 1750°C and became severely distorted when heated to 1650°C, indicating the formation of a low-temperature-melting compound. No evidence of liquid loss was detected after sintering.

A series of experiments[20] was then carried out at various times and temperatures with "prereacted" 70 wt % Gd_2O_3–30 wt % Al_2O_3 powder to overcome the distortion problems encountered when using standard fabrication procedures and to better understand the sintering characteristics of this system.

Final densities as high as 6.09 g/cm^3 were achieved; this is higher than the theoretical value of 5.89 g/cm^3 for a fully dense 70 to 30 wt % mixture of Gd_2O_3 (7.41 g/cm^3) and alpha-Al_2O_3 (3.99 g/cm^3). The higher density and a complex sintering behavior indicated that this compound does not remain in a simple mechanical mixture on heating to 1650°C. X-ray diffraction analysis identified this material as primarily perovskite-type phase $GdAlO_3$ with an excess of alpha-Al_2O_3.

Results of these tests indicate the following qualitative features of the phase diagram in the Gd_2O_3-rich portion of the system.

1. The liquidus temperature for the 70 wt % Gd_2O_3–30 wt % Al_2O_3 mixture is approximately 1750°C.
2. A $GdAlO_3$ phase exists at a composition of approximately 78 wt % Gd_2O_3.
3. Eutectic melting of the compound and an unidentified (probably Al_2O_3-rich) phase occurs between 1500 and 1550°C.
4. The compound melts peritectically between 1600 and 1650°C.
5. The slope of the liquidus curve is large between the eutectic point and the terminus of the peritectic horizontal.

A technique was investigated in which the pressed specimen of prereacted material is supported on a similar but shorter "dummy" specimen so that the frictional restraint that causes the undesirable distortion during sintering is sustained by the supporting member. By this technique it was possible to sinter pieces with good geometrical integrity at temperatures up to 1645°C and with bulk densities of 5.1 to 5.2 g/cm^3. Densities to 5.26 g/cm^3 were attained, with minor dimensional changes, by thermal cycling the parts between 1635 and 1660°C; however, this technique is not considered practical for large quantities of the material.

A prereacted mixture of 80 wt % Gd_2O_3–20 wt % Al_2O_3 was also investigated using similar techniques, except that the mixture was reacted initially at 1750°C rather than at 1650°C. No deformation or tendency to weld was observed in specimens sintered at temperatures as high as 1750°C for 1 hr. X-ray diffraction analysis of these materials revealed $GdAlO_3$ perovskite and an as yet unidentified phase.

The results of this work indicate that fabrication of shapes to controlled size and density can be accomplished with the prereacted 80-20 mixture by a standard cold-pressing and sintering technique, whereas the 70-30 mixture requires rigid temperature control and impractical techniques. The 70-30 mixture can be successfully cold pressed and sintered to form solid shapes or thick-walled hollow shapes and machined to final size.

If composition requirements for MSRE control elements need not be rigidly fixed at 70 wt % Gd_2O_3–30 wt % Al_2O_3, it appears probable that a small shift in composition to something between 70 and 80 wt % Gd_2O_3 would give a mixture with sufficient liquid phase for densification without a major loss in strength of the specimen at the sintering temperature. Such a mixture should be relatively easy to fabricate to controlled sizes and densities.

SAMPLE CONTROL-ROD ELEMENT TESTING

A. Taboada

Prototype control-rod elements consisting of Gd_2O_3-Al_2O_3 (70 to 30 wt %) ceramic bodies canned in austenitic stainless steel were procured

[19] R. B. Briggs *et al.*, *MSRP Semiann. Progr. Rept. Aug. 31, 1962*, ORNL-3369, pp 98–99.

[20] R. B. Briggs *et al.*, *MSRP Semiann. Progr. Rept. Jan. 31, 1963*, ORNL-3419, pp 76–79.

to determine fabricability of the element design. These elements were subjected to general inspection and to testing that included exposure in a control-rod rig test[21] for soundness, dimensional stability, and general suitability for MSRE use.

The element was designed with dimensions that allowed a free fit over a flexible hose moving through a nonlinear path. Difficulty in meeting these dimensions as well as density requirements caused the supplier (Dresser Products, Inc.) to abandon cold-pressing methods for fabricating the ceramic pieces. A hot-pressing technique was developed, the use of which resulted in dimensions within a tolerance of 0.008 in. on the diameter and 0.010 in. in the length. Densities ranged from 96 to 99% of theoretical.

Radiography of uncanned pieces revealed no evidence of cracking or lack of soundness. The canned ceramic bodies showed some axial cracking on the ends, probably caused by dissimilar heating during welding of the end caps.

Two canned elements were exposed to repeated thermal and mechanical shock in the control-rod rig test from room temperature to 1400°F. These were examined radiographically and dimensionally after 24 hr (one cycle), 350 hr, and 600 hr of operation that included approximately 11,000 cycles and 1700 simulated scrams. Holes were made in one can to expose the Gd_2O_3-Al_2O_3 to air for the final 250 hr of test.

No measurable dimensional changes in the metal cans were noted throughout the test. Axial cracks were observed radiographically after the first cycle, and severe cracking in both the axial and transverse direction was observed at the later stages. However, no crumbling or ratchetting was evident, and no condition was observed that might affect the nuclear or mechanical performance of the control-rod elements.

[21] R. B. Briggs *et al.*, *MSRP Semiann. Progr. Rept. Aug. 31, 1962*, ORNL-3369, pp 98–99.

22. High-Flux Isotope Reactor

G. M. Adamson, Jr.

INTRODUCTION

The main function of the High-Flux Isotope Reactor (HFIR) being constructed at ORNL is to provide research quantities of the transplutonium elements. This reactor will be capable of producing 5×10^{15} neutrons cm^{-2} sec^{-1}. Such flux densities are achieved through average power densities of 2000 kw/liter and a total power of 100,000 kw. Both the engineering characteristics and materials problems for this reactor were covered in a group of papers presented at the Fuel Element Conference in Gatlinburg.

Achieving the necessary operating conditions and high performance expected of this reactor has created many difficult materials problems. To minimize flux peaking and thereby reduce the hot-spot temperature, it was necessary that the fuel content of every plate be varied nonlinearly across the width. A burnable poison is added, the concentration of which varies inversely with that of the fuel. Extremely close tolerances are required on both the amount and distribution of the fuel and burnable poison and on all the dimensions that affect the size of the water channels. These tolerances are much closer than those used on other reactor systems. The control rods are also unique, consisting of two large cylinders over 5 ft long, each of which contains four areas of differing absorption characteristics.

FUEL ELEMENT

During the past year, many improvements have been made in the procedures for design and fabrication of the fuel element; these improvements were extensions of those developed for the Puerto Rico Research Reactor.[1] The concentration of uranium has been increased, and changes have been made in the core contours. Powder metallurgy cores will now be used for both annuli, and all the burnable poison will be added in the inner-annulus aluminum filler pieces. The fabrication procedures have been altered so that the duplex cores for both annuli are pressed to size and shape in a single powder metallurgy operation. Elements are now made by sliding the fuel plates into grooved side plates and then joining the plates to the tubes by circumferential welds. During the past year, both inner and outer annuli have been assembled and have met all the required tolerances. Figure 22.1 shows an element that has been assembled to specifications, illustrating the complexity of these reactor cores. The insert shows the configuration of the individual plates.

Core Fabrication

W. J. Werner T. D. Watts
J. P. Hammond

The Powder Metallurgy Laboratory has successfully developed and demonstrated a process for pressing the HFIR duplex cores in a single operation. The basic procedures discussed last year[2]

[1] W. J. Kucera, C. F. Leitten, Jr., and R. J. Beaver, *Specifications and Procedures Used in Manufacturing U_3O_8-Aluminum Dispersion Fuel Elements for Core I of the Puerto Rico Research Reactor,* ORNL-3458 (in press).

[2] T. D. Watts and J. P. Hammond, *Metals and Ceramics Div. Ann. Progr. Rept. May 31, 1962,* ORNL-3313, pp 102–3.

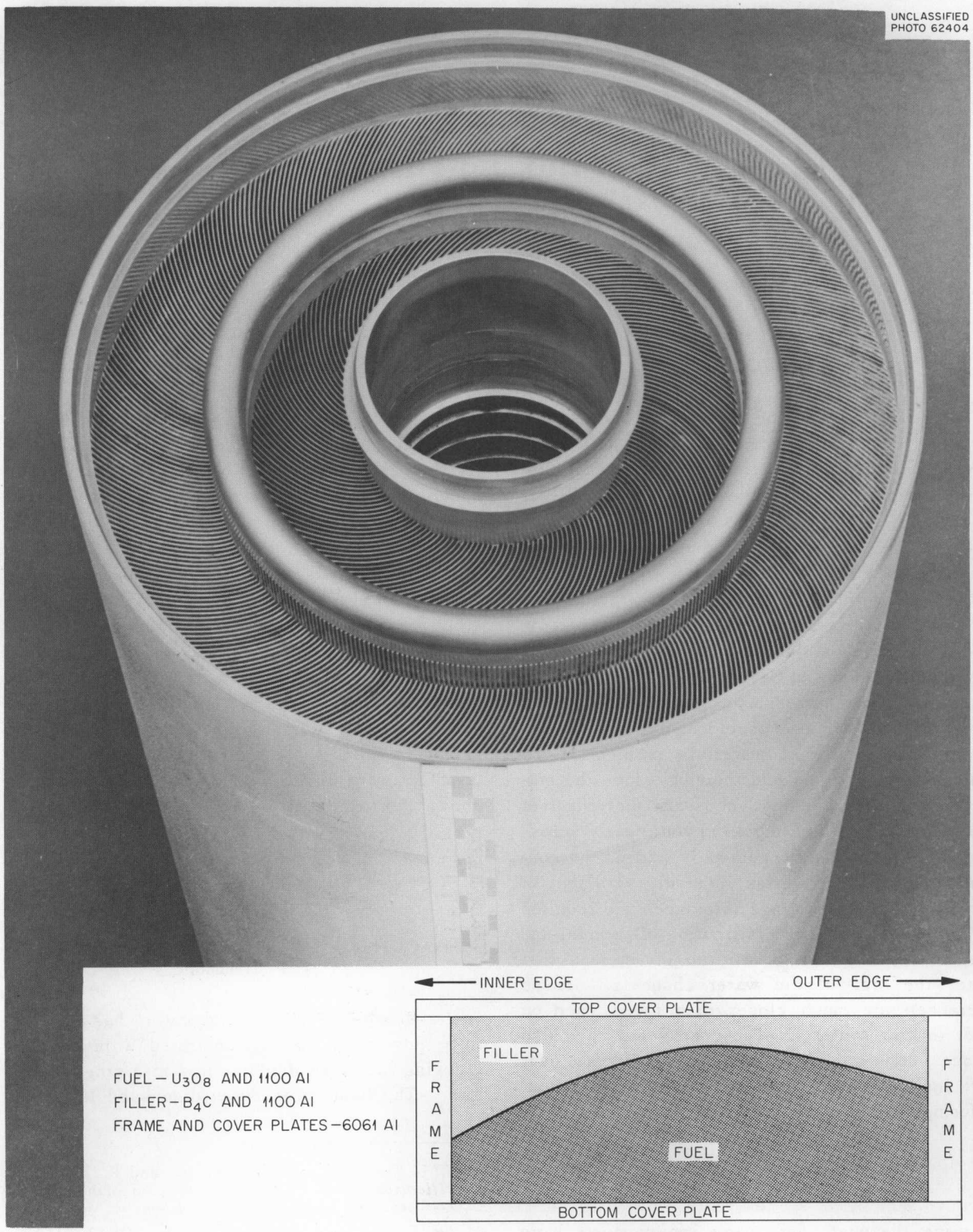

Fig. 22.1. HFIR Fuel Element; Insert Shows the Cross Section of a Flat Inner-Annulus Fuel Plate.

have been modified and improved. Control over dimensional tolerances was achieved primarily by minimizing movement of the powders. A second die top has been added to control the addition of the filler powders. Cores for an entire inner annulus (171 plates) were prepared, and not a single one was rejected.

Procedures have been developed by which the required die-top contours may be calculated. It is necessary to correct for the compressibility of both the fuel and filler sections, for changes in width and length relative to thickness during rolling, and for the relative densities of the powders as poured, as pressed, and as rolled. Data from a statistical analysis from ten as-pressed cores are presented in Fig. 22.2, showing that the approximate desired contour was obtained on the first try.

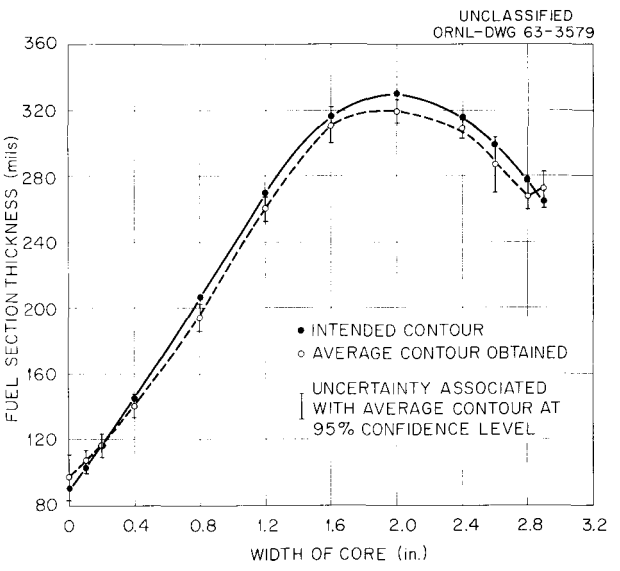

Fig. 22.2. Contour of HFIR Powder Cores.

Fuel Plate Fabrication

M. M. Martin C. F. Leitten, Jr.

In the plate fabrication studies, the major emphasis was on refining the procedures to meet the dimensional specifications. Additional studies were conducted on fuel and burnable-poison distribution.

Fuel plates with forged alloy cores, forged dispersion cores, or direct powder-metallurgy-compacted dispersion cores were all fabricated to the required tight dimensional specifications, with yields in excess of 90%. A sufficient number of plates for assembling entire annuli were prepared for both the dispersion-core techniques. However, because of simplicity of operation, better material control, improved homogeneity, and higher yield, the direct powder-pressing technique was selected as the production procedure.

Thickness variations in the plates were shown to be a major factor in plate forming and were therefore limited to ±0.0002 in. Such control was achieved by grading the hot-rolling schedule of the plate in the later stages to obtain a hot-rolling tolerance of ±0.005 in. Reducing the percent cold reduction per mill pass then permitted a minimum final variation.

One of the most difficult of the plate tolerances to meet is the one on fuel distribution. The specification is complicated in that the contoured core requires a different concentration for every longitudinal traverse. It is further required that the fuel for every 0.005-in.^{2} area be distributed to within 30% of the theoretical concentration and that the line average along the length of a plate be within 10% of theoretical. It has been shown that fuel particle size is an important variable affecting the distribution. With plates prepared from forged cores, fuel variations of ±25 and ±55% were obtained with −170 +325 and −100 +325 mesh U_3O_8 respectively. In the former case the variations were also shown to be inversely proportional to section thickness. A statistical evaluation of the homogeneity data from a typical plate (forged core, −170 +325 mesh) is presented in Table 22.1. Data presenting variations in core thickness and uranium density (both of which are shown to be important contributors to variations in total uranium) are listed. Comparable results were obtained from samples taken from a batch of plates. With the exception of row 1, the spot homogeneity specifications were met. A correction in thickness at the thin edge would bring all values within tolerance.

Fuel Plate Forming

J. H. Erwin C. F. Leitten, Jr.

Obtaining an acceptable yield of involute curved fuel plates has continued to be a major problem. Improvements have been made in the low-pressure

Table 22.1. Statistical Analysis of Fuel Section Profile, Distribution of Uranium, and Homogeneity of Uranium in Experimental Inner-Annulus Plate H-1224

Row No.	Distance from Edge of Plate (in.)	No. of Replicate Punchings	Fuel Section Thickness			Uranium Content			Uranium Density		
			Theoretical (mils)	Average (mils)	Tolerance[a] Limits (%)	Theoretical (mg)	Average (mg)	Tolerance[a] Limits (%)	Theoretical (g/cm^3)	Average (g/cm^3)	Tolerance[b] Limits (%)
1	0.33	10	9.1	5.2	±31	0.54	0.36	±42	0.75	0.84	±25
2	0.66	20	12.6	10.1	±16	0.76	0.66	±23	0.75	0.79	±25
3	0.98	10	16.4	14.6	±11	0.99	0.87	±17	0.75	0.72	±25
4	1.31	10	20.4	19.0	± 8	1.25	1.17	±13	0.75	0.75	±25
5	1.64	3	23.8	23.2	± 7	1.43	1.37	±11	0.75	0.71	ND[c]
6	1.97	3	25.9	26.0	± 6	1.56	1.48	±10	0.75	0.69	ND[c]
7	2.30	3	26.6	26.6	± 6	1.60	1.54	±10	0.75	0.70	ND[c]
8	2.62	3	25.9	25.5	± 6	1.56	1.46	±10	0.75	0.70	ND[c]
9	2.95	3	23.9	22.8	± 7	1.44	1.27	±12	0.75	0.68	ND[c]

[a]Tolerance limits calculated at the 95% confidence level to include at least 99% of the distribution for a sample size of 57.
[b]Calculated overall homogeneity tolerance is 0.76 g/cm^3 ±25%.
[c]Not determined but assumed to be the same as the others.

marforming process and in the development of backup procedures.[3]

In an attempt to achieve the uniform plate properties which have previously been shown to be necessary,[3,4] a variety of conditioning procedures was evaluated. Data from this study are presented in Table 22.2. Variables studied included commercial and composite plates, alloy and dispersion cores, solution heat treatments and anneals, and cold work prior to annealing. The change from 7.4% cold work, previously used, to 20% cold work was made on the basis of results obtained on the Fuel Element Development Program, Part II, Chap. 16, this report. After fabrication, all plates were annealed at 500°C and furnace cooled and were low-pressure marformed at 1600 psi. Data are presented on the reproducibility of curvature at the various positions.

It is apparent in Table 22.2 that the reproducibility was improved by both solution heat treatment and an increased percentage of cold reduction. It is also interesting to note that the percentage rejection of outer-annulus fuel plates decreased when dispersion cores were substituted for the original alloy cores.

Paralleling the low-pressure marforming studies, alternate methods for achieving reproducible fuel plate curvatures were investigated. Experiments were conducted employing high-pressure marforming (approximately 10,000 psi) and electrohydraulic forming coupled with low-pressure marforming to improve the duplication of the fuel plate involute curvatures. A summary of the restrike data obtained in these experiments for plates formed out of tolerance and then restruck is shown in Table 22.3 for both inner- and outer-annulus fuel plates. For comparison the duplication data obtained in low-pressure marforming are also presented. It is apparent that electrohydraulic restrike forming of outer-annulus fuel plates improved the position duplication. In fact, all the plates which were electrohydraulically re-formed were within the desired ±0.004-in. tolerance. Similar duplication was not achieved in the restrike forming of inner-annulus fuel plates, although improvements were definitely noted. It is presently thought that these inferior results with the inner-annulus plates are associated with the plate preforming characteristics. These plates were undersize, whereas the others were oversize.

High-pressure marforming experiments have been conducted to date only on type 6061 clad uranium-aluminum-alloy-bearing outer-annulus fuel plates. As noted in Table 22.3, improvement in duplication was achieved. However, the degree of improvement was less than that obtained by electrohydraulic re-forming. Thus it appears that HFIR fuel plates can be formed within close tolerances, by low-pressure marforming techniques. Experiments have shown that plates initially out of tolerance can be corrected (with high yields) by electrohydraulic or, possibly, by high-pressure marforming techniques.

Assembly and Welding

J. W. Tackett G. M. Slaughter

During the past year, four annular units were manufactured to demonstrate and evaluate improved welding procedures and alternate methods of assembling the HFIR fuel elements.[5] Table 22.4 summarizes the as-built plate-spacing data obtained for each of the four units manufactured. All but one of the annular units (the depleted-uranium fueled unit) met the plate-spacing tolerance requirements. In the case of this unit, only 6 of the 7749 total individual measurements were outside the required dimension, 0.050 ± 0.010 in.

Two units, the fueled (depleted uranium) outer annulus and an unfueled inner annulus, incorporated fuel plates with a bend on the outer edge to establish plate spacing; these plates were installed on and mechanically attached to a grooved inner support tube, as reported previously.[6] These units were used to evaluate an improved circumferential welding procedure and to investigate the possibility of correcting the fuel plate curvature

[3] M. M. Martin, J. H. Erwin, and C. F. Leitten, Jr., "Fabrication Development of the Involute-Shaped High Flux Isotope Reactor Fuel Plates," pp 268–89 in *Research Reactor Fuel Element Conference, September 17–19, 1962, Gatlinburg, Tennessee*, TID-7642, bk 1 (1963).

[4] J. H. Erwin and R. W. Knight, *Metals and Ceramics Div. Ann. Progr. Rept. May 31, 1962*, ORNL-3313, pp 85–87.

[5] J. W. Tackett, J. H. Erwin, C. F. Leitten, Jr., and G. M. Slaughter, "Assembly and Welding Development for the High-Flux Isotope Reactor Fuel Element," pp 290–314 in *Research Reactor Fuel Element Conference, September 17–19, 1962, Gatlinburg, Tennessee*, TID-7642, bk 1 (1963).

[6] J. W. Tackett, *Metals and Ceramics Div. Ann. Progr. Rept. May 31, 1962*, ORNL-3313, pp 113–14.

Table 22.2. Summary of Data from Low-Pressure Marformed HFIR Fuel Plates

Plate Description[a]	Number of Plates	Maximum Spread in Plate Position Measurements (mils)[b]	Average Spread in Plate Position Measurements (mils)[b]	Percent Rejection Based on Position Average ±0.004 in.
Inner Annulus				
Commercial type 6061, annealed from T-6	20	10	9.1	35
Commercial type 6061, solution heat treated after anneal	20	5	4.3	0
Composite type 6061, 7.4% cold reduction	18	22	19.3	83
Composite type 6061, 20% cold reduction	19	10	7.9	0
Composite type 6061, solution heat treated	18	13	8.4	17
Type 6061 clad U_3O_8-Al forged dispersion, 7.4% cold reduction	22	15	13.6	64
Outer Annulus				
Commercial type 6061, annealed from T-6	20	6	4.9	0
Composite type 6061, 7.4% cold reduction	12	12	11.1	42
Type 6061 clad forged U-Al alloy, 7.4% cold reduction	20	16	12.3	50
Type 6061 clad forged U_3O_8-Al dispersion, 7.4% cold reduction	30	13	10.9	13
Type 6061 clad forged U_3O_8-Al dispersion, 20% cold reduction	10	6	5.1	0

[a]All plates heated to 500°C and slow cooled before test.

[b]Measurements taken at seven equidistances along the length of each plate at three radii positions (21 measurements per plate).

Table 22.3. Summary of Restrike Data from Electrohydraulic and High-Pressure Marformed HFIR Fuel Plates

Plate Description	Number of Plates	Maximum Spread in Plate Position Measurements (mils)	Average Spread in Plate Position Measurements (mils)	Percent Rejection Based on Position Average ±0.004 in.
Outer Annulus				
Type 6061 clad U_3O_8-Al dispersion plates, 7.4% cold reduction (standard)	30	13	10.9	13
Type 6061 clad U-Al alloy plates, 7.4% cold reduction (standard)	20	16	12.3	50
Type 6061 clad U_3O_8-Al dispersion plates, 7.4% cold reduction; electrohydraulic restrike, 2400 joules	30	6	4.6	0
Type 6061 clad U-Al alloy plates, 7.4% cold reduction; electrohydraulic restrike, 2400 joules	13	6	4.6	0
Type 6061 clad U-Al alloy plates, 7.4% cold reduction; high-pressure marformed, 10,000 psi	20	9	7.9	25
Inner Annulus				
Type 6061 clad U_3O_8-Al dispersion plates, 7.4% cold reduction (standard)	22	15	13.6	64
Type 6061 clad U_3O_8-Al dispersion plates, 7.4% cold reduction; electrohydraulic restrike, 2400 joules	15	12	7.9	33
Type 6061 clad U_3O_8-Al dispersion plates, 7.4% cold reduction; electrohydraulic restrike, 4300 joules	11	12	9.4	36

Table 22.4. Summary of Plate-Spacing Measurements Obtained from the HFIR Fuel Units Completed During the Current Year

	Inner Annulus (Bent Lip)	Fueled Outer Annulus (Bent Lip)	All-Welded Outer Annulus (Sliding Plate)	All-Welded Inner Annulus (Bent Lip)
Individual Measurements				
Number	3591	7749	7749	3591
Average dimension (mils)	51.4	49.4	48.6	40.9
Maximum/minimum (mils)	56/47	62/35	58/40	58/43
Number not within 50 ±10 mils	0	6[a]	0	0
Number not within 50 ±5 mils	0	115	111	10
Calculated Average Width Dimension				
Number	1197	2583	2583	1197
Average dimension (mils)	51	49.8	48.9	50.4
Maximum/minimum (mils)	53/49	56/45	54/45	53/48
Number not within 50 ±6 mils	0	0	0	0
Number not within 50 ±3 mils	0	11	24	0

[a]Three channels involved.

and resulting water channel by the use of Teflon spacers. In order to establish the tolerance limits required for the as-curved fuel plates, the fueled unit utilized plates that were much beyond the original acceptance limits, in some cases as much as 20 mils out of tolerance. The plate curvature, which was corrected by the Teflon spacers, largely remained corrected after the unit was welded and the spacers were removed. This technique has since been used on all annuli fabricated and has provided excellent control of channel spacing and diametral shrinkage.

A major improvement in assembly procedure was incorporated in the inner-annulus assembly described in column 1 of Table 22.4. The general manufacturing procedures used were similar to the ones used for the banded outer-annulus unit made last year; however, the welding of the outer tube was greatly simplified, and the bands were eliminated. Weld grooves were machined directly into the peripheral surface generated by the bent lips. Each plate was attached to its neighbor by an automatic low-energy welding process. The welds were made manually, the complete circumferential length of each weld being made in one continuous operation. The as-welded annulus is shown in Fig. 22.3.

Another major development involved the successful fabrication of an all-welded annulus (column 3, Table 22.4). This unit utilized lipless plates installed by sliding them between two concentric support tubes. The support tubes were slotted longitudinally for the plates and grooved circumferentially for welding, and the fuel plate edges were fused to the support tubes by circumferential welds, as shown in Fig. 22.4. The 369 fuel plates were installed in a very short time (~2 hr) and without difficulty. A volatile camphor-alcohol mixture, used as a lubricant during plate assembly, was removed by heating. Both the inner and outer welds were made with the low-energy, automatic, consumable-electrode welding process. During welding, the support tubes shrank in length, but the fuel plates were not noticeably distorted.

The final element listed is an all-welded combination of the two methods. The inner attachment

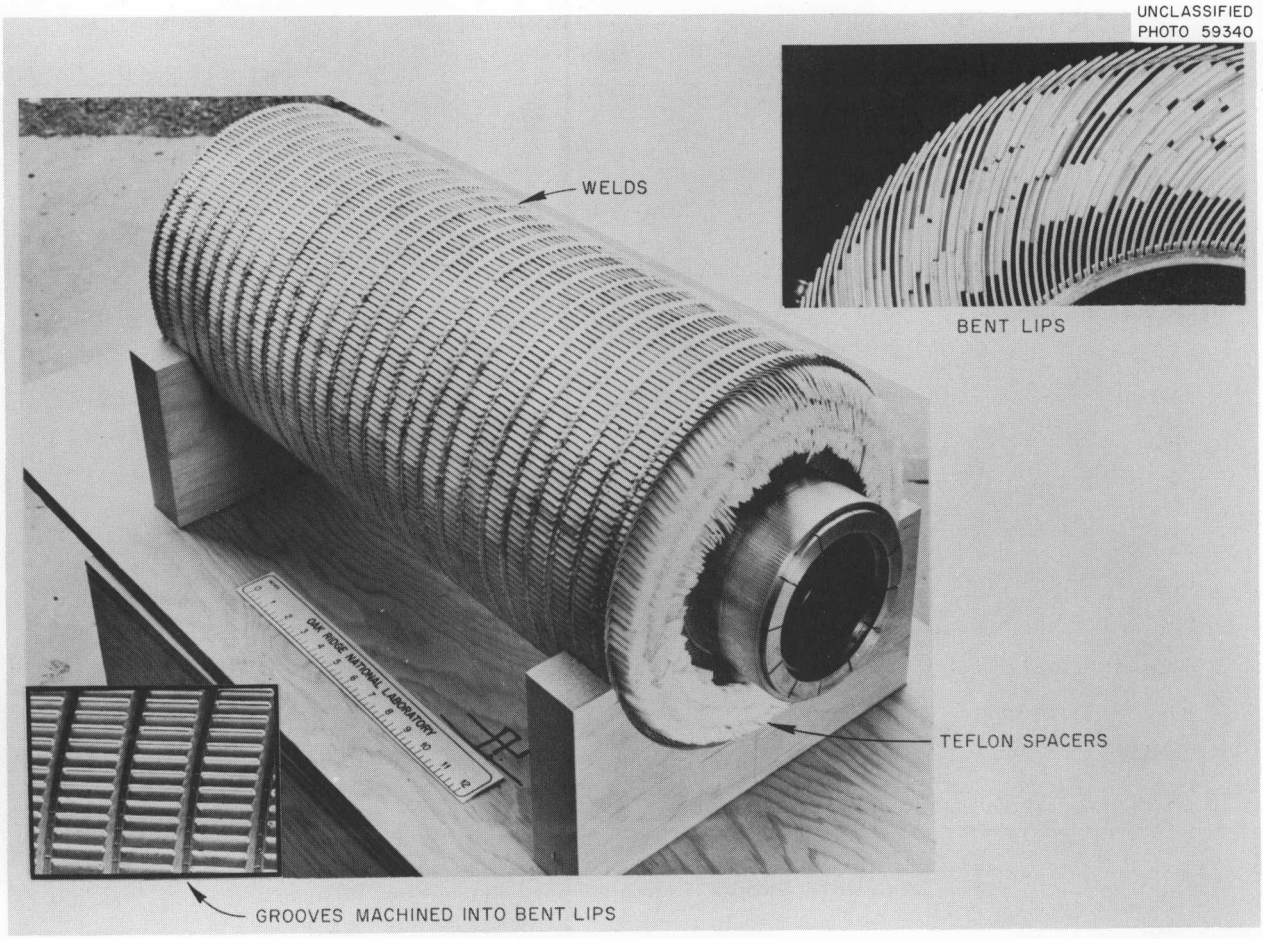

Fig. 22.3. HFIR Inner Annulus Using Plates of the Bent-Lip Design.

was made by welding to a longitudinally slotted tube, while the outer joints were of the bent-lip configuration.

It was demonstrated that elements could be manufactured by the three different procedures and still meet tolerances. The all-welded sliding-plate concept was selected as the first production method. The selection was, however, made primarily for design considerations.

NONDESTRUCTIVE TESTING

R. W. McClung

The HFIR nondestructive testing program has been directed primarily toward the development or application of techniques to evaluate various fuel element properties. Most of the work has been directed to the detection or measurement of those conditions that could cause uneven heat distribution. The developments have included ultrasonic techniques for the detection of nonbonded areas between the core and cladding material in the fuel plates, an x-ray attenuation method as a tool for measuring fuel concentration variations within each fuel plate, an electrical impedance technique for the measurement of coolant channel spacing, and an eddy-current technique for the identification of core orientation. Most of the theories of operation and results of preliminary work were included in a paper[7] presented at the Research Reactor Fuel Element Meeting.

---

[7]R. W. McClung, "Nondestructive Testing of the High-Flux Isotope Reactor and Advanced Test Reactor Fuel Elements," pp 337–59 in *Research Reactor Fuel Element Conference, September 17–19, 1962, Gatlinburg, Tennessee,* TID-7642, bk 1 (1963).

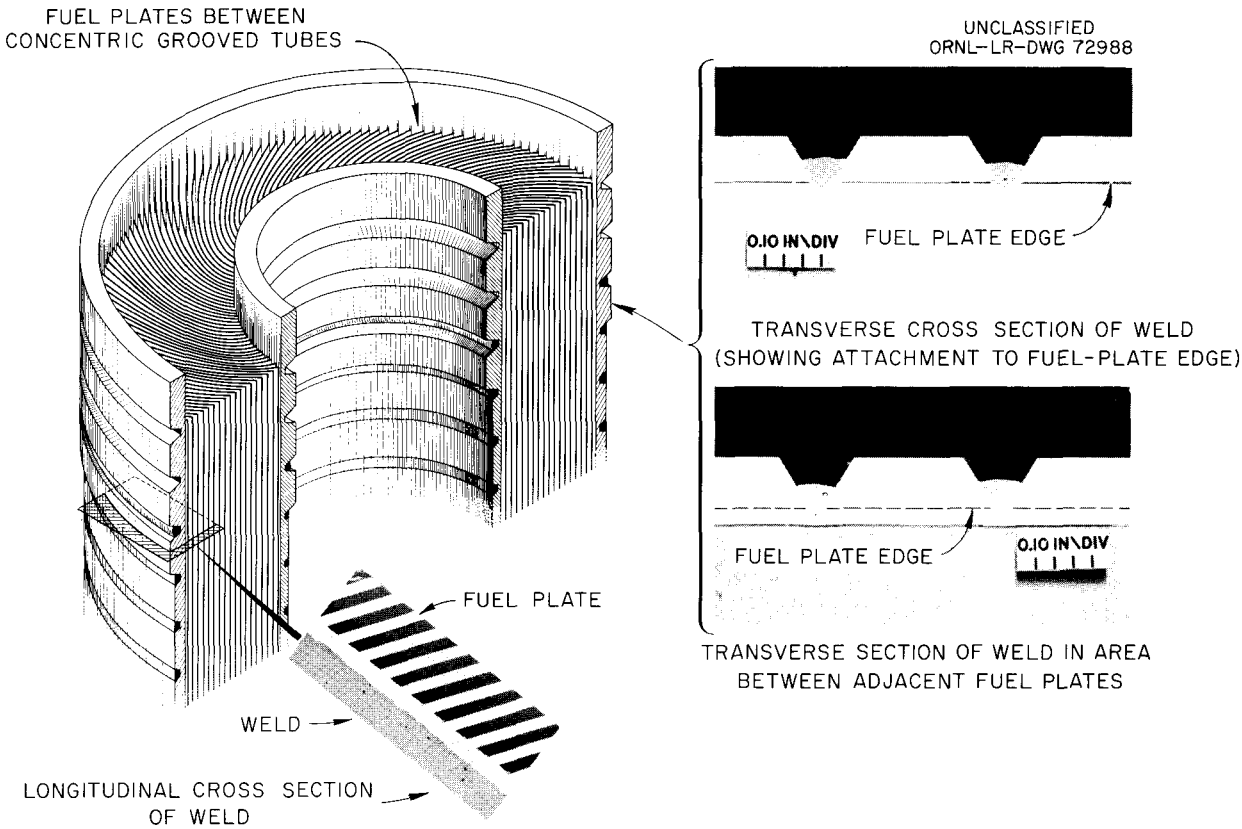

Fig. 22.4. HFIR Annulus of the All-Welded Sliding-Plate Design.

Ultrasonic Nonbond Detection

K. V. Cook

The through-transmission ultrasonic technique has been used for the detection of nonbond areas between the core and cladding. Although this technique had been used successfully for alloy fuel plates, the principal unknown for application to HFIR plates was the effect of the cermet-dispersion core on the ultrasonic transmission and the size defect (1/16 in.) that must be located.

Simulated 1/16-, 3/32-, and 1/8-in.-diam nonbonds were placed in frame and core areas of developmental plates to be used as reference standards. A number of HFIR plates were examined by use of the reference plates to establish the inspection sensitivity and control instrument calibration. Since only a few nonbonds as large as 1/16 in. in diameter have been detected, this seems to be a reasonable inspection requirement. More plates must be evaluated, however, before firm conclusions can be drawn.

Fuel Homogeneity

B. E. Foster S. D. Snyder

A through-transmission x-ray attenuation technique is being developed to measure fuel concentration variations in the HFIR fuel plate. Figure 22.5 is a block diagram of the system that is being used. Careful control of the voltage to the x-ray tube results in a steady, reproducible output of x rays. The array of collimators restricts the primary beam to the spot size of interest on the plate and prevents scattered radiation from reaching the detector. Thus, as fuel concentration varies, the change in transmitted x-ray intensity will be detected, amplified, and recorded. Mechanical X-Y scanning of the plate is necessary to allow full coverage of the entire plate surface.

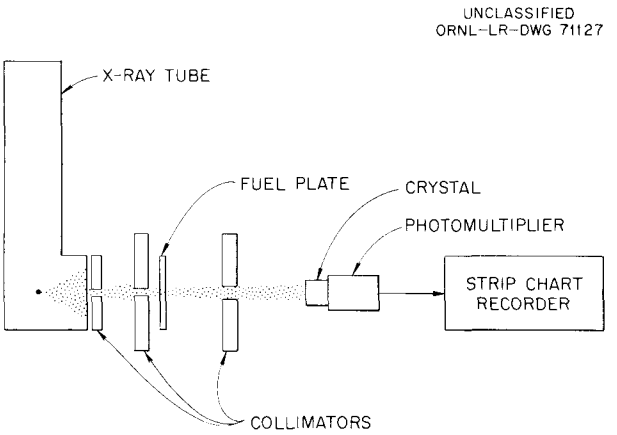

Fig. 22.5. Block Diagram of System for Fuel Homogeneity Determination.

The most difficult and time-consuming part of the effort has been the establishment of adequate, realistic calibration standards so that an accurate relation can be established between fuel concentration and x-ray attenuation. The complexity of the problem is the result of a number of factors, including a fuel concentration gradient across the fuel plate, the measurement of fuel concentration changes in very small areas, the requirement for complete plate scanning to ensure conformance to tolerance, and the necessity for instantaneous calibration to minimize the overall inspection time. An attempt was made to use U_3O_8-Al dispersion foils of known concentration as standard material, but their inhomogeneity prevented single-point calibration and only by extensive scanning and integration of the transmission value could the relation of transmission vs concentration be established. The need for instantaneous calibration demands a homogeneous standard. For this reason, homogeneous materials such as tool steel, 6061 aluminum, and U-Al eutectic alloy have been evaluated to determine the thickness necessary to have the equivalent attenuation to the U_3O_8-Al dispersion core. From such data a prototype tool steel attenuation standard was made using digitally programmed machine tools, but the specimen was so thin (about one-half the core thickness) that it was impractical from the standpoints of accuracy and stability. Both aluminum and the U-Al eutectic seem to be suitable; however, it is felt that a uranium-bearing standard will minimize the effect of small inadvertent changes in the x-ray energy.

The proposed inspection system being studied will have curved calibration standards to match the designed fuel concentration gradient across the plate width. Individual samples will coincide in x-ray attenuation to nominal maximum or minimum allowable fuel concentration. Thus, immediately before each longitudinal scan is made along a plate, the go-no-go conditions will be monitored by the detection systems. Instrumentation is being developed and assembled to provide an indication for out-of-tolerance conditions for both point-to-point variations and the integrated value along any linear scan.

The large, versatile mechanical scanner shown in Fig. 22.6 was developed and fabricated and is being used during the development program. The HFIR plate is mounted in a special holder that accommodates the standards. The mechanism has the capability of scanning the plate in the longitudinal direction at any speed up to 150 in./min. At the end of each longitudinal scan, a transverse indexing step (variable from 0.0005 to 0.500 in.) can be made before a parallel return scan. Data potentiometers are used to provide positional data for the data-processing circuitry.

Core Orientation

C. V. Dodd

To avoid premature element failure, the varying-concentration fuel plate must be assembled in a consistent manner, with every core being oriented identically. An eddy-current technique which can rapidly determine the orientation of the core "hump" has been developed. This development was possible because the thickness of the higher conductivity type 1100 aluminum filler used in the fuel plate fabrication varied.

Coolant Channel Spacing[8]

C. V. Dodd

The nominal coolant channel spacing of 0.050 in. must be maintained to an average tolerance of 0.006 in. at any cross section. Excessive variation in spacing would, of course, prevent uniform heat removal from the plate. Special electrical-impedance test probes have been designed which

[8]C. V. Dodd and R. W. McClung, *Metals and Ceramics Div. Ann. Progr. Rept. May 31, 1962,* ORNL-3313, p 49.

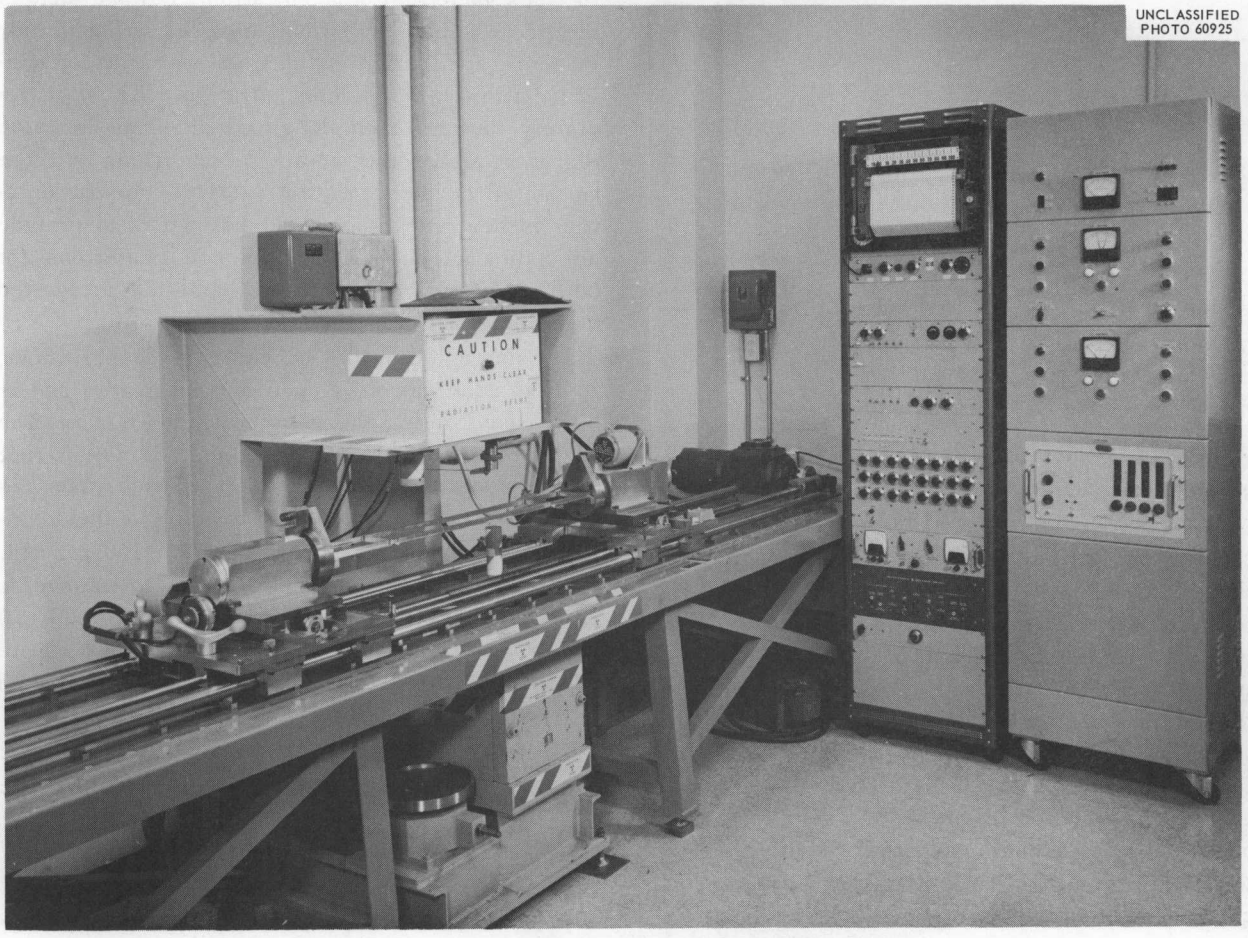

Fig. 22.6. Equipment for *X-Y* Scanning of Fuel Plates to Detect Inhomogeneities.

are inserted into the channel spacing for the measurement. Commercial instrumentation has been used to generate the high frequencies used and to indicate the impedance changes in the active element (coil) as the spacing varies.

MECHANICAL PROPERTIES OF 6061-4043 WELDMENTS AT ELEVATED TEMPERATURE

J. W. Tackett W. R. Martin

High-Flux Isotope Reactor fuel element components that utilize type 6061-T6 aluminum base material welded with type 4043 aluminum filler alloy have been fabricated. Specific sequential steps were required in making the components; for example, the 6061 material was formed and welded in a T0 condition, stress-relief annealed, and re-heat-treated to a T6 condition. The properties of the T6 heat-treated weldments are of interest since both the base metal and welds can be stressed. Data on tensile stress as a function of temperature up to 600°F have been developed, and stress-rupture data are available at 500°F.

A comparison of the yield stress for the weldment and 6061 alloy in the annealed and aged condition is given in Table 22.5. These weldments were given the T6 heat treatment after welding. It is obvious that the strength of the weldment is greater than the 6061-0 and less than the 6061-T6. The tensile ductility of the 4043 alloy was in the range 6 to 10%. The stress-rupture properties of the weldment are compared to 6061-T6 in Table 22.6. The creep strength of the 4043

Table 22.5. Comparison of Yield Stress for 6061 Alloys at Elevated Temperatures

Material	Yield Stress (psi)				
	212°F	300°F	400°F	500°F	600°F
6061-T6	40,000	37,000	32,000	22,000	10,000
6061-T0	8,500	8,200	7,800	6,800	5,300
6061-4043 weld metal (heat treated to T6 condition)	18,600	16,500	13,800	9,000	7,200

Table 22.6. Comparison of Stress-Rupture Properties of 6061 Alloys at 500°F

Material	Stress to Rupture (psi)		
	10 hr	100 hr	1000 hr
6061-T6	12,000	9200	7300
6061-4043 weldment (heat treated to T6 condition)	6,800	5700	4800

is less than that of the 6061-T6 alloy. The creep ductilities of the 4043 were never greater than 2%.

The tensile and creep data show that the strength of 4043 alloy is less than that of 6061-T6 and that, with equivalent stress conditions, it will fracture prior to 6061-T6. The low ductility of 4043 welds must be considered in the designs.

BURNABLE POISONS

T. D. Watts M. M. Martin

Reactor physics calculations have indicated that more-uniform fuel burnup and thereby longer core life may be obtained by the addition of small amounts of burnable poisons. It was desired that small amounts of boron carbide and possibly a cadmium compound be added to each filler piece for the inner annulus. The feasibility of such additions has been demonstrated; however, analytical problems must be solved before the distributions may be shown to achieve the desired accuracy.

Since only meager data existed on the compatibility of various cadmium compounds when present in aluminum-base dispersions, it was necessary to first obtain such data. In these tests, to magnify any reactions, concentrations of both the boron carbide and cadmium materials were increased from <1 wt % to 20 wt % each. Pellets were prepared and held in vacuum ($<1 \times 10^{-3}$ mm Hg) for 24 hr at 600°C. Results are given in Table 22.7. On the basis of these results, $CdSO_4$ and glass sample 1A 9078 were chosen for additional study.

Miniature fuel plates containing either 1 wt % glass or $CdSO_4$ in addition to the B_4C were then prepared using the HFIR inner-annulus fabrication schedule, which included a blister anneal for 1 hr at 500°C. All plates were shown to be satisfactory by both radiographic and metallographic examinations. Any cadmium or boron losses occurring during fabrication were within the experimental accuracy of the test.

A serious problem with both the boron and cadmium additions was that of demonstrating the homogeneity of the fabricated plates. With sample sizes of interest (1/2-in. disks), the boron and cadmium contents were so low that they caused analytical difficulties. Although 27 mg of B_4C was incorporated into a plate, the amount in the 1/2-in. samples varied from 50 to 225 μg. The analytical accuracy in analyzing a full-size plate was found to be ±10%; however, it was shown to be negative bias by 7%. With the small samples, the accuracy was only ±25%. A total of 140 mg of cadmium was present in a plate, with 100 to 600 μg in the 1/2-in. samples. When the cadmium was used as a glass, analytical difficulties were encountered with both concentrations. The accuracy was only ±50%. Both these problems are being considered further, and until the analytical problems are solved, only B_4C will be used as a poison.

Table 22.7. Compatibility of Cadmium Materials in Aluminum Matrices

Cadmium-Bearing[a] Material	Increase in Length and/or Diameter (in.)	Loss in Weight of 4.5-g Pellet (g)	Visual Observations
Cadmium fluoride	0.015	−0.008[b]	Quartz capsule burst in the furnace during heat treatment
Cadmium oxide	0.008	0.15	Bright metallic globules appeared on the interior of the capsule; these deposits were shown to be cadmium
Cadmium phosphate	0.010	0.20	Heavy brown deposit on the walls of the capsule and large amounts of metallic cadmium deposits
Cadmium silicate	0.002	0.15	Cloudy white deposit on capsule wall and formation of metallic cadmium globules
Cadmium sulfide	0.015	0.13	Metallic cadmium particles adhered to both the tube wall and the pellet
Cadmium sulfate (anhydrous)	0.005	0.01	Yellow deposit on tube walls but no metallic particles formed
Glass samples (AVQ, AVR, AVT, AVU, AVW, and AVX)	0.002–0.005	0.002–0.003	All these glass samples behaved more or less alike; in every case, there was deposition of some brown vapor on the walls of the tube and also of a few very minute particles
Glass samples Nos. IA 9079, IA 9080, and IA 9081	0.002–0.003	0.005–0.010	These glasses behaved more or less like the Corning glass samples; sample No. 9080, which had maximum silica, exhibited maximum loss in weight and darkest deposition on the wall
Glass sample No. IA 9078	0.001–0.002	0.000	No deposition of any kind; pellet in sound condition
1100 Al	0.001–0.002	0.000	No deposition of any kind; pellet in sound condition

[a]All pellets were 1/2 in. in diameter by 1/2 in. high and contained 20 wt % Cd-bearing material and 20 wt % B_4C.
[b]Pellets held at 600°C for 24 hr in vacuum, $<1 \times 10^{-3}$ mm Hg.

HFIR METALLURGICAL ENGINEERING ASSISTANCE PROGRAM

J. R. McGuffey

Full-time metallurgical consultation on the HFIR was furnished to the Reactor Division. This program consisted of (1) technical assistance in the preparation of specifications for major components of the primary system; (2) review of the manufacturers' engineering drawings, procedures, and specifications to ensure compliance with the contract; (3) discussions with the fabricators' engineering and shop personnel to resolve interpretations of the specifications; (4) periodic visits to the manufacturers' plants to evaluate the quality of workmanship by inspection of the facilities and equipment and their application to the construction of components such as the primary pressure vessel and heat exchangers, the beryllium reflector, and the flow nozzle; (5) preparation of specifications (covering all phases of procurement of materials of construction, cleaning, forming, welding, heat treatment, inspection, and

records) for components inside the vessel (such as the core, reflector, structural supports, and the control-rod drives); and (6) a metallurgical review of the reactor component drawings. The recommendations for materials of construction were based on mechanical properties, dimensional stability, availability, and corrosion resistance. During this period the corrosion program was expanded to cover the numerous dissimilar metal and nonmetal combinations and possible coatings. The program also included liaison with the Y-12 and ORNL shops to discuss fabrication requirements and current shop practice.

HFIR CONTROL RODS

R. J. Beaver

The neutron absorbers of the HFIR control rods consist of two basic components, the inner control rod and the outer control rod (see Fig. 22.7). The inner control rod consists of four 1/4-in.-thick, 65-in.-long composite plates which are formed and then welded together to form a cylinder. To prevent the weld heat-affected zone from penetrating into the neutron absorber section, a circumferential separation of 3/4 in. of aluminum is permitted between the neutron-absorbing sections of the plates. This inner rod is separated from the outer periphery of the fuel core by a 0.104-in. annulus.

The outer control rod also consists of four curved plates; however, instead of being welded together, they are joined mechanically and are separated by a circumferential distance of 3/4 in. The inner rod is driven from the top, whereas the outer rod is driven from the bottom. The important feature of the design is that they move in opposite directions in such a manner that they maintain symmetry about the fuel core. In both control rods, 1/4-in.-diam holes spaced at 1-in. intervals are drilled, as illustrated, to reduce the hydraulic forces acting on these components while operating in the reactor.

Both inner- and outer-control-rod plates are identical in design with respect to their neutron-absorbing regions. As shown, each plate consists of four regions. For a distance of $27\frac{1}{16}$ in. from the top in the case of the inner rod and $6\frac{5}{8}$ in. for the outer rod, the plate is all aluminum; thus, it is relatively transparent to thermal neutrons and is termed a "white" section. Immediately below this region is a 22-in.-long section containing 33 vol % Eu_2O_3 dispersed in aluminum. This region is very absorbent to thermal neutrons and is termed the "black" section. Below this section is the "gray" section (5 in. long), which only partially absorbs neutrons and consists of 40 vol % tantalum dispersed in aluminum. The balance of the plate is again all aluminum, representing another "white" section. Each plate is clad with 0.031-in.-thick type 6061 aluminum.

It is important that the 0.104-in. annuli between the fuel core and the inner-control rod, as well as between the inner and outer control rods, be controlled as closely as possible. Therefore, rigorous diametric tolerances have been specified on the control-rod components.

A program has been initiated to bond the plates by roll cladding. To achieve the desired contour dimensions, the outer-annulus plates will be explosively sized after preforming. Also, after the inner-control-rod plates have been preformed and welded together, the cylinder will be explosively sized to final dimensions.

POWDER METALLURGY

W. J. Werner

To determine whether or not europium oxide and tantalum are chemically compatible with aluminum when rolled and heat treated at 500°C, samples were made in which 37 vol % Eu_2O_3 and 40 vol % Ta were intimately mixed with aluminum powder, cold pressed into compacts, clad with type 6061 aluminum by rolling at 500°C, and finally heat treated at 500°C for 4 hr. In neither case were any deleterious effects such as swelling and blistering observed during the heat treatment, and, as illustrated in Figs. 22.8 and 22.9, no reaction occurred between either the europium oxide and aluminum or the tantalum and aluminum.

Rather than experiment any further with expensive europium oxide, Lindsay Mix (a cheaper rare-earth mixture of samarium and gadolinium oxides) was chosen as a substitute for europium oxide. The raw material was converted to a more desirable vitreous state by a high-firing operation. The fired oxide was crushed to both −100 +325 mesh sizes. Each size fraction was intimately mixed with aluminum and pressed under 45 tons/in.^{2} at room temperature to a compact density of 93% of theoretical.

UNCLASSIFIED
ORNL-DWG 63-3580

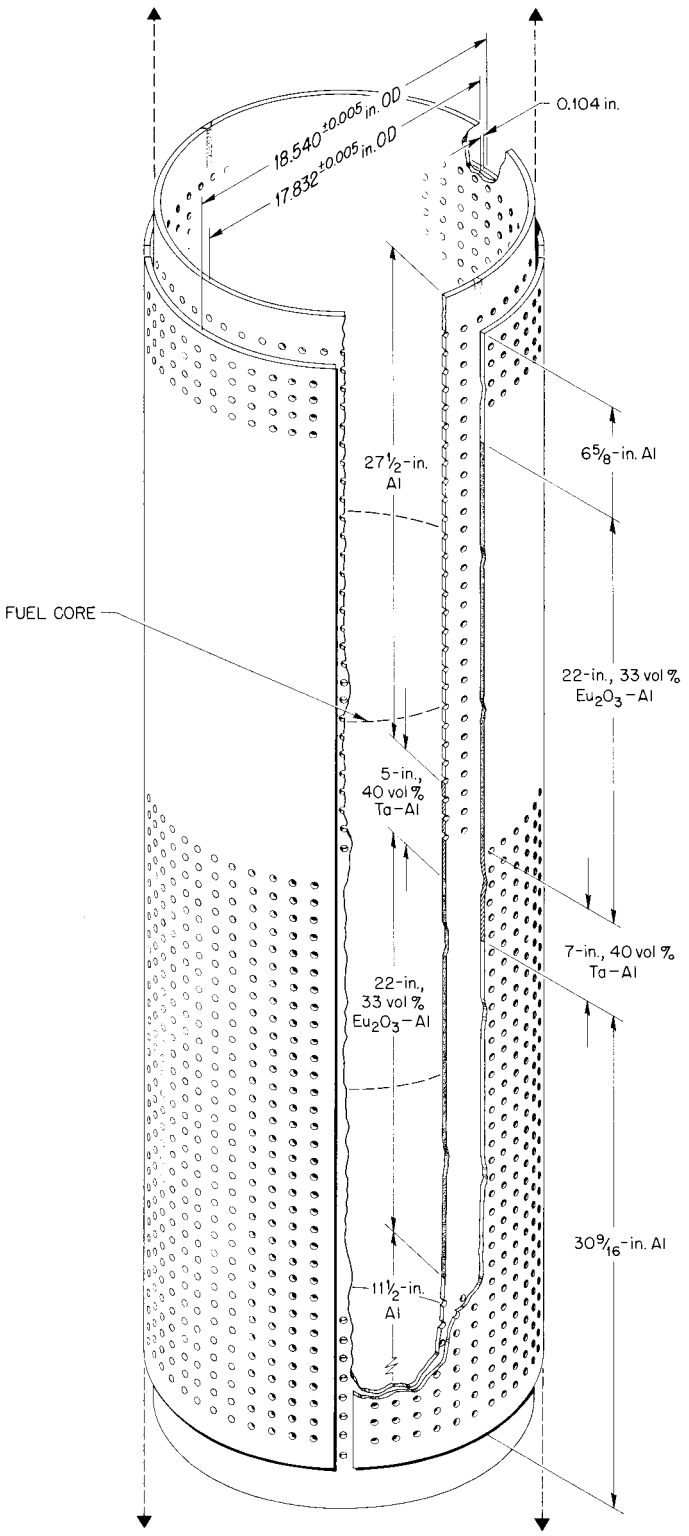

Fig. 22.7. Schematic of Inner and Outer HFIR Control-Rod Components.

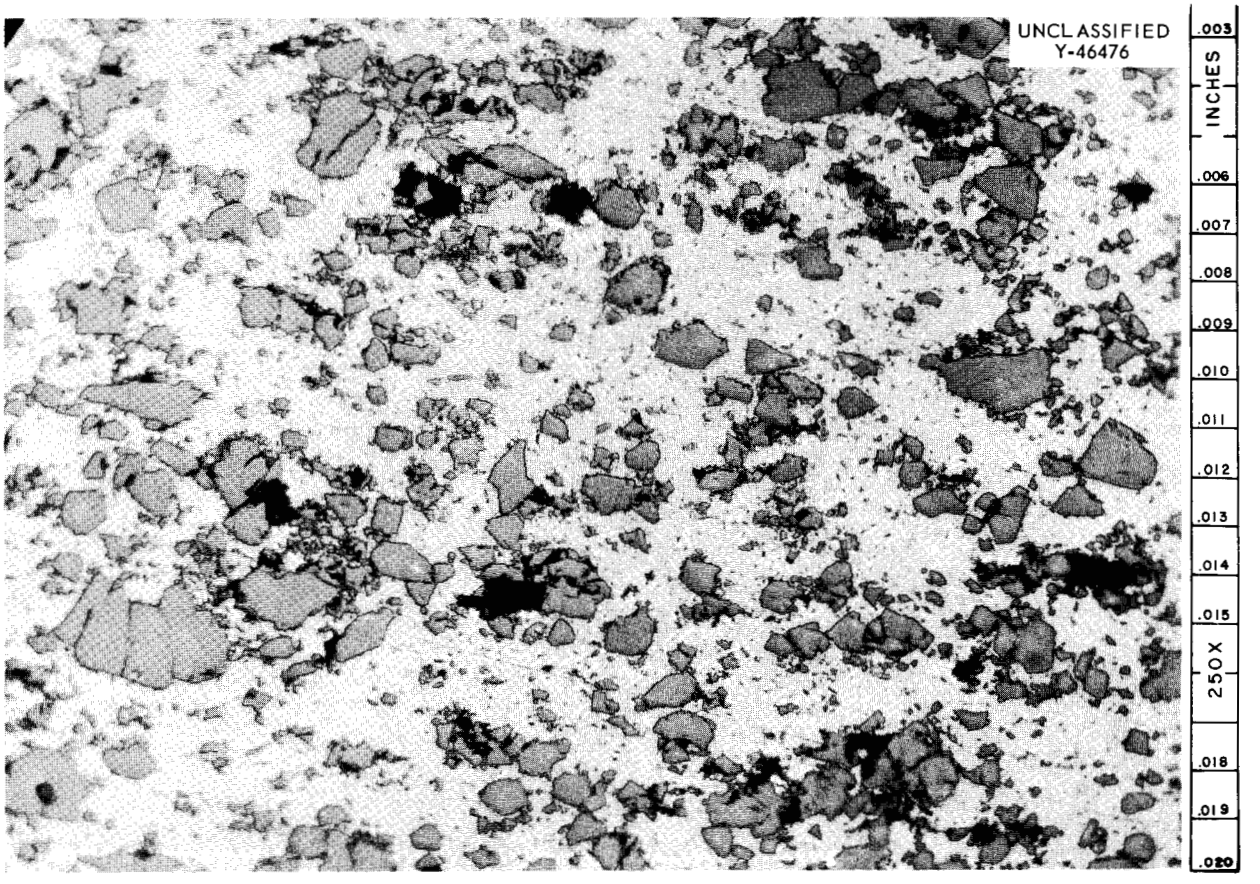

Fig. 22.8. 37 vol % Eu_2O_3 (–325 Mesh) Dispersed in Aluminum, Roll Clad at 500°C, and Heat Treated 4 hr at 500°C. Note that no reaction exists between the Eu_2O_3 and aluminum. As polished.

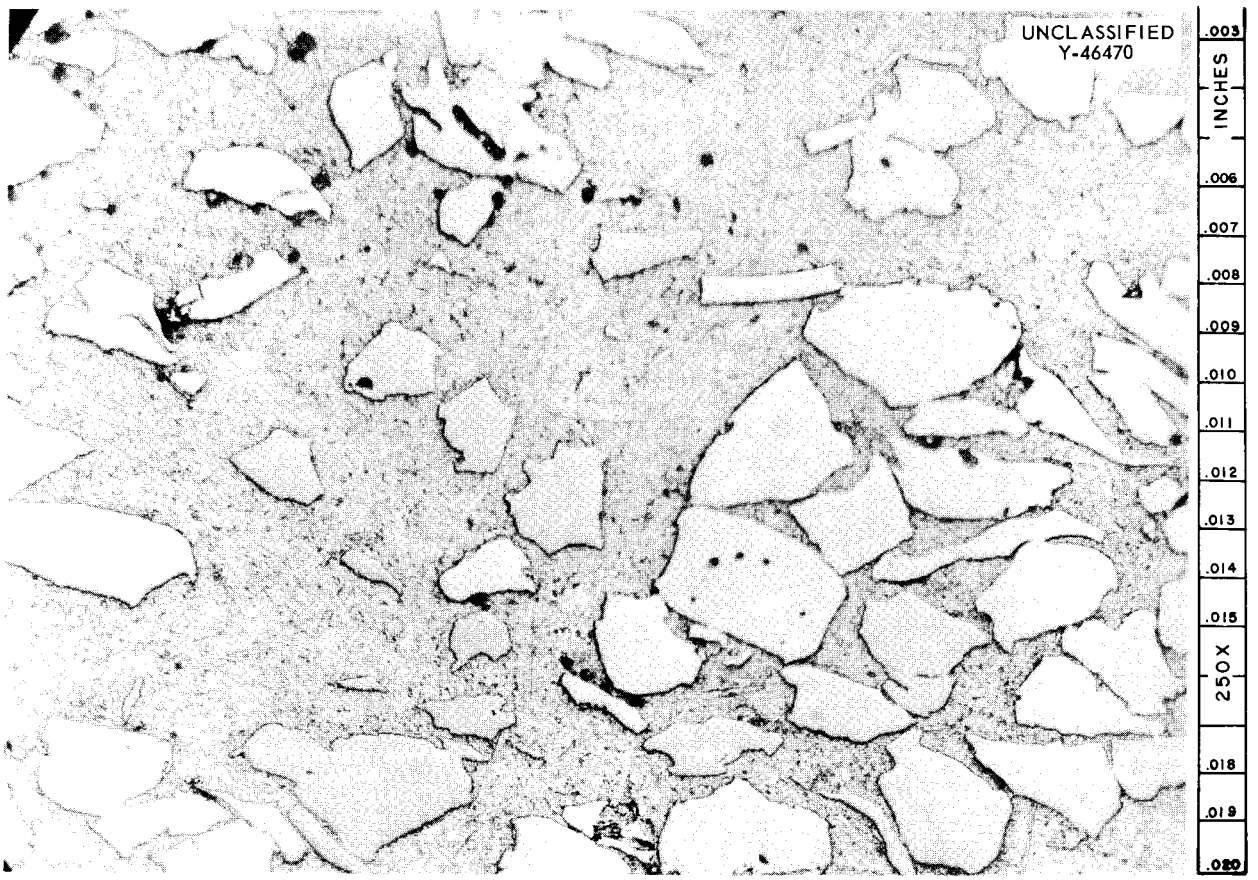

Fig. 22.9. 40 vol % Ta (−200 +325 Mesh) Dispersed in Aluminum, Roll Clad at 500°C, and Heat Treated for 4 hr at 500°C. Note that no reaction exists between tantalum and aluminum. As polished.

PLATE ROLLING AND PREFORMING

C. F. Leitten, Jr. M. M. Martin

The concept in preparing composite control-rod plates is to insert both the Eu_2O_3-Al and the tantalum-aluminum compacts into a single cavity of a billet frame. Billets are prepared by the conventional "picture-frame" technique, and the inner parts are evacuated and sealed from the atmosphere to ensure high-quality bonding when roll clad. Plates are rolled at 500°C to proper width and length using a combination of cross rolling and straight rolling.

Initial work in roll cladding plates containing 40 vol % (vitreous) rare earths and 40 vol % Ta has revealed that well-bonded plates with predictable absorber section dimensions can be fabricated. However, a problem has been encountered in forming the plate at room temperature without propagation of cracks in the rare-earth portion of the plate. As illustrated in Fig. 22.10, the −325 mesh rare-earth particles have a marked tendency to stringer and agglomerate when hot rolled. When either roll formed or marformed, longitudinal cracks were observed, with a deleterious localized thinning of the cladding above the cracks. As shown in Fig. 22.11, in which −100 +325 mesh rare-earth oxide was substituted for the −325 mesh material, an improvement in the distribution of the rare-earth oxide can be seen. This improvement, although noticeable, may not be sufficient to eliminate crack propagation during forming; the volume fraction of the rare-earth constituent therefore is being reduced to 33 vol % to circumvent this problem. A possible alternate also being considered is to hot form.

Microscopic examination showed that the distribution of tantalum particles in the tantalum-aluminum region of the full-size plate was quite

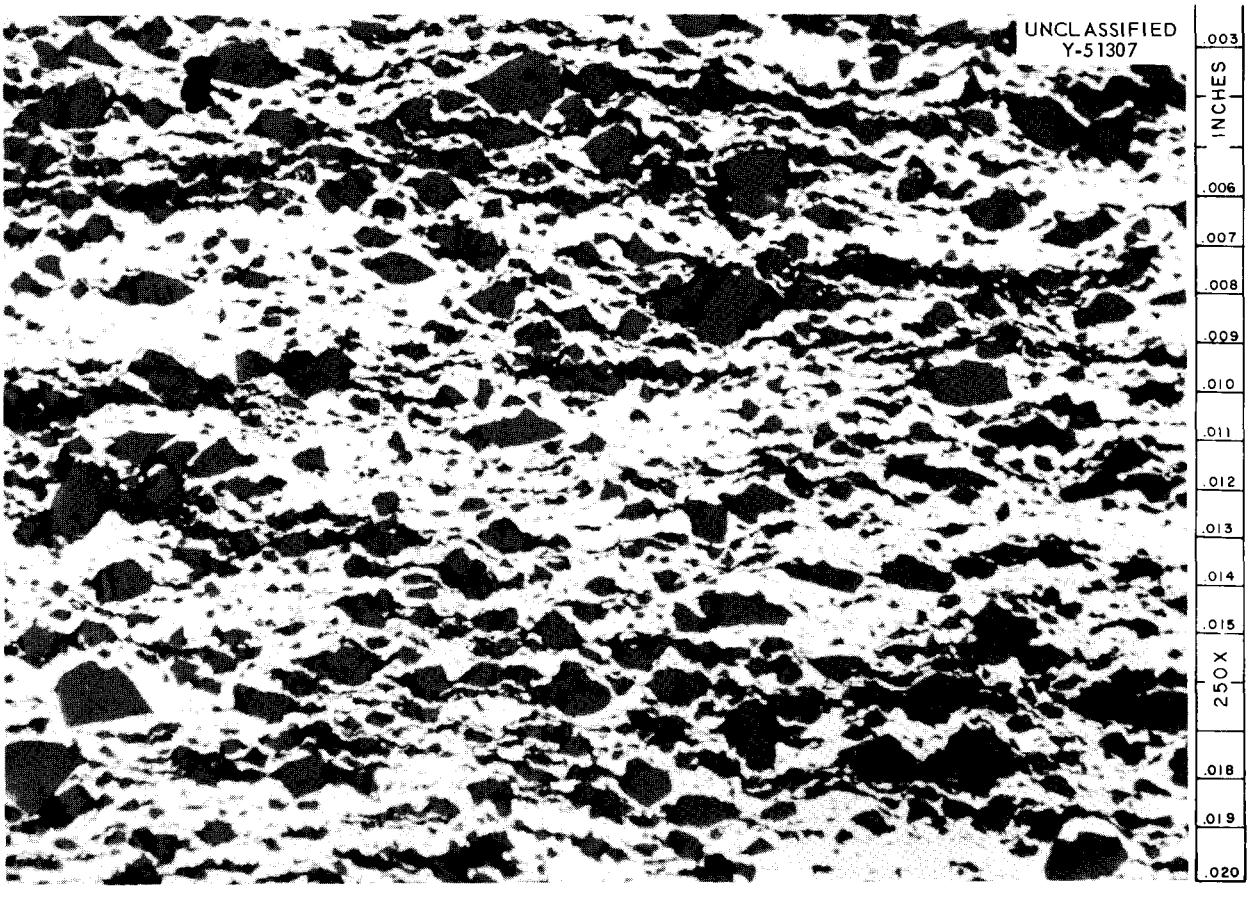

Fig. 22.10. Longitudinal Section of the 40 vol % Rare-Earth–Aluminum Section in a Plate Rolled at 500°C to a 90% Reduction in Thickness (Original Rare-Earth Size Was −325 Mesh), Showing Poor Dispersion Quality. As polished.

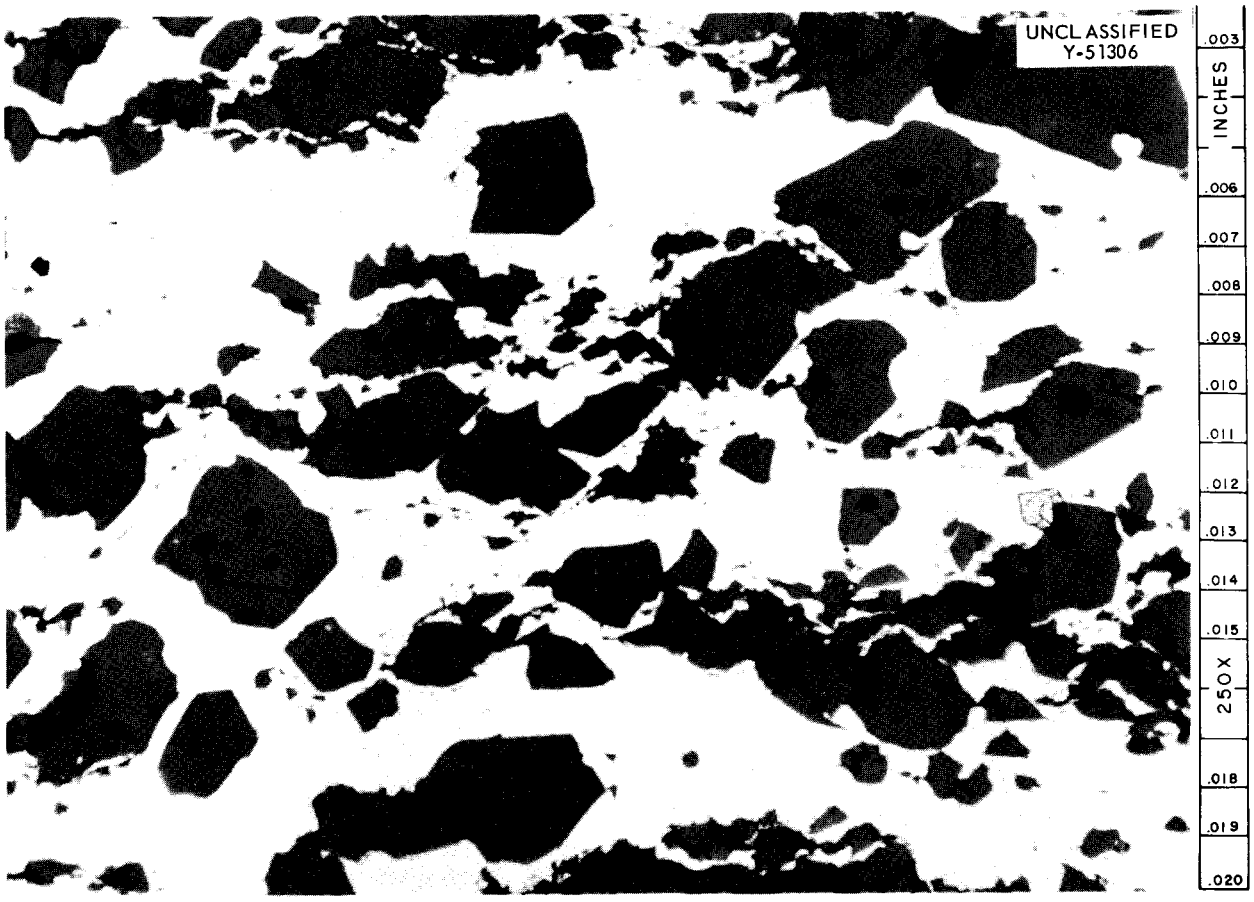

Fig. 22.11. Longitudinal Section of the 40 vol % Rare-Earth–Aluminum Section in a Plate Rolled at 500°C to a 90% Reduction in Thickness (Original Rare-Earth Size Was –100 +325 Mesh), Showing Improvement in Dispersion Quality. As polished.

similar to the compatibility specimen previously illustrated. No difficulty was experienced in this region when the plate was formed.

THERMAL CONDUCTIVITY

T. G. Kollie

Tentative measurements of the thermal conductivities of the fabricated 40 vol % rare-earth–aluminum and 40 vol % Ta–Al dispersions have been made in the thermal comparator. The microstructures of the material examined are similar to those shown in Figs. 22.10 and 22.11. The values at 125°C were 55 and 65 w m^{-1} $°C^{-1}$ for the rare-earth–aluminum mixture and the tantalum-aluminum mixture respectively. Since the calibration curve has not been completely established, the accuracy of these values is considered to be ±20% at this time. The values obtained are lower than would be predicted by calculations based on proportionalities. This indicates that calculated thermal conductivities where significant volume fractions of dispersoids are involved must be considered as purely qualitative estimates with a high degree of uncertainty.

23. Space Power Program

W. C. Thurber

INTRODUCTION

The objective of this program is to provide materials support for the Medium-Power Reactor Experiment. The reactor involved is a single-loop Rankine-cycle system employing boiling potassium as the coolant and working fluid and a stainless-steel-type material for containment. This reactor will produce in excess of 100 kw of electricity for space power application.

Current emphasis is placed on the fabrication of various special components to be used in experimental test rigs and therefore centers primarily on the fields of welding and brazing. Metallurgical engineering assistance in design review, specification preparation, and materials selection is also provided to the project.

COMPONENT FABRICATION

Fabrication of Instrumented Clusters

C. W. Fox

An extensive program has been undertaken to develop procedures for instrumenting electrical heaters used in various boiling-liquid test apparatus. Because it is expected that the tests will be operated at near "burnout" conditions, it is essential that the heater surface temperature be known. To accomplish this, sheathed thermocouples of very small diameters (0.010 and 0.020 in.) are installed in grooves machined in the stainless steel heater sheathing.

The thermocouples are joined to the heaters by soldering or brazing. The development of attachment procedures has progressed through three types of filler metals: (1) high-melting soft solders (mp <750°F), (2) silver brazing alloys (mp 1100 to 1300°F), and (3) high-temperature nickel-base brazing alloys (mp 1900 to 2200°F). Each of these types of filler metals has an application in some phase of the experiments.

Several different methods were investigated to prevent thermocouple buckling during heating to brazing temperature, and the only method found to be completely successful utilized peening. In this process the groove is upset slightly over the thermocouple with a vibrating diamond-point tool. Figure 23.1 shows a 0.010-in.-diam thermocouple peened to a $\frac{1}{2}$-in.-diam "firerod" heater prior to brazing.

During the course of this program, a large number of instrumented assemblies have been successfully fabricated, including 6 units joined with soft solder, 22 with silver brazing alloy, and 15 with a high-temperature nickel-base brazing alloy. Individual firerods contained as many as four thermocouples.

Turbine Pump Fabrication

C. W. Fox

Among the materials that have been proposed for use in high-temperature liquid-metal bearing applications are cermets that contain major amounts of refractory-metal carbides (e.g., tungsten carbide). These cermets are generally difficult to wet, and their coefficients of expansion are so low that there may be serious problems when they are to be joined to metals. A program is under way to develop suitable procedures for attaching these bearings to metal pump components.

Of immediate interest is the fabrication of a small turbine pump in which several cermet bearings must be brazed to a molybdenum alloy impeller shaft. The bearing material selected was 88% WC–12% Co (Kennametal K-94).

In order to choose the best brazing metal for joining the bearings to the impeller, preliminary

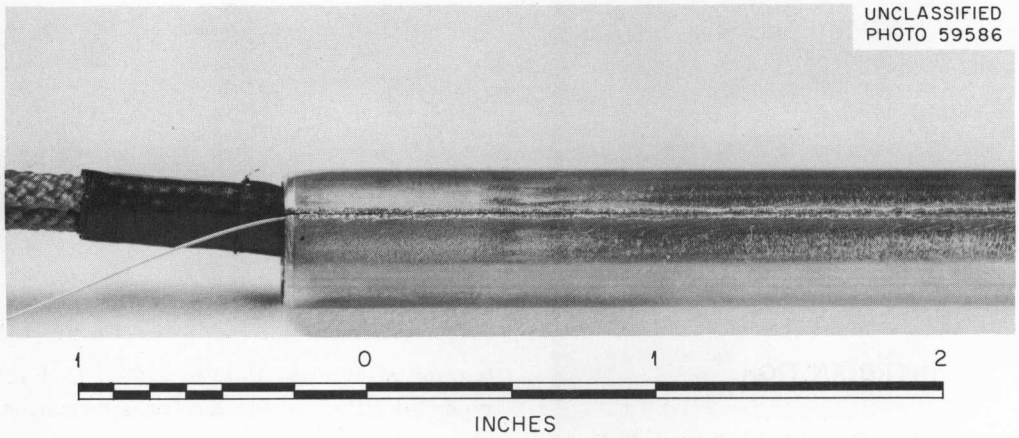

Fig. 23.1. Instrumented "Firerod" Assembly Showing 0.010-in. Stainless-Steel-Sheathed Thermocouple Peened into Groove in Heat Element Prior to Brazing.

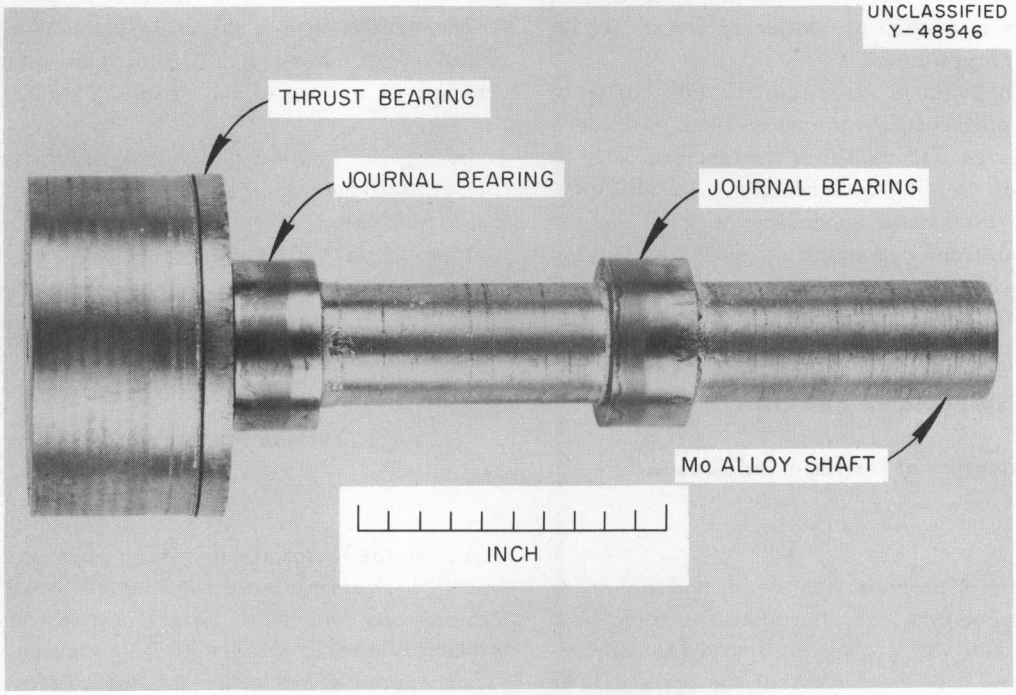

Fig. 23.2. Molybdenum Impeller for Turbine Pump with Cermet (88% WC–12% Co) Bearings Brazed with Nickel-Silicon-Boron Alloy.

studies were conducted using small samples of this cermet and molybdenum. Of the many corrosion-resistant alloys tried, three were found which appear satisfactory: Nicrobraz 50 (Ni-Cr-P), Coast Metals 52 (Ni-Si-B), and a 48 Ti–48 Zr–4 Be (wt %) experimental alloy. The first two alloys are especially promising.

A completed assembly with two radial bearings and one thrust bearing brazed to a molybdenum impeller with the nickel-silicon-boron alloy is shown in Fig. 23.2. Two such assemblies have been constructed for pump usage.

Fabrication of Heat-Transfer Equipment

E. A. Franco-Ferreira

Two large units for the study of fluid heat transfer were fabricated for the Reactor Division.

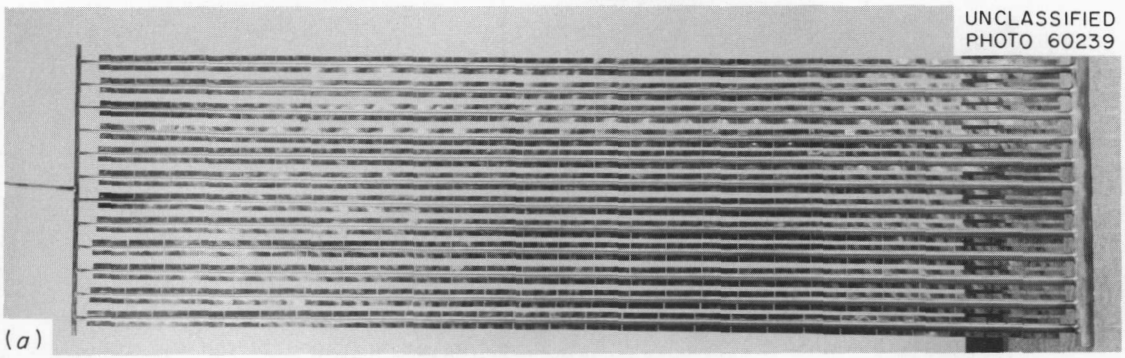

Fig. 23.3(*a*). 12-Tube Finned Radiator; (*b*) 144-Tube Radiator.

Figure 23.3(*a*) shows an overall view of a 12-tube finned radiator. Each tube is tapered from 0.700 in. OD to 0.300 in. OD and is 7 ft long. The tubes and headers are type 316 stainless steel. Fins are brazed the length of each tube, and all fins lie in the same longitudinal plane. The fins were high-conductivity stainless steel-clad copper, 0.008 in. thick.

The fins were attached to the tubes by a combination welding and brazing process. Initially, the fins were spot-welded to the tubes using a condenser discharge welder. After the spot welding, brazing-alloy slurry (Ni-Cr-P) was added to the joints, and the fins were brazed at 1850°F in a hydrogen atmosphere.

To attach the individual tubes to their headers, welding techniques were developed by the ORNL Shops under welding supervision of the Metals and Ceramics Division. All welding was done by Shops personnel.

A 144-tube unfinned condenser, shown in Fig. 23.3(*b*), was also fabricated. The same type of tubes described above was used, the only difference being that no fins were required. Welding techniques developed for the 12-tube radiator were successfully applied to this unit.

24. Thorium Utilization Program

INTRODUCTION

D. A. Douglas

The known reserves of uranium that can be recovered at a relatively low cost are limited. As more and larger power reactors are built, the rate at which these reserves are depleted will rise exponentially. One method for significantly reducing this rate is to design reactors based on a thorium-uranium fuel cycle. Chemical processing can be used to recover the U^{233} isotope from such fuel after irradiation. Once an equilibrium cycle has been achieved, very little additional uranium is required if a high conversion ratio is obtained. The purpose of this program in the Metals and Ceramics Division is to explore the feasibility (technically and economically) of fabricating fuel elements containing this mixture.

One of the major problems which must be resolved stems from the fact that recycled thorium and U^{233} contain significant quantities of Th^{228} and U^{232}. The decay products of these isotopes are energetic gamma emitters; thus, all fabrication must be conducted in shielded and tightly contained cells. The development of equipment capable of conducting each of the fabrication steps without the normal visual and manual control by the operator is an important aspect of this work. Ways must be found to perform these functions economically but to the same high standards of quality always required for satisfactory fuel element performance. The Fuel Rod Facility is the first attempt to solve some of these problems and will be discussed in detail in this chapter. The next advancement will be the Thorium Fuel Cycle Facility, which is in the Title I stage of development. The conceptual designs are being refined and incorporated into the plans of the architect-engineer. Propaedeutic to each of these efforts is the development work carried out in the functional laboratories. Their efforts are reported following descriptions of the two facilities. The performance of the oxide fuel, which is obtained by chemical processing, is being evaluated in irradiation tests. Finally, the possibility of using a metal alloy is being explored, and the current status of this work is reported.

Th-U^{233} FUEL-ROD FACILITY

J. D. Sease J. E. Van Cleve

The design and construction of a facility for fabrication of fuel rods containing low-activity U^{233} and thorium were completed. Although the facility, known as the Oak Ridge National Laboratory Fuel Rod Facility, has sufficient flexibility to accommodate a variety of work, it was specifically designed for making approximately one thousand ½-in.-OD × 48-in.-long Zircaloy-2-clad fuel rods containing $(Th-3\ wt\ \%\ U^{233})O_2$ for criticality experiments at Brookhaven National Laboratory. The 3 wt % U^{233} fuel containing 40 ppm U^{232} can be handled safely in the facility for 30 days after the separation of 99% of the U^{233} daughter products. The entire facility encompasses solvent extraction purification of U^{233}, bulk oxide preparation by the ORNL sol-gel process, and rod fabrication and inspection, with the Metals and Ceramics Division having responsibility for the latter step.

The fabrication process, which is based on the vibratory compaction of sol-gel bulk oxide fuel material, will be carried out in lightly shielded (4-in. armor plate) alpha-tight cubicles (shown in Fig. 24.1), which are located on the bottom two floors of a 20-ft-long, 19-ft-wide, 27-ft-high chemical process cell which serves as secondary containment.

The procedure employed to fabricate the fuel rods (shown in Fig. 24.2) includes the crushing and classification of the oxide according to particle size, vibratory compaction, welding of

UNCLASSIFIED
ORNL-LR-DWG 76196

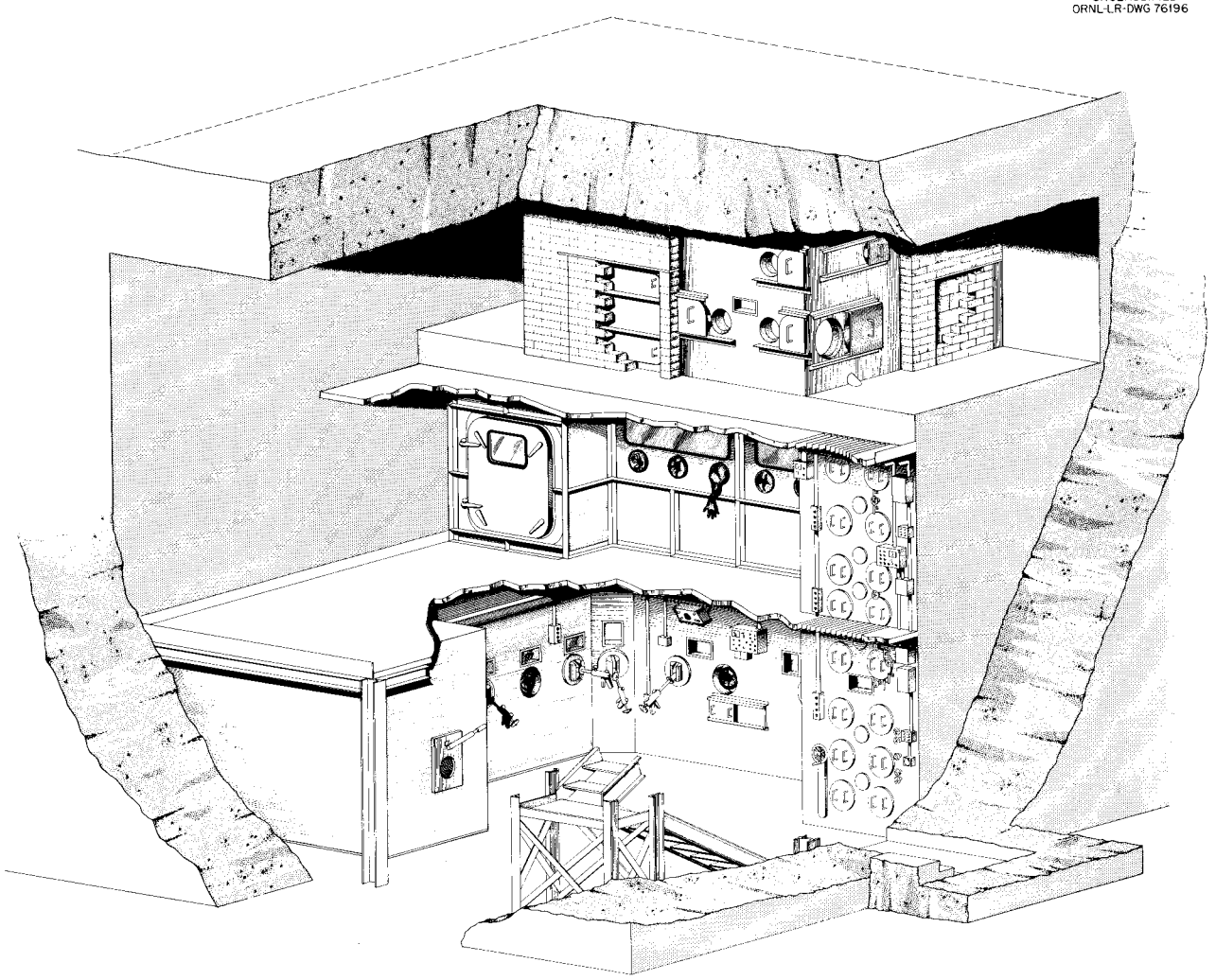

Fig. 24.1. Kilorod Solids Preparation and Rod Fabrication Facility.

end-closure plug, rod decontamination, and rod inspection.[1] The crushing, grinding, classifying, weighing, and blending machines needed for the powder-conditioning operations are positioned in a vertical shaft, with pipe connections so that gravity may be utilized for transferring fuel from one equipment unit to the next. The powder-conditioning operations are controlled either electrically or by flexible shafts. The vibratory compaction unit employs a pneumatic vibrator with the associated chuck and a fuel-loading mechanism. A vertical end-cap welder was developed for making a fusion lip weld. It incorporates, in addition to the inert-gas welding mechanism, a means of backfilling the tube with helium and a press for inserting the end plug after backfilling. Decontamination is accomplished by an ultrasonic cleaner. Inspection of the rods includes helium leak testing of the final closure weld and density checking by a gamma-absorption device. A complete and comprehensive report on the fabrication process and equipment may be reviewed elsewhere.[2]

[1] J. T. Lamartine, *Metals and Ceramics Div. Ann. Progr. Rept. May 31, 1962*, ORNL-3313, pp 107–8.

[2] A. L. Lotts *et al.*, "The Oak Ridge National Laboratory Kilorod Facility," in *Proceedings of the Thorium Fuel Cycle Symposium, Gatlinburg, Tennessee, December 5–7, 1962*, TID-7650 (in press).

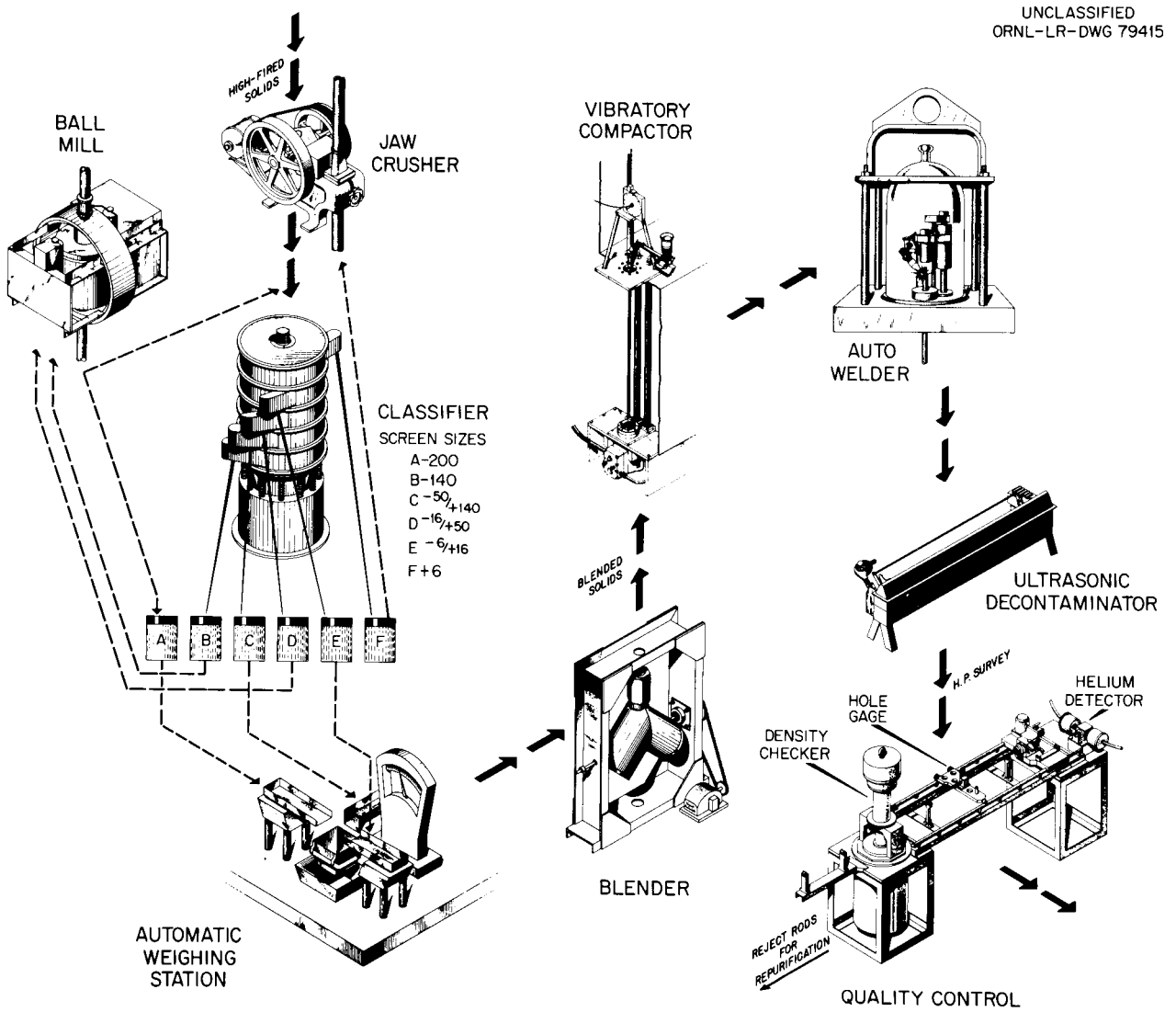

Fig. 24.2. Flow Diagram for Fabrication of Fuel Rods Bearing U^{233}–Thorium Oxide.

In April 1963, the facility and the process equipment were successfully tested, and satisfactory fuel rods were made with depleted uranium substituted for the U^{233} in the (Th–3 wt % U^{233})O_2 fuel.

THORIUM-URANIUM FUEL CYCLE DEVELOPMENT FACILITY

A. R. Irvine[3] A. L. Lotts

The design of the Thorium-Uranium Fuel Cycle Development Facility (TUFCDF) has continued as a joint effort of the Chemical Technology and Metals and Ceramics Divisions. The basic criteria for the design of the building have not changed from those reported previously.[4] The conceptual design[5] was completed by Giffels and Rosetti,

[3]Chemical Technology Division.

[4]A. R. Irvine and A. L. Lotts, *Metals and Ceramics Div. Ann. Progr. Rept. May 31, 1962,* ORNL-3313, pp 106–7.

[5]A. R. Irvine and A. L. Lotts, "The Thorium Fuel Cycle Development Facility Conceptual Design," in *Proceedings of the Thorium Fuel Cycle Symposium, Gatlinburg, Tennessee, December 5–7, 1962,* TID-7650 (in press).

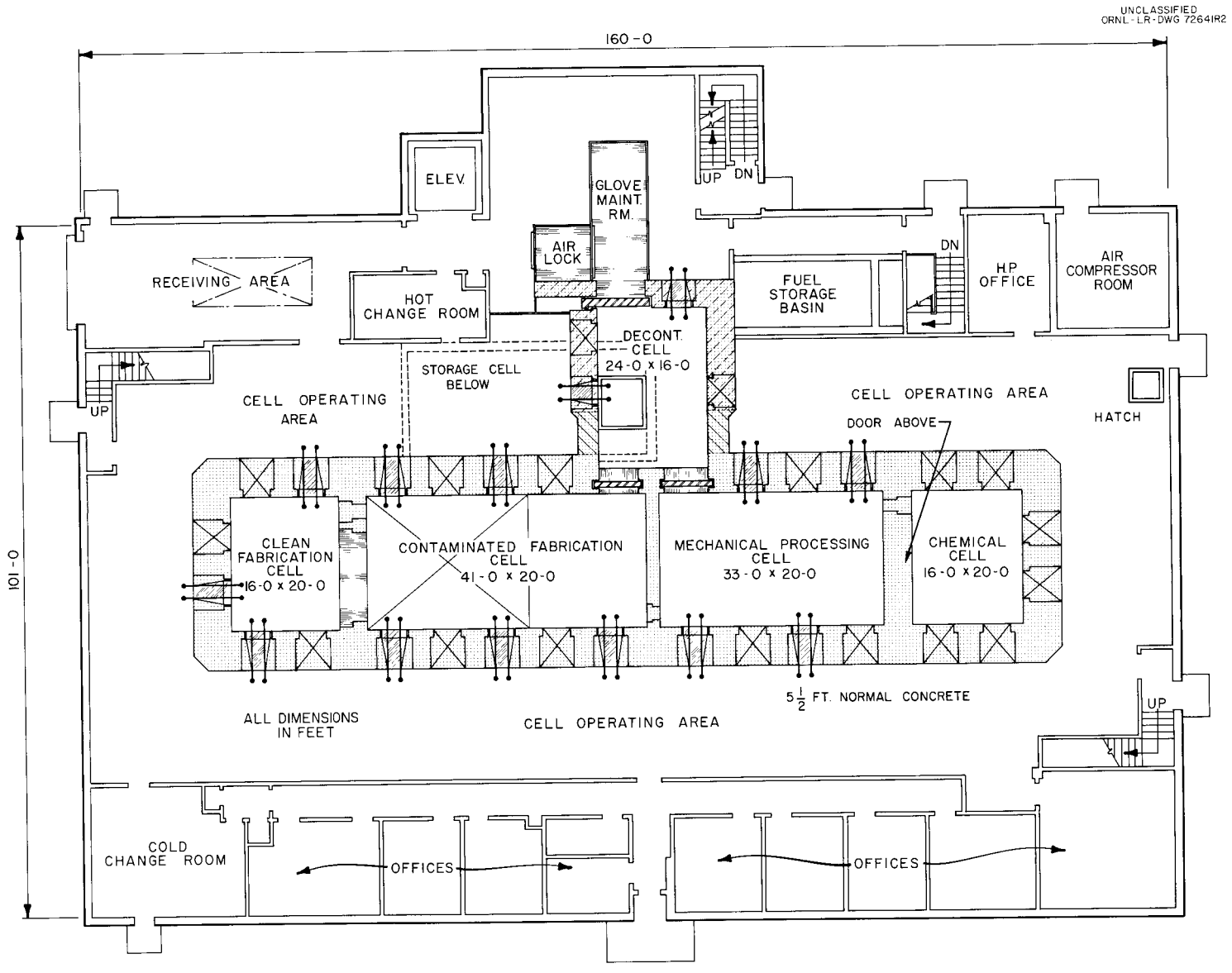

Fig. 24.3. First-Floor Plan, Thorium-Uranium Fuel Cycle Development Facility.

UNCLASSIFIED
ORNL-LR-DWG 75591R

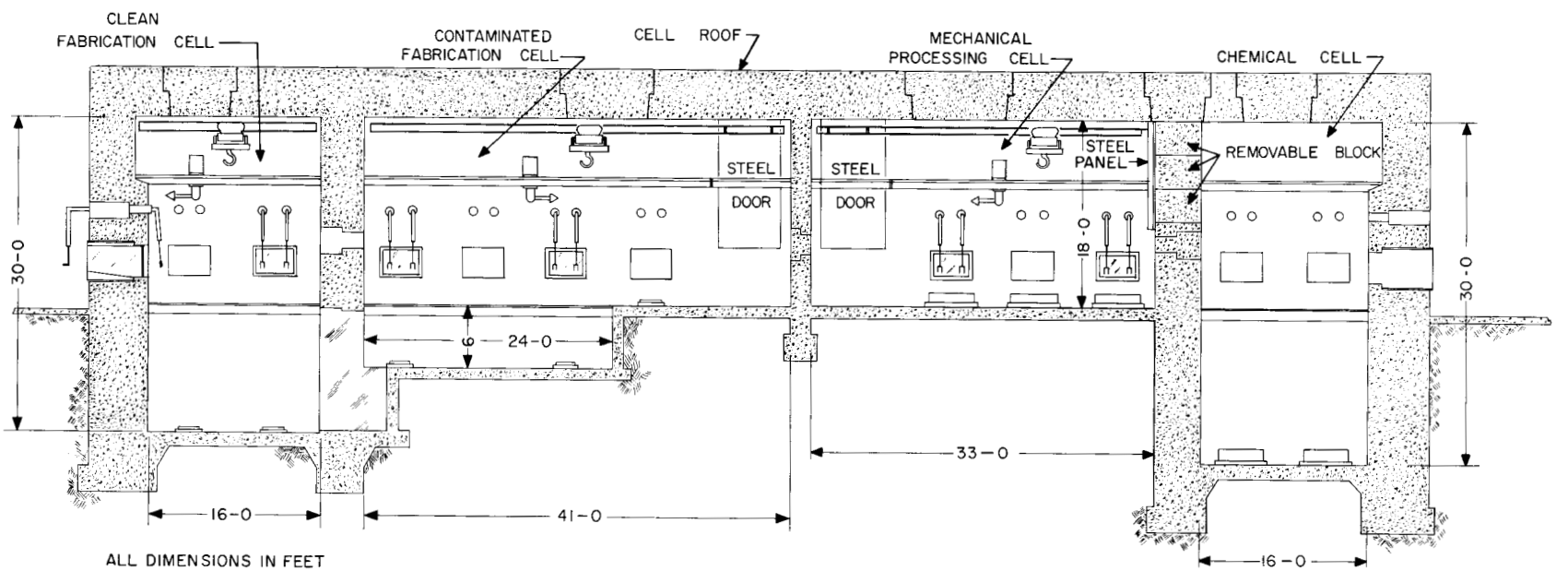

Fig. 24.4. Elevation of Operating Cells, Thorium-Uranium Fuel Cycle Development Facility.

Inc., Detroit, Michigan, with project direction being provided by ORNL. Since completion of the conceptual design, Title I design of the facility has been initiated and, at this reporting, essentially completed.

The TUFCDF is designed to provide a versatile, integrated facility for development of all phases of the thorium fuel cycle. Fuel elements of the type used for the Consolidated Edison Thorium Reactor (CETR) and the High-Temperature Gas-Cooled Reactor (HTGCR) were selected as a basis for design of the facility, since these represent two diverse fuel elements of types anticipated for future reactors utilizing the Th-U^{233} fuel cycle. Although these fuel elements were selected as the basis for design, their selection does not preclude the development of recycle schemes for other fuel materials or geometries.

The heart of the facility is the hot-cell complex, which is depicted in Figs. 24.3 and 24.4. It is composed of a chemical cell, a mechanical processing cell, a contaminated fabrication cell, and a clean fabrication cell. In the chemical cell, irradiated fuels will be processed to separate the fissile and fertile materials. In the mechanical processing cell, those operations will be carried out that are necessary for reconstituting the fissle and fertile materials into a form suitable for fuel element manufacture. In the contaminated fabrication cell, uncontained fuels will be encapsulated. The clean fabrication cell is for inspection, assembly, and handling of contamination-free elements. Also provided by the facility are two service cells: a decontamination cell (which is to be used for decontamination and as a radiation lock) and a storage cell (which is located at the basement level and is to be used for storage of contaminated equipment). A glove maintenance room with an attached air lock is located adjacent to the decontamination cell and is to be used for maintenance of manipulative and process equipment as well as for entry to the cell complex.

Five of the six cells either will be, or can be, maintained entirely by remote devices. The clean fabrication cell is the exception because it is to receive fuels only after they are encapsulated in tubes or other containers. In this cell the installation and repair of equipment will be accomplished by contact methods. Either remote or contact maintenance may be employed in the chemical cell since a doorway is provided, allowing isolation from or connection to the mechanical processing cell.

The transportation and manipulative system is the lifeline of the cell complex. This system consists of a pair of overhead bridge cranes which can travel over essentially all the area in the glove maintenance room and the decontamination, chemical, mechanical processing, and contaminated fabrication cells. A special transfer bridge system in the decontamination cell, which travels in three planes, allows the movement of a hoist between cells and the removal of operating cell bridges to the glove maintenance room for repair. Bridge cranes are provided in the clean fabrication and storage cells. Manipulation in cells is provided by bridge-mounted electromechanical manipulators and master-slave manipulators.

REMOTE FABRICATION EQUIPMENT FOR CLAD OXIDE FUELS

A. L. Lotts

The first fabrication equipment to be installed in the Thorium-Uranium Fuel Cycle Development Facility (TUFCDF) will be that for the demonstration of techniques for remote manufacture of clad oxide fuel elements. The conceptual design of this equipment was started during the latter part of this reporting period and is almost finished. Basic criteria established for the complete line of equipment are as follows:

1. The equipment is to be flexible enough to permit the fabrication of fuel rods ranging from 2 to 10 ft in length and from $\frac{1}{4}$ to $\frac{3}{4}$ in. in diameter. This flexibility will most probably be accomplished by making certain parts of the equipment readily replaceable.
2. The design of the equipment, wherever possible, is to be based on the scaledown of equipment that might be used in a production plant.
3. Although it is not the intent to use automation exclusively, it is desirable to demonstrate its feasibility by incorporating automation in some equipment items.
4. All fuel rods and bundles are to be handled with their axes in a vertical attitude.

A modified Consolidated Edison Thorium Reactor (CETR) fuel element, the fuel rod for which is shown in Fig. 24.5, was used as the design basis. Principal modifications were those affecting the

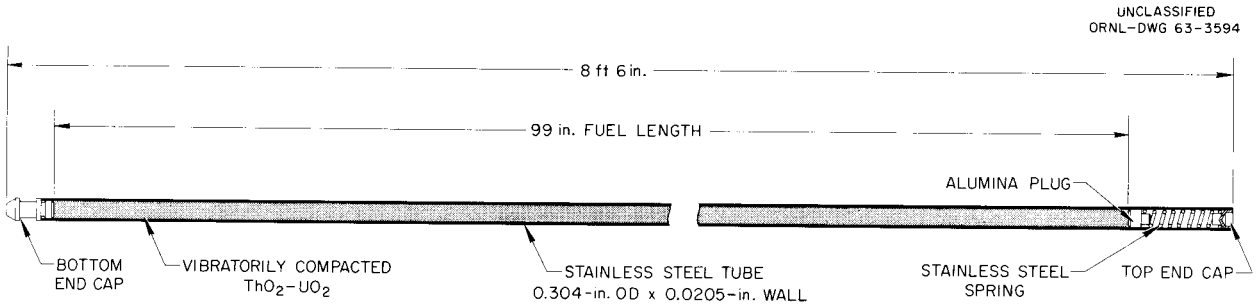

Fig. 24.5. Clad Oxide Fuel Rod, Thorium-Uranium Fuel Cycle Development Facility.

fuel density, end-cap design, and method of assembly. Instead of using a brazed fuel bundle with ferrules as fuel rod spacers, the array of rods is to be obtained through the use of a preassembled lattice which provides spring tabs for holding the rods in position. The fuel bundle can be assembled by simply pushing the rods into the lattice positions.

The procedure for making the clad oxide elements includes oxide powder preparation, vibratory compaction, encapsulation, inspection, and assembly steps as shown in the flowsheet (Fig. 24.6). To summarize the equipment concepts as presently envisioned, sol-gel oxide feed (as received from the calcination step in the mechanical processing cell) will be comminuted and screened; and appropriate size fractions will be blended for vibratory compaction. The equipment for these operations, which is to be installed in the contaminated fabrication cell, will be similar to that being employed in the fabrication of fuel rods for the Brookhaven National Laboratory (see "Brookhaven National Laboratory Kilorod Welding Development" following in this chapter). This powder-conditioning equipment is to be part of a completely sealed system, employing pipes and a vibrational means of conveyance for communication between individual working units to minimize spread of dust.

All process steps in the contaminated fabrication cell involving tubes will be done at process stations which are placed in a linear arrangement. The tubes will be transferred between these stations with two independently operated devices of special design. Each device will cover approximately one-half the process line and is to be designed so that placement of the tubes in the various required positions is automatic. The stations in this line are for vibratory compaction, gamma scanning, and end capping, as well as for the accompanying requirements of tube feeding, rod rejection, and product magazine filling. The product magazine will be used in conveying a number of rods to and through the ultrasonic cleaning unit. The ultrasonic cleaning unit will also serve as a transfer port to the clean fabrication cell.

The concepts for inspection and assembly equipment to be located in the clean fabrication cell are not sufficiently advanced to permit an exact description. It is certain, however, that one or two special manipulative devices will be used to handle the filled fuel rods, that the equipment will be placed in a linear arrangement, and that the rods will be handled with their axes in a vertical attitude. All equipment for the fuel rod inspection steps shown on the flowsheet (Fig. 24.6) and devices for insertion of rods into a preassembled lattice and attachment of fuel element end fittings are currently being designed.

BROOKHAVEN NATIONAL LABORATORY KILOROD WELDING DEVELOPMENT

J. W. Tackett

In connection with the manufacture of the 1000 Zircaloy-2-clad $U^{233}O_2$-ThO_2-fueled rods for the Brookhaven National Laboratory kilorod program, satisfactory welding procedures have been developed for the attachment of top and bottom end

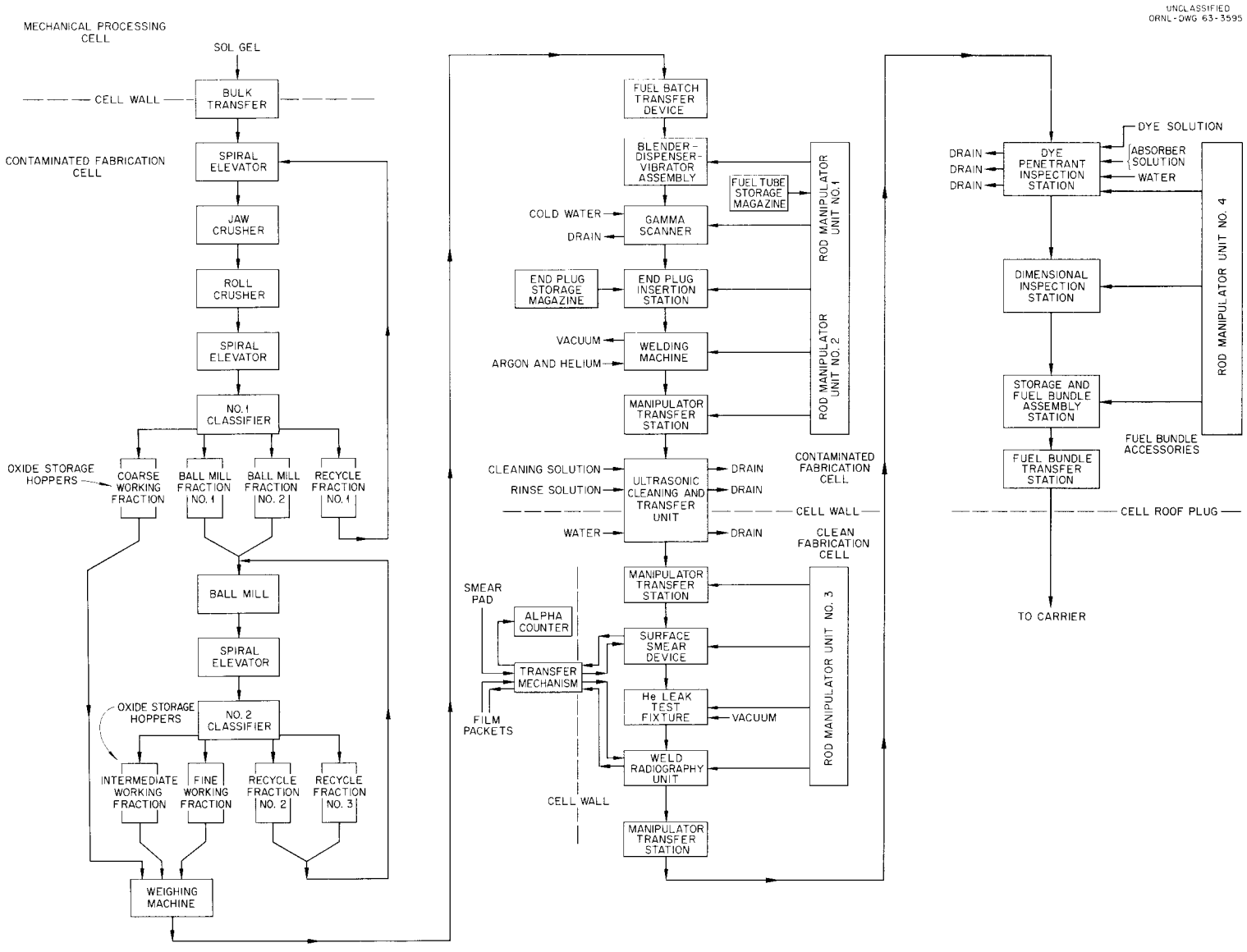

Fig. 24.6. Fabrication Flowsheet for Clad Oxide Fuel Elements, TFCDF.

plugs which are used to seal the fuel rod ends.[6] The bottom end plugs will be circumferentially welded to the bottom ends of the tubes prior to the fuel-loading step. A unique rapid-loading welding chamber [Fig. 24.7(*a*)] was developed for making these bottom welds instead of using the more time-consuming conventional vacuum-purged inert-atmosphere chambers (vacuum-purged equipment is usually used to obtain an atmosphere purity that is suitable for welding Zircaloy-2).

[6]J. W. Tackett, *Status and Progress Report for Thorium Fuel Cycle Development December 31, 1962,* ORNL-3385 (in press).

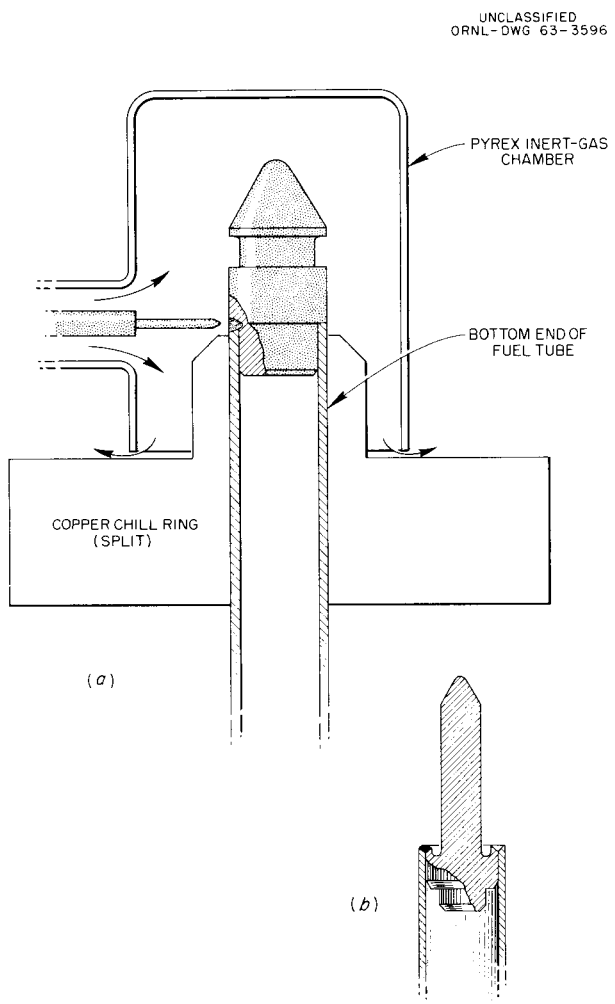

Fig. 24.7. (*a*) Special Chamber Used in Making Bottom End-Plug Welds in Zircaloy-2 Fuel Rods; (*b*) Beveled Joint Design Used in Making Top End-Plug Welds.

After loading the tubes with fuel, the top end plugs will be welded, using an edge-weld joint design. These top welds will be made remotely inside a contamination zone cubicle with special vacuum-purged equipment. This is necessary for this weld in order to backfill the rods with inert gas. The beveled-joint configuration used in the top weld [Fig. 24.7(*b*)] was designed specifically to minimize the problem of weld roll-over. Completely satisfactory welds have been produced with both end-plug designs.

VIBRATORY-COMPACTION STUDIES

W. S. Ernst, Jr.

Vibratory compaction is the preferred method for fabricating recycled $Th\text{-}U^{233}$ oxide fuels. The criteria established for evaluating this fabrication process are concerned with operational simplicity, process yield, bulk fuel density, axial density distribution, and performance. Simultaneous optimization is difficult because these criteria are not mutually compatible. The effect of particle-size distributions, which appears to be the primary controlling factor, on the attainment of simultaneous optimization has been discussed in detail elsewhere.[7]

Experimental studies that relate bulk density with particle-size distributions indicate that there are a number of distributions and systems in the ternary and binary classes that will yield bulk fuel densities between 87 and 90% of theoretical.[8] Thus, it appears that, if vibratory compaction is to attain its maximum potential and meet the criteria mentioned above, it may be necessary to allow several particle-size distributions in a given core loading.

Attainment of a uniform axial fuel distribution within a tight tolerance is still a major problem. Experimental results indicate that the axial density distribution is dependent on many factors, such as the incremental particle-size distribution during the filling operation, the feed rate during filling, the overall particle-size distribution, and the

[7]W. S. Ernst, Jr., "Recent Vibratory-Compaction Studies on Thoria-Urania," in *Proceedings of the Thorium Fuel Cycle Symposium, Gatlinburg, Tennessee, December 5–7, 1962,* TID-7650 (in press).

[8]W. S. Ernst, Jr., "Vibratory-Compaction Studies," in *Status and Progress Report for Thorium Fuel Cycle Development December 31, 1962,* ORNL-3385 (in press).

vibration-energy characteristics. For example, a well-blended fuel charge that does not segregate during filling and is fed at a relatively slow rate has been found to improve the fuel distribution. Results also indicate that a narrow-sized coarse fraction is better than a broad-sized one and an energetic mechanical pulse is much better than a pure sine wave for attaining uniform fuel distribution.

IRRADIATION STUDIES

Neutron-Activation Experiments on Mixed Oxides Produced by the Sol-Gel Process

R. E. Adams

Neutron-activation experiments were made to study fission-gas release from ThO_2-UO_2 produced by the sol-gel process. Samples of sol-gel S (sized to −325 mesh, to −10 +16 mesh, and one containing a mixed size range between 10 and −325 mesh) were irradiated to about 10^{15} fissions at room temperature. The fission gas released during irradiation and that released on subsequent heating for 2 hr at temperatures between 1000 and 2000°C were measured. Data have indicated greater gas release by the smaller-sized particles. These results indicate that gas release was roughly proportional to the total calculated surface area of the particles in the sample. This correlation is not unexpected, since the particles produced in the sol-gel process have a very high density.

In-Pile Tests of Mixed Oxides Produced by the Sol-Gel Process

S. A. Rabin

Significant progress has been made in evaluating the irradiation behavior of ThO_2-base ceramic fuels.[9] Investigations have been conducted with vibratorily compacted sol-gel ThO_2-UO_2 and arc-fused ThO_2-UO_2 and with tamp-packed sol-gel ThO_2-PuO_2 in stainless steel and Zircaloy-2 claddings.

[9]S. A. Rabin *et al.*, "Thorium Fuel Cycle Irradiation Program at the Oak Ridge National Laboratory," in *Proceedings of the Thorium Fuel Cycle Symposium, Gatlinburg, Tennessee, December 5–7, 1962*, TID-7650 (in press).

Irradiation tests performed to date include uninstrumented capsules at process water conditions in the MTR and in the Chalk River Reactor (NRX), instrumented capsules in the ORR poolside facility with 1000 to 1300°F cladding temperatures, and a trefoil cluster in an ORR pressurized-water loop operating at 500°F and 1750 psi. By July 1963, another series of capsules will be inserted in the MTR and the ETR. A summary of the experiments is presented in Table 24.1.

It can be seen that these experiments provide comparisons and assessments of the following parameters: (1) type of oxide, (2) content of fissile material, (3) sol-gel preparation route, (4) fuel rod geometry, (5) irradiation temperature, (6) heat generation rate, and (7) burnup.

Irradiation and examination of two MTR-irradiated rods (from group I) and twelve NRX-irradiated rods (groups I and II) are essentially complete. Successful irradiations to burnups of 14,000 Mwd per metric ton of metal at heat ratings up to 47,600 Btu hr^{-1} ft^{-1} have indicated that these fuels will be acceptable for power reactor applications. Tests imparting more-severe conditions are in progress.

No significant dimensional changes were found as a result of the irradiations. Fission-gas-release data are shown in Table 24.2, together with the burnups and heat ratings. The sol-gel oxide appears to be as good as or better than the arc-fused material in this respect, but there are patent differences among the various sol-gel powders. As shown in Fig. 24.8, there was no evidence of grain growth or central void formation in any of the rods, and the microstructures were similar to those before irradiation. Although the fuel appeared to have agglomerated, there was no metallographic evidence of sintering. This agglomeration was confirmed by powder-particle sieve analyses, which showed that nearly all the fine- and medium-sized particles had coalesced into coarser particles. Actually, this adhesion of contiguous particles can be considered an early stage of sintering.

Vacuum leak-testing experiments on the NRX group II specimens furnished a rather interesting phenomenon. These tests indicated that gas diffusion was unexpectedly poor through the vibratorily-compacted rods. Preliminary out-of-pile tests have verified this observation. The situation warrants

Table 24.1. Summary of Fuel Cycle Irradiations[a]

Experimental Facility	Number of Capsules	Type of Oxide	Vibrated Density (% of Theoretical)	Clad Temperature (°F)	Average External Pressure (psia)	Fuel Rod Dimensions (in.)			Peak Linear Heat Rating (Btu hr^{-1} ft^{-1})	Estimated Burnup (Mwd per metric ton of metal)	Status
						Length	OD	Wall			
ORR poolside	2	Sol-gel D	85–86	1000, 1300	315	7	0.625	0.020	40,000	6,000	Out 9-23-62
NRX (group I)	8	Sol-gel A, B	84–86	~200	130	11	0.312	0.025	10,600–17,500	13,400–16,400	Out 5-22-62
NRX (group II)	4	Arc-fused sol-gel C	84–86	~200	130	22.5	0.312	0.025	14,400–21,900	3,200–5,000	Out 2-16-62
MTR (group I)	7	Arc-fused sol-gel E	86–87	~200	40	11	0.312	0.025	41,800–47,600	12,300–100,000	3-in-pile; 2 out 4-2-62; 2 out 3-25-63
MTR (group II)	2	Sol-gel S	88	220	40	22.5	0.312	0.025	62,000	105,000	In 1-2-63
MTR (group III)	2 2 2	Air fired Nitrogen fired 4% H_2–Ar fired	88–90	225	40	12	0.437	0.025	85,000	22,000–93,000	Fabricated
ETR (group I)	2 1 1	Air fired Nitrogen fired 4% H_2–Ar fired	88–90	280	40	12	0.437	0.025	138,000	22,000	Fabricated
NRX (group III)	6	Sol-gel S	88–89	~200	130	39	0.312	0.025	28,000	23,000	In 5-24-62
NRX (group III)	3	Sol-gel ThO_2-PuO_2	74–76[b]	~200	130	11	0.312	0.025	27,000	22,000	In 5-24-62
ORR loop (L-1)	3-rod cluster	Sol-gel 26	84–85	~500	1750	21.5	0.460	0.015	43,000–52,300	2,500–3,000	Out 10-31-62

[a]Fuel: ThO_2-UO_2 except for three (NRX group III) ThO_2-PuO_2-bearing capsules; cladding: type 304 stainless steel except for experiment L-1 (one clad with type 304 stainless steel and two with Zircaloy-2).

[b]Tamp packed.

Table 24.2. Fuel Cycle Experiment Burnups, Heat Ratings, and Fission-Gas-Release Data

Specimen Group	Rod No.	Fuel	Peak Burnup (Mwd per metric ton of U + Th)	Calculated Peak Heat Rating (Btu hr^{-1} ft^{-1})	Fission-Gas Release (%)
MTR-I	U-1	Arc fused	12,300	38,800	2.4
	Z-5	Sol-gel E	14,000	44,200	0.5
NRX-I	X-1	Sol-gel A	13,400	14,300	2.2
	X-8	Sol-gel A	16,360	17,500	2.8
	O-3	Sol-gel B	15,690	16,800	3.6
	O-5	Sol-gel B	14,450	15,400	2.9
	H-3	Sol-gel B	10,000[a]	10,600[a]	1.6[a]
NRX-II	A-1	Arc fused	3,170	14,400	3.5
	A-2	Arc fused	4,310	19,500	3.3
	C-3	Sol-gel C	4,960	21,900	4.0
	C-4	Sol-gel C	4,160	18,200	Gas lost

[a]Estimate.

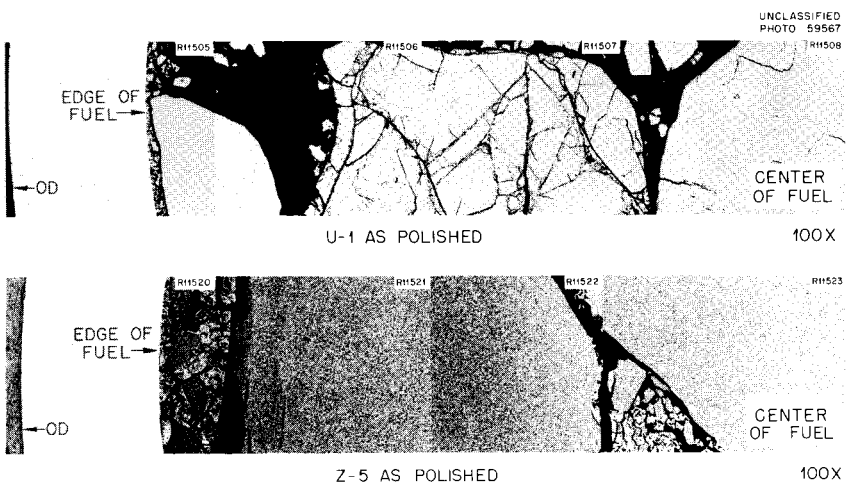

Fig. 24.8. Composite Photomicrographs Showing Typical Transverse Sections of Capsules U-1 and Z-5. Radial area from outside diameter of the cladding to center of the fuel. Reduced 52.5%.

still further investigation since the practical implications in terms of fuel element design may be profound.

Effective thermal-conductivity values for the ThO_2-UO_2 fuel in the two ORR poolside capsules were calculated on the basis of the measured thermal-neutron flux and the continuously monitored central temperature. The results are compiled in Table 24.3, along with some comparative values from the literature for pressed and sintered bodies of ThO_2 and ThO_2–10% UO_{2+x}. It is notable that the conductivities compare favorably for a nonsintered fuel. The postirradiation examination of these capsules is in progress.

Table 24.3. Thermal Conductivity of Thoria-Base Fuels

Source	Composition	Average Temperature (°C)	Average Temperature (°F)	Thermal Conductivity[a] ($w\ cm^{-1}\ °C^{-1}$)	Thermal Conductivity[a] ($Btu\ hr^{-1}\ ft^{-1}\ °F^{-1}$)
ORR (06-5)	ThO_2–2.9% UO_2	990	1815	0.021[b]	1.20
ORR (03-5)	ThO_2–2.9% UO_2	1325	2415	0.017[b]	1.00
Kingery[c]	ThO_2	600	1112	0.046	2.66
	ThO_2	800	1472	0.036	2.08
	ThO_2	1000	1832	0.033	1.91
	ThO_2–10% UO_{2+x}	600	1112	0.032	1.87
	ThO_2–10% UO_{2+x}	800	1472	0.029	1.66
	ThO_2–10% UO_{2+x}	1000	1832	0.025	1.44

[a]Data corrected to same density as vibrated ThO_2–2.9% UO_2 using the relation $k_m = k_t (1 - P)$, where P is pore volume fraction, k_m is the measured conductivity, and k_t is the value corrected to theoretical density.

[b]Based on flux calculated from burnup measurement.

[c]W. D. Kingery, *J. Am. Ceram. Soc.* 4(12), 617 (1959).

The mechanically assembled bundle irradiated in the ORR loop contained two rods clad with Zircaloy-2 (0.460-in.-OD × 0.015-in.-wall) and one clad with type 304 stainless steel with the same dimensions. The element was prematurely discharged from the reactor because of a failure in one of the Zircaloy-2-clad rods. The appearance of the failure (see Fig. 24.9) indicates that it occurred as a result of some corrosion reaction; also, a circumferential crack propagated around the periphery of the rod. Metallographic examination of this area is in progress.

Macroscopic examination of the fuel from this rod revealed that sintering took place, but its extent remains to be determined. In addition to having a higher heat rating (52,000 Btu $hr^{-1}\ ft^{-1}$) than the examined NRX and MTR rods, it should also be borne in mind that the surface temperature was approximately 300°F higher, resulting in an even higher $\int k\, d\theta$. The fuel will be microscopically examined in the near future.

Metallic Fuels

S. A. Rabin

Three thermocouple-instrumented NaK-filled capsules containing Th-U-Zr alloys are being irradiated in the General Electric Test Reactor (GETR) Radially Adjustable Facility Tubes (RAFT). The capsules were designed and fabricated by the Advanced Technology Laboratories (ATL). Each capsule contains a stack of ten ½-in.-diam, 1½-in.-long pellets. Three alloys in two heat treatments (see Table 24.4) are included and are based on an alloy development program performed by ATL.[10]

The specimens are to operate with a 700°C surface temperature and 825°C axial temperature for burnups of 10,000, 20,000, and 30,000 Mwd per metric ton of fuel. The purpose of the experiment is to demonstrate whether the Th-U-Zr alloys, which possess improved elevated-temperature strength compared with Th-U alloys, exhibit sufficient resistance to radiation-induced swelling at the operating temperatures. This objective is based on the determination of an AEC task force[11] in 1959 that, to provide low fuel cycle costs, Th-U alloys capable of operating at central temperatures of from 835 to 1085°C were required.

[10]R. H. Cole and L. E. Wilkinson, *Development of High-Strength Ternary and Quaternary Thorium-Uranium Base Alloys*, ATL-A-128 (Nov. 1, 1961).

[11]Civilian Reactor Fuel Element Review Group, AEC, *Report on Civilian Reactor Fuel Elements*, TID-8505 (June 1959).

UNCLASSIFIED
PHOTO 60810

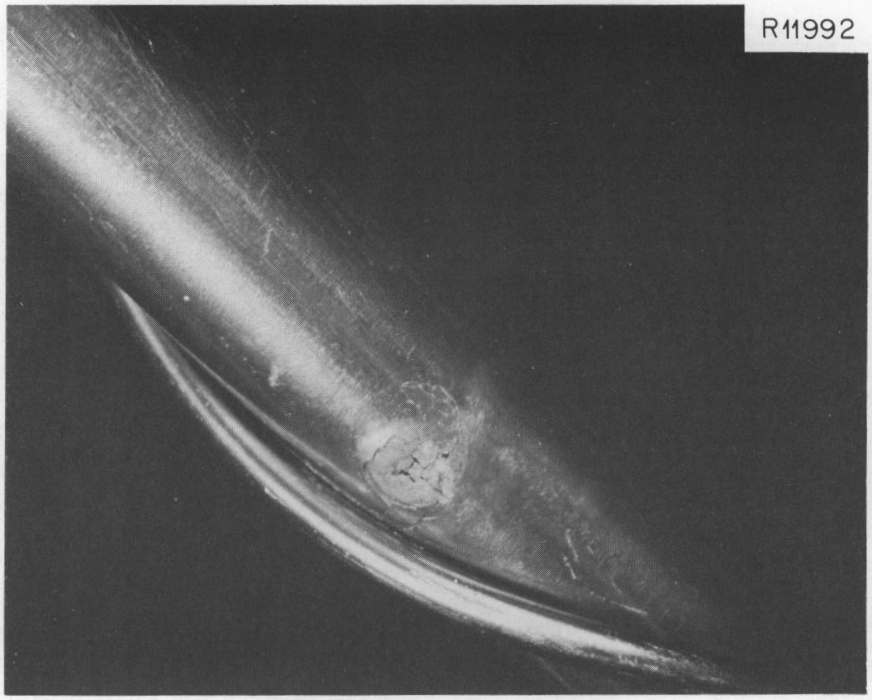

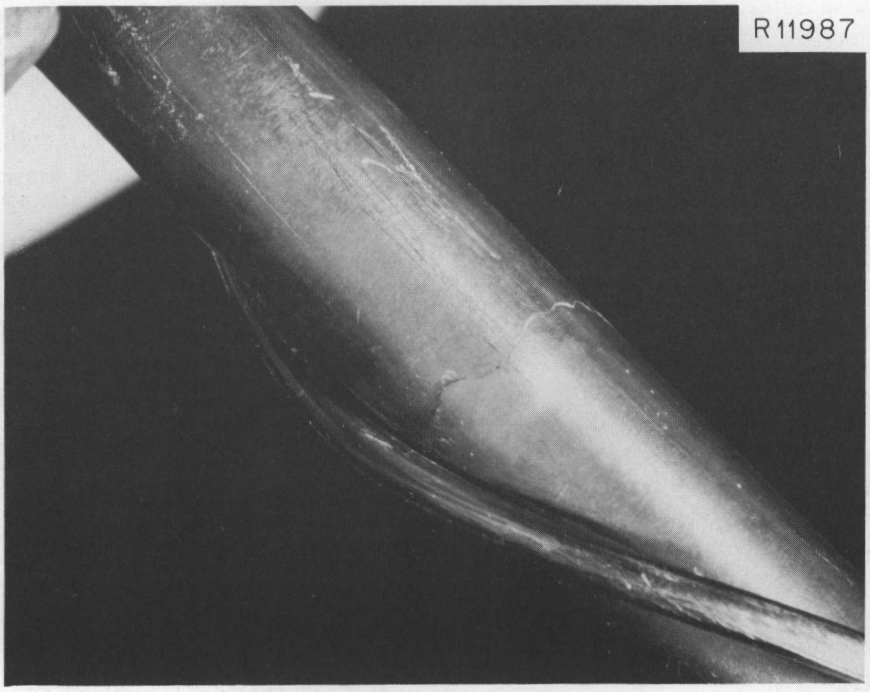

Fig. 24.9. Failure in Zircaloy-2-Clad Fuel Rod, Approximately $2\frac{1}{2}$ in. from Top End.

Table 24.4. ATL Specimens: Composition and Heat Treatment

Specimen Code[a]	Alloy Composition (%)	Heat Treatment
I-A	90 Th–10 U	Solution heat treated 3½ hr at 1320°C; He quenched; annealed 2 hr at 850°C
I-B	90 Th–10 U	Annealed 2 hr at 850°C
II-A	88 Th–10 U–2 Zr	Solution heat treated 3½ hr at 1320°C; He quenched; annealed 2 hr at 850°C
II-B	88 Th–10 U–2 Zr	Annealed 2 hr at 850°C
III-A	85 Th–10 U–5 Zr	Solution heat treated 3½ hr at 1320°C; He quenched; annealed 2 hr at 850°C
III-B	85 Th–10 U–5 Zr	Annealed 2 hr at 850°C

[a]Codes with I prefix are for one specimen per capsule; prefix II or III denotes two specimens per capsule.

DISPERSION HARDENING OF THORIUM

J. A. Burka J. P. Hammond

Efforts to develop dispersion-hardened thorium have been undertaken in order to increase the operating temperature and burnup of thorium-base fuels in power reactors. The method chosen for the dispersion hardening of thorium is that of distributing ultrafine particles of thoria in thorium. The role of the thoria particles is to increase the creep strength of thorium [similar to the effect produced by fine Al_2O_3 particles in aluminum (SAP)] and to provide a multitude of sites for the nucleation of inert fission-gas bubbles so that they will remain small in size.

Procedures for the preparation of thorium hydride–metal oxide mixtures and consolidation of the powders produced were given in the previous year's report,[12] with some initial results. Further studies have been made using thorium hydride and an ultrafine thoria powder (average particle size 0.04 μ) obtained from Vitro Laboratories. Ball milling was used to comminute the hydride and also to blend the thoria. Some preliminary investigations were necessary to determine a method of producing powders of the finest possible particle size. The effects of ball milling time and the use of ethyl alcohol as a grinding aid on the particle size of the thorium hydride were determined. Particle size analysis indicated that there was no significant effect produced by the use of ethyl alcohol compared to dry milling. Milling of the hydride dry for periods of time to 24 days produced average particle diameters of $\sim 1\ \mu$ at the maximum milling time.

Thorium hydride and 10 vol % thoria were milled together for the same times used in the particle size study. A total of five compacts were made by vacuum hot pressing the powders at 1000°C, with dehydriding occurring concurrently. The compacts were extruded in steel billets with intervening Inconel encasement to reduce alloying between iron and thorium. Extrusion was done at 900°C, with a 9:1 reduction in area. Hot-hardness tests[13] on the extruded bars indicated that the highest degree of hardness at all temperatures was gained by milling the powders for 24 days. Figure 24.10 is an electron micrograph at 84,000X, showing the dispersion of the thoria particles in thorium obtained after 24 days of milling. The particle size of thoria is 0.1 μ or less, and interparticle spacing averages between 0.2 and 0.4 μ. Stress-rupture tests at 800°C have been made on this

[12]J. A. Burka and J. P. Hammond, *Metals and Ceramics Div. Ann. Progr. Rept. May 31, 1962*, ORNL-3313, pp 95–98.

[13]G. Hallerman and R. J. Gray, *Equipment for Hardness Testing at Elevated Temperatures*, ORNL-3448 (in press).

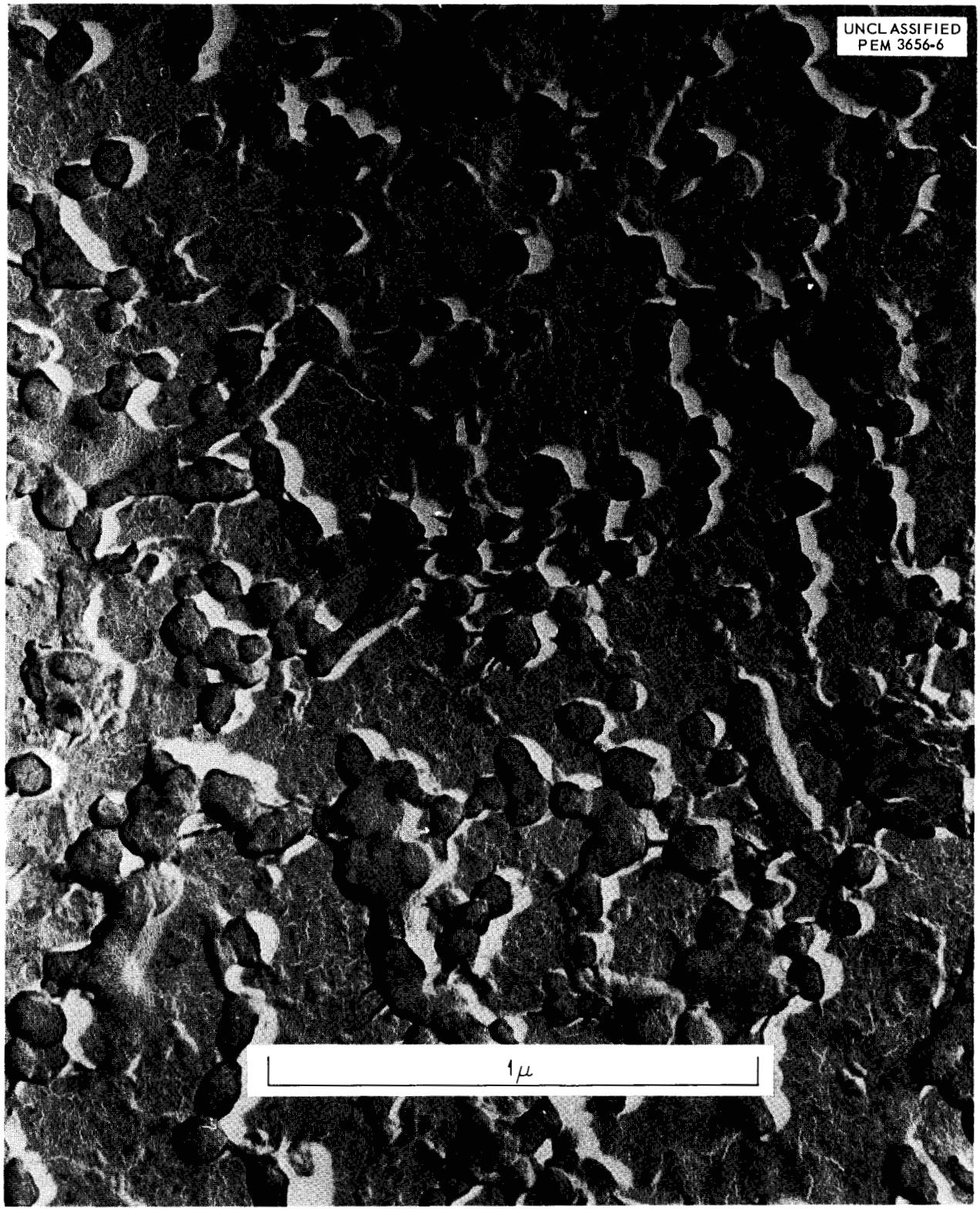

Fig. 24.10. Electron Micrograph of Th–10 vol % ThO_2 Extrusion Prepared from Thorium Hydride and Ultrafine Thoria Ball Milled for 24 Days. Specimen as-polished. PVA carbon replica, chromium shadowed. 84,000X.

extrusion, and the results are given in Table 24.5. For comparison, the best results reported by Cole and Wilkinson[14] for a thorium-base alloy are shown.

These preliminary data show that dispersion-hardened thorium has a creep rate that is one-third to one-sixth of the lowest creep rate reported. The rupture times of the two alloys are similar. A third specimen was tested at 3500 psi but failed prematurely outside the gage length.

Studies on the dispersion hardening of thorium metal powder prepared commercially by calcium reduction have started in an attempt to reduce fuel cycle costs. Initial milling experiments have shown that average particle sizes below 1 μ can be obtained by use of stearic acid as a surfactant to prevent welding of particles together. However, the complete removal of the stearic acid has been unsuccessful, causing embrittlement by the formation of thorium carbides. Other more-volatile surfactants are being tested to eliminate this problem.

Another method investigated for reducing the fuel cycle cost for thorium-base fuels has been the co-reduction of thorium and zirconium oxides to form directly a solution-strengthened thorium-zirconium alloy powder. The alloy powder could be used directly for preparing fuels or given still further strengthening by dispersion hardening. The Y-12 Development Section has prepared eight small batches of the co-reduced powder. The zirconium content ranged from 2.5 to 4.6 wt %, with an intended composition of 5 wt %; oxygen contents were from 0.09 to 0.58 wt %. Attempts to dispersion harden the alloy with additions of thoria have not been successful as yet because of the occurrence of carbide contamination similar to that in the commercial metal powder. Preliminary results on hot pressings of Th–5 wt % Zr alloys prepared from the hydrides of the two elements have shown that dispersion hardening increases the hot hardness of the base alloy by 50% at 800°C.

[14] R. H. Cole and L. E. Wilkinson, *Development of High Strength Ternary and Quaternary Thorium-Uranium Base Alloy*, ATL-A-128 (Nov. 1, 1961) p 138.

THORIA-PELLET DEVELOPMENT

A. J. Taylor R. A. Potter

Investigations directed toward the development of techniques for preparing and characterizing ThO_2 pellets for use in fluidized-blanket systems were terminated during this report period. The results of these investigations were reported[15] and are summarized here.

Fabrication methods were developed whereby pellet density and grain size could be controlled. The effects of these properties on attrition resistance were determined previously.[16]

Coatings of Al_2O_3 and zirconium metal were evaluated on the basis of spouted-bed tests.[17] The coatings were applied to $\frac{1}{8}$-in.-diam ThO_2 spheroids at Battelle Memorial Institute under a subcontract arrangement. In one instance, it was found that an 80-μ coating of Al_2O_3 increased attrition resistance by a factor of 6. However, the lack of integrity displayed by some of the coated pellets suggests that extreme control must be maintained during the coating process.

[15] R. A. Potter and A. J. Taylor, *Status and Progress Report for Thorium Fuel Cycle Development December 31, 1962*, ORNL-3385 (in press).

[16] A. J. Taylor, R. A. McNees, and R. A. Potter, *Metals and Ceramics Div. Ann. Progr. Rept. May 31, 1962*, ORNL-3313, p 74.

[17] Attrition resistance tests performed by S. Reed, Reactor Chemistry Division.

Table 24.5. Stress-Rupture Results at 800°C of Th-ThO_2 and Th-U-Zr Alloy

Stress (psi)	Minimum Creep Rate (%/hr)		Rupture Time (hr)	
	Th–10 vol % ThO_2	Th–5 wt % U–2 wt % Zr	Th–10 wt % ThO_2	Th–5 wt % U–2 wt % Zr
4000	4.0×10^{-3}	2.5×10^{-2}	69.5[a]	143.4
5000	2.8×10^{-2}	9.0×10^{-2}[b]	29.2	40.0[b]

[a] Stress increased to 5000 psi after 65.5 hr at 4000 psi.
[b] Extrapolated data.

25. Advanced Test Reactor

R. J. Beaver

INTRODUCTION

The Advanced Test Reactor (ATR), under construction at the National Reactor Testing Station, was designed to provide additional experimental loop irradiation space for the AEC testing program. Perturbed neutron fluxes exceeding 10^{15} thermal neutrons cm^{-2} sec^{-1} and 1.5×10^{15} epithermal neutrons cm^{-2} sec^{-1} will be produced. The core configuration provides for nine flux-trap regions in a geometry similar to that of a four-leaf clover, with one flux trap in each leaf, one at the intersection of the leaves, and one between each pair of leaves. The nominal power level will be 250 Mw. Oak Ridge National Laboratory is supporting the design effort and has the responsibility of developing the fuel element technology.

FUEL ELEMENT DEVELOPMENT

This program has essentially been completed, and a prebid meeting was held with prospective vendors for the procurement of fuel elements for the Critical Test Facility. The ATR fuel element that was developed is illustrated in Fig. 25.1. The detailed design of this element has been described previously.[1] Since that time, modifications were made to strengthen the overall component to better resist the hydraulic forces anticipated in the reactor when exposed to the water coolant velocity of 45 fps. The thickness of the top plate was increased from 0.080 to 0.100 in., and 6061-0 aluminum was substituted as the cladding in preference to the weaker X8001 type aluminum.

[1]R. J. Beaver, *Metals and Ceramics Div. Ann. Progr. Rept. May 31, 1962*, ORNL-3313, p 15.

The objectives of the fabrication development have been mainly to determine the feasibility of (1) roll cladding the long fuel plates to the desired dimensional specifications, (2) forming plates to exact and reproducible radii of curvature, and (3) assembling and mechanically joining elements to within the required spacing and other dimensional tolerances. It was also desirable that fuel homogeneity and bonding of the plates be evaluated by nondestructive techniques. An appreciable portion of the program was devoted to preparing fuel element specimens for associated testing programs.

Powder Metallurgical Preparation of Fuel Cores

W. J. Werner T. D. Watts

In the ATR fuel element, the width of the fuel sections increases from plate No. 1 (the narrowest plate) to plate No. 19 (the widest plate). To conserve die costs during development, only three types of fuel cores were made rather than a core for each specific plate. By cross rolling these cores when roll cladding the plates, it was possible to fabricate plates with the required dimensions. In order to produce a 48-in. length in the finished product, most plates required two cores in tandem. Details of the processing have been reported previously.[2] Briefly, U_3O_8 (−100 +325 mesh particle size) is blended dry with −100 mesh X8001 powder and pressed into compacts (dimensions are listed in Table 25.1).

Previous experience had shown that it was important to control variations of thickness in any

[2]R. L. Heestand, C. F. Leitten, Jr., and R. W. Knight, "Fabrication Development of the Advanced Test Reactor Fuel Element," pp 315–36 in *Research Reactor Fuel Element Conference, September 17–19, 1962, Gatlinburg, Tennessee*, TID-7642, bk 1, (1963).

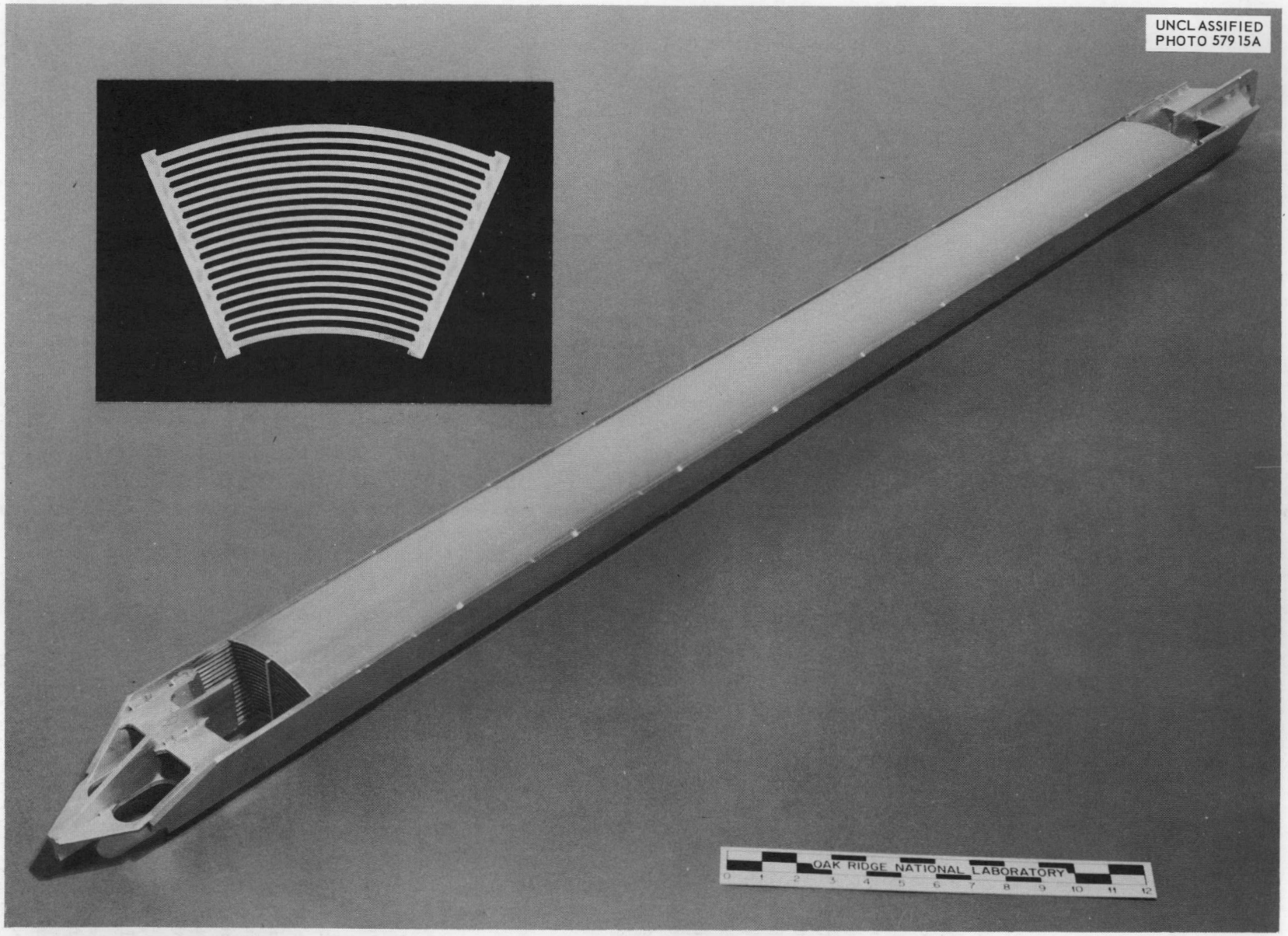

Fig. 25.1. Overall View of ATR Fuel Element.

Table 25.1. Pertinent Design Parameters in Fabricating ATR Fuel Plates

Plate Number	Type of Core[a]	Number of Cores per Plate	Core Thickness (in.)	Thickness Reduction Ratio During Cross Rolling	Total Thickness Reduction Ratio
1	A	1	0.320	1.00/1	14/1
2	A	1	0.330	1.081/1	14.6/1
3	A	1	0.348	1.132/1	15.4/1
4	A	1	0.365	1.183/1	16.1/1
5	B	2	0.191	1.024/1	8.4/1
6	B	2	0.200	1.035/1	8.9/1
7	B	2	0.208	1.129/1	9.4/1
8	B	2	0.217	1.165/1	9.9/1
9	B	2	0.226	1.224/1	10.4/1
10	B	2	0.235	1.282/1	10.9/1
11	B	2	0.243	1.329/1	11.3/1
12	B	2	0.252	1.354/1	11.1/1
13	C	2	0.298	1.022/1	13.9/1
14	C	2	0.308	1.044/1	14.4/1
15	C	2	0.318	1.072/1	14.8/1
16	C	2	0.328	1.109/1	15.3/1
17	C	2	0.338	1.153/1	15.8/1
18	C	2	0.348	1.199/1	15.4/1
19	A	2	0.297	1.007/1	14.3/1

[a]A cores, 1.655 × 3.47 in.; B cores, 2.059 × 2.795 in.; and C cores, 2.880 × 1.750 in.

individual core to avoid "rainbowing" of the plate when rolled. Recently it was also found that, because of density variations from one core to another, difficulty was experienced in rolling plates to within the specified length tolerances. By increasing the pressing pressure from 33 to 45 tons/in.^{2} and by improving the dimensional tolerances of the die components, it was possible to produce 95% of the fuel cores with a theoretical density of (93.5 ± 0.5)% and with thickness variations within ±0.002 in.

Fuel Plate Fabrication

D. O. Hobson C. F. Leitten, Jr.

Changes in fuel element design and selection of type 6061 aluminum as the cladding material necessitated additional evaluation of the ATR fuel plate fabrication process.

The basic process for roll cladding the modified ATR fuel plates was essentially the same method reported previously, with the exception that 5%

Alclad 6061 was substituted for X8001 aluminum[3] as the frame and cladding. Alclad 6061 aluminum was selected instead of conventional 6061 grade to ensure more complete bonding by having type 1100 aluminum at the mating surfaces. The hot-rolling and annealing temperature was 500°C; and, as mentioned previously, to produce plates to the specified widths, different degrees of cross rolling and other variations in processing parameters were required. These are listed in Table 25.1.

By applying experience developed on the HFIR and Fuel Element Development Projects, no unusual difficulties were experienced in fabricating the 6061-clad plates. Blister rejections were less than 1% in the 210 fuel plates produced. Of these plates, 98.6% were rolled to within the desired fuel section width tolerances. Only 63.8% were rolled to within the length specifications, but variations in fuel core densities (which have subsequently been controlled) were mainly responsible for the low yield. There is little question that on a production basis, having once established the process and taking advantage of the plate thickness tolerance, yields as high as 95% or possibly better are likely.

The homogeneity of the U_3O_8 in aluminum appears, in most cases, to be adequate, based on radiographic inspection and confirmed in part by chemical samples from several fabricated plates. These data indicate that a variation of ±20% (in a local area of 0.080 in. diam) from the nominal concentration is possible. The results also revealed that the fuel concentration at the interface between the two tandem cores was always considerably lower than the nominal fuel concentrations. Additional information by the nondestructive technique of x-ray attenuation scanning will provide a better basis for a more quantitative evaluation.

[3]M. M. Martin and R. L. Heestand, *Metals and Ceramics Div. Ann. Progr. Rept. May 31, 1962*, ORNL-3313, pp 83–85.

Fuel Plate Forming

J. H. Erwin C. F. Leitten, Jr.

The main effort in forming ATR fuel plates has been directed to low-pressure marforming (a process in which the plate is placed on a flat bed of rubber and pressed with a steel ram contoured to a fixed radius). In low-pressure marforming, pressure is generally limited to a range of 800 to 1600 psi. The development of this forming method for the ATR element is complicated by having 19 different entities, since each plate in this fuel element has its own specific radius, which is approximately 0.130 in. different from its neighboring plates in the element. Control must be exercised to reproducibly form each type of plate to its specific radius. This causes difficulty in forming since variations in curvature are not the same in each

Table 25.2. Effect of Prior Cold-Working History on Forming of ATR Fuel Plates in Two-Strike Marforming

	Maximum Variation of *h* in Any Individual Plate (in.)	Maximum Variation of *h* in a Group of Plates (in.)	Maximum Variation in Radius in a Group of Plates (in.)	Average Radius in a Group of Plates (in.)	Intended Plate Radius (in.)
Plates Cold Worked 7.4% Followed with a 500°C Anneal[a]					
Preformed	0.013	0.025	0.144	4.630	
Final formed	0.015	0.018	0.066	4.500	4.503
Plates Cold Worked 20% Followed with a 500°C Anneal[a]					
Preformed	0.003	0.006	0.074	4.783	
Final formed	0.003	0.006	0.053	3.991	3.985

[a]Data based on six plates.

plate and therefore fail to compensate for each other as they do in MTR-type fuel elements. It is also important that, within a group of plates of a specific radius, acceptable reproducibility must be maintained.

Other results (reported in Part II, Chap. 16, this report) revealed that introduction of 20% cold work into U_3O_8-Al fuel plates, prior to the final annealing, aided reproducible plate forming. The data presented in Table 25.2 show the effectiveness of this development when translated to forming ATR fuel plates. The parameter used to detect reproducibility is the chord height *h*, and the reported radii are calculated from the conventional equation relating chord height and length. Neither the *h* values shown for 7.4% cold-worked plates nor the variation in radius are acceptable. By re-forming the plate, a significant improvement occurred in the variation in radius from one plate to another, and it was possible to form to the desired radius within tolerable limits. However, deviations in the *h* values were not satisfactory. By an increase in the amount of cold working during fabrication of the plate from 7.4 to 20%, the *h* variations were also brought to acceptable levels, and an additional improvement in the radius variation occurred. Thus, a process which appears feasible in forming ATR fuel plates is that of (1) preforming the plate to a somewhat larger radius than desired; (2) measuring the plate radius; (3) from experimental data, selecting the die radius that will produce the final plate radius desired; and (4) re-forming to the desired radius.

Fuel Element Assembly

R. W. Knight[4] C. F. Leitten, Jr.

The fuel element specifications require that any individual measurement of channel spacing differ no more than ±0.010 in. and the average for any channel no more than ±0.006 in. from 0.78 in. Twist and bow in the element must be limited to <0.015 in. The plates are mechanically joined to side pieces, and the strength of the joint must be a minimum of 150 lb per lineal inch.

The basic process and equipment for mechanically joining fuel plates to side plates have been reported in detail previously.[5] The procedure is shown schematically in Fig. 25.2; briefly, it consists in assembling plates in the grooves of the side plates and mechanically rolling the edge of the land into the edge of the fuel plate, in effect, "cold welding" the fuel plate to the side plate. Notches in the land edge keep the swager in position as it rolls horizontally along the joint; thus a uniform force is maintained, and good quality control is exercised. A typical roll-swaged joint is also depicted in this illustration. The equipment for this process has been improved by modifications that (1) maintain constant load in forming the joint by using air pressure instead of a spring and (2) increase production by roll swaging both edges of the plate simultaneously. Another added feature is a fuel plate holddown fixture that maintains the plate in position during roll swaging, thus allowing better control of the plate spacings. These improvements are illustrated in Fig. 25.3.

[4]On loan from Engineering and Mechanical Division.

[5]R. L. Heestand, C. F. Leitten, Jr., and R. W. Knight, "Fabrication Development of the Advanced Test Reactor Fuel Element," pp 315–16 in *Research Reactor Fuel Element Conference, September 17–19, 1962, Gatlinburg, Tennessee*, TID-7642, bk 1 (1963).

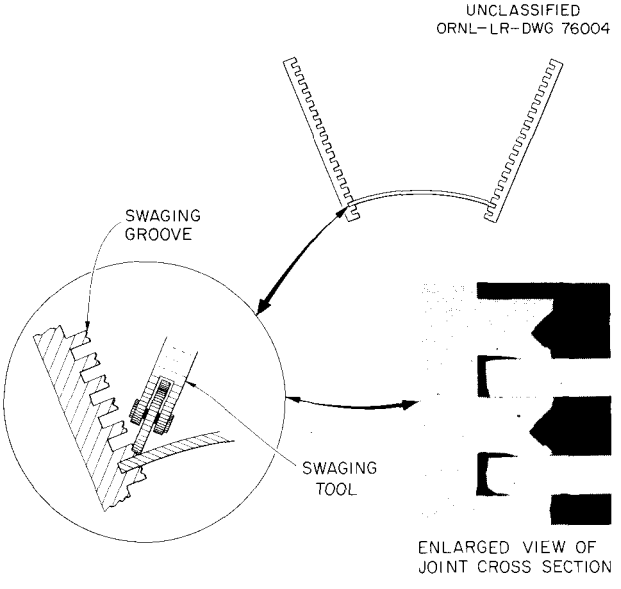

Fig. 25.2. Roll-Swaging Attachment Process Used for Joining Fuel Plates to Side Plates in the ATR Fuel Element.

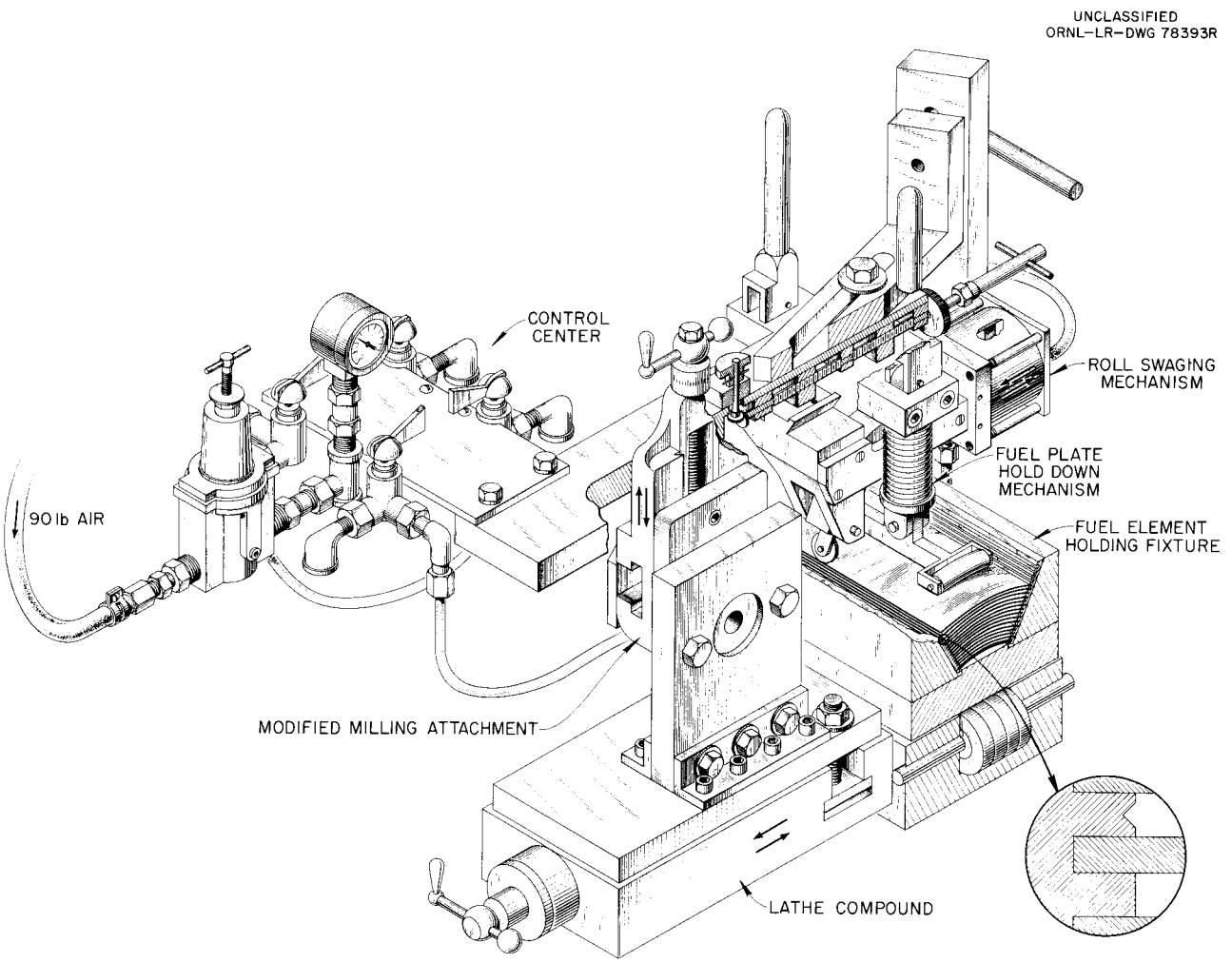

Fig. 25.3. Improved Fixture for Assembling and Joining ATR Fuel Element.

Table 25.3. Optimum Groove Depth and Width

Fuel Plate Thickness (in.)	Groove Depth (in.)	Groove Width (in.)	Strength (lb/lineal in.)
0.050	0.070	0.057	300
0.080	0.100	0.087	350
0.100	0.100	0.107	500

Studies were conducted to select optimum depth and width (dimensions) for the grooves in the side plate. From these studies the dimensions given in Table 25.3 were found to be optimum for producing maximum joint strengths, which ranged from 300 to 500 lb per lineal inch, using an air pressure of 50 psi or a calculated tool force of 353 lb. Six elements have been assembled and mechanically joined, with final dimensions well within the specifications. It is anticipated that several more will be produced before this project is completed.

MECHANICAL PROPERTIES

W. R. Martin J. R. Weir

The tensile, creep, and other pertinent mechanical properties of the fuel plates have been reported

previously.[6,7] The creep properties of X8001 cladding, the U_3O_8-Al dispersions, and the composite fuel plate in uniaxial tension were measured in the temperature range 400 to 600°F for maximum strains of 1.0% and times of 450 hr. The tensile properties were measured from 70 to 500°F.

The fuel dispersion is stronger in creep than the X8001-0 cladding material. The creep strength of the fuel plate in uniaxial tension is intermediate between the strength of the dispersion and the cladding. The tensile strength of the fuel dispersion is approximately twice that of the X8001-0. The tensile strength and ductility of the fuel plate are limited by the low ductility of the fuel dispersion.

Recently, additional studies have been made to establish a relation between static recovery of cold-worked 6061 and age-hardened 6061 aluminum alloys to the T6 condition. Room-temperature hardness was used to determine percent recovery of these materials after heat treatment for 1, 10, 100, and 500 hr at 150, 200, 250, and 300°C respectively.

The Larson-Miller parameter θ was calculated using the relation

$$\theta = T(C + \log t) ,$$

where

θ = Larson-Miller parameter,

T = exposure temperature (°K),

C = material constant (17.7 for this alloy),

t = time of exposure (hr).

The relation is presented in Table 25.4. This information should prove useful in predicting recovery in cold-worked 6061 or age-hardened 6061 aluminum alloy while exposed at elevated temperatures. For example, in an actual yield-strength test, 6061-T6 showed 9% recovery after 10 hr at 232°C. The data available in Table 25.4 would have predicted 10% recovery.

NONDESTRUCTIVE TESTING

R. W. McClung

The desirable homogeneity and nonbond specifications for the ATR fuel plate are quite similar to the HFIR fuel plate requirements. X-ray attenuation techniques for detection of fuel homogeneity and through-transmission ultrasonic techniques for nonbond surveys of plates have been mainly developed on other programs and are reported elsewhere in this report (Part II, Chap. 18, and Part III, Chap. 22).

Scanning of ATR fuel plates for fuel homogeneity by x-ray attenuation has not been initiated although standards have been prepared and fixturing equipment procured. It is expected that a statistical

[6] W. R. Martin, *Metals and Ceramics Div. Ann. Progr. Rept. May 31, 1962*, ORNL-3313, p 34.

[7] W. R. Martin and J. R. Weir, "Mechanical Properties of X-8001 Aluminum Cladding and X8001 Aluminum-Base Fuel Dispersion at Elevated Temperatures," pp 549–64 in *Research Reactor Fuel Element Conference, September 17–19, 1962, Gatlinburg, Tennessee*, TID-7642, bk 2 (1963).

Table 25.4. Static Recovery of 6061 Aluminum Alloy

Alloy Condition	θ Necessary to Obtain a Given Percent Recovery for 6061 Aluminum (% Recovery)					
	10	20	30	40	50	60
6061-0						
5% cold worked	10,700	11,500	11,700	11,800	11,950	12,100
10% cold worked	11,200	11,700	11,900	12,050	12,200	12,300
25% cold worked	10,500	10,850	11,150	11,400	11,600	11,800
50% cold worked	9,150	9,800	10,100	10,300	10,350	10,450
6061-T6	9,450	9,900	10,250	10,450	10,600	

number of plates will be evaluated before the close of this program.

Several ATR fuel plates have been scanned by the through-transmission ultrasonic method using $\frac{1}{16}$-, $\frac{3}{32}$-, and $\frac{1}{8}$-in. artificial nonbonds as reference standards for response comparison and equipment calibration. It has been found that the average background variation in ultrasonic transmission due to core variables is slightly less than that caused by a $\frac{1}{16}$-in. nonbond. On plates run thus far, only a few nonbonds have been detected which were equal to or greater than $\frac{1}{16}$ in. in diameter. It will be necessary, however, to examine a large sampling of plates before firm conclusions can be reached on realistic sensitivity levels.

26. Army Package Power Reactor

R. J. Beaver

INTRODUCTION

To support the materials field of the Army Package Power Reactor (APPR) program, effort was originally directed toward advancing the technology of UO_2–stainless steel dispersion fuels, as well as burnable-poison and neutron absorber materials, the major constituents of typical Army reactor cores.

The initial core loading for the first Army reactor, designated SM-1, was fabricated by the Metals and Ceramics Division. The fuel element consists of 18 composite plates containing a dispersion of 26.16 wt % UO_2 and 0.23 wt % B_4C in type 302, grade B stainless steel.

This program is undergoing a change in direction that should become even more pronounced in the coming year. Until recently, the principal effort has been directed toward improving the fuel elements and control rods for reactors using the flat-plate, stainless steel dispersion element that is similar to the SM-1. Future materials work for the APPR program will be concentrated on systems adaptable to standard plant concepts and, most likely, to those using tubular fuel elements.

During the past year, the fuel element work has consisted primarily of hot-cell examinations of fuel elements that have been irradiated to burnups beyond design expectations. Irradiated fuel plate samples were studied to further understand radiation damage in such dispersions. The second area of study has been that of burnable-poison and control materials. New materials for such applications have been developed and tested. Engineering assistance has been provided to the Army Power Reactor Branch in their fuel element procurement.

CONTROL AND POISON MATERIALS

Europium Oxide Consolidation Studies

C. F. Leitten, Jr. R. E. McDonald

The basic process developed for consolidating Eu_2O_3 for use as a control material in the APPR involved the hydrogen-atmosphere high firing of the as-received material and subsequent hand crushing of the conditioned oxide to the desired particle-size range. Experience has shown that the consolidation of Eu_2O_3 by this method often resulted in oxide particles with varying densities and with varying physical and chemical characteristics. In addition, the processing costs of the oxide are relatively high. A program was therefore initiated to explore the possibility of consolidating Eu_2O_3 by arc melting in an effort to reduce the consolidation costs and to improve the reproducibility of the oxide particle density and characteristics.

Exploratory studies were conducted using Lindsay Mix (a rare-earth mixture of gadolinium and samarium oxides) as a substitute for the europium oxide to reduce costs. The initial attempt to melt the compacted Lindsay Mix by a tungsten arc resulted in severe arc scatter and the subsequent reaction with, and pitting of, the copper hearth. The arc scatter was attributed to the extremely low surface tension of the molten oxide. The use of a deep, hemispherical mold cavity greatly reduced the arc scatter since it prevented the spreading out of small droplets of the oxide mixture. Electropolishing the hearth prior to melting minimized wetting of the hearth by the Lindsay Mix. During the initial phase of melting, the oxide vaporized some, but the evaporation rate decreased rapidly after the mixture became consolidated. That the total amount of

oxide vaporized during the consolidation was low is demonstrated by the fact that it was not sufficient to obstruct viewing of the melt through the chamber sight port. Complete fusion of a 30-g pellet of the mixed oxides was accomplished at a power level of approximately 300 amp at 15 v.

The present arc-melted oxides are vitreous in nature but slightly deficient in oxygen. Experiments have shown that the oxygen can be restored easily to the stoichiometric value by heating the crushed fused oxide in an oxidizing atmosphere at 1000°C. The fused oxide pellets can be readily attritioned in a mechanical disk grinder to various desired particle size ranges ($<10\ \mu$) with a minimum of fines.

The arc-melting practice is also amenable to the production of the more-corrosion-resistant compound $Eu_{5.3}MoO_{11}$. Although this compound can be made by another process, reported previously,[1,2] the method is inherently expensive because of the high cost of crucibles. Employing procedures developed to arc melt Eu_2O_3, a mixture of 85% Eu_2O_3–15% MoO_3 was successfully melted. Little material loss was encountered in melting, particularly after the initial consolidation of the material. The compound, like arc-melted Eu_2O_3, is slightly deficient in oxygen but can be restored by a similar oxidizing treatment.

Cursory experiments indicated that this material could also be shape-cast into small-diameter cylinders such as would be required for use as a lump control material. Figure 26.1 shows such a casting.

Based on these initial studies, attempts were also made to arc-fuse pellets of Sm_2O_3 and Eu_2O_3. Both these materials behaved similarly to the Lindsay Mix, except that stabilization of the melting arc became a problem. Better arc stability was attained with 20 mm of high-purity argon flowing through the furnace. The addition of the argon also reduced vaporization. There is little question that melting parameters can be established to produce large quantities of oxide by this arc-fusion technique with minimum hearth contamination and a high recovery.

[1]R. A. Potter and R. A. McNees, *Metals and Ceramics Div. Ann. Progr. Rept. May 31, 1962*, ORNL-3313, pp 76–77.

[2]R. A. Potter, *Army Reactors Program Ann. Progr. Rept. Oct. 31, 1962*, ORNL-3386, pp 16–18.

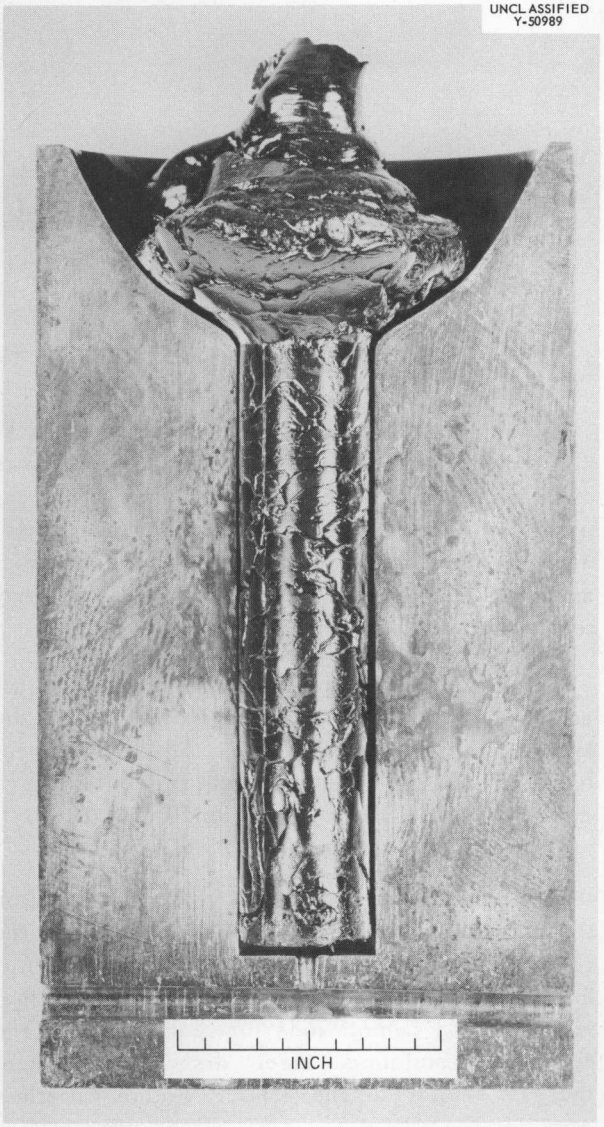

Fig. 26.1. Cast Rare-Earth Oxide Rod. Such a casting would be ideal for use as a bulk poison.

Europium Oxide Stability Studies

R. A. Potter

Investigations of the aqueous corrosion resistance of Eu_2O_3 as used in Eu_2O_3-bearing stainless steel absorber plates in contact with 250°C water were continued.[1] A method was developed for stabilizing the oxide against corrosion in the event a plate becomes defective. Details of the investigations have been reported[2] and are summarized here.

Mixtures of Eu_2O_3 and 15 wt % MoO_3, heated in air, reacted to form a single phase, which was identified by x-ray diffraction[3] as a face-centered cubic structure with a parameter of 5.43 A. Pellets made from the compound ($Eu_{5.3}MoO_{11}$) were tested for aqueous corrosion resistance in 100°C water for periods up to 1250 hr and were found to be essentially inert. In 250°C water a weight gain of only 4% was observed after 850 hr. The pellets remained physically intact, and there were no visible signs of attack.

It was found that WO_3 could be substituted for MoO_3, with the resultant formation of a similar face-centered cubic compound.

Irradiation Testing of Stainless-Steel-Clad Dispersions of Eu_2O_3

A. E. Richt C. F. Leitten, Jr.

Irradiation testing results on miniature stainless-steel-clad Eu_2O_3 dispersion absorber plates continue to be encouraging.[4] Specimens containing 20, 30, or 40 wt % Eu_2O_3 dispersed in stainless steel have been irradiated in the ETR at surface temperatures of 170°F to exposures of up to 4.5×10^{21} nvt (unperturbed), with no evidence of dimensional or structural changes. A comparison of microstructures of unirradiated and irradiated dispersions of 40 wt % Eu_2O_3 in stainless steel after an estimated exposure of 4×10^{21} thermal neutrons/cm^2 is shown in Fig. 26.2(*a*), unirradiated sample, and (*b*), irradiated sample. A complete absence of any reaction between the two phases may be noted. The absence of irradiation damage is further confirmation that silicon in the stainless steel matrix was probably responsible for the damage observed previously in this system by KAPL.[5] The stainless steel used for the ORNL samples contained less than 0.02 wt % Si.

Postirradiation corrosion tests on sections from these specimens have shown that samples containing 30 and 40 wt % Eu_2O_3 cores are susceptible to gross swelling when exposed to water at 570°F and 1200 psi pressure for short periods of time.[6] However, as shown in Table 26.1, corrosion tests on both irradiated and control specimens indicate that swelling is predominantly a function of the Eu_2O_3 loading; irradiation, even at these high burnups, has no effect on the swelling characteristics of the defected specimen. Microstructural examination of the corrosion-tested specimens showed that, even though the Eu_2O_3 was exposed to the water of the autoclave and hydration effects were observed, no leaching of the Eu_2O_3 could be seen. This was also confirmed by analysis of the water after the test. The possibility of a cladding failure in the SM-1 neutron absorber plate is remote because of the nature of the fabrication process and the thick

[3]X-ray diffraction performed by L. A. Harris of the X-Ray Diffraction Group.

[4]A. E. Richt, *Army Reactors Program Ann. Progr. Rept. Oct. 31, 1962,* ORNL-3386, pp 84–88 (Apr. 2, 1963).

[5]W. K. Anderson and D. N. Dunning, *Nucl. Sci. Eng.* 4(3), 458–66 (September 1958).

[6]C. F. Leitten, Jr., and A. E. Richt, *Metals and Ceramics Div. Ann. Progr. Rept. May 31, 1962,* ORNL-3313, p 88.

Table 26.1. Corrosion-Test Results on Defected Eu_2O_3 Dispersions in Water at 570°F and 1200 psi Pressure

Specimen No.	Unperturbed Dose (*nvt*) $\times 10^{21}$	Weight Change (%)	Thickness Change (%)
	20 wt % Eu_2O_3		
2 (control)		+0.03	0
39-1	7.0	+0.04	+0.9
39-2	12.1	+0.01	+0.8
39-3	28.4	+0.05	+2.5
39-4	45.0	+0.04	+0.7
	30 wt % Eu_2O_3		
39-5	7.6	+0.42	+13.3
39-6	14.6	+0.62	+15.4
39-7	27.9	+0.71	+11.3
39-8	45.0	+0.61	+12.0
	40 wt % Eu_2O_3		
4 (control)		+1.53	+27.3
39-9	7.2	+0.24	+34.0
39-10	14.8	+1.58	+30.5
39-11	28.7	+1.51	+31.3
39-12	42.8	+1.60	+29.5

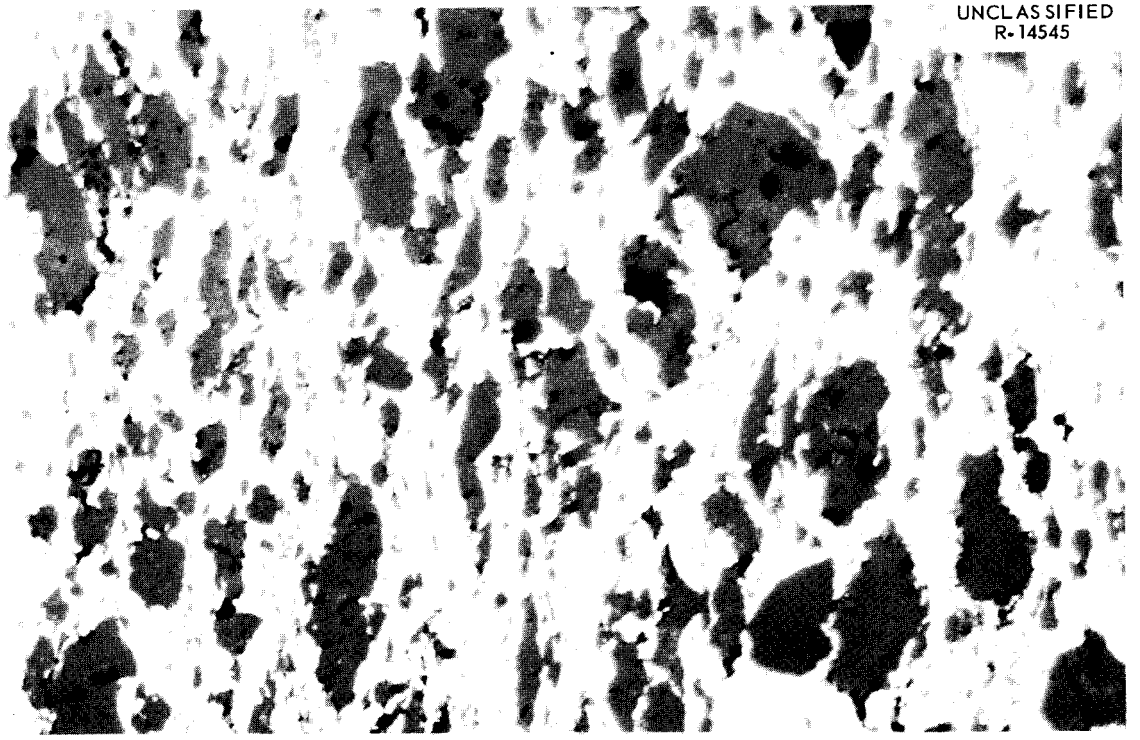

(*a*)

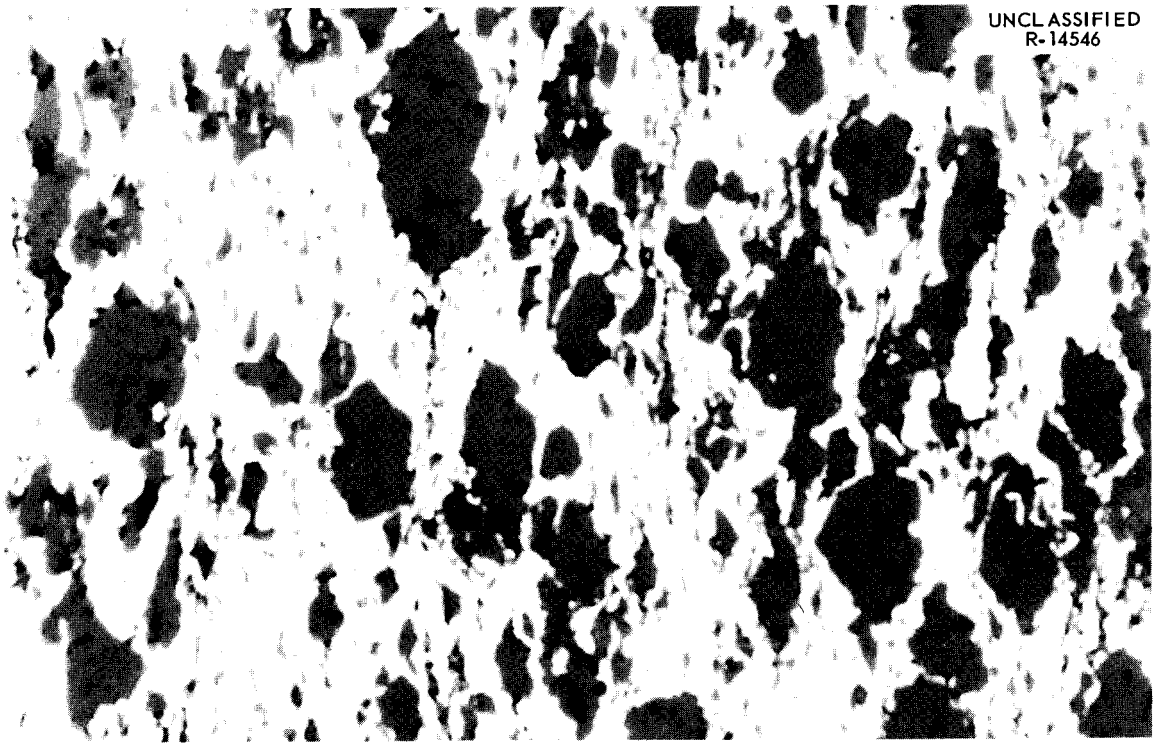

(*b*)

Fig. 26.2. Stability of Irradiated Eu_2O_3–Stainless Steel Dispersions. Note absence of any reaction around Eu_2O_3 particles. (*a*), unirradiated sample; (*b*), irradiated sample.

cladding. If a defect occurred, it is extremely unlikely that the failure would be catastrophic.

FUEL MATERIALS

Postirradiation Examination of SM-1 Core 1 Fuel Elements

A. E. Richt

The effects of irradiation on the dimensional stability and structural integrity of SM-1 core 1 fuel elements are being studied. In this work, fuel elements are subjected to a thorough post-irradiation examination after various exposures in the active lattice of the SM-1 reactor. As reported previously,[7,8] two stationary fuel elements (S-72 and S-79) have been examined after 10.5 and 16.4 Mwyr of reactor operation respectively. The examination of a third fuel element (S-81) is under way. This element was removed from the reactor core after 19.5 Mwyr of operation, 30% beyond designed core life.

Preliminary results of the examination of fuel element S-81 indicate that rippling of the two outer fuel plates of the assembly was more severe than that noted in the examination of the previous elements.[9] Changes in the thickness of individual fuel plates were found to be directly proportional to burnup, with increases of 0.003 in. being noted in regions of maximum burnup. For a nominal 0.030-in.-thick fuel plate, this represents a 10% increase in plate thickness at 62% depletion of U^{235} (2.2×10^{21} fissions/cm^3). Metallographic examination revealed no evidence of matrix cracking or gross deterioration of the UO_2 fuel dispersion. The frequency of cracks in the cladding was significantly greater than that noted in previous examinations. Occasionally, the cracks propagated through the cladding to the surface of the fuel section; however, in no instance did they penetrate any further.

Postirradiation Examination of SM-2 Fuels Development Specimens

A. E. Richt

The postirradiation examination of 34 plate-type miniature fuel specimens from the SM-2 fuels development program has been completed.[10] These specimens, fabricated and irradiated by Battelle Memorial Institute (BMI), contained cermet fuel cores of either 34 wt % UN or 24, 26, or 38 wt % UO_2 dispersed in and clad with type 347 stainless steel. The fuel cores also contained various additions of B_4C, NbB_2, or ZrB_2 as a burnable poison. The specimens were irradiated in the ETR in six NaK-filled capsules which were designed to maintain the surface temperature of the specimens at 600°F.[11]

Postirradiation examination results revealed that 11 of the 34 specimens were damaged in degrees varying from blistering to complete disintegration. However, these failures appear to be mainly related to the fact that, at some times during the irradiation, temperatures of several specimens far exceeded 600°F. Although the results are clouded by the questionable thermal histories, examination of the undamaged specimens revealed that the 24 and 26 wt % UO_2 cermets can sustain a U^{235} depletion of 67% (2.6×10^{21} fissions/cm^3) at surface temperatures of approximately 600°F, with adequate dimensional stability and no loss of structural integrity. The changes in microstructure were similar to those previously found in the examination of the SM-1 fuel elements.[8] As shown in Fig. 26.3, the density of the 24 and 26 wt % UO_2 fuel cores appears to decrease linearly with increasing burnup at a rate corresponding to approximately 4.3% per 10^{21} fissions/cm^3. Within this range of burnups, the growth rate appears to be independent of the type of UO_2 (spherical and hydrothermal) used in fabrication of the cermet fuel cores. Reactions with the stainless steel matrix were found with

[7] *APPR Ann. Progr. Rept. Jan. 31, 1960*, ORNL-2907, pp 37–41.

[8] A. E. Richt, *Army Reactors Program Progr. Rept.*, ORNL-3231, pp 33–38 (Jan. 31, 1962).

[9] A. E. Richt, *Army Reactors Program Ann. Progr. Rept. Oct. 31, 1962*, ORNL-3386, pp 82–84.

[10] A. E. Richt and L. D. Schaffer, *Army Reactors Program Ann. Progr. Rept. Oct. 31, 1962*, ORNL-3386, pp 53–82.

[11] D. B. Hamilton *et al.*, *Irradiation-Capsule Study for SM-2 Reference and Alternate Dispersion Fuels*, BMI-1916 (May 25, 1961).

the UN fuels and ZrB_2 poisons.[10] No reaction was noted with Eu_2O_3, confirming the data in the previous section.

An additional discussion of the effects of irradiation on dispersion fuels may be found in Part III, Chap. 27, this report.

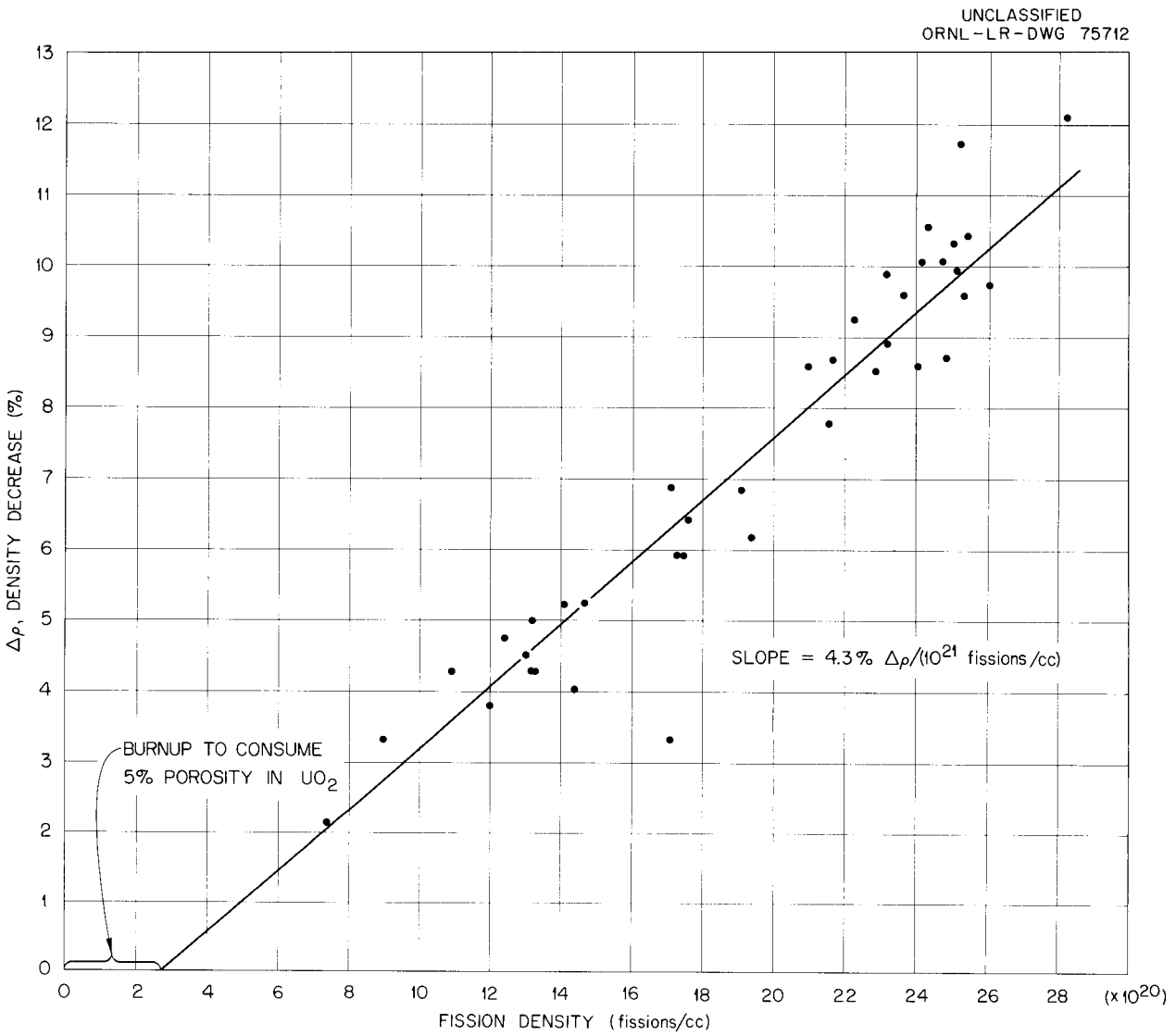

Fig. 26.3. Matrix Swelling of UO_2–Stainless Steel Dispersion Fuels Irradiated at <700°F.

27. Enrico Fermi Fast-Breeder Reactor

W. C. Thurber R. J. Beaver

INTRODUCTION

The Laboratory has been working with Atomic Power Development Associates (APDA) in developing an improved fuel element for use as core B in the Enrico Fermi Reactor. This fuel element is for service in sodium at temperatures up to 900°F. The element consists of brazed bundles of 14 stainless-steel-clad plates, each fueled with a dispersion of 35 wt % spheroidal UO_2 in a type 347 stainless steel matrix. The major efforts at ORNL during the past year consisted in demonstrating the developed fabrication techniques by fabricating elements for test by APDA and in conducting an irradiation testing program.

FUEL ELEMENT FABRICATION

R. G. Donnelly

The Fermi core B fuel elements, which contain 14 plates of UO_2 dispersed in stainless steel as well as a complexity of other components, are furnace brazed in a dry hydrogen atmosphere or vacuum in a single brazing operation.[1] As a result of the developmental work completed this year, procedures have been worked out to fabricate these complex fuel elements. Seven prototype fuel-bearing elements have been assembled and have met all tolerances and requirements imposed by APDA[2] except for two problem areas: (1) the stack-up height of 2.270 ± 0.005 in. and (2) the coolant channel width of 2.246 ± 0.002 in.

The stack-up height problem results from a buildup of tolerances on the 14 fuel plates and 13 layers of wire spacers. Of the seven prototype fuel elements fabricated, none exhibited a measurement below the nominal, four were within +0.005 in., and the remaining three were within +0.010 in. Stack-up heights this close to the nominal, however, could only be obtained by using very high bolting forces, which hindered flow of the brazing alloy. This does not appear to be a serious problem and should be solved by reducing the thickness of the spacers by only ½ mil. This small change will not affect the plate spacing tolerance.

The internal coolant channel widths were measured on the last element with a newly developed caliper device with an eddy-current coil developed by the Nondestructive Testing group (Fig. 27.1). The correct channel width was held when the spacers were spot-welded to the plates. However, after the element components were bolted into the assembly fixture and brazed, only about 50% of all measurements were within the acceptable ±0.002-in. range and about 90% were within ±0.005 in. from nominal.

A topical report[3] relates all procedures and techniques used in fabricating this complex fuel element and also details recommendations for further work needed to eliminate the few problems remaining.

[1] R. G. Donnelly, *Metals and Ceramics Div. Ann. Progr. Rept. May 31, 1962*, ORNL-3313, pp 114–15.

[2] J. G. Duffy, "Core B Design Data and Description," Appendix C in *Minutes of the Fourth Semiannual Information Meeting of the ORNL Fast Breeder Assistance Program*, Atomic Power Development Associates, Inc., 1961.

[3] R. G. Donnelly, W. C. Thurber, and G. M. Slaughter, *Development of Fabrication Procedures for Core B Fuel Elements for the Enrico Fermi Fast Breeder Reactor*, ORNL-3475 (in press).

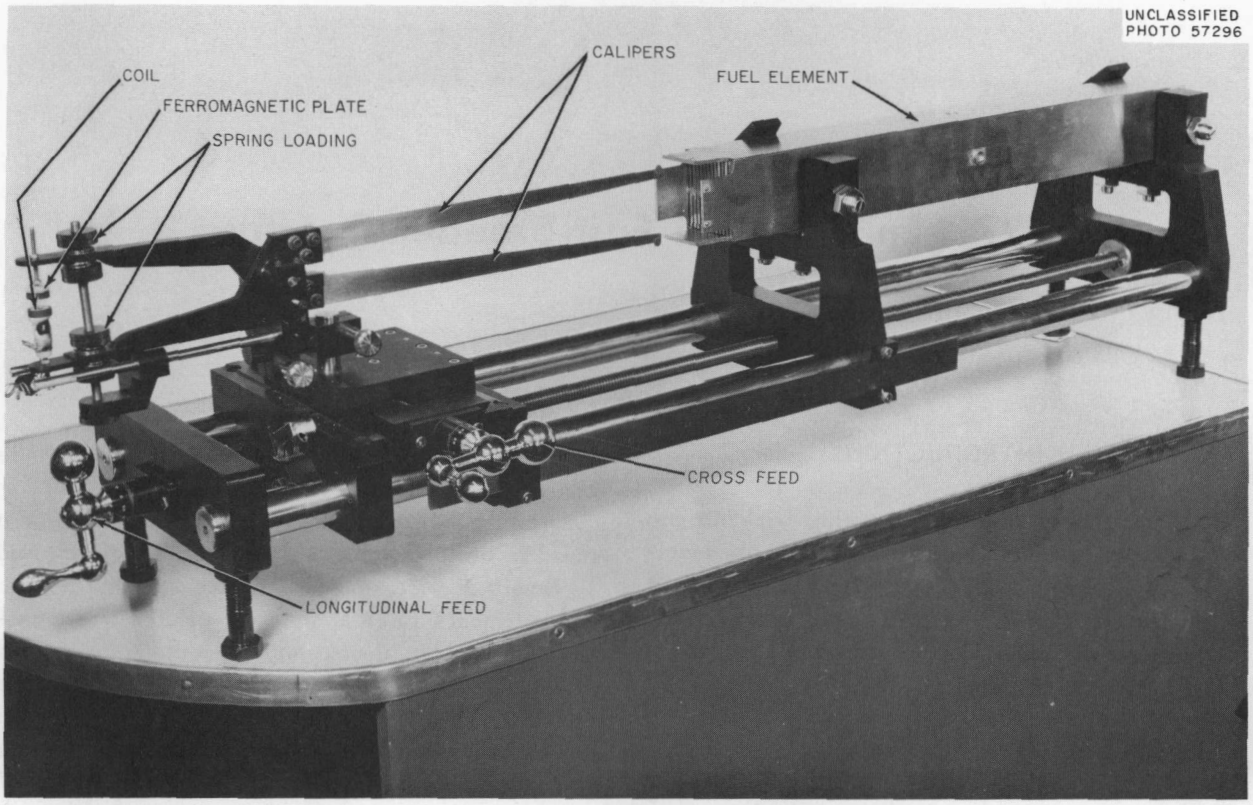

Fig. 27.1. Partially Completed Enrico Fermi Core B Fuel Element with Instrument Used for Measuring Internal Coolant Channel Widths.

IRRADIATION TESTING OF FERMI CORE B MINIATURE FUEL SPECIMENS

W. C. Thurber F. R. McQuilkin[4]

As previously noted, the fuel element selected for core B of the Enrico Fermi Fast Breeder Reactor consists of a brazed array of 14 flat plates, each containing approximately 35 wt % ($27\frac{1}{2}$ vol %) spheroidal UO_2 dispersed in and clad with type 347 stainless steel. The reference plates are 0.112 in. thick and have 0.005 in. of cladding on either surface. One of the major criteria in the selection of this fuel system was the proven irradiation stability of UO_2–stainless steel dispersion fuel over wide ranges of temperature and burnup. Thermal and nuclear analyses of core B indicate that the flat-plate fuel elements should operate at a nominal maximum center-line temperature of 1040°F to a throughput fission burnup of 20% of the U^{235} atoms (12.5×10^{20} fissions/cm^3). The peak center-line temperature including hot-channel factors to a three-sigma limit would increase this temperature approximately 100°F, and the peak burnup would be on the order of 25% of the U^{235} atoms (15.5×10^{20} fissions/cm^3). To provide experimental confirmation of the anticipated irradiation stability, a modest irradiation test program has been conducted.

Capsule and Specimen Design

The irradiation program consisted of three instrumented, temperature-controlled capsules exposed in the MTR to nominal fission burnups of 9, 16, and 26% of the U^{235} atoms.

Temperatures were monitored and controlled by two pairs of sheathed Chromel-P–Alumel thermocouples in contact with the specimen surfaces at the center and at the edge. During operation, considerable difficulty was encountered with the thermocouples.

[4]Reactor Division.

Each capsule contained two specimens of the design outlined below:

Nominal overall dimensions (in.)	2.0 × 0.50 × 0.116
Nominal core dimensions (in.)	1.5 × 0.38 × 0.102
Cladding and matrix material	Type 347 stainless steel
Fuel material	UO_2
Shape	Spheroidal
Particle size (mesh)	−100 + 140
Loading (wt %)	33.2

The specimens were prepared by procedures analogous to those used in fabricating core B prototype fuel plates.[5] The lower fuel plate in each capsule contained a small bushing which penetrated entirely through the fuel-bearing section. Leakage of fission products from around this bushing was prevented by sealing with Coast Metals No. 60 brazing alloy.

Operating History

Since two MTR reflector positions were available to this program, the nominal 9 and 16% burnup irradiations were initiated simultaneously. At the completion of the exposure of the low-burnup capsule, it was replaced by the third capsule in the program, which then ran to a nominal 26% burnup.

The temperature history of each capsule, as determined from the operational thermocouples, is summarized in Table 27.1.

The peak center-line temperature is calculated to be approximately 130°F more than the maximum surface temperature noted above. It is apparent that for a portion of the irradiation period the temperatures in capsules 46-2 and 46-5 were in excess of the core B hot-spot temperature of 1140°F.

The calculated fission burnup for capsule 46-4 was 9.32% U^{235}, whereas the measured burnup was 6.35%. On the basis of this discrepancy between predicted and actual burnup, a correction factor of 0.68 was applied to the calculated burnup for the other two capsules to predict the discharge dates (i.e., the exposures were increased by a factor of 1.47).

Table 27.1. Temperature History of Capsules Irradiated in the MTR

Capsule	Temperature Range (°F)	Maximum Average Temperature (°F)[a]
46-2	715–1220	1015
46-4	780–1010	945
46-5	700–1160	1000

[a]The cycle-to-cycle average of the hottest thermocouple.

Postirradiation Examination

As indicated in Table 27.2, virtually no change was detected for the specimens in capsule 46-4. However, the upper specimen in capsule 46-2 had a large hole melted through it, and the lower specimen swelled drastically. The overheating associated with specimen 6 could possibly have resulted from inadequate sodium coverage or shrinkage of the sodium away from the fuel during solidification on reactor shutdown. A matrix crack, which propagated entirely across the transverse section, was metallographically observed in specimen 5.

Swelling of both specimens in capsule 46-5 occurred, although the swelling was not so severe as that noted for specimen 5 in capsule 46-2. The specimens in capsule 46-5 contained microcracks in the matrix, but these had not propagated to produce gross structural defects.

From the burnup values, it may be noted that the exposure in capsule 46-2 is significantly greater than predicted. In fact, it is about that which would have been calculated had no experience factor been applied. With capsule 46-4, the reverse situation was obtained; application of the experience factor permitted close prediction of the actual burnup. The burnup-temperature relations for capsules 46-2 and 46-5 are in a range where existing information would lead one to question the suitability of this fuel. Since these conditions are somewhat more severe than the

[5]J. H. Cherubini, R. J. Beaver, and C. F. Leitten, Jr., *Fabrication Development of UO_2–Stainless Steel Composite Fuel Plates for Core B of the Enrico Fermi Fast Breeder Reactor*, ORNL-3077 (Apr. 4, 1961).

Table 27.2. Summary of Irradiation Tests on Fermi Core B Fuel Specimens

Capsule No.	Specimen No.	Surface Temperature (°F)	Fission Burnup (% U^{235})		Maximum Thickness Increase (%)	Density Decrease (%)	Observations
			Calculated	Measured			
46-4	1	780–935	9.32	6.11	0.9	0.6	No significant changes
	10	800–1010	9.32	6.60	0.6	0.4	No significant changes
46-2	5	715–1165	16.5[a]	25.9	63	12.6	Specimen swelled and blistered
	6	850–1220	16.5[a]				Specimen partially melted
46-5	8	850–1160	26.4[a]	28.4	27	8.5	Specimen swelled severely; microcracks in matrix
	9	700–1100	26.4[a]	28.9	31	6.2	Specimen swelled severely; microcracks in matrix

[a]A correction factor of 0.68 was applied, based on burnup results from capsule 46-4.

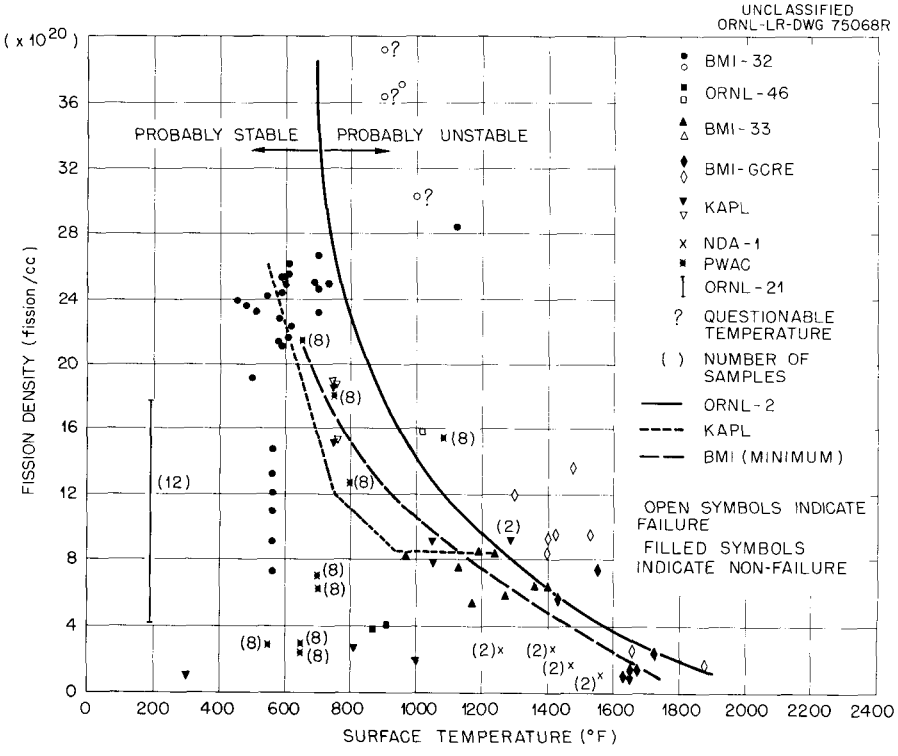

Fig. 27.2. Irradiation Stability of UO_2–Stainless Steel Dispersions.

predicted Fermi core B maxima, it is apparent that additional experiments at intermediate burnups are required to fully define capability of this fuel.

In an effort to support the above data, a study was made of the information available in the literature showing the temperature-burnup limitations for UO_2–stainless steel dispersion fuels. These results are summarized in Fig. 27.2. From the available experimental information, only those specimens for which the burnup was measured and the temperature reasonably well documented are included. It should also be noted that those fuels listed as being stable (no blistering or gross changes) often exhibited some swelling. Additional data on the effects of irradiation on UO_2–stainless steel dispersions are presented in Chap. 26, this report. Applying these data to conditions expected in core B would indicate a necessity for additional irradiation work at the specific conditions expected.

28. Water Desalination Program

D. A. Douglas

INTRODUCTION

A study of nuclear-powered seawater distilling plants is being conducted by ORNL. This study has already shown that very large reactors supplying heat to evaporators can probably produce fresh water from the sea more inexpensively than any other method presently proposed.

Nuclear and conventional power plants of today appear to have promise for saline water conversion for municipal and industrial use. However, to economically supply large quantities of water for agricultural use, the cost must be appreciably reduced. A cost reduction of the magnitude required seems possible for very large stations with inexpensive fuel cycles; R.P. Hammond and co-workers[1] recently observed that large reactor stations in the range of 25,000 Mw (thermal) may be capable of producing heat at a cost low enough to permit seawater desalination for irrigation use.

In this study, the Metals and Ceramics Division has evaluated the cost of fabricating the appropriate fuel elements for various reactor types as a function of production throughput.

Only reactors close to current technology were considered in the ORNL study; one reactor, fueled with natural uranium, moderated with D_2O, and cooled by light water seemed to provide the lowest heat cost. A reference reactor station of this type is described in Hammond's report;[1] and the proposed fuel-element design for such a reactor is shown in Fig. 28.1. In brief, the proposed element can be described as a series of concentric tubes. The annuli formed between adjacent tubes serve as containers for the fuel or as channels for the coolant; end caps are attached to encapsulate the fuel; and spacers are introduced along the length of the

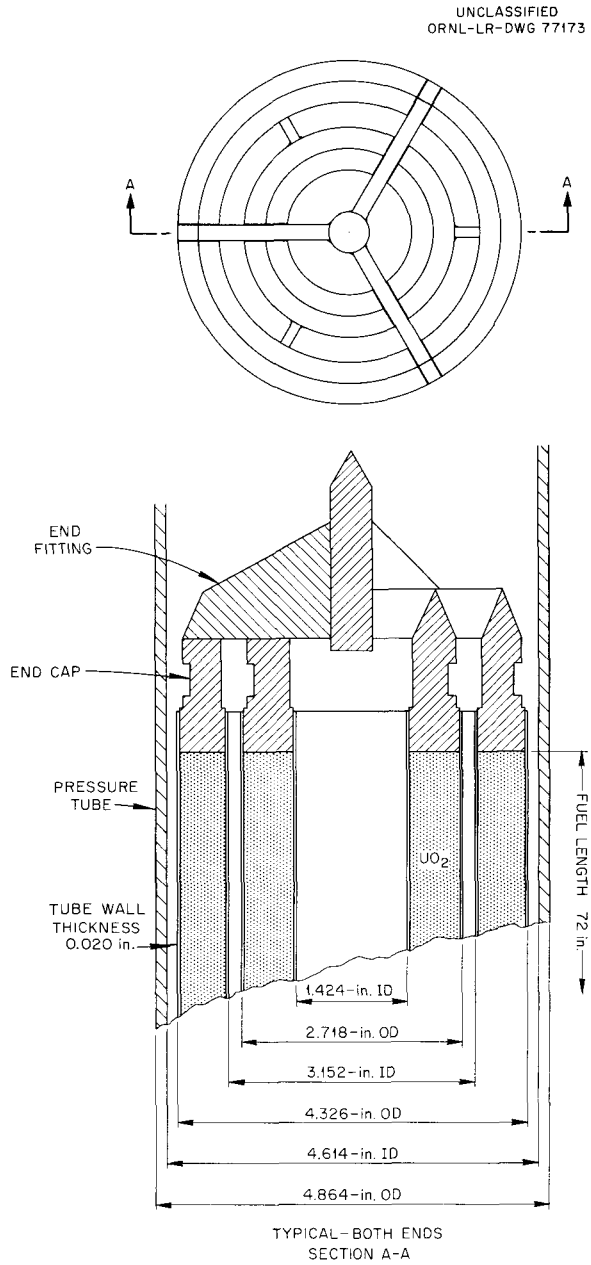

Fig. 28.1. Proposed Fuel-Element Design for Reference Reactor.

[1] R. P. Hammond, Irving Spiewak, and Gale Young, *Prospects for Sea-Water Desalination with Nuclear Energy, An Evaluation Program,* ORNL TM-465 (January 1963).

coolant channel for structural rigidity. Fuel fabrication costs developed in several case studies used this concept as the reference.

FUEL FABRICATION COSTS

Zircaloy-Clad Natural-UO_2 Elements

A. L. Lotts

Fuel fabrication costs were estimated for 3500-, 25,000-, and 100,000-Mw (thermal) reactors. With a 90% availability factor, the required production rate of a manufacturing plant would be 0.65, 4.6, and 18.4 metric tons of uranium per day to fuel these reactors.

The following procedure was used to establish cost data for elements produced in each of these plants. A fabrication line was envisioned; the capital equipment needs for each production rate were predicted; and equipment costs were then estimated. Some scaling factors conventionally employed in the construction industry were used in deriving the cost of the capital structure. The proper personnel quota for each plant was determined on the basis of experience and observation. Also considered in the cost estimates were such factors as interest, depreciation, inventory, and insurance charges; in addition, the incremental costs of rejects and shipping were included. Total costs, expressed as dollars per kilogram of uranium, are shown in the lower curve on Fig. 28.2. Since no fabrication plants designed to produce the reference element exist at any scale, the exactness of the values presented is open to question. However, the effect of production rates and the general trends illustrated appear quite valid. A complete discussion of the study can be reviewed in a forthcoming report.[2]

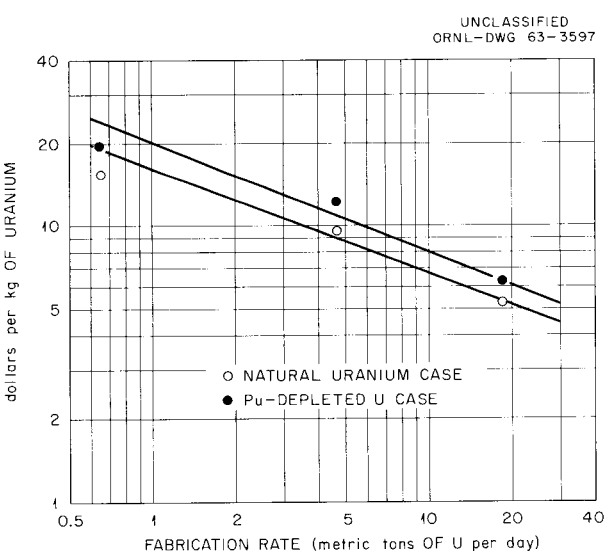

Fig. 28.2. Effect of Plant Size on the Fabrication Cost of Zircaloy-Clad-Oxide, Concentric-Tube Fuel Element.

Zircaloy-Clad Plutonium-Depleted UO_2

A. L. Lotts

Also as a part of the desalination study by ORNL, the Metals and Ceramics Division has considered the effect of processing 6 g of plutonium per kilogram of depleted uranium on the cost of fabricating the fuel element described previously. The data and information developed in the above analysis were used to estimate these costs (represented by the top curve in Fig. 28.2) for the 3500-, 25,000-, and 100,000-Mw (thermal) reactors respectively. The increased cost of the plutonium-bearing fuel element reflects the difference in mode of operation between the plutonium–depleted-uranium case and the natural-uranium case. Whereas equipment for the uranium case can be maintained and operated by contact techniques, the plutonium-fabrication equipment requires remote location, 1 ft of concrete shielding, and a larger number of maintenance personnel to cope with the more difficult maintenance required.

Because of the inaccuracies which may be inherent in these cost analyses, a more detailed conceptual study for three sizes of processing plants is now being conducted for both the plutonium–depleted-uranium case and the natural-uranium case. The operating costs of such plants are also being reevaluated.

Clad Uranium-Metal Elements

R. J. Beaver

Interest was expressed in the possibility of using uranium in the metallic rather than the ceramic

[2] A. L. Lotts and D. A. Douglas, *A Preliminary Study of Fuel Fabrication Costs for Large Heavy-Water Moderated Reactors,* ORNL TM-587 (in press).

form. Principal deterrents to the use of the metal fuel are the reduced operating temperatures and limited exposure traditionally experienced. The same general approach to the problem of estimating costs was taken as before. Extrusion and pressure bonding were examined independently as fabricating techniques; and aluminum, as well as Zircaloy, was considered for cladding material. Because of the poor performance capabilities, no serious attention is being given this concept. However, very attractive fuel costs were estimated.[3]

[3]R. J. Beaver, *Estimated Fabrication Costs for Large-Scale Production of Metal Fuel Elements,* ORNL TM-596 (in press).

GENERAL ECONOMIC STUDIES

A. L. Lotts

As an outgrowth of economic evaluations made in the ORNL Water Desalination Program, the Atomic Energy Commission, in cooperation with other governmental agencies, has undertaken a more generalized economic study of reactor systems having potential for large-scale power and water-desalination application. The Metals and Ceramics Division has provided consultation services in this study by estimating the cost of various fuel elements and the effect of production rate on their cost. The results of the study are given in Fig. 28.3.

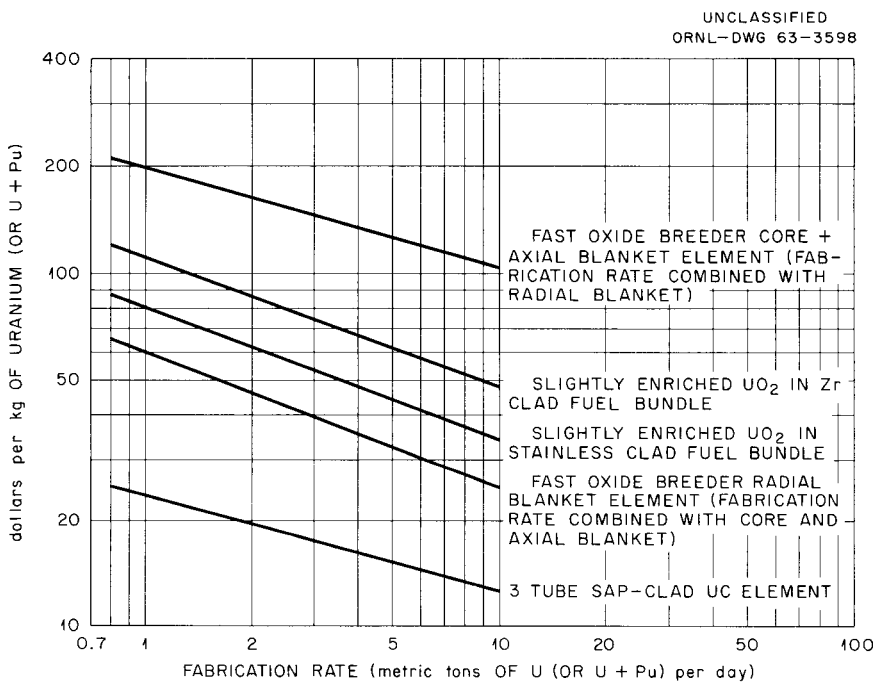

Fig. 28.3. Effect of Plant Size on the Fabrication Cost of Several Fuel Elements.

Part IV.
Other Program Activities

29. Thermonuclear Project

R. E. Clausing

INTRODUCTION

The ultimate goal of the Thermonuclear Project is to harness the energy available from the controlled fusion of the hydrogen isotopes, deuterium and tritium. This requires the production and containment of dense, high-temperature plasmas. Experiments at ORNL and elsewhere are being conducted to explore the various schemes for accomplishing this end and to discover and develop the basic plasma physics that must provide the foundation for the eventual production and practical application of thermonuclear power.

VACUUM

The present experimental work requires the achievement and maintenance of ultrahigh vacuum conditions inside the experimental machines in spite of the influx of relatively large amounts of hydrogen or hydrogen isotopes. The use of evaporated metal getter films has proved very useful. The Metals and Ceramics Division has carefully explored the use of evaporated titanium films and has developed procedures and techniques capable of very greatly improved performance. Last year, the sorption rate of these films was improved for hydrogen to a value 25 times that obtained in commercial titanium pumps.[1] During this year, data have been obtained that tend to confirm a qualitative correlation between sorption rate and film structure. This is to imply only that in a controlled series of experiments, films with certain structural features have much larger sorption rates; it is not to imply that other variables are unimportant.

Figure 29.1 illustrates the surface features of films deposited by several techniques. There appears to be a qualitative correlation between the surface areas, or roughness, of these films and their sorption rates. The sticking probabilities for hydrogen on these films immediately after preparation (and at the temperature of preparation) are, typically: (*a*) 0.05, (*b*) 0.20, (*c*) 0.25, and (*d*) 0.85. X-ray and electron diffraction studies of the films indicate either that the deposits made in the presence of helium have a very seriously distorted

Table 29.1 Sticking Probability for Various Gases on Vapor-Deposited Titanium Films[a] [(Gas Molecules Sorbed per Second)/ (Gas Molecules Striking the Film per Second)]

Gas	Substrate at −195°C		Substrate at 10°C	
	Baked[b]	Unbaked[c]	Baked[d]	Unbaked[e]
H_2	0.84	0.24	>0.11	0.07
H_2O			0.25	0.20
D_2	0.75		0.27	(0.07 for H_2)
N_2	0.90	0.85	0.15	0.08
CO	0.98	0.95	0.38	0.38
CO_2			0.6	>0.4
O_2	0.98			

[a]The titanium deposition rate was between 2×10^{14} and 4×10^{14} atoms cm^{-2} sec^{-1} for all deposits. The normal thickness before the sticking probability measurement was about 2×10^{18} atoms/cm^2.

[b]System pressures were between 2×10^{-10} and 2×10^{-9} torr during evaporation.

[c]System pressures were between 2×10^{-8} and 7×10^{-8} torr during evaporation.

[d]System pressures were between 5×10^{-9} and 8×10^{-8} torr during evaporation.

[e]System pressures were between 1×10^{-7} and 3×10^{-7} torr during evaporation.

[1]R. E. Clausing, *A Large-Scale Getter Pumping Experiment Using Vapor Deposited Titanium Films*, ORNL-3217 (Oct. 24, 1961).

UNCLASSIFIED
PHOTO 57576

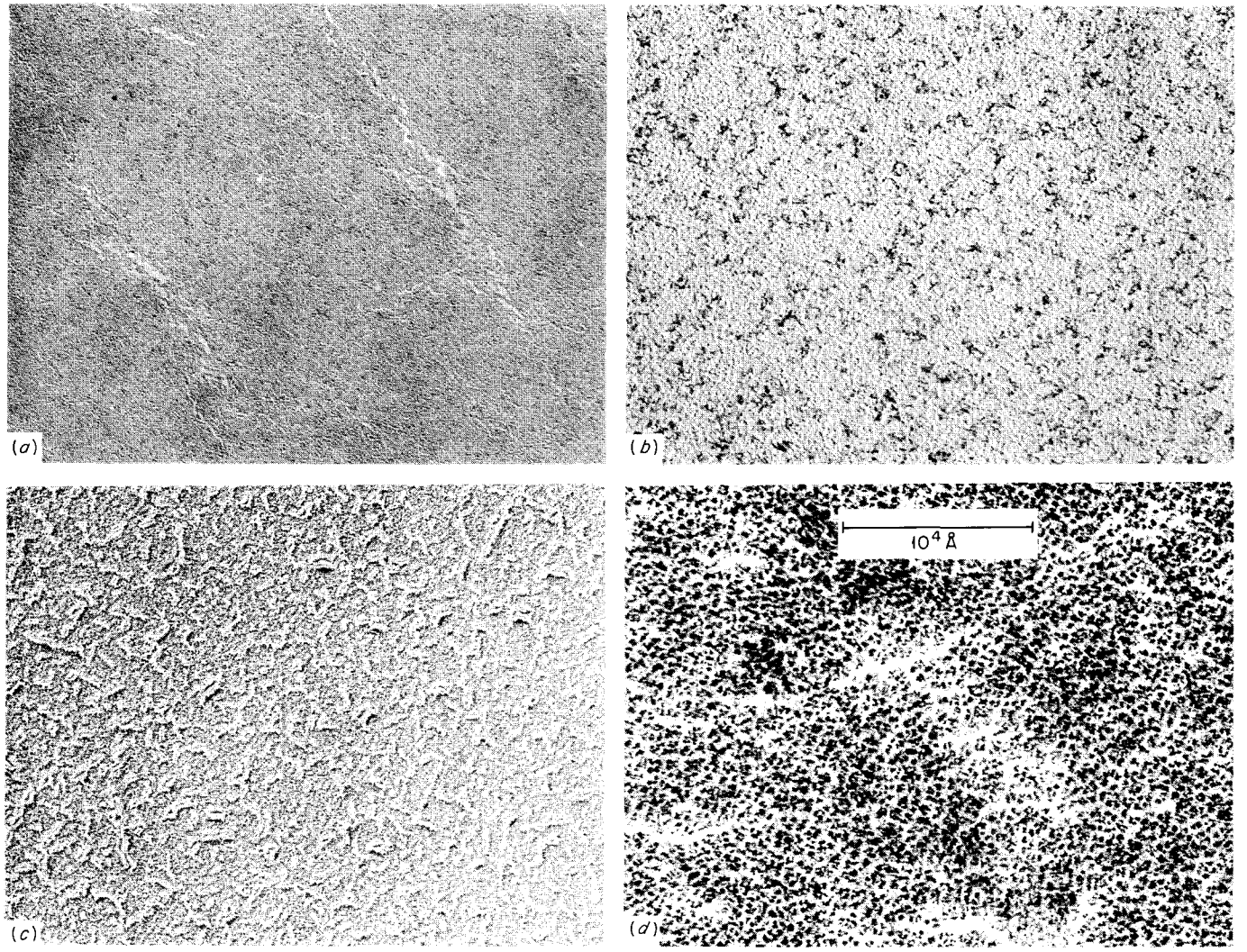

Fig. 29.1. Electron Photomicrographs Showing the Topography of Titanium Films Prepared at Various Temperatures and Pressures. (*a*) 10°C, 5×10^{-8} torr; (*b*) 10°C, 2×10^{-3} torr of helium; (*c*) −195°C, 5×10^{-8} torr; (*d*) −195°C, 2×10^{-3} torr of helium. The substrates were NaCl; the titanium deposition rates were 5×10^{14} atoms sec^{-1} cm^{-2}; the films were shadowed with palladium before exposure to high pressure and are shown at 35,000X. (*a*) and (*b*) were 10-min titanium evaporations; (*c*) and (*d*) were 1-hr titanium evaporations. Reduced 22%.

crystal structure or that each of the particles shown in the electron photomicrographs is composed of many smaller ones. That is to say, the size of the particles in the photomicrographs is too large to account for the observed broadening of the diffraction patterns.

The techniques of film formation have been further improved to permit the deposition of films with very good sorption characteristics without the need for inert gases.[2] Typical deposition conditions and sorption data are shown in Table 29.1. A detailed report of the entire study has been prepared.[3]

SUPERCONDUCTIVITY

The discovery of superconducting materials suitable for use in very high magnetic fields is of very great importance to the ultimate achievement of economical thermonuclear power. It makes the cost of obtaining the very high magnetic fields required for plasma containment very much less than that of any other method. The development of inexpensive, reproducible, and reliable superconducting magnets is thus of great importance. The Metals and Ceramics Division is conducting a series of investigations on the metallurgy of superconductors. Part of this work is supported by Thermonuclear Project funds. These investigations combine the practical problems of production and inspection of conductors (which are of immediate interest to the Thermonuclear Project) with a more basic investigation of superconducting alloys and phenomena.

Among the problems expected in the manufacture of large-volume, high-field superconducting magnets are two of immediate and major interest related to the metallurgy of superconducting materials. One of these is the problem of making joints between sections of superconducting wire and between normal and superconducting materials. It will be impossible to manufacture as one continuous length the thousands of feet to thousands of miles of wire that will be required in the large-volume magnets. It is necessary that the joints be capable of introducing the required currents from normal-state materials (e.g., copper) into the superconducting material without heating the joint to a temperature such that the superconductor is driven to the normal state. This condition can be met only if the contact resistance between the two materials is kept low. Several joint designs and materials are being investigated for metallurgical quality and current-carrying capacity. The principal problem in the joints between two superconductors is that of keeping or regaining the current density and field capabilities of the parent material. This research is being conducted as part of the study of the physical metallurgy of superconducting materials, reported in Part I, Chap. 11.

The second major problem is that of determining wire quality in a nondestructive way. The current density of the coil may be limited by small, randomly located defects of several types in any individual wire length. These defects may be mechanical in nature (i.e., cracks, internal voids or core fractures, folds, laps, seams, die marks, reduced cross sections, etc.) or they may be metallurgical in nature (i.e., variations in composition along the wire length or diameter, variations in amount of cold working or heat treatment, or variations in transformation morphology). Several methods of nondestructive examination are being developed. Most of the work to date has been concentrated on developing and using an electrical-resistance measurement in which the resistance of a 1/4-in.-high increment is measured continuously as the wire is drawn from one spool to another. The resistance is continuously recorded on a strip chart, driven at a speed which is a known ratio of the wire speed. The results obtained to date have shown resistance variations of as much as 10% in some lots of wire. Specimens have been cut from regions of low, average, and high resistance for superconducting property testing. These tests will be followed by destructive examination to determine the cause of the resistance variation.

ENGINEERING

The construction, alterations, and maintenance of a variety of experimental machines require the establishment of specifications, review of metallurgical details of construction, establishment of heat treatment procedures, and the solutions of joining and other problems on a routine basis. Although these tasks deserve mention, they are not suitable for detailed reporting.

[2] R. E. Clausing, *Thermonuclear Div. Semiann. Progr. Rept. Oct. 31, 1962*, ORNL-3392, p 86.

[3] R. E. Clausing, *Sorption of Gases by Vapor Deposited Titanium Films*, ORNL-3481 (in press).

30. Transuranium Program

D. A. Douglas

INTRODUCTION

The Transuranium Program is being carried out in two parts. One is the design and construction of the High Flux Isotope Reactor (HFIR), for which the development of the fuel element is a responsibility of the Metals and Ceramics Division. The description of this work can be found in Part III, Chap. 22, this report. The second phase of the program is the development of the criteria and the requisite equipment for the remote fabrication of the target elements. Progress on this phase is reported below.

The initial targets will contain plutonium oxide. Following their exposure in the reactor, desired isotopes will be chemically separated and suitably processed to provide material for inclusion in new targets for additional exposure. Through these sequential steps, gram quantities of the higher actinide oxides (americium, curium, berkelium, and californium) can be produced. Since the material to be processed will be highly radioactive and toxic, a heavily shielded and contained facility is required for carrying out the chemical processing and fabrication steps.

The work in the Metals and Ceramics Division consists in developing fabrication procedures that will produce a satisfactory element, conducting irradiation tests to demonstrate the adequacy of the fabrication techniques, and inventing or modifying equipment to carry out the fabrication in enclosed and shielded cubicles. Two of the more troublesome developmental problems have been the pressing of aluminum pellets containing an ideal dispersion of oxides and making satisfactory end closures by welding. A résumé of the progress achieved on the facility and these two problem areas during the past year follows.

TRANSURANIUM TARGET FABRICATION EQUIPMENT

M. K. Preston, Jr.[1]

The HFIR target elements, shown schematically in Fig. 30.1, consist of a 3/8-in.-OD finned tube and a 5/8-in. hexagonal can which is roll swaged to the fins as a spacer and coolant channel. The target is 35 in. long with 1/4-in.-diam, 0.571-in.-long pellets contained in the 20-in. active length of the rod. The remainder of the 35-in. tube consists of end caps and void space for accumulation of fission gas. The pellets will consist of an actinide oxide and aluminum powder mixture with a density that is approximately 89% of theoretical. In the pressing operation, each pellet will be completely encapsulated in an aluminum can.

The fabrication and inspection of the HFIR target elements will employ a combination of powder, metallurgical, welding, and chemical techniques. The various operations have been assigned to the three available cubicles, or cells, according to the degree of contamination expected from them. To minimize the recontamination of the target elements, auxiliary enclosures of some items of equipment will be provided within the cubicles. The basic criteria and mode of operation of the equipment have not changed substantially from those outlined previously.[2] To summarize these criteria and the operational mode, all equipment is to be designed to operate semiautomatically, requiring only minimum recourse to the manipulators. To minimize the spread of contamination, special transfer arms or similar devices will be used to effect transfer

[1] On loan from Engineering and Mechanical Division.

[2] M. K. Preston, *Metals and Ceramics Div. Ann. Progr. Rept. May 31, 1962*, ORNL-3313, pp 108-11.

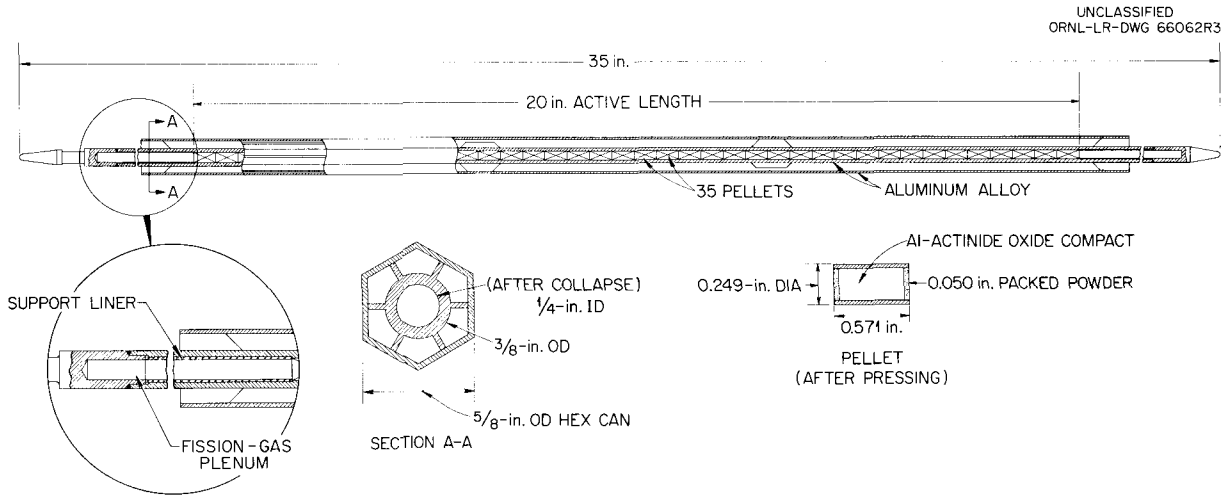

Fig. 30.1. HFIR Target Rod.

of components between steps in the process. Sensitive parts of the equipment must be easily removable and of a size such that they can be transported by the intercell conveyer for discharge and replacement. Further, all equipment will be so mounted that it can be removed from the cubicle through the 35- by 18-in. equipment transfer hatch located in the cell roof.

The following is a résumé of the status of the design and development of the target fabrication and inspection equipment for TRU, all of which is depicted in Fig. 30.2. More detailed information is available in other reports.[3-5]

Cubicle No. 3

Design and development of equipment for cubicle 3, which includes all operations up to completion of the pellets, are further advanced than those for any of the other cubicles. Conceptual design is 75% complete; conceptual study is still required on the batch weighing scale, the actinide calciner, and the piping and electrical layouts. Design of the pellet ultrasonic cleaner, pellet dryer, blender-dispenser, transfer arm, and the cap powder loader has been completed. Cubicle 3 equipment that has been constructed is the pellet press, which has been extensively tested and had design improvements incorporated; the die magazine feeder; the die loading scale; and two commercial items that combine to make the pellet ultrasonic cleaner and vibratory transfer track. All the latter equipment is being tested.

Cubicle No. 2

Conceptual design of equipment for cubicle 2 is 65% complete; the end-cap welding machine still requires conceptual study. The complete apparatus will include devices for helium filling, end cleaning, end capping, and the welding and electrical and piping layouts. Detail design of the pellet inspection and loading equipment, the hydrostatic collapse equipment, and the helium leak-test equipment is complete. Detail design of the target ultrasonic cleaner, a device for transfer of the target from cubicle 2 to cubicle 1, and the target auxiliary enclosure has started. The concept of the target transfer arm for cubicle 2 is complete, but detail design is being delayed until more processing equipment has been developed.

---

[3] W. C. Thurber and A. L. Lotts, "Development of Procedures and Equipment for Fabrication of the High Flux Isotope Reactor Target Rods," pp 27–38 in *Proceedings of the 10th Conference on Hot Laboratories and Equipment (ANS, Washington, Nov. 26–28, 1962)*, American Nuclear Society, Chicago, 1962.

[4] A. L. Lotts, *Transuranium Quart. Progr. Rept. Aug. 31, 1962*, ORNL-3375, pp 34–35.

[5] M. K. Preston, A. L. Lotts, and R. I. Deaderick, *Transuranium Quart. Progr. Rept. Nov. 30, 1962*, ORNL-3408, pp 55–65.

UNCLASSIFIED
ORNL-DWG 63-6185

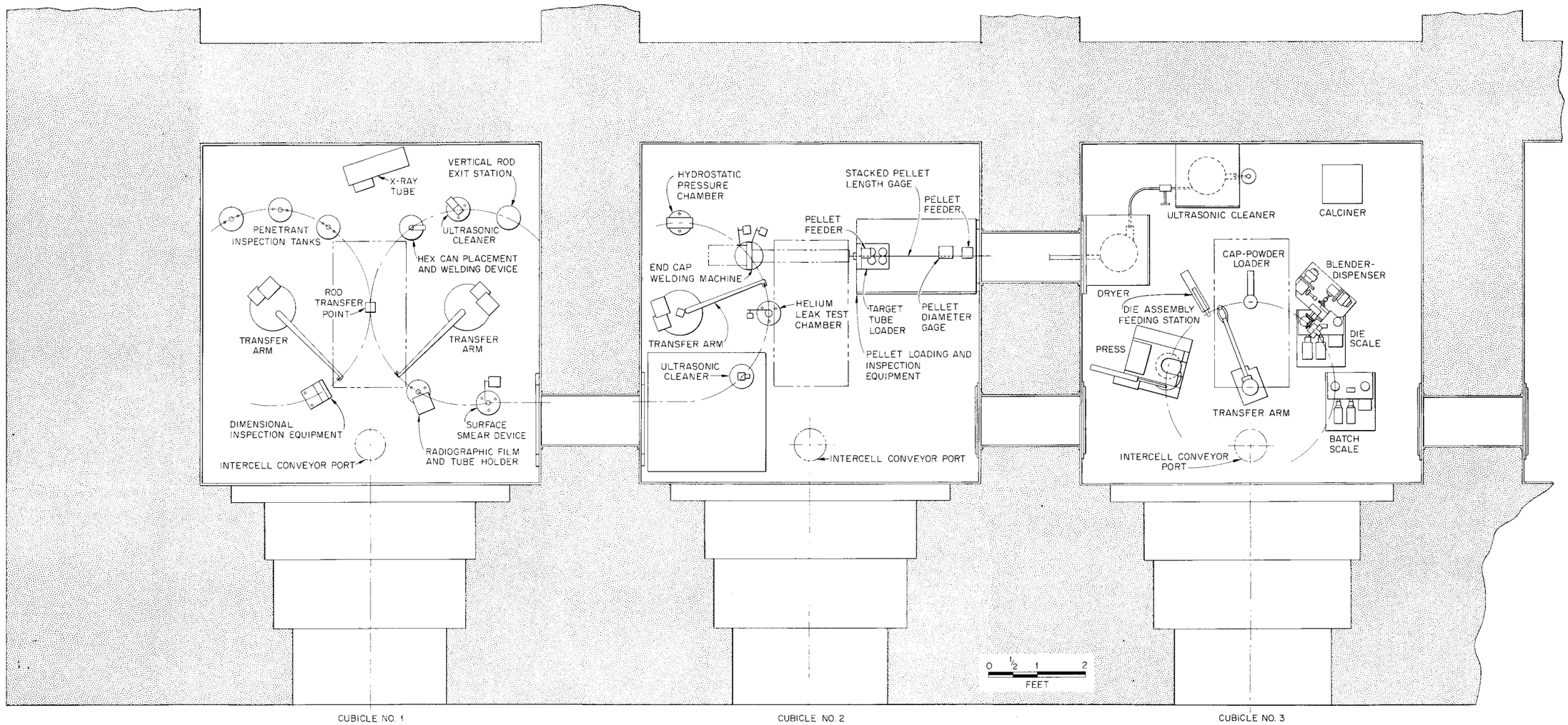

Fig. 30.2. Plan View of Transuranium Target Fabrication Equipment.

The pellet inspection and loading equipment and a prototype helium leak-test system have been assembled. Testing of the loading and inspection equipment has not started; however, the prototype helium leak-test system has been exhaustively tested, and design improvements have been initiated to simplify the overall operation of this apparatus.

Cubicle No. 1

Conceptual design of cubicle 1 equipment is just now getting under way. No significant detail design of this equipment has been accomplished.

PLUTONIUM TARGET FABRICATION EQUIPMENT

A. L. Lotts

The Pu^{242}-bearing target elements will constitute the first loadings for the HFIR flux trap. They will have the same design as those to be fabricated in the Transuranium Processing Facility (TRU). Therefore, fabrication will be essentially the same, and the equipment required is very similar. The principal difference lies in the relative simplicity of the plutonium target fabrication equipment, which can be maintained and operated by gloved hands.

Procurement and construction of part of the equipment required for the fabrication of HFIR target elements containing Pu^{242} were accomplished. Completion of this line of equipment awaits the results of process development that will allow reliable selection of the remaining equipment components. Items which were either purchased or built are all glove boxes, pellet fabrication equipment, an automatic welding outfit, a helium leak-test system, and hydrostatic collapse equipment. The glove boxes were installed in an area where complete installation and test of process equipment can be accomplished prior to installation of the equipment in an alpha laboratory.

By use of the procedures outlined above, six prototype elements were fabricated in a glove-box arrangement. These were inserted in a test reactor for irradiation.

PELLET PRESSING

D. M. Hewette II

In work accomplished over the last year,[6–8] powder-blending and pellet-pressing techniques have been developed further. Studies of the physical and mechanical properties of the target pellets were carried out to determine pellet resistance to thermal shock, thermal expansion of the composite pellet, thermal conductivity of the pellet core, and compressive yield strength of the composite pellet.

In the remote fabrication sequence, calcination, blending, and metering are to be done using a single container. A mockup of three proposed container configurations and the blending-metering equipment have been constructed. Preliminary tests performed with this equipment have demonstrated the feasibility of the blending and metering conceptual design.

Pellets are to be pressed so that the actinide oxide–aluminum core is completely contained by a cladding of aluminum and the outside surface is contamination free. Therefore, the blended actinide and aluminum powders are loaded into short, thin-walled aluminum tubes capped at each end with pure aluminum powder; this entire configuration is pressed to form the target pellet.

Thermal conductivity measurements on Al-Gd_2O_3 pellets containing 0, 10, 15, 20, and 25 vol % Gd_2O_3 have shown that the thermal conductivity decreases rapidly with increasing oxide concentration.[9] The cause of this behavior was shown to be due to the oxide being the continuous phase. The Gd_2O_3 used in these experiments was prepared by a technique similar to that which was expected to be used for processing the actinide oxides in the TRU Facility. The resulting oxide had an average particle size of 6 μ, whereas the −325 mesh aluminum has an average particle size of 20 μ. The much smaller particles tended to coat the aluminum particles as the oxide concentration

[6] E. E. Barton, R. G. Gilliland, D. M. Hewette II, and R. W. McClung, *Transuranium Quart. Progr. Rept. Feb. 28, 1962*, ORNL-3290, pp 14–19.

[7] D. M. Hewette II, *Transuranium Quart. Progr. Rept. Aug. 31, 1962*, ORNL-3375, p 24.

[8] D. A. Douglas, *Transuranium Quart. Progr. Rept. Nov. 30, 1962*, ORNL-3408, p 54.

[9] D. L. McElroy, W. Fulkerson, and T. Kollie, *Transuranium Quart. Progr. Rept. Aug. 31, 1962*, ORNL-3375, pp 25–26.

increased beyond 8 vol %. The desired loading is 17 vol %.

Thus, experiments have been directed toward obtaining a microstructure with a continuous aluminum phase to achieve a higher thermal conductivity.

Although other techniques were developed, the most desirable solution to this problem is obtained by increasing the oxide particle size and thereby ensuring a continuum of aluminum with oxide concentrations as high as 25 vol %. The ability to produce a PuO_2 powder tailored to size has been indicated.[10] A particle size range between −170 and +325 mesh has been specified tentatively for the PuO_2 loading, based on homogeneity studies performed in conjunction with the HFIR fuel element.[11] Increasing the oxide particle size increases the compactability of the pellet matrix, and the pressing pressure must be lowered from 30 to 10 tons/in.^{2} to obtain a core density of 89 to 92% of theoretical.

No pellet degradation or dimensional changes were noted on thermally cycling pellets of the original design concept between room temperature and 300°C for 40 cycles. Linear thermal-expansion measurements were made on target pellets of the original design concept between 25 and 400°C. The average coefficient of thermal expansion over this temperature range is 24.85×10^{-6} in. in.$^{-1}$ °C^{-1}. This compares very closely with the average coefficient of thermal expansion for wrought type 1100 aluminum (29.6 in. in.$^{-1}$ °C^{-1}) over the same temperature range. No permanent axial or radial expansion was observed with the composite pellets. Target pellets of the original design concept were tested in compression at room temperature in order to obtain compressive yield strengths. Six determinations of 0.2% offset yield strength gave an average value of 19,840 psi. This approaches the compressive yield strength of type 1100 aluminum H-18, which is 22,000 psi.

[10]Personal communication with R. E. Leuze, Chemical Technology Division, ORNL.

[11]Personal communication with W. J. Werner.

TARGET END CLOSURES

C. H. Wodtke

There are several reasons why the closures at the ends of the target rods must possess far greater than normal reliability. For instance, the target

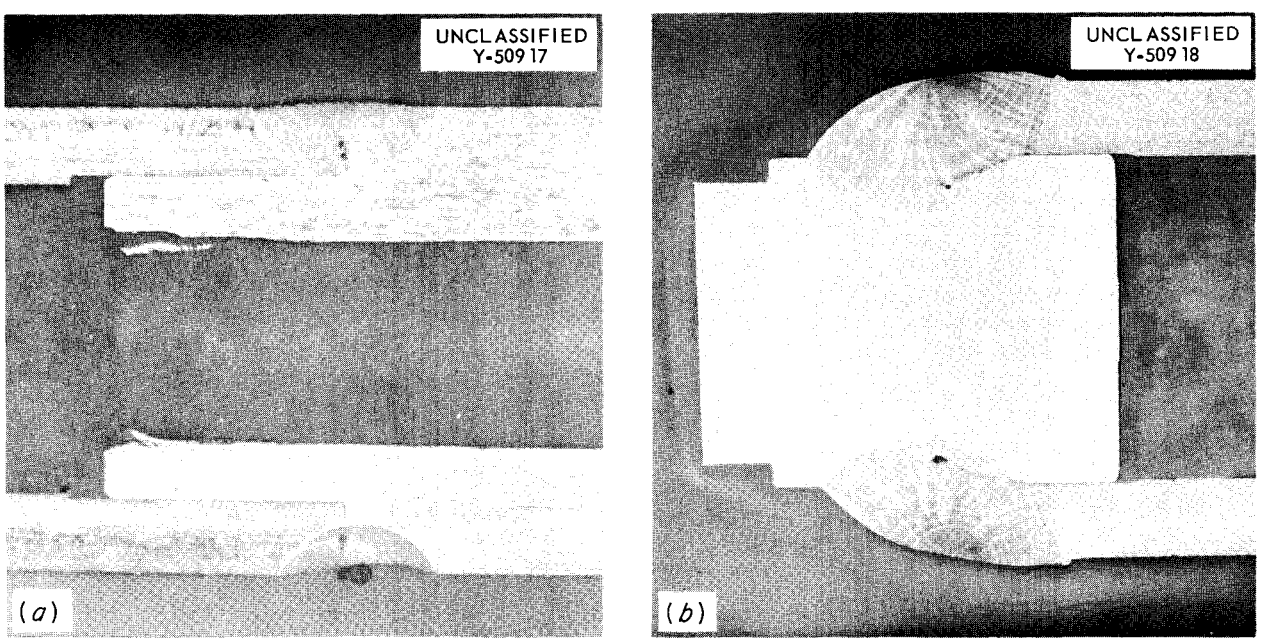

Fig. 30.3. (*a*) Typical Defects Found in Early Welds; Uneven Weld Penetration, Porosity, and Root Cracks Are Evident. (*b*) Improved Weld Made with More Suitable Welding Conditions.

service life will extend for ~18 months, and during this period will undergo many cycles of thermal and mechanical stresses. After one or two recycles, the product contained in the targets will be extremely valuable, even on a microgram scale. The product will be very toxic and highly radioactive. For these reasons, means are being sought to effect a double seal at each end of the target to obtain added strength and integrity. Welding will be the method selected for the final closure. Brazing and mechanical bonding are being investigated for the initial seal.

Welding

A fusion-welding technique of the tungsten inert-gas type will be employed. The welding problem is a difficult one. Typical defects frequently noted are weld blowout, incomplete fusion, root cracking, and cratering. Chill blocks and high rotational speed combined with high amperage are two of the necessary modifications required to reduce the frequency and magnitude of these defects. A controlled power supply and a programmed welding cycle are being developed to ensure reproducible quality. Typical defects found in the early stages of the program are shown in Fig. 30.3(*a*), and, for comparison, more recent welds are shown in 30.3(*b*).

Brazing

An aluminum-silicon alloy has been used for brazing plate-type aluminum fuel elements for many years. Its use for achieving a primary seal and adding strength to the end closure appears worth considering. Either induction heating or a furnace could be employed to obtain the required

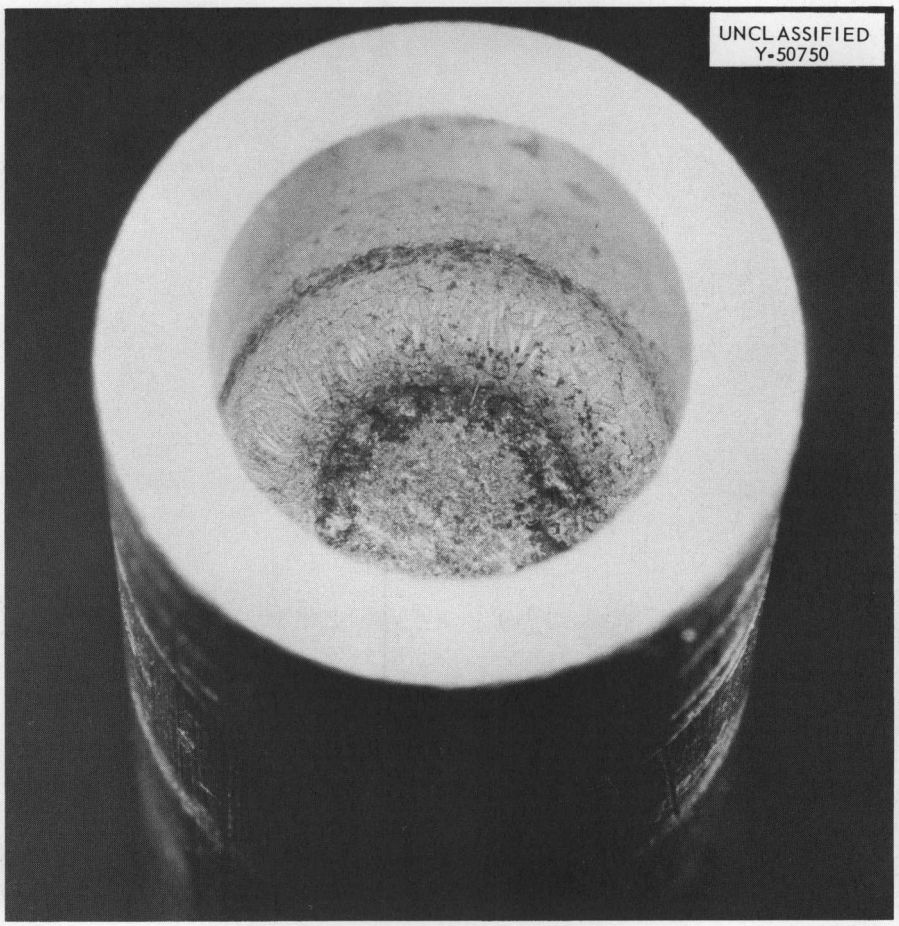

Fig. 30.4. Brazed End Closure in Aluminum Tube. Good filleting and flow of the brazing alloy are evident.

temperature. Examples of brazed end plugs are shown in Fig. 30.4. The major deterrent to the use of this technique is the problem of remotely fluxing the tubes and completely removing excess flux after brazing.

COLLAPSE OF TARGET TUBES

A. L. Lotts

At the stage of fabrication when the pellets have been pressed and inserted into the finned tubes and the end closure has been made, there is an average radial clearance of 3 mils between the pellet wall and the inside diameter of the finned tubing. A paradox now confronts the designer. If heat is not removed at a sufficient rate from the pellets, the center temperature may closely approach or exceed the melting point of aluminum. The heavy actinide oxides would then tend to settle and concentrate, leading to higher temperatures and additional melting. Preliminary heat transfer calculations have indicated that this will probably not occur if the radial gap is of the order of 3 mils. However, to add some additional margin of safety, collapse of the external tube around the pellets has been recommended.

Tubes have been collapsed around pellets by use of hydraulic pressure at ambient and elevated temperatures and by use of a "Magneform" machine. Typical results are shown in Fig. 30.5

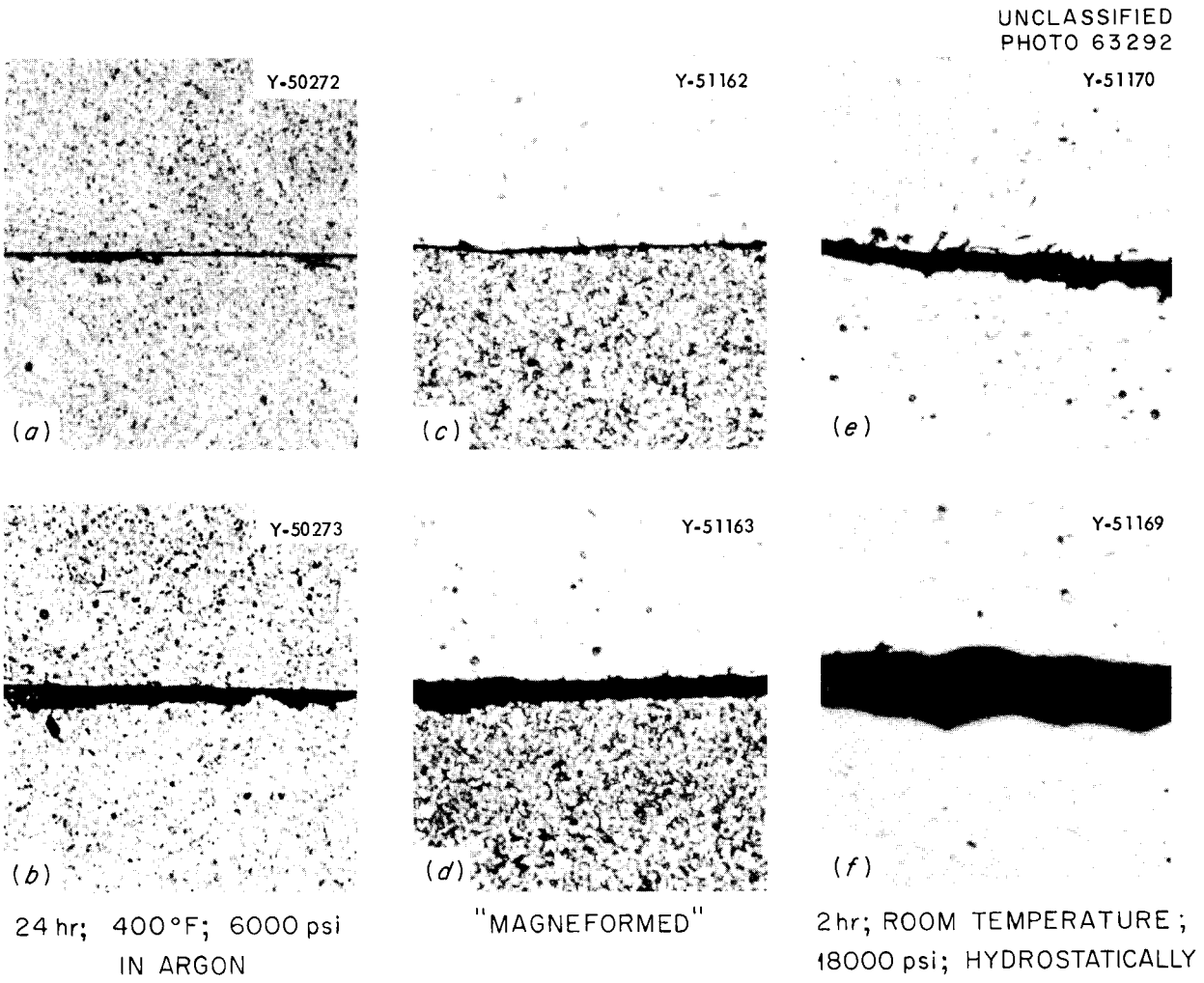

Fig. 30.5. Transverse Sections of HFIR Target Specimens. 500X. (*a*) Minimum pellet-clad gap, 0.00005 in. (*b*) Maximum pellet-clad gap, 0.0002 in. (*c*) Minimum pellet-clad gap, 0.0004 in. (*d*) Maximum pellet-clad gap, 0.0001 in. (*e*) Minimum pellet-clad gap, 0.0005 in. (*f*) Maximum pellet-clad gap, 0.0009 in.

(composite). Although use of the "Magneform" technique or hydraulic pressure at elevated temperatures provides a more uniform and closer fit, the results at ambient temperature with hydraulic pressure are considered adequate.

Although collapse aids heat transfer when contact between the pellet and tube is produced, two other undesirable phenomena may occur. Swelling of the pellet from fission-gas retention after long exposure may occur, and interaction between the pellet and tube wall during thermal cycles may cause a ratchetting effect. Under proper conditions, either may lead to failure of the tube wall. Results of the irradiation tests will be required before these questions can be resolved.

ATTACHMENT OF THE HEXAGONAL SLEEVE TO THE FINNED TUBING

M. K. Preston

The complete target loading in the HFIR will consist of three tubes inserted into individual, hexagonally shaped sleeves. The purpose of the sleeves is to prevent bowing of the tubes from hot-spot regions and to provide a channel for the coolant water. Because of the likelihood of fretting corrosion, the fins on the target tubes must be rigidly fastened to the hexagonal sleeve. Welding, brazing, and pinning have all been explored as possible means of effecting this attachment. All were discarded, owing to problems of indexing and control during remote fabrication. Thus a tool by which a good mechanical bond can be readily achieved was developed, based on the concept of roll swaging (conceived by R. W. Knight) for attaching HFIR fuel elements to side plates. The technique has been successfully demonstrated in the laboratory, and no difficulties are expected in adapting it to remote operation.

RÉSUMÉ

D. A. Douglas

The problem is to conceive of a process by which toxic and radioactive oxides in the transplutonium actinide series can be remotely fabricated into target elements. Requirements are that the final product be free from contamination on the external surface and capable of surviving ~18 months of exposure to the operating conditions of the HFIR. The status of the development has been described. The adequacy of the solutions proposed awaits the results of irradiation tests.

31. Postirradiation Examination Laboratory

A. R. Olsen

INTRODUCTION

During the past year the Postirradiation Examination Group was disbanded, and the primary responsibility for its various functions was transferred to the Hot-Cell Operations Group of the Operations Division and various functional laboratories in the Metals and Ceramics Division. From the end of the last reporting period until October 1, 1962, the date of transfer, the Group continued its service functions in the Building 4501 hot-cell facilities. The design, construction, and testing of equipment were continued, as well as the development of techniques for use in existing and future hot-cell facilities.

The construction contractor completed his work on the new High-Radiation-Level Examination Laboratory (HRLEL)[1-3] on November 5, 1962. Those portions of the construction program for which ORNL was responsible, which could not be done until after the fixed-price contractor had completed his work, were completed on May 17, 1963. With the completion of this work – which included the installation of ORNL-procured equipment, the tie-in of all services including the radioactive hot-drain system, and the repair of certain deficiencies in the prime contractor's work – the facility is now ready for the installation and integration of the experimental equipment. Actually, most of the experimental equipment has been moved to the facility, and a number of items have been installed along with the construction project equipment.

The HRLEL, as constructed, meets all of the design criteria. It provides the first high-level alpha-gamma facility at ORNL with adequate shielding for the previously established sizes of irradiated fuel elements, including that of a fully irradiated High-Flux Isotopes Reactor core after five months of cooling to permit its safe handling in air. The cell complex provides complete primary containment for all alpha-emitting materials. A safety analysis report of the entire facility is in preparation and will be issued soon.[4] This report will cover, in detail, all of the safety features and presents a proposed operational philosophy.

DEVELOPMENT OF POSTIRRADIATION EXAMINATION TECHNIQUES

R. E. McDonald D. E. Wilson

Remote Replication

R. E. McDonald

The remote replication techniques developed by the Postirradiation Examination Group[5-8] have been expanded to include complete replication of

[1] A. R. Olsen and R. E. McDonald, *Met. Div. Ann. Progr. Rept. July 1, 1960*, ORNL-2988, pp 436–37.

[2] *Technical Function and Operation of the High-Radiation-Level Examination Laboratory, Bldg. 3525*, ORNL CF-61-1-75 (Jan. 31, 1961).

[3] A. R. Olsen, "A New Postirradiation Examination Laboratory at the Oak Ridge National Laboratory," p 3 in *Proceedings of the Ninth Conference on Hot Laboratories and Equipment*, American Nuclear Society, Chicago, 1961.

[4] A. R. Olsen, J. P. Nichols, and S. Peterson, *Safety Analysis of the Operation of the High-Radiation-Level Examination Laboratory*, ORNL-3479 (in press).

[5] E. L. Long, Jr., *GCR Quart. Progr. Rept. Sept. 30, 1961*, ORNL-3210, pp 147–52.

[6] A. R. Olsen and R. E. McDonald, *Met. Div. Ann. Progr. Rept. May 31, 1961*, ORNL-3160, pp 150–52.

[7] R. E. McDonald, B. W. McCollum, and G. A. Moore, "Replication of Surfaces for Hot-Cell Applications," p 166 in *Proceedings of the Ninth Conference on Hot Laboratories and Equipment*, American Nuclear Society, Chicago, 1961.

[8] A. R. Olsen and R. E. McDonald, *Metals and Ceramics Div. Ann. Progr. Rept. May 31, 1962*, ORNL-3313, pp 127–28.

sections of the HRT core wall, both pre- and post-irradiation replications of experimental fuel capsules, and a large variety of components involving nonradioactive materials where surface topography must be recorded and filed for future reference.

To date, eleven sections of the HRT core wall from various locations have been replicated. Using the epoxy replicas, the orientation of core- and blanket-side damage can be clearly defined, and sections were designated for further metallographic examination. Work on this program is essentially complete. As a result of these replications and some laboratory experiments, it was determined that dimensional changes cannot be predictably controlled for reliable measurements. Replica thickness dimensions varied from −2% to as high as −15% of the piece dimensions on a single large replica, approximately $3 \times 7 \times \frac{1}{4}$ in. No single variable was found to be controlling. Surface reproduction was equally good at all locations regardless of the dimensional variations.

Ultrasonic Cleaning

R. E. McDonald D. E. Wilson

Although there were no unique findings in the established ultrasonic cleaning procedures for small objects, the principle was expanded to a feasibility study of the ultrasonic cleaning of large waste and storage cans for use in the HRLEL. Utilizing a 55-gal drum as a cleaning tank, three 30-in.-long racks, each supporting three submersible zirconium titanate transducers, were inserted in the tank in an equilateral triangle arrangement. With this equipment, tests have been run on cleaning 6-in.-diam aluminum cans up to 24 in. in length. Results to date indicate that gross decontamination of objects this size is no problem provided the object is traversed past the transducers. Tests with small individual samples distributed throughout the tank are being made to determine the exact cleaning patterns. No nulling effects have been found with this arrangement of transducers.

DEVELOPMENT OF REMOTE EQUIPMENT

R. E. McDonald J. R. Parrott
D. E. Wilson J. E. Van Cleve

Concurrent with the start of design on the HRLEL, a review was made of the various functions which the new facility was expected to provide. From this review, a list of equipment requirements was developed. The original list was restricted to multipurpose items; that is, items which could perform the required function on a variety of different irradiated experiments. The original listing was presented in a staff report[9] and has been reviewed, modified, and updated through the years. At this time, out of the 82 different items in the original listing, two have been dropped (the automet polisher and the inspection-molding device), no significant development or design work has been done on six items (four advanced types of nondestructive testing, a simple capacitor-discharge spot welder, the need of which is questioned, and an impact tester, because of the existence of a suitable unit in another facility), and eleven items are in an incomplete state of development (i.e., the design is complete but either the fabrication and/or mockup testing is not complete). Some 63 items have been developed, designed, constructed, and at least mockup tested. Many of the items have been in use in existing facilities for as long as three years. The development status and more recently detailed information on most of these items have been reported elsewhere.[10–15] In addition to these reports and others in preparation, detailed operational and maintenance manuals have been prepared for each equipment item which has been mockup tested.

Of all items tested and operated during the past year, four deserve special recognition. These are

---

[9] *Technical Function and Operation of the High-Radiation-Level Examination Laboratory, Bldg. 3525*, ORNL CF-61-1-75 (Jan. 31, 1961).

[10] E. L. Long, Jr., J. E. Van Cleve, and R. J. Gray, *Met. Div. Ann. Progr. Rept. July 1, 1960*, ORNL-2988, pp 348–60.

[11] A. R. Olsen, R. E. McDonald, J. R. Parrott, and J. E. Van Cleve, *Met. Div. Ann. Progr. Rept. May 31, 1961*, ORNL-3160, pp 152–57.

[12] A. R. Olsen, R. E. McDonald, J. R. Parrott, and J. E. Van Cleve, *Metals and Ceramics Div. Ann. Progr. Rept. May 31, 1962*, ORNL-3313, pp 128–32.

[13] R. E. McDonald, D. E. Wilson, and J. L. Wilson, *A Remotely Operated Measuring Device*, ORNL TM-548 (May 31, 1963).

[14] R. E. McDonald and J. L. Wilson, *In-Cell Sound Transmission System*, ORNL TM-565 (in press).

[15] A. R. Olsen, R. E. McDonald, and J. L. Wilson, *Kollmorgen Periscope Adaptations for Use in the High-Radiation-Level Examination Laboratory at the Oak Ridge National Laboratory*, ORNL TM-529 (May 17, 1963).

the x-ray diffraction unit, the fission-gas sampling device, the pinhole camera, and the gamma-ray spectrometer.

The x-ray diffraction unit, described in detail last year,[16] has been in continuous operation in one of the existing facilities providing information on a variety of samples with activity low enough to permit loading in the unshielded area.

The fission-gas sampling apparatus was developed as a prototype of the HRLEL equipment and to meet a specific need in the Molten-Salt Reactor experimental program. Of particular importance on this apparatus has been the leak-tightness of the remote puncturing head over prolonged periods of time. A standard Veeco valve was modified to provide a small-diameter O-ring sealing surface on the bottom of the body. The sealing washer on the bellows-sealed stem was replaced with a hardened tool-steel needle that pierced the capsule through the center of the O-ring. This valve was mounted on a stand above a vise with replaceable jaw inserts. The vise containing the capsules to be sampled was forced up against the O-ring with the needle retracted. The entire in-cell portion of the apparatus could be then evacuated to less than 10 μ of pressure before the needle was lowered to puncture the capsule. Repeated leak checks on a number of experiments indicated overall system leak rates of less than 2 μ/min at pressures less than 100 μ. Twice for experimental reasons[17] the capsules, after puncturing, were left sealed to this apparatus for periods of days with no detectable change in leak rates. The percentage of air in samples obtained with this system averaged less than 2% with a single high reading of 11%. A comprehensive report on this system is in preparation.

The pinhole camera which was constructed was based on a design developed by others.[18] The apparatus consisted of a cored-lead casting with the pinhole developed by the core conformation. Specimens with activities as low as 10 r/hr at 6 in. and with film-to-specimen distances as great as 40 in. were autoradiographed. These radiographs, using type AA Kodak film, provided sufficient resolution to first show the existence of smooth-surfaced voids in the bottom of the MSRE fuel capsules.[19]

The gamma-ray spectrometer installation is made up of three basic components – the spectrometer, a collimating shield functioning through a penetration in the cell wall, and an in-cell positioning mechanism. Preinstallation tests on the collimator have indicated collimation and background or scatter attenuation well beyond the design characteristics. The heart of the collimator for very high-level work consists of three removable right cylinders of tungsten. Two of these were made in two sections to provide centered 0.002 × 0.200 in. slots along their axis. One of these cylinders can be remotely rotated to provide an ultrafine collimation slot only 0.000004 in. in cross-sectional area. The third cylinder has a 0.250-in. hole bored along its axis. The tests to date indicate that the scanner will easily accommodate specimens with the design activity of 2×10^9 dis sec^{-1} cm^{-2} and will probably, with the use of the incorporated absorption features, accommodate specimens with activities at least two orders of magnitude higher. This will permit detailed nondestructive burnup analysis of any fuel element that the HRLEL shielding can accommodate.

INSTALLATION OF SHIELDED METALLOGRAPHS

R. J. Gray E. L. Long, Jr.

Shielded research metallographs manufactured by Bausch & Lomb, Rochester, New York, and Reichert, Vienna, Austria, and shown in Fig. 31.1 were installed in the HRLEL. Each metallograph is designed for alpha-beta-gamma shielding with 8 in. of steel. All offset joints in the shielding are sealed with neoprene and all the operational adjustments are relayed through the shielding as sealed rotary movements to minimize particulate contamination. A shield cover (not shown in Fig. 31.1) contains a leaded glass window for observing the stage. Mounted specimens $1\frac{1}{4}$ in. in diameter are carried to the stage of each metallograph by individual specimen relays. This operation is semiautomatic since there are no manipulators available to the operator. After the specimen is positioned on the stage, normal and X and Y movements are available to the operator.

[16] H. L. Yakel, *Metals and Ceramics Div. Ann. Progr. Rept. May 31, 1962*, ORNL-3313, pp 130–32.

[17] W. R. Grimes, *Radiation Chemistry of the Molten Salt Reactor System*, ORNL TM-500, pp 11–17 (Mar. 13, 1963).

[18] W. N. Beck, *A Pinhole Camera Autoradiographic Technique for Encapsulated Irradiated Fuel Specimens*, ANL-6533 (April 1962).

[19] *Ibid.*, p 19.

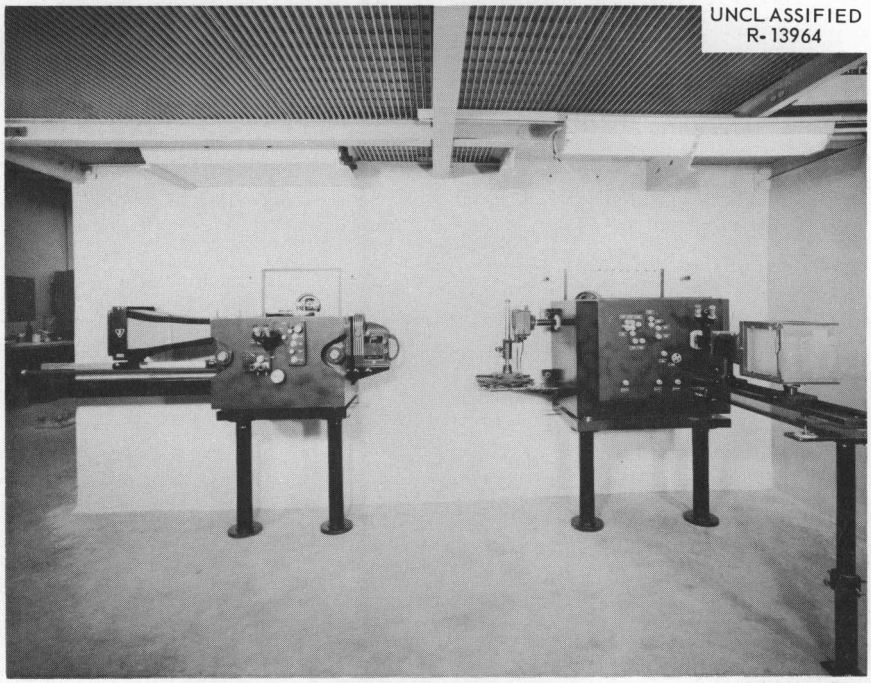

Fig. 31.1. Shielded Metallographs for HRLEL. The Bausch & Lomb unit is on the left, and the Reichert unit is on the right.

Papers, Oral Presentations, and Open-Literature Publications

Papers and Oral Presentations Given at Scientific and Technical Meetings

Nuclear Congress and International Exposition, New York, June 4–7, 1962

R. W. McClung, "Ultrasonic Methods for Examination and Acceptance of Components"

International Atomic Energy Agency, Conference on the Corrosion of Reactor Materials, Salzburg, Austria, June 4–9, 1962

J. H. DeVan* and R. B. Evans III, "Corrosion Behavior of Reactor Materials in Fluoride Salt Mixtures"

J. R. DiStefano and E. E. Hoffman,* "Relationship Between Oxygen Distribution and Corrosion in Some Refractory Metal–Lithium Systems"

H. Inouye, "High-Temperature Reactions of Type 304 Stainless Steel in Low Concentrations of Carbon Dioxide and Carbon Monoxide"

H. E. McCoy, Jr., "The Influence of Various Gaseous Environments on the Creep-Rupture Properties of Nuclear Materials Selected for High-Temperature Service"

Pacific Northwest Metals Conference, Seattle, Wash., June 7–9, 1962

P. Patriarca, "Joining of Exotic Materials for Nuclear Fuel Elements"

American Nuclear Society, Annual Meeting, Boston, Mass., June 18–20, 1962

J. S. Eldridge* and R. E. McDonald, "Use of a High-Level Gamma Spectrometer System for Nondestructive Inspection"

M. F. Osborne,* A. E. Goldman, E. L. Long, Jr., F. R. McQuilkin, and J. G. Morgan, "Beryllium Sheathed UO_2 Fuel Element Irradiation Tests"

Seventh International Conference on Coordination Chemistry, Stockholm and Uppsala, Sweden, June 25–29, 1962

G. P. Smith, Jr.,* and C. R. Boston, "Cation-NO_3^- Coordination in Fused Nitrates by Means of Shifts in the UV Spectrum of NO_3^-"

Eleventh Annual Conference on Applications of X-Ray Analysis, Denver, Colo., Aug. 8–10, 1962

C. J. Sparks, Jr.,* and B. S. Borie, "An X-Ray Determination of Debye-Waller Factors for Cu_2O and UO_2 and the Atomic Scattering Factor for Cu in Cu_2O"

Advanced Institute on Materials for Nuclear Reactors, General Electric Company, Richland, Wash., Aug. 20, 1962

W. O. Harms, "Coated Particle Fuels"

---

*Speaker

Atomic Energy Commission, Second Beryllium Oxide Coordination Meeting, Canoga Park, Calif., Aug. 23–24, 1962

W. O. Harms* and R. L. Hamner, "Fabrication and Characterization of BeO Specimens for ORNL Irradiation Tests in the Engineering Test Reactor"

R. W. Swindeman, "The Australian BeO Program"

Symposium on Measurement of Thermal Radiation Properties of Solids, Dayton, Ohio, Sept. 5–7, 1962

D. L. McElroy* and T. G. Kollie, "The Total Hemispherical Emittance of Pt, Cb–1% Zr, and Polished and Oxidized INOR-8 in the Range 100 to 1200°C"

Research Reactor Fuel Element Meeting, Gatlinburg, Tenn., Sept. 17–19, 1962

R. L. Heestand,* C. F. Leitten, Jr., and R. W. Knight, "Fabrication Development of the Advanced Test Reactor Fuel Element"

M. M. Martin,* J. H. Erwin, and C. F. Leitten, Jr., "Fabrication Development of the Involute-Shaped High Flux Isotope Reactor"

W. R. Martin* and J. R. Weir, "Mechanical Properties of X8001 Aluminum Cladding and X8001 Aluminum-Base Fuel Dispersion at Elevated Temperatures"

R. W. McClung, "Nondestructive Testing on HFIR and ATR Fuel Elements"

A. E. Richt,* C. F. Leitten, Jr., and R. J. Beaver, "Radiation Performance and Induced Transformations in Aluminum-Base Fuels"

J. W. Tackett,* J. H. Erwin, C. F. Leitten, Jr., and G. M. Slaughter, "Assembly and Welding Development for the High-Flux Isotope Reactor Fuel Element"

Zirconium Association, Discussion on Zirconium Alloy Development, Cleveland, Ohio, Sept. 26, 1962

M. L. Picklesimer, "Zirconium Alloy Research at the Oak Ridge National Laboratory"

American Society for Testing Materials, Fourth Pacific Area National Meeting, Los Angeles, Calif., Oct. 1–5, 1962

C. R. Kennedy, "The Effect of Stress State on High-Temperature Low-Cycle Fatigue"

National Association of Corrosion Engineers, Northeast Regional Meeting, Albany, N.Y., Oct. 1–3, 1962

J. H. DeVan, "Corrosion in Molten-Salt Reactor Systems"

American Welding Society, National Fall Meeting, Milwaukee, Wis., Oct. 1–4, 1962

K. V. Cook* and R. W. McClung, "Development of Ultrasonic Techniques for the Evaluation of Brazed Joints"

Sixth Conference on Analytical Chemistry in Nuclear Reactor Technology and Third Conference on Nuclear Reactor Chemistry, Gatlinburg, Tenn., Oct. 9–11, 1962

E. L. Compere, W. J. Leonard, and S. A. Reed,* "Hydriding of Zirconium Alloys in Circulating High-Temperature Aqueous ThO_2 and Thorium-Uranium Oxide Slurries"

Conference on Thermal Conductivity Methods, Second, Ottawa, Ontario, Canada, Oct. 10–12, 1962

D. L. McElroy,* T. G. Kollie, W. Fulkerson, T. G. Godfrey, and H. B. Godbee, "Progress Report on Thermal Conductivity Measurements at the Oak Ridge National Laboratory"

American Ceramic Society, 15th Pacific Coast Regional Meeting, Seattle, Wash., Oct. 17–19, 1962

W. C. Thurber, "Irradiation Studies on Nonsintered Oxide Fuels"

---

*Speaker

Metallurgical Society of AIME, Fall Meeting, New York, Oct. 28–Nov. 1, 1962

D. S. Easton* and J. O. Betterton, Jr., "The Phase Diagram of Zirconium-Gallium"

T. S. Lundy and J. I. Federer,* "Diffusion of Zr^{95} and Nb^{95} in Body-Centered Cubic Iodide Zirconium"

C. J. McHargue and H. E. McCoy,* "Effect of Interstitial Elements on Twinning and Fracture of Columbium"

R. O. Williams* and J. A. Wheeler, Jr., "The Stored Energy of Cold Work of Alloys as a Function of Composition and Temperatures"

American Society for Metals, 44th Metal Show and National Congress, New York, Oct. 29–Nov. 2, 1962

J. W. Tackett* and G. M. Slaughter, "Welding of High-Flux Isotope Reactor Fuel Elements"

American Chemical Society, Southeastern Regional Meeting, Gatlinburg, Tenn., Nov. 1–3, 1962

C. R. Boston and G. P. Smith,* "A Spectroscopic Search for Evidence of Tetrahedral Nickel(II) Complexes in Molten Salts"

D. W. James, "Orientation of Nitrate Ions in Molten Salts"

A. F. Saturno, H. W. Joy,* and L. C. Snyder, "A Test of Dewar's Split *p*-Orbital (SPO) Method"

G. P. Smith, "Anomalous Intensity of the Spectra of Octahedral-Like Complexes in Molten Salts"

Symposium on Zirconium Alloy Development, Pleasanton, Calif., Nov. 12–14, 1962

M. L. Picklesimer, "A Preliminary Examination of the Formation and Utilization of Textures and Anisotropy in Zircaloy-2"

Geological Society, Annual Meeting, Houston, Tex., Nov. 12–14, 1962

O. C. Kopp,* L. A. Harris, and G. W. Clark, "The Hydrothermal System: Alkali Hydroxide-Silica-Water in the Presence of Iron"

High-Temperature Fuels Committee, 15th, Los Alamos, N. Mex., Nov. 13–15, 1962

J. L. Scott* and W. C. Thurber,* "High-Temperature Fuel Work at the Oak Ridge National Laboratory"

Society of Aerospace Material and Process Engineers, Hollywood, Calif., Nov. 14–15, 1962

R. G. Donnelly,* R. G. Gilliland, C. W. Fox, and G. M. Slaughter, "The Development of Alloys and Techniques for Brazing Graphite"

Hot Laboratory and Equipment Conference, 10th, Washington, Nov. 26–29, 1962

W. C. Thurber* and A. L. Lotts, "Development of Procedures and Equipment for Fabrication of the High-Flux Isotope Reactor Target Rods"

American Nuclear Society Thorium Fuel Cycle Symposium, Gatlinburg, Tenn., Dec. 5–7, 1962

W. S. Ernst, Jr., "Recent Vibratory Compaction Studies in Thoria-Urania"

A. R. Irvine* and A. L. Lotts, "The Thorium Fuel Cycle Development Facility Conceptual Design"

A. L. Lotts,* J. D. Sease, R. E. Brooksbank, A. R. Irvine, and F. W. Davis, "The Oak Ridge National Laboratory Kilorod Facility"

S. A. Rabin,* S. D. Clinton, M. F. Osborne, and J. W. Ullmann, "Thorium Fuel Cycle Irradiation Program at the Oak Ridge National Laboratory"

---

*Speaker

American Physical Society, Stanford, Calif., Dec. 26–29, 1962

J. O. Betterton, Jr.,* and D. S. Easton, "Magnetoresistance and Transverse Voltage, That Is Even with Respect to the Field, in Tungsten"

Metallurgical Engineering Seminar, Purdue University, Lafayette, Ind., Jan. 29, 1963

B. S. Borie, "An X-Ray Diffraction Study of Epitaxially Induced Strains in Oxide Films Grown on Copper"

DRAGON Project Fuel Element Symposium, Bournemouth, England, Jan. 28–29, 1963

E. S. Bomar,* F. L. Carlsen, Jr., and W. O. Harms, "Development of Fueled Graphite Elements Containing Carbon-Coated Particles for Nonpurged, Gas-Cooled Systems"

American Physical Society, New York, Jan. 22–25, 1963

G. D. Kneip, Jr.,* J. O. Betterton, Jr., and J. O. Scarbrough, "The Specific Heats of Zirconium Alloys"

American Institute of Mining, Metallurgical, and Petroleum Engineers, Annual Meeting, Dallas, Tex., Feb. 24–28, 1963

R. Arsenault* and J. Weirtman, "Low-Temperature Creep in Alpha Iron"

D. O. Hobson* and C. J. McHargue, "Twinning in Columbium-Vanadium Alloys"

J. F. Murdock* and T. S. Lundy, "Diffusion of Ti^{44} and V^{48} in Body-Centered Cubic Titanium"

J. O. Stiegler* and C. J. McHargue, "Transmission Electron Microscope Study of Dislocations and Deformation Twins in Columbium and Columbium-Vanadium Alloys"

National Association of Corrosion Engineers, International Congress on Metallic Corrosion, 2d, New York, Mar. 11–15, 1963

J. R. DiStefano* and E. E. Hoffman, "The Effect of Impurities in Some Refractory Metal–Alkali Metal Systems"

AIME Conference on Deformation Twinning, Gainesville, Fla., Mar. 22, 1963

J. O. Stiegler* and C. J. McHargue, "The Effect of Impurities on Mechanical Twinning and Dislocation Behavior in Body-Centered Cubic Metals"

Society for Nondestructive Testing, Western National Meeting, Los Angeles, Calif., Mar. 18–22, 1963

C. V. Dodd, "Applications of a New Phase-Sensitive Eddy-Current Instrument"

Electrochemical Society, 123d National Meeting, Pittsburgh, Pa., Apr. 14–18, 1963

J. V. Cathcart* and G. F. Petersen, "The Characterization of Very Thin Oxide Films Formed on Copper Single Crystals"

R. E. Pawel,* J. V. Cathcart, and J. J. Campbell, "Stress Generation in Tantalum During Oxidation"

American Nuclear Society National Topical Meeting, Cincinnati, Ohio, Apr. 17–19, 1963

G. M. Slaughter, "Joining of Exotic Materials"

American Welding Society, 44th Annual Meeting, Philadelphia, Pa., Apr. 22–26, 1963

R. G. Gilliland, "Investigations on the Wettability of Various Pure Metals and Alloy Systems on Beryllium"

R. G. Gilliland* and G. M. Slaughter, "Influence of Minor Alloying Additions on INOR-8 Welds"

---

*Speaker

American Ceramic Society Annual Meeting, Pittsburgh, Pa., Apr. 28–May 2, 1963

W. S. Ernst, Jr., "Optimization of Process Parameters for Remote Fabrication of Nuclear Fuels by Vibratory Compaction"

F. L. Carlsen,* E. S. Bomar, and W. O. Harms, "Coated-Particle Development for Fueled-Graphite, Gas-Cooled Nuclear Reactors"

A. T. Chapman, "Studies on Volatility of UO_{2+x} and Phase Relations in the Uranium-Oxygen System"

Atomic Energy Commission Metallography Group, 17th, Los Alamos, N. Mex., May 21–23, 1963

R. S. Crouse, "A Portable Metallography Laboratory"

R. S. Crouse, "Replication of Microstructures Using Silicone Rubber and Epoxy Resins"

T. M. Kegley* and B. C. Leslie, "A New Microhardness Technique"

E. J. Manthos, "Replication of Irradiated Specimens with Room-Temperature Vulcanizing Silicones"

Atomic Energy Commission 12th Annual Corrosion Symposium, Pleasanton, Calif., May 20–22, 1963

J. R. DiStefano, "Refractory Metal–Lithium Corrosion Studies"

D. H. Jansen* and E. E. Hoffman, classified.

A. P. Litman* and J. R. DiStefano, "Oxygen Partitioning in Potassium-Oxygen Refractory Metal Systems"

Atomic Energy Commission Fourth Uranium Carbide Meeting, Rensselaer Polytechnic Institute Graduate Center, South Windsor, Conn., May 20–21, 1963

J. P. Hammond,* J. D. Sease, and C. Hamby, Jr., "Uranium Carbide Fabrication with UAl_2 as Sintering Aid"

AGR/EGCR Thin Can Symposium, Risley, England, May 27–29, 1963

C. R. Kennedy, "Strain Fatigue in Fuel Element Cladding"

C. R. Kennedy* and W. R. Martin, "The Effects of Irradiation on the Mechanical Properties of Metal Alloys at High Temperatures"

W. R. Martin, "Failure Mechanisms for Metal-Clad Fuel Elements"

High-Temperature Fuels Committee, 16th, Brookhaven National Laboratory, New York, May 15–17, 1963

J. L. Scott* and W. C. Thurber,* "High-Temperature Fuel Work at the Oak Ridge National Laboratory"

---

*Speaker

Publications

Adamson, G. M., Jr., R. J. Beaver, and J. E. Cunningham, "Radiation Performance and Fabrication Advances with Aluminum Dispersion Fuel Elements," pp 433–66 in *Plansee Proceedings 1961, Powder Metallurgy in the Nuclear Age* (ed. by F. Benesovsky), Springer-Verlag, Berlin, 1962.

Betterton, J. O., Jr., G. D. Kneip, Jr., D. S. Easton, and J. O. Scarbrough, "Size Effect and Interstitial Impurities in Nb_3Zr Superconductors. Superconducting Solenoids with Metal Insulation," pp 61–68 in *Superconductors* (ed. by M. Tanenbaum and W. Wright), Interscience-Wiley, New York, 1962; also published as ORNL-3303 (Aug. 28, 1962).

Borie, B. S., C. J. Sparks, Jr., and J. V. Cathcart, "Epitaxially Induced Strains in Cu_2O Films on Copper Single Crystals. I. X-Ray Diffraction Effects," *Acta Met.* **10**(8), 691–97 (1962).

Boston, C. R., and G. P. Smith, "Spectra of Dilute Solutions of Bismuth Metal in Molten Bismuth Trihalides. I. Evidence for Two Solute Species in the System Bismuth–Bismuth Trichloride," *J. Phys. Chem.* **66**(6), 1178–81 (1962).

Boston, C. R., and G. P. Smith, *Spectrophotometric Study of Dilute Solutions of Bismuth in Molten $BiCl_3$*, ORNL-3316 (Sept. 4, 1962).

Boston, C. R., and G. P. Smith, "Tetrahedral $NiCl_4^{2-}$ in Molten Salts. The Complete Spin-Allowed Spectrum of *3d* Orbital Transitions," *J. Am. Chem. Soc.* **85**(7), 1006 (1963).

Bourgette, D. T., *Preparation of Stoichiometric Uranium Monocarbide Cylinders*, ORNL TM-309 (Oct. 4, 1962).

Carden, A. E., *Thermal Fatigue – An Analysis of the Experimental Method*, ORNL TM-405 (Jan. 4, 1963).

Cathcart, J. V., J. E. Epperson, and G. F. Petersen, "Epitaxially Induced Strains in Cu_2O Films on Copper Single Crystals. II. Optical Effects," *Acta Met.* **10**(8), 699–703 (1962).

Chapman, A. T., "Phase Studies in BeO–Metal Oxide Systems Using a Porous-Collector Technique," *J. Am. Ceram. Soc.* **46**(4), 171–74 (1963).

Cherubini, J. H., and S. Peterson, *A Technique for the Quantitative Characterization of Dispersions*, ORNL TM-446 (Feb. 28, 1963).

Clausing, R. E., "A Large-Scale Getter Pumping Experiment Using Vapor Deposited Titanium Films," pp 345–56 in *1961 Transactions of the Eighth Vacuum Symposium and Second International Congress*, Pergamon Press, New York, 1962.

Clausing, R. E., *Calculation of the Requirements for Operation of Refractory-Metal Components at High Temperature in Vacuum*, ORNL TM-334 (Sept. 18, 1962).

Coobs, J. H., "Materials Development for Core I Fuel Assemblies for the Experimental Gas-Cooled Reactor," *Nucl. Sci. Eng.* **14**(1), 53–68 (1962).

Coobs, J. H., N. A. Brown, R. M. Evans, and G. M. Tolson, *Specifications and Drawings for the Control Rods for the Experimental Gas-Cooled Reactor*, ORNL TM-547 (May 29, 1963).

Coobs, J. H., E. A. Wick, R. M. Evans, and G. M. Tolson, *Specifications for Fuel Assemblies for Core I of the Experimental Gas-Cooled Reactor*, ORNL TM-546 (May 29, 1963).

Cook, K. V., and R. W. McClung, "Development of Ultrasonic Techniques for the Evaluation of Brazed Joints," *Welding J.* **41**(9), 404-s–408-s (1962); also published as ORNL TM-356 (Oct. 23, 1962).

DeVan, J. H., and R. B. Evans III, "Corrosion Behaviour of Reactor Materials in Fluoride Salt Mixtures," pp 557–79 in *Conference on Corrosion of Reactor Materials, June 4–8, 1962, Proceedings,* vol II, International Atomic Energy Agency, Vienna, 1962; also published as ORNL TM-328 (Sept. 19, 1962).

DiStefano, J. R., and E. E. Hoffman, "Relation Between Oxygen Distribution and Corrosion in Some Refractory Metal–Lithium Systems," pp 431–49 in *Conference on Corrosion of Reactor Materials, June 4–8, 1962, Proceedings,* vol II, International Atomic Energy Agency, Vienna, 1962; also published as ORNL TM-327 (Oct. 4, 1962).

Donnelly, R. G., R. G. Gilliland, C. W. Fox, and G. M. Slaughter, "The Development of Alloys and Techniques for Brazing Graphite," *Proceedings of the Fourth National SAMPE Symposium Materials Compatibility and Contamination Control Process, November 13–15, 1962, Hollywood, California,* Society of Aerospace Material and Process Engineers, 1963.

Easton, D. S., *The Phase Diagram of Zirconium-Gallium,* ORNL TM-304 (Dec. 12, 1962).

Ernst, W. S., Jr., and R. L. Beatty, "Vibratory Compacted Studies at the Oak Ridge National Laboratory," pp II-D-1–II-D-14 in *Symposium on Powder Packed Uranium Dioxide Fuel Elements, November 30 and December 1, 1961,* CEND-153 (1962), vol I.

Ferguson, D. E., E. P. Arnold, and W. S. Ernst, Jr., "Preparation and Fabrication of ThO_2 Fuels," pp 513–37 in *Il Ciclo Combustible U-Th VI Congresso Nucleare di Roma, 13–15 giugno 1961,* Comitate Nazionale Energia Nucleare, 1962.

Fleischer, B., J. H. DeVan, and J. H. Coobs, *Graphite–Stainless Steel Compatibility Studies,* ORNL TM-338 (Sept. 25, 1962).

Foster, B. E., and J. W. Evans, "X-Ray Mass Attenuation Coefficients in the Range of 50 to 150 kvp," *Nondestructive Testing* **21**(1), 51–58 (1963).

Fox, C. W., *Progress Report – Brazing of Ceramics,* ORNL TM-413 (Nov. 8, 1962).

Franco-Ferreira, E. A., and G. M. Slaughter, "Welding of Columbium–1% Zirconium," *Welding J.* **42**(1), 18-s–24-s (1963).

Gilliland, R. G., *Investigation of the Wettability of Various Pure Metals and Alloys on Beryllium,* ORNL-3438 (May 29, 1963).

Gilliland, R. G., and E. A. Franco-Ferreira, "Joining of Columbium and Tantalum," pp 169–97 in *Columbium and Tantalum,* Wiley, New York, 1963.

Gilliland, R. G., and G. M. Slaughter, "Fusion Welding of End Caps in Beryllium Tubes," *Welding J.* **42**(1), 29–36 (1963).

Gordon, P., and R. A. Vandermeer, "The Mechanism of Boundary Migration in Recrystallization," *Trans. Met. Soc. AIME* **224**(5), 917 (1962).

Grimes, W. R., G. M. Watson, J. H. DeVan, and R. B. Evans, "Radio-Tracer Techniques in the Study of Corrosion by Molten Fluorides," pp 559–74 in *Conference on the Use of Radioisotopes in the Physical Sciences and Industry, Sept. 6–17, 1960, Proceedings,* vol III, International Atomic Energy Agency, Vienna, 1962.

Harms, W. O., "Coated-Particle Fuel Development at Oak Ridge National Laboratory," pp 71–104 in *Ceramic Matrix Fuels Containing Coated Particles, Proceedings of a Symposium Held at Battelle Memorial Institute, November 5 and 6, 1962,* TID-7654 (1963); also published as ORNL TM-431 (Feb. 14, 1963).

Harris, L. A., R. A. Potter, and H. L. Yakel, "Preliminary Observations of Mixed Oxide Compounds Containing BeO," *Acta Cryst.* **15**(6), 615 (1962).

Heestand, R. L., C. F. Leitten, Jr., and R. W. Knight, "Fabrication Development of the Advanced Test Reactor Fuel Element," pp 315–36 in *Research Reactor Fuel Element Conference, September 17–19, Gatlinburg, Tennessee, 1962,* TID-7642, Bk 1 (1963).

Inouye, H., "High-Temperature Reactions of Type 304 Stainless Steel in Low Concentrations of Carbon Dioxide and Carbon Monoxide," pp 317–42 in *Conference on Corrosion of Reactor Materials, June 4–8, 1962, Proceedings,* vol I, International Atomic Energy Agency, Vienna, 1962; also published as ORNL TM-293 (Aug. 29, 1962).

Joy, H. W., "Integrals of Products of Associated Legendre Functions," *J. Chem. Phys.* **37**(12), 3018 (1962).

Kegley, T. M., Jr., and A. P. Litman, *Corrosion of Nickel-Base Specimens Exposed in the Volatility Pilot Plant Mark III Fluorinator,* ORNL TM-411 (Jan. 4, 1963).

Kennedy, C. R., *The Effect of Stress State on High-Temperature Low-Cycle Fatigue,* ORNL-3398 (Mar. 7, 1963).

Kennedy, C. R., and J. T. Venard, "Collapse of Tubes by External Pressure," pp 421–42 in *Developments in Theoretical and Applied Mechanics, Proceedings First Southeastern Conference,* vol 1, Plenum Press, New York, 1963.

Kneip, G. D., Jr., J. O. Betterton, Jr., D. S. Easton, and J. O. Scarbrough, "Superconductivity in Heat-Treated Nb-Zr Alloys," *J. Appl. Phys.* **33**(2), 754–55 (1962).

Kopp, O. C., L. A. Harris, G. W. Clark, and H. L. Yakel, "A Hydrothermally Synthesized Iron Analog of Pollucite – Its Structure and Significance," *Am. Mineralogist* **48**(1/2), 100–109 (1963).

Lefever, R. A., and G. W. Clark, "Multiple-Tube Flame Fusion Burner for the Growth of Oxide Single Crystals," *Rev. Sci. Instr.* **33**(7), 769–70 (1962).

Leitten, C. F., Jr., "Iron-Base Dispersions," pp 330–41; "Stainless-Steel-Base Dispersions," pp 341–51; "Copper-Base Dispersions," pp 384–92; "Selection of Matrix Material," pp 571–78; "Properties of Lanthanon Dispersions," pp 578–80; "Chemical Stability of Lanthanon Dispersions," pp 580–84; "Rectangular Box-Shaped Control Rods for the Stationary Medium Power Reactor," pp 636–46; "Stainless Steel–Uranium Dioxide–Boron Dispersions for Fuel Components of the Stationary Medium Power Reactor," pp 714–17 in *Neutron Absorber Materials for Reactor Control* (ed. by W. K. Anderson and J. S. Theilacker), Naval Reactors, Division of Reactor Development, USAEC, Washington, 1962.

Lichter, B. D., "Electrical Properties of Mg_2Sn Crystals Grown from Nonstoichiometric Melts," *J. Electrochem. Soc.* **109**(9), 819–24 (1962).

Lundy, T. S., and J. I. Federer, "A Method for Separating Grain-Boundary and Lattice Diffusion Effects in Polycrystalline Materials," *Trans. Met. Soc. AIME* **224**(6), 1285 (1962).

Lundy, T. S., and J. I. Federer, *Diffusion of Zr^{95} in Body-Centered Cubic Iodide Zirconium,* ORNL-3339 (Aug. 22, 1962).

Manly, W. D., and J. H. Coobs, "The Experimental Gas-Cooled Reactor," pp 49–82 in *Nuclear Metallurgy,* vol 8, IMD Spec. Rept. Ser. No. 11, the Metallurgy Society of AIME, 1962.

Martin, M. M., J. H. Erwin, and C. F. Leitten, Jr., "Fabrication Development of the Involute-Shaped High Flux Isotope Reactor Fuel Plates," pp 268–89 in *Research Reactor Fuel Element Conference, September 17–19, 1962, Gatlinburg, Tennessee,* TID-7642, bk 1 (1963).

Martin, W. R., and H. E. McCoy, "Effect of CO_2 on the Strength and Ductility of Type 304 Stainless Steel at Elevated Temperatures," *Corrosion* **19**(5), 157t–64t (1963); also published as ORNL TM-339 (Sept. 27, 1962).

Martin, W. R., and J. R. Weir, "Mechanical Properties of X8001 Aluminum Cladding and X8001 Aluminum-Base Fuel Dispersion at Elevated Temperatures," pp 549–64 in *Research Reactor Fuel Element Conference, September 17–19, 1962, Gatlinburg, Tennessee,* TID-7642, bk 2 (1963).

McClung, R. W., "Inspection of Nuclear Components," *Ultrasonic News* **6**(3), 8–15 (1962).

McClung, R. W., "Nondestructive Testing of High Flux Isotope Reactor and Advanced Test Reactor Fuel Elements," pp 337–59 in *Research Reactor Fuel Element Conference, September 17–19, 1962, Gatlinburg, Tennessee,* TID-7642, bk 1 (1963).

McClung, R. W., "Techniques for Low-Voltage Radiography," *Nondestructive Testing* **20**(4), 248–53 (1962); and *Metals Eng. Quart.* **2**(2), 68–75 (1962).

McCoy, H. E., Jr., "The Influence of Various Gaseous Environments on the Creep-Rupture Properties of Nuclear Materials Selected for High-Temperature Service," pp 263–94 in *Conference on Corrosion of Reactor Materials, June 4–8, 1962, Proceedings,* vol I, International Atomic Energy Agency, Vienna, 1962; also published as ORNL TM-326 (Sept. 19, 1962).

McCoy, H. E., Jr., *Influence of CO-CO_2 Environments of the Calibration of Chromel-P-Alumel Thermocouples,* ORNL TM-481 (Mar. 28, 1963).

McCoy, H. E., Jr., and D. A. Douglas, Jr., *Effect of Environment on the Creep Properties of Type 304 Stainless Steel at Elevated Temperatures,* ORNL-2972 (Sept. 5, 1962).

McCoy, H. E., Jr., and J. F. Murdock, "Influence of Argon and Hydrogen Environments on the Rate of Diffusion of Cobalt-60 in Nickel," *Am. Soc. Metals, Trans. Quart.* **56**(1), 11–15 (1963); also published as ORNL TM-235 (July 27, 1962).

McDonald, R. E., A. R. Olsen, D. E. Wilson, and J. L. Wilson, *A Remotely Operated Measuring Device,* ORNL TM-548 (May 31, 1963).

McElroy, D. L., T. G. Godfrey, and T. G. Kollie, "The Thermal Conductivity of INOR-8 Between 100 and 800°C," *Am. Soc. Metals, Trans. Quart.* **55**(3), 749–51 (1962).

McElroy, D. L., T. G. Kollie, and T. G. Godfrey, "Progress Report on Thermal Conductivity Measurements at Oak Ridge National Laboratory," pp 17–29 in *Proceedings of the Second Conference on Thermal Conductivity, October 10, 11, and 12, 1962,* Division of Applied Physics, National Research Council, Ottawa, Ontario, 1963.

Morgan, C. S., "Influence of Powder Properties in Sintering of Thoria," pp 126–32 in *Plansee Proceedings 1961, Powder Metallurgy in the Nuclear Age* (ed. by F. Benesovsky), Springer-Verlag, Berlin, 1962.

Murdock, J. F., "Reaction Between Beryllium and Uranium Monocarbide," *J. Nucl. Mater.* **7**(3), 192–96 (1962).

Olsen, A. R., "Trends in Hot-Cell Design," *Nucleonics* **21**(3), 66 (1963).

Olsen, A. R., R. E. McDonald, and J. L. Wilson, *Kollmorgen Periscope Adaptations for Use in the High Radiation Level Examination Laboratory at the Oak Ridge National Laboratory,* ORNL TM-529 (May 17, 1963).

Pawel, R. E., and T. S. Lundy, *A Submicron Sectioning Technique for Analyzing Diffusion Specimens of Tantalum and Niobium,* ORNL TM-575 (May 27, 1963).

Peterson, S., "Combustion of Reactor Materials," *Nucl. Safety* **4**(2), 55–62 (1962).

Picklesimer, M. L., "A Note on Some of the Intermediate Phases in the Nb-Sn System," *Appl. Phys. Letters* **1**(3), 64 (1962).

Picklesimer, M. L., "A Preliminary Examination of the Formation and Utilization of Texture and Anisotropy in Zircaloy-2," sec 13 in *Proceedings of the USAEC Symposium on Zirconium Alloy Development, Castlewood, Pleasanton, California, November 12–14, 1962,* GEAP-4089, vol II (Nov. 30, 1962); also published as ORNL TM-460 (Feb. 28, 1963).

Picklesimer, M. L., "Superconducting Transition Temperature of Purified Technetium," *Phys. Rev. Letters* **9**(6), 254 (1962).

Potter, R. A., and L. A. Harris, "Stability of $Ca_2Be_3O_5$ in the System BeO-CaO," *J. Am. Ceram. Soc.* **45**(12), 615–16 (1962).

Prislinger, J. J., *Evaluation of Subsize Izod Specimen Designs for Determining the Notch Toughness of Zircaloy-2,* ORNL TM-336 (Oct. 1, 1962).

Prislinger, J. J., *Results of Tensile Tests Performed on Materials Exposed in the Homogeneous Reactor Experiment No. 2 Blanket and Low-Flux-Core Region,* ORNL TM-337 (Oct. 2, 1962).

Richt, A. E., C. F. Leitten, Jr., and R. J. Beaver, "Radiation Performance and Induced Transformations in Aluminum-Base Fuels," pp 469–88 in *Research Reactor Fuel Element Conference, September 17–19, 1962, Gatlinburg, Tennessee,* TID-7642, bk 2 (1963).

Slaughter, G. M., C. W. Fox, E. A. Franco-Ferreira, and R. G. Gilliland, "Joining of Refractory Metals for Space Power Application," pp 728–46 in *Materials Science and Technology for Advanced Applications* (ed. by D. R. Mash), Prentice-Hall, Englewood Cliffs, N.J., 1962.

Stiegler, J. O., and C. J. McHargue, "Comments on Stacking Fault Energy of Thorium," *Acta Met.* **11**(3), 225 (1963).

Stiegler, J. O., and C. J. McHargue, *The Effect of Impurities on Mechanical Twinning and Dislocation Behavior in Body-Centered Cubic Metals,* ORNL TM-542 (May 28, 1963).

Stiegler, J. O., and T. S. Noggle, "Nitrogen Ion Bombardment of Thin Pt Films," *J. Appl. Phys.* **33**(5), 1894–95 (1962).

Tackett, J. W., J. H. Erwin, C. F. Leitten, Jr., and G. M. Slaughter, "Assembly and Welding Development for the High Flux Isotope Reactor Fuel Element," pp 290–314 in *Research Reactor Fuel Element Conference, September 17–19, 1962, Gatlinburg, Tennessee,* TID-7642, bk 1 (1963).

Taylor, A. J., "Characterization of Uranium Dioxide Powders for Sintering," pp 31–42 in *Meeting on Characterization of Uranium Dioxide Held at Oak Ridge National Laboratory, Oak Ridge, Tennessee, December 12–13, 1961,* TID-7637 (Oct. 1, 1962).

Taylor, A. J., M. P. Haydon, J. M. Robbins, and W. O. Harms, "Characterization of Spheroidal Uranium Dioxide Particles," pp 354–64 in *Meeting on Characterization of Uranium Dioxide Held at Oak Ridge National Laboratory, Oak Ridge, Tennessee, December 12–13, 1961,* TID-7637 (Oct. 1, 1962).

Thurber, W. C., "Compacted Powder Fuel Irradiation Studies at the Oak Ridge National Laboratory," pp IV-C-1–IV-C-27 in *Symposium on Powder Packed Uranium Dioxide Fuel Elements, November 30 and December 1, 1961,* CEND-153, vol II (1962).

Thurber, W. C., and A. L. Lotts, "Development of Procedures and Equipment for Fabrication of the High Flux Isotope Reactor Target Rods," pp 27–38 in *Proceedings of the 10th Conference on Hot Laboratories and Equipment,* American Nuclear Society, Inc., Chicago, 1962; and *Trans. Am. Nucl. Soc.* **5**(2), 298–99 (1962).

Williams, R. O., "Stored Energy and Release Kinetics in Lead, Aluminum, Silver, Nickel, Iron, and Zirconium After Deformation," *Trans. Met. Soc. AIME* **224**(4), 719–26 (1962).

Yakel, H. L., "High-Temperature X-Ray Diffraction Study of the Order-Disorder Transition in a Cu–32.2 Atomic Percent Gold Alloy," *J. Appl. Phys.* **33**(8), 2439–43 (1962).

Yakel, H. L., and I. Fankuchen, "Systematic Multiple Diffraction in Equi-Inclination Weissenberg Geometry," *Acta Cryst.* **15**, pt 11, 1188 (1962).

METALS AND CERAMICS DIVISION

AT

THE OAK RIDGE NATIONAL LABORATORY

AUGUST 1, 1963

DIRECTOR — J. H. FRYE, JR.
BERTIE BYRUM

ASSISTANT DIRECTOR — J. E. CUNNINGHAM
MARGE WHITE

RADIATION CONTROL OFFICER
A. R. OLSON[1]

ADMINISTRATIVE ASSISTANT
L. E. BANKER
MARY YAGGI

FUNDAMENTAL RESEARCH

B. S. BORIE[1]
FRANCES LOVING

CRYSTAL PHYSICS
G. W. CLARK
C. B. FINCH
S. D. FULKERSON
C. SCHOENE[2]

DEFORMATION OF CRYSTALLINE SOLIDS
R. O. WILLIAMS
R. ARSENAULT

REACTIONS AT METAL SURFACES
J. V. CATHCART
R. E. PAWEL
G. F. PETERSEN
J. J. CAMPBELL

SPECTROSCOPY OF IONIC MEDIA
G. P. SMITH, JR.
C. R. BOSTON
T. R. GRIFFITHS[3]
D. W. JAMES[4]
H. W. JOY
W. M. EWING

STRUCTURE OF METALS
C. J. MCHARGUE[1]
R. E. REED, SR.
R. A. VANDERMEER
J. C. OGLE

THEORY OF ALLOYING
J. O. BETTERTON, JR.
G. V. CZJZEK
D. S. EASTON
L. G. PATTERSON[2]
J. R. PENLAND[3]
J. O. SCARBROUGH

X-RAY DIFFRACTION
H. L. YAKEL, JR.
O. B. CAVIN
L. A. HARRIS
R. M. STEELE

X-RAY STUDIES OF CRYSTALLINE DEFECTS
B. S. BORIE[1]
J. S. FAULKNER
C. J. SPARKS, JR.

APPLIED RESEARCH

C. J. MCHARGUE[1]
MARY COMBS
DOLORES POE

PROJECT COORDINATION SHERWOOD
R. E. CLAUSING

ELECTRON MICROSCOPY
J. O. STIEGLER
C. K. H. DUBOSE
J. T. HOUSTON

METALLOGRAPHY
R. J. GRAY
R. S. CROUSE
E. L. LONG, JR.
W. H. BRIDGES
G. HALLERMAN
T. M. KEGLEY, JR.
E. J. MANTHOS
A. E. RICHT
M. D. ALLEN
L. A. AMBURN
N. M. ATCHLEY
E. D. BOLLING
E. R. BOYD
W. E. DENNY
W. H. FARMER
J. C. GOWER
E. P. GRIGGS
C. P. HALTOM
T. J. HENSON
R. J. HUNTER
E. H. LEE
B. C. LESLIE
R. J. LOCKETT
Z. R. MCNUTT
R. G. SHRADER
E. D. SIMS
S. E. SPENCER
H. R. TINCH
C. E. WADDELL, JR.
R. M. WALLACE
M. A. WHEELER
C. E. ZACHARY

METALLURGY OF SUPERCONDUCTING MATERIALS
M. L. PICKLESIMER[1]
E. E. BARTON, JR.
G. R. LOVE
J. A. WHEELER, JR.
J. P. GORDON

PHYSICAL PROPERTIES
D. L. MCELROY
T. G. KOLLIE
J. P. MOORE
W. FULKERSON
R. S. GRAVES
W. LAING[2]
W. P. MURRAY[2]

SINTERING STUDIES
C. S. MORGAN, JR.
C. S. YUST
L. L. HALL

SOLID REACTION STUDIES
T. S. LUNDY
W. K. BIERMANN[5]
D. HEITKAMP[5]
J. F. MURDOCK
F. R. WINSLOW
T. L. BOSWELL
R. A. PADGETT, JR.

ZIRCONIUM ALLOY DEVELOPMENT
M. L. PICKLESIMER[1]
J. C. BANTER
S. PETERSON
P. L. RITTENHOUSE
J. C. WILSON
P. J. JONES
G. C. NELSON

RESEARCH AND DEVELOPMENT

P. PATRIARCA
W. C. THURBER[1]
ANN HOBBS
EDITH TAYLOR

PROJECT COORDINATION CE-NYTA-SPACE-MSRP
A. E. GOLDMAN
A. TABOADA[1]
W. C. THURBER[1]
J. B. PHILLIPS

CERAMICS LABORATORY
W. O. HARMS
R. L. BEATTY
E. S. BOMAR, JR.
F. L. CARLSEN, JR.
JI YOUNG CHANG[7]
A. T. CHAPMAN
J. L. COOK
W. S. ERNST, JR.
T. O. GODFREY, JR.
R. L. HAMNER
NIGEL HILL[2]
R. E. MEADOWS
R. A. POTTER
J. M. ROBBINS
A. J. TAYLOR
S. J. ACRES
B. R. CHILCOAT
C. M. FITZPATRICK
J. A. GRIFFIN
F. P. JEFFERS
J. E. POPE
W. W. PROAPS
D. E. ROSSON
W. H. SMITH, JR.

CORROSION ENGINEERING
A. TABOADA[1]
B. FLEISCHER
G. M. TOLSON
E. J. LAWRENCE
M. A. REDDEN

MATERIALS COMPATIBILITY
J. H. DEVAN
E. E. HOFFMAN
W. H. COOK
J. R. DISTEFANO
D. H. JANSEN
A. P. LITMAN
J. L. GRIFFITH
J. W. HENDRICKS
B. W. MCCOLLUM
R. E. POTTER
L. R. TROTTER

PHYSICAL METALLURGY
H. INOUYE
D. T. BOURGETTE
T. K. ROCHE
J. F. NEWSOME
S. H. WHEELER

SPECIAL ASSIGNMENTS
J. H. COOBS[8]
W. J. LEONARD
J. R. MCGUFFEY[1]
J. J. PRISLINGER[9]
G. D. BRADY

RESEARCH AND DEVELOPMENT

G. M. ADAMSON[1]
FREDA FINN

PROJECT COORDINATION ATR-HFIR-APPR-FERMI
G. M. ADAMSON, JR.[1]
R. J. BEAVER
J. R. MCGUFFEY[1]

METAL FORMING AND CASTING
C. F. LEITTEN, JR.
J. H. ERWIN
J. I. FEDERER
R. L. HEESTAND
D. O. HOBSON
R. W. KNIGHT[10]
M. MARTIN
R. E. MCDONALD
N. P. PIENAAR[11]
G. E. ANGEL
K. P. BAYNE
C. E. DUNN
J. B. FLYNN
J. W. GEER
G. D. GOLDSTON
J. N. HIX
C. R. HOLLAND, JR.
L. QUEENER
E. R. TURNBULL
H. J. WALLACE

POWDER METALLURGY
J. P. HAMMOND
J. A. BURKA
D. M. HEWETTE II
K. K. SAHA[12]
W. J. WERNER
T. W. COFFEY
C. HAMBY, JR.
W. R. JOHNSON
J. H. TERRY

WELDING AND BRAZING
G. M. SLAUGHTER
R. G. DONNELLY
C. W. FOX
E. A. FRANCO-FERREIRA
R. G. GILLILAND
J. W. TACKETT
C. H. WODTKE
L. G. BRYSON
F. J. CUZZE[2]
J. D. HUDSON
H. H. SCOTT[2]
R. G. SHOOSTER
L. C. WILLIAMS
J. J. WOODHOUSE, JR.

RESEARCH AND DEVELOPMENT

D. A. DOUGLAS, JR.[1]
JANE MORRISON
LOUIE MAE PYATT

PROJECT COORDINATION FUEL CYCLE – TRANSURANIUM
D. A. DOUGLAS, JR.[1]
A. R. OLSEN[1]
S. A. RABIN
J. T. EAST

FUEL EVALUATION
J. L. SCOTT
R. E. ADAMS
R. B. FITTS
C. MICHELSON[13]
R. A. BOWMAN
G. A. MOORE[14]

MECHANICAL PROPERTIES
J. R. WEIR, JR.
W. W. DAVIS
C. W. DOLLINS
D. G. HARMAN
C. R. KENNEDY
W. R. MARTIN
H. E. MCCOY, JR.
R. L. STEPHENSON
R. W. SWINDEMAN[6]
J. T. VENARD
J. W. WOODS
J. C. ZUKAS
F. L. BEELER
K. W. BOLING
E. BOLLING
V. R. BULLINGTON
D. G. GATES
V. G. LANE
A. G. LYON[2]
B. MCNABB, JR.
E. B. PATTON, JR.
C. K. THOMAS
R. D. WADDELL, JR.
C. W. WALKER
B. C. WILLIAMS

NONDESTRUCTIVE TESTING
R. W. MCCLUNG
K. V. COOK
C. V. DODD III
B. E. FOSTER
S. D. SNYDER
L. D. CHITWOOD
O. E. CONNER
R. A. CUNNINGHAM, JR.
R. L. FITZGERALD
W. J. MASON

REMOTE FABRICATION
A. L. LOTTS
R. L. PILLOTON
R. B. PRATT
M. K. PRESTON[10]
J. D. SEASE
J. E. VAN CLEVE, JR.
J. E. EVE
C. M. SMITH, JR.[15]
M. E. WOODWARD

DIVISION SERVICES

BUDGET AND TIMEKEEPING
R. G. CARDWELL, JR.
H. W. HOOVER

PROCUREMENT AND MAINTENANCE
R. J. STEERE
RUTH HENGSTLER

REPORTS OFFICE
M. R. HILL
GENEVA HARRIS
FRANCES SCARBORO
SUSAN THOMPSON
EMILY WELLS

[1]DUAL CAPACITY
[2]CO-OP STUDENT
[3]VISITOR FROM ENGLAND
[4]VISITOR FROM NEW ZEALAND
[5]VISITOR FROM GERMANY
[6]ON LOAN TO AAEC, RES. ESTABLISHMENT, LUCAS HEIGHTS
[7]VISITOR FROM KOREA
[8]ON LOAN TO AEE, WINFRITH, ENGLAND
[9]ON LOAN TO P AND E DIVISION
[10]ON LOAN FROM P AND E DIVISION
[11]VISITOR FROM AFRICA
[12]VISITOR FROM INDIA
[13]ON LOAN FROM TVA
[14]ON LOAN FROM REACTOR DIVISION
[15]ON LOAN TO REACTOR DIVISION

ORNL-3470
UC-25 – Metals, Ceramics, and Materials
TID-4500 (23rd ed.)

INTERNAL DISTRIBUTION

1. Biology Library
2–4. Central Research Library
5. Reactor Division Library
6–7. ORNL–Y-12 Technical Library, Document Reference Section
8–57. Laboratory Records Department
58. Laboratory Records, ORNL R.C.
59. Laboratory Shift Supervisor
60. G. M. Adamson, Jr.
61. L. G. Alexander
62. R. J. Beaver
63. J. O. Betterton, Jr.
64. D. S. Billington
65. A. L. Boch
66. E. G. Bohlmann
67. B. S. Borie
68. R. B. Briggs
69. J. V. Cathcart
70. G. W. Clark
71. R. E. Clausing
72. J. H. Coobs
73. J. A. Cox
74. F. L. Culler
75. J. E. Cunningham
76. J. H. DeVan
77. D. A. Douglas, Jr.
78. J. H. Erwin
79. J. H. Frye, Jr.
80. J. H. Gillette
81. A. E. Goldman
82. R. J. Gray
83. B. L. Greenstreet
84. W. R. Grimes
85. J. P. Hammond
86. W. O. Harms
87. C. S. Harrill
88–97. M. R. Hill
98. N. E. Hinkle
99. A. Hollaender
100. A. S. Householder
101. A. P. Huber (K-25)
102. H. Inouye
103. R. G. Jordan (Y-12)
104. M. T. Kelley
105. R. B. Korsmeyer
106. J. A. Lane
107. C. E. Larson
108. C. F. Leitten, Jr.
109. R. S. Livingston
110. A. L. Lotts
111. T. S. Lundy
112. H. G. MacPherson
113. W. D. Manly
114. R. W. McClung
115. D. L. McElroy
116. C. J. McHargue
117. A. J. Miller
118. E. C. Miller
119. C. S. Morgan
120. K. Z. Morgan
121. M. L. Nelson
122. A. R. Olsen
123. R. B. Parker
124. P. Patriarca
125. M. L. Picklesimer
126. H. W. Savage
127. A. W. Savolainen
128. L. D. Schaffer
129. J. L. Scott
130. H. E. Seagren
131. M. J. Skinner
132. G. M. Slaughter
133. C. O. Smith
134. G. P. Smith, Jr.
135. P. E. Stein
136. J. O. Steigler
137. J. A. Swartout
138. A. Taboada
139. E. H. Taylor
140. W. C. Thurber
141. M. S. Wechsler
142. A. M. Weinberg
143. J. R. Weir, Jr.
144. G. C. Williams
145. R. O. Williams
146. J. C. Wilson
147. H. L. Yakel
148. A. A. Burr (consultant)
149. J. R. Johnson (consultant)
150. C. S. Smith (consultant)
151. R. Smoluchowski (consultant)

EXTERNAL DISTRIBUTION

152. D. E. Baker, General Electric Company, Hanford
153–154. David F. Cope, Oak Ridge Operations Office
155. Ersel Evans, General Electric Company, Hanford
156. J. L. Gregg, Cornell University
157. E. G. Haas, Department of the Navy, Washington, D.C.
158. E. E. Hoffman, General Electric Flight Propulsion Laboratory Operations, Cincinnati
159. R. W. McNamee, Union Carbide Corporation, New York
160. R. R. Nash, Code 423, Metallurgy Branch, Office of Naval Research
161. Henry M. Otte, RIAS Research Institute
162–165. J. Pheline, Centre d'Etudes Nucleaires de Saclay
166. H. B. Rahner, Savannah River Operations
167. Thomas A. Read, University of Illinois
168. J. Simmons, U.S. Atomic Energy Commission, Washington, D.C.
169. Lawrence M. Slifkin, University of North Carolina
170. E. E. Stansbury, University of Tennessee
171. D. K. Stevens, U.S. Atomic Energy Commission, Washington, D.C.
172. Dorothy Smith, Division of Research, U.S. Atomic Energy Commission, Washington, D.C.
173. Watt Webb, Union Carbide Metals
174. Division of Research and Development, AEC, ORO
175–756. Given distribution as shown in TID-4500 (23rd ed.) under Metals, Ceramics, and Materials category (75 copies – OTS)